PERFORMANCE STUDIES OF THE

TUBULAR FILTER PRESS

Gunter Eduard Rencken

Submitted in partial fulfilment of the requirements for the degree of Doctor of Philosophy in the Department of Chemical Engineering, University of Natal, Republic of South Africa.

Durban
January 1992

ABSTRACT

The tubular filter press is a novel tubular configured filter press for the filtration or dewatering of sludges.

The unique features of the filter press are :

(i) during the cake deposition cycle, cake is deposited on the internal walls of a self-supporting array of *horizontal* collapsible porous fabric tubes;

(ii) during the cake removal cycle, cake is dislodged from the tube walls by means of a roller cleaning device and the dislodged flakes of cake are hydraulically transported out of the tubes by the feed sludge which is simultaneously re-circulated at a high flow rate through the tubes.

The two main problems experienced on a prototype tubular filter press, which was erected at a water treatment plant to dewater the sludge from the clarifier underflow, were :

(i) tube blockage problems during the filtration cycle;

(ii) low cake recoveries (high cake losses) during the cake removal cycle.

The following objectives which were defined for this study, were regarded as fundamental prerequisites for any solution of the two main problems :

(i) to develop a predictive dead-end internal *cylindrical* model for compressible cake filtration inside a porous tube;

(ii) to investigate the cake losses during the cake removal cycle of the tubular filter press;

(iii) to develop a predictive unsteady-state internal cylindrical cross-flow microfiltration model for a non-Newtonian sludge which, when filtered, produces a very compressible cake. (An alternative to dead-end filtration during the filtration cycle of a tubular filter press is low axial velocity cross-flow filtration).

On the basis of the objectives the study was divided into three separate investigations.

To date no one has developed a model which incorporates the cylindrical configuration of the filter medium for dead-end compressible cake filtration *inside* a porous tube. The most comprehensive model for dead-end *external* cylindrical compressible cake filtration is that of Tiller and Yeh (1985). This model was adapted for *internal* cylindrical compressible cake filtration.

In essence the model by Tiller and Yeh (1985) requires the solution of a system of two ordinary differential equations in order to calculate the radial variation of solids compressive and liquid pressures in a compressible filter cake deposited externally on a cylindrical surface. The relevant equations were derived for internal cylindrical compressible cake filtration and it was found that one of the differential equations changes from :

$$\frac{dp_l}{dr} = \frac{\mu_l Q}{2\pi r K} \qquad (external\ cylindrical)$$

to

$$\frac{dp_i}{dr} = -\frac{\mu_f Q}{2\pi r K} \qquad (internal\ cylindrical)$$

The other differential equation remains unaltered for internal cylindrical compressible cake filtration.

A batch of waterworks clarifier sludge from the prototype tubular filter press was used for experiments to evaluate the performance of the internal cylindrical filtration model. The cake produced by the filtration of this sludge had to be characterized for the model. Compression-permeability data were obtained over a wide solids compressive pressure range. A Compression-Permeability (C-P) cell was used for high solids compressive pressures (10 kPa $\leq p_s \leq$ 400 kPa) and settling tests were used for low solids compressive pressures (0,0065 Pa $\leq p_s <$ 525,6 Pa). The cake was found to be very compressible (compressibility coefficient = 0,989). Empirical equations of the form, $K = F p_s^{\delta}$ and $(1-\epsilon) = B p_s^{\beta}$, were derived from the C-P cell and settling tests to relate permeability and porosity to solids compressive pressure. The equations were slightly different to those proposed by Tiller and Cooper (1962).

The predictions by the internal cylindrical compressible cake filtration model were compared to the results of constant pressure internal cylindrical filtration experiments, at filtration pressures of 100 kPa, 200 kPa and 300 kPa, using the waterworks clarifier sludge. The internal diameter of the filter tube which was used for the experiments was 26,25 mm. The model accurately described the results of the filtration experiments in terms of volume of filtrate, average cake dry solids concentration, filtrate flux and internal cake diameter.

The differences between external cylindrical, internal cylindrical and planar compressible cake filtration were highlighted.

Since the tubular filter press is a novel process, the cake losses during the cake removal cycle have not been investigated before. An investigation was therefore conducted into the cake losses which occur during the cake removal cycle.

The same batch of clarifier sludge was also used for the investigation of cake losses during the cake removal cycle at filtration pressures of 100 kPa and 300 kPa. It was found that significant cake losses occurred due to :

(i) the shear of the cleaning fluid prior to the action of the rollers (losses varied between 10 % to 20 % of the deposited cake dry solids);

(ii) the combined action of the rollers when dislodging the cake and the hydraulic conveyance of the dislodged flakes of cake (losses varied between 30 % to 40 % of deposited cake dry solids).

A new shear model, which was developed, accurately predicted the cake losses and increase in internal cake diameter and average cake dry solids concentration, which occurred due to the

shear of the cleaning fluid. For the shear model the sludge (cake) rheology was determined using a capillary-tube viscometer. It was found that the sludges exhibited Bingham plastic behaviour in the solids concentration range : 3,58 % m/m $\leq c_s \leq$ 16,71 % m/m.

The cake losses due to the action of the rollers and hydraulic conveyance of the dislodged flakes of cake decreased markedly as filtration pressure and filtration time were increased, while a decrease in path length for hydraulic conveyance of dislodged cake flakes resulted in a mild decrease in these cake losses.

A literature review revealed that to date only one mathematical model (Pearson and Sherwood, 1988) is available for the unsteady-state cross-flow microfiltration of a non-Newtonian sludge which, when filtered, produces a compressible cake. A new unsteady-state internal cylindrical axial convection shear model (for laminar flow of the feed sludge) was developed for cross-flow microfiltration of a Bingham plastic sludge which, when filtered, produces a very compressible cake. Similar to the approach by Pearson and Sherwood (1988) this model is a combination of the dead-end internal cylindrical compressible cake filtration model and the "cleaning fluid" shear model. The major difference between the new model and the model by Pearson and Sherwood (1988) is that unlike the convection-diffusion model of Pearson and Sherwood (1988), diffusive and shear induced diffusive back-mixing of particles were assumed to be negligible. The existence of a shear plane within the cake forms the basis of the model. Those cake layers with a yield stress less than the shear stress exerted by the flowing feed sludge at the inner cake wall are convected along the shear plane. It was assumed that the *axial convection* of the solids in the moving cake layer along the shear plane is the sole mechanism for removal of solids deposited at the cake surface.

The model was compared to the results of cross-flow microfiltration experiments at one filtration pressure (300 kPa) and cross-flow flow rates of 0,84 ℓ/min; 1,58 ℓ/min; 2,43 ℓ/min and 4,44 ℓ/min. The model accurately described the variation of filtrate flux, internal cake diameter and average cake dry solids concentration during the unsteady-state time period. The model, however, had to be "extended" by incorporating empirical equations for changes in permeability and porosity (due to further cake compaction) to obtain a good fit between the model and experimental results during the pseudo steady-state time period.

The results of all three investigations provide a greater understanding of the cake deposition process (during both dead-end and cross-flow filtration modes) and the cake removal process for the tubular filter press. This should assist in finding solutions to the two main problems which were experienced on the prototype tubular filter press.

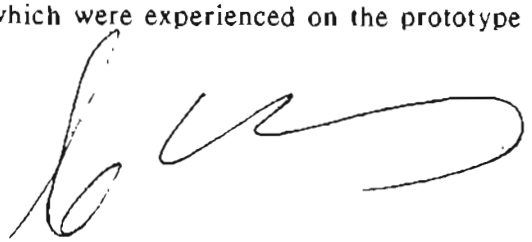

STATEMENT

Most of the work presented in this thesis was carried out in the Department of Chemical Engineering of the University of Natal. The work is my own except where otherwise stated in the text and has not been submitted to any other university for degree purposes.

G.E. RENCKEN

January 1992

ACKNOWLEDGEMENTS

The guidance and supervision of Prof. C.A. Buckley and Prof. J.D. Raal during this project is gratefully acknowledged. Their enthusiasm and experience were of great assistance throughout the investigation.

The management of Umgeni Water, especially Mr. W.N. Richards, Director of Scientific Services, supported my part-time secondment from Umgeni Water to the Pollution Research Group at the University of Natal.

This investigation and my part-time secondment were financed by the Water Research Commission under Project No. 238, *Research on the Design Criteria for Cross-flow Microfiltration*. Explochem Water Treatment (Pty) Ltd. contributed a significant sum of money towards the procurement of equipment for the experimental apparatus.

The advice from and discussions held with staff and postgraduate students in the Department of Chemical Engineering are also acknowledged. My sincere gratitude is especially due to Mr. C.J. Brouckaert, Mr. V.L. Pillay, Mr. K. Treffry-Goatley and Prof. V.G. Jenson for the invaluable advice and assistance offered during numerous discussions. The input by the workshop staff who constructed the experimental apparatus and assisted in so many ways is also acknowledged.

I would also like to express my appreciation for the assistance from staff of Umgeni Water with experiments at the prototype tubular filter press. Mr. R. Rajagopaul helped with many experiments.

The credit for the typing of the thesis goes to Mrs. N. Kissoon and Mrs. M. Thotharam.

The valuable assistance of the staff of the CCWR (Computing Centre for Water Research) at the University of Natal is also acknowledged. Without this facility many numerical calculations would have been impossible.

Last but certainly not least, I would like to thank my wife and daughters for their patient endurance during the period of this study.

TABLE OF CONTENTS

LIST OF FIGURES

LIST OF TABLES

CHAPTER 1
INTRODUCTION

1.1 BACKGROUND TO THE TUBULAR FILTER PRESS PROCESS

The tubular filter press is a novel tubular configured filter press for the filtration or dewatering of sludges. Before the objectives of this study are defined (see Chapter 2) it is necessary to give a brief background to and process description of the tubular filter press process.

The tubular filter press was developed by the Pollution Research Group, University of Natal, under a Water Research Commission grant (Treffry-Goatley and Buckley, 1987). The unique features of this filter press are :

(i) during the cake deposition stage, sludge is fed under pressure into a self-supporting array of horizontal collapsible porous fabric tubes. The cake is deposited on the internal walls of the tubes;

(ii) during the cake removal stage, sludge is pumped through the array of tubes at a high velocity and the cake is dislodged from the tube walls by means of a roller cleaning device which traverses the length of the array of porous tubes. The dislodged cake, which is in the form of flakes, is simultaneously hydraulically transported out of the tubes, drained and conveyed to a collection hopper.

After a joint agreement between the Water Research Commission, University of Natal and Umgeni Water, a prototype unit was constructed at Umgeni Water's H.D. Hill Water Treatment Plant and commissioned in January 1987. The prototype unit was designed to dewater thickened clarifier waste sludge resulting from the treatment of surface water at the water treatment plant.

Since the commissioning of the prototype unit, a number of units have been installed and are currently operating at various water treatment plants, treating clarifier waste sludge.

A process description of the tubular filter press process is given in section 1.2.

The only other filter press which employs the principle of filtering sludges inside collapsible porous fabric tubes is the dual functional or Uni-flow filter (Henry et al., 1976). The difference between the tubular filter press and the Uni-flow filter is that for the Uni-flow filter the porous tubes are mounted vertically. Also, cake deposited inside the tubes is dislodged by a shock wave which is generated by the sudden opening of the bottom valve, instead of a roller cleaning device.

A process description of the Uni-flow filter is given in section 1.3.

1.2 PROCESS DESCRIPTION OF THE TUBULAR FILTER PRESS PROCESS

The process schematic of the tubular filter press process is shown in Figure 1.1. The process consists of a sludge balancing or collection sump, a feed tank, a filtrate collection tray, a MONO pressing pump, a tube flushing or cleaning pump, the filter tube array and cleaning rollers mounted on a carriage.

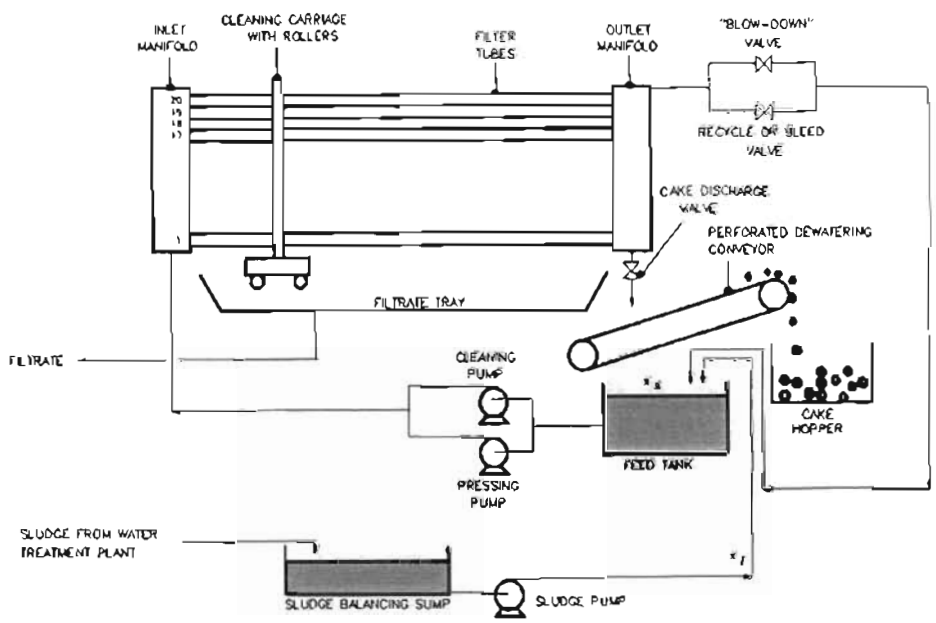

FIGURE 1.1 : Process Schematic for Tubular Filter Press Process

The tube array is made up of filter tube curtains. Each tube curtain consists of a number of filter tubes manifolded in parallel, between an inlet and a reject manifold. The tubes are flexible and collapsible and are constructed from woven polyester fabric (Downing and Squires, 1986). (On the prototype unit the length of each of the tube curtains was 10 m and the internal diameter of the individual tubes was 25 mm. Each tube curtain consisted of 20 tubes. The prototype unit had two tube curtains installed.)

The sludge pump supplies thickened sludge on demand from the balancing sump to the feed tank. The sludge is pumped into the tube array by the pressure pump. When the cake discharge valve is closed the pressure in the tube array increases and the filtrate permeates through the tube walls (for operation of "blow-down" valve and recycle valve see section 2.1.1). The sludge solids are simultaneously deposited as a cake on the inner walls of the tubes (see Figure 1.2). All units have been

designed for constant pressure filtration. As the thickness of the cake increases the filtrate flow rate decreases. The cake thickness can be estimated from the filtration rate and is limited to a maximum thickness in order to prevent tube blockages.

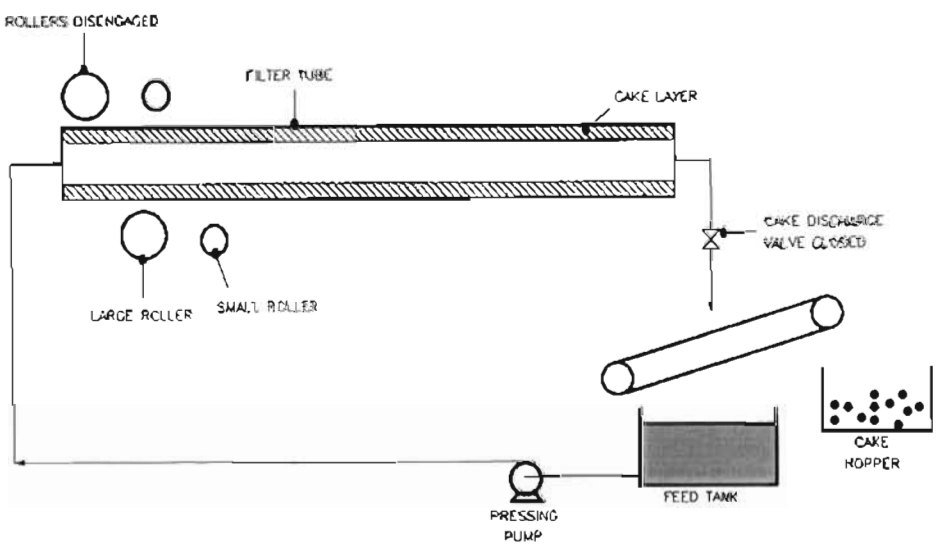

FIGURE 1.2 : Deposition of Cake Layer

When it is estimated that the desired cake thickness has been achieved, the cake discharge valve is opened, the flush or cleaning pump is started (to pump sludge from the feed tank through the tube curtains), the rollers are engaged and the cake is dislodged from the inner tube surface by the action of the rollers moving along the tube surface (see Figure 1.3). The rollers create a restriction in the tubes. (The gap between the two large rollers on the prototype unit was set at 3 mm. For more details of the rollers see Figure 4.8 in Chapter 4.) The high fluid velocity, reduced pressure and turbulence created at the point of restriction are sufficient to dislodge the cake from the tube surface. The cake is simultaneously hydraulically conveyed out of the tubes and is separated from the bulk fluid on a perforated conveyor belt.

Not all the deposited cake is recovered during the cake removal phase. Some cake is re-slurried or re-dispersed by the action of the flowing fluid and the moving rollers. This leads to an increase in the solids concentration of the feed sludge in the feed tank.

The process operation is therefore cyclic. Each cycle consists of a cake deposition and a cake removal stage. The duration of the cake deposition stage is typically 10 to 60 minutes depending on the feed sludge solids concentration and specific filtration

resistance of the cake, while the duration of the cake removal stage is typically 2 to 3 minutes for a 10 m long curtain. The entire process is micro-processor controlled and requires a minimum of operator attention.

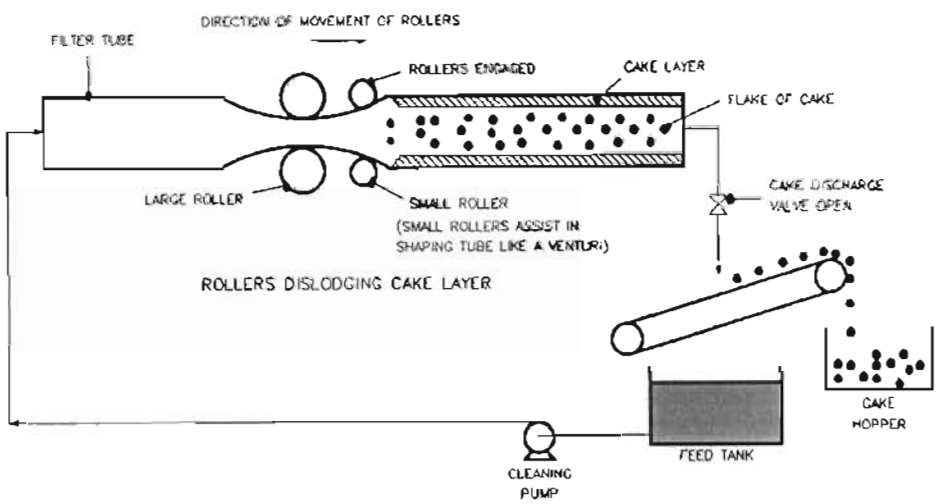

FIGURE 1.3 : Dislodging of Cake Layer and Separation of Cake Particles on a Perforated Conveyor Belt

The major advantages of the tubular filter press are, that :

(i) no plates and frames are required as for a conventional plate and frame filter press. This makes the equipment less bulky and decreases costs relative to a plate and frame filter press;

(ii) the cleaning cycle is short and the cleaning operation relatively simple. The filter is particularly suitable for sludges which produce cakes with a high specific filtration resistance, since the rapid and simple cleaning allows the deposition and removal of relatively thin cakes. The rapid cyclic operation leads to significantly higher overall filtration rates;

(iii) the process is modular because of the concept of tube curtains. This facilitates maintenance and allows for inexpensive and easy upgrading of plant.

1.3 PROCESS DESCRIPTION OF THE UNI-FLOW FILTER

A process schematic of the Uni-flow filter (Henry et al., 1976) is shown in Figure 1.4.

The Uni-flow filter consists of an array of vertical collapsible porous hoses and a settling tank or thickener. Each cycle consists of three phases :

(i) a filtration phase;

(ii) a cake removal or dump phase;

(iii) a settling phase.

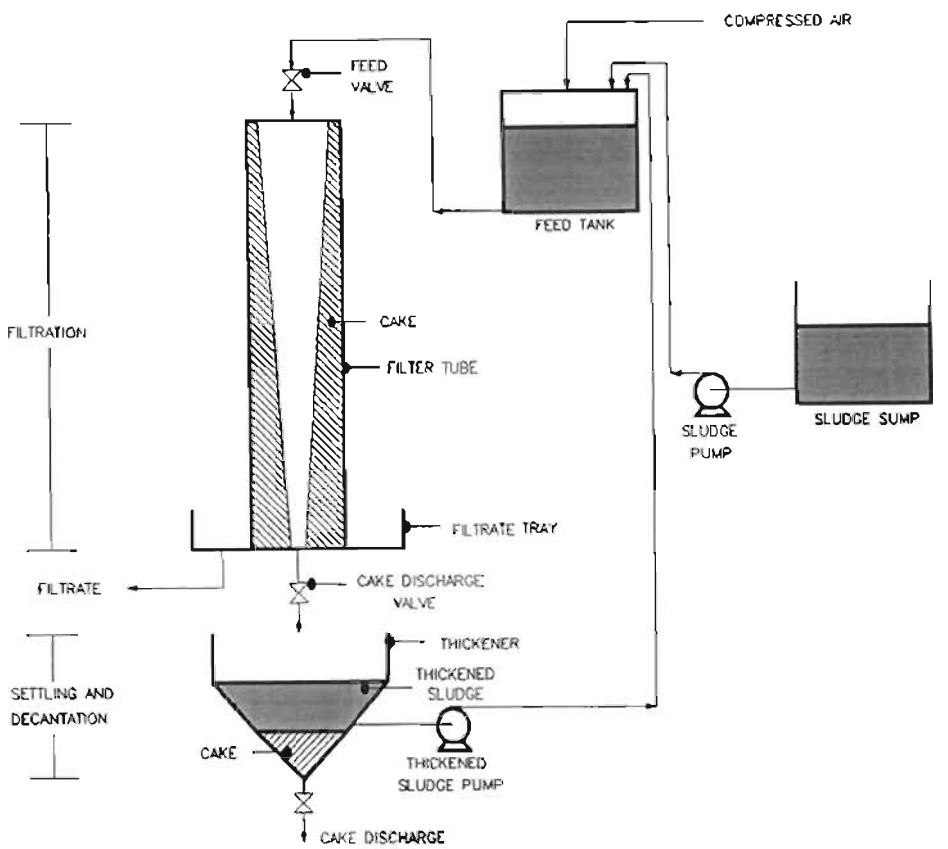

FIGURE 1.4 : Process Schematic for the Uni-flow Filter

During the filtration phase, sludge is introduced at the top of the tubes and the valves at the bottom are closed. The filter cake is deposited on the interior walls of the tubes. Filtrate permeates through the porous walls of the hoses. The cake thickness is limited to a maximum thickness in order to prevent tube blockages. During the filtration phase, the feed tank can be pressurized by means of compressed air.

The cake removal or dump phase of the cycle is initiated by closing the feed valve at the top of a tube and by opening the cake discharge valve. The resulting pressure shock wave causes the cake and feed slurry in the vertical tube to be dumped to the

thickener. The heterogeneous material in the thickener is composed of cake and a thickened sludge; i.e. some of the cake re-disperses into the interior core of feed sludge during dumping.

During the third phase of the cycle, the cake is allowed to settle in the thickener. The thickened sludge in the thickener is decanted and mixed with dilute sludge from the sludge sump. The solids concentration of the decanted sludge is greater than that of the sludge from the sludge sump, because of the re-dispersion of a portion of the filter cake into the inner core of feed sludge during dumping.

Henry et al. (1976) developed a mathematical model for the Uni-flow filter. Unlike the tubular filter press there is a significant axial pressure gradient along the tubes of the Uni-flow filter, because of the vertical mounting of the tubes. The model of Henry et al. (1976) included both the effects of axial variation of the pressure driving force and filter cake compressibility.

The model accurately predicted the axial variation of cake thickness and filtrate flux for a neutralized acid mine slurry.

A fundamental assumption of the model was that the cake thickness is thin compared to the internal diameter of the tube. This allowed the use of standard filtration equations which are valid for *planar* filtration configurations. No cylindrical filtration model was incorporated into the overall model.

Henry et al. (1976) also did not investigate the cake recovery or re-dispersion of cake in great detail. They found that there was a decrease in the degree of re-dispersion of cake as the filtration pressure was increased. They ascribed this to an increase in cake consolidation as the filtration pressure was increased.

1.4 OBJECTIVES OF THIS STUDY

Some of the results which were obtained and the problems which were encountered on the prototype tubular filter press are discussed in Chapter 2. These results and problems provided the framework for, and assisted in defining the objectives of, this study.

These objectives are defined and discussed in Chapter 2.

CHAPTER 2
OBJECTIVES OF STUDY AND RESULTS ACHIEVED ON PROTOTYPE TUBULAR FILTER PRESS

2.1 OBJECTIVES OF STUDY

Some of the results achieved and problems encountered on the prototype tubular filter press are discussed in this chapter. The objectives of this study were defined on the basis of the results achieved and the two main problems encountered on the prototype tubular filter press. The two main problems experienced on the prototype tubular filter press were :

(i) tube blockages during the pressing or filtration cycle;

(ii) low cake recoveries (high cake losses) during the cake removal cycle.

The objectives of this study were classified into three categories :

(i) The first objective was to develop a predictive model for *dead-end* constant pressure compressible cake filtration inside a horizontal porous tube, since such an internal cylindrical model is currently not available (see Chapter 3). As discussed in sections 2.2.1 and 2.2.2.1, such a model is required to predict the variation of internal cake diameter (in the filter tubes) with filtration time when the tubular filter press is operated in dead-end mode during the filtration cycle. This is fundamental to any solution of the tube blockage problems experienced during the dead-end filtration mode on the tubular filter press;

(ii) The second objective was to investigate the cake recovery (cake losses) during the cake removal cycle of the tubular filter press process. Since the tubular filter press is a novel process, the cause of these losses has not been investigated before;

(iii) As discussed in section 2.2.1, an alternative to dead-end filtration during the filtration cycle is to operate the tubular filter press in low axial velocity cross-flow filtration mode during the filtration cycle. The third objective of the study was therefore to develop a predictive unsteady-state internal cylindrical cross-flow filtration model for a sludge which has a non-Newtonian rheology and which, when filtered, produces a very compressible cake. As discussed in Chapter 5, no satisfactory model is currently available.

It must be stressed at the outset that the objective of this study was not to solve the tube blockage or low cake recovery problems. It was the intention to provide a greater insight or understanding of the cake deposition process

(during both dead-end and cross-flow filtration modes) and the cake removal process. A greater understanding of these processes is essential before these problems may be solved.

This thesis deviates from the usual thesis layout i.e. *Introduction, Literature Review, Theory, Experimental, Discussions and Conclusions.* Each objective above involved a "self contained" independent investigation with its own literature review and experimental procedure. It was therefore decided to present each study (objective) as a separate chapter.

In the subsequent sections of this chapter, some of the results achieved and the main problems encountered on the prototype tubular filter press are discussed in greater detail. These discussions should give greater clarity on the definition of the objectives of this study, as well as a better assessment of what the contribution of this study is towards the solution of these problems.

2.2 RESULTS ACHIEVED AND PROBLEMS ENCOUNTERED ON PROTOTYPE TUBULAR FILTER PRESS

2.2.1 Tube Blockages

One of the main problems which was experienced on the prototype tubular filter press was that of tube blockages. The tube blockage problem was peculiar in that not all but only some tubes would occasionally be blocked before the cake removal cycle. This meant that no fluid could flow through such tubes during the cake removal cycle and therefore the cake could not be dislodged by the rollers. These problems were particularly serious because the only way to dislodge such tube blockages was to disconnect the tubes and to manually force a high pressure water nozzle down the blocked tubes. This meant lost production time since the process had to be halted until such blockages were cleared. On average it took approximately 15 minutes to clear a single blocked tube.

An investigation was launched to establish whether there was some form of recurring pattern in the occurrence of the tube blockages in a tube curtain or whether the blockages were randomly dispersed between the tubes in a curtain.

The total number of blockages experienced per tube over the period January 1987 to April 1989, is shown in Figures 2.1 and 2.2 for curtains 1 and 2, respectively, on the prototype unit. Curtain 2 was only commissioned in September 1988 and therefore did not have the same number of operating hours as curtain 1. The convention was adopted to number the tubes in a curtain from the bottom to the top i.e. the bottom tube was tube number 1 while the top tube was tube number 20 (see Figure 1.1).

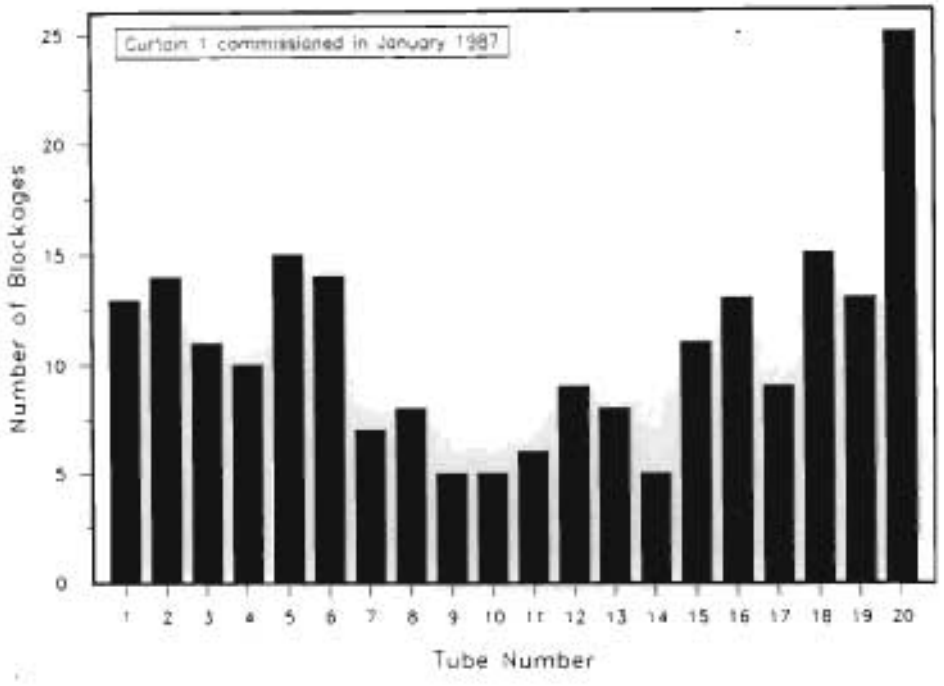

FIGURE 2.1 : Total Blockages Per Tube for Curtain 1 Over Period January 1987 to April 1989

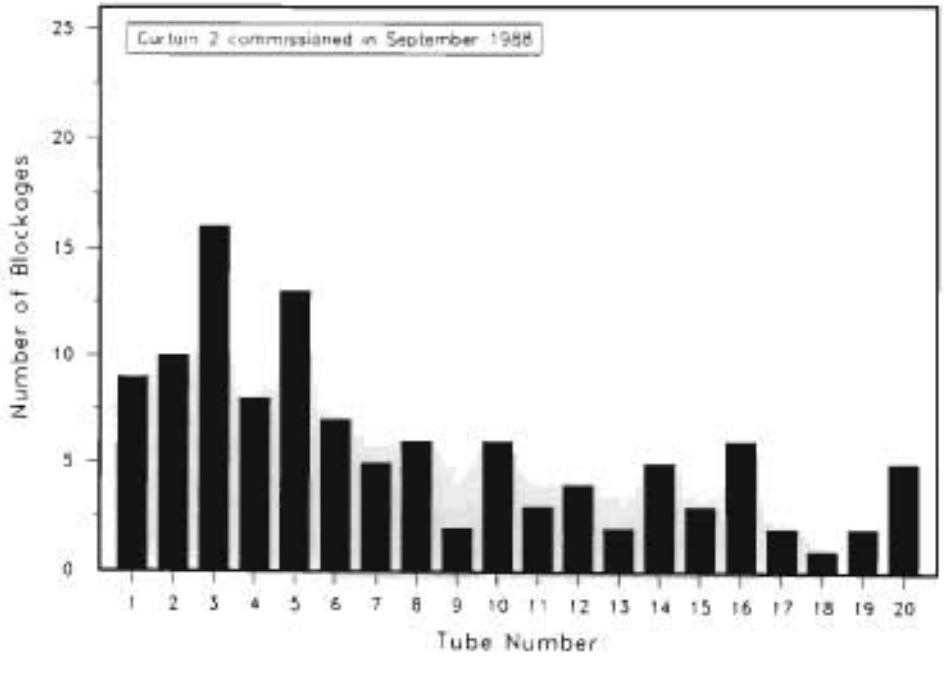

FIGURE 2.2 : Total Blockages Per Tube for Curtain 2 Over Period September 1988 to April 1989

For curtain 1 the number of blockages in the lower tubes (tubes 1 to 6) and in the upper tubes (tubes 16 to 20) was higher than for the centre tubes. For curtain 2 the number of blockages in the lower tubes (tubes 1 to 6) was higher than the number of blockages in the rest of the tubes.

During some periods the turbidity of the raw water at the water treatment plant was very low (1 to 3 Nephelometric Turbidity Units (NTU)). During such periods sodium bentonite was dosed at the head of the works as a coagulant aid. It was found that the incidence of tube blockages increased significantly during the periods when the ratio of the bentonite dose to the concentration of suspended solids in the raw water was relatively high. The nature of the sludge therefore seemed to affect the incidence of tube blockages.

In an attempt to solve the tube blockage problem on the prototype unit, it was decided to introduce a "blow-down" or purge at 5 minute intervals during the filtration or pressing cycle.

This involved opening of the "blow-down" valve (see Figure 1.1) for 15 seconds on each curtain at 5 minute intervals. During a "blow-down" the pressure inside a curtain was released suddenly and the full flow of the pressing pump was then passed through the curtain for the duration of the "blow-down".

The aim of the "blow-down" was to prevent tube blockages by passing a flow through all the tubes in a curtain at regular intervals. However, the tube blockage problem persisted even after the introduction of the "blow-down".

In another attempt to solve the tube blockage problem, experiments were done whereby a small bleed flow was continuously passed through the curtain during the pressing or filtration cycle. The flow rate of this bleed stream was regulated manually by a small valve on the "blow-down" line (see Figure 1.1). It was thought that a small axial flow in a tube would eventually limit cake growth. It is well known that this occurs in cross-flow filtration processes such as cross-flow microfiltration. Ideally, if the flow rate in all tubes were identical then the internal cake diameter would eventually reach an identical equilibrium value in all tubes and theoretically it would then be impossible for tube blockages to occur.

If on the other hand, the flow rate were too high, cake deposition would be hindered. This would lead to thickening of the sludge in the feed tank and to reduced efficiency of the dewatering process. Also, as the axial flow rate is increased, the energy consumption per unit mass of cake dry solids in the product cake increases.

There were, however, still incidents of tube blockages during these low axial velocity experiments.

It is well known that under certain conditions an uneven distribution of flow between tubes can occur in conventional manifold systems with *impermeable* tubes (Bajura and Jones, 1976; Datta and Majumdar, 1980). A mathematical model was developed to determine the effect of manifold configuration in cross-flow microfiltration systems

(with an array of *permeable* tubes) (Rencken, 1989) (see section 2.2.4). The model predicted that manifold configuration had a significant effect on flow distribution between the various tubes in a cross-flow microfiltration system. This model (see section 2.2.4) predicted that the tubes which had a high flow rate had a relatively thin cake, while those with a low flow rate had a thick cake. It was postulated that such maldistributions of flow could have occurred during the "blow-down" and low axial velocity experiments on the prototype unit (see section 2.2.5). Such variations in flow rate could have led to variations in cake thickness throughout the tubes in a curtain. This could possibly explain why some tubes became blocked while others remained open.

To summarize, the prototype tubular filter press was thus operated in three different modes during the pressing or filtration cycle :

(i) dead-end filtration without regular "*blow-down*";

(ii) dead-end filtration with regular "*blow-down*";

(iii) cross-flow filtration with low *bleed* flow through the tubes.

Tube blockages were experienced during all three modes of operation.

It should be pointed out that the waterworks clarifier sludges, which were dewatered on the prototype unit, produced very compressible cakes (see Chapter 3) and had non-Newtonian rheology (see Chapter 4).

The tube blockage problem highlighted the need for models for :

(i) the dead-end filtration of a compressible cake inside a porous tube;

(ii) the unsteady-state internal cylindrical cross-flow filtration of a sludge which has a non-Newtonian rheology and, when filtered, produces a very compressible cake.

No internal *cylindrical* model is currently available for dead-end compressible cake filtration inside a porous tube (see Chapter 3). As discussed in section 2.1, one of the objectives of this study was to develop a model. Such a model, which is developed in Chapter 3, allows the accurate prediction of the internal cake diameter at various filtration times. This is fundamental to any solution of the tube blockage problem for the dead-end filtration mode. The model used hitherto (see section 2.2.2.1) was based on conventional *planar* equations and for the model it was assumed that the thickness of the cake is thin compared to the internal diameter of a filter tube.

Similarly no satisfactory predictive model is currently available for the unsteady-state internal cylindrical cross-flow filtration of a non-Newtonian sludge, which (when filtered) produces a very compressible cake (see Chapter 5). As discussed in section 2.1, one of the objectives of this study was to develop a model. Such a model, which is developed in Chapter 5, allows the prediction of the internal cake diameter at various filtration times. This is fundamental to any solution of the tube blockage problem for the cross-flow filtration mode.

2.2.2 Cake Deposition and Recovery

2.2.2.1 Cake deposition

Cake deposition in the tubular filter press process has been modelled hitherto, by assuming dead-end filtration and that the cake is thin compared to the internal diameter of a filter tube, so that the filtration equations for a *planar* configuration are valid (see, for example, Rencken et al., 1990). As discussed in Chapter 1, Henry et al. (1976) adopted a similar approach for the modelling of cake deposition in the Uni-flow filter.

As derived in Appendix G and discussed in Chapter 3, the conventional planar filtration equation for both a compressible and an incompressible cake is :

$$\frac{dv}{dt} = \frac{P}{\mu_f (\alpha_{av} w_c + R_m)} \qquad (G.10)$$

where P = applied filtration pressure, (Pa)
R_m = resistance of medium, (m^{-1})
t = time, (s)
v = volume of filtrate per unit medium area, (m^3/m^2)
w_c = total mass of cake dry solids deposited per unit medium area, (kg/m^2)
α_{av} = average specific filtration resistance of cake, (m/kg)
μ_f = viscosity of liquid (filtrate), (Pa.s)

If it is assumed that the resistance of the medium, R_m, is negligible compared to the resistance of the cake (as was true for the fabric used and the cakes obtained on the prototype unit), equation G.10 can be written as :

$$\frac{dt}{dv} = \frac{\mu_f \alpha_{av} w_c}{P} \qquad (2.1)$$

However :

$$w_c = c\,v \qquad (2.2)$$

where c = mass of cake dry solids per unit volume of filtrate, (kg/m^3)

Substituting equation (2.2) in equation (2.1) gives :

$$\frac{dt}{dv} = \frac{\mu_f \alpha_{av} c\,v}{P} \qquad (2.3)$$

For constant pressure filtration (which is the current practice on all installed tubular filter presses) and assuming c is constant (Leu, 1981), equation (2.3) may be integrated to give :

$$t = \frac{\mu_f \alpha_{av} c\,v^2}{2P} \qquad (2.4)$$

Substituting equation (2.2) in equation (2.4) :

$$t_d = \frac{\mu_f \alpha_{av} w_c^2}{2 P_c} \qquad (2.5)$$

where t_d = time to deposit cake, (s)

From equation (2.5) the time to deposit any cake mass, w_c, for a given value of c may be determined.

The internal radius of the cake for a certain value of w_c can be determined from the following equation :

$$r_2 = \sqrt{r_1^2 - \left(\frac{2 w_c r_1}{f_s \rho_w}\right)} \qquad (2.6)$$

where f_s = mass fraction of solids in cake, (-)

r_1 = internal radius of filter medium, (m)

r_2 = internal radius of cake, (m)

ρ_w = average bulk density of wet cake, (kg/m^3)

As has been discussed before, the planar cake deposition model which is presented above has some severe limitations when it is applied to the filtration of a sludge inside a porous tube. The model assumes that the cake thickness is thin compared to the internal diameter of a tube. It therefore cannot be used to accurately predict the variation of the internal cake diameter with filtration time, except for relatively thin cakes. The question immediately arises as to the definition of a thin and a thick cake and as to when the model is valid or not.

As mentioned before, the cake which resulted from the filtration of the waterworks clarifier sludge on the prototype unit was very compressible (see Chapter 3).

A cylindrical model for the filtration of a compressible cake inside a porous tube, such as developed in Chapter 3, allows the accurate prediction of the variation of internal cake diameter with filtration time. From such a model the maximum filtration time which will still result in a "safe" internal cake diameter, so that there is no danger of a tube blockage, may be calculated for a specific sludge. This will be of great assistance in the operation of a tubular filter press (in dead-end mode) and should minimize the occurrence of tube blockages. As discussed in section 2.1, one of the objectives of this study was to develop a model for constant pressure dead-end compressible cake filtration inside a horizontal porous tube.

2.2.2.2 Cake recovery

As a result of the cake removal and recovery process a fraction of the cake is re-slurried.

The fraction of the deposited cake dry solids that is recovered from the filter tubes is defined as :

$$R = \frac{w_r}{w_c} \qquad (2.7)$$

where R = fraction of deposited cake dry solids recovered from the filter tubes, (-)

w_r = mass of cake dry solids recovered per unit medium area, (kg/m^2)

As a result of the re-slurrying of the cake during the cake removal and recovery process, the average steady-state solids concentration of the sludge fed to the array of curtains, (x_s), is greater than the concentration of solids in the feed to the plant (x_f) (see Figure 1.1).

A liquid balance around the feed tank for a tubular filter press in dead-end filtration mode yields (see Figure 2.3) :

$$V_f + V_c = V_s \qquad (2.8)$$

where V_c = volume of liquid in cake which is not recovered per cycle, (m^3)

V_f = volume of liquid in feed sludge which is pumped to the plant per cycle, (m^3)

V_s = volume of liquid in sludge which is filtered during pressing cycle, (m^3)

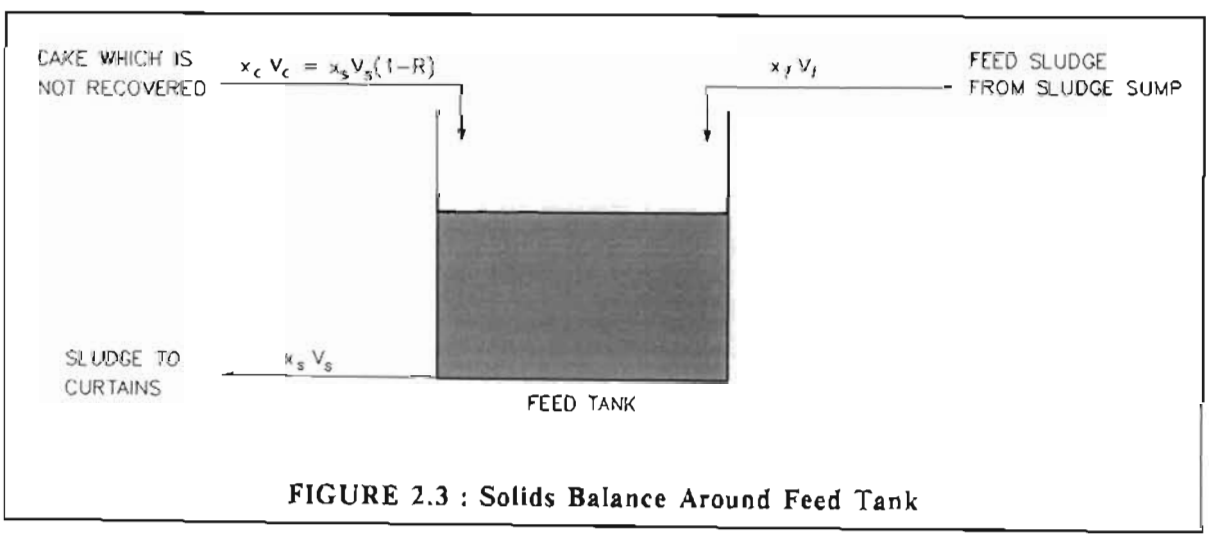

FIGURE 2.3 : Solids Balance Around Feed Tank

From a solids balance around the feed tank (see Figure 2.3) :

$$x_f V_f + x_c V_c = x_s V_s \qquad (2.9)$$

where x_c = mass of dry solids per unit volume of liquid in cake which is not recovered, (kg/m^3)

x_f = mass of dry solids per unit volume of liquid in feed sludge which is pumped to the plant, (kg/m^3)

x_s = average steady-state mass of dry solids per unit volume of liquid in sludge which is filtered during pressing cycle, (kg/m^3)

The mass of cake dry solids deposited per cycle is :

$$W_c = x_s V_s \tag{2.10}$$

where W_c = mass of cake dry solids deposited per cycle, (kg)

The mass of cake dry solids which is returned to the feed tank per cycle is :

$$(1 - R) W_c = (1 - R) x_s V_s = x_c V_c \tag{2.11}$$

Substituting equation (2.11) in equation (2.9) yields :

$$x_f V_f + (1 - R) x_s V_s = x_s V_s \tag{2.12}$$

Therefore :

$$x_s = \frac{x_f V_f}{R V_s} \tag{2.13}$$

If it is assumed that V_c is negligible compared to V_f, then from equation (2.8) :

$$V_f \simeq V_s$$

and equation (2.13) becomes :

$$x_s = \frac{x_f}{R} \tag{2.14}$$

On the prototype unit over the period January 1987 to October 1990 the value of R varied between 0 and 0,8. It was found that during those periods when the bentonite dose into the raw water at the head of the waterworks was high, the values of R were significantly lower than during periods when the bentonite dose was low or when no bentonite was dosed.

From equation (2.14) it is evident that low values of R can result in a significantly increased solids concentration in the feed tank relative to the solids concentration in the feed to the plant. On the prototype unit it was found that low values of R led to a very viscous sludge in the feed tank. These sludges are undesirable since they are difficult to pump and also increase the risk of tube blockages, especially if such sludges have a significant yield stress. A low value of R can lead to further complications, as discussed in Chapter 4.

It is therefore very important that cake recovery during the cake removal cycle be further investigated. As discussed in section 2.1, one of the objectives of this study was to investigate the cake recovery during the cake removal cycle.

2.2.3 Process Optimization for Dead-end Filtration

For conventional constant pressure dead-end planar filtration it is possible to show (Leu, 1981) that, if it is assumed that the resistance of the filter medium is negligible, the optimum cake dry solids production occurs when :

$$t_d = t_c \qquad (2.15)$$

where t_c = time to remove cake during cake removal cycle, (s)

For the tubular filter press process the cake dry solids production rate (J_s) may be calculated from the following equation :

$$J_s = \frac{3\,600\, R\, w_c}{(t_d + t_c)} \qquad (2.16)$$

where J_s = mass of cake dry solids produced per unit medium area per hour, (kg/m^2.h)

It has been shown (Rencken et al., 1990) that for a constant filtration pressure (P), fractional cake recovery (R) and cleaning time (t_c) and assuming planar and not cylindrical filtration the optimum cake dry solids production rate for the tubular filter press should also occur when :

$$t_d = t_c \qquad (2.15)$$

This was, however, not found to be generally true on the prototype unit. For the waterworks sludge, cake recovery was not constant, but was found to be a complex function of the mass of dry solids deposited (w_c). On the prototype unit, cake recovery was found to increase drastically as w_c was increased (see Figure 2.4). For the specific test shown in Figure 2.4, the optimum cake dry solids production rate (J_s) occurred at a value of w_c of 0,74 kg/m^2 (see Figure 2.5). For a cleaning time (t_c) of 150 s, the optimum t_d was 700 s :

i.e. $t_d = 4.67\, t_c$

The strong variation of R with w_c and the use of a planar instead of an internal cylindrical filtration model were probably the main reasons for a different result on the prototype unit to that predicted theoretically by Rencken et al. (1990), for the optimum cake dry solids production rate. Yeh (1985), who developed a model for the external cylindrical filtration of a compressible cake on a tube (as in a candle filter), found that for external cylindrical filtration, the determination of the optimum cake dry solids production rate was far more complex than the relatively simple equation (2.15) for the planar case.

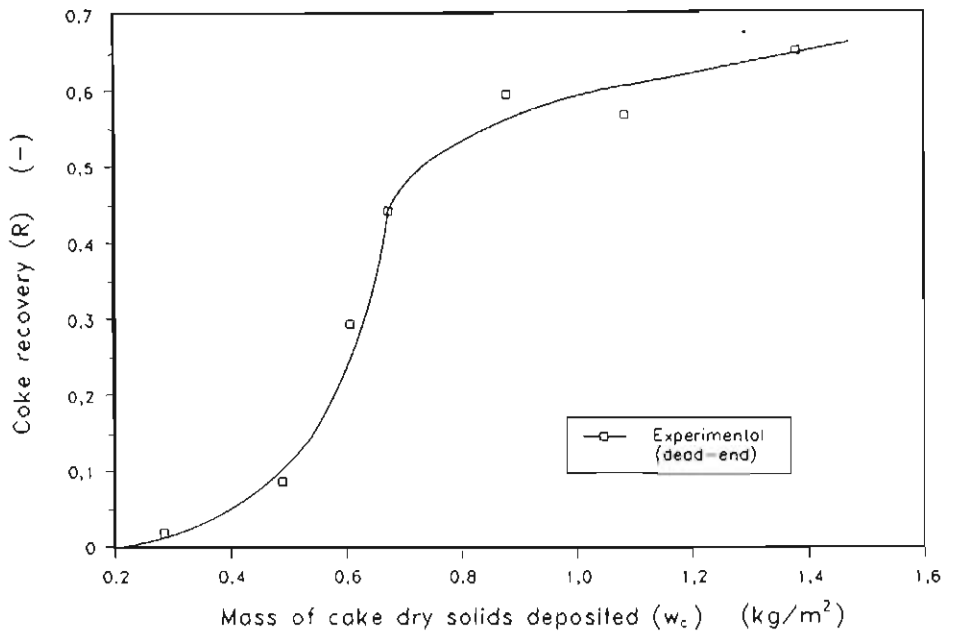

FIGURE 2.4 : Variation of Cake Recovery with Mass of Cake Dry Solids Deposited for Prototype Tubular Filter Press

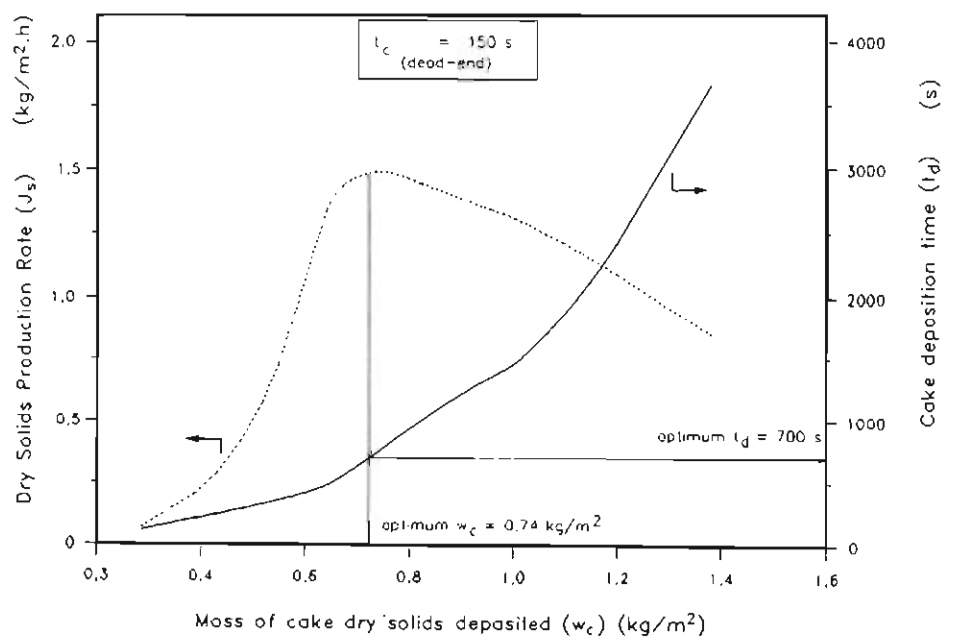

FIGURE 2.5 : Determination of the Optimum Dry Solids Production Rate for Prototype Tubular Filter Press

Thus the result achieved on the prototype unit for the optimum cake dry solids production rate further reinforced the need for an investigation into cake recovery during the cake removal cycle and for an internal cylindrical filtration model rather than a simple model based on planar filtration equations. As discussed in section 2.1, two of the objectives for this study were to investigate cake recovery (cake losses) during the cake removal process and to develop a predictive model for constant pressure dead-end compressible cake filtration inside a horizontal porous tube.

2.3 THE EFFECT OF MANIFOLD CONFIGURATION AND DESIGN ON FLOW DISTRIBUTION WITHIN MANIFOLD SYSTEMS

As explained in Chapter 1, for the tubular filter press the filter tubes in a tube curtain are manifolded in parallel between an inlet and an outlet manifold.

As discussed in section 2.2.1, it was postulated that uneven flow distributions in the interconnected filter tubes (manifold systems) on the prototype tubular filter press, could have been responsible for a variation in cake thickness in the tubes of a curtain during the pressing cycle.

Consequently it was decided to investigate the effect of manifold configuration and design on flow distribution in a manifold system. The initial design of the prototype unit was such that during the "blow-down", and for the low axial velocity experiments the manifold configuration was parallel (see section 2.3.1 and Figure 2.8) and during the cake removal or cleaning cycle the manifold configuration was reverse (see section 2.3.1 and Figure 2.9) (see also Figure 1.1).

2.3.1 Description of Manifold Headers and Coupled Systems

Manifold headers can be classified into two main types :

(i) the dividing flow or "blowing" manifold header for the distribution of a fluid to multiple laterals (see Figure 2.6), and;

(ii) the combining flow or "sucking" manifold header in which fluid is collected from the laterals (see Figure 2.7).

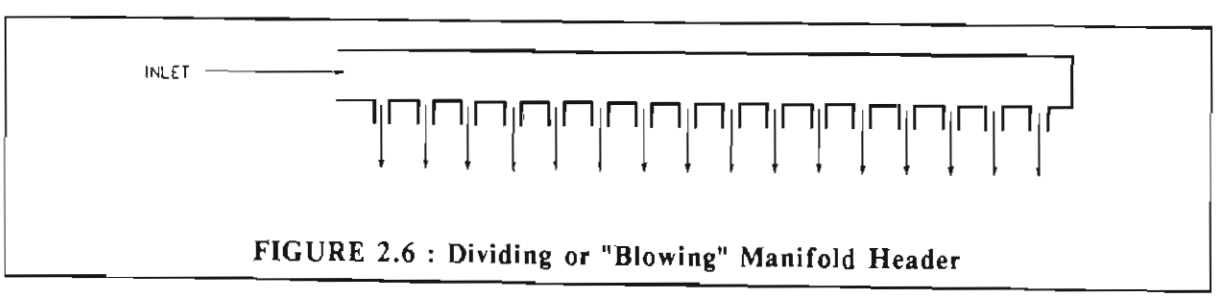

FIGURE 2.6 : Dividing or "Blowing" Manifold Header

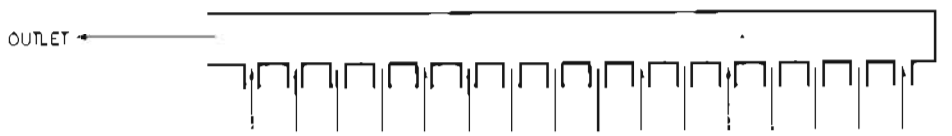

FIGURE 2.7 : Combining or "Sucking" Manifold Header

As already discussed, for the tubular filter press process the dividing and combining headers are connected through an array of filter tubes. Coupled manifolds can form either a *parallel* (also known as a Z) coupled system (see Figure 2.8) or a *reverse* (also known as a U) coupled system (see Figure 2.9).

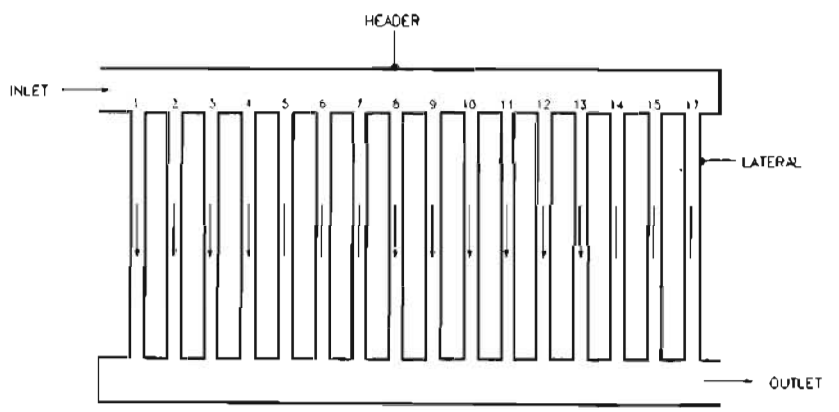

FIGURE 2.8 : Parallel or Z Configuration

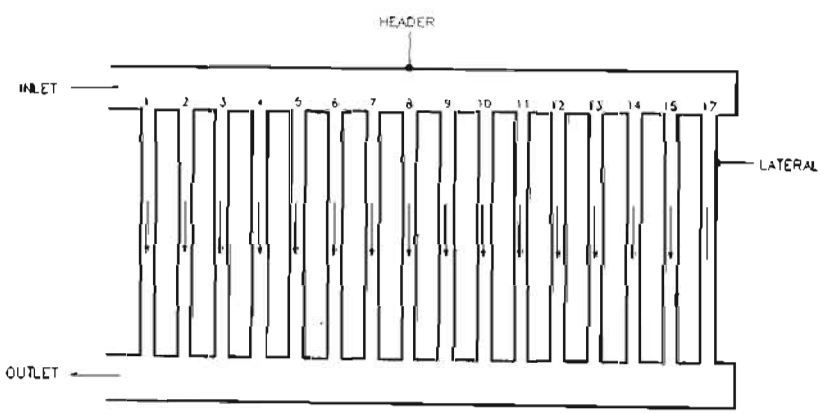

FIGURE 2.9 : Reverse or U Configuration

2.3.2 Modelling of Flow Distribution in Conventional Manifold Systems with *Impermeable* Laterals

It is not the intention to give a detailed description of the various mathematical models which are available in the literature for conventional manifold systems with *impermeable* laterals.

A comprehensive review of such models has been given elsewhere (Nuijens, 1983 and Rencken, 1989). Two types of mathematical models are found in the literature :

(i) a continuum model;

(ii) a discrete model.

A continuum model treats the manifold as a pipe with uniform porosity and is applicable to manifolds with closely spaced laterals.

In a discrete model the flow "splits" at individual laterals are considered. A discrete flow distribution model describes the physical situation better than a continuum model, because of the discontinuous character of manifold flow.

The main advantage of a continuum model is its relative simplicity, but in most cases such a model is only an approximation. Moreover, geometric non-uniformities and larger lateral spacings cannot be dealt with.

The most comprehensive discrete model to date is that of Datta and Majumdar (1980).

The model is a fairly complex iterative finite difference model. A report by Rencken (1989) gives calculation procedures and computer programs.

The ordinary differential equation (2.17) is the basis of the Datta and Majumdar (1980) model :

$$C_t \rho_{fl} v_h \frac{dv_h}{dx_h} = -\frac{dP_h}{dx_h} - \frac{f \rho_{fl} v_h^2 S}{2a_h} \qquad (2.17)$$

where a_h = cross-sectional area of manifold header, (m)
C_t = turning loss coefficient, (-)
f = friction factor, (-)
P_h = pressure of fluid along header, (Pa)
S = perimeter of header, (m)
v_h = average axial velocity in header, (m/s)
x_h = distance along header, (m)
ρ_{fl} = density of fluid, (kg/m^3)

Equation (2.17) may be derived by applying Newton's second law of motion to a fluid element (see Figure 2.10) in the dividing or combining header. There are three force components :

(i) since there is a loss of fluid from the dividing header to the laterals, the fluid velocity decreases as the fluid flows along the length of the header. For a combining header there is a gain of fluid as the fluid flows along the length of the header. This increase or decrease in fluid velocity or change in momentum results in a net force being exerted on an element of fluid;

(ii) there is a frictional force exerted on an element of fluid which flows along a header;

(iii) there is a net pressure force across an element of fluid.

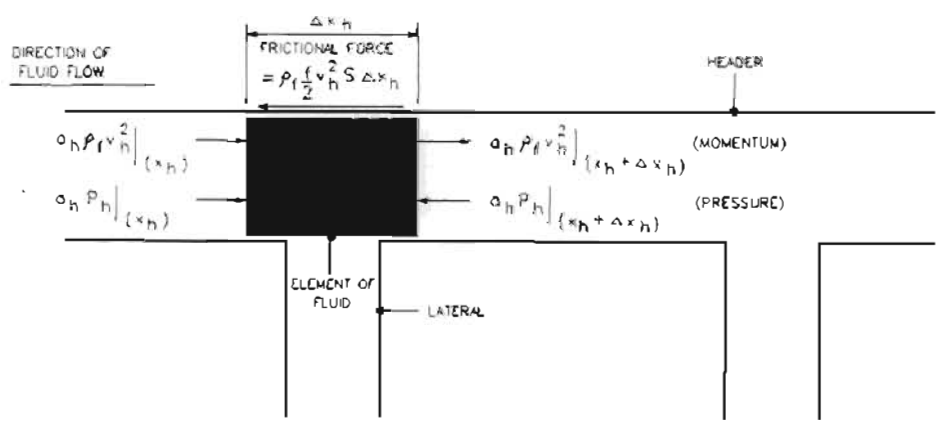

FIGURE 2.10 : Various Force Components Acting on an Element of Fluid in a Manifold Header

The turning loss coefficient was introduced into equation (2.17) by Datta and Majumdar (1980) to account for changes in pressure due to turning of the fluid stream at a lateral/header junction. Datta and Majumdar (1980) used the values of the turning coefficient which were determined by Sherman (1949) and used by Bajura and Jones (1976) for their manifold experiments. The turning coefficients used by Datta and Majumdar (1980) were :

C_t (for dividing header) = 1,05

C_t (for combining header) = 2,66

It is evident from equation (2.17) that if the frictional force component is small (for closely spaced laterals, say) the fluid pressure may rise in the direction of fluid flow along the dividing header, because of deceleration of the fluid.

For the combining header the opposite is true. The fluid pressure will decrease in the direction of the flow along the combining header, because of acceleration of the fluid. This effect is larger for the combining than the dividing header, because of the larger turning coefficient, C_t, for the combining header (see equation 2.17).

Figure 2.11 shows the typical pressure distribution in both dividing and combining headers for a parallel configuration with 30 laterals, as predicted by the Datta and Majumdar (1980) model. For the dividing header the static pressure rises steadily as lateral number increases while for the combining header the opposite is true. Note that the convention has been adopted that lateral number increases as one moves away from the inlet point for both parallel and reverse configurations (see Figures 2.8 and 2.9).

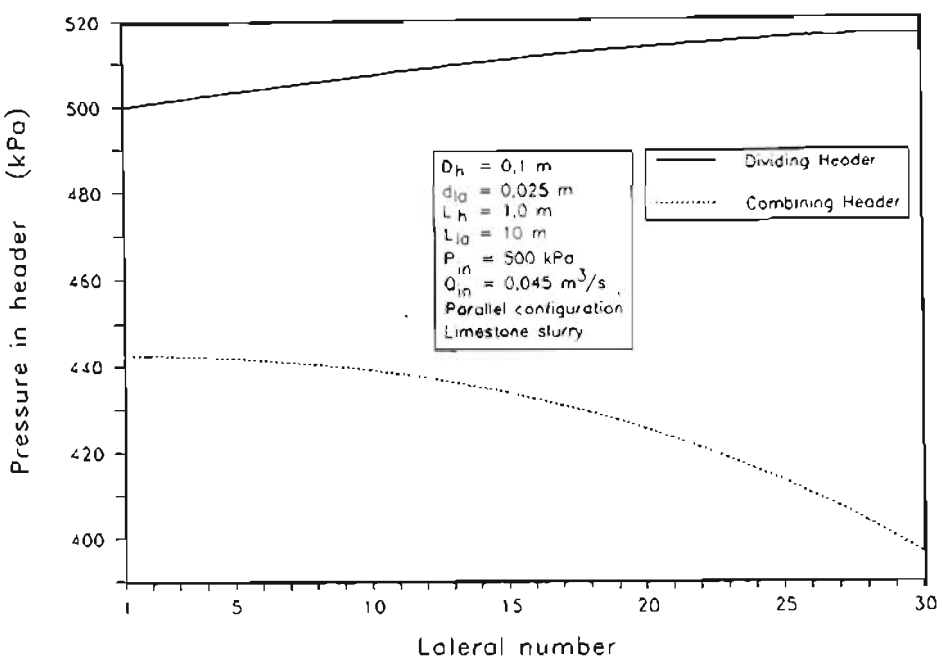

FIGURE 2.11 : Graph Showing Predicted Pressure Distribution in Dividing and Combining Headers (Parallel Configuration with Impermeable Laterals)

The flow rate in a lateral is governed by the pressure difference between the inlet and the exit of the lateral. In Figure 2.11 it can be seen that for the parallel configuration the pressure difference across a lateral increases as the lateral number increases. Therefore, in general, for the parallel configuration, the flow rate in a lateral increases as lateral number increases.

For the reverse configuration, the pressure in the dividing header increases in a similar way as the pressure in the dividing header for the parallel configuration. However, because of the difference in outlet orientation, the pressure in the combining header decreases with decreasing lateral number. This is demonstrated in Figure 2.12.

Since the pressure difference between the dividing and combining headers for the reverse configuration does not vary as drastically as for the parallel configuration, the flow distribution is generally better for the reverse configuration. This is demonstrated in Figure 2.13. The reverse configuration clearly has a better flow distribution than the parallel configuration, all factors being equal. Normalized flow rate was defined as the inlet flow rate for a specific lateral divided by the maximum lateral inlet flow rate in the system.

As shown in Figure 2.13, for the parallel configuration the flow rate in a lateral generally increases as lateral number increases, while for the reverse configuration the opposite is true.

There was good agreement between the model of Datta and Majumdar (1980) for combined manifold systems and the experimental results of Bajura and Jones (1976) for air.

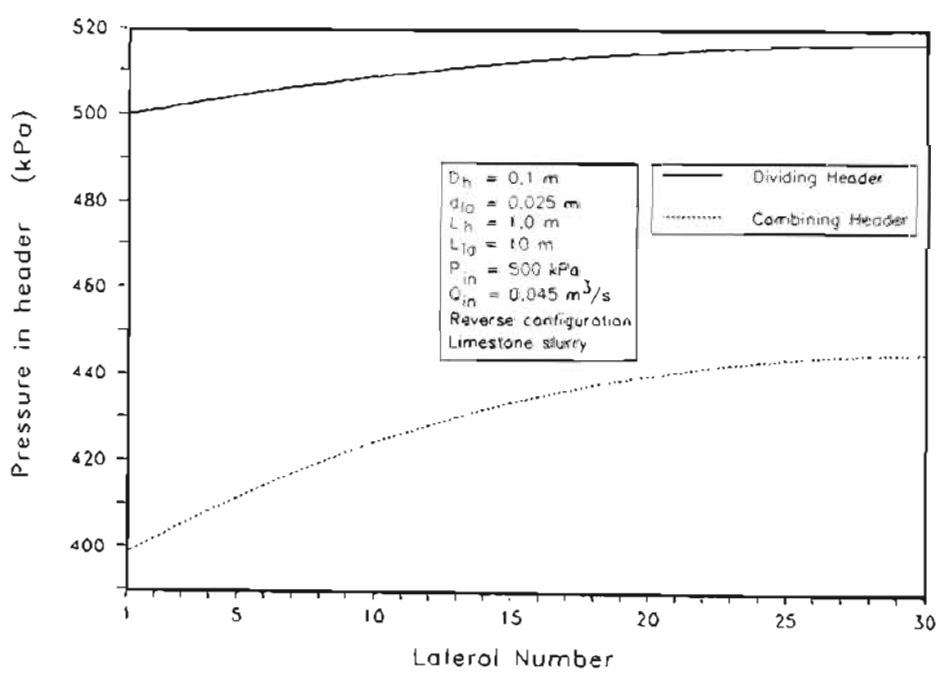

FIGURE 2.12 : Graph Showing Predicted Pressure Distribution in Dividing and Combining Headers (Reverse Configuration with Impermeable Laterals)

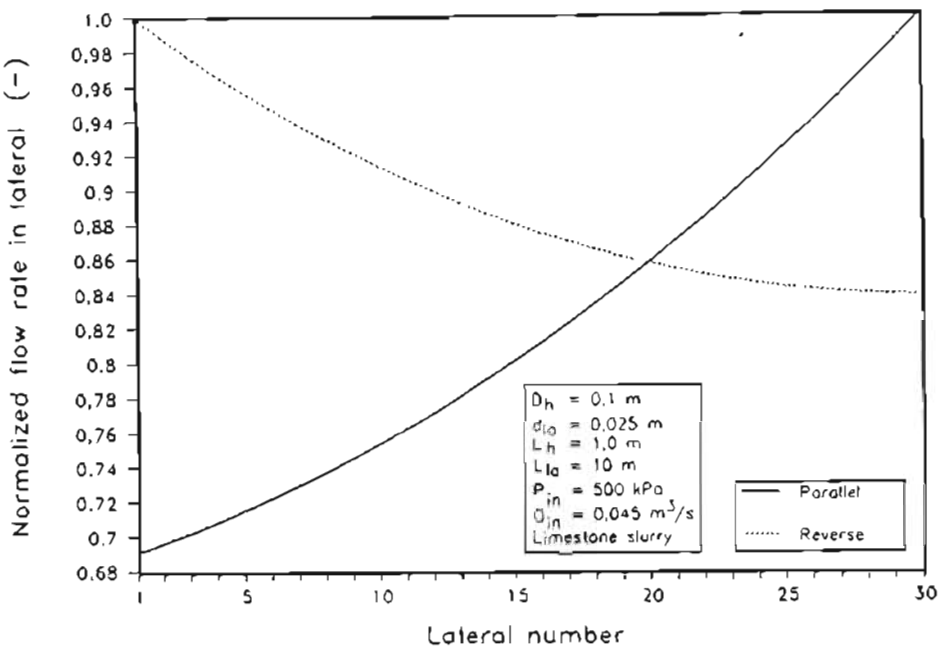

FIGURE 2.13 : Graph Showing Effect of Type of Manifold Configuration on Predicted Flow Distribution (Impermeable Laterals)

2.3.3 The Main Factors Affecting the Flow Distribution in Conventional Manifold Systems with *Impermeable* Laterals

Datta and Majumdar (1980) in common with other researchers such as Bajura and Jones (1976) found that the following parameters had the greatest effect on lateral flow distribution :

(i) the variation in the lateral flow distribution increases as the ratio of the sum of cross-sectional areas for all the laterals to the header cross-sectional area increases. This means that for fixed header and lateral diameters, the variation in the lateral flow distribution increases as the number of laterals increases. Also for a fixed header diameter and a fixed number of laterals, the variation in the lateral flow distribution will increase as the diameter of the laterals increases;

(ii) the higher the frictional resistance of the laterals the more even the lateral flow distribution;

(iii) a reverse configuration provides a more uniform flow distribution than a parallel configuration for an otherwise identical flow and geometric configuration;

(iv) for a parallel configuration, lateral flow rate increases with lateral number, while for a reverse configuration, lateral flow rate decreases with lateral number.

2.3.4 Amalgamation of Hunt (1987) Cross-flow Microfiltration Model and Datta and Majumdar (1980) Manifold Model

A literature survey revealed that to date nobody has modelled the flow or cake thickness distribution in a manifold system with an array of interconnected filter tubes. In a preliminary investigation to model the flow and cake thickness distribution in a manifold system with cross-flow filtration in an array of interconnected *permeable* tubes, the Hunt (1987) model for the turbulent cross-flow microfiltration of a limestone slurry was amalgamated with the Datta and Majumdar (1980) model for conventional manifold systems with *impermeable* tubes or laterals. It is not the intention to give all the details here, but only to mention some of the main findings of the theoretical study. Hunt (1987) used similar filter tubes for his cross-flow microfiltration experiments as were used for the prototype tubular filter press and for this study. Hunt (1987) found that for the cross-flow microfiltration of a limestone slurry, the slurry flow rate, filtration pressure and the solids concentration of the slurry had a significant effect on the cake thickness and filtrate flux. Pillay et al. (1989) numerically integrated Hunt's model for a differential length of filter tube, to predict cake thickness, filtrate flux and solids concentration profiles along a *single* long filter tube, for the cross-flow microfiltration of a limestone slurry. In order to model the flow distribution in cross-flow microfiltration manifold systems (for a limestone slurry), the computer program of Pillay et al. (1989) was used as a subroutine of the main manifold program. The calculation and computer program details were given by Rencken (1989).

During the theoretical study, it was found that the variation of cake thickness with pressure and flow rate was the prime cause of a significant difference between the flow distribution in a conventional manifold system with impermeable tubes and that in a manifold system with cross-flow microfiltration.

As shown in Figure 2.14, inlet flow rate has a significant effect on flow distribution. For the parallel system in Figure 2.14, the greater the flow rate, the worse the flow distribution. The main reason for this is the decrease in cake thickness (increase in internal cake diameter) as the flow rate increases (see Figure 2.15 for variation in cake thickness at the inlet of the tubes). As mentioned in section 2.3.3, for a conventional manifold system with impermeable tubes, the internal diameter of the laterals has a marked effect on flow distribution; the greater the internal diameter of the laterals, the worse the flow distribution. Under certain circumstances the flow distribution in a manifold system with cross-flow filtration may be worse than for an equivalent conventional system with impermeable tubes. This is shown in Figure 2.16 for a parallel configuration.

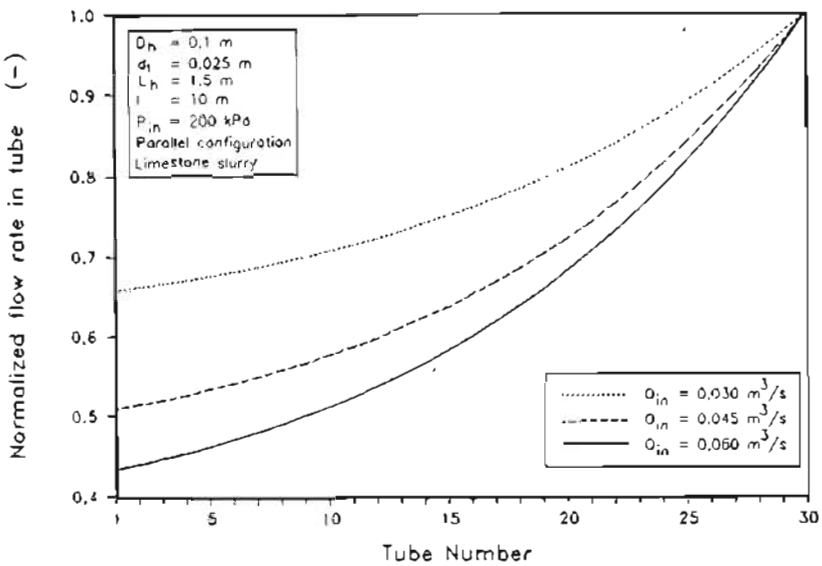

FIGURE 2.14 : Graph Showing Effect of Inlet Flow Rate (Q_{in}) on Predicted Flow Distribution in a Parallel Cross-flow Microfiltration Manifold System

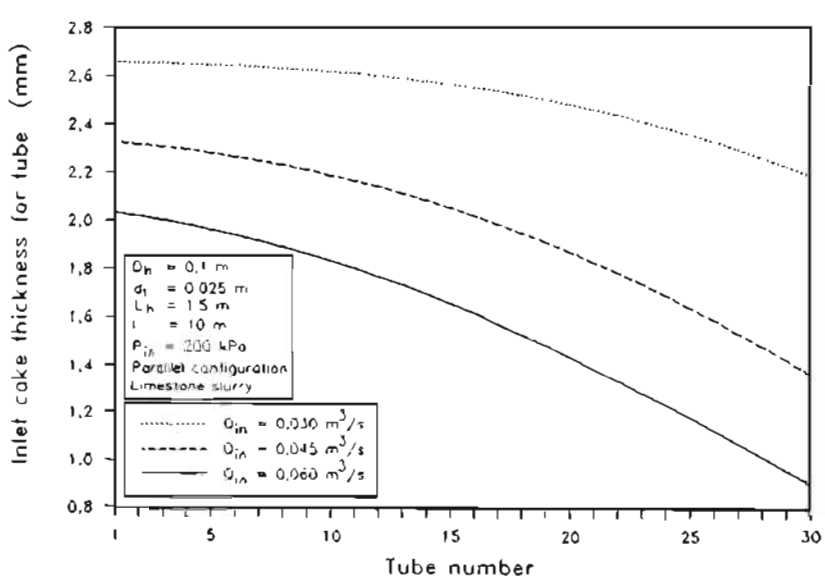

FIGURE 2.15 : Graph Showing Effect of Inlet Flow Rate (Q_{in}) on Predicted Cake Thickness at Inlet of Filter Tubes for a Parallel Cross-flow Microfiltration Manifold System

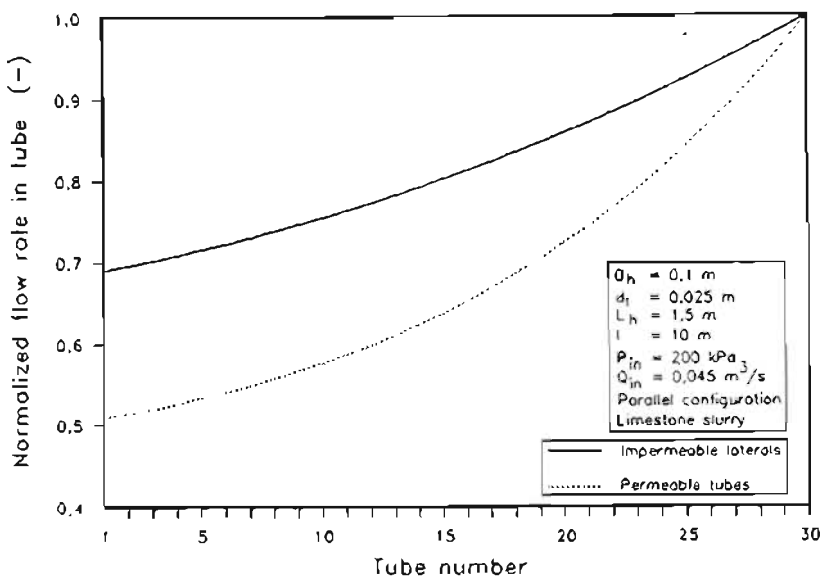

FIGURE 2.16 : Graph Showing Difference in Predicted Flow Distribution Between a Manifold System with *Impermeable* Laterals and One with *Permeable* Filter Tubes

Pressure also has a significant effect on flow distribution because of its effect on cake thickness (internal cake diameter). As shown in Figure 2.17, the flow distribution becomes more even as the pressure is increased. The effect of inlet pressure on inlet cake thickness for the various tubes is shown in Figure 2.18.

As is the case for conventional manifold systems with impermeable laterals, the reverse configuration yields a more even flow distribution than the parallel configuration, for a manifold system with cross-flow microfiltration.

In general, the main factors affecting the flow distribution in a conventional manifold system with impermeable laterals (see section 2.3.3) were also found to be valid for manifold systems with cross-flow microfiltration.

2.3.5 Measurement of Flow Distribution in a Tubular Filter Press Manifold System

After the theoretical study on the distribution of flow in manifold systems was concluded, and the possibility of a variation of cake thicknesses (internal cake diameters) in the various tubes was demonstrated for the cross-flow microfiltration of a limestone slurry, it was decided to study the flow distribution in the manifold systems of the tubular filter press prototype unit. A survey on flow meters indicated that magnetic induction flow meters were the only suitable type. Unfortunately, because of their high cost only two could be purchased. It was therefore only

possible to measure the flow rate in two tubes at any given time. Ideally, a flow meter should have been connected to every tube in the manifold system. The details of these measurements have been reported (Rencken, 1990).

The measurements were done both with the recycle valve closed (and a "blow-down" at regular intervals) (see Figure 1.1) and with the recycle valve open (and the "blow-down" valve closed) to give a low axial velocity in the filter tubes during the pressing cycle.

A typical result with the recycle valve closed and the "blow-down" valve operating, is shown in Figure 2.19. As already mentioned, the original design of the prototype unit was such that during the "blow-down" cycle and the low bleed flow experiments, the manifold system was parallel, while during the cake removal cycle the system was reverse. For Figure 2.19 one flow meter was connected to tube 1 while the other was connected to tube 20 (on curtain 2). Tube 1 was closest to the sludge entry point of the manifold system (bottom tube on the prototype unit), while tube 20 was furthest from the manifold entry point (top tube on the prototype unit).

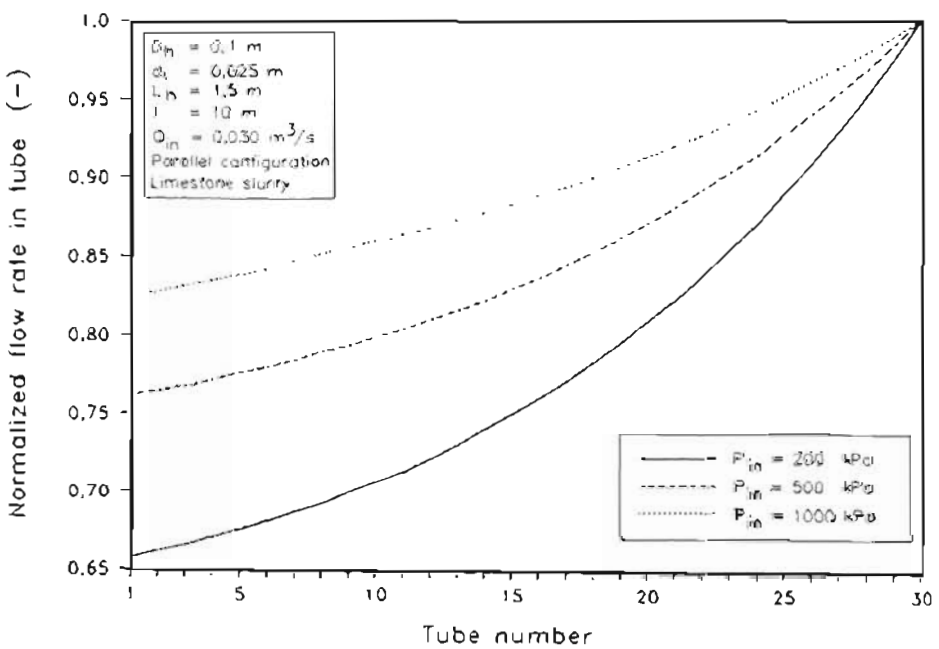

FIGURE 2.17 : Graph Showing Effect of Inlet Pressure (P_{in}) on Predicted Flow Distribution In a Parallel Cross-flow Microfiltration Manifold System

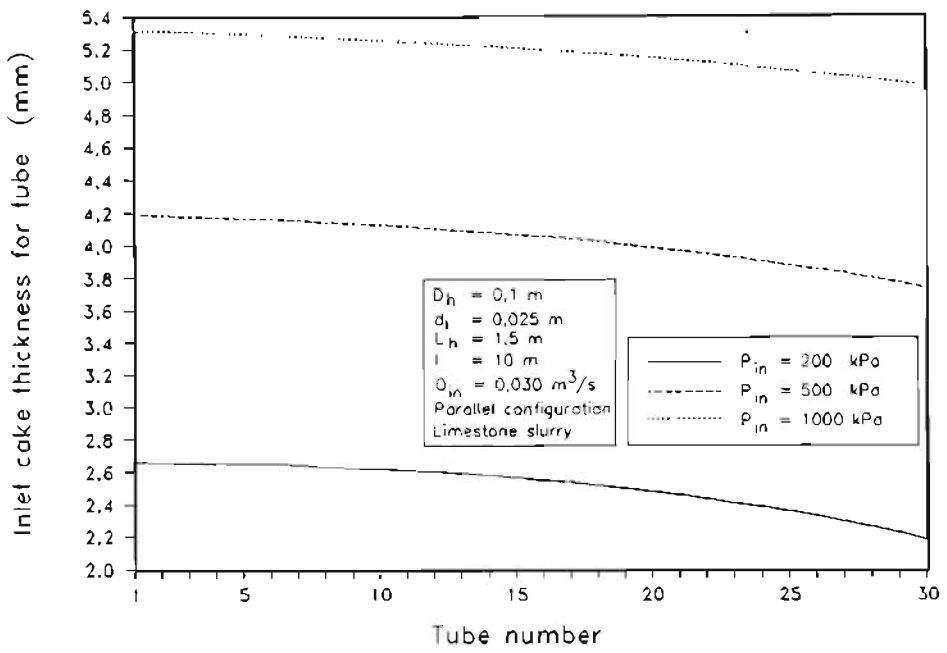

FIGURE 2.18 : Graph Showing Effect of Inlet Pressure (P_{in}) on Predicted Cake Thickness at Inlet of Filter Tubes for a Parallel Cross-flow Microfiltration Manifold System

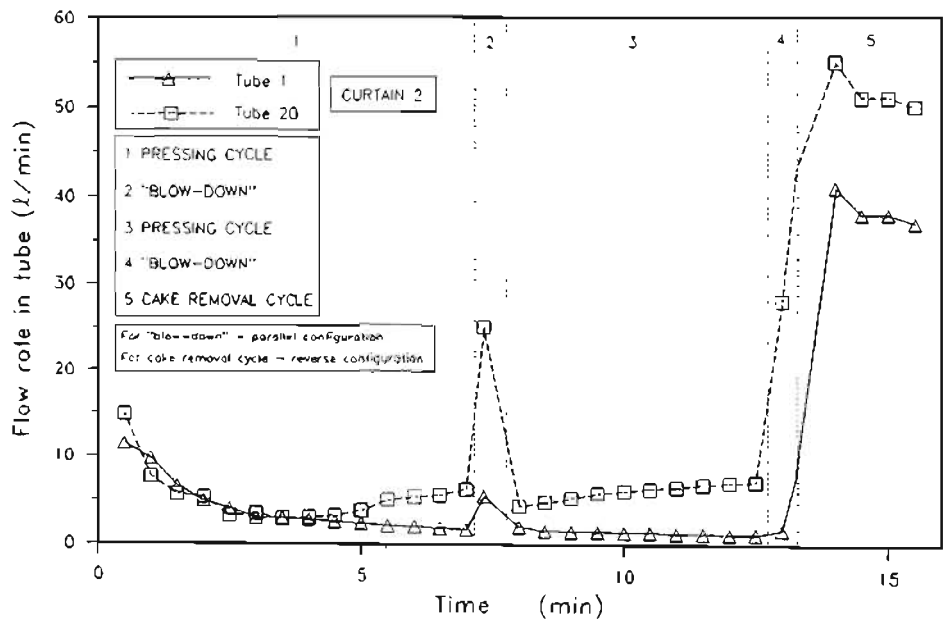

FIGURE 2.19 : Flow Rates in Two Tubes During Various Cycles on Prototype Tubular Filter Press (With "Blow-down" Valve Operating)

As shown in Figure 2.19, the flow rate in tube 20 first decreased and then increased steadily during the pressing cycle, while the flow rate in tube 1 decreased steadily. During the "blow-down" cycles the flow rate in tube 20 was far higher than in tube 1, as would be expected for a conventional parallel manifold configuration. For the cake removal cycle (reverse manifold configuration) the difference between the flow rates in tubes 1 and 20 was reduced, as would be expected for a conventional reverse manifold system.

After these experiments, it was postulated that a significant fraction of the (very compressible) cake in a tube was probably removed due to the shear of the flowing sludge during the "blow-down" and cake removal cycles. This would lead to an increase in internal cake diameter in a tube. Moreover, if the increase in internal cake diameter were dependent on the flow rate in a tube, then an uneven flow distribution in a tube curtain during the "blow-down" cycle, would lead to a variation in internal cake diameters throughout the tube curtain after a "blow-down" cycle. If this occurred, the maldistribution of flow (and the variation in internal cake diameters) in the curtain would become worse from one "blow-down" cycle to the next. This could possibly explain the occurrence of tube blockages and also account for a portion of the cake losses which were measured on the prototype unit.

Experiments were also done with a continuous low purge or bleed flow through the curtain during the pressing cycle i.e. with the recycle valve open (see Figure 1.1) during the pressing cycle and the "blow-down" valve closed. For these experiments the flow meters were connected at the inlet of tubes 15 and 20 on curtain 1. It was found that the flow distribution became less uniform as the bleed flow rate was decreased. This trend is shown in Figures 2.20 and 2.21 for an *average* flow rate per tube of 5,31 ℓ/min and 1,89 ℓ/min, respectively. For the experiment with an average flow rate of 1,89 ℓ/min per tube, the flow rate into tube 15 was higher than that into tube 20. This is contrary to the flow distribution for a conventional parallel manifold configuration.

After several experiments and sometimes conflicting results, the conclusion was reached that before any meaningful conclusions could be drawn from any low bleed flow experiments in a tubular filter press manifold system on the prototype unit, the low velocity cross-flow filtration for a very compressible cake inside a single tube had to be investigated. The prediction of internal cake diameter as a function of axial flow rate for a single tube was particularly important before any modelling of flow (and therefore cake thickness) distribution in a tube curtain was possible.

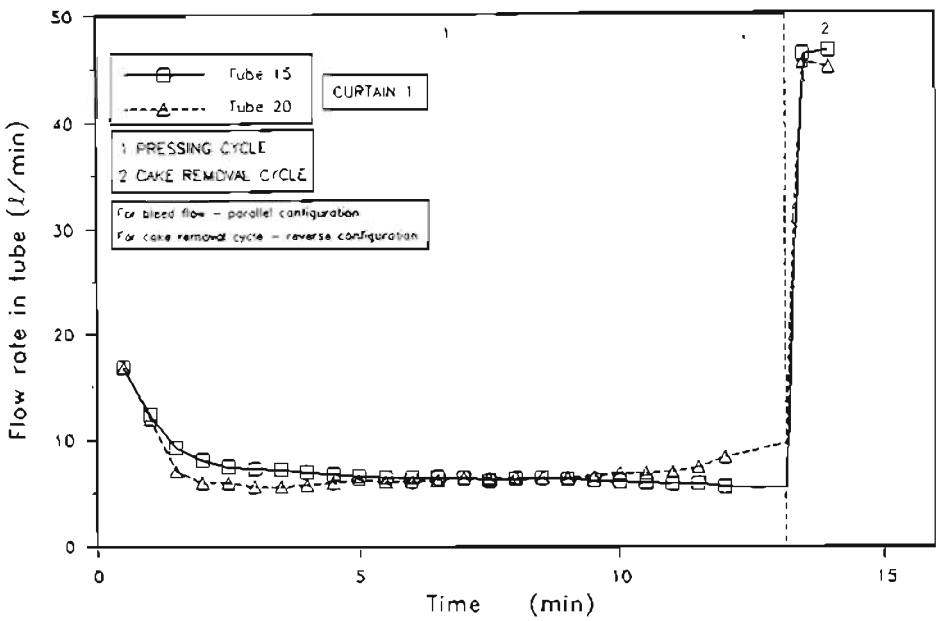

FIGURE 2.20 : Flow Rates in Two Tubes with an *Average* Flow Rate of 5,31 ℓ/min per Tube (Low Bleed Flow Experiments)

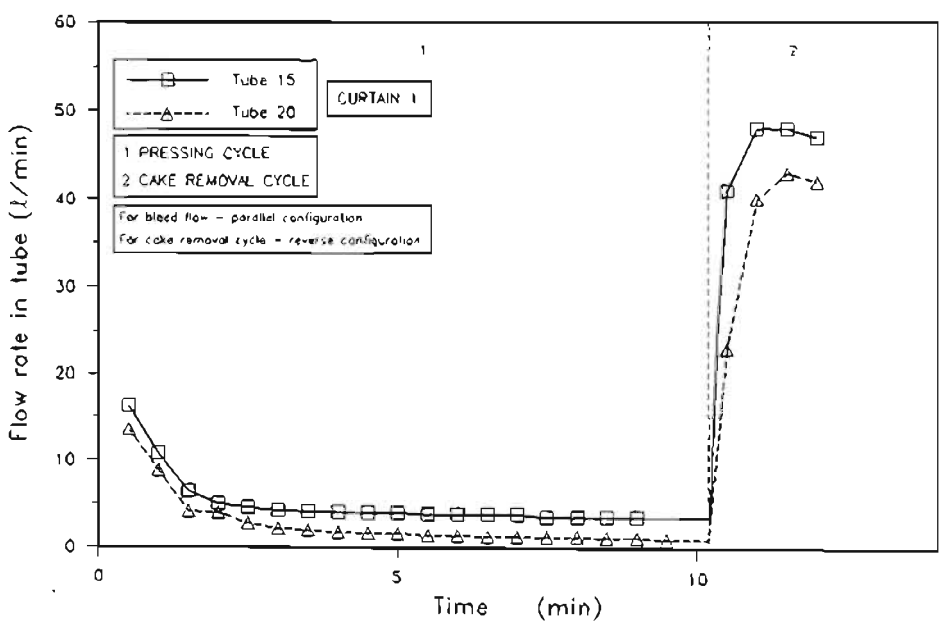

FIGURE 2.21 : Flow Rates in Two Tubes with an *Average* Flow Rate of 1,89 ℓ/min per Tube (Low Bleed Flow Experiments)

As discussed in section 2.1, one of the objectives of this study was to develop a predictive unsteady-state cross-flow microfiltration model for a sludge which has a non-Newtonian rheology and which (when filtered) produces a very compressible cake. Such a model for a single tube could then be amalgamated with a conventional manifold model (such as that of Datta and Majumdar (1980)) in a similar manner as the Hunt (1987) model (see section 2.3.4). Such an amalgamated model could then be used for predicting the distribution of flow and cake thicknesses in a tube curtain.

2.4 THESIS APPROACH AND LAYOUT

In the context of the comprehensive discussion of the results achieved and problems experienced on the prototype unit, the objectives of this study were classified into three distinct categories, as discussed in section 2.1.

As mentioned in section 2.1, this thesis deviates from the usual thesis layout. Each of the three objectives defined in section 2.1, involved a "self contained" independent investigation with its own literature review and experimental procedure. It was therefore decided to present each study (objective) as a separate chapter.

Chapter 3 concerns the development of a model for the *dead-end* constant pressure compressible cake filtration inside a horizontal porous tube. The results of experiments were compared with the predictions of the internal cylindrical filtration model for a very compressible cake.

In Chapter 4 cake losses during the cake removal cycle are investigated. It was found that for a very compressible cake there are two sources of cake losses during the cleaning or cake removal cycle in the tubular filter press process :

(i) cake losses due to the shear of the cleaning fluid prior to the action of the rollers;

(ii) cake losses due to the action of the rollers and hydraulic conveyance of dislodged flakes of cake.

A model was developed to predict the cake losses which are due to the shear of the cleaning fluid only. The combined cake losses due to the action of the rollers and hydraulic conveyance are far more complex and are very difficult, if not impossible, to predict accurately. Various parameters were found to have a significant effect on the combined cake losses due to the action of the rollers and hydraulic conveyance of dislodged flakes of cake.

In Chapter 5 the cross-flow filtration of a sludge, which has a non-Newtonian (Bingham plastic) rheology and which (when filtered) produces a very compressible cake, is investigated. An unsteady-state predictive model was developed.

Finally, in Chapter 6, the major findings of the various studies are summarized, and suggestions for future research are made.

CHAPTER 3
CONSTANT PRESSURE COMPRESSIBLE CAKE FILTRATION INSIDE A HORIZONTAL POROUS TUBE

3.1 INTRODUCTION

The objectives for this study were defined in Chapter 2. One of the objectives was to develop a predictive model for dead-end constant pressure compressible cake filtration inside a horizontal porous tube. Such a model is developed in this chapter.

The most common example of cylindrical or tubular geometry in conventional dead-end or static cake filtration is the external deposition of cakes on candle filters. Another example of cylindrical or tubular geometry is the tube press which was described by Brown (1979). For the tube press external cylindrical filtration is followed by external cylindrical expression. Although there are numerous examples in the literature of continuous cross-flow ultrafiltration and microfiltration processes, in which a cake is deposited internally, in a porous hose or tube, rather than externally, there are only two examples of internal cylindrical dead-end or static filtration which have been reported. These are the Uni-flow filter and the tubular filter press process. Both were described in Chapter 1.

Literature related to the modelling of cake filtration has almost exclusively been devoted to one-dimensional planar filtration. Moreover, most studies in non-unidimensional filtration have concentrated on incompressible cake filtration. Very few have considered compressible cake filtration. Except for Henry et al. (1976) who developed a model for the Uni-flow filter (see Chapter 1), all studies have only considered external cylindrical filtration.

For internal cylindrical compressible cake filtration, no one to date has developed a model which incorporates the *cylindrical* nature of the filter element. As discussed in Chapter 2, such a model is required for the satisfactory operation of a tubular filter press in dead-end filtration mode. For this study, the model by Tiller and Yeh (1985) for external compressible cake filtration was adapted for internal cylindrical compressible cake filtration. Experiments were conducted to evaluate the performance of this adapted model.

3.2 LITERATURE REVIEW ON CYLINDRICAL CAKE FILTRATION

3.2.1 Cylindrical Incompressible Cake Filtration

Shirato et al. (1968) developed a mathematical model for external and internal cylindrical filtration to relate filtrate flux to applied filtration pressure. This model

assumed incompressible filter cakes and negligible filter medium resistance. The basis of the model was the definition of an effective filtration area factor, which was derived as follows.

The conventional Ruth equation (Ruth, 1935) for planar incompressible and compressible cake filtration, assuming negligible filter medium resistance, is written as :

$$\frac{dv}{dt} = \frac{P}{\mu_f \alpha_{av} w_c} \tag{3.1}$$

where P = applied filtration pressure, (Pa)

t = time, (s)

v = volume of filtrate per unit medium area, (m^3/m^2)

w_c = total mass of cake dry solids deposited per unit medium area, (kg/m^2)

α_{av} = average specific filtration resistance of cake, (m/kg)

μ_f = viscosity of liquid (filtrate), (Pa.s)

Equation (3.1) is derived from equation (G.10) in Appendix G.

The equation developed by Shirato et al. (1968) for external incompressible cake filtration on a cylindrical element is :-

$$\frac{dv}{dt} = \frac{2\left(\frac{v_c}{r_3}\right) P}{\ln\left[1 + 2\left(\frac{v_c}{r_3}\right)\right] \mu_f \alpha_{av} w_c} \tag{3.2}$$

where r_3 = external radius of filter medium, (m)

v_c = volume of cake per unit medium area, (m^3/m^2)

For internal cylindrical filtration the equation according to Shirato et al. (1968) is :

$$\frac{dv}{dt} = \frac{-2\left(\frac{v_c}{r_1}\right) P}{\ln\left[1 - 2\left(\frac{v_c}{r_1}\right)\right] \mu_f \alpha_{av} w_c} \tag{3.3}$$

where r_1 = internal radius of filter medium, (m)

Since the effective filtration area changes with time for both internal and external cylindrical filtration, equation (3.1) was modified by Shirato et al. (1968) to account for this :

$$\frac{dv}{dt} = \frac{P}{\mu_f \alpha \frac{w}{A}}$$

$$= \frac{P}{\mu_f \alpha_{av} \left(\frac{w}{A}\right)\left(\frac{A}{A_0}\right)}$$

$$= \frac{P}{\mu_f \alpha_{av} \frac{w_c}{f}} \tag{3.4}$$

where A = area of filter medium, (m^2)

A_e = effective filtration area, (m^2)

j = effective filtration area factor defined by equation (3.4), (-)

W = total mass of dry solids in cake, (kg)

Note that for planar filtration A_e is equal to A (equations (3.1) and (3.4)).

A comparison of equations (3.2) and (3.4) shows that the effective filtration area factor, j, for external cylindrical filtration is :

$$j = \frac{2\left(\frac{v_c}{r_3}\right)}{\ln\left[1 + 2\left(\frac{v_c}{r_3}\right)\right]} \tag{3.5}$$

while j for internal radial filtration (from equations (3.3) and (3.4)) is :

$$j = \frac{-2\left(\frac{v_c}{r_1}\right)}{\ln\left[1 - 2\left(\frac{v_c}{r_1}\right)\right]} \tag{3.6}$$

Therefore external and internal incompressible cake filtration on or inside a tubular element can be modelled fairly easily by using the equations for planar filtration and incorporating the effective filtration area factor. Shirato et al. (1968) gave examples of calculations.

Shirato and Kobayashi (1967) and Shirato et al. (1966) found that there was good correlation between the mathematical model (equations (3.4) and (3.5)) and the results of external filtration experiments on a cylindrical element using almost incompressible Filter-cel slurry (compressibility coefficient, n, of cake = 0,03) and slightly compressible Mitsukuri silica sand (compressibility coefficient, n, of cake = 0,33 (see equation (3.34)).

Yelshin and Tiller (1989) provided a model for optimizing the design and performance of candle filters. This model was presented for incompressible cakes, although the authors claim that it could in principle be extended to compressible cakes.

3.2.2 Cylindrical Compressible Cake Filtration

Only minimal attention has been focused on compressible cake filtration on cylindrical surfaces. Shirato and Aragaki (1969) presented relationships between solids compressive and liquid pressures within compressible filter cakes deposited on non-unidimensional filtration configurations. The configurations considered were leaf, spherical and cylindrical filters.

For cylindrical filter tubes they derived the following equation for the radial relationship between solids compressive and liquid pressures for internal and external cylindrical filtration :

$$p_s + p_l = P + \int_r^{r_1} \frac{(1 - k_o)}{r} p_s \, dr \qquad (3.7a)$$

where k_o = coefficient of earth pressure at rest, (-)

p_l = liquid pressure, (Pa)

p_s = solids compressive pressure, (Pa)

r = radius, (m)

Equation (3.7a) may be written in differential form as :

$$\frac{dp_l}{dr} + \frac{dp_s}{dr} + (1 - k_o) \frac{p_s}{r} = 0 \qquad (3.7b)$$

This equation was also derived by Tiller and Yeh (1985), using a far simpler derivation than that of Shirato and Aragaki (1969). The derivation of Tiller and Yeh (1985) is shown later in this section.

Aragaki et al. (1989) derived a *general* relationship between solids compressive and liquid pressures within a filter cake. This general relationship is valid for any filter cake of whatever geometry. Aragaki et al. (1989) showed how equation (3.7b) for external cylindrical filtration may be derived from the general relationship.

Shirato et al. (1973) used equation (3.7b) to develop a model for compressible cake filtration on a tubular element. They conducted experiments with a slurry which was a 1 : 1 mixture of Filter-Cel and Mitsukuri Gairome clay. They used fairly sophisticated experimental equipment which allowed the measurement of the radial variation of local liquid pressures within the cake by means of strain gauges. They also had equipment to measure the radial variation of porosity within the cake.

They obtained good agreement between predicted and measured filtrate fluxes. There was also good agreement between the predicted and measured radial variation in liquid pressure and porosity within the cake. The agreement between the predicted and measured growth of external cake radius with time, was not too good, however.

Tiller and Yeh (1985) developed the most comprehensive model to date for the external deposition of compressible cakes on cylindrical surfaces.

There are three main differences between external compressible cake filtration on a cylindrical surface and planar compressible cake filtration.

For a cylindrical element with external cake deposition, flow is directed radially inward toward the origin as shown in Figure 3.1.

External cylindrical filtration differs from planar filtration in that the liquid velocity increases as the radius decreases towards the medium.

As the cake grows for external cylindrical filtration, the total force exerted at the cake/medium interface for constant pressure filtration, increases as the outer cake radius increases.

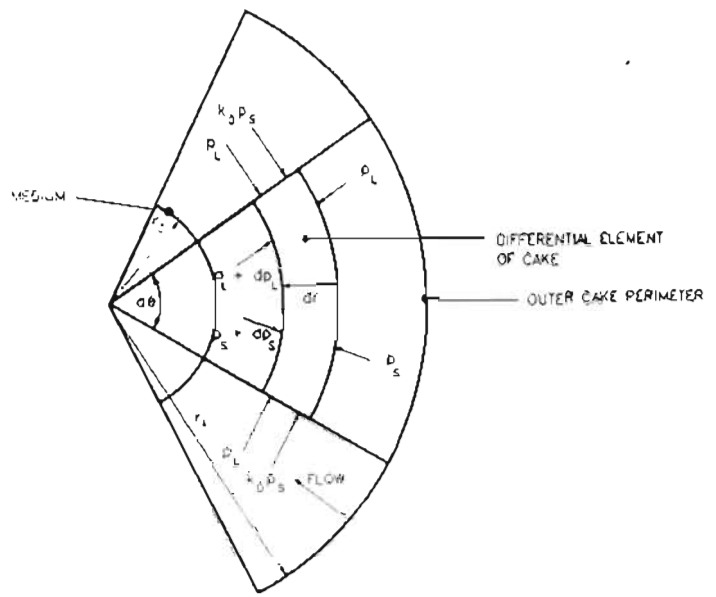

FIGURE 3.1 : Schematic Diagram of Forces Acting on a Differential Element of Cake for External Cylindrical Filtration

Before the derivation by Tiller and Yeh (1985) of equation (3.7b) for external cylindrical filtration is shown, the relationship between liquid pressure and solids compressive pressure for planar filtration will be considered very briefly.

In cake filtration, solid particles form a filter cake on the filter medium, and liquid flows through the interstices of the cake in the direction of decreasing liquid pressure. Each particle is subjected to frictional drag due to flow of the liquid. The forces on the particles are communicated from particle to particle at points of contact.

Since the solid particles are assumed to be in point instead of area contact, the liquid pressure, p_L, is effective over the entire cross-sectional area, A (Leu, 1981). The forces acting on a differential element, dx, of the filter cake are shown in Figure 3.2. The following equation may be derived from Newton's second law of motion, assuming that inertial effects and acceleration are negligible in filtration (Tiller et al., 1986) :

$$dF_s + A dp_L = 0 \qquad (3.8)$$

where F_s = accumulated frictional drag on particles, (N)

The solids compressive pressure is defined as :

$$p_s = \frac{F_s}{A} \qquad (3.9)$$

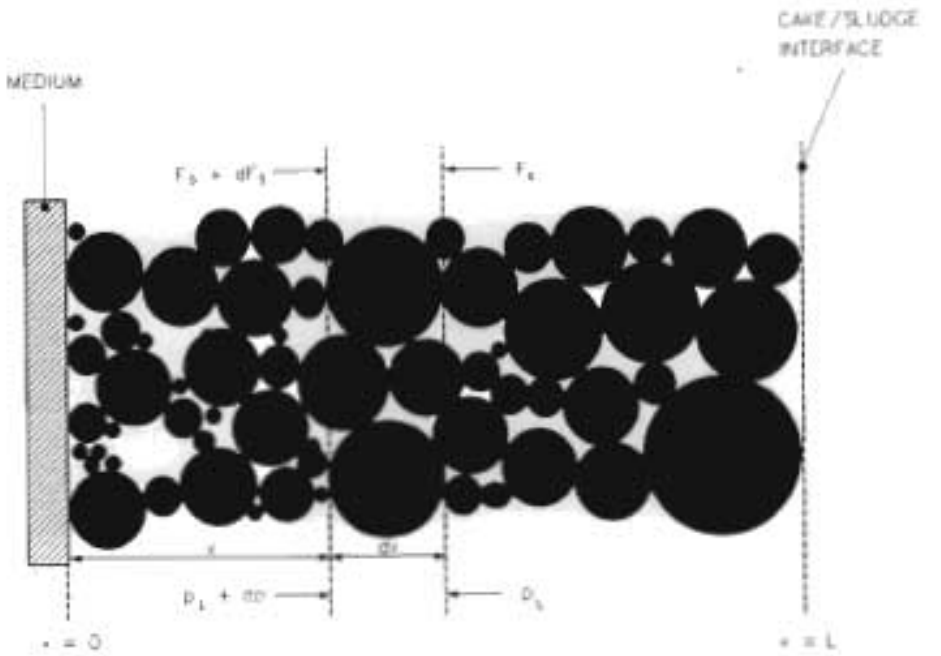

FIGURE 3.2 : Diagram Showing the Forces Acting on a Differential Element of Cake for Planar Filtration

Therefore from equation (3.8) :

$$dp_s + dp_l = 0 \qquad (3.10a)$$

or

$$\frac{dp_s}{dx} + \frac{dp_l}{dx} = 0 \qquad (3.10b)$$

where x = distance from medium for planar filtration, (m)

Equations (3.10a) and (3.10b) state that the frictional drop of the liquid is offset by a corresponding increase in the solids compressive pressure.

The variation of liquid pressure and solids compressive pressure is shown in Figure 3.3 for planar filtration. In Figure 3.3 the following boundary conditions apply :

p_l at cake/sludge interface	$= P$
p_l at medium	$= p_1$
p_s at cake/sludge interface	$= 0$
p_s at medium	$= P - p_1$

where p_1 = liquid pressure at medium, (Pa)

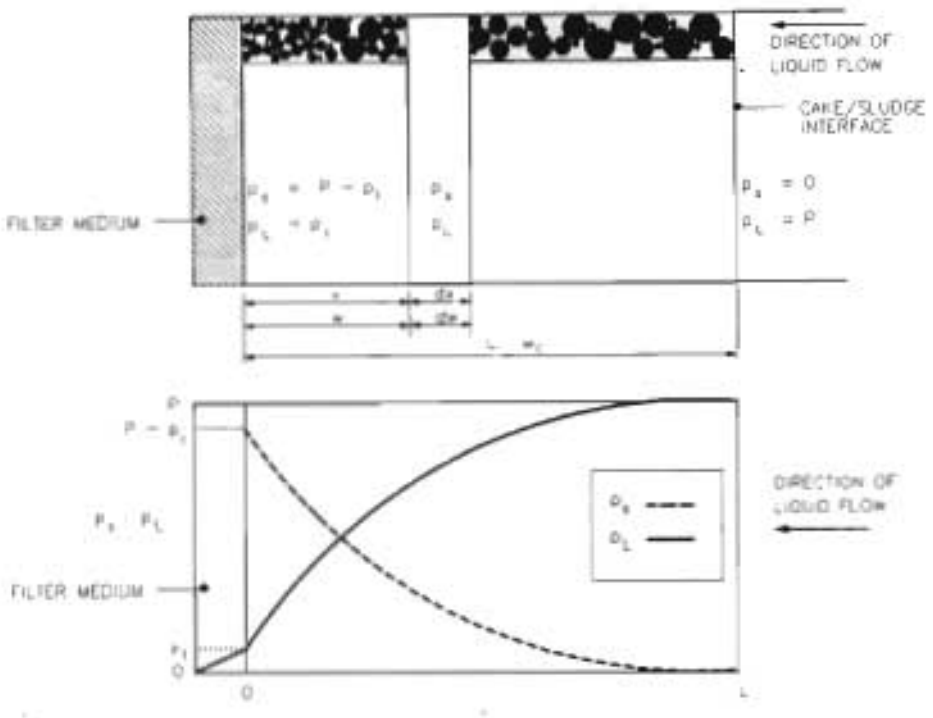

FIGURE 3.3 : Schematic Diagram of a Filter Cake and its Liquid and Solids Compressive Pressure Profiles for Planar Filtration

As already mentioned, for external cylindrical filtration, growth in external cake surface area leads to an increasing total stress at the cake/medium interface. The stress in the radial direction induces a transverse or lateral stress as shown in Figure 3.1. In soil mechanics, if an element of soil is subjected to a vertical (major principal stress), a minor principal stress will be induced in a horizontal direction, as shown in Figure 3.4. The ratio of horizontal to vertical stress is known as the coefficient of earth pressure at rest, k_s (Whitlow, 1983).

As mentioned earlier, Tiller and Yeh (1985) also derived equation (3.7b), describing the relationship between liquid and solids compressive pressure for external cylindrical compressible cake filtration. Their derivation was as follows.

The forces acting on a small element of cake are shown in Figure 3.1. The following equation may be derived from Newton's second law of motion, assuming that inertial effects and acceleration are negligible in filtration (Tiller et al., 1986) :

$$d(r\,p_L)d\theta + d(r\,p_s)d\theta = (p_L + k_s p_s)dr\sin(d\theta) \qquad (3.11)$$

where θ = cylindrical co-ordinate in cylindrical filtration, (radians)

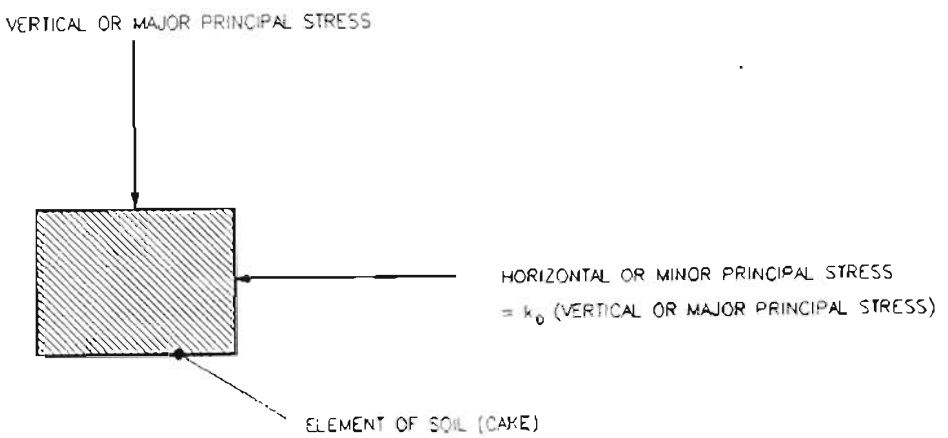

FIGURE 3.4 : Diagram to Explain the Coefficient of Earth Pressure at Rest, k_o

For small $d\theta$, $d\theta \cong \sin(d\theta)$, and equation (3.11) reduces to :

$$\frac{dp_l}{dr} - \frac{dp_s}{dr} + (1 - k_o)\frac{p_s}{r} = 0 \qquad (3.7b)$$

Therefore, summarizing, equation (3.10b) describes the relationship between liquid and solids compressive pressure for planar filtration, while equation (3.7b) is valid for external filtration on a cylindrical element.

Reported values of k_o vary from 0,3 to 1,0 (Yeh, 1985). Tiller and Lu (1972) obtained values for k_o of 0,34 and 0,45 for Solkafloc (which is very compressible) and sand, respectively. Whitlow (1983) quoted values of k_o for sand and saturated clay of 0,5 and 1,0 respectively.

The model of Tiller and Yeh (1985) predicted that for external cylindrical compressible cake filtration the effect of k_o was negligible.

Tiller and Yeh (1985) presented both analytical and numerical solutions for the ordinary differential equations of their model for constant *pressure* and constant *rate* external cylindrical compressible cake filtration. However, no experiments were done to evaluate the performance of the model.

Yeh (1985) demonstrated how the external cylindrical compressible filtration model may be used to determine the optimum design and performance for compressible cake filtration on cylindrical elements.

As discussed in Chapter 1, Henry et al. (1976) developed a model for compressible cake filtration *inside* the porous *vertical* filter tubes of the uni-flow filter. However, as already discussed, this model has limitations, since it incorporates the filtration equations for *planar* filtration and one of the assumptions for the model is that the thickness of the cake is thin compared with the internal diameter of a filter tube.

It should also be mentioned that models have also been developed for external cylindrical *expression* as opposed to *cake filtration.* Murase et al. (1985) modelled the expression of a compressible cake on a cylindrical element. Good agreement between predicted and experimental volumes of expressed liquid at various consolidation times, was achieved. Bömkes and Wagener (1990) compared external and internal cylindrical expression at pressures up to 15 MPa in a press filter. In some instances the final water content of the cake for internal expression was lower than that for external expression. The expression operation is, however, too different from that of cake filtration, for these models to be applied to cylindrical cake filtration.

3.2.3 Conclusions of Literature Review on Cylindrical Cake Filtration

The literature review revealed that all the models for cylindrical compressible cake filtration (except the one by Henry et al. (1976) for the Uni-flow filter) are for an external cylindrical configuration. Shirato and Aragaki (1969) developed a relationship between solids compressive and liquid pressures within a filter cake for external and internal cylindrical compressible cake filtration. However, they did not develop a model for internal cylindrical compressible cake filtration.

Except for the experiments by Henry et al. (1976) for the Uni-flow filter, all the experimental studies for cylindrical incompressible and compressible cake filtration have been for external cylindrical configurations.

For internal cylindrical compressible cake filtration, no one to date has developed a model which incorporates the *cylindrical* configuration of the filter element.

For this study, the model by Tiller and Yeh (1985) for external cylindrical compressible cake filtration was adapted for internal cylindrical compressible cake filtration. Experiments were conducted to evaluate the performance of this adapted model.

3.3 THEORY FOR CONSTANT PRESSURE COMPRESSIBLE CAKE FILTRATION INSIDE A POROUS TUBE

The theory for compressible cake filtration inside a porous tube, which is presented in the following sections, is based on and is almost identical to that developed by Tiller and Yeh (1985) for external cylindrical filtration. Their model has been adapted for internal cylindrical filtration, where necessary.

For this research project only constant pressure filtration has been considered, since all the tubular filter presses which are currently installed were designed for constant pressure filtration. Also, the limited filtration area available on the test rig combined with the relatively high resistance of the cake, made it almost impossible to locate a positive displacement slurry pump to accurately pump the small flow rates required for constant rate filtration (approximately 1 mℓ/s).

3.3.1 Relationship Between p_l and p_s for Filtration Inside a Porous Tube

As was mentioned in section 3.2.2, Shirato and Aragaki (1969) derived equation (3.7b) for internal and external cylindrical compressible cake filtration. Equation (3.7b) will be derived again for internal cylindrical filtration using a derivation which is similar to that given by Tiller and Yeh (1985) for external cylindrical filtration.

The forces acting on a small element of cake for internal cylindrical compressible cake filtration are shown in Figure 3.5(a). The effective solids compressive pressure, $k_o p_s$, acting on both sides of the element of cake, may be resolved into two components as shown in Figure 3.5(b). The same applies to the liquid pressure, p_L, acting on both sides of the element of cake.

The following equation may be derived from Newton's second law of motion, assuming that inertial effects and acceleration are negligible in filtration (Tiller et al., 1986) :

$$[(p_L + dp_L)(r + dr) - p_L r]d\theta + [(p_s + dp_s)(r + dr) - p_s r]d\theta$$

$$= 2(p_L + k_o p_s)dr \sin\left(\frac{d\theta}{2}\right) \qquad (3.12)$$

When $d\theta$ is small, $\sin(d\theta/2) \cong d\theta/2$, so that equation (3.12) reduces to :

$$\frac{d(rp_L)}{dr} + \frac{d(rp_s)}{dr} - (p_L + k_o p_s) = 0 \qquad (3.13)$$

Equation (3.13) may be re-written to give equation (3.7b) :

$$\therefore \frac{dp_L}{dr} + \frac{dp_s}{dr} + (1 - k_o)\frac{p_s}{r} = 0 \qquad (3.7b)$$

3.3.2 Relationship Between Liquid Pressure Gradient and Liquid and Solids Velocities

D'Arcy's law (D'Arcy, 1856) is utilised for the study of the flow of liquids through porous media. It states that the superficial velocity, u, of the liquid is proportional to the liquid pressure gradient and inversely proportional to the liquid viscosity, μ_f. Therefore, for planar filtration, D'Arcy's law (D'Arcy, 1856) may be expressed in spatial co-ordinates as follows :

$$\frac{dp_L}{dx} = \frac{\mu_f u}{K} \qquad (3.14)$$

where

$$u = \frac{Q_f}{A} \qquad (3.15)$$

where K = local permeability of cake or sediment, (m^2)

Q_f = overall volumetric flow rate of liquid (filtrate), (m^3/s)

u = superficial velocity of liquid (filtrate), (m/s)

For equation (3.14) the direction of increasing x, is as shown in Figure 3.2.

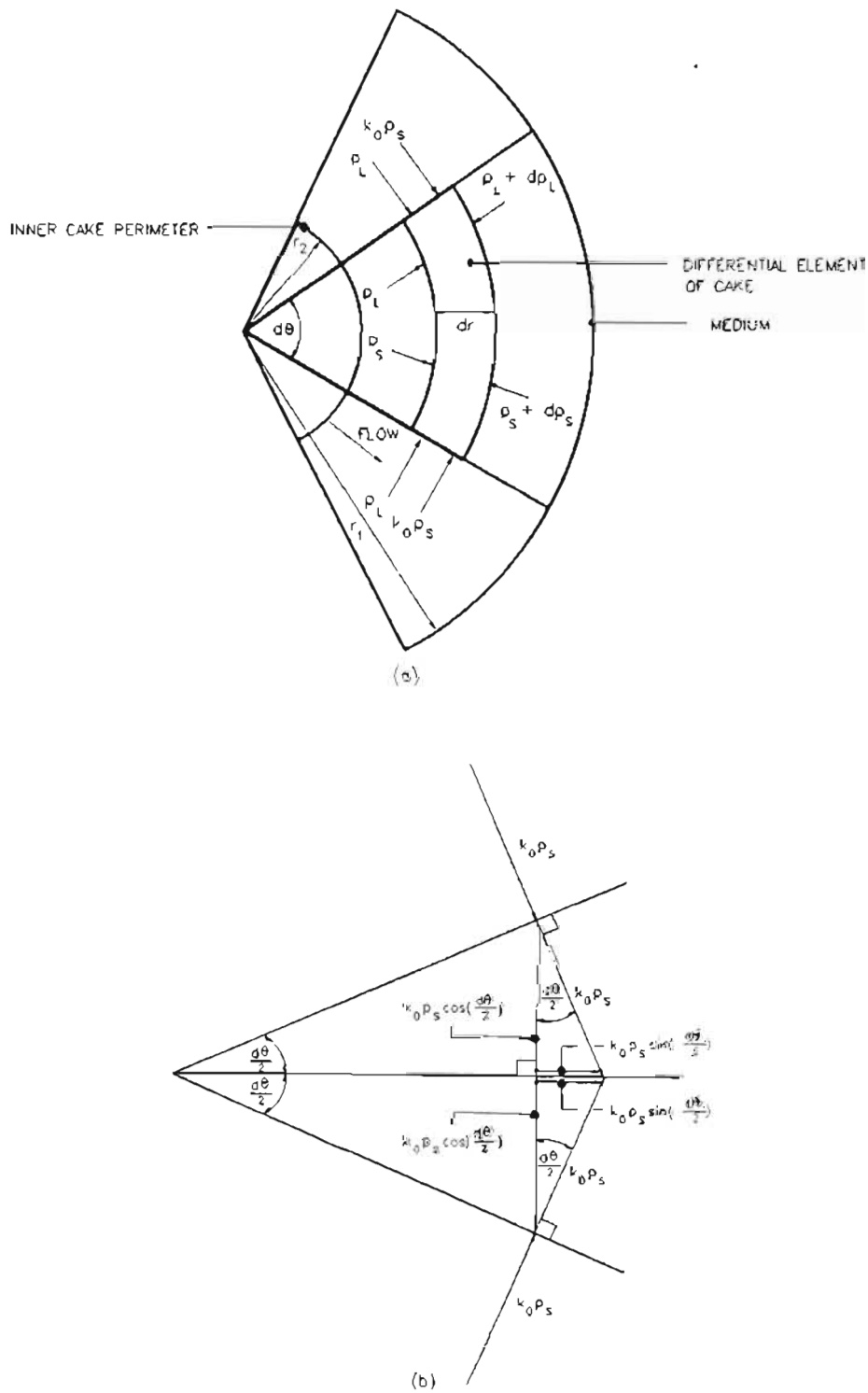

FIGURE 3.5 : Schematic Diagram of Forces Acting on a Differential Element of Cake for Internal Cylindrical Filtration

D'Arcy's law (D'Arcy, 1856) is frequently expressed in terms of material co-ordinates in the form :

$$\frac{dp_L}{dw} = \mu_f \alpha u \tag{3.16}$$

where w = mass of cake dry solids per unit medium area deposited in thickness x from medium (planar filtration), (kg/m^2)

α = local specific filtration resistance of cake or sediment, (m/kg)

Since,

$$dw = \rho_s(1-\epsilon)dx \tag{3.17}$$

from equations (3.14) and (3.16) :

$$K = \frac{1}{\rho_s \alpha (1-\epsilon)} \tag{3.18}$$

where ϵ = local porosity of cake or sediment, (-)

ρ_s = solids density, (kg/m^3)

D'Arcy's law (D'Arcy, 1856) may also be written in terms of the average pore or true velocity of liquid, u_L, which for planar filtration is defined as follows :

$$u_L = \frac{Q_f}{A\epsilon} \tag{3.19}$$

where u_L = average pore or true velocity of liquid, (m/s)

From equation (3.14), D'Arcy's law (D'Arcy, 1856) in terms of u_L is :

$$\frac{dp_L}{dx} = \frac{\mu_f \epsilon u_L}{K} \tag{3.20}$$

For an incompressible cake, the solid particles are stationary, and the superficial velocity of the solids is assumed independent of distance x through the cake. With compressible cakes, the solids move towards the medium as the cake is compressed and the local porosity changes. Strictly speaking D'Arcy's law (D'Arcy, 1856) must be modified to account for the relative velocity of the liquid with respect to the solids.

The modified D'Arcy equation (D'Arcy, 1856) is known as the D'Arcy-Shirato equation (Shirato et al., 1969) and is written as :

$$\frac{dp_L}{dx} = \frac{\mu_f \epsilon}{K}(u_L - u_s) \tag{3.21}$$

where u_s = average solids velocity, (m/s)

According to Shirato et al. (1969), equation (3.21) should be used for the filtration of highly concentrated slurries where the rate of growth of cake is rapid and total filtration time is measured in tens of seconds. In terms of this definition, the slurry used during this study was relatively dilute and the solids velocity term was omitted, from all equations relevant to this study.

For external and internal cylindrical filtration, the average pore or true liquid velocity at radius, r, in the cake (see Figures 3.1 and 3.5(a)) is :

$$u_L = \frac{Q_f}{2\pi r l \epsilon} \tag{3.22}$$

where l = length of filter tube, (m)

u_L may also be written in terms of Q :

$$u_L = \frac{Q}{2\pi r \epsilon} \tag{3.23}$$

where

$$Q = \frac{Q_f}{l} \tag{3.24}$$

Q = overall volumetric flow rate of liquid (filtrate) per unit length of filter tube, ($m^3/m.s$)

D'Arcy's law (D'Arcy, 1856) for *external* cylindrical filtration may be written (Tiller and Yeh, 1985) as :

$$\frac{dp_L}{dr} = \frac{\mu_f \epsilon u_L}{K} \tag{3.25}$$

The direction of increasing r for equation (3.25) is as defined in Figure 3.1.

For *internal* cylindrical filtration equation (3.25) becomes :

$$\frac{dp_L}{dr} = -\frac{\mu_f \epsilon u_L}{K} \tag{3.26}$$

The direction of increasing r for equation (3.26) is as shown in Figure 3.5(a).

By combining equation (3.23) with equations (3.25) and (3.26) respectively, D'Arcy's equation (D'Arcy, 1856) for external and internal cylindrical filtration may be written in terms of Q as :

$$\frac{dp_L}{dr} = \frac{\mu_f Q}{2\pi r K} \qquad (external) \tag{3.27}$$

$$\frac{dp_L}{dr} = -\frac{\mu_f Q}{2\pi r K} \qquad (internal) \tag{3.28}$$

For compressible cake filtration, when a thin layer of cake is deposited at the free surface of the filter cake (cake/sludge interface), the porosity is relatively high. As fresh layers build up, the previous surface becomes a part of the cake interior, and its porosity decreases. Liquid which is initially deposited is later partially removed. This "squeezing" action of the cake will result in an increase in liquid flow rate as the filter medium is approached. Equations (3.27) and (3.28) assume that Q is constant throughout the cake thickness.

A general continuity equation for the liquid must include this squeezing action of the cake. For internal cylindrical filtration, the liquid contained in an internal portion of the cake between an arbitrary radius r and r_1, the internal radius of the porous tube, is given by :

$$\frac{Volume\ of\ liquid}{Length\ of\ tube} = 2\pi \int_r^{r_1} \epsilon r\, dr \qquad (3.29)$$

The liquid flow rate, Q_1 at r_1, minus the liquid flow rate, Q at r, is equal to the rate of accumulation of liquid or :

$$Q_1 - Q = \frac{\partial}{\partial t}\left[2\pi \int_r^{r_1} \epsilon r\, dr\right] \quad : \quad \text{where } Q = Q(r;t) \text{ and } Q_1 = Q_1(t)$$

$$= 2\pi \int_r^{r_1} \frac{\partial \epsilon}{\partial t} r\, dr \qquad (3.30)$$

where Q_1 = overall volumetric flow rate of liquid (filtrate) per unit length of filter tube at r_1, ($m^3/m.s$)

Differentiating equation (3.30) with respect to r yields :

$$\frac{\partial Q}{\partial r} = -2\pi r \frac{\partial \epsilon}{\partial t} \qquad (3.31)$$

Equations (3.29) to (3.31) were derived by Tiller and Yeh (1985) for external cylindrical filtration and have been modified for internal cylindrical filtration.

The porosity at a fixed spatial co-ordinate decreases with time because of cake compaction; consequently $\partial\epsilon/\partial t < 0$ and Q increases as r increases from the internal cake radius r_2 to r_1, for internal cylindrical filtration.

Like Tiller and Yeh (1985), it was assumed for this study that $\partial\epsilon/\partial t$ is small and Q is independent of r. The assumption of constant Q throughout the cake at any time, t, leads to ordinary rather than complex partial differential equations and greatly simplifies the required numerical calculations. Leu (1981) derived the full partial differential continuity equations for planar compressible cake filtration. He had difficulty in solving the full equations and had to make various simplifications.

3.3.3 Empirical Equations Relating Permeability and Porosity to Solids Compressive Pressure

Equations relating permeability (K) and porosity (ϵ) to solids compressive pressure, are required if the filtration equations for compressible cake filtration are to be solved.

Tiller and Cooper (1962) proposed the following equations to relate permeability (K), porosity (ϵ) and specific filtration resistance (α) to solids compressive pressure :

$$\begin{aligned} K &= F p_s^{-\delta} && p_s \geq p_{sl} \\ K &= K_l = F p_{sl}^{-\delta} && p_s \leq p_{sl} \end{aligned} \qquad (3.32)$$

$$\begin{aligned} (1-\epsilon) &= B p_s^{\beta} && p_s \geq p_{sl} \\ (1-\epsilon_l) &= B p_{sl}^{\beta} && p_s \leq p_{sl} \end{aligned} \qquad (3.33)$$

$$\begin{aligned} \alpha &= C p_s^{n} && p_s \geq p_{sl} \\ \alpha &= \alpha_l = C p_{sl}^{n} && p_s \leq p_{sl} \end{aligned} \qquad (3.34)$$

where B = empirical constant in set of equations (3.33)

C = empirical constant in set of equations (3.34)

F = empirical constant in set of equations (3.32)

K_l = permeability of cake when $p_s \leq p_{sl}$, (m^2)

n = empirical constant in set of equations (3.34) (compressibility coefficient)

p_{sl} = solids compressive pressure below which permeability, porosity and specific filtration resistance of cake are assumed constant, (Pa)

α_l = specific filtration resistance of cake when $p_s \leq p_{sl}$, (m/kg)

β = empirical constant in set of equations (3.33)

δ = empirical constant in set of equations (3.32)

ϵ_l = porosity of cake when $p_s \leq p_{sl}$, (-)

There is some experimental evidence that permeability, porosity and specific filtration resistance are constant below some low solids compressive pressure, p_{sl} (Tiller and Leu, 1980). According to Tiller and Leu (1980) the location of p_{sl} is entirely

empirical and relatively arbitrary, the main problem being that Compression-Permeability (C-P) cells (see section 3.3.7.1) are not very accurate at the low solids compressive pressures required to locate p_{si} accurately.

Tiller and Leu (1980) proposed the following set of alternative empirical equations :

$$K = K_o\left(1 + \frac{p_s}{p_a}\right)^{-\delta_1} \tag{3.35}$$

$$1 - \epsilon = (1 - \epsilon_o)\left(1 + \frac{p_s}{p_a}\right)^{\beta_1} \tag{3.36}$$

$$\alpha = \alpha_o\left(1 + \frac{p_s}{p_a}\right)^{n_1} \tag{3.37}$$

where K_o = permeability of cake when $p_s = 0$, (m^2)

n_1 = empirical constant in equation (3.37)

p_a = empirical constant, (Pa)

α_o = specific filtration resistance of cake when $p_s = 0$, (m/kg)

β_1 = empirical constant in equation (3.36)

δ_1 = empirical constant in equation (3.35)

ϵ_o = porosity of cake when $p_s = 0$, (-)

3.3.4 Solids Compressive Pressure and Liquid Pressure as a Function of Radius

By combining equations (3.7b) and (3.28) the following equation is obtained :

$$\frac{dp_s}{dr} + (1 - k_0)\frac{p_s}{r} = -\frac{dp_L}{dr} = \frac{\mu_f Q}{2\pi r K} \tag{3.38}$$

Equation (3.38) represents a system of two ordinary differential equations :

$$\frac{dp_s}{dr} = \frac{\mu_f Q}{2\pi r K} - (1 - k_0)\frac{p_s}{r} \tag{3.39}$$

and

$$\frac{dp_L}{dr} = -\frac{\mu_f Q}{2\pi r K} \tag{3.28}$$

with initial values :

$$p_s(r_2) = O \tag{3.40}$$

$$p_L(r_2) = P \tag{3.41}$$

where r_2 = internal radius of cake, (m)

For planar filtration the pressure drop across the medium is defined (Leu, 1981) as :

$$\Delta p_m = \frac{\mu_f Q_f R_m}{A} \tag{3.42}$$

where Δp_m = pressure drop across the medium, (Pa)

R_m = resistance of medium, (m^{-1})

In the same manner the pressure drop across the medium for internal cylindrical filtration is :

$$\Delta p_m = \frac{\mu_f Q_f R_m}{2\pi r_1 l} \tag{3.43}$$

If the liquid pressure drop across the cake is given by Δp_c, then :

$$P = \Delta p_c + \Delta p_m \tag{3.44}$$

where Δp_c = pressure drop across the cake, (Pa)

The pressure drop across the cake may be obtained by the simultaneous numerical integration of equations (3.39) and (3.28) with initial value conditions (3.40) and (3.41), respectively. For the correct filtrate flow rate, Q, the sum of the pressure drops across the cake and the medium is equal to the filtration pressure, according to equation (3.44). Since the correct filtrate flow rate, Q, is not known, a priori, a FORTRAN computer program was written to solve for the correct Q, by using an interval halving technique. The flowsheet of this program is shown in Appendix E and this technique is further discussed in section 3.5.7.

Tiller and Yeh (1985) derived analytical solutions for the system of equations (3.28) and (3.39). For this study it was found to be far easier to resort to numerical techniques.

3.3.5 Mass Balances

Once the solids compressive pressure profile through the cake has been calculated, the porosity profile may be obtained by using an empirical equation such as equation (3.33) or (3.36).

The average porosity is given by :

$$\epsilon_{av} = \frac{2\pi \int_{r_2}^{r_1} \epsilon r dr}{\pi (r_1^2 - r_2^2)} \tag{3.45}$$

where ϵ_{av} = average porosity of cake, (-)

Since the solids and liquid are incompressible, a total mass balance on a volumetric basis gives :

$$\left\{\begin{array}{c}Volume\ of\\ slurry\ per\ unit\\ medium\ area\end{array}\right\} = \left\{\begin{array}{c}Volume\ of\\ cake\ per\ unit\\ medium\ area\end{array}\right\} + \left\{\begin{array}{c}Volume\ of\\ filtrate\ per\ unit\\ medium\ area\end{array}\right\}$$

or

$$\frac{\omega_c}{\phi_s} = \frac{\omega_c}{(1-\epsilon_{av})} + v \qquad (3.46)$$

where ϕ_s = volume fraction of solids in feed sludge, (-)

ω_c = volume of cake dry solids per unit medium area, (m^3/m^2)

Also,

$$\omega_c = \frac{(1-\epsilon_{av})(r_1^2 - r_2^2)}{2r_1} \qquad (3.47)$$

Solving for v using equations (3.46) and (3.47) gives :

$$v = \frac{(1-\epsilon_{av}-\phi_s)}{\phi_s}\frac{(r_1^2 - r_2^2)}{2r_1} \qquad (3.48)$$

3.3.6 Time Relationships for Constant Pressure Filtration

In general, in order to obtain filtrate volume or cake volume as a function of time, the relationship between P and Q as determined by the pumping mechanism must be known. As already mentioned, only constant pressure filtration was considered for this study.

For constant pressure filtration, filtration time is calculated from equation (3.49) :

$$t = \int_0^V \frac{dV}{Q} \qquad (3.49)$$

where V = volume of filtrate per unit length of tube, (m^3/m)

Numerical integration of equation (3.49) requires that Q be known as a function of V. V may be calculated from equation (3.48) :

$$V = \frac{(1-\epsilon_{av}-\phi_s)\pi(r_1^2 - r_2^2)}{\phi_s} \qquad (3.50)$$

In order to calculate the filtration time for this study, the corresponding values of Q were calculated for various values of the internal cake radius, r_2, as outlined in section 3.5.7. Once the values of Q had been found for the various values of r_2, t was found by numerical integration of equation (3.49) (see section 3.5.7).

3.3.7 Determination of Compression-permeability Data

For a very compressible cake (like the cake formed from the waterworks clarifier sludge used in this study) a highly resistant layer or skin is formed near the medium (Tiller and Green, 1973), while the bulk of the cake is not very well consolidated. The solids compressive pressure is relatively low in this "sloppy" cake region.

Therefore, for very compressible cakes, like the cake formed from the waterworks clarifier sludge used in this study, it is important to have accurate data in the relatively low solids compressive pressure region.

Although C-P cells have been used down to very low solids compressive pressures, for example down to 2 kPa by Tiller and Cooper (1962), serious reservations have been expressed by many authors on the accuracy of the C-P cell data in the low solids compressive pressure region (e.g. Shirato et al., 1983 and Tiller and Lu, 1972). The main reason for inaccurate results is friction between the inner wall of the C-P cell and the compressed cake.

Shirato et al. (1983) proposed a batch settling technique for the determination of porosity and permeability at very low solids compressive pressures. Shirato et al. (1983) obtained porosity data for three different sludges (zinc oxide, Mitsukuri Gairome clay and ferric oxide) for the p_s range, $100\,Pa \leq p_s \leq 1000\,Pa$. Permeability data for the same sludges were determined for the p_s range, $0.1\,Pa \leq p_s \leq 100\ Pa$.

Murase et al. (1989) proposed a centrifuge method for the determination of porosity data for intermediate solids compressive pressures. Murase et al. (1989) obtained porosity data for zinc oxide and ferric oxide slurries for the p_s range, 10^3 Pa $< p_s <$ 10^5 Pa.

Since the cake obtained from the waterworks clarifier sludge which was used for this study, was very compressible, it was decided to use all three methods (i.e. settling (low p_s); centrifuge (intermediate p_s) and C-P cell (high p_s)) in order to obtain porosity and permeability data over a wide range of solids compressive pressures. These three methods are discussed below in greater detail.

3.3.7.1 Determination of compression-permeability data using a Compression-Permeability (C-P) cell for high solids compressive pressures

As can be seen from empirical equations (3.32) to (3.37), a multitude of constants has to be determined for a particular sample of sludge or cake, before any modelling can be undertaken. Compression-Permeability (C-P) cells have been employed extensively to determine the variation of porosity and permeability with solids compressive pressure for compressible cakes. The C-P cell used in this study is described in section 3.4.2.1.1.

At a certain solids compressive pressure, the liquid permeability is calculated from the D'Arcy equation (D'Arcy, 1856) (see equation (3.14)) :

$$K = \frac{\mu_f Q_f \Delta l_c}{A_c \Delta p_c} \tag{3.51}$$

where A_c = area of cake in C-P cell, (m^2)

Δl_c = thickness of cake in C-P cell, (m)

For equation (3.51) it is assumed that the resistance of the filter paper in the C-P cell is negligible compared to the resistance of the cake, as was true for the cakes in this study.

The specific filtration resistance, α , at a certain solids compressive pressure may be calculated from the permeability by using equation (3.18) :

$$\alpha = \frac{1}{\rho_s K(1-\epsilon)} \tag{3.52}$$

The porosity of the cake at the end of a C-P cell test may be calculated from the final moisture content of the cake from the following equation :

$$\epsilon = \frac{Volume\ of\ liquid}{Volume\ of\ liquid + Volume\ of\ solids}$$

$$= \frac{\frac{z}{\rho_l}}{\frac{z}{\rho_l} + \frac{(1-z)}{\rho_s}} \tag{3.53}$$

where z = mass fraction of moisture in cake, (-)

ρ_l = liquid density, (kg/m^3)

3.3.7.2 Settling method for determining porosity at low solids compressive pressures

The following technique for the determination of porosities at low solids compressive pressures was developed by Shirato et al. (1983).

When a suspension containing the dry solids volume, ω_o , per unit area settles in a cylinder, the final equilibrium height of the sediment is denoted by H_∞ , as shown in Figure 3.6(a). When the initial volume of solids is increased by the volume $d\omega_o$, as shown in Figure 3.6(b), the final height of the sediment will be given by $(H_\infty + dH_\infty)$. The porosity variation of the suspension AB in Figure 3.6(a) is identical to that of the suspension A$^-$B$^-$ in Figure 3.6(b). Consequently, the total solids volume $(\omega_o + d\omega_o)$ in the sediment A$^-$C$^-$ can be represented by :

$$\omega_o + d\omega_o = \omega_o + dH_\infty(1-\epsilon) \tag{3.54}$$

where H_∞ = final equilibrium height of sediment, (m)

ω_o = total volume of dry solids per unit cross-sectional area of tube or cylinder, (m^3/m^2)

Solving for ϵ in equation (3.54) :

$$\epsilon = 1 - \frac{d\omega_o}{dH_\infty} \tag{3.55}$$

ω_o is related to the solids compressive pressure p_s by the relation :

$$p_s = (\rho_s - \rho_l) g \omega_o \tag{3.56}$$

where g = constant of gravitational acceleration, (m/s^2)

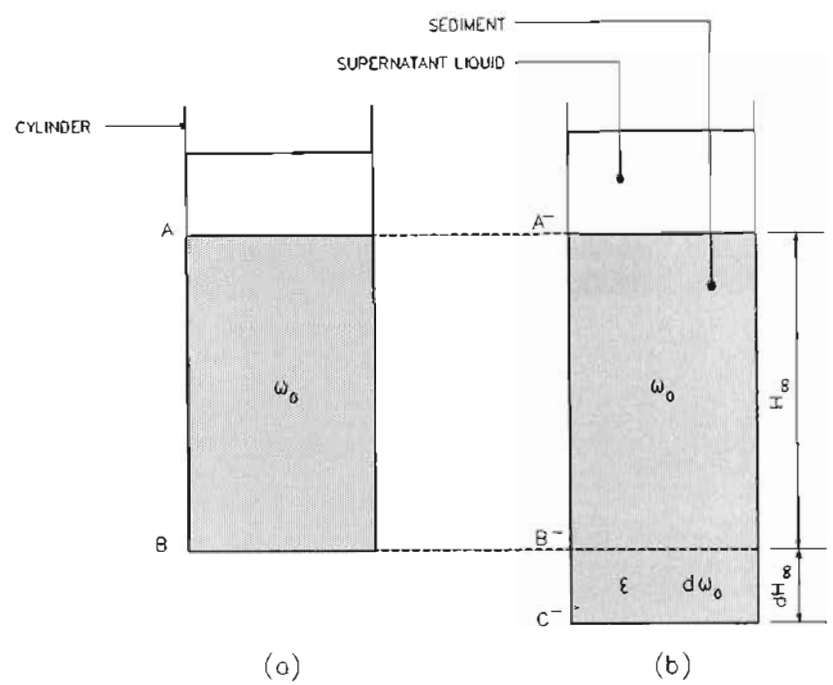

FIGURE 3.6 : Schematic Diagram Showing the Relationship Between Height of Sediment and Volume of Dry Solids per Unit Area (ω_0)

Shirato et al. (1983) found that on the basis of experimental data, H_∞ could be represented in terms of ω_0 by the following equation :

$$H_\infty = a\omega_0^b \tag{3.57}$$

where a = empirical constant in equation (3.57)
b = empirical constant in equation (3.57)

Substituting equation (3.57) into equation (3.55) and eliminating ω_0 by means of equation (3.56), one obtains equation (3.33) :

$$(1-\epsilon) = Bp_s^\beta \tag{3.33}$$

where

$$B = \frac{1}{ab[(\rho_s-\rho_l)g]^{(1-b)}} \tag{3.58a}$$

and

$$\beta = 1-b \tag{3.58b}$$

The values of empirical constants a and b may be obtained from a linear regression using the experimental results of log H_∞ and log ω_o. From equation (3.57) :

$$\log H_\infty = \log a + b \log \omega_o \qquad (3.59)$$

The values of B and β are calculated from equations (3.58a) and (3.58b), respectively. The relationship between porosity and solids compressive pressure can be calculated from equation (3.33).

3.3.7.3 Settling method for determining permeability at low solids compressive pressures

The following technique for determining permeability at low solids compressive pressures, was also developed by Shirato et al. (1983).

Michaels and Bolger (1962) investigated the sedimentation behaviour of flocculated suspensions of kaolin. For their sedimentation model they assumed that for flocculated suspensions, the basic flow units or settling entities are small clusters of particles or flocs. For gravity settling the flocs group into clusters of flocs called particle or floc aggregates. Michaels and Bolger (1962) found that the floc aggregates determine the sedimentation behaviour of flocculated suspensions. Shirato et al. (1983) confirmed the results of Michaels and Bolger (1962).

By using zinc oxide, Mitsukuri Gairome clay and ferric oxide slurries, they showed that sedimentation behaviour may be classified into three general regions according to the initial porosity of a suspension, ϵ_{in}, as shown in Figure 3.7.

In the dilute concentration region, $\epsilon_{in} > \epsilon_L$, free or hindered settling of individual particles or aggregates of particles may occur. In the intermediate concentration region, $\epsilon_{if} < \epsilon_{in} < \epsilon_L$, sedimentation behaviour becomes unstable owing to partial collapse of particle aggregates. In the higher concentration region, $\epsilon_{in} < \epsilon_{if}$, the supernatant liquid/sediment interface subsides slowly due to slow *consolidation* or *compression* of the sediment. In order to describe the sedimentation behaviour in the dilute concentration region, Michaels and Bolger (1962) modified an equation which Richardson and Zaki (1954) developed for the hindered settling of uniform, spherical particles. According to the modified equation, for dilute suspensions ($\epsilon_{in} > \epsilon_L$) of small clusters or aggregates of particles, the initial settling velocity of the surface of the sediment, v_o, can be related to the initial porosity, ϵ_{in}, of the original suspension :

$$v_o^{\frac{1}{4.65}} = \left\{ \frac{g d_f^2 (\rho_s - \rho_l)}{18 \mu_l (1 - \epsilon_{if})^{3.65}} \right\}^{\frac{1}{4.65}} (\epsilon_{in} - \epsilon_{if}) \qquad (3.60)$$

where d_f = mean diameter of particle aggregates, (m)

v_o = initial settling velocity of surface of sediment, (m/s)

ϵ_{if} = internal porosity of particle aggregates, (-)

ϵ_{in} = initial porosity of suspension, (-)

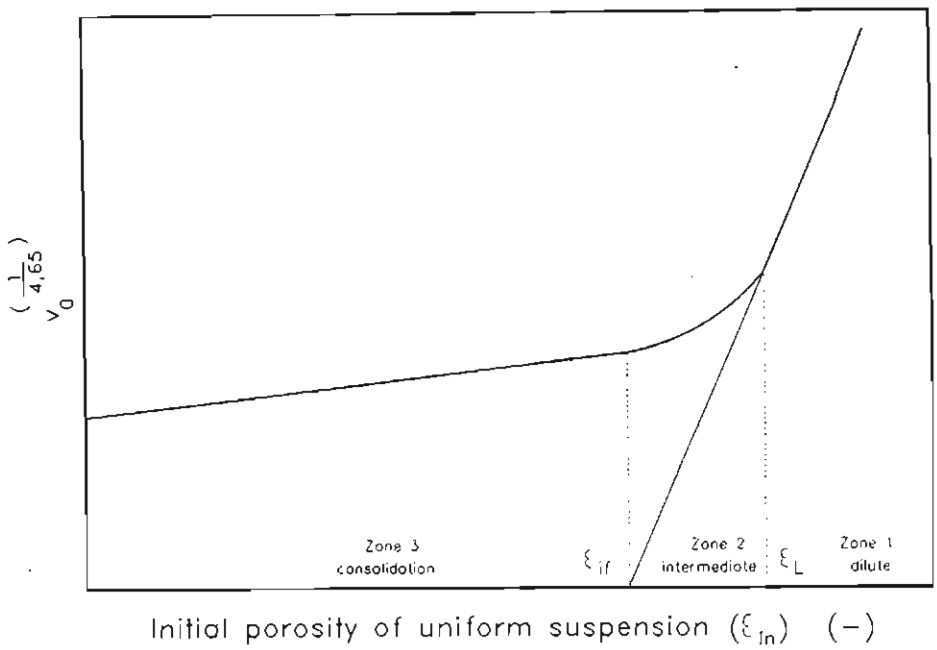

FIGURE 3.7 : Diagram Showing the Various Settling Regimes for a Sludge or Slurry

As shown in Figure 3.7, a straight line is obtained in the dilute region ($\epsilon_{in} > \epsilon_L$) in accordance with equation (3.60).

The technique for measuring porosity (as mentioned in section 3.3.7.2) and permeability at low solids compressive pressures is only valid for the concentration region, $\epsilon_{in} < \epsilon_{if}$, where sedimentation occurs due to *consolidation* of the sediment (Shirato et al., 1983).

For batch sedimentation of a concentrated suspension inside a cylinder, the liquid pressure, p_L, and the solids compressive pressure, p_s, increase towards the bottom of the cylinder. When a thin layer of the suspension settles due to consolidation, liquid has to flow through the thin layer due to the liquid pressure gradient across the layer as shown in Figure 3.8. The liquid pressure gradient across an element is caused by the weight of the particles lying above the element.

The D'Arcy equation (D'Arcy, 1856) may be used to describe the liquid flow through the thin layer :

$$u_l = -\frac{K}{\mu_l}\frac{\partial p_L}{\partial y} \qquad (3.61)$$

where u_l = apparent liquid velocity relative to solids, (m/s)

y = distance measured from bottom of cylinder, (m)

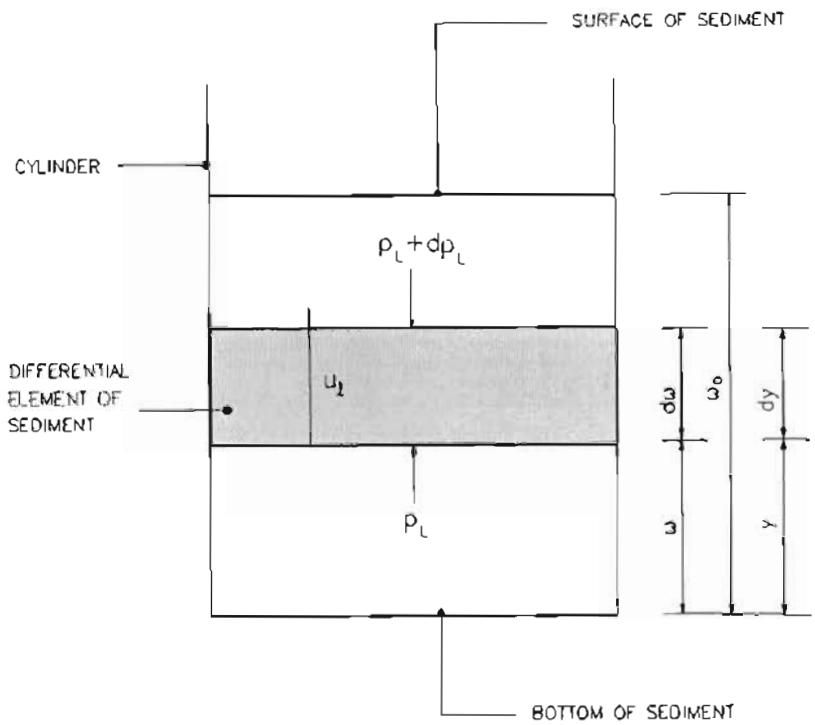

FIGURE 3.8 : Schematic Diagram Showing Up-flow of Liquid Due to Liquid Pressure Gradient in "Consolidation" Settling Regime

But

$$d\omega = (1-\epsilon)dy \tag{3.62}$$

where ω = volume of dry solids per unit cross-sectional area of tube or cylinder measured from bottom of tube or cylinder, (m^3/m^2)

Therefore equation (3.61) may be written in terms of ω, as follows :

$$\mu_l = -\frac{K(1-\epsilon)}{\mu_f}\frac{\partial p_L}{\partial \omega} \tag{3.63}$$

The forces acting on a differential element, $d\omega$, are shown in Figure 3.9. The following equation may be derived from Newton's second law of motion (assuming acceleration and inertial effects to be negligible) :

$$\frac{\partial p_L}{\partial \omega} + \frac{\partial p_s}{\partial \omega} = -(\rho_s - \rho_f)g \tag{3.64}$$

Wall friction is assumed to be negligible.

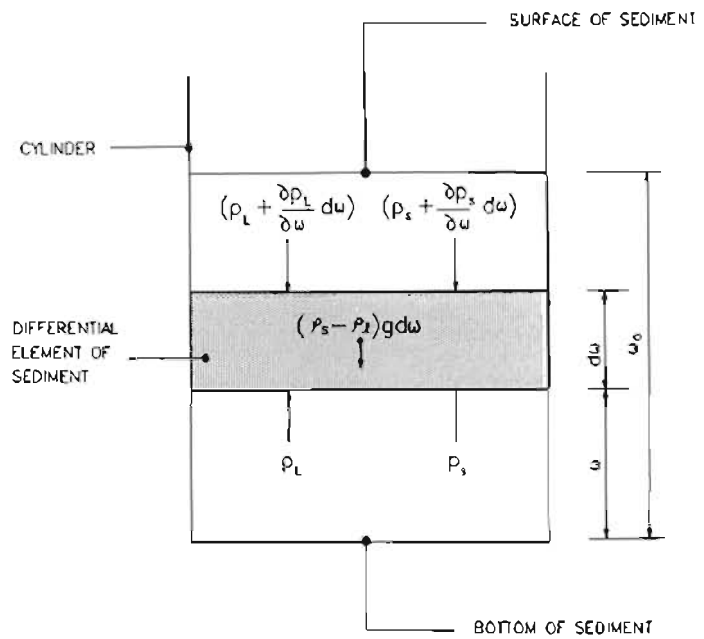

FIGURE 3.9 : Forces Exerted on a Differential Element, $d\omega$, in the "Consolidation" Settling Regime

Since the solids compressive pressure, p_s, can be assumed to be constant throughout the height of the cylinder at the beginning of a settling test when the suspension is uniform (Shirato et al., 1983), the initial liquid pressure gradient can be obtained from equation (3.64).

$$\left(\frac{\partial p_l}{\partial \omega}\right)_{t=0} = -(\rho_s - \rho_l)g \tag{3.65}$$

At time, $t = 0$, u_l in equation (3.63) can be considered as a constant which is equal to the initial settling velocity of the sediment surface, v_o. Combining equations (3.63) and (3.65) :

$$K = \frac{v_o \mu_l}{(\rho_s - \rho_l)(1 - \epsilon_{in})g} \tag{3.66}$$

But from equation (3.18) :

$$K = \frac{1}{\rho_s \alpha (1 - \epsilon_{in})} \tag{3.67}$$

Therefore,

$$\alpha = \frac{(\rho_s - \rho_l)g}{\mu_l \rho_s v_o} \tag{3.68}$$

On the assumption that the initial settling velocity depends only on the initial concentration of a suspension, equations (3.66) and (3.68) in conjunction with batch sedimentation data permit the calculation of permeability and specific filtration resistance, respectively.

Shirato et al. (1983) obtained the initial settling velocity, v_o, of a suspension by plotting (H/H_i) versus (t/H_i) for different initial heights, H_i, in a cylinder (see Figure B.1 in Appendix B). H is the height of the interface between the supernatant liquid and the sediment at time, t, while H_i is the initial height of the uniform suspension in the cylinder. For the experimental results of Shirato et al. (1983), the initial settling velocity of a suspension, v_o, was not affected by the initial height of the uniform suspension in a cylinder, H_i.

3.3.7.4 Centrifuge method for determining porosity in the intermediate solids compressive pressure range

Shirato et al. (1983) found good agreement between the compression-permeability results from a C-P cell (at high solids compressive pressure) and those obtained using the settling technique (at low solids compressive pressure). However, Murase et al. (1989) did not find good correlation between the porosity results using the settling technique and those obtained from a C-P cell and a new centrifuge technique. They ascribed this to friction between the suspension and the inner wall of the cylinder during batch settling. Murase et al. (1989) gave results of $(1-\epsilon)$ versus p_s for zinc oxide and ferric oxide slurries for all three techniques. The results for the settling tests were in the p_s range, $30\,\text{Pa} < p_s < 1000\,\text{Pa}$, for the centrifuge tests the results were in the p_s range, $10^3\,\text{Pa} < p_s < 10^5\,\text{Pa}$, and for the C-P cell tests the results were in the p_s range, $10^5\,\text{Pa} < p_s < 10^7\,\text{Pa}$. They recommended the centrifuge technique for determining the variation of porosity with solids compressive pressure in the intermediate p_s range.

The theory for the centrifuge technique is outlined below .

Figure 3.10 shows a suspension which has reached an equilibrium thickness in a rotating centrifuge tube. The forces acting on a thin element of sediment, Δr_c, are shown in Figure 3.10. The following equation may be derived from Newton's second law of motion (at equilibrium) :

$$F_c(r+\Delta r) - F_c(r) = (\rho_s - \rho_l)(1-\epsilon)(\pi r_t^2 \Delta r_c) r_c \Omega^2 \qquad (3.69)$$

where F_c = solids compressive force, (N)

r_c = distance from centre of centrifuge, (m)

r_t = radius of centrifuge tube, (m)

Δr_c = thickness of differential element of sediment, (m)

Ω = angular velocity, (rad/s)

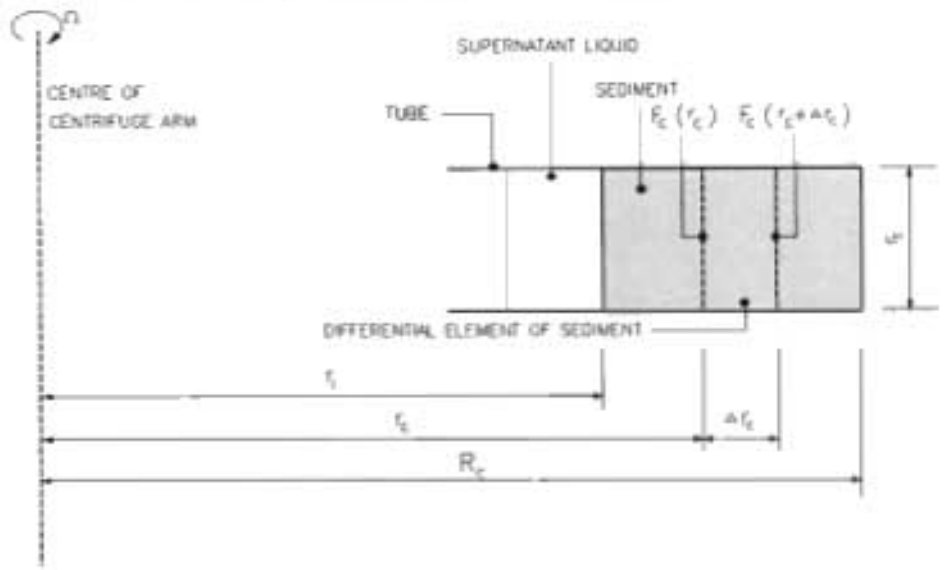

FIGURE 3.10 : Forces Acting on Differential Element of Sediment in Centrifuge Tube

In the limit, as $\Delta r_c \rightarrow 0$, equation (3.69) becomes :

$$\frac{dp_s}{dr_c} = (\rho_s - \rho_l)(1-\epsilon) r_c \Omega^2 \tag{3.70}$$

Integration of equation (3.70) with respect to r_c yields the following equation for the solids compressive pressure at the bottom of the tube, $p_s(R_c)$:

$$p_s(R_c) = (\rho_s - \rho_l)\Omega^2 \int_{r_l}^{R_c} (1-\epsilon) r_c dr_c \tag{3.71}$$

where R_c = distance between centre of centrifuge and bottom of centrifuge tube, (m)

r_l = distance from centre of centrifuge to surface of sediment, (m)

If $R_c \gg (R_c - r_l)$, the variable r_c in equation (3.71) can be approximated by $\frac{(R_c + r_l)}{2}$.

Therefore

$$p_s(R_c) = (\rho_s - \rho_l)\Omega^2 \frac{(R_c + r_l)}{2} \int_{r_l}^{R_c} (1-\epsilon) dr_c$$

$$= (\rho_s - \rho_l)\Omega^2 \left(\frac{R_c + r_l}{2}\right) \omega_u \tag{3.72}$$

where ω_o = total volume of dry solids per unit cross-sectional area of tube or cylinder, (m^3/m^2)

As shown in section 3.3.3, set of equations (3.33) has generally been used to model the variation of porosity with solids compressive pressure, p_s:

$$(1-\epsilon) = B p_s^{\beta} \qquad p_s \geq p_{si}$$

$$(1-\epsilon_i) = B p_{si}^{\beta} \qquad p_s \leq p_{si} \tag{3.33}$$

Combining equations (3.70) and (3.33) and integrating equation (3.70) over the entire sediment layer one obtains :

$$\int_o^{p_{si}} \frac{dp_s}{B p_{si}^{\beta}} + \int_{p_{si}}^{p_s(R_c)} \frac{dp_s}{B p_s^{\beta}} = (\rho_s - \rho_l)\Omega^2 \int_{r_i}^{R_c} r_c dr_c \tag{3.73}$$

Therefore,

$$\frac{p_{si}^{(1-\beta)}}{B} + \frac{p_s(R_c)^{(1-\beta)} - p_{si}^{(1-\beta)}}{B(1-\beta)} = (\rho_s - \rho_l)\Omega^2 \frac{(R_c + r_i)}{2}(R_c - r_i) \tag{3.74}$$

Combining equations (3.72) and (3.74) yields the following equation :

$$R_c - r_i = \frac{\omega_o^{(1-\beta)}}{B(1-\beta)} \left\{(\rho_s - \rho_l)\frac{(R_c + r_i)}{2}\Omega^2\right\}^{-\beta} - \frac{\beta p_{si}^{(1-\beta)}}{B(1-\beta)} \left\{(\rho_s - \rho_l)\frac{(R_c + r_i)}{2}\Omega^2\right\}^{-1} \tag{3.75}$$

Murase et al. (1989) found that for their results the second term on the right hand side of equation (3.75) was negligible. They obtained a good linear correlation when they plotted $\log (R_c - r_i)$ versus $\log \left\{(\rho_s - \rho_l)\frac{(R_c + r_i)}{2}\Omega^2\right\}$. From such a plot and by ignoring the second term of equation (3.75), the values of the constants B and β can be determined. The porosity versus p_s relationship can then be obtained from set of equations (3.33).

3.4 EXPERIMENTAL STUDY OF COMPRESSIBLE CAKE FILTRATION INSIDE A POROUS WOVEN TUBE

3.4.1 Introduction

The objectives in this experimental study were :

(i) to establish the variation of permeability and porosity with solids compressive pressure over a wide p_s range for a batch of waterworks clarifier sludge obtained from the prototype tubular filter press unit;

(ii) to determine the variation of filtrate flux, average cake dry solids concentration and internal radius of the cake with time, for the filtration of the same batch of clarifier sludge inside a porous woven tube;

(iii) to compare the experimental results with those predicted by the internal cylindrical filtration model.

In order to evaluate the permeability and porosity data, which were obtained from the C-P cell, settling and centrifuge experiments in (i), the data were incorporated into a conventional *planar* filtration model (see section 3.5.5). Results obtained from planar filtration experiments were compared with the predictions by the planar filtration model (with the incorporated permeability and porosity data).

3.4.2 Experimental System

3.4.2.1 Apparatus

3.4.2.1.1 C-P cell

A process schematic of the C-P cell which was used during this study, is shown in Figure 3.11. The C-P cell was constructed according to the design given by Rowe et al. (1966).

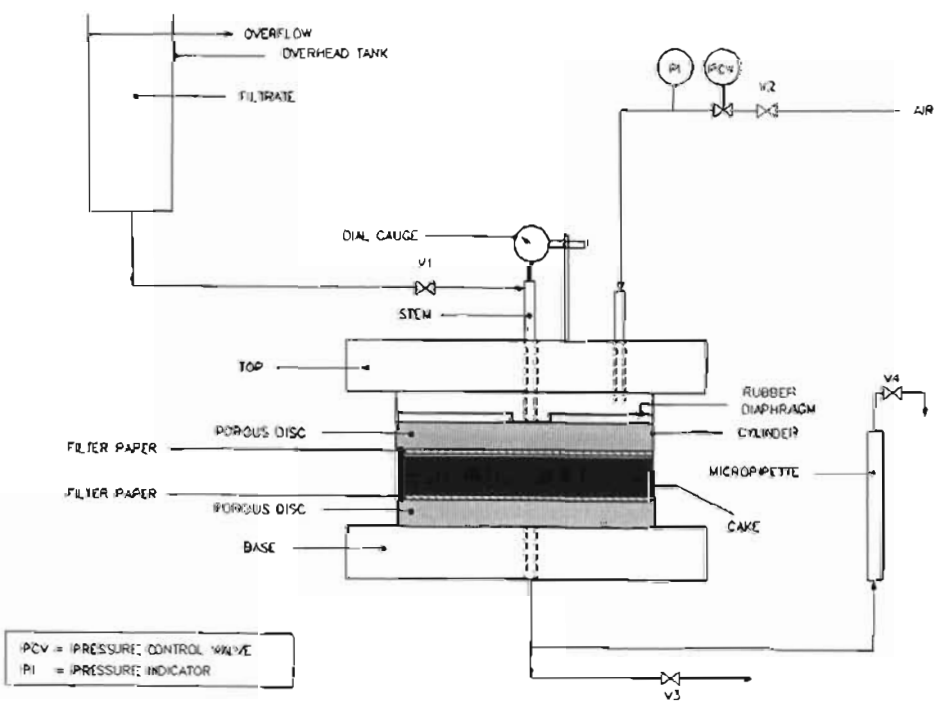

FIGURE 3.11 : Schematic Diagram of the Compression-Permeability (C-P) Cell

A top and a bottom filter paper separated the cake from the two porous discs. After the cell was assembled, the rubber diaphragm was pressurized with air. The cake was compressed by the pressure exerted by the rubber diaphragm on the top porous disc. The air pressure was controlled with a pressure control valve.

Filtrate from the internal cylindrical filtration experiments was stored in a header tank and was allowed to flow down the stem, through the cake and then through a micropipette for the measurement of volumetric flow rate of filtrate.

The level of filtrate in the header tank was fixed by an overflow pipe.

The movement of the stem under air pressure was measured with a dial gauge.

3.4.2.1.2 Internal cylindrical filtration apparatus

A schematic diagram of the internal cylindrical filtration apparatus is presented in Figure 3.12.

A stirrer in the sludge tank allowed the feed sludge to be thoroughly mixed before a run. At the start of an experiment, feed sludge was pumped by a MONO C22M pump into the cylindrical sludge container which had a capacity of 10 ℓ. The MONO pump was driven by a 2,1 kW d.c. motor, the speed of which was governed by a BRUNO ELECTRONIC TECHNIQUES d.c. variable speed drive. Once the cylindrical sludge container was filled with sludge, sludge was pumped by the MONO pump into the porous woven tube assembly.

During a filtration experiment, sludge was forced into the porous woven tube by applying air pressure to the cylindrical sludge container. The air pressure to the container was regulated with a pressure control valve.

The filtrate flowed down a gutter into a filtrate measuring cylinder which was located on a SARTORIUS electronic mass balance.

In order to clean the pipes after a series of experiments, water was pumped from the water tank by the centrifugal pump.

The porous woven tube, which could be dismantled after a filtration experiment and re-assembled before a subsequent filtration run, is shown in Figure 3.13. The porous woven tube assembly was constructed as follows. Holes of 6 mm were drilled at 50 mm intervals into two 1 m lengths of angle iron. The holes coincided exactly when the two lengths were placed on top of each other with the ends flush. A rectangular piece of woven polyester fabric supplied by Gelvenor[1] was folded and stretched tightly over a 25 mm O.D. PVC pipe. The two lengths of angle iron were placed over the two ends of the fabric so that the ends were flush with the fabric. Holes of 6 mm were burnt through the fabric at the position of the holes in the angle iron. After the holes had been burnt, the two ends of the fabric were clamped

1 Gelvenor Textiles (Pty) Ltd, Hammarsdale, Republic of South Africa.

tightly between the angle iron, by bolting the two lengths of angle iron together. The PVC pipe was removed and two 25 mm O.D. PVC end pieces that had been cut before, were secured at either end of the fabric by short lengths of wire.

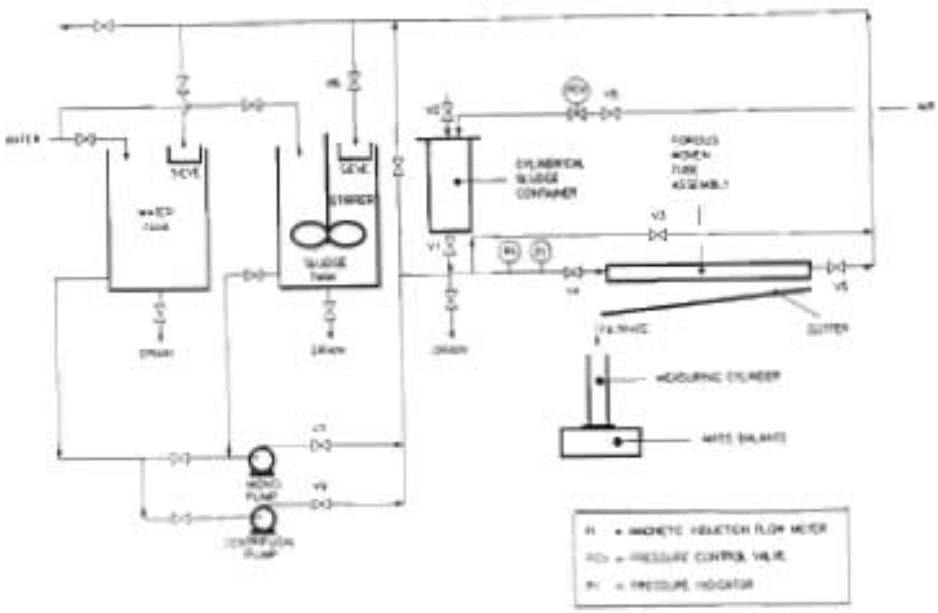

FIGURE 3.12 : Schematic Diagram of the Experimental Apparatus for Internal Cylindrical Filtration Experiments

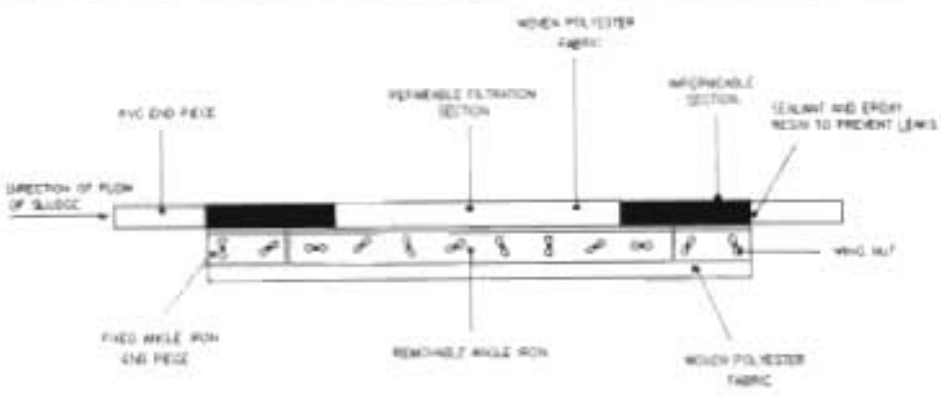

FIGURE 3.13 : Diagram of the Porous Woven Tube Assembly

A sealant was injected between the fabric and the outer perimeter of the end pieces so that there were no leaks. Each length of angle iron was cut into two end pieces of equal length and a central removable piece. The end pieces of angle iron were bolted permanently together. After an experiment only the central piece of angle

iron was removed to open the tube. The fabric at the end pieces was impregnated with an epoxy resin, to ensure that the end pieces were securely held together. After the resin had dried, the end pieces of the fabric were rendered impermeable by the application of a commercial resin. These non-porous regions served to minimize entrance and exit effects.

The effective length of the porous section of the tube was 0,442 m.

3.4.2.1.3 Planar filtration apparatus

A schematic diagram of the cylindrical pressure filter, which was used for the planar filtration experiments, is shown in Figure 3.14. The internal diameter of the cylindrical container was 145 mm. The filter medium was the same woven polyester fabric which was used for the internal cylindrical filtration experiments.

During an experiment, the filtrate flowed into a measuring cylinder which was located on a SARTORIUS electronic mass balance.

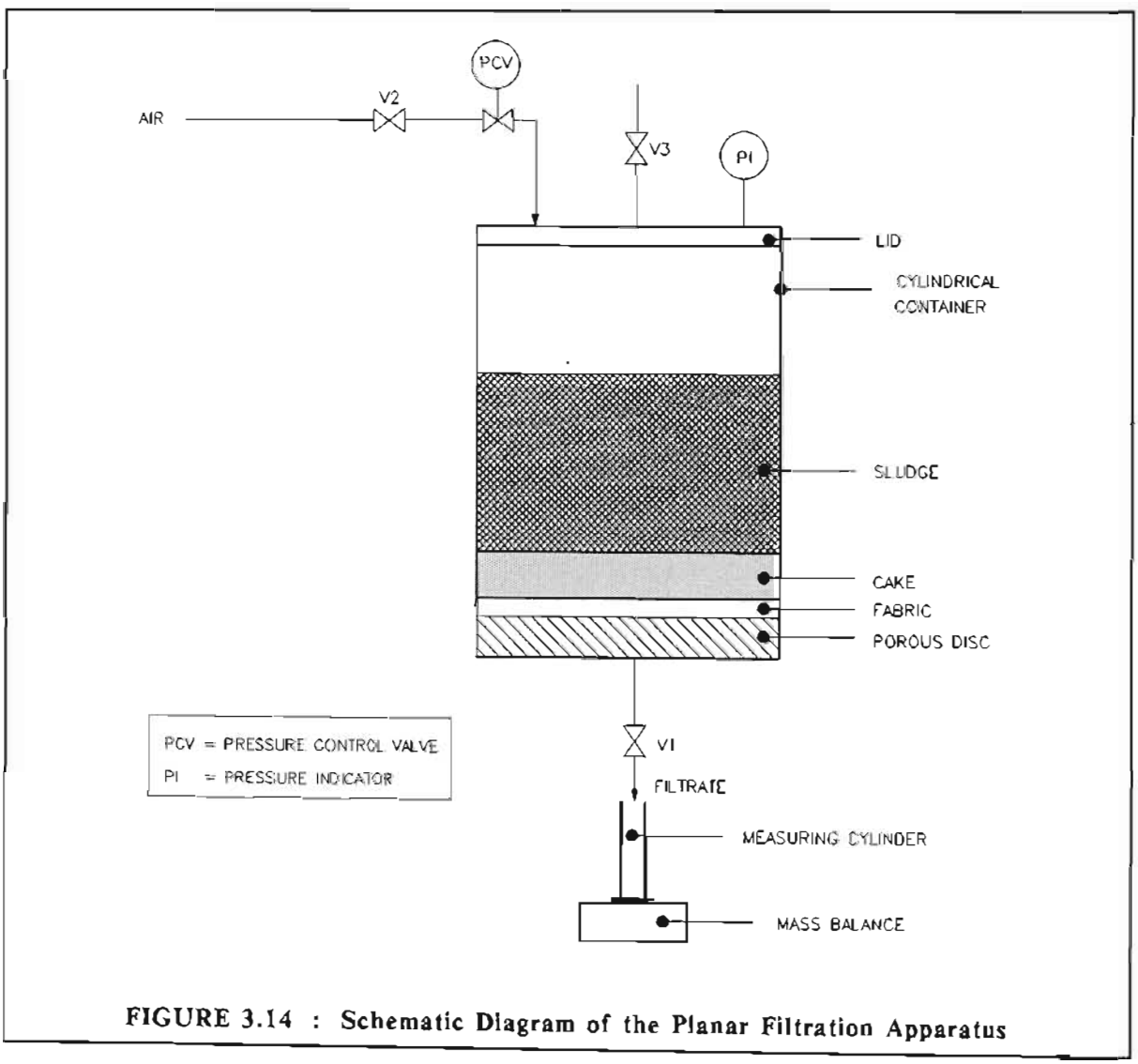

FIGURE 3.14 : Schematic Diagram of the Planar Filtration Apparatus

3.4.2.2 Measurement of main parameters

3.4.2.2.1 C-P cell

(i) Pressure : The air pressure was measured with a pressure gauge. The maximum error in these measurements was estimated to be 5 %.

(ii) Temperature : The temperature of the filtrate to the C-P cell was measured with a thermometer at regular intervals. The maximum error in these measurements was estimated to be 2 %.

(iii) Filtrate flow rate : The filtrate flow rate was measured by timing the displacement of a fixed volume of filtrate in a 1 mℓ micropipette, using a stop-watch. The maximum error for these measurements was estimated to be 3 %.

3.4.2.2.2 Internal cylindrical and planar filtration rigs

(i) Pressure : On the internal cylindrical filtration rig, the filtration pressure was measured with a WIKA electronic pressure transducer. On the planar filtration rig, filtration pressure was measured with a WIKA pressure gauge. The accuracy of the pressure measurement was estimated to be within 1 %.

(ii) Temperature : The temperature of the feed sludge and filtrate was measured with a thermometer at regular intervals during a filtration experiment. The maximum error in these measurements was estimated to be 2 %.

(iii) Concentration : The solids concentration of the feed sludge and the cake was measured using a gravimetric method. The maximum error in these measurements was estimated to be 3 %.

(iv) Filtrate flow rate : The filtrate flow rate was measured by recording the total accumulated mass of filtrate (as measured by a SARTORIUS mass balance) at regular intervals during an experiment. The accuracy of these measurements was estimated to be within 1 %.

3.4.3 Experimental Procedure

3.4.3.1 C-P cell

The cylinder was placed on the base after a thin film of grease had been applied on the bottom rim of the cylinder to ensure a proper seal between the base and the cylinder (see Figure 3.11).

The cylinder was half-filled with filtrate which had been obtained from filtration experiments on the internal cylindrical filtration rig. Air bubbles were expelled from the feed line to the micropipette and from the micropipette by-pass line by allowing filtrate to flow through these lines. The bottom porous disc was carefully

inserted and filter paper which had been cut to a slightly larger diameter than the internal diameter of the cylinder was placed on top of the porous disc. Care was taken to ensure that the filter paper formed a proper seal at its outer edge.

Approximately 150 mℓ of sludge was then introduced on top of the filter paper. A cake was allowed to form and any slurry adhering to the walls of the cylinder was washed with filtrate. A second filter paper which had been cut to a slightly larger diameter than the internal diameter of the cylinder, was placed on top of the cake ensuring a proper seal at the outer perimeter of the filter paper. The cylinder was then filled with clear filtrate.

A second porous disc was placed on top of the top filter paper. The cylinder was again filled with filtrate until it overflowed. Valve V1 was opened to allow filtrate to flow from the header tank (which had previously been filled with filtrate) through the stem. The diaphragm and top assembly was carefully lowered onto the top of the cylinder and the top was firmly bolted onto the base thereby clamping the diaphragm between the top and the cylinder. The dial gauge was fixed to the stem and its arm was secured to the top of the cell.

The header tank was then filled with filtrate. The level in the header tank was fixed by an overflow pipe. Valve V4 was opened to allow filtrate to flow through the micropipette (Valve V3 was closed).

The diaphragm was inflated to the desired pressure with air by opening valve V2. The air pressure was adjusted by means of the pressure control valve. In order to measure the flow rate of filtrate, bypass valve V3 was opened slightly to allow the level in the micropipette to drop. Filtrate flow rate was measured by closing valve V3 and by allowing the level in the micropipette to rise. Filtrate flow rate and the dial gauge reading were recorded every 15 minutes. It was found that for the waterworks clarifier sludge, both readings stabilized within 90 to 120 minutes. The level in the feed tank was also checked every 15 minutes and if required the tank was filled with filtrate.

After the dial gauge and the filtrate flow rate readings had stabilized, the air pressure in the diaphragm was increased and further readings were obtained in a similar manner.

At the end of the run the cell was dismantled and the cake was carefully removed and weighed. The cake was re-weighed after drying at 105 °C for at least 5 hours. The final thickness of the cake was calculated using the final porosity, cross-sectional area of the cell and the particle density, ρ_s, of the solids in the cake (see Appendix A). The variation of cake thickness with solids compressive pressure was determined from the final thickness of the cake and the readings on the dial gauge at the various pressures.

All the runs were carried out at ambient temperature.

3.4.3.2 Internal cylindrical filtration apparatus

Approximately 500 kg of wet cake was collected in four containers at the prototype tubular filter press over a period of two days. After collection the cake was immediately transported to a controlled environment room. The temperature in this room was controlled at between 2 and 5 °C. The cake was stored in this controlled environment to limit microbiological activity and degradation.

Prior to this, attempts had been made to prepare synthetic sludges using sodium bentonite and also various proportions of bentonite and kaolin. All these attempts were unsuccessful, however. For the pure bentonite the average specific filtration or cake resistance was so high that filtration runs would have been exceedingly long, while for the bentonite/kaolin mixtures it was found that the settling rates for sludges with a solids concentration in the range 50 g/ℓ to 100 g/ℓ were relatively high. These high settling rates resulted in significantly higher cake thicknesses at the bottom than at the top of the horizontally mounted porous tube of the filtration rig. Feed sludges with solids concentrations higher than 100 g/ℓ resulted in very short filtration runs in the porous tube which had an internal diameter of 26,25 mm. Consequently, it was decided to collect a large batch of wet cake from the prototype tubular filter press, since a great deal of experience had been gained using the waterworks clarifier sludge on the prototype unit.

Before a series of experiments, a known mass of cake was added to a known volume of tap water to yield approximately the desired feed solids concentration. The cake and the tap water were homogenized by switching on the high speed stirrer in the feed tank for 20 to 30 minutes. Thereafter the resultant sludge was passed twice through a 425 μm sieve by pumping all the sludge from the feed tank through the sieve to the water tank and vice versa. This was done to remove any undesirable larger lumps of cake or particles which had not been homogenized. The solids concentration of the feed sludge was then re-determined by a gravimetric method. If the feed solids concentration was *higher* than desired, a calculated volume of water was added to the feed tank. If it was *lower* than the desired value, a calculated amount of water was siphoned from the top of the feed tank after overnight settling of the solids in the feed tank.

Before an experiment the feed sludge was homogenized by switching on the stirrer in the feed tank (see Figure 3.12). Immediately after homogenization of the feed sludge, the cylindrical sludge container was filled by pumping feed sludge from the feed tank using the MONO pump. After filling the sludge container, valves V1 and V2 at the bottom and top of the container respectively, were closed. Thereafter, sludge was circulated by the MONO pump from the feed tank through the system and back to the feed tank by opening valve V3 and keeping valves V4 and V5 closed. This was done to fill all pipes with sludge and to expel any air bubbles from the system.

After 5 minutes of pumping, valves V4 and V5 were opened and bypass valve V3 was closed to allow circulation of sludge through the porous tube for a short time period of 30 seconds. This allowed filling of the porous-woven tube assembly and the expelling of any air bubbles from the assembly.

The pump was then switched off. Valves V5 and V7 were closed and valve V1 was opened. Valve V8 was opened and the air pressure was regulated to the pre-set desired filtration pressure with the pressure control valve.

The filtrate flowed down the gutter and into a measuring cylinder which was located on a SARTORIUS electronic mass balance. The accumulated mass of filtrate was recorded at an interval of 30 seconds. The solids concentration of the feed sludge was sufficiently high for the solids in the sludge to be in the consolidation settling regime (see section 3.3.7.3). Consequently the settling rate of the solids in the feed sludge was very low. There was therefore minimal settling in the pipework and the porous filter tube over the filtration period, which was a maximum of 30 minutes (see Appendix D).

At the end of a filtration experiment, valve V8 was closed and the pressure in the system was released by opening valve V2. Care was taken not to release the pressure too suddenly, to avoid disturbing the cake in the filter tube.

Once the pressure had been released, valve V4 was closed and the filter tube was disconnected from the pipework. The filter tube assembly was tipped slightly and either valve V4 or V5 was opened slightly to allow any feed sludge remaining inside the tube to be drained very slowly. Care was taken to avoid disturbing the cake inside the tube.

After drainage of the filter tube, the tube was opened by unbolting the two central lengths of angle iron. If the cake was sufficiently robust so as not to be broken during handling, the internal diameter of the cake was measured with a vernier calliper. The internal cake diameter was also calculated from the mass of wet cake and average cake dry solids concentration, as detailed in Appendix D.

Care was taken to remove all the cake from the tube. The mass of the wet cake was determined and the average dry solids concentration of the cake was determined by drying the cake in an oven at 105 °C for 12 hours.

The fabric was washed thoroughly using a high pressure spray and the filter tube was re-assembled and returned to the filtration rig.

The experimental procedure was repeated for subsequent filtration experiments.

At the end of a day the pipes in the system were purged of sludge by pumping water from the water tank through the system using the centrifugal pump.

The internal diameter of the tube (filter medium) was determined as follows. A filtration run was allowed to continue for an extended time period, until the tube was solidly blocked and the cake was hard and robust. The tube was dismantled and the outer diameter of the cake was measured with a vernier calliper at various

points along the length of the tube. The *average* outer diameter of the cake (internal diameter of the tube) was found to be 26,25 mm. The variation in outer diameter along the length of the tube was 0,5 mm.

3.4.3.3 Planar filtration apparatus

Prior to an experiment a batch of waterworks clarifier sludge, which had been prepared for the internal cylindrical filtration experiments, was removed from the sludge tank of the internal cylindrical filtration apparatus.

Valve V1 (see Figure 3.14) was closed and the porous disc and woven polyester filter fabric (which had been cut to a slightly larger diameter than the internal diameter of the cylindrical container) were carefully located at the bottom of the cylindrical container. The batch of feed sludge was homogenized using a laboratory stirrer and the required volume of sludge was carefully poured into the cylindrical container. The lid was bolted on and valve V2 was opened. The air pressure was regulated to the desired filtration pressure with the pressure control valve.

Valve V1 was opened and the filtrate flowed into a measuring cylinder which was located on a SARTORIUS electronic mass balance. The accumulated mass of filtrate was recorded at an interval of 30 seconds (see Appendix D). The solids concentration of the feed sludge was sufficiently high for the solids in the sludge to be in the consolidation settling regime (see section 3.3.7.3). Consequently the settling rate of the solids in the feed sludge was very low.

At the end of a filtration experiment, valves V1 and V2 were closed and the pressure in the system was released by opening valve V3.

Once the pressure had been released, the lid was removed and the bulk of the remaining sludge was pumped out of the cylindrical container using a small peristaltic pump. The remaining sludge was then removed by tipping the cylindrical container to the side. Care was taken to avoid disturbing the cake.

All the cake was then removed. The mass of wet cake was determined. The average dry solids concentration of the cake was determined by drying the cake in an oven at 105 °C for 12 hours.

The fabric, porous disc and cylindrical container were washed thoroughly using a high pressure spray.

The experimental procedure was repeated for subsequent filtration experiments.

The cake thickness for each experiment was calculated as shown in Appendix D.

3.4.3.4 Determination of compression-permeability data at low solids compressive pressure using the settling technique

3.4.3.4.1 Determination of variation of porosity with solids compressive pressure using the settling technique

Various quantities of homogenized sludge were introduced into eight perspex cylinders with an internal diameter of 60 mm. The initial heights of the sludge in the cylinders were in the range of approximately 0,05 m to approximately 1,5 m. The initial solids concentration of the sludge was sufficiently high so as to be in the region where settling occurs due to compaction or consolidation from the beginning of the experiment (see section 3.3.7.3).

The heights of the interfaces between the sediment and supernatant liquid in the cylinders were measured at regular intervals. It was found that there was no further compaction or consolidation after approximately 2 weeks of standing.

The final equilibrium heights were recorded. The results were then analysed according to the model proposed by Shirato et al. (1983) which was described in section 3.3.7.2.

3.4.3.4.2 Determination of variation of permeability with solids compressive pressure using the settling technique

Various quantities of homogenized sludge were introduced into 4 polypropylene measuring cylinders with a capacity of 1 ℓ and an internal diameter of 50 mm. The initial solids concentration of the sludge was sufficiently high for sedimentation to occur by compaction or consolidation from the beginning of the experiment (see section 3.3.7.3).

The initial heights of the sludge were 159 mm; 239 mm; 318 mm and 397 mm for all initial solids concentrations which were tested. The heights of the interfaces between the sediment and the supernatant liquid were measured at regular time intervals for various initial solids concentrations.

The results were analysed according to the model proposed by Shirato et al. (1983), which was described in section 3.3.7.3.

3.4.3.5 Determination of variation of porosity with solids compressive pressure in the intermediate solids compressive pressure range using the centrifuge technique

Equal amounts of homogenized sludge were introduced into four flat-bottomed centrifuge tubes. The details of the tubes are shown in Appendix C. The tubes were placed in their holders in the centrifuge and were then spun at a fixed speed for 1 hour. Previous experiments had shown that the thickness of the sediments in the tubes did not change significantly after rotating for more than 1 hour.

The thickness of the sediments in the tubes was then measured. The tubes were then again placed in their holders in the centrifuge and were then spun at a higher rotational speed.

The rotational speed was varied in the range 500 r.p.m. (52,36 rad/s) to 4 000 r.p.m. (418,88 rad/s).

3.4.3.6 Determination of sludge and cake parameters

3.4.3.6.1 Determination of solids content of the sludge

A 50 mℓ aliquot of a representative sample of the sludge was measured into a weighed crucible. The sample was dried at 105 °C for 5 to 12 hours and then cooled in a dessicator and re-weighed. The results were expressed in terms of mass of dry solids per unit volume of sludge.

3.4.3.6.2 Determination of the average cake dry solids concentration

A representative sample of wet cake was placed into a small glass beaker and weighed. The cake was re-weighed after drying at 105 °C for 12 hours.

3.4.3.6.3 Determination of the density of the solids in the sludge

A representative sample of the sludge was dried at 105 °C for 12 hours. The dry solids were allowed to cool and were then ground in a mortar using a pestle.

Four density cells were thoroughly cleaned with acetone and then dried. The mass of each cell was determined. The cells were then filled with distilled water and inserted into a water bath at 25 °C. After half an hour the tops were inserted into each cell. The cells were then removed from the water bath and dried on the outside. The mass of water which each cell could hold at 25 °C was determined. From this the volume of each cell was determined. The water from each cell was discarded.

After thorough drying with acetone the mass of each cell was determined again. A representative sample of finely ground, dried sludge solids was added to each cell and the mass of solids in each cell was determined by difference.

The cells were then filled with distilled water and re-inserted into the water bath at 25 °C. After half an hour the tops were inserted into each cell; the cells were removed from the water bath and dried on the outside. The mass and volume of water in each cell was determined.

The volume of solids in each cell was equal to the difference between the volume of the cell and the volume of the water in each cell. The density of the solids in each cell could be calculated from the mass and volume of the solids in each cell. The solids density was taken as the average of the results for the four cells.

The average density of the solids was found to be 2 380,1 kg/m^3.

3.4.3.6.4 Determination of the average particle size and particle size distribution of the particles in the sludge

The average particle size and the particle size distribution of the particles in a representative sample of the sludge were determined using a Malvern particle size analyser type 3600 E. The mass average particle size was found to be 5,90 μm. The results and further details are tabulated in Appendix F.

3.4.3.6.5 Measurement of the resistance of the woven filter fabric used for the internal cylindrical filtration experiments

Prior to a test to determine the resistance of the woven polyester filter fabric, which was used for the internal cylindrical filtration experiments, the pipes of the experimental apparatus and the filter fabric were washed thoroughly with tap water.

Tap water was then allowed to permeate through the fabric at a constant pressure of 50 kPa. The flow rate of filtrate was determined.

The resistance of the medium was then determined using equation (3.43).

$$\Delta p_m = \frac{\mu_f Q_f R_m}{2\pi r_i} \qquad (3.43)$$

Several tests were done and the *average* resistance of the filter fabric was found to be 5,353 x 10^{10} m^{-1}.

Leu (1981) showed that because of migration of fine particles and continued deposition of particles in the medium, medium resistance increases with time during a filtration run. However, for this study it was assumed that medium resistance remained constant during a filtration experiment. This was a fair assumption since the cake from the clarifier sludge had a very high resistance compared to the medium resistance.

3.5 RESULTS

3.5.1 Results of the C-P Cell Experiments

The results of two C-P cell tests are tabulated in Appendix A.

Plots of permeability versus solids compressive pressure and solids volume fraction $(1 - \epsilon)$ versus solids compressive pressure for the two tests are shown in Figures 3.15 and 3.16 respectively.

Linear regressions using the permeability versus solids compressive pressure data for tests A.1 and A.2 yielded values for F and δ (see set of equations (3.32)) as shown in Table 3.1.

Linear regressions using the solids volume fraction $(1 - \epsilon)$ versus solids compressive pressure data for tests A.1 and A.2 yielded values for B and β (see set of equations (3.33)) as shown in Table 3.2.

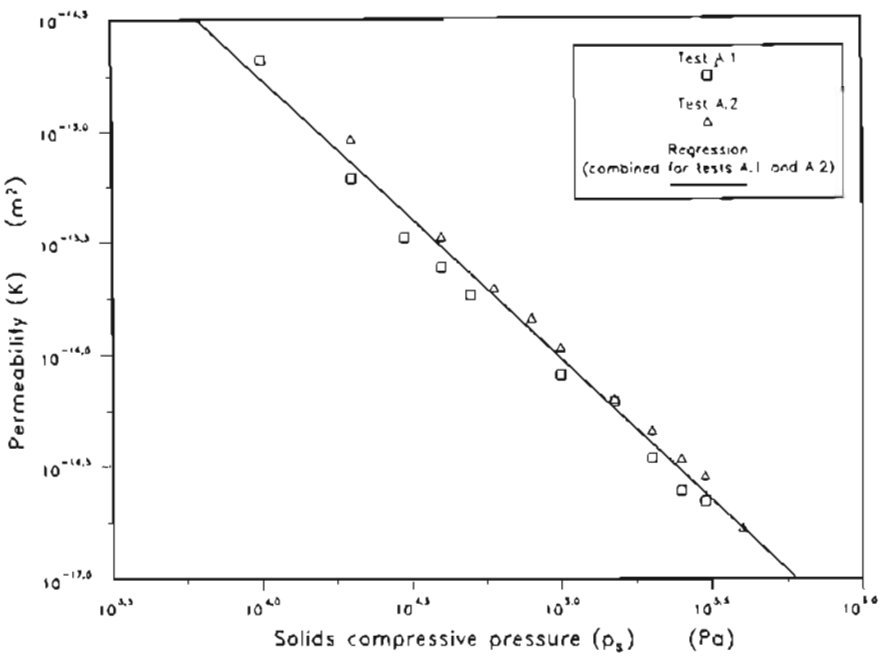

FIGURE 3.15 : Graph of Permeability (K) versus Solids Compressive Pressure (ρ_s) for the C-P Cell Experiments

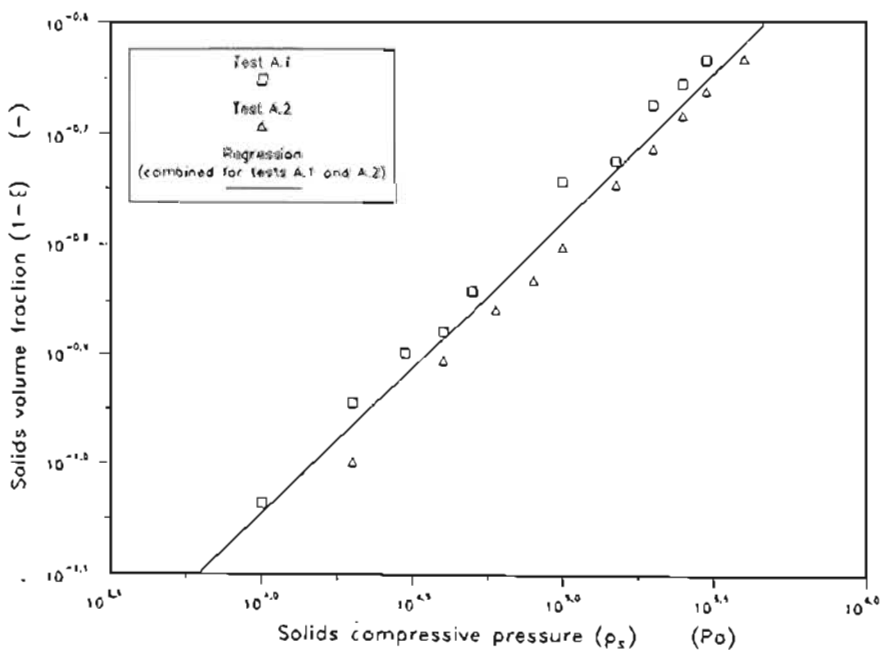

FIGURE 3.16 : Graph of Solids Volume Fraction ($1 - \epsilon$) versus Solids Compressive Pressure (ρ_s) for the C-P Cell Experiments

TABLE 3.1
Linear Regression Values for F , δ and Correlation Coefficient (r_r^2) for C-P Cell Test A.1, Test A.2 and Tests A.1 and A.2 *Combined*

	Test A.1	Test A.2	Tests A.1 and A.2 *Combined*
F	2,129 x 10^{-10}	2,922 x 10^{-10}	1,779 x 10^{-10}
δ	1,281	1,286	1,254
r_r^2	0,991	0,998	0,985

TABLE 3.2
Linear Regression Values for B , β and Correlation Coefficient (r_r^2) for C-P Cell Test A.1, Test A.2 and Tests A.1 and A.2 *Combined*

	Test A.1	Test A.2	Tests A.1 and A.2 *Combined*
B	0,00771	0,00621	0,00785
β	0,271	0,282	0,265
r_r^2	0,996	0,999	0,974

For specific filtration resistance the values of C and n in set of equations (3.34) (for *combined* tests A.1 and A.2) were calculated in Appendix G :

$$C = 3,008 \times 10^{8}$$

$$n = 0,989$$

The cake was therefore very compressible.

3.5.2 Results of the Low Solids Compressive Pressure Settling Experiments

3.5.2.1 Determination of porosity at low solids compressive pressure

The results of two settling tests (tests B.1 and B.2) to determine the relationship between porosity and solids compressive pressure at low solids compressive pressure are tabulated in Appendix B.

A plot of H_∞ versus ω_0 for both tests is shown in Figure 3.17. Linear regressions using the H_∞ versus ω_0 data for tests B.1 and B.2 yielded values for a and b (see equation (3.57)) as shown in Table 3.3.

TABLE 3.3
Linear Regression Values for a , b and Correlation Coefficient (r_r^2) for Settling Test B.1, Test B.2 and Tests B.1 and B.2 *Combined*

	Test B.1	Test B.2	Tests B.1 and B.2 *Combined*
a	17,108	17,391	17,248
b	0,9201	0,9235	0,9218
r_r^2	0,999	0,999	0,999

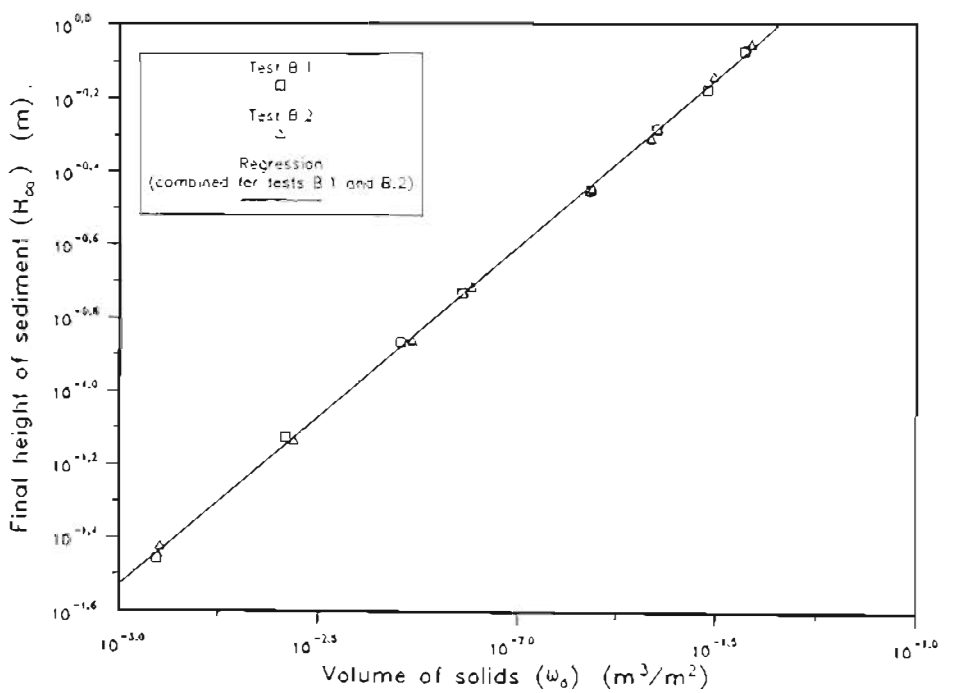

FIGURE 3.17 : Graph of Final Height of Sediment (H_∞) versus Volume of Solids (ω_o) for the Settling Experiments

As explained in section 3.4.3.6.3, the density of the solids in the sludge was found to be 2380,1 kg/m^3. Taking the density of water as 997,69 kg/m^3 (at 22,5 °C; Perry, 1973), the value for B for the *combined* regression data may be calculated from equation (3.58a) for the values of a and b for the *combined* H_∞ versus ω_o data.

$$B = \frac{1}{ab[(\rho_s - \rho_l)g]^{(1-b)}}$$

$$= \frac{1}{(17,248)(0,9218)[(2380,1 - 997,69)(9,81)]^{(1-0,9218)}}$$

$$= 0,0299$$

From equation (3.58b) :

$$\beta = 1 - b$$

$$= 1 - 0,9218$$

$$= 0,0782$$

From set of equations (3.33) :

$$1 - \epsilon = B p_s^{\beta}$$

$$= 0,0299\, p_s^{0,0782} \qquad \left(\begin{array}{c} for\ combined\ regression\ data \\ for\ tests\ B.1\ and\ B.2 \end{array}\right)$$

The values of B and β for test B.1, test B.2 and tests B.1 and B.2 *combined* are shown in Table 3.4 :

TABLE 3.4
Values for B and β for Settling Test B.1, Test B.2 and Tests B.1 and B.2 *Combined*

	Test B.1	Test B.2	Tests B.1 and B.2 *Combined*
B	0,0297	0,0301	0,0299
β	0,0799	0,0765	0,0782

A plot of solids volume fraction $(1 - \epsilon)$ versus solids compressive pressure for the settling experiments, is shown in Figure 3.18.

The solids compressive pressure range for these experiments was, $16,9\ Pa \leq p_s \leq 525,6\ Pa$, as shown in Appendix B.

3.5.2.2 Determination of permeability at low solids compressive pressure

The results of the settling tests to determine the variation of permeability with solids compressive pressure at low solids compressive pressures are tabulated in Appendix B. As shown in Figure B.1 in Appendix B, for the clarifier sludge :

$\epsilon_L = 0,991$

$\epsilon_{ll} = 0,982$ (see section 3.3.7.3)

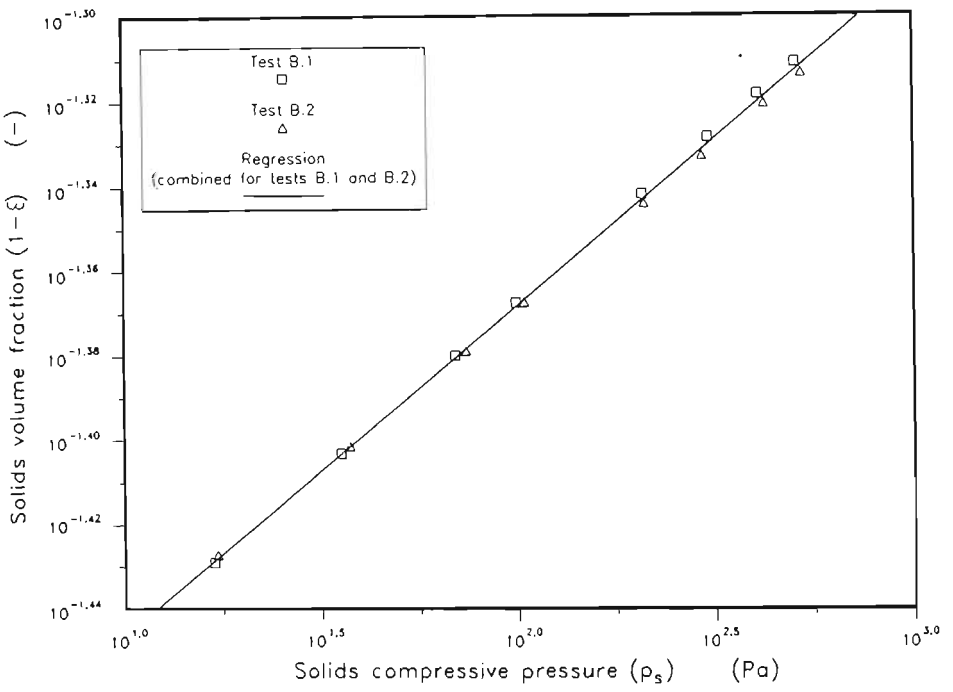

FIGURE 3.18 : Graph of Solids Volume Fraction ($1 - \epsilon$) versus Solids Compressive Pressure (p_s) for the Settling Experiments

A plot of permeability versus solids compressive pressure is shown in Figure 3.19. The solids compressive pressure range for these experiments was, $0.0065\,\text{Pa} \leq p_s \leq 22.55\,\text{Pa}$.

A linear regression using the permeability versus solids compressive pressure data yielded the following values for F and δ (see set of equations (3.32)) in the solids compressive pressure range which was investigated :

$$F = 6.621 \times 10^{-13}$$

$$\delta = 0.575$$

The correlation coefficient, r_r^2, for the regression was 0,977.

The values of C and n for specific filtration resistance (see set of equations (3.34)) were calculated in Appendix G for the settling experiments :

$$C = 2.122 \times 10^{10}$$

$$n = 0.497$$

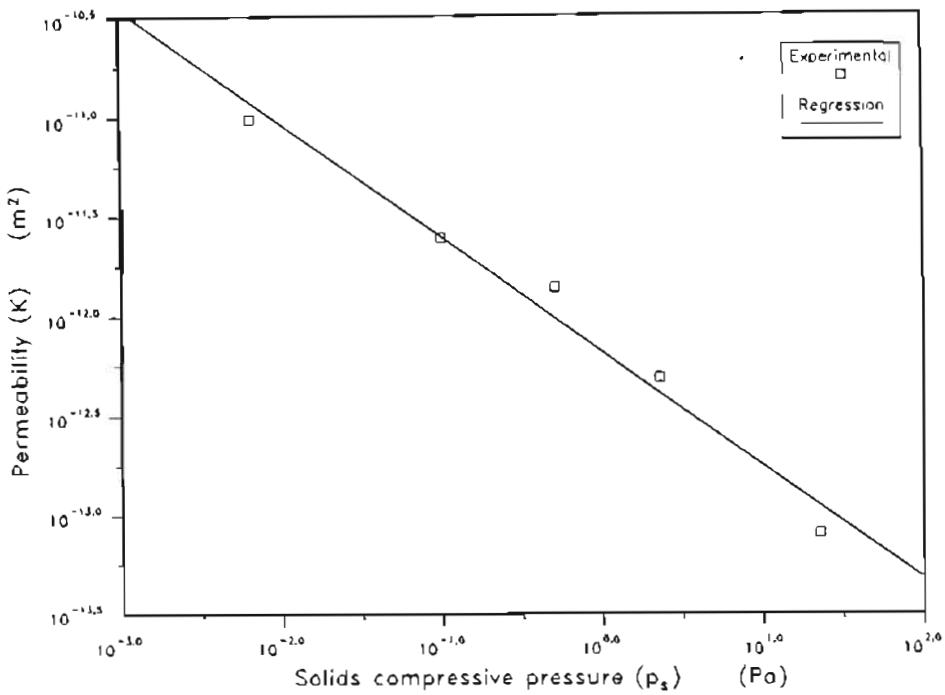

FIGURE 3.19 : Graph of Permeability (K) versus Solids Compressive Pressure (p_s) for the Settling Experiments

3.5.3 Results of the Centrifuge Experiments to Determine Porosity in the Intermediate Solids Compressive Pressure Range

The results of two centrifuge tests are tabulated in Appendix C.

As stated in section 3.3.7.4, Murase et al. (1989) found that the second term on the right hand side of equation (3.75) could be ignored. This gives the following equation :

$$(R_c - r_i) = \frac{\omega_0^{(1-\beta)}}{B(1-\beta)} \left\{ (\rho_s - \rho_l) \frac{(R_c + r_i)}{2} \Omega^2 \right\}^{-\beta} \qquad (3.76)$$

By plotting $(R_c - r_i)$ versus $\left\{ (\rho_s - \rho_l) \frac{(R_c - r_i)}{2} \Omega^2 \right\}$ on a log scale, a straight line should be obtained.

A graph of $(R_c - r_i)$ versus $\left\{ (\rho_s - \rho_l) \frac{(R_c - r_i)}{2} \Omega^2 \right\}$, for the tests C.1 and C.2 shown in Appendix C, is shown in Figure 3.20.

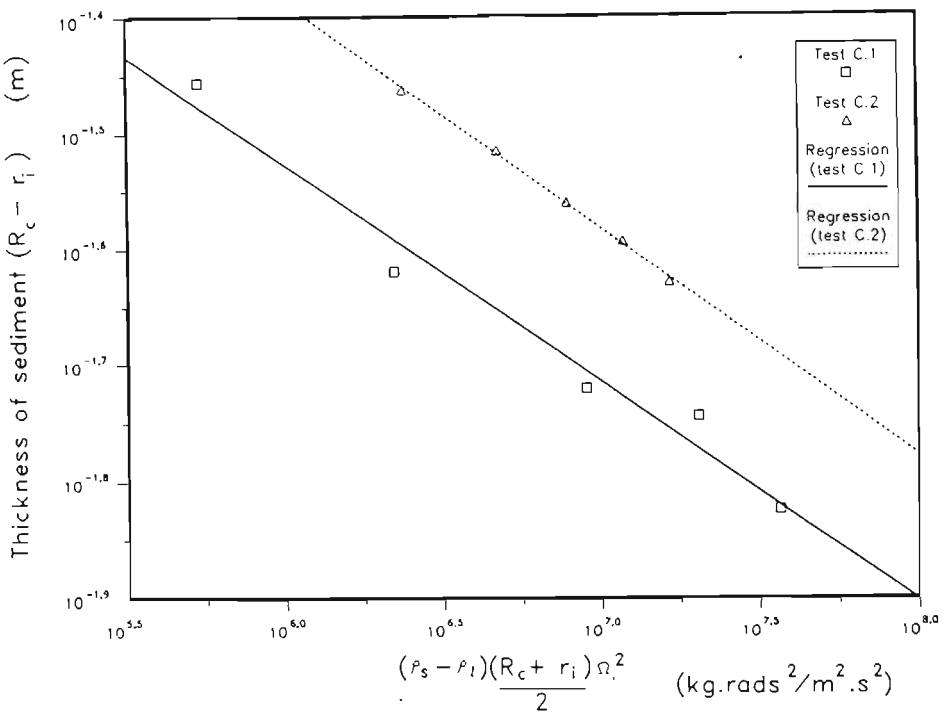

FIGURE 3.20 : Graph of Thickness of Sediment $(R_c - r_i)$ versus $\left\{(\rho_s - \rho_l)\left(\frac{R_c + r_i}{2}\right)\Omega^2\right\}$ for the Centrifuge Experiments

The values for B and β, which were obtained from linear regressions using the data for tests C.1 and C.2, are shown in Table 3.5 :

TABLE 3.5
Linear Regression Values for B, β and Correlation Coefficient (r_r^2) for Centrifuge Test C.1, Test C.2 and Tests C.1 and C.2 *Combined*

	Test C.1	Test C.2	Tests C.1 and C.2 *Combined*
B	0,0177	0,0175	0,0169
β	0,187	0,196	0,196
r_r^2	0,973	0,998	0,981

A plot of solids volume fraction $(1 - \epsilon)$ versus solids compressive pressure for the centrifuge tests is shown in Figure 3.21.

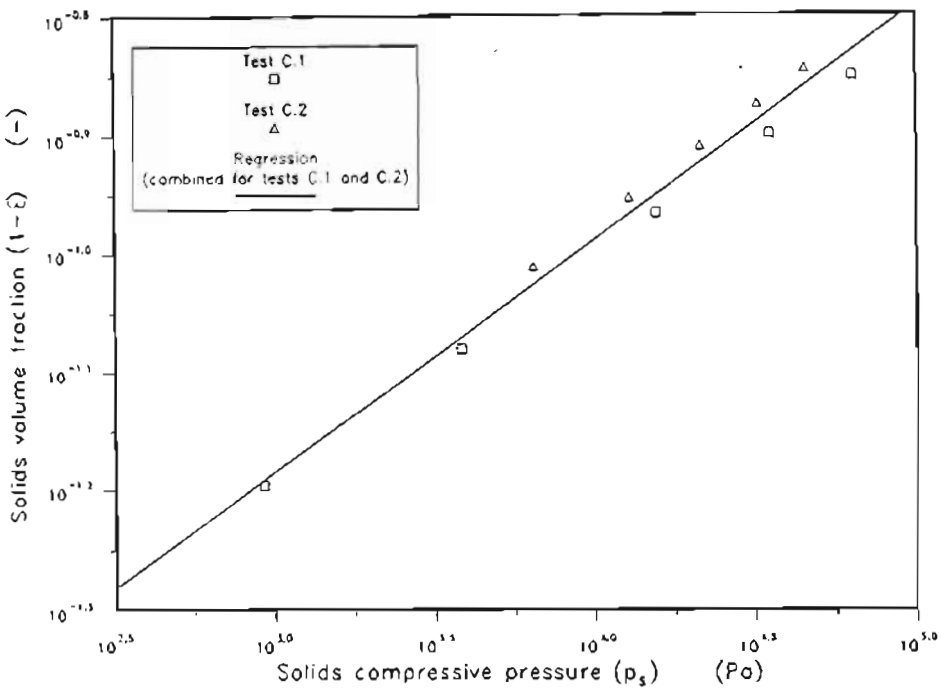

FIGURE 3.21 : Graph of Solids Volume Fraction ($1 - \epsilon$) versus Solids Compressive Pressure (p_s) for the Centrifuge Experiments

3.5.4 Fitting of Porosity and Permeability Data to Standard Equations

3.5.4.1 Permeability data

A graph of permeability versus solids compressive pressure for the settling tests and the two C-P cell tests is shown in Figure 3.22(a). The regression lines for the settling and *combined* C-P cell data are also shown. From Figure 3.22(a) it is evident that the slopes of the regression lines are different. The two lines intersect at a solids compressive pressure of 3781,7 Pa.

The following equations are based on the linear regression results of the *combined* C-P cell and settling data, as shown in sections 3.5.1 and 3.5.2.2, respectively :

$$K = 6.621 \times 10^{-13} p_s^{-0.575} \qquad p_s \leq 3781.7 \text{ Pa}$$

$$K = 1.779 \times 10^{-10} p_s^{-1.254} \qquad p_s \geq 3781.7 \text{ Pa} \qquad (3.77)$$

From set of equations (3.77); $K \rightarrow \infty$ as $p_s \rightarrow 0$. In order to prevent this it was assumed that below the solids compressive pressure, p_{sf}, the permeability is constant. Solids compressive pressure, p_{sf}, was defined as follows from set of equations (3.33) :

$$p_{sf} = \left(\frac{1 - \epsilon_f}{B} \right)^{\frac{1}{\delta}} \qquad (3.78)$$

where p_{sl} = solids compressive pressure corresponding to porosity of feed sludge, (Pa)

ϵ_l = porosity of feed sludge, (-)

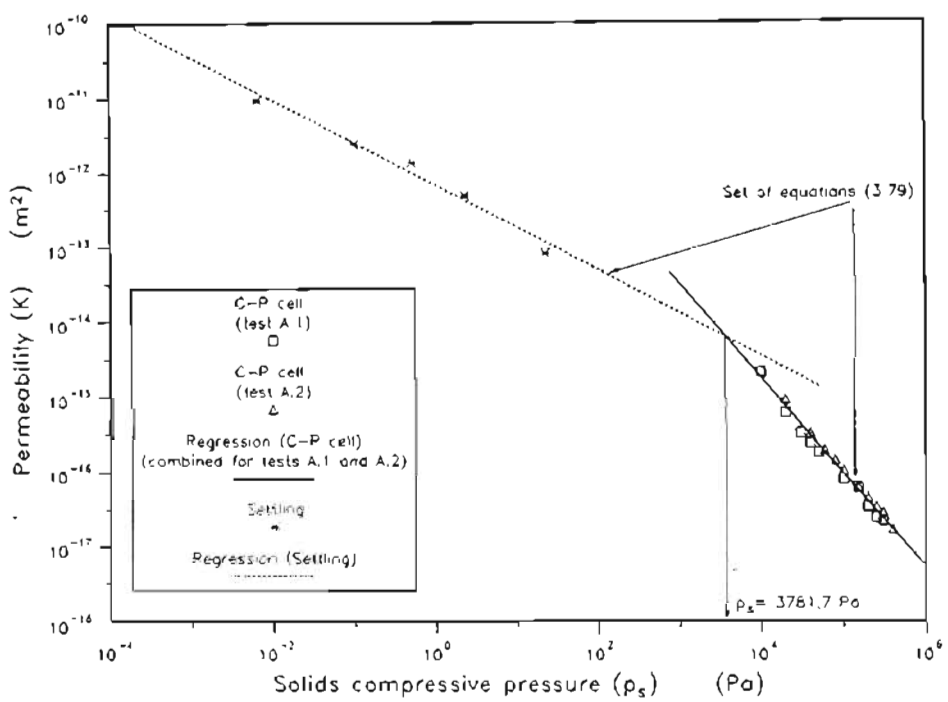

FIGURE 3.22(a) : Graph of Permeability (K) versus Solids Compressive Pressure (p_s) for the C-P Cell and Settling Experiments Showing the Basis for Set of Equations (3.79)

The equations which were used to describe the permeability versus solids compressive pressure relationship for the clarifier sludge, were therefore :

$$K = 6.621 \times 10^{-13} p_{sl}^{-0.575} \qquad 0 \leq p_s \leq p_{sl}$$

$$K = 6.621 \times 10^{-13} p_s^{-0.575} \qquad p_{sl} \leq p_s \leq 3781.7 \text{ Pa} \qquad (3.79)$$

$$K = 1.779 \times 10^{-10} p_s^{-1.254} \qquad p_s \geq 3781.7 \text{ Pa}$$

Unless the solids concentration of the feed sludge is very high, the value of p_{sl} will be small. For a feed sludge solids concentration of 49 g/ℓ, as was used in this study, and using the regression results of the settling tests :

$$p_{sl} = \left(\frac{1 - 0.9794}{0.0299} \right)^{\frac{1}{0.0782}}$$

$$= 0.0085 \text{ Pa}$$

The set of equations (3.79) is similar to the set of equations (3.32) which was proposed by Tiller and Cooper (1962).

Murase et al. (1989) also reported different slopes for settling data and C-P cell data. They ascribed this to network formation between aggregates of particles in the concentration range where settling occurs due to consolidation or compaction. According to them the network formation leads to significant friction between particles and the inner wall of the cylinder and therefore to erroneous results. However, a good fit between experimental results and the planar and internal cylindrical filtration models, using set of equations (3.79), was obtained. For further discussions see section 3.6.4.

The resistance of the cake was very high. As shown in Appendix G, the average specific filtration resistance (for planar filtration) was calculated to be 1,351 x 10^{13} m/kg for an applied filtration pressure of 300 kPa.

3.5.4.2 Porosity data

A graph of $(1-\epsilon)$ versus p_s for the settling data, centrifuge data and the C-P cell data is shown in Figure 3.22(b). It is evident that the three sets of data for the three different methods all have significantly different slopes. The agreement between the C-P cell data and the centrifuge data is not nearly as good as that reported by Murase et al. (1989). A linear regression using the *combined* centrifuge and C-P cell data yielded the following results :

$$B = 0,0125$$

$$\beta = 0,226$$

The correlation coefficient, r_r^2, for the linear regression was 0,966.

The *combined* centrifuge and C-P cell regression line intersects that of the settling data at a solids compressive pressure of 365,3 Pa. If the centrifuge data are ignored, the regression line of the *combined* C-P cell data intersects that of the settling data at 1 285,1 Pa. Sets of equations (3.80) and (3.81) were used for the porosity versus solids compressive pressure relationship in the planar and internal cylindrical filtration models. Set of equations (3.80) incorporates the centrifuge data as discussed above, while for set of equations (3.81) the centrifuge data are ignored. In the same manner as for permeability, the porosity of the cake was assumed to be constant and equal to ϵ_f below p_{sf}.

$$\begin{aligned} 1-\epsilon &= 0,0299 p_{sf}^{0,0782} && 0 \leq p_s \leq p_{sf} \\ 1-\epsilon &= 0,0299 p_s^{0,0782} && p_{sf} \leq p_s \leq 365,3\,\text{Pa} \\ 1-\epsilon &= 0,0125 p_s^{0,226} && p_s \geq 365,3\,\text{Pa} \end{aligned} \qquad (3.80)$$

$$
\begin{aligned}
1-\epsilon &= 0.0299\,p_{sl}^{0.0782} && 0 \le p_s \le p_{sl} \\
1-\epsilon &= 0.0299\,p_s^{0.0782} && p_{sl} \le p_s \le 1285.1\ \text{Pa} \\
1-\epsilon &= 0.00785\,p_s^{0.265} && p_s \ge 1285.1\ \text{Pa}
\end{aligned}
\qquad (3.81)
$$

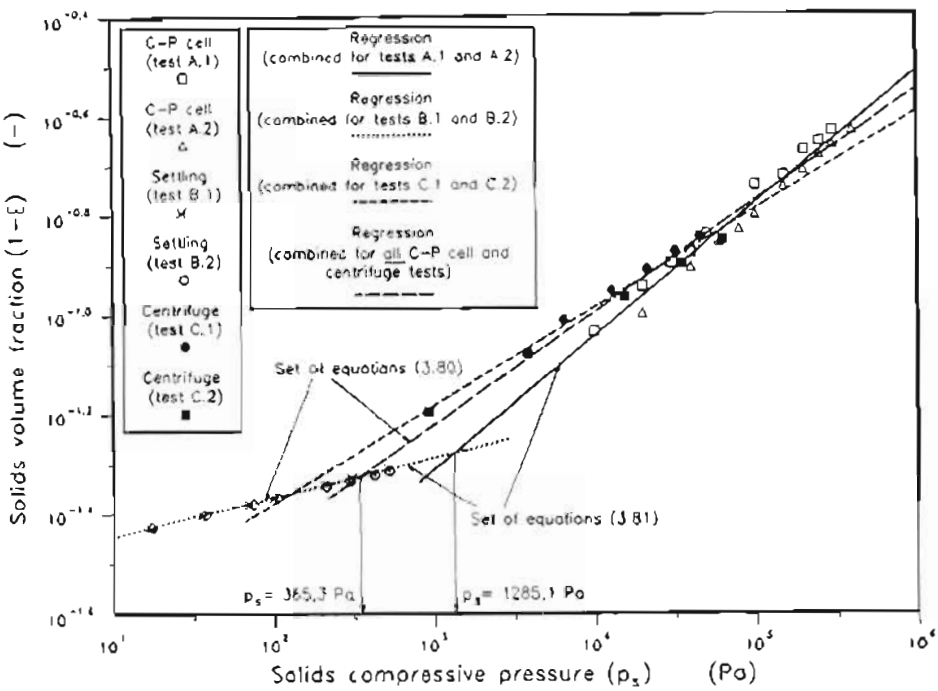

FIGURE 3.22(b) : Graph of Solids Volume Fraction ($1-\epsilon$) versus Solids Compressive Pressure (p_s) for the Settling, Centrifuge and C-P Cell Experiments Showing the Basis for Sets of Equations (3.80) and (3.81)

Sets of equations (3.80) and (3.81) are similar to set of equations (3.33), which was proposed by Tiller and Cooper (1962).

As shown in sections 3.5.5 and 3.5.7, set of equations (3.81) gave a better correlation between experimental and predicted average cake dry solids concentrations, when used in the planar and internal cylindrical filtration models, than set of equations (3.80).

An attempt was also made to fit all the permeability and porosity data to equations (3.35) and (3.36) respectively. Equations (3.35) and (3.36) were proposed by Tiller and Leu (1980). However, the fit between a non-linear regression (using equations (3.35) and (3.36)) and the experimental data, was not very good. Also, when the non-linear regression equations (for equations (3.35) and (3.36)) were incorporated into the planar and internal cylindrical filtration models, the correlation between experimental and predicted values was not very good.

3.5.4.3 Porosity and permeability data for error analysis

As shown in Figures 3.15 and 3.16 for permeability and solids volume fraction ($1-\epsilon$), respectively, there was a significant "scatter" of experimental points around the regression lines for the *combined* C-P cell data for tests A.1 and A.2.

In subsequent error analyses (see sections 3.5.5 and 3.5.7) it was found that this "scatter" was significant when incorporated into the planar and internal cylindrical filtration models. The error or uncertainty limits for the C-P cell data were determined by using the permeability versus solids compressive pressure relationship for test A.1 with the porosity versus solids compressive pressure relationship for test A.2 and vice versa.

The resultant sets of equations (similar to sets of equations (3.79) and (3.81)) for the uncertainty limits are :

$$
\begin{aligned}
1-\epsilon &= 0.0299\, p_{sf}^{0.0782} && 0 \le p_s \le p_{sf} \\
1-\epsilon &= 0.0299\, p_s^{0.0782} && p_{sf} \le p_s \le 2249.3\,Pa \\
1-\epsilon &= 0.00621\, p_s^{0.282} && p_s \ge 2249.3\,Pa
\end{aligned}
\qquad (3.82)
$$

$$
\begin{pmatrix} Uncertainty \\ limit\ 1 \end{pmatrix}
$$

$$
\begin{aligned}
K &= 6.621 \times 10^{-13}\, p_{sf}^{-0.575} && 0 \le p_s \le p_{sf} \\
K &= 6.621 \times 10^{-13}\, p_{sf}^{-0.575} && p_{sf} \le p_s \le 3567.4\,Pa \\
K &= 2.129 \times 10^{-10}\, p_s^{-1.281} && p_s \ge 3567.4\,Pa
\end{aligned}
$$

$$
\begin{aligned}
1-\epsilon &= 0.0299\, p_{sf}^{0.0782} && 0 \le p_s \le p_{sf} \\
1-\epsilon &= 0.0299\, p_s^{0.0782} && p_{sf} \le p_s \le 1145.9\,Pa \\
1-\epsilon &= 0.00771\, p_s^{0.271} && p_s \ge 1145.9\,Pa
\end{aligned}
\qquad (3.83)
$$

$$
\begin{pmatrix} Uncertainty \\ limit\ 2 \end{pmatrix}
$$

$$
\begin{aligned}
K &= 6.621 \times 10^{-13}\, p_{sf}^{-0.575} && 0 \le p_s \le p_{sf} \\
K &= 6.621 \times 10^{-13}\, p_{sf}^{-0.575} && p_{sf} \le p_s \le 5245.3\,Pa \\
K &= 2.922 \times 10^{-10}\, p_s^{-1.286} && p_s \ge 5245.3\,Pa
\end{aligned}
$$

The basis for sets of equations (3.82) and (3.83) is plotted in Figures 3.23(a) and (b).

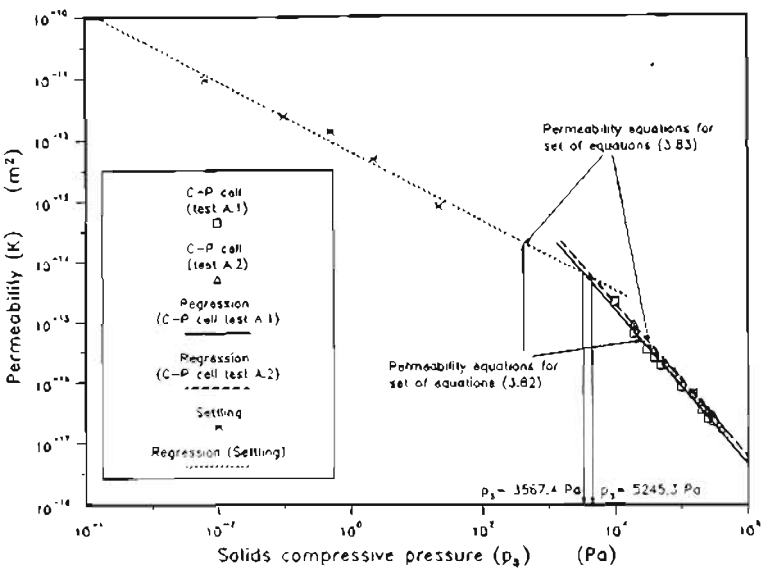

FIGURE 3.23(a) : Graph of Permeability (K) versus Solids Compressive Pressure (p_s) for the C-P Cell and Settling Experiments Showing the Basis for Sets of Equations (3.82) and (3.83)

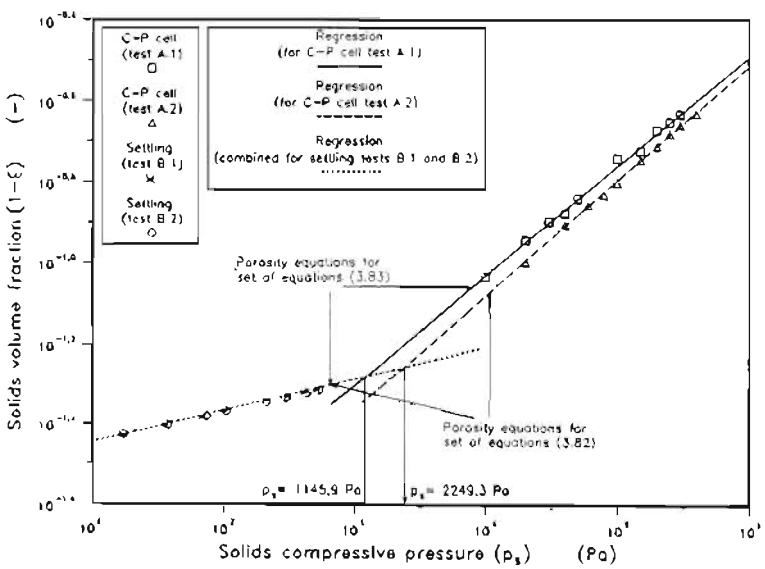

FIGURE 3.23(b) : Graph of Solids Volume Fraction ($1-\epsilon$) versus Solids Compressive Pressure (p_s) for the Settling and C-P Cell Experiments Showing the Basis for Sets of Equations (3.82) and (3.83)

3.5.5 Results of Constant Pressure Planar Filtration Experiments

3.5.5.1 Conventional model for planar compressible cake filtration

In order to evaluate the permeability and porosity data, which were obtained from the C-P cell, settling and centrifuge experiments, the data were incorporated into the conventional planar filtration model which was presented in sections 3.2.2 and 3.3.2. The model is summarized below :

$$\frac{dp_s}{dx} + \frac{dp_l}{dx} = 0 \qquad (3.10b)$$

From D'Arcy's law (D'Arcy, 1856) :

$$\frac{dp_l}{dx} = \frac{\mu_f u}{K} \qquad (3.14)$$

But

$$u = \frac{Q_f}{A} \qquad (3.15)$$

Combining equations (3.14) and (3.15) :

$$\frac{dp_l}{dx} = \frac{\mu_f Q_f}{AK} \qquad (3.84)$$

Combining equations (3.10b) and (3.84) :

$$\frac{dp_s}{dx} = -\frac{\mu_f Q_f}{AK} \qquad (3.85)$$

A FORTRAN computer program was written to numerically integrate equations (3.84) and (3.85) in order to obtain the p_l and p_s profiles within the cake. The computer program was similar to that which was written for the internal cylindrical filtration model, and which is discussed in detail in section 3.5.7. Equations (3.84) and (3.85) were integrated by incorporating the permeability data from set of equations (3.79) and the porosity data from set of equations (3.80) or (3.81) into a Runge-Kutta numerical integration technique.

3.5.5.2 Comparison between planar filtration model and experimental results

The results of the constant pressure planar filtration experiments are tabulated in Appendix D. The experiments were conducted at three filtration pressures, namely, 100 kPa, 200 kPa and 300 kPa, using the waterworks clarifier sludge. The filtration times were in increments of 5 minutes up to 30 minutes and the solids concentration of the feed sludge was approximately 49 g/ℓ.

The predicted and experimental average cake dry solids concentrations are shown in Figures 3.24(a) to (d). As shown in Figure 3.24(a) there was a slight increase in *experimental* average cake dry solids concentration with filtration pressure. Set of equations (3.80), which incorporates the porosity data of the centrifuge tests, was

used to generate the curves for the *predicted* average cake dry solids concentrations in Figures 3.24(a) to (d). As shown in Figures 3.24(b) to (d) the predicted values were significantly higher than the experimental results.

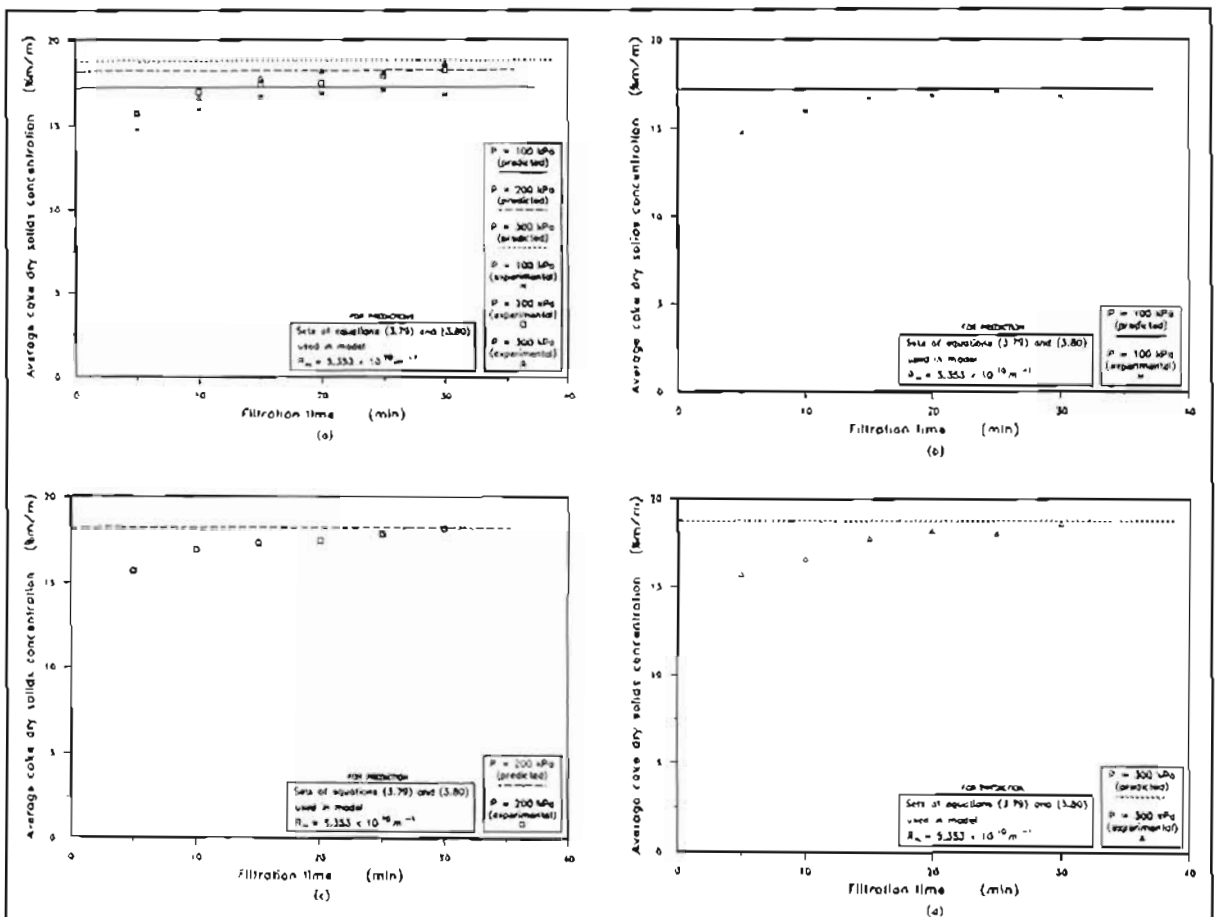

FIGURE 3.24 : Comparison Between Experimental and Predicted Average Cake Dry Solids Concentrations for Planar Filtration (Centrifuge Data Included) : (a) Combined Results; (b), (c) and (d) Individual Results for P = 100 kPa, P = 200 kPa and P = 300 kPa, respectively

When the porosity data of the centrifuge tests were ignored and set of equations (3.81) (instead of set of equations (3.80)) was incorporated into the model, almost all the experimental average cake dry solids concentrations fell within the range of uncertainty for the model predictions, as shown in Figures 3.25(b) to (d). The uncertainty limits shown in Figures 3.25(b) to (d) were determined by using sets of equations (3.82) and (3.83) to describe the variation of permeability and porosity with solids compressive pressure in the planar model (see section 3.5.4.3).

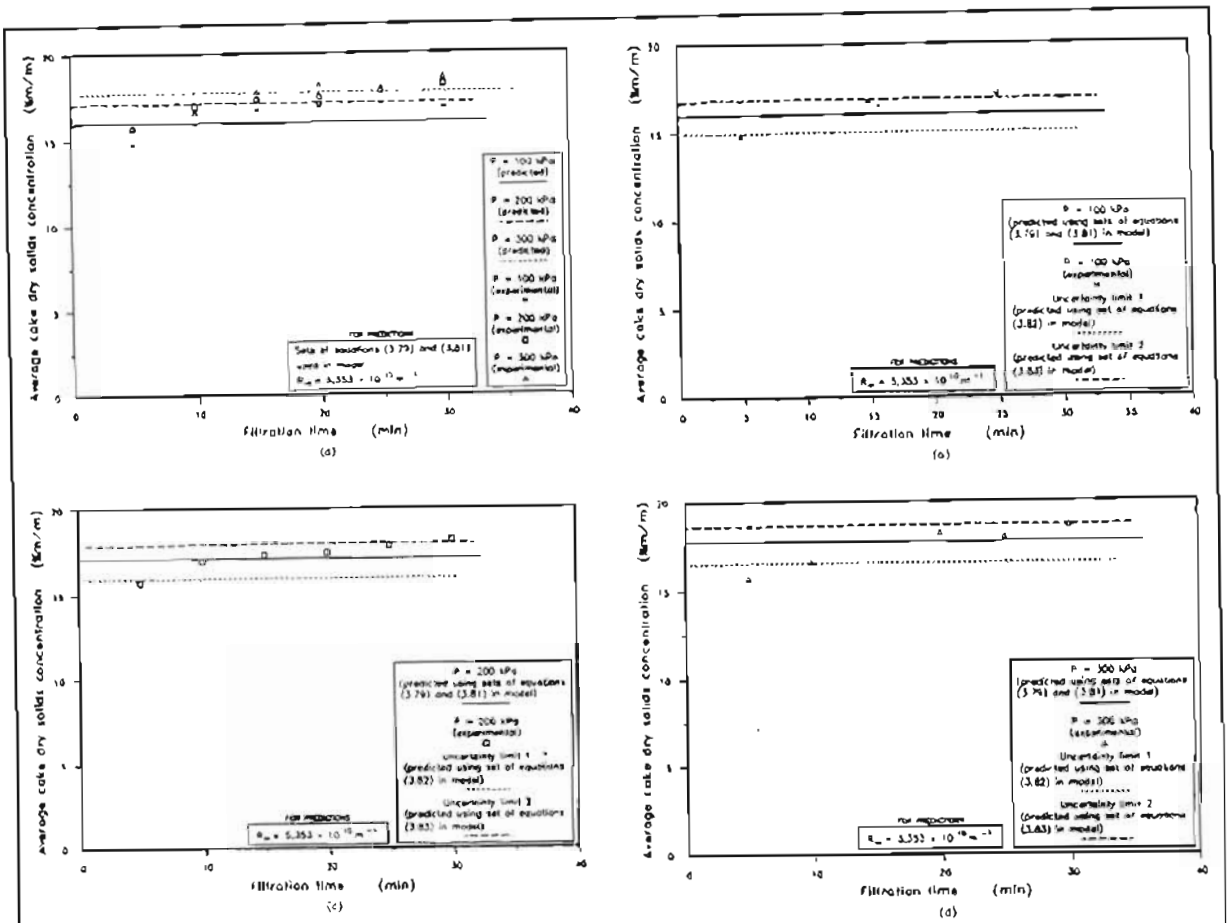

FIGURE 3.25 : Comparison Between Experimental and Predicted Average Cake Dry Solids Concentrations for Planar Filtration (Centrifuge Data Excluded) : (a) Combined Results; (b), (c) and (d) Individual Results for P = 100 kPa, P = 200 kPa and P = 300 kPa, respectively

The predicted and experimental filtrate fluxes are shown in Figures 3.26(a) to (d). As shown in Figure 3.26(a) there was a marginal increase in filtrate flux with filtration pressure. Except for a few experimental points for P = 100 kPa (see Figure 3.26(b)), all the experimental filtrate fluxes fell within the range of uncertainty for the model predictions, as shown in Figures 3.26(b) to (d). The uncertainty limits shown in Figures 3.26(b) to (d) were determined by using sets of equations (3.82) and (3.83) to describe the variation of permeability and porosity with solids compressive pressure in the planar model (see section 3.5.4.3).

As shown in Appendix D, for each filtration pressure the filtrate volumes for the experiments at shorter filtration times, were very close to those for the experiment with the longest filtration time. For this reason only the filtrate fluxes for the experiments with the longest total filtration time are given in Figures 3.26(a) to (d).

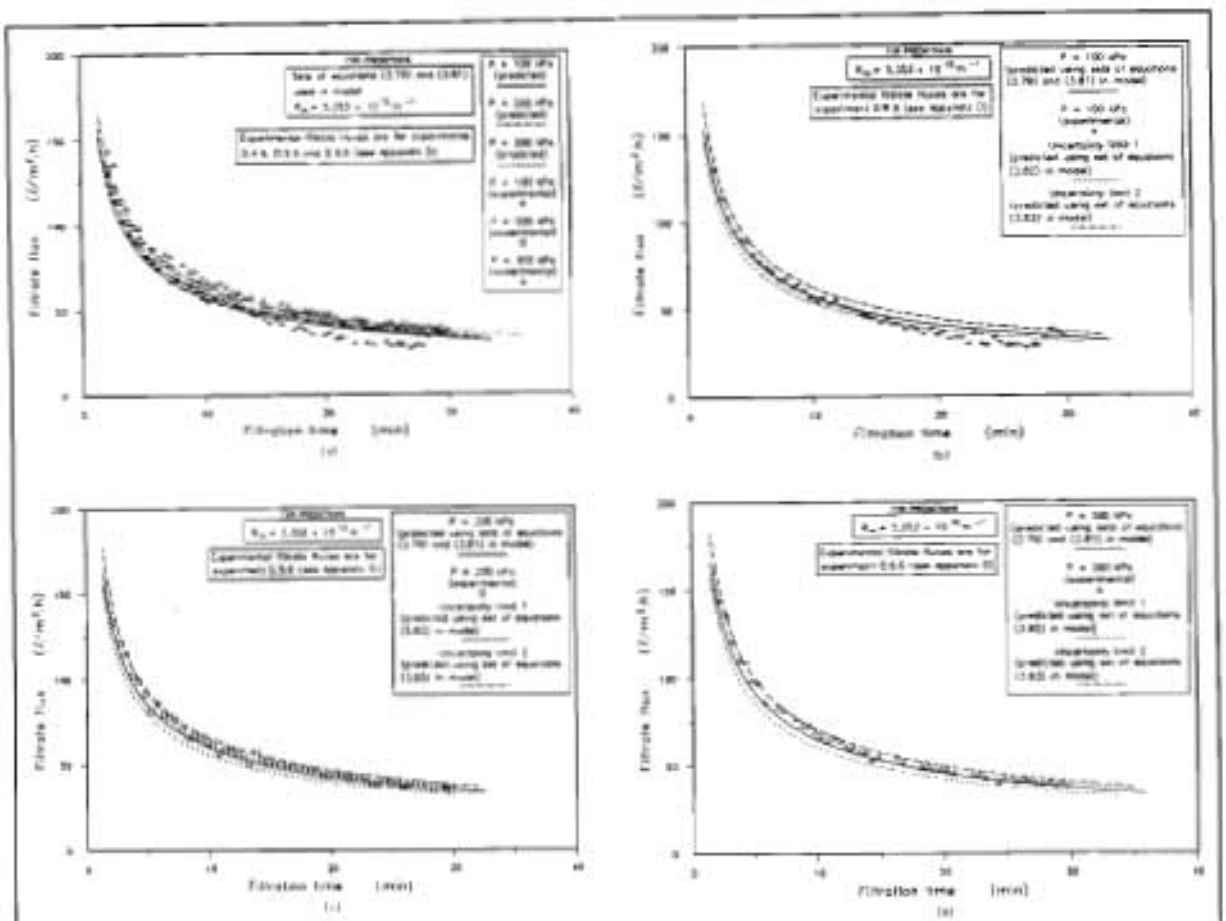

FIGURE 3.26 : Comparison Between Experimental and Predicted Filtrate Fluxes for Planar Filtration :
(a) Combined Results; (b), (c) and (d) Individual Results for P = 100 kPa, P = 200 kPa and P = 300 kPa, respectively

3.5.6 Results of Constant Pressure Internal Cylindrical Filtration Experiments

The results of the constant pressure internal cylindrical filtration experiments are tabulated in Appendix D. Three series of experiments were done at filtration pressures of 100 kPa, 200 kPa and 300 kPa. The filtration times were in increments of 5 minutes up to 30 minutes and the solids concentration of the feed sludge was approximately 49 g/ℓ. The results of the following variables versus filtration time are shown in Figures 3.27 to 3.30, respectively :

(i) total volume of permeate;
(ii) average cake dry solids concentration;
(iii) filtrate flux;
(iv) calculated and measured experimental internal cake diameters.

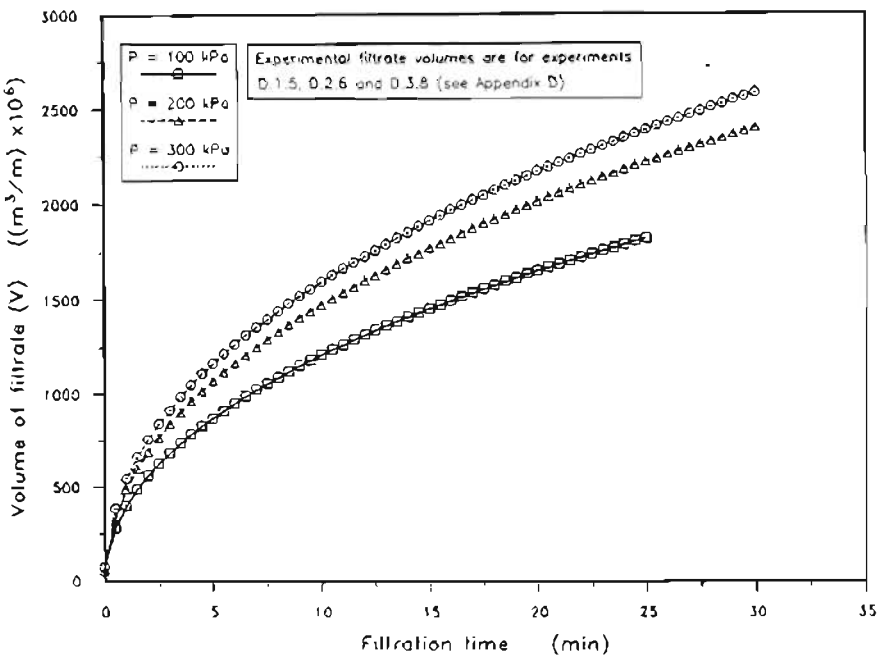

FIGURE 3.27 : Effect of Filtration Pressure on Volume of Filtrate for Internal Cylindrical Filtration (Experimental)

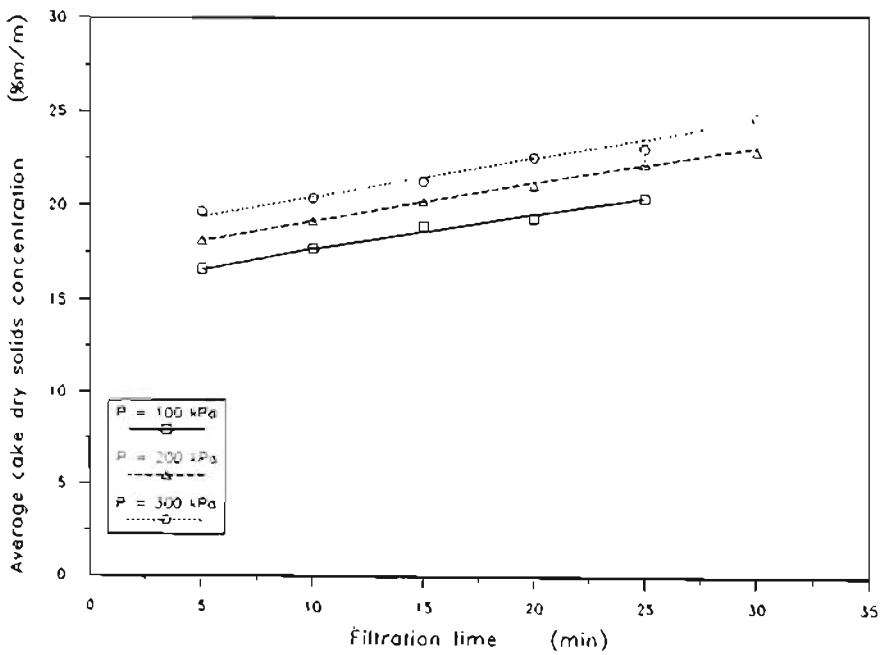

FIGURE 3.28 : Effect of Filtration Pressure on Average Cake Dry Solids Concentration for Internal Cylindrical Filtration (Experimental)

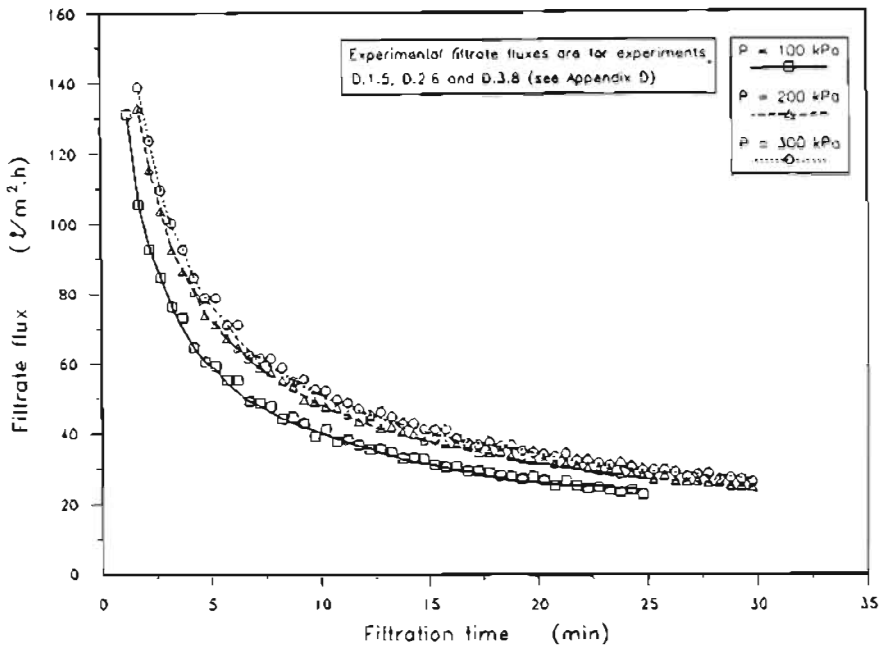

FIGURE 3.29 : Effect of Filtration Pressure on Filtrate Flux for Internal Cylindrical Filtration (Experimental)

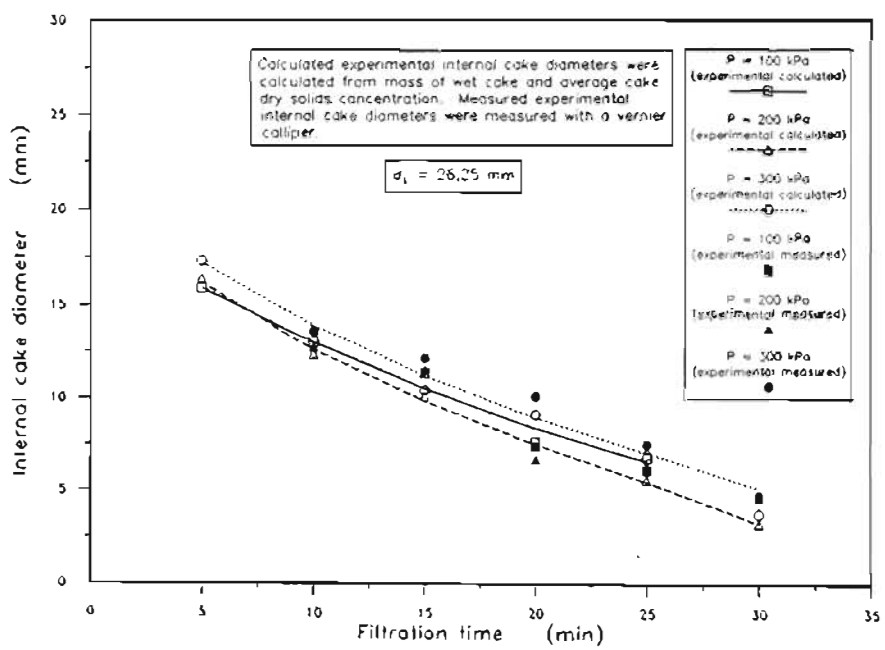

FIGURE 3.30 : Effect of Filtration Pressure on Measured and Calculated Experimental Internal Cake Diameters for Internal Cylindrical Filtration

The experimental internal diameters of the cake were both *calculated* (from mass of wet cake and average cake dry solids concentration, as shown in Appendix D) and *measured* using a vernier calliper (if the cake was not broken, see Appendix D).

The variation of filtrate volume with filtration time and pressure is shown in Figure 3.27. For each filtration pressure in Figure 3.27, the filtrate volumes are given for the experiment with the longest total filtration time. For each filtration pressure, the filtrate volumes for the experiments at shorter filtration times were very close to those for the experiment at the longest total filtration time, as shown in Appendix D. Filtrate volume increased with filtration pressure, as shown in Figure 3.27.

As shown in Figure 3.28, the average cake dry solids concentration increased with filtration time and with filtration pressure.

As would be expected for a very compressible cake, the effect of filtration pressure on filtrate flux was not very great, as shown in Figure 3.29. There was, however, a slight increase in filtrate flux as filtration pressure was increased.

In the same manner as for the filtrate volumes shown in Figure 3.27, the filtrate fluxes shown in Figure 3.29 are given for the experiment with the longest total filtration time, for each filtration pressure.

As shown in Appendix D, the *experimental* internal cake diameters were calculated (from mass of wet cake and average cake dry solids concentration) and also measured with a vernier calliper where possible. In general, there was good agreement between calculated (from mass of wet cake and average cake dry solids concentration) and measured experimental internal cake diameters, as shown in Figure 3.30. The decrease of the calculated and measured experimental internal cake diameters with filtration time is shown in Figure 3.30. The difference between the experimental internal cake diameters (calculated and measured) for the various filtration pressures was not very significant.

Three experiments were done at a filtration pressure of 300 kPa and for a filtration time of 20 minutes to determine the repeatability of the experiments. These experiments were experiments D.3.4, D.3.5 and D.3.6, as given in Appendix D. As discussed in section 3.6.2, the maximum deviation of average cake dry solids concentrations for these three experiments was 3,14 %, while for the *calculated* (from mass of wet cake and average cake dry solids concentration) experimental internal cake diameters the maximum deviation was 9,53 %. The maximum deviation of the filtrate volumes at the end of the experiments was 0,96 %.

A graph of inverse flow rate of filtrate (dt/dv) versus mass of cake dry solids deposited (w_c), for a filtration pressure of 300 kPa, is shown in Figure 3.31 for both internal cylindrical and planar filtration. Both curves are based on experimental values. For planar filtration the curve is a straight line as would be expected from equation (2.1) (see Appendix G) :

$$\frac{dt}{dv} = \frac{\mu_f \alpha_{av} w_c}{P} \qquad (2.1)$$

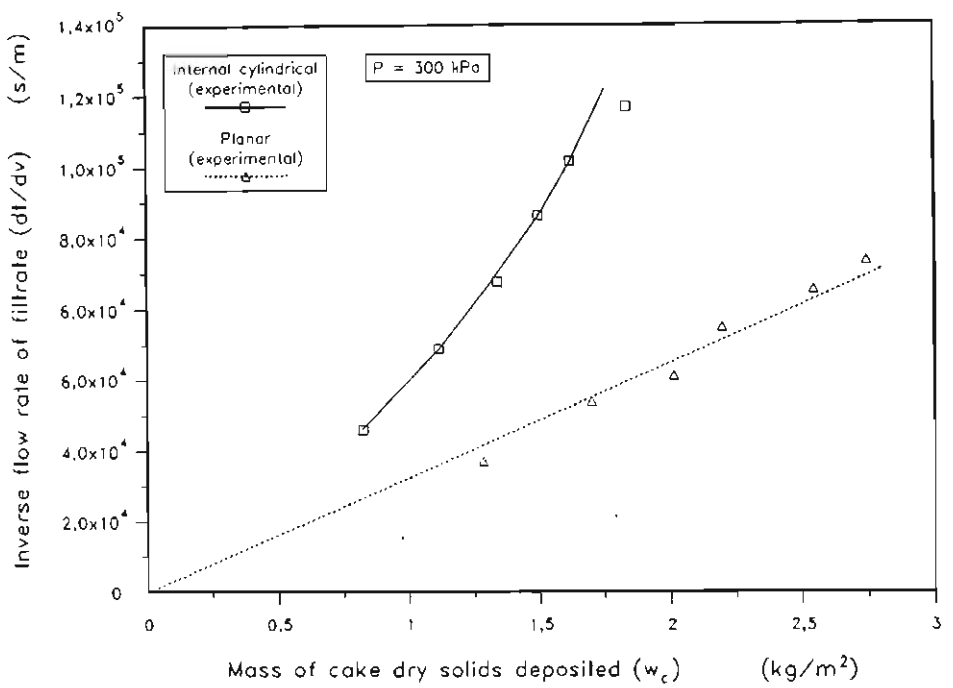

FIGURE 3.31 : Example of Graph of Inverse Flow Rate of Filtrate (dt/dv) versus Mass of Cake Dry Solids Deposited (w_c) for Internal Cylindrical and Planar Filtration (Experimental)

Unlike planar filtration, the curve for internal cylindrical filtration curves upwards as w_c increases. This is mainly due to the diminishing internal filtration area as the internal cake diameter decreases with increasing w_c.

3.5.7 Comparison Between Internal Cylindrical Filtration Model and Experimental Results

A FORTRAN computer program was written to numerically integrate equations (3.28) and (3.39) (see section 3.3.4), in order to obtain p_l and p_s profiles within the cake. Equations (3.28) and (3.39) were integrated by incorporating the permeability data from set of equations (3.79) and the porosity data from set of equations (3.80) or (3.81). The predictions by the internal cylindrical filtration model were then compared to the experimental results for internal cylindrical filtration. The flowsheet for the computer program is shown in Appendix E.

Unlike planar or external cylindrical filtration, it is possible for internal cylindrical filtration for p_s at the medium (and also in the cake layers in close proximity to the medium) to decrease as the internal diameter decreases (see section 3.5.8). As shown in the computer flowsheet in Appendix E, the Euler finite difference technique was used to numerically integrate the ordinary differential equations (3.28) and (3.39) in order to obtain the p_s and p_l profiles through the cake for various internal cake diameters. It was assumed that the cake is deposited in thin layers of equal thickness, Δr, as shown in Figure 3.32. For the numerical integration, the number of mesh points per layer of cake was kept constant. This meant that the radial distance between the various mesh points, h, was constant throughout each layer irrespective of the internal cake diameter.

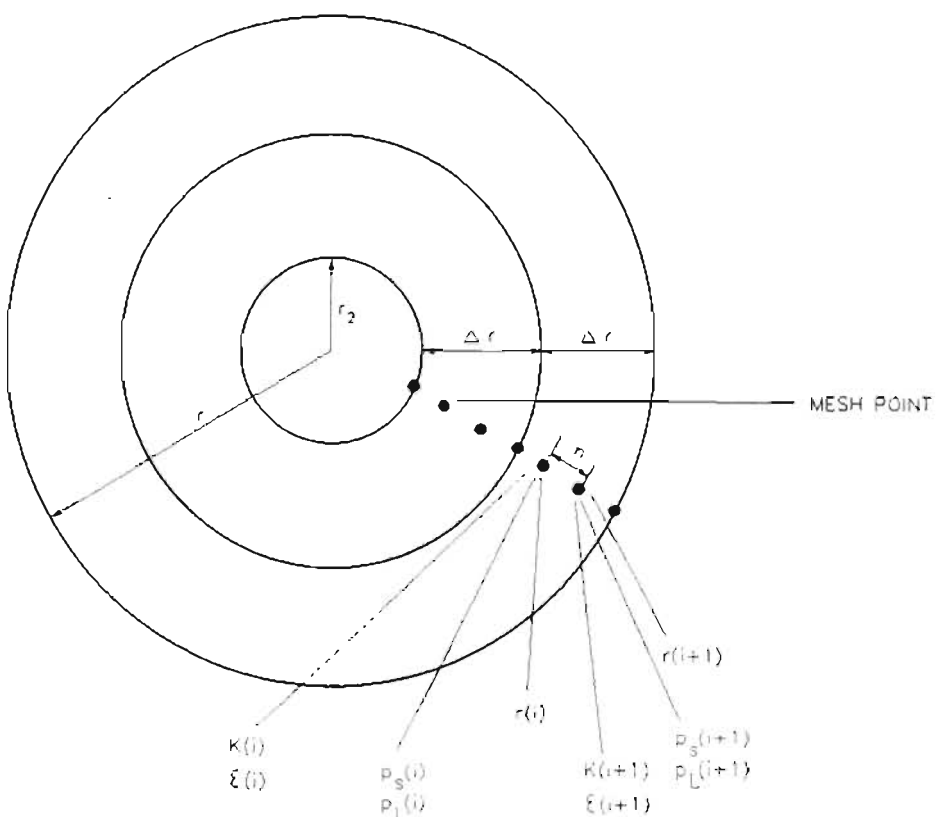

FIGURE 3.32 : Diagram to Illustrate Euler Finite Difference Numerical Integration Technique for the Internal Cylindrical Filtration Model

As mentioned earlier, for internal cylindrical filtration it is possible for p_s at the medium (and also in the cake layers in close proximity to the medium) to decrease as the internal cake diameter decreases (see Figure 3.40).

For the calculations in the program it was assumed that the permeability, K, and porosity, ϵ, at a certain point remain at those values which are determined by the *maximum* p_s experienced at that particular point. In other words, if the p_s reaches a maximum at a certain point and then declines as the internal cake diameter decreases, the permeability and porosity do not increase as p_s decreases. Since it proved very difficult to incorporate the above into the computer program for internal cylindrical filtration using more sophisticated techniques such as the Runge-Kutta finite difference numerical integration technique, the Euler finite difference technique was used. The Euler technique is generally less accurate than more sophisticated finite difference techniques such as the Runge-Kutta technique. In order to limit inaccuracy, the effect of step size, h, on model predictions was tested. The step size, h, was chosen to be very small (3,125 x 10^{-5} m) to limit inaccuracy.

Similar FORTRAN programs were written for planar and external cylindrical filtration (see section 3.5.5.1 and 3.5.11 respectively). As mentioned before, for external cylindrical filtration equation (3.39) still holds, while equation (3.27) must be used instead of equation (3.28) :

$$\frac{dp_l}{dr} = \frac{\mu_l Q}{2\pi r K} \qquad (3.27)$$

For planar and external cylindrical filtration, the ordinary differential equations were integrated using the Runge-Kutta finite difference technique. For planar and external cylindrical filtration, p_s at a point in the cake increases continuously throughout a filtration run. Therefore, the same complexity as for internal cylindrical filtration was not experienced.

The following were taken as variables to compare the predictions of the internal cylindrical filtration model with the experimental results :

(i) total volume of filtrate;
(ii) average cake dry solids concentration;
(iii) filtrate flux;
(iv) internal diameter of the cake.

The value of k_o was taken to be 0,34. As mentioned in section 3.2.2, this was the same value Tiller and Lu (1972) had measured for Solkafloc, which is also a very compressible material. However, as shown in section 3.5.8 the value of k_o has no great effect on the results generated by the internal cylindrical filtration model, except for small cake diameters or long filtration times. Tiller and Yeh (1985) found that for external cylindrical filtration the effect of k_o was also not very significant.

The experimental filtrate volumes, V, at various filtration times for filtration pressures of 100 kPa, 200 kPa and 300 kPa are shown in Figure 3.33(a), together with the predictions of the internal cylindrical filtration model.

As discussed in section 3.5.4.3, there was a significant "scatter" in the experimental results of the two C-P cell tests. The uncertainty limits for the C-P cell data shown in Figures 3.33(b) to (d), were determined by using sets of equations (3.82) and (3.83) to describe the variation of permeability and porosity with solids compressive pressure in the model. As shown in Figures 3.33(b) to (d) the experimental results fell within this uncertainty range.

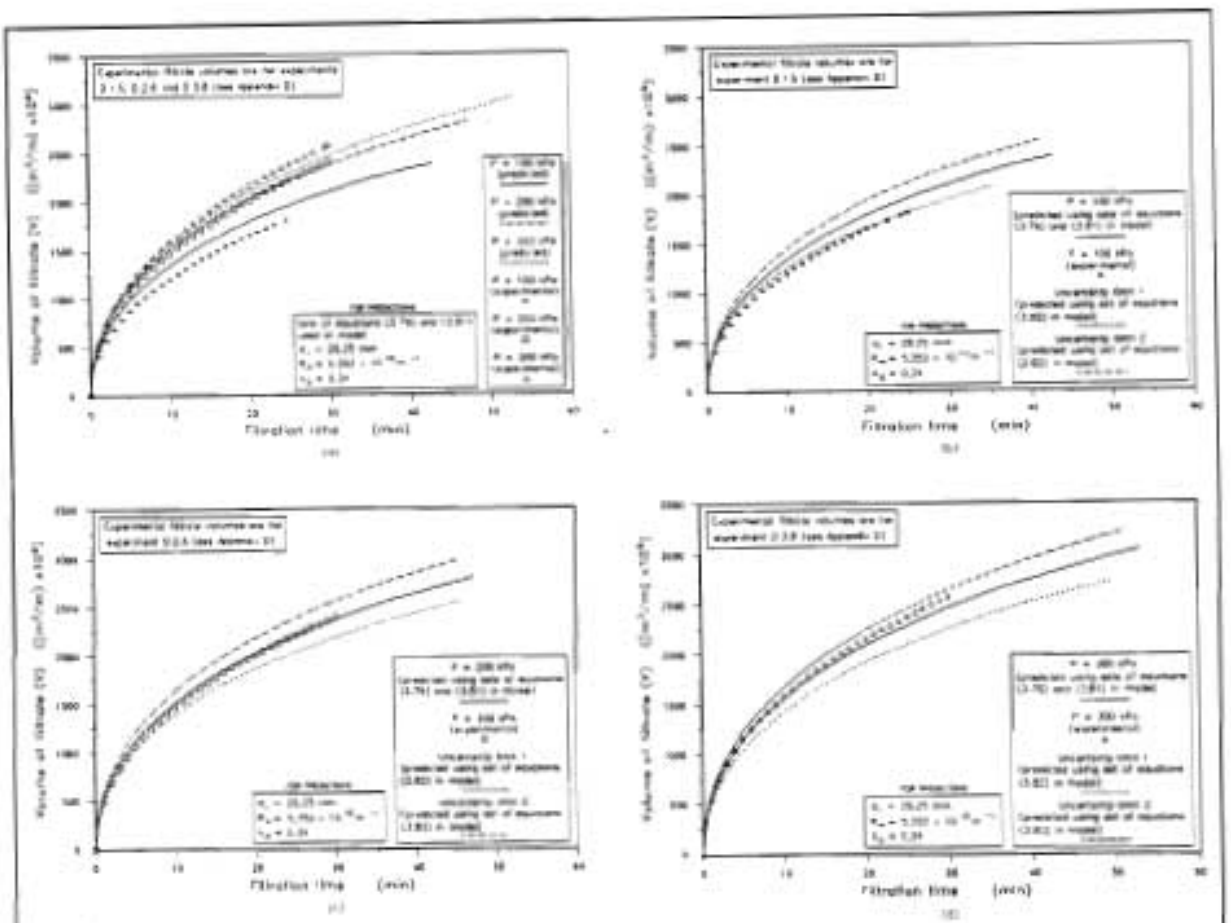

FIGURE 3.33 : Comparison Between Experimental and Predicted Filtrate Volumes for Internal Cylindrical Filtration :
(a) Combined Results; (b), (c) and (d) Individual Results for P = 100 kPa, P = 200 kPa and P = 300 kPa, respectively

The experimental average cake dry solids concentrations at various filtration times for filtration pressures of 100 kPa, 200 kPa and 300 kPa are shown in Figure 3.34(a), together with the predictions of the internal cylindrical filtration model. As discussed in sections 3.5.6 and 3.6.2, the results of three experiments to determine repeatability, showed that the maximum deviation of the average cake dry solids concentrations was 3,14 %. The degree of uncertainty in the experimental values is shown in

Figures 3.34(b), (c) and (d) by means of error bars for P = 100 kPa, 200 kPa and 300 kPa, respectively. Set of equations (3.80), which incorporates the porosity data of the centrifuge tests (as explained in section 3.5.4.2), was used to generate the curves in Figures 3.34(a) to (d). As shown in Figures 3.34(b), (c) and (d), the agreement between predicted and experimental average cake dry solids concentrations was not very good compared to that in Figures 3.35(b), (c) and (d).

When the porosity data of the centrifuge tests were ignored and set of equations (3.81) was used in the model, the agreement between predicted and experimental average cake dry solids concentrations was better. This is shown in Figures 3.35(a) to (d). For this reason the porosity data of the centrifuge tests were ignored in subsequent modelling.

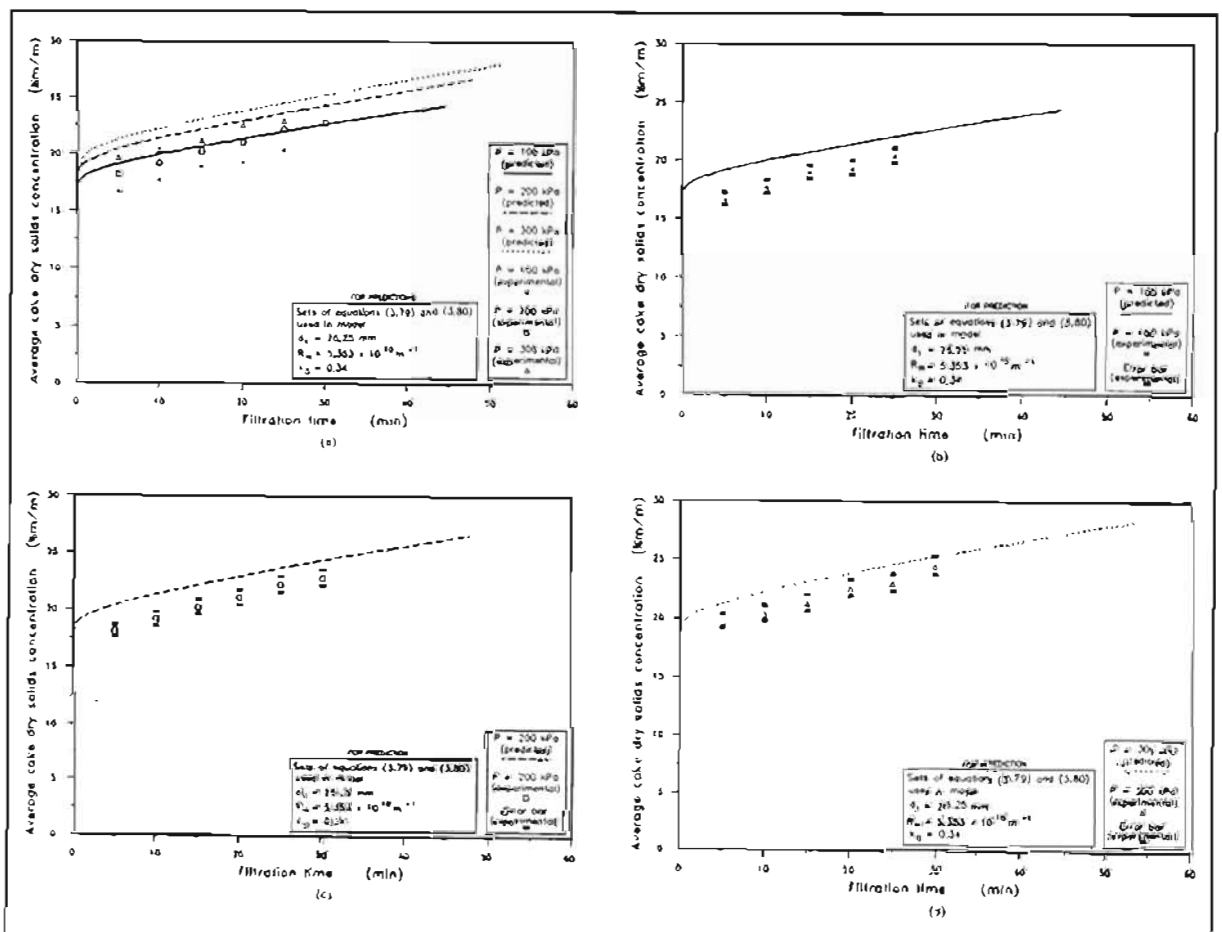

FIGURE 3.34 : Comparison Between Experimental and Predicted Average Cake Dry Solids Concentrations for Internal Cylindrical Filtration (Centrifuge Data Included) : (a) Combined Results; (b), (c) and (d) Individual Results for P = 100 kPa, P = 200 kPa and P = 300 kPa, respectively

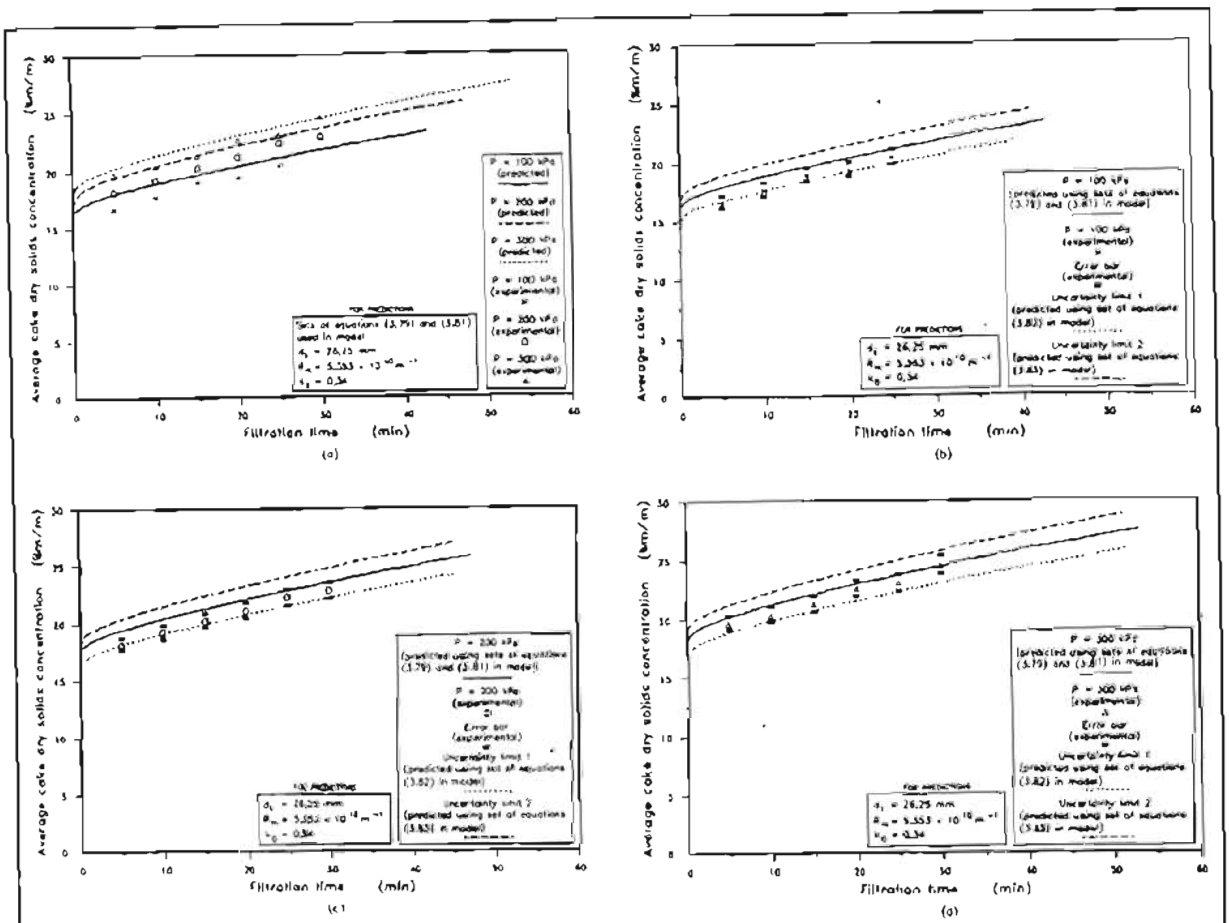

FIGURE 3.35 : Comparison Between Experimental and Predicted Average Cake Dry Solids Concentrations for Internal Cylindrical Filtration (Centrifuge Data Excluded) : (a) Combined Results; (b), (c) and (d) Individual Results for P = 100 kPa, P = 200 kPa and P = 300 kPa, respectively

As discussed in section 3.5.4.3, there was a significant "scatter" in the experimental results of the two C-P cell tests. The uncertainty limits for the C-P cell data shown in Figures 3.35(b) to (d), were determined by using sets of equations (3.82) and (3.83) to describe the variation of permeability and porosity with solids compressive pressure, in the model. As shown in Figures 3.35(b) to (d) the experimental results fell within this uncertainty range.

There was a good fit between the experimental values for filtration flux and those determined by the internal cylindrical filtration model, for all three pressures which were investigated. This is shown in Figures 3.36(a) to (d). As shown in Appendix D and discussed in sections 3.5.6 and 3.6.2, the results of three experiments to determine repeatability, showed that the maximum deviations of filtrate volume and filtrate flux were minimal. For this reason no error bars for experimental points have been

included in Figures 3.33 and 3.36. As shown in Figures 3.36(b) to (d), the experimental results fell within the uncertainty range for the C-P cell data, as determined by sets of equations (3.82) and (3.83).

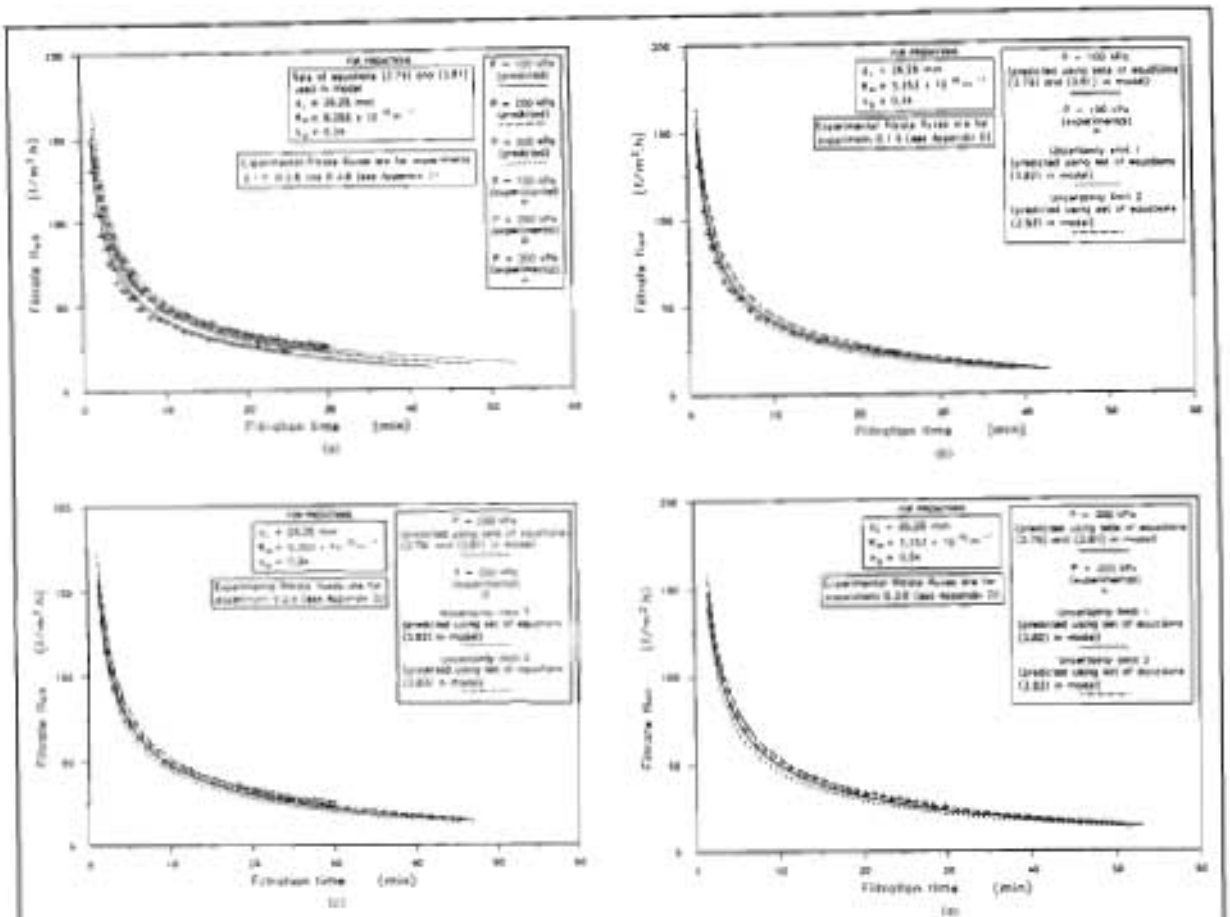

FIGURE 3.36 : Comparison Between Experimental and Predicted Filtrate Fluxes for Internal Cylindrical Filtration :
(a) Combined Results; (b), (c) and (d) Individual Results for P = 100 kPa, P = 200 kPa and P = 300 kPa, respectively

The variation of the experimental and predicted internal cake diameters with filtration time and filtration pressure is shown in Figure 3.37(a) for P = 100 kPa, 200 kPa and 300 kPa. Only the calculated (from mass of wet cake and average cake dry solids concentration, see Appendix D) experimental internal cake diameters are shown in Figure 3.37(a). The model predicts a marginal increase in internal cake diameter with an increase in pressure. As discussed in sections 3.5.6 and 3.6.2, the results of repeatability experiments showed that the maximum deviation of the average cake dry solids concentrations was 3,14 %, while the maximum deviation of mass of wet cake was 2,08 %. Since the average cake dry solids concentration and mass of wet

cake were used for determining the calculated experimental internal cake diameters (see Appendix D), the experimental variations in these two variables had a significant effect on the range of uncertainty for the calculated experimental internal cake diameters (especially for the smaller internal cake diameters). The degree of uncertainty in calculated experimental internal diameters is shown by means of error bars in Figures 3.37(b), (c) and (d) for P = 100 kPa, 200 kPa and 300 kPa, respectively. The measured experimental internal cake diameters are also shown in Figures 3.37(b), (c) and (d). For all three pressures the experimental results fell within the uncertainty range for the C-P cell data, as determined by sets of equations (3.82 and (3.83).

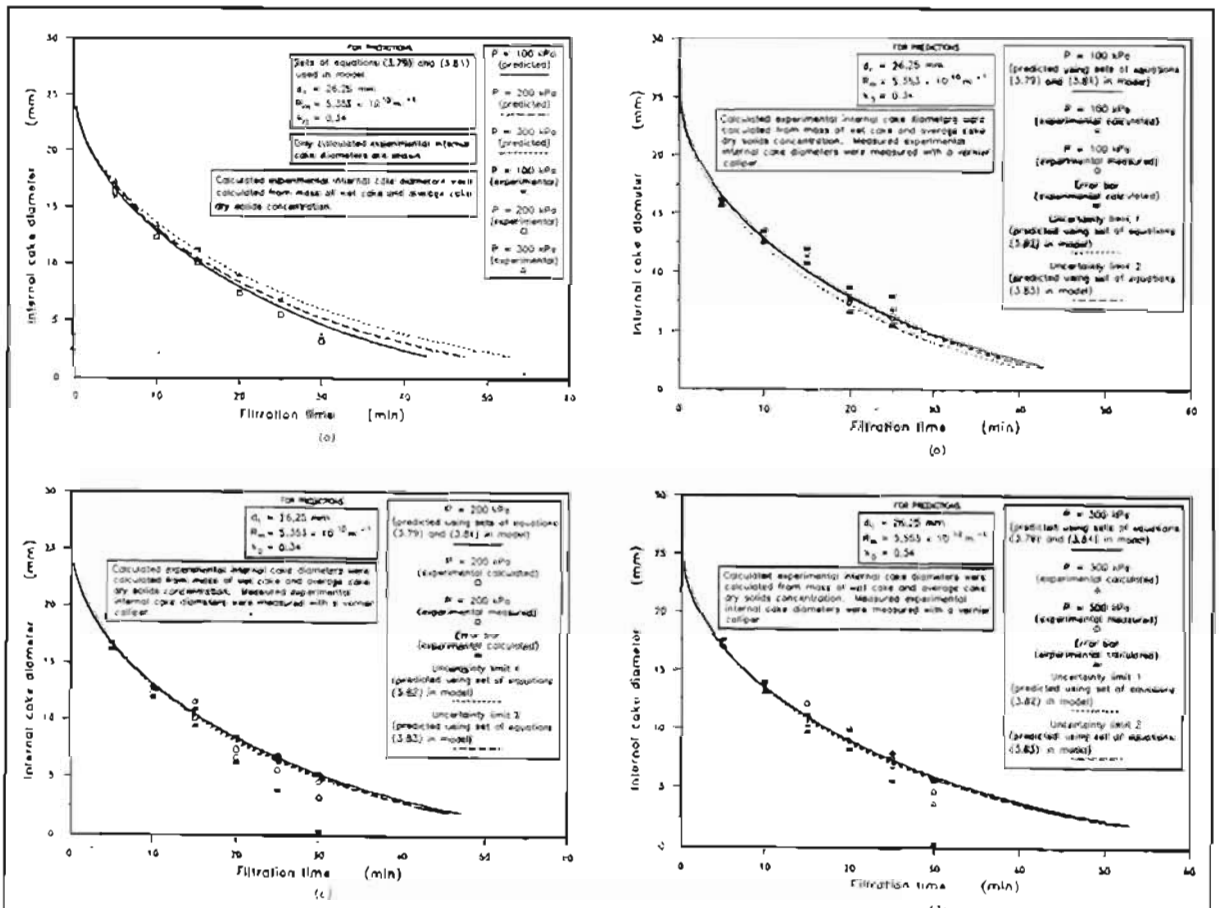

FIGURE 3.37 : Comparison Between Experimental (Measured and Calculated) and Predicted Internal Cake Diameters for Internal Cylindrical Filtration : (a) Combined Results; (b), (c) and (d) Individual Results for P = 100 kPa, P = 200 kPa and P = 300 kPa, respectively

3.5.8 The Effect of the Coefficient of Earth Pressure at Rest, k_o, for Internal Cylindrical Filtration

The effect of the coefficient of earth pressure at rest, k_o, was only found to be significant for long filtration times. This is shown in Figures 3.38 and 3.39 for predicted internal cake diameter and average cake dry solids concentration, respectively. The filtration time required to reach an internal cake diameter of 2 mm, for example, is significantly higher for $k_o = 1$ than for $k_o = 0$. However, over the practical range of internal cake diameters, as applicable to the tubular filter press, the coefficient of earth pressure at rest, k_o, was found to have no significant effect on the determinands of filtrate flux, average cake dry solids concentration and internal cake diameter.

The coefficient of earth pressure at rest, k_o, has a significant effect on the variation of solids compressive pressure at the filter medium, p_{sm}, with cake thickness, as shown in Figure 3.40. For thin cake layers p_{sm} increases sharply as the pressure drop across the cake, Δp_c, increases. For $k_o = 0$ and $k_o = 0,5$, p_{sm} reaches a maximum and as the cake thickness increases, p_{sm} decreases. This can be explained as follows. As the cake thickness increases, the filtration area decreases, which leads to a decrease in stress or force on the cake at the filter medium. The decrease in stress on the cake at the medium leads to a decrease in p_{sm}. The effect is more drastic for $k_o = 0$ than it is for $k_o = 0,5$. For $k_o = 1$ there is no maximum in the curve and p_{sm} increases continuously as the cake thickness increases, as is the case for conventional planar filtration. When $k_o = 1$, equation (3.7b) becomes :

$$\frac{dp_s}{dr} + \frac{dp_L}{dr} = 0 \qquad (3.86)$$

Equation (3.86) is identical to equation (3.10b), which is used for planar filtration.

The effect of a maximum in the p_s curve is limited to the cake layers in close proximity to the filter medium. The effect on the overall filtration performance was therefore found to be negligible.

As one moves away from the filter medium towards the centre of the filter tube, the maximum in the p_s versus cake thickness curve becomes less marked or vanishes completely, as shown in Figure 3.40 for the solids compressive pressure at an internal radius of r = 13 mm (r_1 = 13,125 mm) for k_o = 0; 0,5 and 1. The curve for $k_o = 0$ has a slight maximum while the curve for $k_o = 0,5$ shows no distinct maximum. The curve for $k_o = 1$ increases steadily. For further discussions see section 3.6.3.

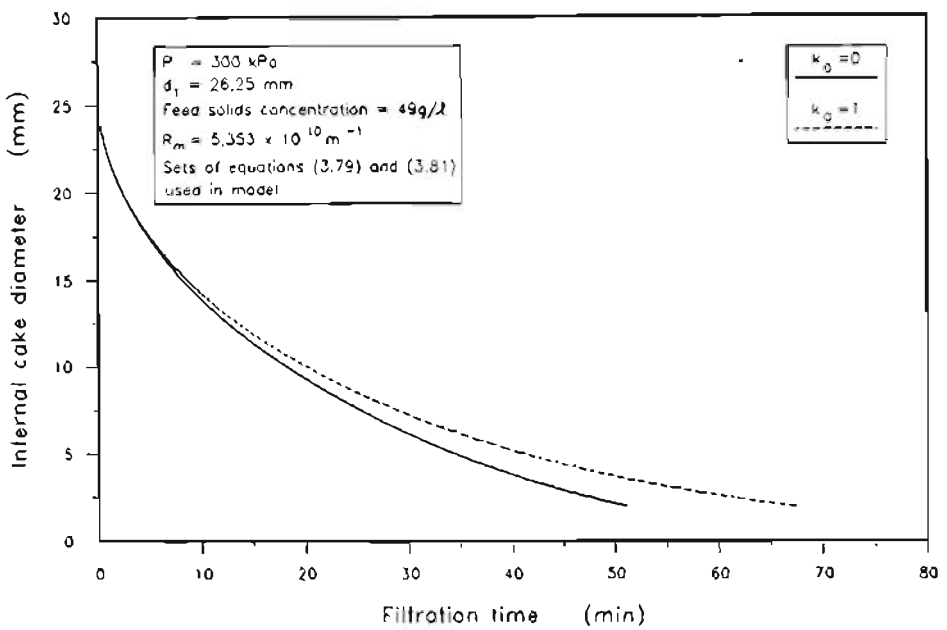

FIGURE 3.38 : Effect of the Coefficient of Earth Pressure at Rest (k_o) on the Predicted Internal Cake Diameter for Internal Cylindrical Filtration

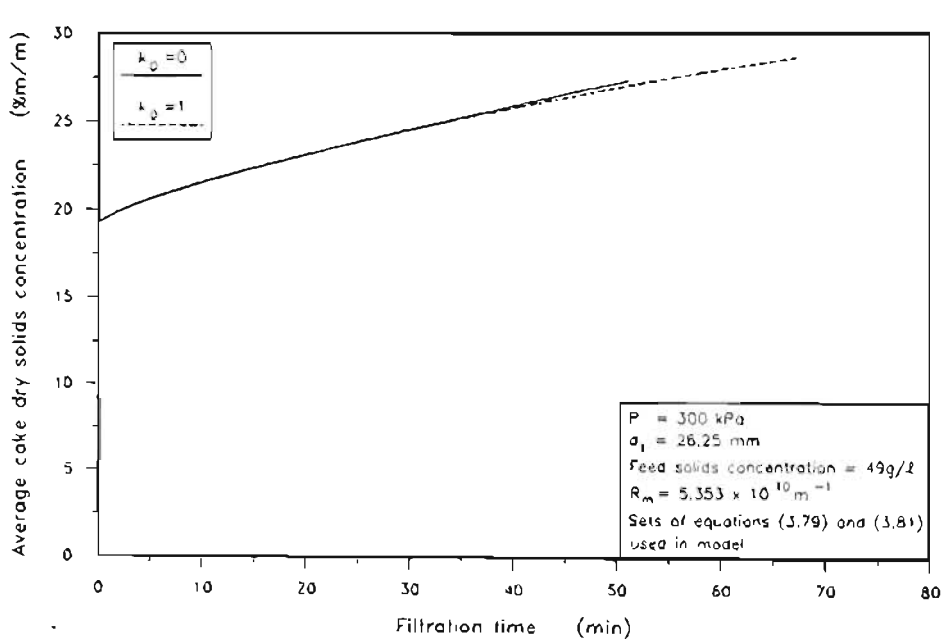

FIGURE 3.39 : Effect of the Coefficient of Earth Pressure at Rest (k_o) on the Predicted Average Cake Dry Solids Concentration for Internal Cylindrical Filtration

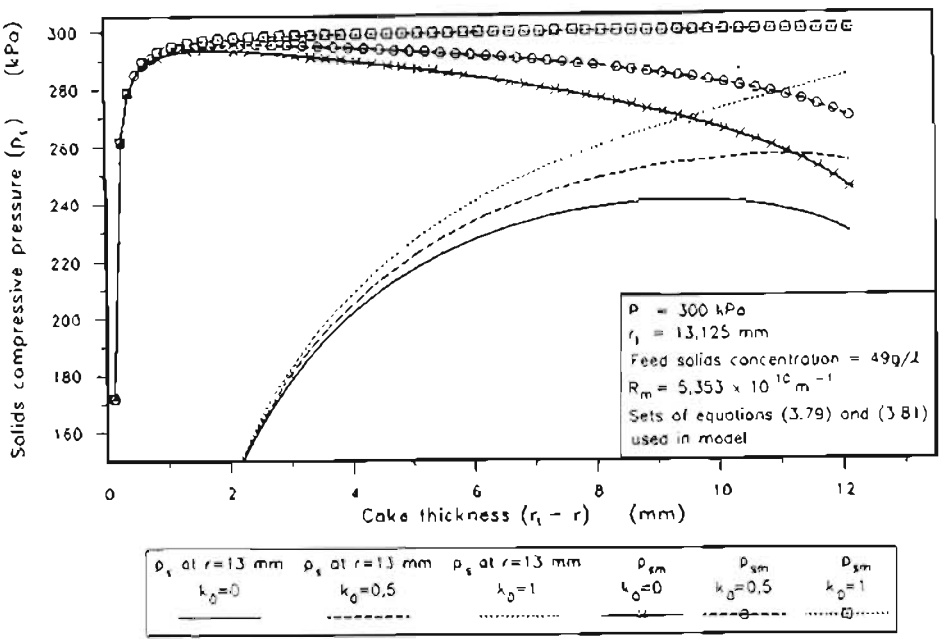

FIGURE 3.40 : The Predicted Variation of the Solids Compressive Pressure at the Medium (p_{sm}) and the Solids Compressive Pressure at the Internal Radius, r = 13 mm, with Cake Thickness for Different Values of k_o

3.5.9 The Variation of p_s and p_l with Radius for Internal Cylindrical Filtration

The predicted variation of p_s and p_l with radius for internal cake radii (r_2) of 1,125 mm; 5,625 mm and 10,125 mm is shown in Figure 3.41 for the waterworks clarifier sludge at a filtration pressure of 300 kPa. These values for r_2 correspond to cake thickness values of 12,0 mm; 7,5 mm and 3,0 mm, respectively.

The cake is very compressible. Following the p_l curve for r_2 = 1,125 mm, for example, it can be seen that the liquid pressure drops by approximately 50 % to 150 kPa in passing from r = 1.125 *mm* to r = 11,6 *mm*. Approximately 50 % of the total liquid pressure drop occurs in the last 1,5 mm, or 12,5 % of the total cake thickness. The p_s curves show similar trends. Thus a highly resistant layer or skin is formed near the filter medium. The bulk of the cake is not well compressed and offers comparatively little resistance to flow compared to the thin skin. The fractional liquid pressure drop across the cake was defined as :

$$\Delta p_f = \frac{P - p_l(r)}{\Delta p_c} \qquad (3.87)$$

where Δp_f = fractional liquid pressure drop across the cake as defined by equation (3.87), (-)

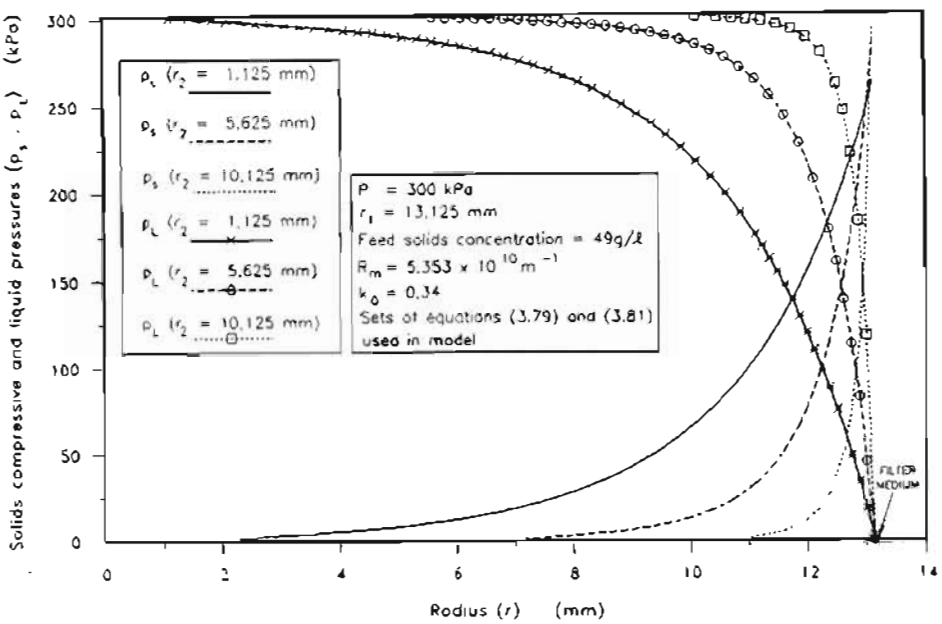

FIGURE 3.41 : The Predicted Variation of Solids Compressive Pressure (p_s) and Liquid Pressure (p_L) with Radius for Various Internal Cake Radii (r_2)

The variation of predicted fractional pressure drop with radius is shown in Figure 3.42 for the same values of r_2 as in Figure 3.41. The inordinately high resistance of the thin skin is clearly evident from Figure 3.42.

The variation of predicted cake dry solids concentration with radius is shown in Figure 3.43 for an internal cake radius of 5,625 mm. As shown in Figure 3.43, the bulk of the cake consists of "mushy" or "sloppy" cake layers, while near the filter medium the cake solids concentration increases significantly.

3.5.10 Comparison of the p_s and p_L Profiles for Internal Cylindrical and Planar Filtration

For conventional planar constant pressure filtration, p_s, p_L and ϵ are unique functions of the fractional distance through the cake, if the pressure drop across the cake, Δp_c, is constant.

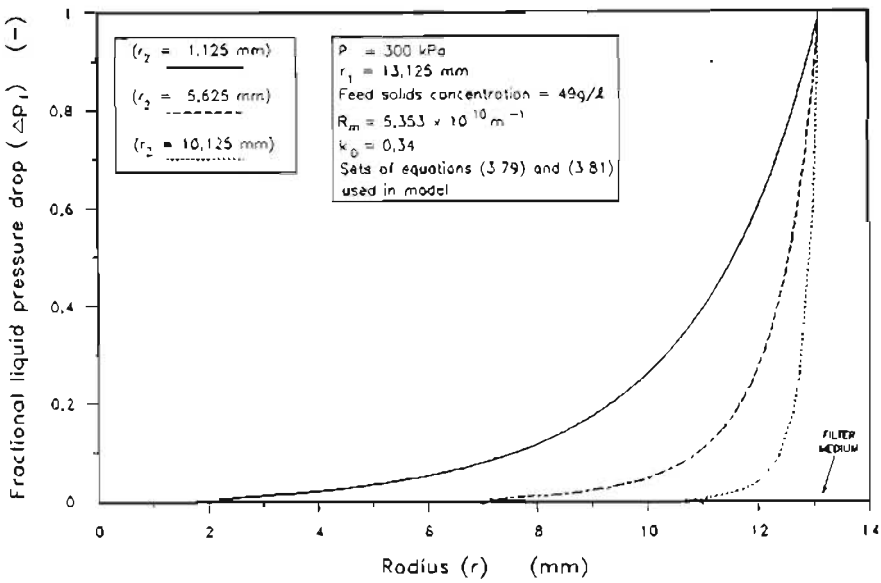

FIGURE 3.42 : The Predicted Variation of Fractional Liquid Pressure Drop (Δp_f) With Radius for Various Internal Cake Radii (r_2)

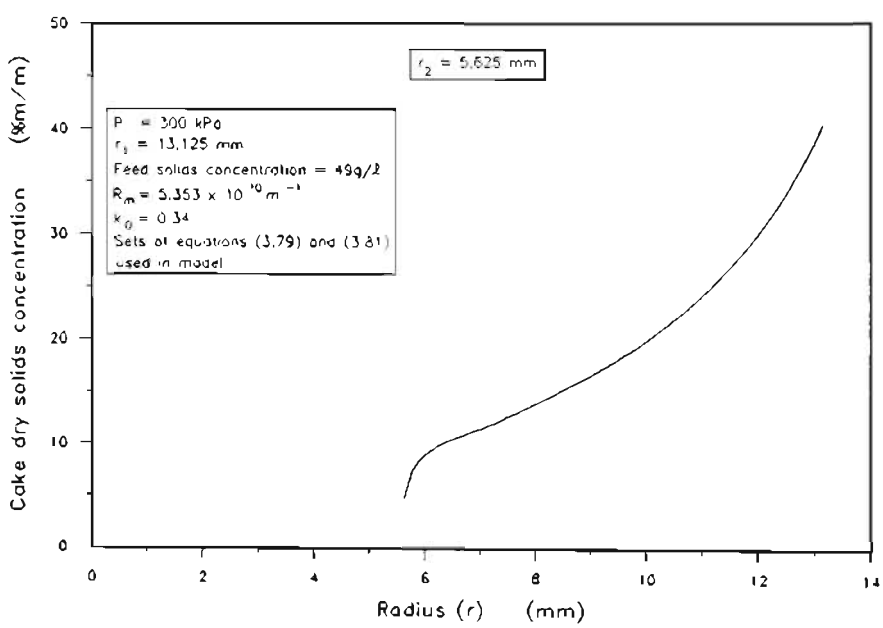

FIGURE 3.43 : The Predicted Variation of Cake Dry Solids Concentration With Radius for Internal Cylindrical Filtration

As explained in section 3.5.5.1, a computer program was written to simulate the planar filtration of the waterworks clarifier sludge. As shown in Figure 3.44, the computer program predicted that for planar filtration, p_s and p_l are unique functions of the fractional distance through the cake, (x/L). The curves were in fact plotted for cake thickness values of 3,0 mm; 7,5 mm and 12,0 mm. The p_s and p_l curves for the three cake thicknesses are in fact superimposed so that only one curve for p_s and one for p_l is visible.

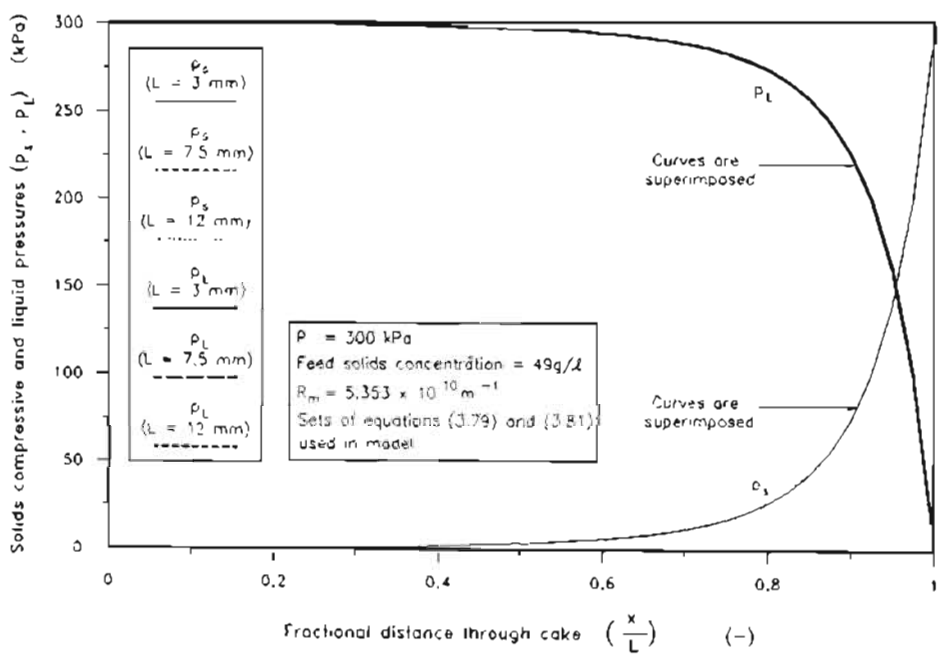

FIGURE 3.44 : The Predicted Variation of Solids Compressive Pressure (p_s) and Liquid Pressure (p_l) with Fractional Distance Through Cake, $\left(\frac{x}{L}\right)$, for Planar Filtration (The Curves for the Three Cake Thicknesses are Superimposed)

The same is not true for internal cylindrical filtration. The variation of p_l and p_s, with the fractional distance through the cake, $(r - r_2)/(r_1 - r_2)$, is shown in Figures 3.45 and 3.46, respectively, for the same three values of cake thickness as shown in Figure 3.44. As shown in Figure 3.45, for the same fractional distance through the cake, the liquid pressure decreases as the cake thickness increases (and the internal cake radius decreases). This may be explained as follows. As the internal cake radius decreases, the ratio of the liquid pressure drop across the inner cake layers (small r) to the liquid pressure drop across the outer cake layers (large r) will increase. This is evident from equation (3.28).

$$\frac{dp_l}{dr} = -\frac{\mu_l Q}{2\pi r K} \qquad (3.28)$$

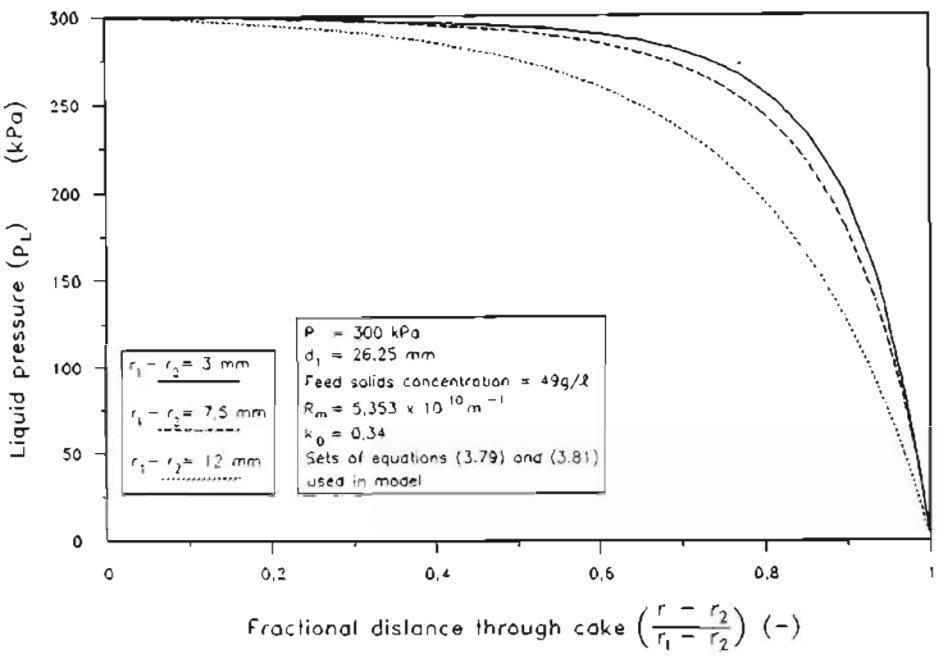

FIGURE 3.45 : The Predicted Variation of Liquid Pressure (p_L) with Fractional Distance Through Cake, $(r - r_2)/(r_1 - r_2)$, for Internal Cylindrical Filtration

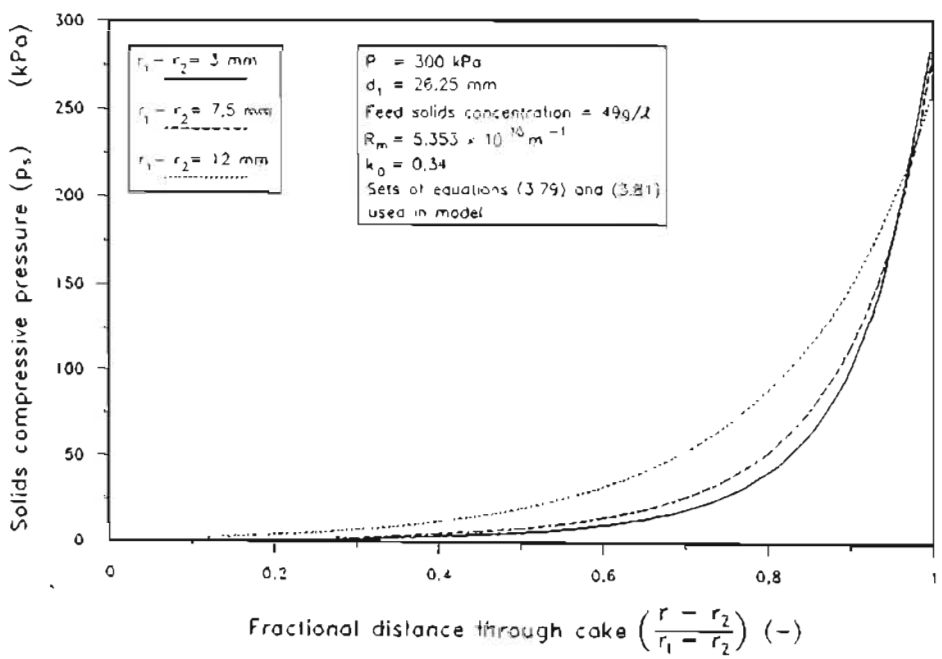

FIGURE 3.46 : The Predicted Variation of Solids Compressive Pressure (p_s) with Fractional Distance Through Cake, $(r - r_2)/(r_1 - r_2)$, for Internal Cylindrical Filtration

The relative increase in p_L across the inner cake layers as the internal cake radius decreases, leads to a concomitant increase in p_s across these layers (see equation (3.7b)). This explains the increase in p_s as the cake thickness increases, as shown in Figure 3.46.

3.5.11 Comparison Between External Cylindrical, Internal Cylindrical and Planar Filtration

As explained in section 3.5.7, a computer program was written to simulate external cylindrical filtration on a tube.

A comparison between the average cake dry solids concentrations for external cylindrical, internal cylindrical and planar filtration of the waterworks sludge, is shown in Figure 3.47. For internal cylindrical filtration and planar filtration the *experimental* and *predicted* values are shown, while for external cylindrical filtration the values were only *predicted*.

The cake thickness for external cylindrical filtration was defined as, $r_4 - r_3$, while that for internal cylindrical filtration was defined as, $r_1 - r_2$. For external cylindrical filtration, r_3 is the external radius of the filter medium.

As shown in Figure 3.47, for very small cake thicknesses, the average cake dry solids concentration is approximately the same for all three filtration configurations. As the cake thickness increases, the average cake dry solids concentration for internal cylindrical filtration increases, that for planar filtration remains essentially constant, while for external cylindrical filtration the average cake dry solids concentration decreases.

These trends may be explained as follows. As was shown in section 3.5.9, a well consolidated cake skin with a high resistance forms near the filter medium. The bulk of the cake, however, consists of "sloppy" cake which is not well consolidated or compressed. For external cylindrical filtration the outer diameter increases (cake thickness increases) as the filtration progresses. As the external diameter increases, the mass of the "sloppy" outer cake layers as a fraction of the total cake mass increases, while the mass fraction of the relatively well consolidated inner cake layers decreases. Thus the *average* cake dry solids concentration decreases as the cake thickness increases. For internal cylindrical filtration the converse is true. The mass fraction of the "sloppy" inner cake layers decreases as the internal cake diameter decreases and the cake thickness increases. The increase in p_s throughout the bulk of the cake, as the internal cake diameter decreases (as shown in Figure 3.46), further contributes to an increase in average cake dry solids concentration for small internal cake diameters. This is probably the cause of the slight upwards turn in the internal cylindrical filtration curve in Figure 3.47, for large cake thicknesses (small internal cake diameters).

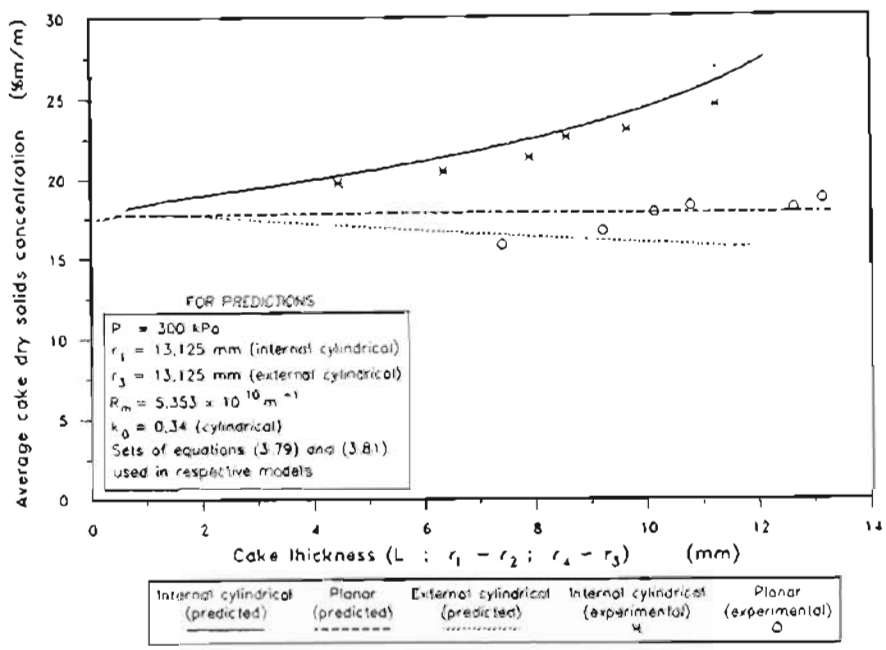

FIGURE 3.47 : The Variation of Average Cake Dry Solids Concentration with Cake Thickness for External Cylindrical, Internal Cylindrical and Planar Filtration

For planar filtration, the mass of the "sloppy" cake layers as a fraction of the total mass of cake, remains essentially constant, irrespective of cake thickness. Therefore the average cake dry solids concentration remains essentially constant.

The variation of cake thickness with filtration time for the waterworks clarifier sludge is shown in Figure 3.48 for all three filtration configurations. For internal cylindrical and planar filtration the *experimental* and *predicted* values are shown, while for external cylindrical filtration the values were *predicted*. For small cake thicknesses, there is no significant difference between the three configurations. For greater cake thicknesses, the filtration time for internal cylindrical filtration is higher than that for external cylindrical and planar filtration. This is due to the significant reduction in filtration area, for large cake thicknesses, during internal filtration.

The variation of dry solids production rate with cake thickness for the waterworks clarifier sludge is shown in Figure 3.49, for the three filtration configurations. For internal cylindrical and planar filtration the *experimental* and *predicted* dry solids production rates are shown, while for external cylindrical filtration the dry solids production rates were *predicted*. The dry solids production rate in Figure 3.49 was defined as :

$$\text{Dry solids production rate } (kg/m^2.h) = \frac{\text{Mass of dry solids in cake for certain cake thickness}}{(\text{Area of filter medium} \times \text{Filtration time})} \qquad (3.88)$$

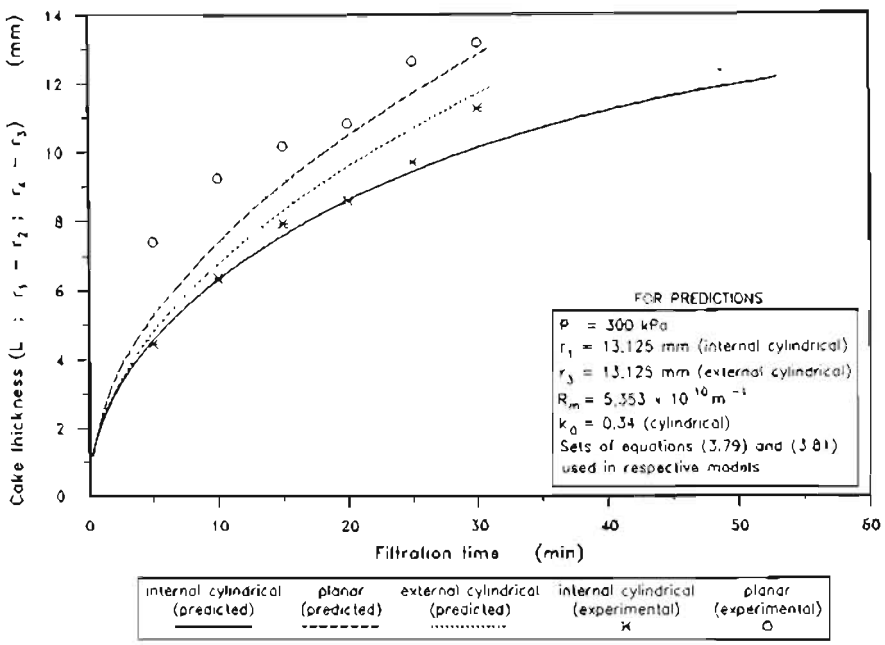

FIGURE 3.48 : Graph of Cake Thickness versus Filtration Time for External Cylindrical, Internal Cylindrical and Planar Filtration

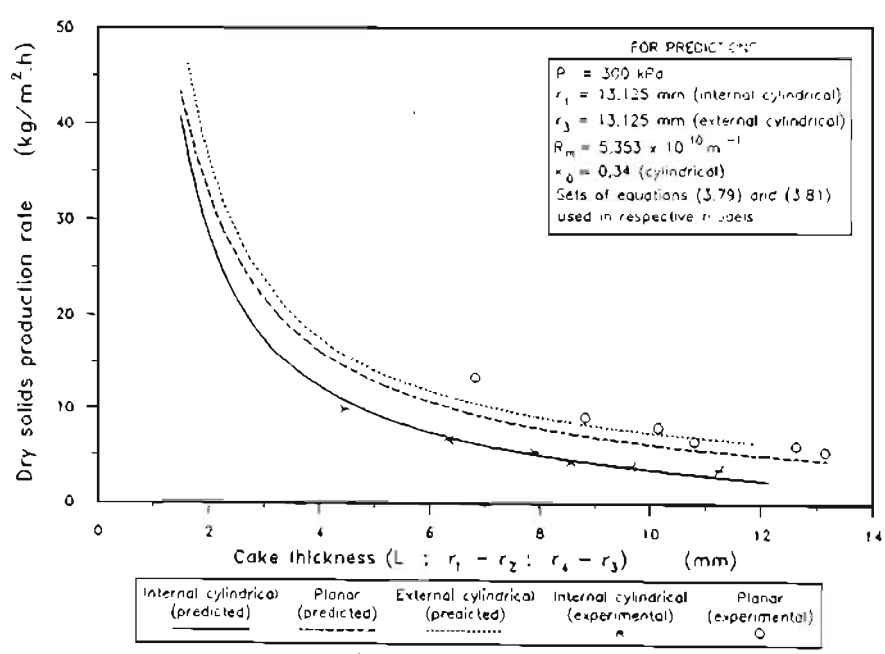

FIGURE 3.49 : Graph of Dry Solids Production Rate versus Cake Thickness for External Cylindrical, Internal Cylindrical and Planar Filtration

This definition of dry solids production rate is based on filtration time only and ignores time for cake removal which would be required in practice. Any cake losses due to cake removal (see Chapter 4) are also ignored.

The dry solids production rate for external cylindrical filtration is slightly higher than that for planar filtration. This is due to the increase in external filter area as cake thickness increases.

The dry solids production rate for internal cylindrical filtration is close to that for planar filtration, for small cake thicknesses. For greater cake thicknesses the dry solids production rate for internal cylindrical filtration is significantly lower than that for planar filtration. This is due to the decrease in internal filtration area as cake thickness increases.

3.5.12 The Effect of Internal Tube Diameter on Internal Cylindrical Filtration

The effect of internal tube diameter on predicted average cake dry solids concentration for internal cylindrical filtration is shown in Figure 3.50, for the waterworks clarifier sludge. Internal tube diameters of 25 mm; 50 mm; 75 mm and 100 mm are shown in Figure 3.50. The predicted average cake dry solids concentration for planar filtration is also shown.

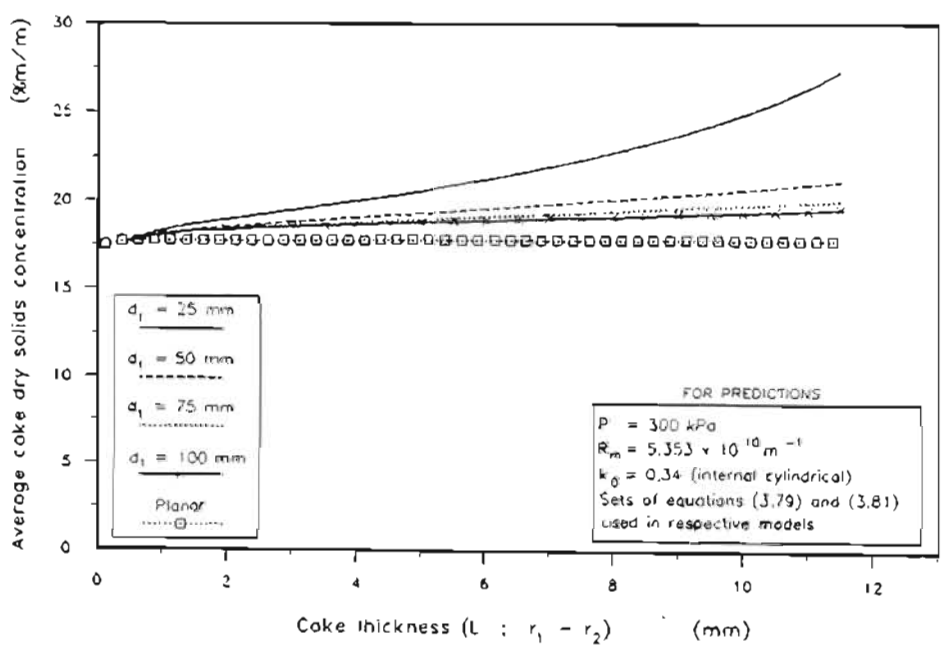

FIGURE 3.50 : Effect of Internal Tube Diameter on Predicted Average Cake Dry Solids Concentration for Internal Cylindrical Filtration

For a given cake thickness the average cake dry solids concentration decreases, as the internal tube diameter increases, for internal cylindrical filtration. As the internal tube diameter increases, the average cake dry solids concentration tends towards that for planar filtration.

The explanation for the trends shown in Figure 3.50 is similar to the one in section 3.5.11. For a given cake thickness the ratio of the internal cake diameter to the internal tube diameter (d_2/d_1), increases as the internal tube diameter increases. As the ratio (d_2/d_1) increases the mass fraction of the "sloppy" inner cake layers, which are not well compressed, increases. This leads to a decrease in the *average* cake dry solids concentration, as observed in Figure 3.50.

3.6 DISCUSSION OF RESULTS

3.6.1 Comparison Between Experimental Results and Planar and Internal Cylindrical Filtration Models

3.6.1.1 Planar filtration

There was good agreement between the experimental filtrate fluxes and those predicted by the planar filtration model, as shown in Figure 3.26.

For average cake dry solids concentration, the agreement between the model and experimental results was significantly better when the centrifuge data were ignored (see Figures 3.24 and 3.25). As shown in Figures 3.25(b) to (d), the experimental average cake dry solids concentrations were within the uncertainty range for the C-P cell data, as determined by sets of equations (3.82) and (3.83). However, although the planar filtration model predicted that the average cake dry solids concentration remains constant with filtration time, the experimental results indicated a slight increase in average cake dry solids concentration with filtration time.

For the very compressible cake obtained from the filtration of the clarifier sludge it was inevitable that some "sloppy" cake layers were lost when the remaining feed sludge was pumped and drained from the filter after an experiment. This had an effect on the accuracy of the results for average cake dry solids concentration.

3.6.1.2 Internal cylindrical filtration

As shown in Figures 3.34 to 3.37, the agreement between the internal cylindrical filtration model and the experimental results was good.

As was true for planar filtration, the fit between the internal cylindrical model and the experimental average cake dry solids concentrations was significantly better when the centrifuge data were ignored (see Figures 3.34 and 3.35). As shown in Figure 3.22(b) the centrifuge method gave lower values of porosity than the settling and C-P cell methods. The reason for this could not be established. The centrifuge tests were repeated several times, and the trend was found to be consistent. The centrifuge method is a relatively new method and it may be that it has limitations

which have not yet been determined. Some of the assumptions in the theory (see section 3.3.7.4) may not be valid. It was decided that for the purpose of this study, the centrifuge method did not warrant further investigation, since the settling and C-P cell data gave acceptable correlations between both the internal cylindrical and planar models and the respective experimental results.

3.6.2 Determination of Internal Cake Diameter and Repeatability of Experiments for Internal Cylindrical Filtration

For the very compressible cake obtained from the filtration of the clarifier sludge it was inevitable that some "sloppy" cake layers were lost when the feed sludge was drained from the tube after an experiment. This affected the accuracy of the measurement or calculation (from mass of wet cake and average cake dry solids concentration) of the internal cake diameter and the average cake dry solids concentration.

During this study great care was taken in draining the feed sludge from the tube after an experiment. The feed sludge was drained very slowly in order to minimize cake losses. Some cake losses also occurred when the cake was removed from the filter medium after an experiment. Mass balance calculations between the dry solids deposited during a filtration experiment and those recovered in the cake after an experiment indicated that the dry solids losses were of the order of 0,5 to 1,5 %.

The experimental internal cake diameters as shown in Figures 3.30 and 3.37, were both measured (with a vernier calliper) and calculated (from mass of wet cake and average cake dry solids concentration) as shown in Appendix D. As discussed in section 3.4.3.2, the average internal diameter of the medium, d_i, was measured to be 26,25 mm. This value was used to determine the calculated experimental internal cake diameters. Although great care was taken to bolt the cloth into the same position for each experiment, slight shifts in the cloth did occur between experiments and these must have resulted in variations in d_i. Although these variations in d_i introduced slight errors in the calculation of the internal cake diameters, they were ignored for the calculation of the error bars shown in Figures 3.37(b), (c) and (d). In order to overcome this problem, attempts were made to measure the external diameter of the cake (and therefore, d_i) with a vernier calliper for each experiment. However, the cake was soft and sometimes broke so that an accurate determination of d_i was impossible. If the cake was not broken, the internal cake diameter was measured with a vernier calliper. Although accurate measurements proved very difficult, because of the sloppy nature of the cake, this procedure served the purpose of "verifying" the calculated internal cake diameters.

The repeatability of the experiments was fair. For the three identical experiments D.3.4, D.3.5 and D.3.6, the average cake dry solids concentrations varied between 21,94 % and 22,63 %, (maximum deviation of 3,14 %), while the total mass of wet cake varied between 238,85 g and 243,93 g (maximum deviation of 2,08 %). The average cake dry solids concentration and the total mass of wet cake were used for

the calculation of the internal cake diameter (see Appendix D). The experimental variations in these two determinands had a significant effect on the range of uncertainty for the calculated internal cake diameters (especially for small internal cake diameters) (see Figures 3.37(b), (c) and (d)). The filtrate volumes at the end of the experiment varied between 900,8 mℓ and 909,4 mℓ (maximum deviation of 0,96 %).

For dead-end filtration inside a tube there is an axial velocity gradient of the feed sludge along the tube. At the outlet end of the tube the axial velocity of the feed sludge is zero while at the entrance of the tube, the axial velocity is at a maximum. If the difference in axial velocity between the entrance and the end of the tube is significant, it could result in a cake thickness gradient along the tube. Since the tube used during this study was short, it was assumed that these effects were negligible. This was also confirmed by measurements of the cake thickness along the tube using a vernier calliper.

3.6.3 The Effect of the Coefficient of Earth Pressure at Rest, k_o, for Internal Cylindrical Filtration

As already discussed in section 3.5.8, k_o only has a significant effect at relatively long filtration times when the internal cake radius is small (cake thickness is large) ($r_2 < 2.5$ mm for the results in section 3.5.8). Such small internal cake radii would not be practical for the tubular filter press, since the probability of tube blockages would be great. For this reason it was decided that any tests to determine the value of k_o for the clarifier sludge were not warranted. The value of k_o was taken to be 0,34, which was the value Tiller and Lu (1972) had found for Solkafloc, which is also a very compressible material.

As shown in Figure 3.40, k_o has a significant effect on the solids compressive pressure at the medium, p_{sm}. For $k_o = 0$ and $k_o = 0.5$, p_{sm} decreased significantly as the cake thickness increased. As discussed in section 3.5.7, for the computer program for internal cylindrical filtration, it was assumed that the permeability and porosity at a certain point in the cake remain at those values which are determined by the maximum p_s experienced at that particular point. However, the significance of this was found to be negligible. There was almost no difference in the results when the permeability and porosity at a particular point in the cake were allowed to increase as p_s decreased, which is obviously unrealistic. The reason for this is that p_s was only found to decrease at the medium and in the cake layers very close to the medium. Throughout the bulk of the cake, p_s was found to increase consistently as the internal cake diameter decreased (cake thickness increased).

3.6.4 Permeability and Porosity Data

3.6.4.1 Permeability data

There was a significant variation in the permeability data for the two C-P cell tests as discussed in section 3.5.4.3.

For the settling test, permeability data were only obtained for very low values of p_s ($0.0065\,Pa \leq p_s \leq 22.63\,Pa$), while the p_s range for the C-P cell tests was ($10\,kPa \leq p_s \leq 400\,kPa$). As discussed in section 3.5.4.1, the point of intersection between the regression line of the *combined* C-P cell permeability data for tests A.1 and A.2 and that of the settling data occurred at a p_s of 3781,7 Pa.

For the computer model the permeability data for the settling tests was assumed to be valid for $p_s \leq 3781.7\,Pa$. The cake permeability for the low p_s region was therefore extrapolated far out of the experimental p_s range.

Attempts were made to increase the experimental p_s range by doing settling tests for sludges with solids concentrations greater than 90,8 g/ℓ, which corresponded to $p_s = 22.55\,Pa$ (see Appendix B). However, the solids hardly settled and the interface between the supernatant liquid and the sediment was barely visible and very difficult to measure accurately.

Murase et al. (1989) expressed reservations about the accuracy of the settling test, since for their results the settling data had a different slope to the C-P cell data, on a log K versus log p_s plot. They ascribed the inaccuracy to network formation between particles and aggregates of particles. They claimed that this network formation leads to significant friction between particles and the inner wall of the cylinder. However, for this study a good fit between the experimental filtration results and the internal cylindrical and planar filtration models was achieved even with the extraordinary extrapolation of the low p_s permeability data. It is probably more realistic than the conventional assumption that permeability is constant below an arbitrary p_s (see set of equations 3.32).

3.6.4.2 Porosity data

The repeatability for the settling and centrifuge tests was good, as shown in Figures 3.18 and 3.21, respectively. For the C-P cell tests there was a significant variation in the porosity data for the two tests A.1 and A.2, as was discussed in section 3.5.4.3.

As has already been mentioned the slopes of the regression lines for the C-P cell data and those for the centrifuge data on a logarithmic K versus p_s plot were significantly different (see Figure 3.22(b)). This was different to the results of Murase et al. (1989) who found close agreement between the centrifuge data and the C-P cell data. The centrifuge data were ignored as explained in section 3.6.1.2.

The settling tests gave porosity data in the range, $16.3\,Pa \leq p_s \leq 525.6\,Pa$, while for the C-P cell tests the p_s range was $10\,kPa \leq p_s \leq 400\,kPa$. The intersection of the regression line for the settling data and that for the *combined* C-P cell data (for tests A.1 and A.2) on a logarithmic $(1-\epsilon)$ versus p_s plot, occurred at 1285,1 Pa. Similar to the permeability data the porosity data for the settling tests was assumed to be valid for $p_s \leq 1285.1\,Pa$. In this case the extrapolation for the settling data was not as great as for the permeability data.

The reservations of Murase et al. (1989) with regard to the accuracy of the settling tests have already been mentioned in section 3.6.4.1.

The combination of the C-P cell and settling data gave a satisfactory fit between the experimental filtration results and the internal cylindrical and planar filtration models, even with the extrapolation of both data sets.

3.7 CONCLUSIONS

A literature review revealed that to date no one has developed a model which incorporates the internal cylindrical configuration of the filter medium, for dead-end internal cylindrical compressible cake filtration. Henry et al. (1976) developed a model for compressible cake filtration inside the filter tubes of the Uni-flow filter. This model has shortcomings, however, since it is based on the assumption that the cake thickness is thin compared to the internal diameter of a filter tube. This allowed the use of standard planar filtration equations for the model of Henry et al. (1976).

The most comprehensive model to date for dead-end *external* cylindrical compressible cake filtration is that of Tiller and Yeh (1985).

For this study, the external cylindrical model by Tiller and Yeh (1985) was adapted for compressible cake filtration *inside* a cylindrical or tubular filter medium.

In essence the model by Tiller and Yeh (1985) for external cylindrical compressible cake filtration requires the solution of a system of two ordinary differential equations. The first differential equation relates the liquid (filtrate) flow rate to the radial liquid pressure drop :

$$\frac{dp_l}{dr} = \frac{\mu_l Q}{2\pi r K} \qquad (external) \qquad (3.27)$$

The second equation gives a relationship between solids compressive and liquid (filtrate) pressures :

$$\frac{dp_s}{dr} = \frac{\mu_l Q}{2\pi r K} - (1-k_0)\frac{p_s}{r} \qquad (3.39)$$

The relevant equations for internal cylindrical filtration were derived and it was found that for internal cylindrical filtration, equation (3.27) changes to :

$$\frac{dp_L}{dr} = -\frac{\mu_f Q}{2\pi r K} \qquad (internal) \qquad (3.28)$$

Equation (3.39) for external cylindrical compressible cake filtration remains unaltered for internal cylindrical compressible cake filtration.

A waterworks clarifier sludge was used for experiments to evaluate the performance of the internal cylindrical compressible cake filtration model. For the model, it was necessary to characterize the cake which was produced by the filtration of the sludge. Since the cake was found to be very compressible, it was decided to obtain porosity and permeability data over a wide range of solids compressive pressures.

A C-P cell was used to obtain cake permeability and porosity data in the high solids compressive pressure range, while a settling technique was used to determine permeability and porosity in the low solids compressive pressure range. A recently developed centrifuge technique was used to obtain porosity data in the intermediate solids compressive pressure range. In order to evaluate the permeability and porosity data, the data was incorporated into a conventional *planar* filtration model. It was found that when the centrifuge data were ignored, there was close agreement between the planar filtration model and the results of constant pressure planar filtration experiments. Incorporation of the centrifuge data into the internal cylindrical filtration model also resulted in significant discrepancies between predictions by the model and experimental results. The centrifuge data were therefore ignored.

The following empirical equations to relate permeability and porosity, respectively, to solids compressive pressure were used in the internal cylindrical filtration model :

$$\begin{aligned} K &= 6.621 \times 10^{-13} p_{sf}^{-0.575} && 0 \le p_s \le p_{sf} \\ K &= 6.621 \times 10^{-13} p_s^{-0.575} && p_{sf} \le p_s \le 3781.7\ \text{Pa} \\ K &= 1.779 \times 10^{-10} p_s^{-1.254} && p_s \ge 3781.7\ \text{Pa} \end{aligned} \qquad (3.79)$$

$$\begin{aligned} 1-\epsilon &= 0.0299 p_{sf}^{0.0782} && 0 \le p_s \le p_{sf} \\ 1-\epsilon &= 0.0299 p_s^{0.0782} && p_{sf} \le p_s \le 1285.1\ \text{Pa} \\ 1-\epsilon &= 0.00785 p_s^{0.265} && p_s \ge 1285.1\ \text{Pa} \end{aligned} \qquad (3.81)$$

Sets of equations (3.79) and (3.81) are similar to the equations proposed by Tiller and Cooper (1962) (see section 3.3.3).

The predictions by the internal cylindrical filtration model were compared to the results of constant pressure filtration experiments inside a porous woven tube, which could be dismantled. The same waterworks clarifier sludge, which when filtered produced a very compressible cake, was used for the experiments. The model accurately described the experimental results.

The main findings of this study were as follows.

As for external cylindrical filtration, it was found that for internal cylindrical filtration the effect of the coefficient of earth pressure at rest, k_o, is small, except for small internal cake diameters (long filtration times). For the tubular filter press such small internal cake diameters are not practical, because of the risk of tube blockages and since cake particles have to be transported through the inner cake diameter during the cake removal cycle.

It was found that k_o had a significant effect on the solids compressive pressure at and very close to the filter medium. For $k_o < 1$, as the filtration progresses and the cake thickness increases, it is possible for the solids compressive pressure at or near the filter medium to increase to a maximum and to decrease thereafter. This may be explained as follows. Initially, solids compressive pressure at the internal surface of the filter medium increases as the pressure drop across the cake, Δp_c, increases. As the cake thickness increases (internal cake diameter decreases), the stress or force at or near the filter medium decreases, resulting in a decrease in the solids compressive pressure. For $k_o = 1$, the maximum in the p_s curve does not occur. However, this phenomenon was found not to have a significant effect on the overall performance of the internal cylindrical filtration model.

For internal cylindrical filtration, the solids compressive pressure, p_s, and liquid pressure, p_L, are not unique functions of the fractional distance through the cake, as is the case for planar filtration with negligible filter medium resistance.

It was found that there was a significant difference between the average cake dry solids concentration for internal cylindrical, external cylindrical and planar filtration. For planar filtration the average cake dry solids concentration remains essentially constant as the cake thickness increases. For external cylindrical filtration the average cake dry solids concentration decreases, while for internal cylindrical filtration the average cake dry solids concentration increases with cake thickness. The dry solids production rate per unit filter medium area is lower for internal cylindrical filtration than for planar filtration or external cylindrical filtration. This is due to the decrease in available filtration area as the cake thickness increases and the internal cake diameter decreases.

The internal tube diameter has a significant effect on the average cake dry solids concentration for internal cylindrical filtration. For the same cake thickness the average cake dry solids concentration decreases as the internal tube diameter increases.

Finally, as discussed in Chapter 2, one of the reasons for developing a dead-end internal cylindrical compressible cake filtration model, was to prevent or minimize tube blockages in a tubular filter press. Since the model, which was developed accurately predicted the variation of internal cake diameter with filtration time, it should be of great assistance in preventing or minimizing tube blockages in a tubular filter press.

CHAPTER 4
INVESTIGATION INTO CAKE RECOVERY DURING THE CAKE REMOVAL CYCLE OF THE TUBULAR FILTER PRESS

4.1 INTRODUCTION

The objectives of this study were defined in Chapter 2. One of the objectives was to investigate cake recovery (cake losses) during the cake removal cycle of the tubular filter press. The motivation for this objective was that, at various times, low cake recoveries (high cake losses) were experienced during the cake removal cycle on the prototype tubular filter press. Low cake recoveries are undesirable since they can result in a reduced dry solids production rate and an excessive increase in solids concentration in the feed tank.

Since the tubular filter press is a novel process, the cake losses during the cake removal cycle have not been investigated before. For this reason, an investigation was conducted into cake recovery during the cake removal cycle of a tubular filter press, using the same batch of clarifier sludge that was used for the internal cylindrical filtration experiments, discussed in Chapter 3. During this study the cake losses due to the shear of the cleaning fluid and the losses due to the action of the rollers and hydraulic conveyance of flakes of dislodged cake were quantified. The effects of various parameters such as filtration pressure and path length for the hydraulic conveyance of flakes of cake were investigated.

4.2 LITERATURE REVIEW

A literature review revealed only two references which deal with the removal or erosion of deposited filter cakes due to the *subsequent* shear of a flowing fluid. Rushton et al. (1979) conducted experiments with various grades of magnesium carbonate. For one set of experiments, water was allowed to permeate through cakes of constant thickness at a constant flux or velocity. The cakes were simultaneously subjected to increasing water flow rates tangentially across the cake surface. Movements of surface layers were observed visually through a window in the side of a rectangular test rig.

For another set of experiments, it was found that as filtrate flux was increased the minimum tangential water flow rate across the cake surface required for erosion of the cake, increased. It was also found that above a certain filtrate flux the minimum tangential water flow rate required to move cake layers, increased as particle size was decreased.

Linear equations relating the tangential water flow rate to permeation velocity or filtrate flux were given for two particle size ranges.

The tests were purely investigative in nature and were not intended for the development of a predictive model. Also, the investigation concentrated on the minimum water flow rate required for erosion of the cake rather than quantifying the cake losses. As has already been mentioned the quantification of cake losses during the cake removal cycle is important for the tubular filter press.

Berger et al. (1990) developed a very simple test to determine the resistance of filter cakes to erosion caused by the shear of a flowing fluid. The objective of the test was to assist filtration plant operators in minimizing cake losses resulting from the introduction of wash fluid during cake washing in the filtration or cake washing cycle of a filter.

The test was conducted as follows. A filter cake was allowed to form under a sub-atmospheric pressure on a filter medium. After a certain cake thickness had been deposited, a regulated flow of water was allowed to impinge on the upper cake surface from a pipe which was located at a certain height above the cake (see Figure 4.1). The pressure differential was maintained across the cake for the duration of the test. Berger et al. (1990) found that cake erosion commenced on a circle or ring which was concentric with the impinging water jet, but did not coincide with the outer boundary of the jet. From this they concluded that cake erosion was not caused by the stagnation pressure of the impinging jet, but rather by the shear of the water layer which flowed from the jet parallel to the upper cake surface (see Figure 4.1). The relationship between shear stress and the distance from the jet is shown in Figure 4.2. Berger et al. (1990) found that the "erosion ring" in the cake coincided approximately with the maximum in the shear stress versus distance curve.

During a series of experiments with limestone, it was found that the velocity in the water layer parallel to the cake surface at incipient erosion, was independent of the diameter of the pipe and the volumetric flow rate of water. It was, however, found that the minimum velocity for incipient erosion increased significantly as the pressure difference across the cake was increased. Particle size and particle size distribution had a significant effect on the minimum velocity for incipient erosion. For various fractions of milled quartz it was found that the minimum velocity increased significantly as the mean particle size was decreased. The effect of particle size distribution on the resistance of the cake to erosion was found to be very complex.

It was stressed by Berger et al. (1990) that the simple test which was developed by them could not be used as an accurate predictive tool or model. It could merely serve as a tool to highlight trends and give a rough or approximate indication of performance on a full-scale plant. Although the compressibility of the quartz and limestone cakes used during their experiments was not indicated, it is generally known that such cakes are not very compressible, (for example, Tiller and Cooper, 1962).

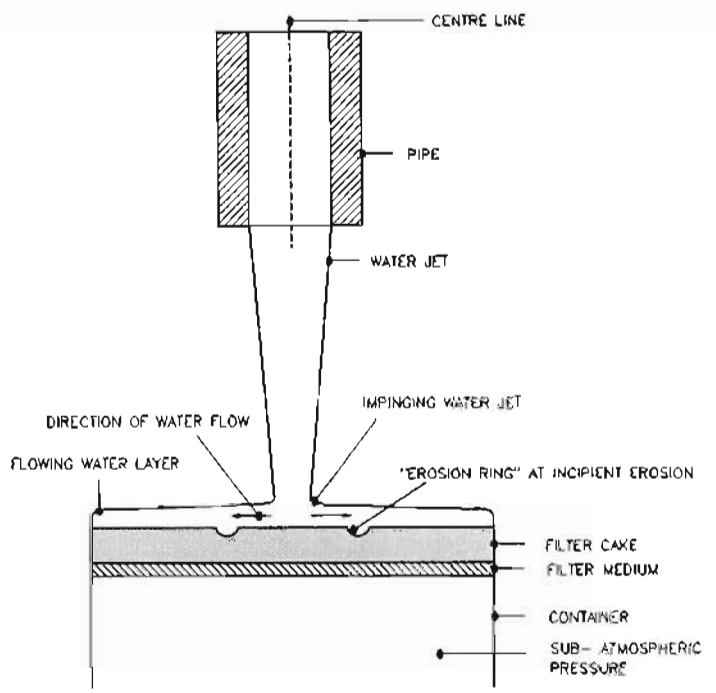

FIGURE 4.1 : Experimental Apparatus of Berger et al. (1990)

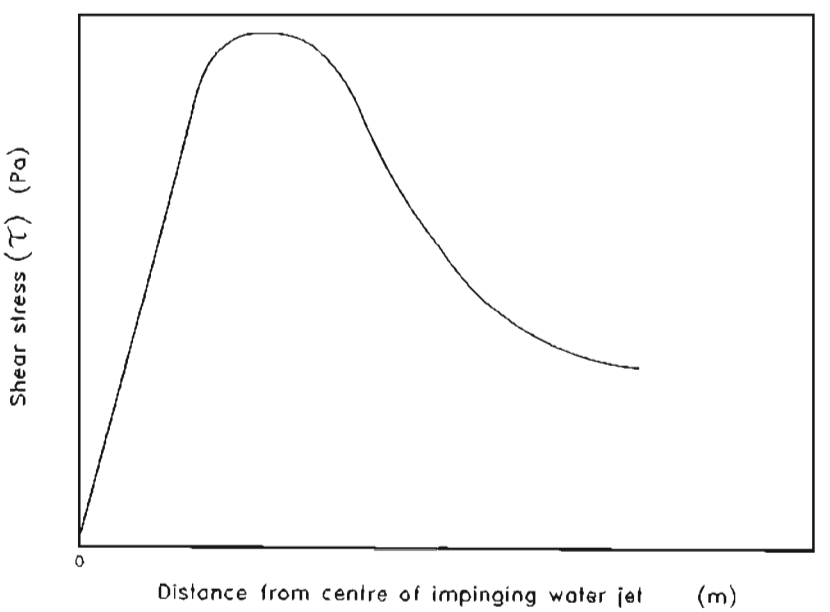

FIGURE 4.2 : Relationship Between Shear Stress and Distance from the Centre of the Impinging Water Jet for Experiments Conducted by Berger et al. (1990)

In the light of the constraints and limitations of the tests by Rushton et al. (1979) and Berger et al. (1990), it was decided to develop a predictive shear model for the erosion of a *compressible* cake which is deposited inside a porous tube and to test the validity of such a model. This model would then allow the prediction of cake losses due to the shear of the cleaning fluid prior to the action of the rollers during the cake removal cycle on a tubular filter press.

Since the tubular filter press is a novel process, the cake losses due to the action of the rollers and the hydraulic conveyance of dislodged flakes of cake have not been investigated.

4.3 PROPOSED SHEAR MODEL FOR THE EROSION OF A COMPRESSIBLE FILTER CAKE BY A FLOWING FLUID INSIDE A POROUS TUBE

4.3.1 Radial Variation of Cake Yield Stress (τ_{oc})

The variation of solids compressive pressure with radius is shown in Figure 3.41 for the very compressible cake obtained during the internal cylindrical filtration experiments using the clarifier sludge (see Chapter 3). The relationship may be written as :

$$p_s = f_u(r) \qquad (4.1)$$

where f_u = function of, (-)

p_s = solids compressive pressure, (Pa)

r = radius, (m)

The variation in solids compressive pressure results in a corresponding variation in cake solids concentration with radius, as shown in Figure 3.43 in Chapter 3 :

$$cake\ solids\ concentration = f_u(r) \qquad (4.2)$$

As is shown later in section 4.6.4 , the waterworks clarifier sludge exhibited a yield stress for all solids concentrations which were investigated. It was found that the yield stress was a strong function of sludge (cake) solids concentration, i.e.

$$\tau_{oc} = f_u(solids\ concentration) \qquad (4.3)$$

where τ_{oc} = yield stress of cake, (Pa)

There was a significant increase in yield stress as the solids concentration of the sludge was increased (see Figure 4.28(a)).

Combining equations (4.2) and (4.3) :

$$\tau_{oc} = f_u(r) \qquad (4.4)$$

4.3.2 Radial Variation of the Shear Stress Exerted by the Flowing Fluid at the Internal Cake Wall (τ_w)

The main hypothesis of the proposed shear model is that if a fluid flows inside a deposited cake annulus (as prior to the action of the rollers during the cake removal cycle of the tubular filter press) then for a *compressible* cake the inner cake layers will be eroded until the shear stress, τ_w, exerted by the fluid at the "new" or exposed cake surface is equal to the yield stress of the cake at this surface. This is shown in Figure 4.3.

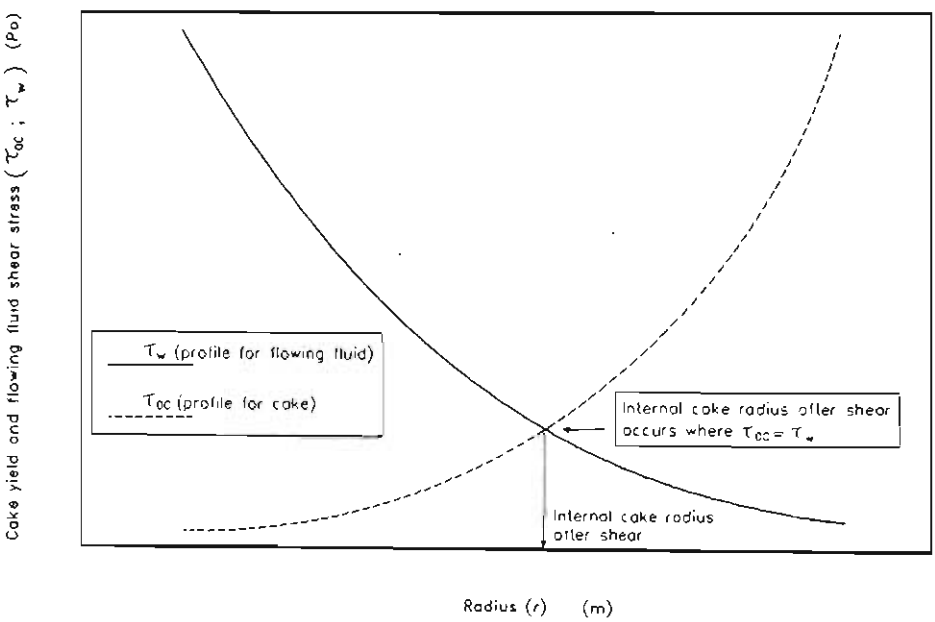

FIGURE 4.3 : Diagram to Show Variation of Shear Stress Exerted by the Flowing Fluid at the Inner Cake Wall (τ_w) and Cake Yield Stress (τ_{oc}) with Radius

The shear stress exerted at the inner cake wall by the flowing fluid for turbulent flow is :

$$\tau_w = \frac{f}{2} \rho_{ff} \bar{u}_{ff}^2 \qquad (4.5a)$$

where f = friction factor, (-)
$\bar{u}_{ff}$ = average velocity of fluid, (m/s)
ρ_{ff} = density of fluid, (kg/m^3)
τ_w = shear stress exerted by flowing fluid at internal wall of tube or cake, (Pa)

For a fluid flowing inside a cake annulus, equation (4.5a) may also be written as :

$$\tau_w = 8 f \rho_{ll} \frac{Q_{ll}^2}{\pi^2 d_2^4} \qquad (4.5b)$$

where d_2 = internal cake diameter, (m)

Q_{ll} = flow rate of fluid, (m^3/s)

The Moody equation for the friction factor for the turbulent flow of a *Newtonian* fluid is (Massey, 1979) :

$$f = 0,001375\left[1 + \left(2 \times 10^4 \frac{k}{d_2} + \frac{10^6}{Re}\right)^{\frac{1}{3}}\right] \qquad (4.6)$$

where k = surface roughness, (m)

Re = Reynolds number, (-)

For a Newtonian fluid flowing inside a cake annulus :

$$Re = \frac{\rho_{ll} \bar{u}_{ll} d_2}{\mu_{ll}} \qquad (4.7)$$

where μ_{ll} = viscosity of fluid, (Pa.s)

It should be noted that the effect of filtrate flux on cake losses has been ignored for the shear model. The reason for this is that during the cake removal cycle the pressure in the porous tubes is significantly lower than the *filtration* pressure, so that the filtrate flux during the cake removal cycle is negligible.

4.4 THEORY FOR ANALYSIS OF BINGHAM PLASTIC RHEOLOGY IN A CAPILLARY-TUBE VISCOMETER

In order to determine the variation of yield stress (τ_o) with sludge (cake) solids concentration (see equation (4.3)), the rheology of the waterworks clarifier sludge was determined over a wide solids concentration range using a capillary-tube viscometer. The capillary-tube viscometer is described in section 4.5.1.3. As is shown later in section 4.6.4, all the sludges (cakes) (over the concentration range which was investigated) exhibited Bingham plastic behaviour.

The rheology for the ideal Bingham plastic is described by the following set of equations :

$$\tau = -\eta \frac{du_{ll}}{dr} + \tau_o \qquad for\ \tau \geq \tau_o$$

$$-\frac{du_{ll}}{dr} = 0 \qquad for\ \tau \leq \tau_o \qquad (4.8)$$

where u_{fl} = axial velocity of fluid at radius r, (m/s)

η = coefficient of rigidity, (Pa.s)

τ = shear stress, (Pa)

τ_o = yield stress, (Pa)

The *true* shear diagram for an ideal Bingham plastic is shown in Figure 4.4.

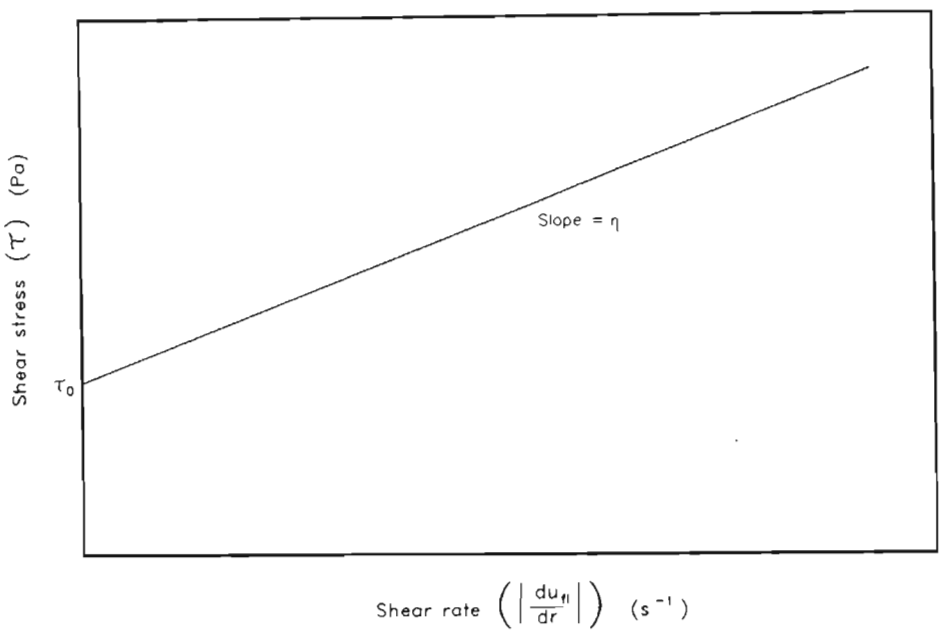

FIGURE 4.4 : *True* Shear Diagram for an Ideal Bingham Plastic

The essential feature of a capillary-tube viscometer is the measurement of the friction loss associated with the *laminar* flow of a fluid at a known rate through a tube of known dimensions.

The primary output from a capillary-tube viscometer is the *pseudo-shear* diagram, which is a plot of the shear stress at the *inner wall* of the capillary tube versus the *average* shear rate in the capillary tube. For a Bingham plastic the coefficient of rigidity (η) and the yield stress (τ_o) may be determined from a pseudo-shear diagram.

The pseudo-shear diagram for an ideal Bingham plastic will be derived next. The derivation is based on that given by Wasp et al. (1979) and Brodkey (1967).

For tube or pipe flow a general rheology equation may be written as :

$$-\frac{du_{fl}}{dr} = f_u(\tau) \qquad (4.9)$$

For the steady flow of a fluid in a tube with a circular cross-section and length, L_t, (as shown in Figure 4.5), the following equation may be derived from Newton's second law of motion (with no acceleration) (see Appendix I for effect of gravity) :

$$\pi R_t^2 \Delta p_t = 2\pi R_t L_t \tau_w \qquad (4.10)$$

where L_t = length of tube, (m)
Δp_t = pressure difference between ends of tube, (Pa)
R_t = internal radius of tube, (m)
τ_w = shear stress exerted by flowing fluid at internal wall of tube or cake, (Pa)

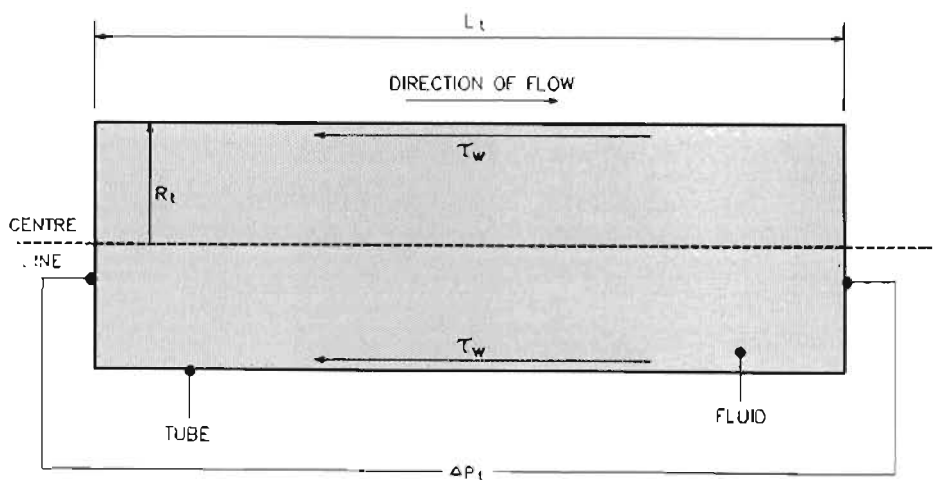

FIGURE 4.5 : Forces Acting on Element of Fluid Within Tube

From equation (4.10) :

$$\tau_w = \frac{\Delta p_t R_t}{2 L_t} \qquad (4.11)$$

Similarly, the shear stress at any arbitrary radius, r, may be written as :

$$\tau = \frac{\Delta p_t r}{2 L_t} \qquad (4.12)$$

Combining equations (4.11) and (4.12) gives the following relationship between τ and τ_w:

$$\tau = \tau_w \frac{r}{R_t} \qquad (4.13)$$

The fluid flow rate in the tube is given by :

$$Q_{ll} = \int_o^{R_t} 2\pi r u_{ll}(r)\, dr \tag{4.14}$$

Equation (4.14) can be integrated by parts which gives :

$$Q_{ll} = \pi\left[r^2 u_{ll}(r) - \int r^2 \frac{d\bar{u}_{ll}(r)}{dr} dr \right]_o^{R_t} \tag{4.15}$$

Since $u_{ll} = 0$ at $r = R_t$, the first term on the right hand side of equation (4.15) is zero. By substituting $\frac{du_{ll}}{dr}$ and r from equations (4.9) and (4.13) respectively, and after transformation of the variables in equation (4.15) :

$$\frac{Q_{ll}}{\pi R_t^3} = \frac{1}{\tau_w^3}\int_o^{\tau_w} \tau^2 f_u(\tau)\, d\tau \tag{4.16}$$

From equation (4.13) the shear stress increases linearly from zero at the centre of the tube to τ_w at the tube wall. For a Bingham plastic fluid flowing in a tube an unsheared plug of fluid moves in the centre of the tube. This is because inside the unsheared central plug the local value of the shear stress is less than the yield stress, τ_o, so that no shearing of the fluid takes place inside this plug.

Therefore :

$$\begin{aligned} f_u(\tau) &= -\frac{du_{ll}}{dr} = 0 \qquad \text{for } \tau_o \geq \tau \geq 0 \\ f_u(\tau) &= -\frac{du_{ll}}{dr} = \frac{\tau - \tau_o}{\eta} \qquad \text{for } \tau_w \geq \tau \geq \tau_o \end{aligned} \tag{4.17}$$

Also :

$$\bar{u}_{ll} = \frac{Q_{ll}}{\pi R_t^2} \tag{4.18}$$

Substituting set of equations (4.17) and equation (4.18) in equation (4.16) gives :

$$\frac{Q_{ll}}{\pi R_t^3} = \frac{2\bar{u}_{ll}}{D_t} = \frac{1}{\eta \tau_w^3}\int_{\tau_o}^{\tau_w} \tau^2(\tau - \tau_o)\, d\tau \tag{4.19}$$

where D_t = internal tube diameter, (m)

$$\frac{2\bar{u}_{ll}}{D_t} = \frac{1}{\eta \tau_w^3}\left[\frac{\tau^4}{4} - \frac{\tau^3 \tau_o}{3}\right]_{\tau_o}^{\tau_w} \tag{4.20}$$

Therefore :

$$\frac{8\bar{u}_{ll}}{D_t} = \frac{\tau_w}{\eta}\left[1 - \frac{4}{3}\left(\frac{\tau_o}{\tau_w}\right) + \frac{1}{3}\left(\frac{\tau_o}{\tau_w}\right)^4\right] \tag{4.21}$$

This is the Buckingham-Reiner equation (Bird et al., 1960) for the *laminar* flow of an ideal Bingham plastic in a tube. For relatively high-fluid flow rates the ratio (τ_o/τ_w) is relatively small and the final term of equation (4.21) may be omitted. For relatively high fluid flow rates (still in the laminar flow regime) equation (4.21) may therefore be written as (Wasp et al., 1979) :

$$\tau_w = \eta\left(\frac{8\bar{u}_{fl}}{D_t}\right) + \frac{4}{3}\tau_o \qquad (4.22)$$

From equation (4.22), the pseudo-shear diagram (which represents a plot of the *shear stress* at the internal wall of the capillary tube (τ_w) versus the average *shear rate* $(8\bar{u}_{fl}/D_t)$) for an ideal Bingham plastic is as shown in Figure 4.6. The curve is linear for relatively high values of $(8\bar{u}_{fl}/D_t)$ and the intercept of the linear portion, extended back to zero shear rate, intercepts the Y-axis at $\frac{4}{3}\tau_o$.

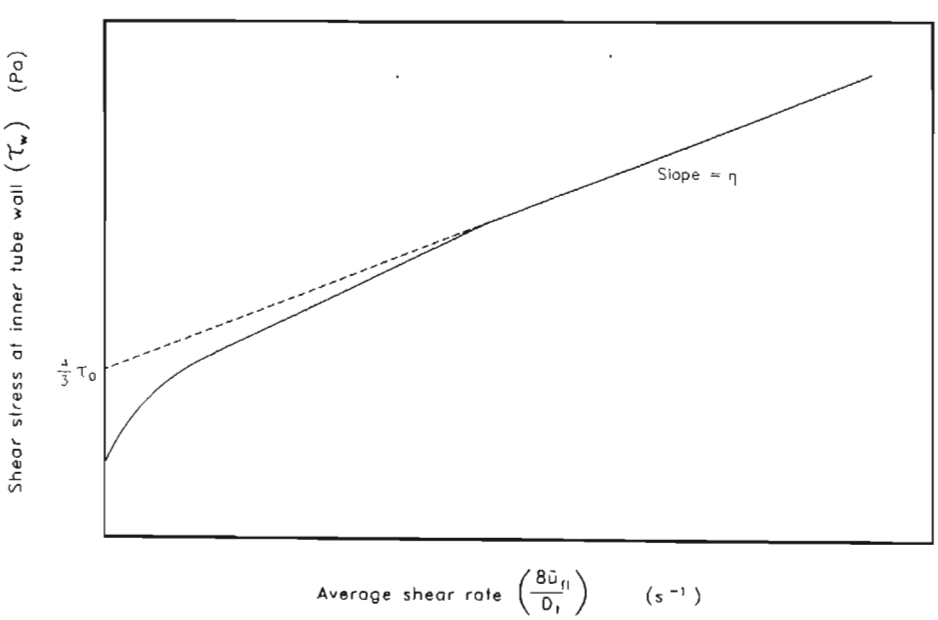

FIGURE 4.6 : *Pseudo-shear* **Diagram for Ideal Bingham Plastic for Capillary-tube Viscometer**

The coefficient of rigidity (η) and the yield stress (τ_o) for an ideal Bingham plastic may therefore be determined from a pseudo-shear diagram which is obtained from capillary-tube viscometer experiments.

As has been mentioned previously, the theory for determining η and τ_o from a pseudo-shear diagram is only valid for *laminar* flow. It is therefore necessary to determine the Reynolds number for a Bingham plastic so that the flow regime may

be determined. According to Thomas (1960) the flow will be laminar for values of Reynolds number less than 2 100, where Reynolds number for a Bingham plastic is defined as :

$$Re = \frac{\rho_{fl}\,\bar{u}_{fl}\,D_t}{\mu_e} \tag{4.23}$$

where Re = Reynolds number, (-)
μ_e = effective viscosity, (Pa.s)
ρ_{fl} = density of fluid, (kg/m^3)

The effective viscosity for a Bingham plastic may be defined as follows. The Hagen-Poiseuille equation describes the pressure drop (friction loss) of a *Newtonian* fluid flowing in a tube. The Hagen-Poiseuille equation may be written as (Bird et al., 1960) :

$$Q_{fl} = \frac{\pi \Delta p_t R_t^4}{8\mu L_t} \tag{4.24}$$

where μ = viscosity, (Pa.s)

Using equations (4.11) and (4.18), equation (4.24) may be written as :

$$\tau_w = \mu\left(\frac{8\bar{u}_{fl}}{D_t}\right) \tag{4.25}$$

or

$$\frac{\tau_w}{\left(\frac{8\bar{u}_{fl}}{D_t}\right)} = \mu \tag{4.26}$$

In the same manner, equation (4.22) for a Bingham plastic may be written as :

$$\frac{\tau_w}{\left(\frac{8\bar{u}_{fl}}{D_t}\right)} = \eta\left(1 + \frac{\tau_o D_t}{6\eta\bar{u}_{fl}}\right) \tag{4.27}$$

Comparing equations (4.26) and (4.27), the effective viscosity, μ_e, of a Bingham plastic is therefore :

$$\mu_e = \eta\left(1 + \frac{\tau_o D_t}{6\eta\bar{u}_{fl}}\right) \tag{4.28}$$

Combining equations (4.23) and (4.28), the Reynolds number for a Bingham plastic is :

$$Re = \frac{\rho_{fl}\,\bar{u}_{fl}\,D_t}{\eta\left(1 + \frac{\tau_o D_t}{6\eta\bar{u}_{fl}}\right)} \tag{4.29}$$

4.5 EXPERIMENTAL

The experiments to determine cake losses during the cake removal cycle were divided into two parts. The objective of the first part was to determine the cake losses due to the shear of the cleaning fluid only. The objective of the second part was to determine the combined cake losses due to the action of the rollers and hydraulic conveyance of dislodged flakes of cake.

4.5.1 Experimental Apparatus

4.5.1.1 Apparatus to determine cake losses due to shear of cleaning fluid

The apparatus used for these experiments was the same as that used for the internal cylindrical filtration experiments, as shown in Figure 3.12.

4.5.1.2 Apparatus to determine cake losses due to action of rollers and hydraulic conveyance

The apparatus for the internal cylindrical filtration experiments was amended slightly so that two different lengths of straight tube could be inserted immediately after the filter tube. The two lengths of tube were 1 m and 4 m long and the internal diameter of the tubes was 25 mm. A 425 μm sieve was placed on a stand at the outlet of these tubes to capture the flakes of cake which were dislodged by the rollers during the cake removal cycle. A process schematic of the amended apparatus is shown in Figure 4.7. After a cake of desired thickness had been deposited, a set of rollers was lowered over the tube (see Figure 4.8) and then aligned or engaged so that the gap between the two larger rollers (with an outer diameter of 25 mm) was 3 mm. The dimensions of the rollers and the gap size were identical to those on the prototype unit. The diameter of the rollers and the gap size between the rollers was not varied during this study.

4.5.1.3 Capillary-tube viscometer to determine cake (sludge) rheology

A capillary-tube viscometer was constructed to determine the cake or sludge rheology at various sludge (cake) solids concentrations. A schematic diagram of the capillary-tube viscometer is shown in Figure 4.9.

The internal diameter of the cylindrical sludge container was 150 mm and its capacity was approximately 8 ℓ. The material of construction was 316 stainless steel. All parts in contact with fluid were polished. The nipple at the bottom was tapered so as to minimize entrance effects.

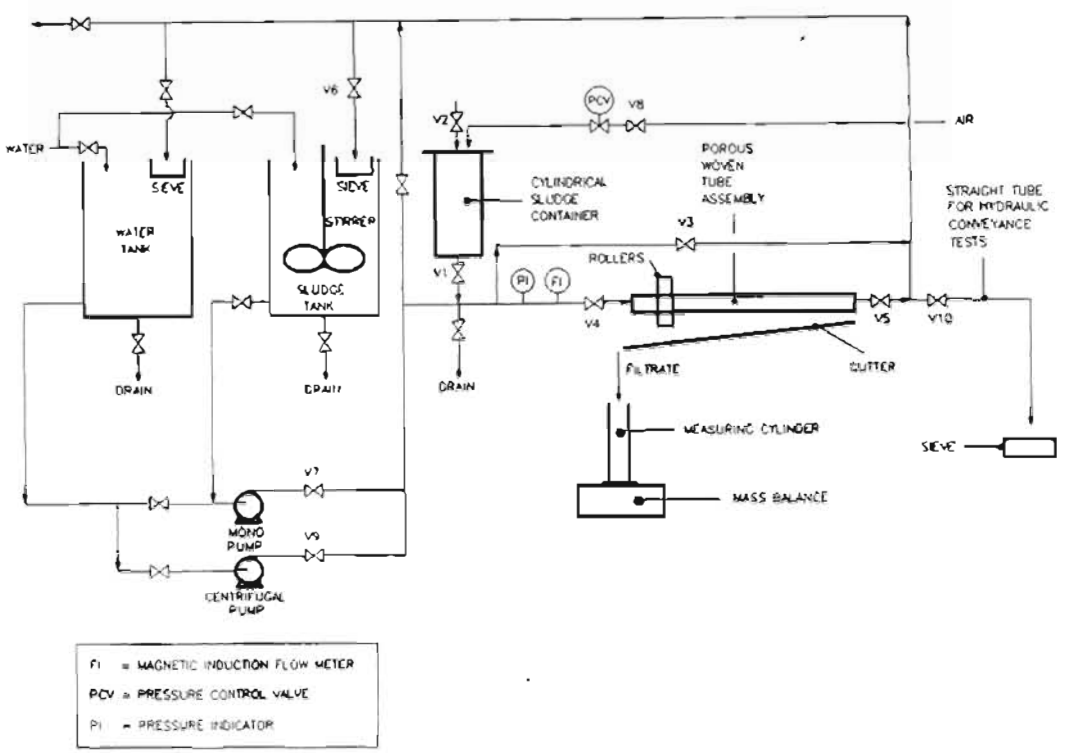

FIGURE 4.7 : Process Schematic of Amended Internal Cylindrical Filtration Apparatus

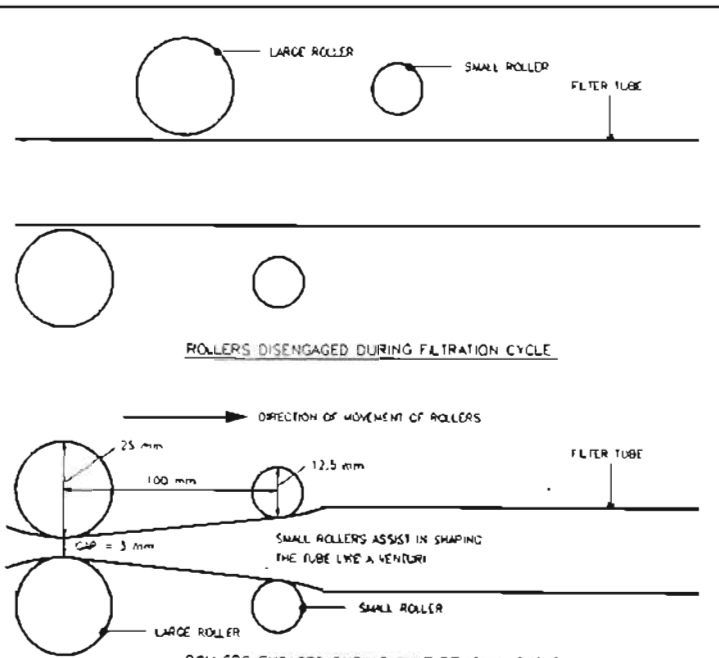

FIGURE 4.8 : Dimensions of Rollers and Gap Size Between Rollers

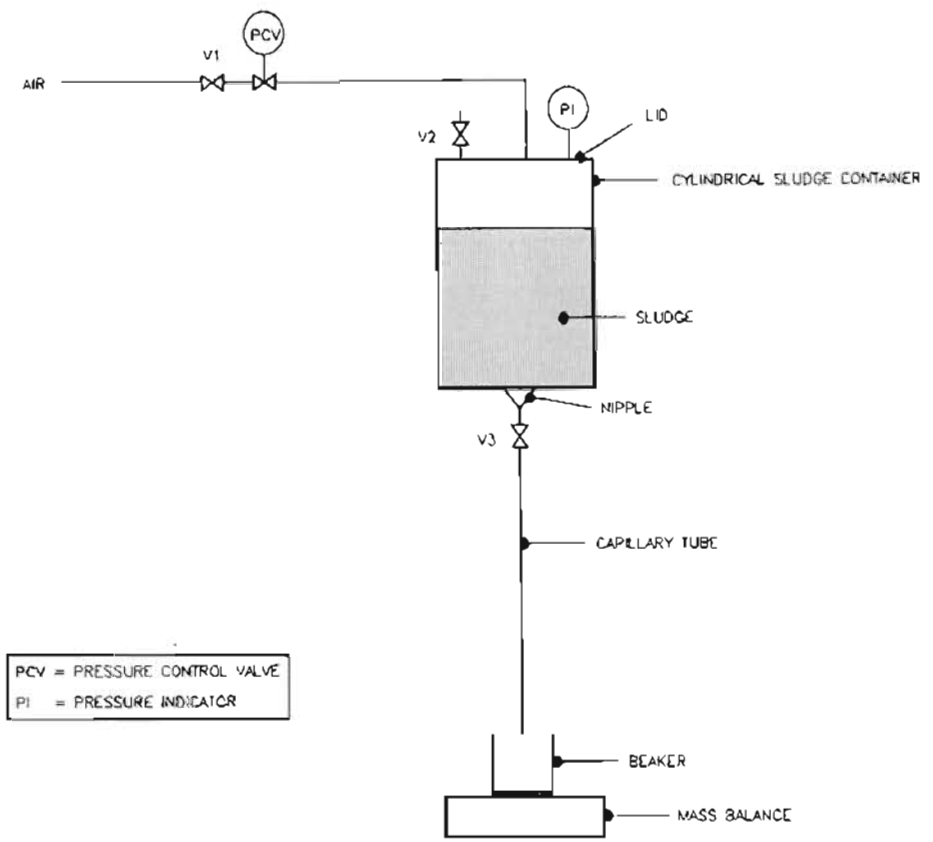

FIGURE 4.9 : Schematic Diagram of Capillary-tube Viscometer

The lid of the sludge container was removable. The tubes used were smooth nylon tubes with uniform internal bore (manufactured to DIN standard 74324) and with an internal diameter of 3,98 mm and an outer diameter of 6 mm. The internal diameter of a representative sample of the tubes was measured accurately by filling an accurately determined length of the tube with mercury. The internal diameter was calculated from the mass of mercury. This method was recommended by Bowen (1961). The tube lengths were varied between 1 m and 9,9 m. The length to internal diameter ratios were therefore in the range $250 < \frac{L_t}{D_t} < 2\ 500$. Since the length to diameter ratios $\left(\frac{L_t}{D_t}\right)$ were large for all the experiments, end effects were ignored for the experiments. The details of the experiments are shown in Appendix I.

The sludges (cakes) were allowed to discharge from the tube into a beaker which was situated on a SARTORIUS mass balance.

The air pressure was measured using a 0 to 500 kPa pressure gauge and the temperature of the sludge was measured with a thermometer.

4.5.2 Experimental Procedure

4.5.2.1 Experiments to determine cake losses due to shear of cleaning fluid

The clarifier sludge which was used for the internal cylindrical filtration experiments (see Chapter 3) was also used for these experiments. The procedure for depositing a cake inside the porous tube was identical to that described in section 3.4.3.2 for the internal cylindrical experiments (see Figure 3.12). After a cake was deposited, the pressure in the cylindrical sludge container and the filtration assembly was released very slowly. Valve V4 was closed and bypass valve V3 was opened. The centrifugal pump was then switched on and water (for some experiments feed sludge) was pumped through the system via the bypass to the porous tube assembly.

It was decided to use water rather than the feed sludge as cleaning fluid for the bulk of the shear experiments, since the rheology of water is well known. (Current practice on all operating filter presses is to use feed sludge as cleaning fluid). This simplified the calculation of the shear stress exerted at the inner cake wall (τ_w) by the flowing cleaning fluid. One set of experiments was however done using the feed sludge as the cleaning fluid (see section 4.7.2).

The flow rate (which was measured with a KROHNE magnetic induction flow meter) was adjusted to the desired value by adjusting valve V9. Once the flow rate had been adjusted to the desired value, valves V4 and V5 were opened very carefully while valve V3 was closed to direct the flow through the filter tube. The flow was allowed to pass through the filter tube for 3 minutes, which was the cleaning time which was found suitable on the prototype tubular filter press. For a few experiments the cleaning time was increased to 10 minutes. No significant difference between the cake losses obtained at a cleaning time of 3 minutes and those at 10 minutes was observed.

After an experiment the centrifugal pump was switched off and the filter tube assembly was drained and dismantled as described in section 3.4.3.2. The cake was carefully removed and the mass of cake remaining after scouring was determined. The solids concentration of the cake was determined in the same manner as for the internal cylindrical filtration experiments. The internal diameter of the remaining cake after scouring was measured with a vernier calliper (where possible) and also calculated (from the mass of wet cake and average cake dry solids concentration) in the same manner as for the internal cylindrical filtration experiments.

The mass of cake remaining after scouring was compared with that which was deposited (from the internal cylindrical filtration experiments) and the cake losses due to shear of the cleaning fluid were calculated.

4.5.2.2 Experiments to determine the total cake losses and the combined cake losses due to the action of the rollers and hydraulic conveyance of dislodged flakes of cake

The clarifier sludge was also used for these experiments. The experimental procedure for these experiments was identical to the procedure described above (in section 4.5.2.1) to determine the cake losses due to the shear of cleaning fluid, except that after the centrifugal pump was switched on, valve V10 was opened (see Figure 4.7) and a set of rollers was slowly moved manually along the porous tube while water was flowing through the porous tube. The dislodged flakes of cake were hydraulically conveyed by the water onto a 425 μm sieve. The flakes of cake were separated from the water by the sieve.

After an experiment the centrifugal pump was switched off and the sieve with the flakes of cake was left to stand for at least 15 minutes. This allowed any excess water to drain from the interstices between flakes of cake. The mass of the wet cake was then determined. The cake was dried in an oven for 12 hours at 105 °C and the mass of the dry cake was determined. The average cake dry solids concentration was calculated. The results of these experiments gave the *overall* cake recovery, R, or *total* cake losses. The combined cake losses due to the action of the rollers and the hydraulic conveyance of dislodged flakes of cake, were calculated by subtracting the cake losses due to the shear of the cleaning fluid (as obtained in section 4.5.2.1) from the *total* cake losses (as obtained from the experiments described above).

4.5.2.3 Experiments to determine sludge (cake) rheology at various solids concentrations

Prior to an experiment a very thick sludge was prepared in the following manner. A portion of cake was taken from the batch which was collected from the prototype tubular filter press and which was used for the internal cylindrical filtration experiments described in Chapter 3. Tap water was added to this portion of cake and the cake was re-slurried using a laboratory stirrer. After the bulk of the cake had been re-slurried, the resultant sludge was passed twice through a 425 μm sieve to remove any lumps of cake or large particles. A fraction of the sieved sludge was then transferred to the beakers of a laboratory centrifuge for thickening. The centrifuge was then started and the speed was adjusted so that the sediment in the centrifuge beakers had a solids concentration of approximately 20 % (m/m) after 15 minutes. The centrifuge was switched off and the beakers were removed. The supernatant liquid was decanted from the beakers, while the sediment was retained for the rheology experiments. This process was repeated until all the sieved sludge had been thickened.

The thickened sludge was then diluted to the desired solids concentration for the first experiment, by adding tap water to the sludge. The sludge was homogenized using the laboratory stirrer. A portion of the sludge was then poured into the cylindrical sludge container of the capillary-tube viscometer. The sludge in the

cylindrical container was stirred and the temperature of the sludge was determined using a thermometer. The height difference between the level of the sludge in the cylindrical container and the discharge level of the capillary tube was measured. The lid of the cylindrical sludge container was then placed on top of the container and was bolted down. The desired air pressure was applied to the cylinder by opening valve V1 (see Figure 4.9) and adjusting the pressure by means of the pressure control valve. The mass of the beaker was recorded. Valve V3 was opened and a stop-watch was started simultaneously. The sludge was discharged from the capillary tube into the beaker situated on the mass balance. After an acceptable time interval valve V3 was closed and the stop-watch was stopped simultaneously. The final combined mass of the sludge and the beaker was recorded. The volumetric flow rate of the sludge was calculated as shown in Appendix I. Before another experiment valve V1 was closed and valve V2 opened to release the air. The lid of the cylindrical container was removed and the sludge was stirred. (The solids concentrations for these experiments were high and the settling rates were very low. Therefore it was not necessary to stir the sludge continuously). The lid of the cylindrical container was bolted down for the next experiment. The height difference between the level of the sludge in the container and the discharge level of the capillary tube was calculated for the next experiment at a higher shear rate (as shown in Appendix I).

The experiment was repeated at a higher shear rate by increasing the applied air pressure in the cylindrical sludge container.

After a number of experiments had been done over a wide shear rate range for a fixed solids concentration, a pseudo-shear diagram (see section 4.4) was prepared. At the end of an experiment with a fixed sludge solids concentration, the portion of sludge was removed from the cylindrical sludge container and the sludge was then diluted to the desired solids concentration for the next set of experiments. The capillary-tube viscometer was cleaned thoroughly before a batch of diluted sludge was placed in the cylindrical sludge container. The experiments were then repeated for the batch of diluted sludge and a pseudo-shear diagram was prepared for the diluted sludge in the same manner as described above.

This process was continued until pseudo-shear diagrams had been prepared for all desired sludge solids concentrations.

4.6 RESULTS

As mentioned in section 4.5.2.2, the experiments with the rollers gave the total cake losses (or overall cake recovery, R). The combined cake losses due to the action of the rollers and hydraulic conveyance of dislodged flakes of cake were calculated by subtracting the cake losses due to the shear of the cleaning fluid from the total cake losses.

In this results section the experimental results are given in the following sequence :

(i) overall cake recovery (total cake losses);

(ii) cake losses due to the shear of the cleaning fluid only;

(iii) combined cake losses due to the action of the rollers and hydraulic conveyance of dislodged flakes of cake only.

4.6.1 Results of Experiments to Determine the Effect of Various Variables on *Overall* Cake Recovery, R

Experiments were conducted to determine the effect of the following variables on *overall* cake recovery, R, (see equation (2.7)) during the cake removal cycle :

(i) filtration pressure;
(ii) cleaning fluid flow rate;
(iii) path length for hydraulic conveyance of flakes of cake.

The investigation of cake losses due to the hydraulic conveyance of the flakes of cake to the collecting sieve is important, since if such losses are significant, then it is advantageous to design plants with filter tubes which are as short as possible. As explained before, water was used as a cleaning fluid for these experiments. Cake recoveries were determined at filtration pressures of 100 kPa and 300 kPa, cleaning water flow rates of approximately 25 ℓ/min (see Appendix H for exact flow rates for each experiment) and approximately 50 ℓ/min. These cleaning water flow rates represented axial velocities of approximately 0,77 m/s and 1,54 m/s, respectively, based on the internal diameter of the filter medium (d_1 = 26,25 mm for the porous tube used during these experiments).

The cleaning velocities used on the prototype tubular filter press were in the range of 1 to 1,5 m/s, based on the internal diameter of the filter medium. For the experiments to investigate the effect of path length on overall cake recovery, two path lengths were used, namely 1 m and 4 m.

The experiments were done at the same feed solids concentration and filtration times as the internal cylindrical filtration experiments in Chapter 3. The results for the experiments are shown in Appendix H.

4.6.1.1 The effect of cleaning fluid flow rate and filtration pressure on overall cake recovery, R

The effect of cleaning fluid flow rate and filtration pressure on overall cake recovery, R, is shown in Figure 4.10 for various filtration times.

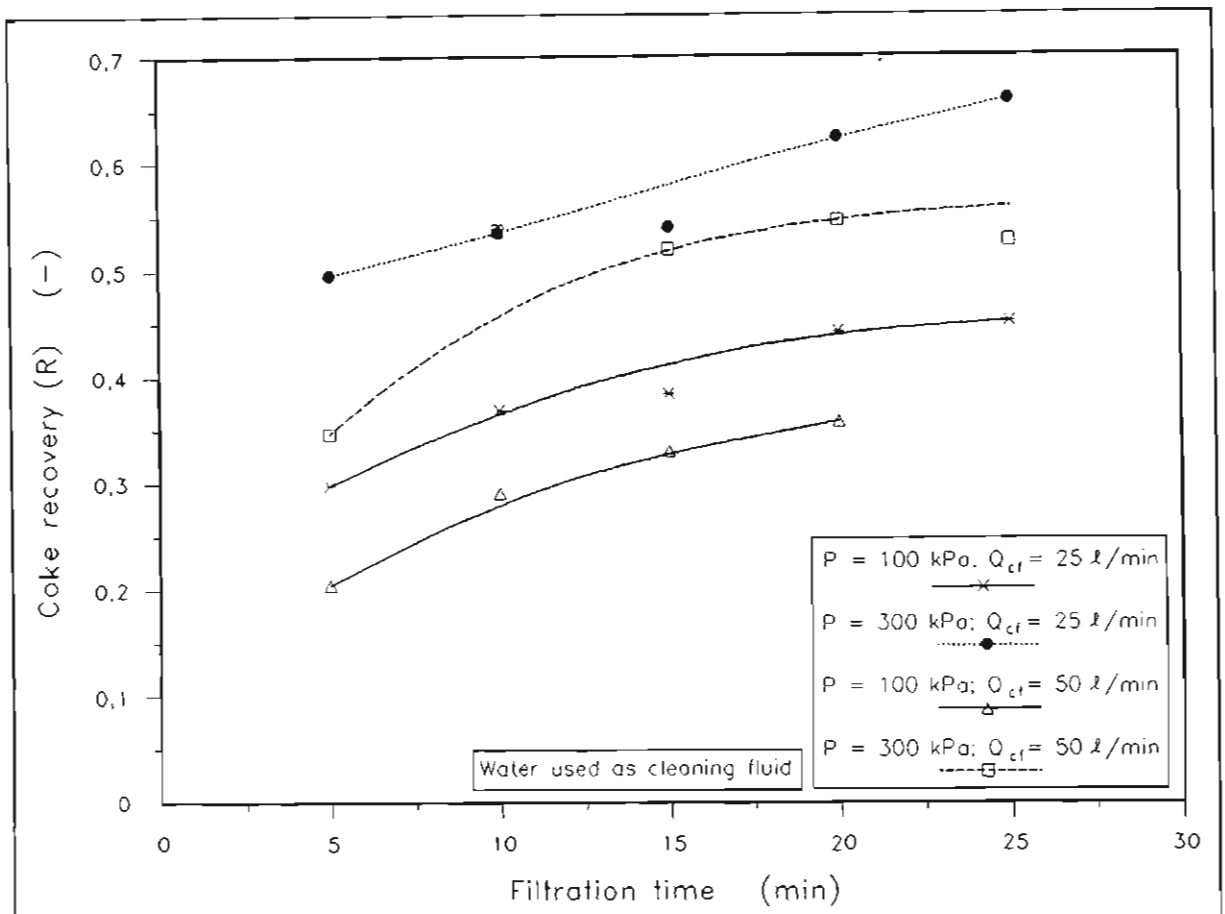

FIGURE 4.10 : Effect of Cleaning Fluid Flow Rate and Filtration Pressure on Cake Recovery (R)

As shown in Figure 4.10, cleaning fluid (water) flow rate, filtration pressure and filtration time (or mass of dry solids deposited per unit medium area, w_c) had an effect on overall cake recovery. An increase in filtration pressure resulted in a significant increase in overall cake recovery, while in general an increase in cleaning fluid (water) flow rate led to a decrease in cake recovery. It was also found that the longer the filtration time (or the higher w_c), the higher the overall cake recovery. This trend with filtration time (or w_c) was also found on the prototype unit, as shown in Figure 2.4 in Chapter 2.

The relationship between mass of dry solids deposited per unit medium area, w_c, and filtration time is shown in Figure 4.11 for filtration pressures of 100 kPa and 300 kPa. The values for w_c were obtained from the internal cylindrical filtration experiments in Chapter 3.

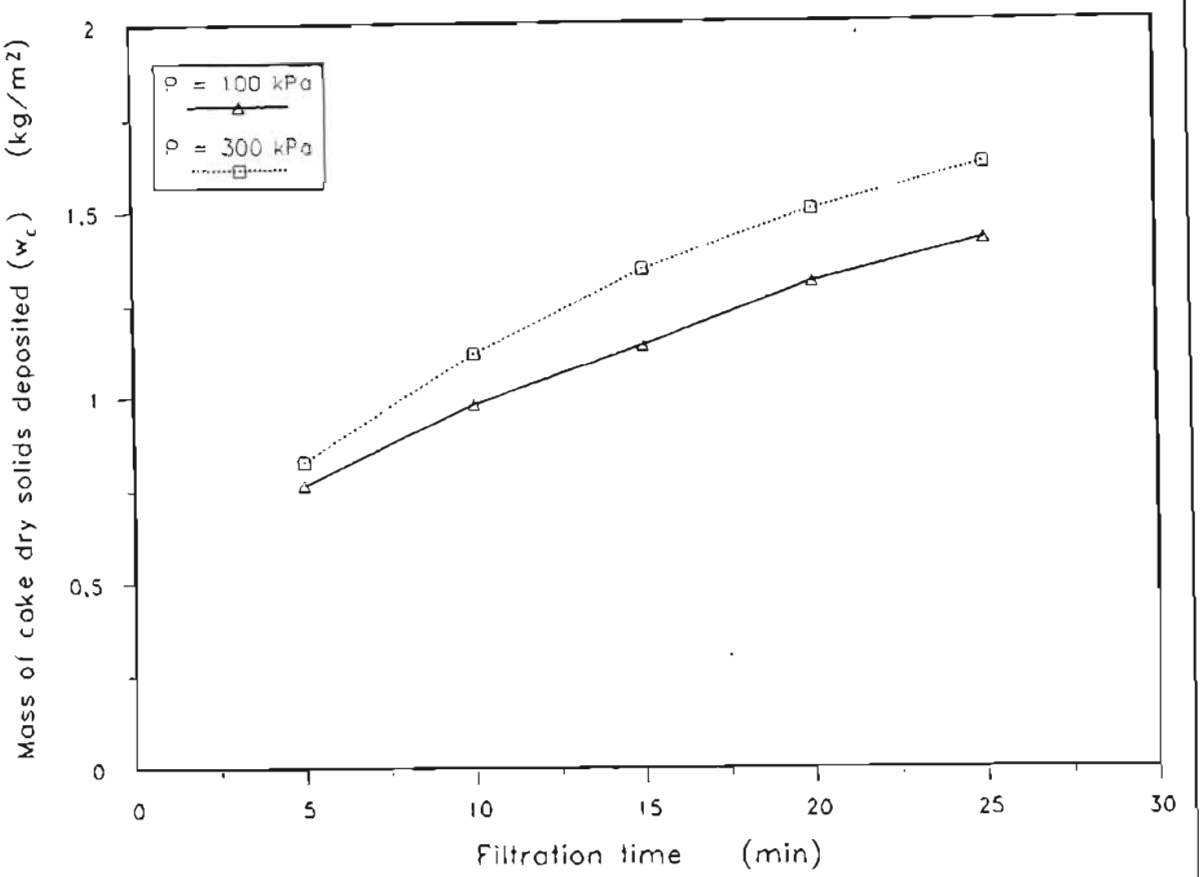

FIGURE 4.11 : Relationship Between Mass of Cake Dry Solids Deposited (w_c) and Filtration Time

4.6.1.2 <u>The effect of path length for hydraulic conveyance of flakes of cake on overall cake recovery, R</u>

The effect of path length on overall cake recovery is shown in Figures 4.12 and 4.13 for cleaning fluid (water) flow rates of 25 ℓ/min and 50 ℓ/min, respectively. The filtration pressure for the results given in Figures 4.12 and 4.13 was 300 kPa.

For both flow rates the cake recovery for the shorter path length of 1 m was higher than that for the longer path length of 4 m. The effect of path length on overall cake recovery decreased as the filtration time was increased for both cleaning fluid (water) flow rates. In fact as shown in Figure 4.13, at a filtration time of 25 minutes the cake recovery for the longer path length was slightly *less* than that for the shorter one.

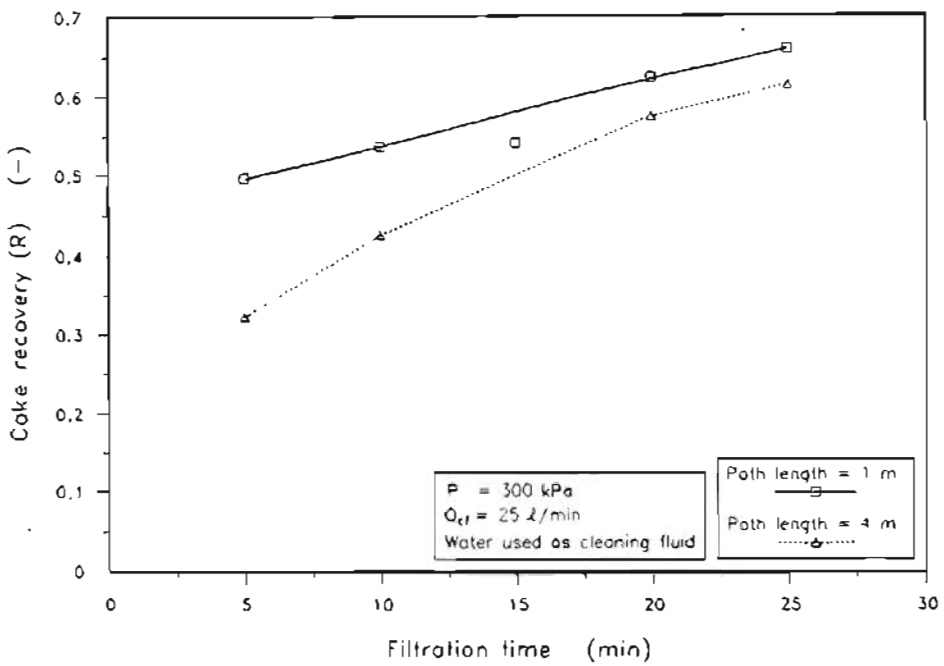

FIGURE 4.12 : Effect of Path Length on Cake Recovery for a Cleaning Fluid Flow Rate of 25 ℓ/min

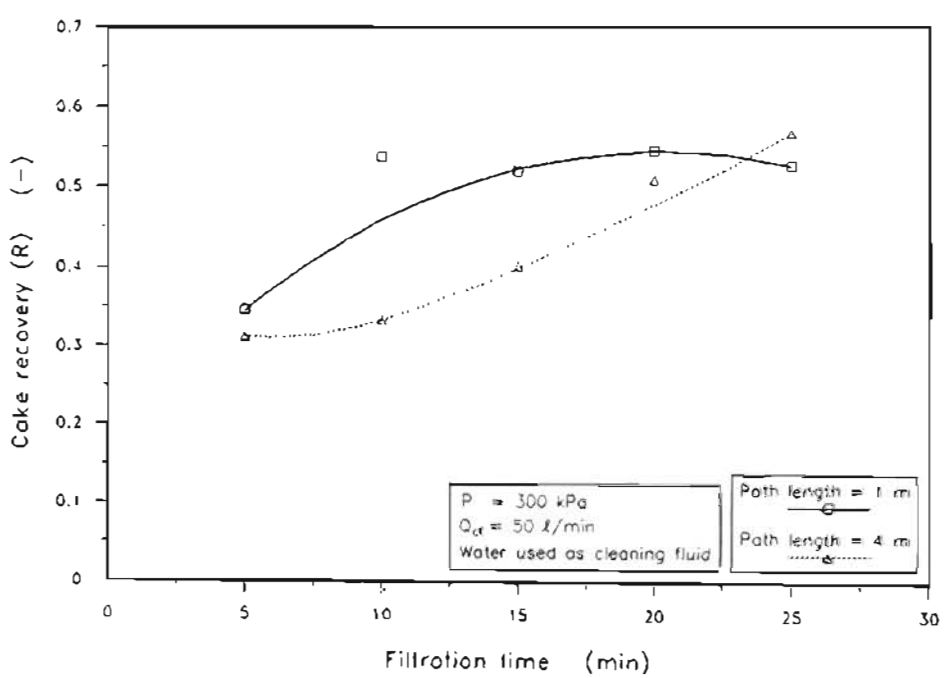

FIGURE 4.13 : Effect of Path Length on Cake Recovery for a Cleaning Fluid Flow Rate of 50 ℓ/min

4.6.2 Results of Experiments to Determine Cake Losses Due to the Shear of the Cleaning Fluid

As shown in the previous section significant cake losses occurred during the cleaning or cake removal process. One of the prime objectives of this study was to quantify the cake losses due to the shear of the cleaning fluid prior to the action of the rollers, and the combined losses due to the action of the rollers and the conveyance of the dislodged flakes of cake.

The cake losses due to the shear of the cleaning fluid were determined at two filtration pressures (100 kPa and 300 kPa) and two cleaning fluid (water) flow rates (approximately 25 ℓ/min and 50 ℓ/min).

The results for the shear experiments are shown in Appendix H. The fractional cake losses (on a dry solids basis) due to the shear of the cleaning fluid were defined as follows :

$$CL_s = 1 - \frac{w_s}{w_c} \qquad (4.30)$$

where CL_s = fraction of cake dry solids which is lost due to the shear of the cleaning fluid, (-)

w_c = total mass of cake dry solids deposited per unit medium area, (kg/m^2)

w_s = mass of cake dry solids per unit medium area remaining after shear of cleaning fluid, (kg/m^2)

4.6.2.1 Effect of cleaning fluid flow rate and filtration pressure on cake losses due to the shear of the cleaning fluid

The effect of cleaning fluid flow rate on cake losses due to shear is shown in Figures 4.14 and 4.15 at various filtration times for filtration pressures of 100 kPa and 300 kPa, respectively.

For both filtration pressures there was a significant increase in cake losses due to shear as the cleaning fluid flow rate was increased. There was no clear trend of cake losses with filtration time, however. The cake losses at a filtration pressure of 100 kPa were slightly higher than those at 300 kPa.

The cake losses due to shear for a set of experiments with feed sludge as cleaning fluid are also shown in Figure 4.15. Except for a filtration time of 20 minutes, there was no great difference between the water and feed sludge experiments.

For a filtration time of 20 minutes there were ripples on the internal cake surface (after shear) for the water experiments, while the internal cake surface (after shear) for the feed sludge experiments had a smooth appearance.

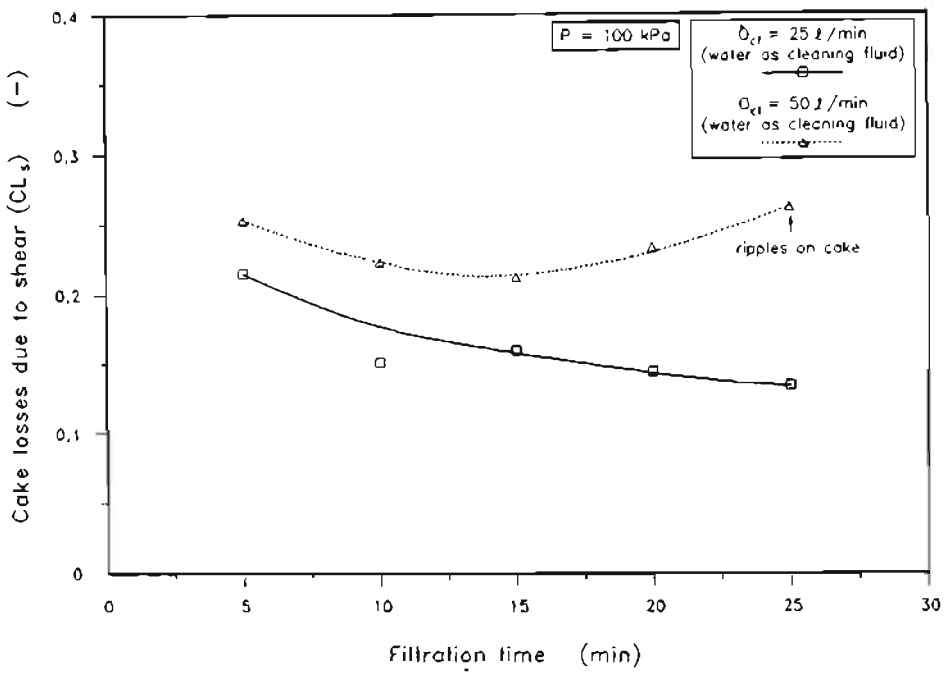

FIGURE 4.14 : Effect of Cleaning Fluid Flow Rate on Cake Losses Due to Shear at a Filtration Pressure of 100 kPa

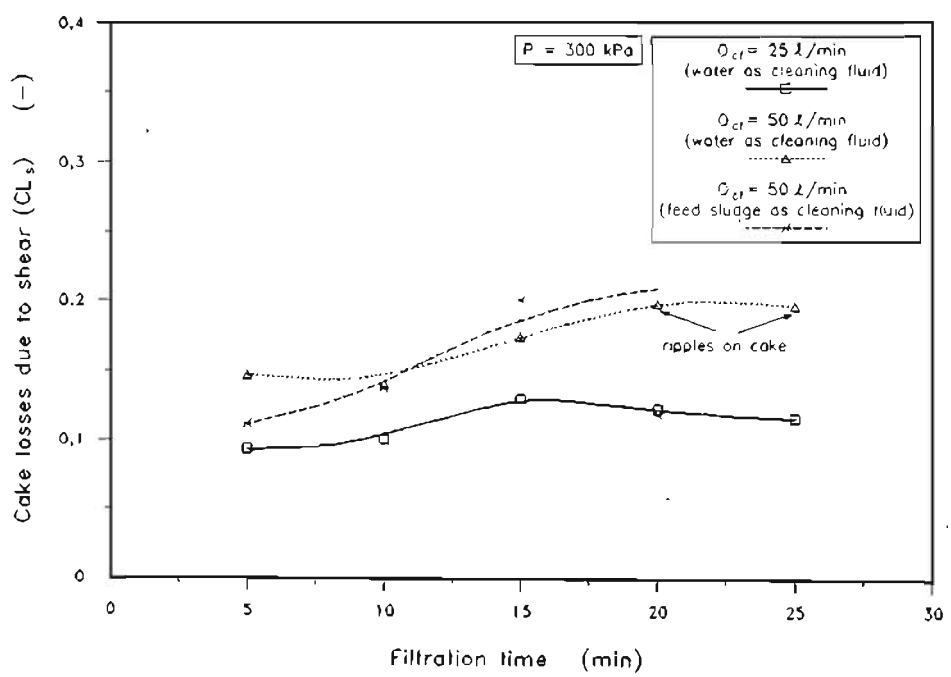

FIGURE 4.15 : Effect of Cleaning Fluid Flow Rate on Cake Losses Due to Shear at a Filtration Pressure of 300 kPa

4.6.2.2 Effect of shear of cleaning fluid on average cake dry solids concentration and internal cake diameter

The shear of the cleaning fluid resulted in significantly increased average cake dry solids concentrations when compared with those of the deposited (unscoured) cakes (as determined for the internal cylindrical filtration experiments in Chapter 3). This is shown for both cleaning fluid flow rates (25 ℓ/min and 50 ℓ/min) in Figures 4.16 and 4.17 for filtration pressures of 100 kPa and 300 kPa, respectively. As shown in Figures 4.16 and 4.17 the average cake dry solids concentration after shear was significantly higher than that for *planar* filtration. For both filtration pressures there was a slight increase in average cake dry solids concentration as the cleaning fluid (water) flow rate was increased.

The average cake dry solids concentrations for a set of experiments with feed sludge as cleaning fluid are also shown in Figure 4.17. There was no great difference between the water and feed sludge experiments.

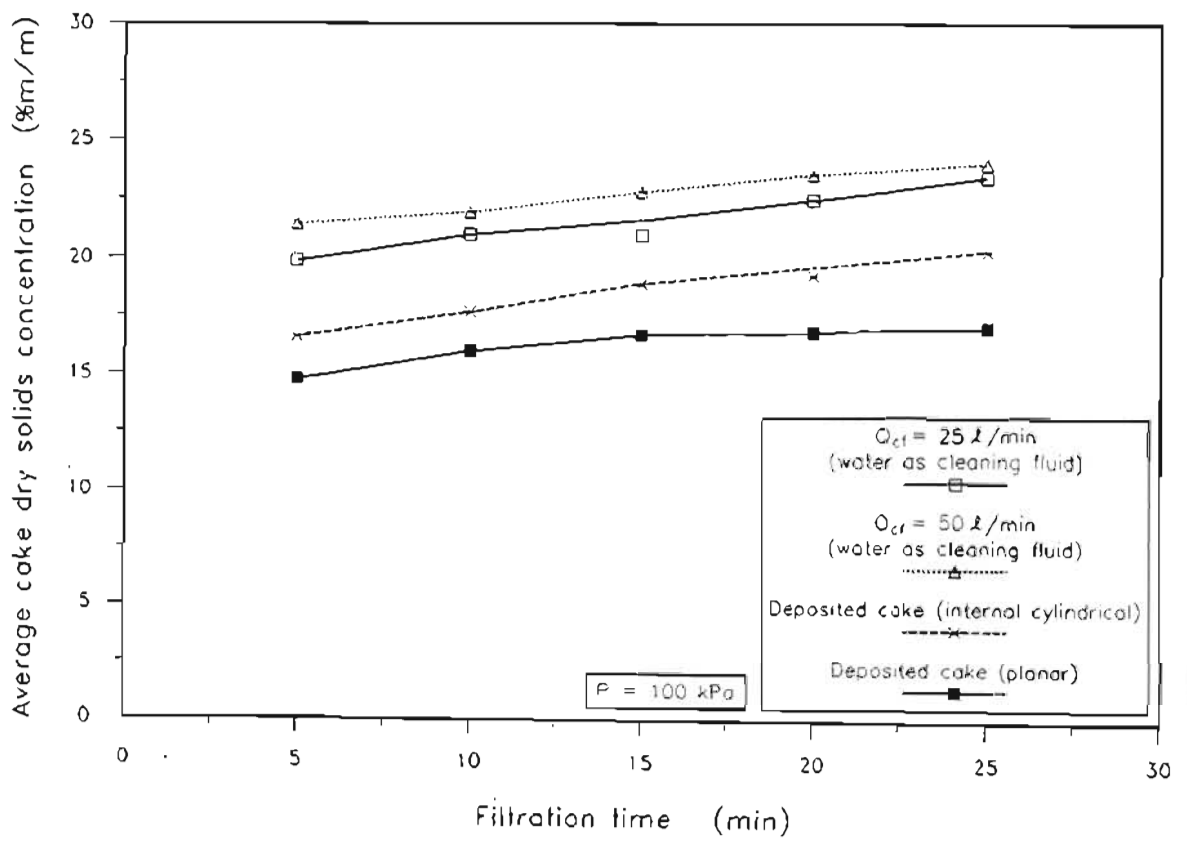

FIGURE 4.16 : Diagram Showing Increase in Average Cake Dry Solids Concentration Due to Shear of Cleaning Fluid at a Filtration Pressure of 100 kPa

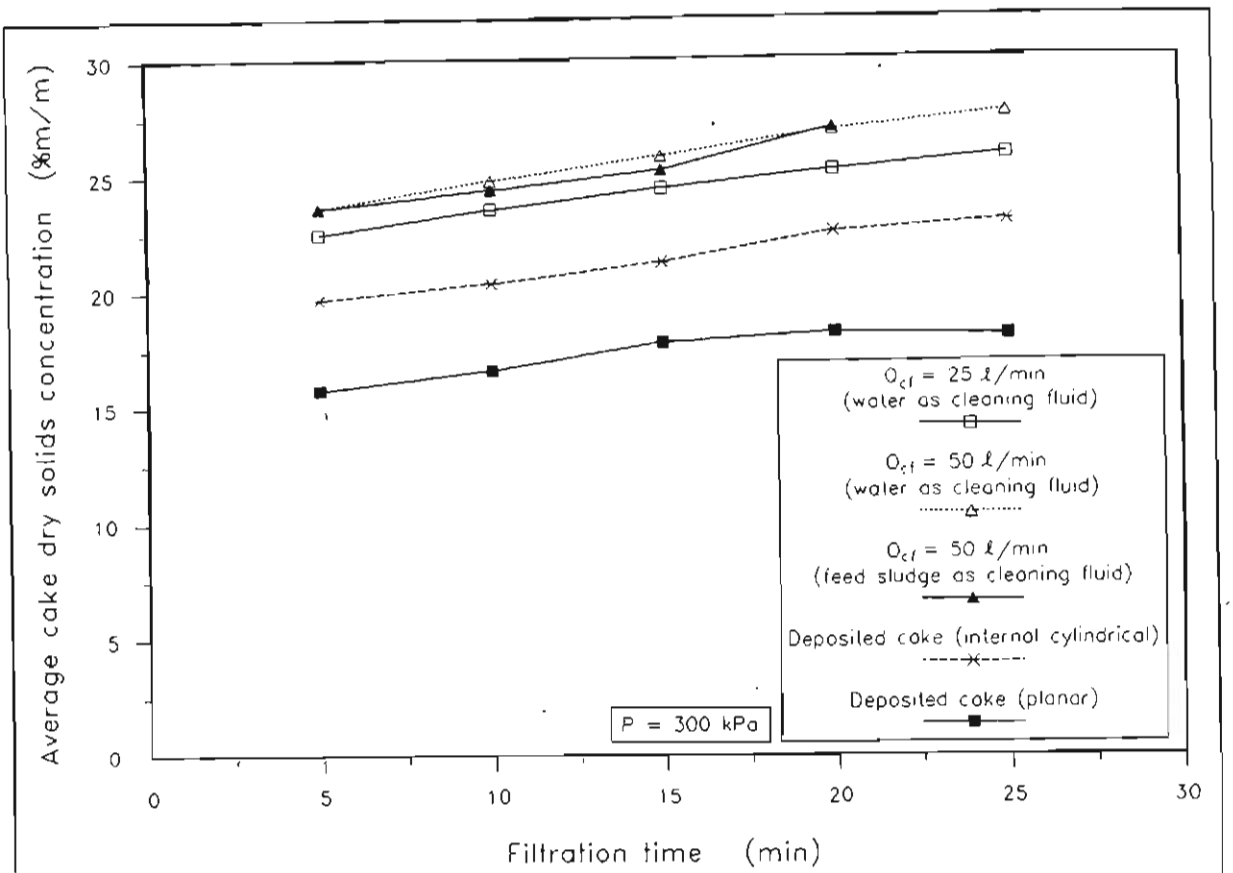

FIGURE 4.17 : Diagram Showing Increase in Average Cake Dry Solids Concentration Due to Shear of Cleaning Fluid at a Filtration Pressure of 300 kPa

The shear of the cleaning fluid also resulted in significantly increased internal cake diameters when compared with those of the deposited (unscoured) cakes (as determined for the internal cylindrical filtration experiments in Chapter 3). This is shown in Figures 4.18 and 4.19 for both cleaning fluid flow rates which were investigated and for filtration pressures of 100 kPa and 300 kPa, respectively.

The internal cake diameters for a set of experiments with feed sludge as cleaning fluid are also shown in Figure 4.19. Except for a filtration time of 20 minutes, the internal cake diameters for the feed sludge experiments were almost identical to those for the water experiments. The internal cake diameters shown in Figures 4.18 and 4.19 were calculated from the mass and the average cake dry solids concentration of the cake which remained inside the filter tube after a shear experiment. This method was used for the internal cylindrical filtration experiments and was mentioned in section 3.5.6 and outlined in Appendix D.

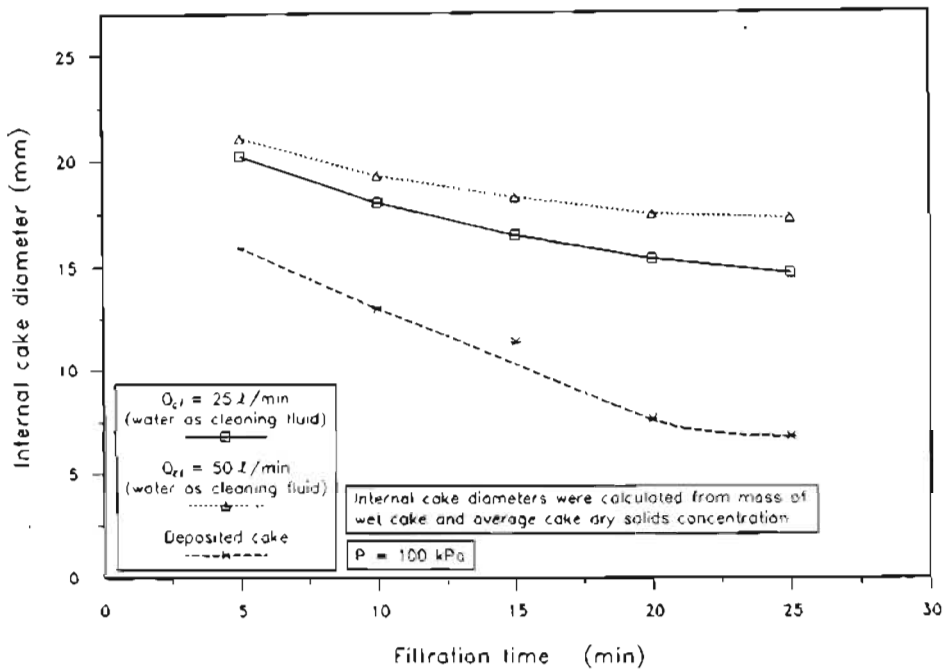

FIGURE 4.18 : Diagram Showing Increase in Internal Cake Diameter (Calculated) Due to Shear of Cleaning Fluid at a Filtration Pressure of 100 kPa

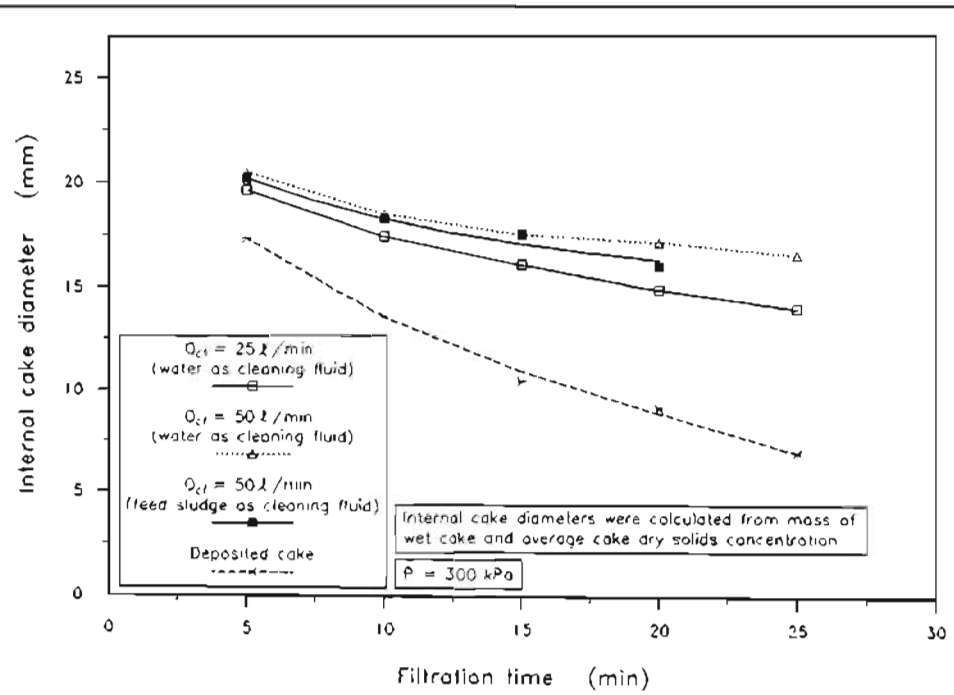

FIGURE 4.19 : Diagram Showing Increase in Internal Cake Diameter (Calculated) Due to Shear of Cleaning Fluid at a Filtration Pressure of 300 kPa

4.6.3 Results of Experiments to Determine Combined Cake Losses Due to Action of Rollers and Hydraulic Conveyance of Flakes of Cake

As shown in section 4.6.1.2, it was found that the longer the path length for the conveyance of the dislodged flakes of cake to the collecting sieve, the lower the cake recovery, R. This means that there are cake losses associated with the conveyance of flakes of cake in a pipe or porous tube. Unfortunately it was not possible to totally isolate the cake losses due to the action of the rollers when dislodging the cake from the inner tube wall from the hydraulic conveyance losses. For this reason it was decided to report all cake losses other than those ascribable to the shear of the cleaning fluid (prior to roller action), as *combined* cake losses due to the action of the rollers and hydraulic conveyance of flakes of cake.

The combined losses due to the action of the rollers and the hydraulic conveyance of the cake flakes from the porous tube onto the cake collecting sieve are given by the following equation :

$$CL_r = 1 - R - CL_s \qquad (4.31)$$

where CL_r = fraction of cake dry solids which is lost due to the action of the rollers and hydraulic conveyance of flakes of cake, (-)

4.6.3.1 Effect of filtration pressure on combined cake losses due to the action of the rollers and hydraulic conveyance of flakes of cake

The combined cake losses due to the action of the rollers and hydraulic conveyance of flakes of cake are shown in Figures 4.20 and 4.21 for filtration pressures of 100 kPa and 300 kPa and cleaning fluid (water) flow rates of 25 ℓ/min and 50 ℓ/min, respectively. The path length for results given in Figures 4.20 and 4.21 was 1 m.

As shown in both Figures 4.20 and 4.21, the cake losses for a filtration pressure of 300 kPa were significantly lower than those for a filtration pressure of 100 kPa.

Also, the combined cake losses due to the action of the rollers and hydraulic conveyance of flakes of cake decreased as filtration time was increased.

4.6.3.2 Effect of cleaning fluid flow rate on combined cake losses due to the action of the rollers and hydraulic conveyance of flakes of cake

The effect of cleaning fluid flow rate on combined cake losses due to the action of the rollers and hydraulic conveyance of flakes of cake is shown in Figures 4.22 and 4.23 for filtration pressures of 100 kPa and 300 kPa, respectively. The path length for the results given in Figures 4.22 and 4.23 was 1 m.

For a filtration pressure of 100 kPa there was no significant difference in cake losses between the two cleaning fluid flow rates which were investigated. For a filtration time of 5 minutes the losses at the higher flow rate were slightly higher than those at the lower flow rate.

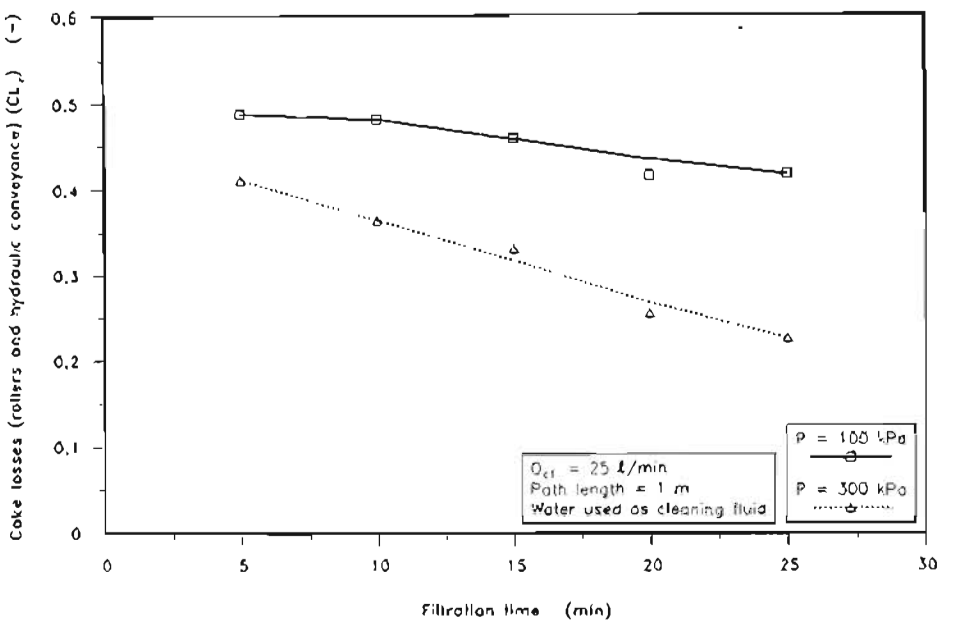

FIGURE 4.20 : Effect of Filtration Pressure on Combined Cake Losses Due to Action of Rollers and Hydraulic Conveyance of Cake Flakes at a Cleaning Fluid Flow Rate of 25 ℓ/min

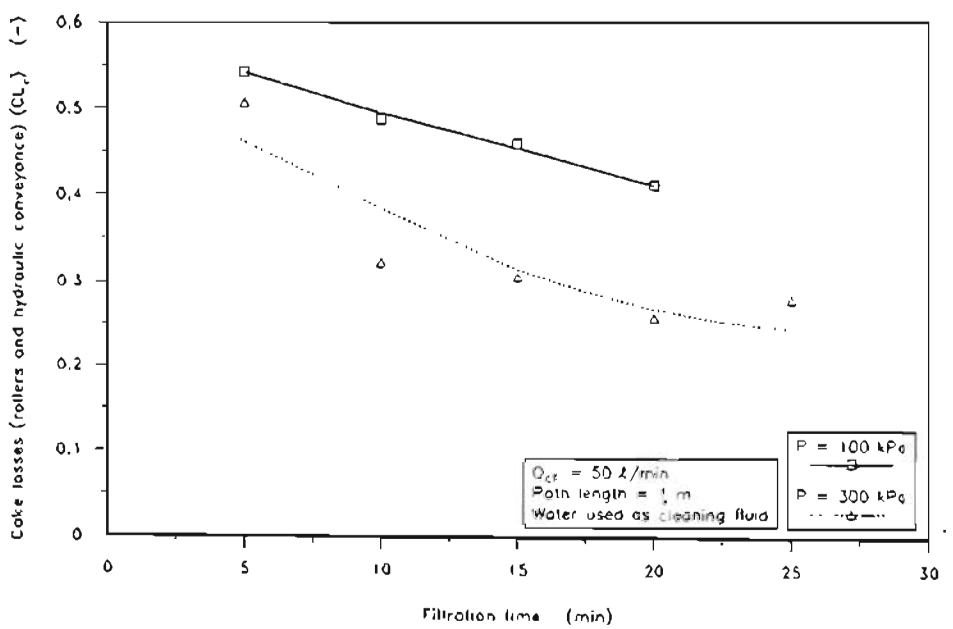

FIGURE 4.21 : Effect of Filtration Pressure on Combined Cake Losses Due to Action of Rollers and Hydraulic Conveyance of Cake Flakes at a Cleaning Fluid Flow Rate of 50 ℓ/min

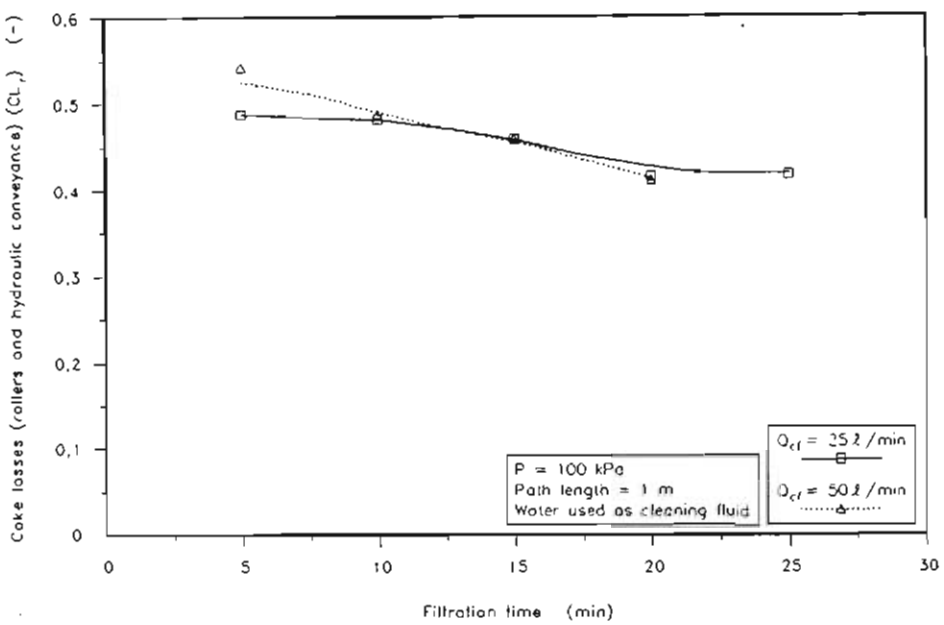

FIGURE 4.22 : Effect of Cleaning Fluid Flow Rate on Combined Cake Losses Due to Action of Rollers and Hydraulic Conveyance of Cake Flakes at a Filtration Pressure of 100 kPa

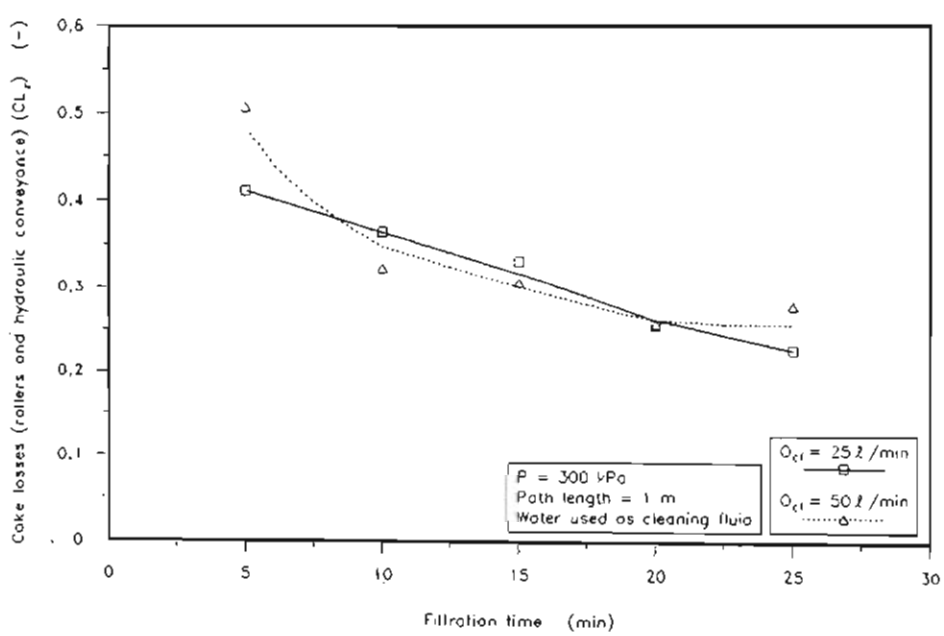

FIGURE 4.23 : Effect of Cleaning Fluid Flow Rate on Combined Cake Losses Due to Action of Rollers and Hydraulic Conveyance of Cake Flakes at a Filtration Pressure of 300 kPa

For a filtration pressure of 300 kPa the effect of cleaning fluid (water) flow rate was inconclusive, as shown in Figure 4.23. However, within the accuracy of the tests, the effect of cleaning fluid (water) flow rate on these cake losses was not very significant.

4.6.3.3 Breakdown of cake losses

The results of the previous sections have shown that cake losses during the cake removal cycle originate from three sources :

(i) shear action of the cleaning fluid prior to the removal of cake by the rollers;

(ii) action of the rollers when dislodging the cake, and;

(iii) hydraulic conveyance of dislodged flakes of cake.

An example of a breakdown of the various cake losses and the overall cake recovery is shown in Figure 4.24 for various filtration times. The filtration pressure for this example was 300 kPa, while the cleaning fluid (water) flow rate was 50 ℓ/min and the path length was 1 m.

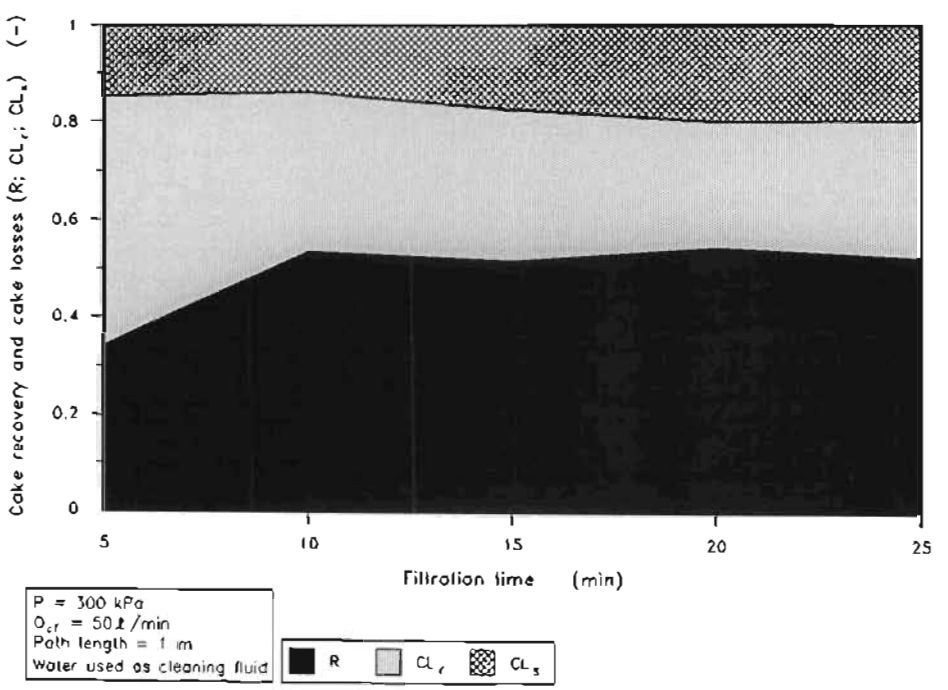

FIGURE 4.24 : Example of Breakdown of Cake Losses Showing the Fraction of the Cake which is Recovered (R), the Fraction which is Lost Due to the Shear of the Cleaning Fluid (CL_s) and the Fraction which is Lost Due to the Rollers and Hydraulic Conveyance (CL_r)

As shown in Figure 4.24, approximately half of the deposited cake was recovered (on the sieve) after roller action and hydraulic conveyance, while approximately half of the deposited cake was lost (due to cleaning fluid shear, roller action and hydraulic conveyance). The cake recovery, R, initially increased with filtration time and thereafter remained essentially constant. The greater portion of the cake losses for this specific case was due to the action of the rollers and hydraulic conveyance. The fraction of these cake losses decreased with filtration time, however, while the losses due to the shear of the cleaning fluid increased with filtration time.

4.6.3.4 Average cake dry solids concentration of *recovered* cake

A reasonable correlation was found between the average dry solids concentration of the cake which remained inside the filter tube after the shear of the cleaning fluid (prior to roller removal) and that which was recovered on the sieve after removal by the rollers and hydraulic conveyance. This is illustrated in Figures 4.25 and 4.26 for various filtration times and for filtration pressures of 100 kPa and 300 kPa, respectively. The average cake dry solids concentrations for the *deposited* cakes (from the internal cylindrical filtration experiments in Chapter 3) are also shown in Figures 4.25 and 4.26.

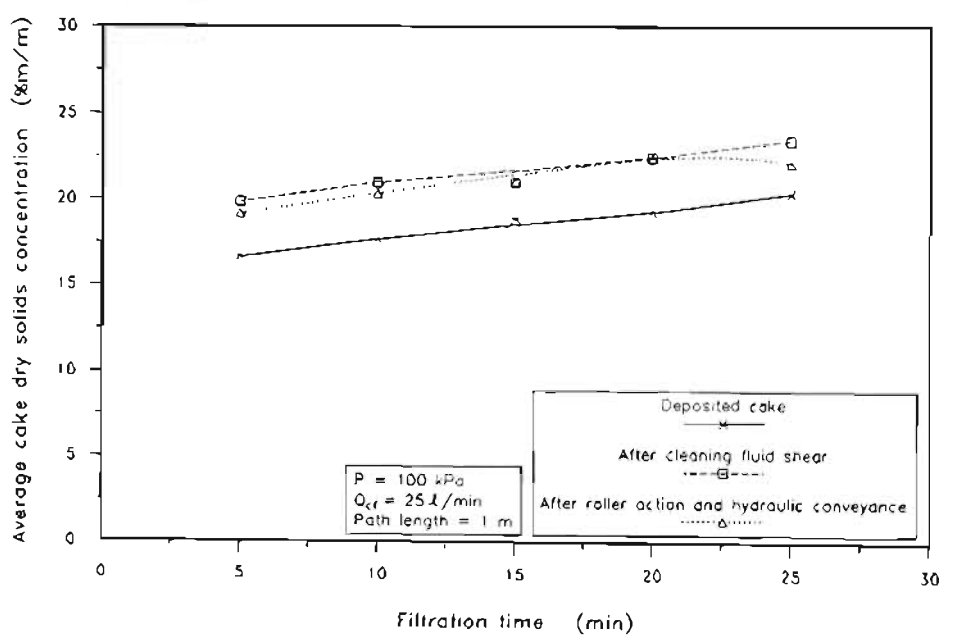

FIGURE 4.25 : Comparison Between Experimental Average Cake Dry Solids Concentrations at a Filtration Pressure of 100 kPa and a Cleaning Fluid Flow Rate of 25 ℓ/min

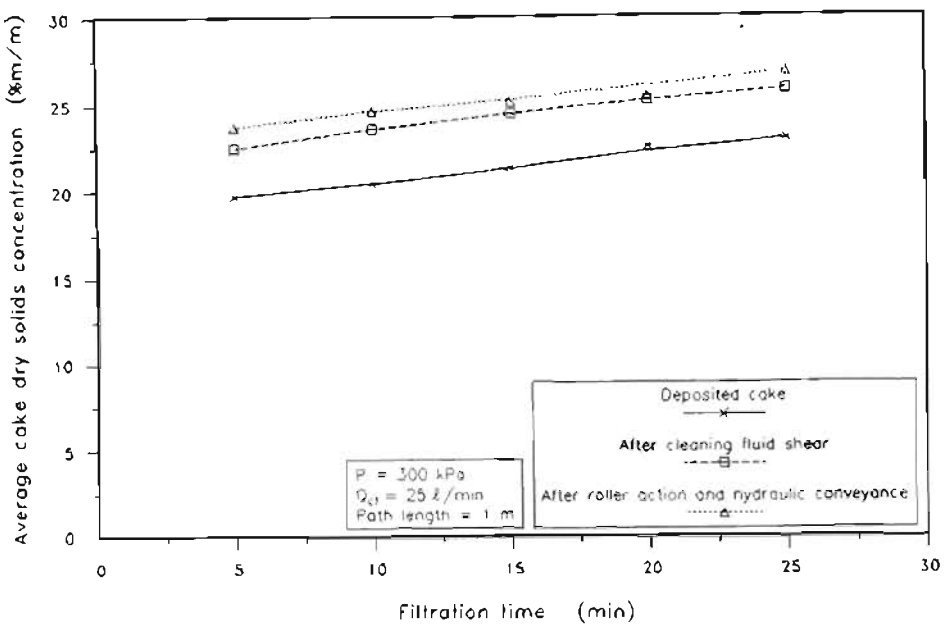

FIGURE 4.26 : Comparison Between Experimental Average Cake Dry Solids Concentrations at a Filtration Pressure of 300 kPa and a Cleaning Fluid Flow Rate of 25 ℓ/min

4.6.4 Results of the Rheology Experiments

4.6.4.1 Examples of pseudo-shear diagrams obtained from capillary-tube viscometer experiments

The results of the capillary-tube viscometer experiments are tabulated in Appendix I.

As illustrative examples, the pseudo-shear diagrams for two sludges with solids concentrations of 12,80 % m/m and 16,71 % m/m are shown in Figure 4.27. The pseudo-shear diagrams for these two solids concentrations are very close to those for an ideal Bingham plastic (see Figure 4.6). The τ_w axis intercept and the slope of the linear portion of the pseudo-shear diagram were calculated from a linear regression using the points of the linear portion of the pseudo-shear diagram. From equation (4.22) :

$$\tau_o = \frac{3}{4}(Y\text{-}axis\ (\tau_w)\ intercept) \qquad (4.32)$$

and

$$\eta = slope\ of\ linear\ portion\ of\ pseudo\text{-}shear\ diagram \qquad (4.33)$$

This procedure was followed for each solids concentration.

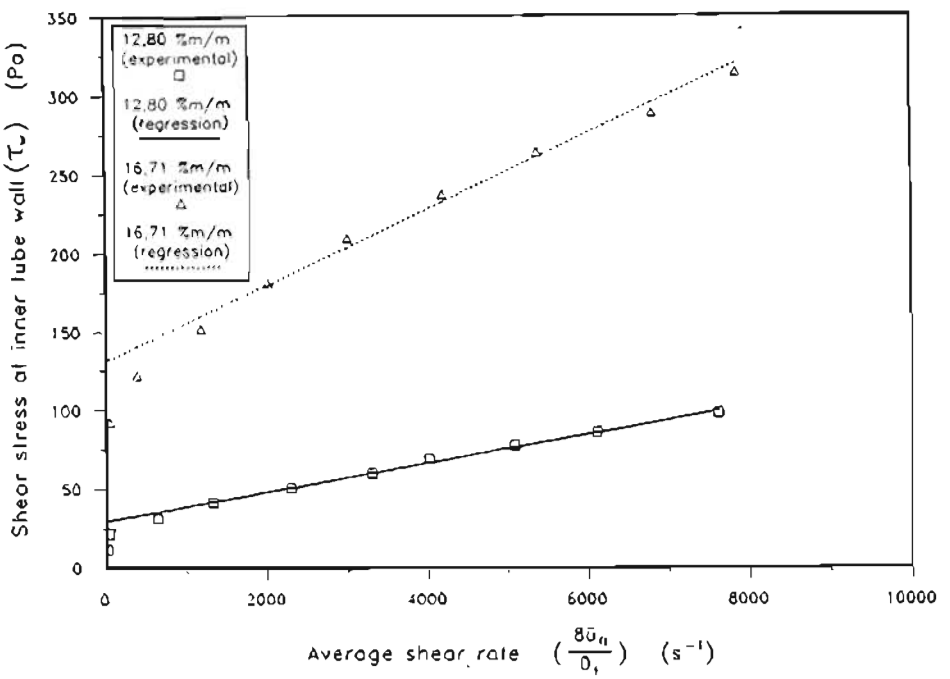

FIGURE 4.27 : Pseudo-shear Diagram for Two Sludge Solids Concentrations

TABLE 4.1
The Variation of Yield Stress (τ_o) and Coefficient of Rigidity (η) with Solids Concentration

Solids concentration (% m/m)	τ_o (Pa)	η (Pa.s x 10^3)	r^2 (-)
3,58	0,12	3,10	0,988
4,66	0,16	3,71	0,998
5,00	0,16	3,92	0,997
5,73	0,68	4,38	0,988
6,04	0,79	4,20	0,994
7,01	1,44	5,13	0,996
7,85	2,62	6,11	0,992
8,72	3,21	6,81	0,992
9,90	6,51	8,17	0,993
11,10	15,17	8,94	0,993
12,80	22,43	9,09	0,996
14,27	38,14	14,58	0,998
15,31	64,05	17,89	0,997
16,71	98,37	24,03	0,987

The yield stresses (τ_o) and coefficients of rigidity (η) for all the solids concentrations are summarized in Table 4.1, together with the regression coefficients for the linear regressions.

The regression coefficients shown in Table 4.1 indicate that a good linear fit was obtained for all solids concentrations which were investigated.

It was found that there was a reasonable fit between the yield stress (τ_o) data and the following equation, as shown in Figure 4.28(a).

$$\tau_o = \frac{7.3268 \times 10^{-4} e^{0.1270 c_s}}{1.4292 c_s^{-3.5805}} \qquad (4.34)$$

where c_s = solids concentration of sludge (cake), (% m/m)

The constants in equation (4.34) were obtained from a SAS[1] least squares non-linear regression package.

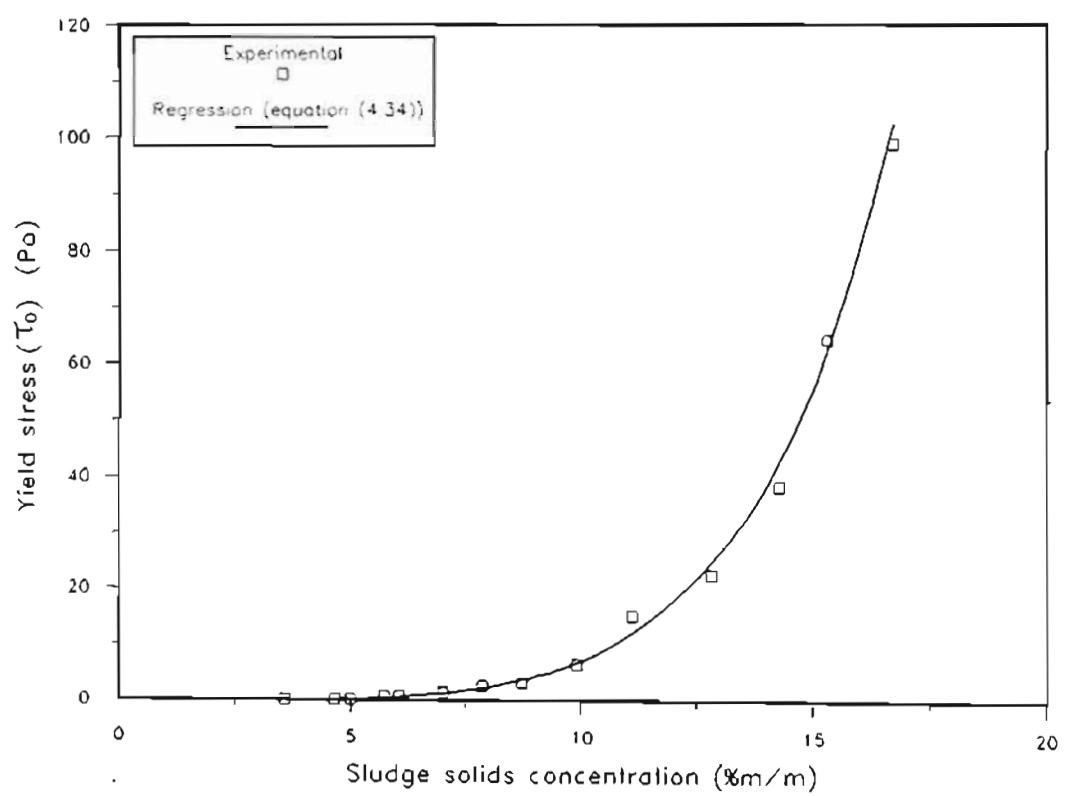

FIGURE 4.28(a) : Graph Showing the Variation of Yield Stress with Sludge Solids Concentration (Experimental and Regression)

1 SAS Institute Incorporated, Cary, North Carolina, USA.

From a linear regression it was found that for the solids concentration range, 3,58 % m/m $\leq c_s \geq$ 11,1 % m/m, there was a reasonable fit between the coefficient of rigidity (η) and the following equation, as shown in Figure 4.28(b) :

$$\eta = 8.1422 \times 10^{-4} c_s - 2.1914 \times 10^{-4} \qquad (4.35)$$

The square of the correlation coefficient, r^2, for the linear regression was 0,980.

The solids concentration range for equation (4.35) (3,58 % m/m $\leq c_s \geq$ 11,1 % m/m) was found to be sufficient for the cross-flow microfiltration model which was developed in Chapter 5 (see Figure 5.29). (It should be noted that the coefficient of rigidity for the sludge was not required for the shear model which was developed in section 4.3).

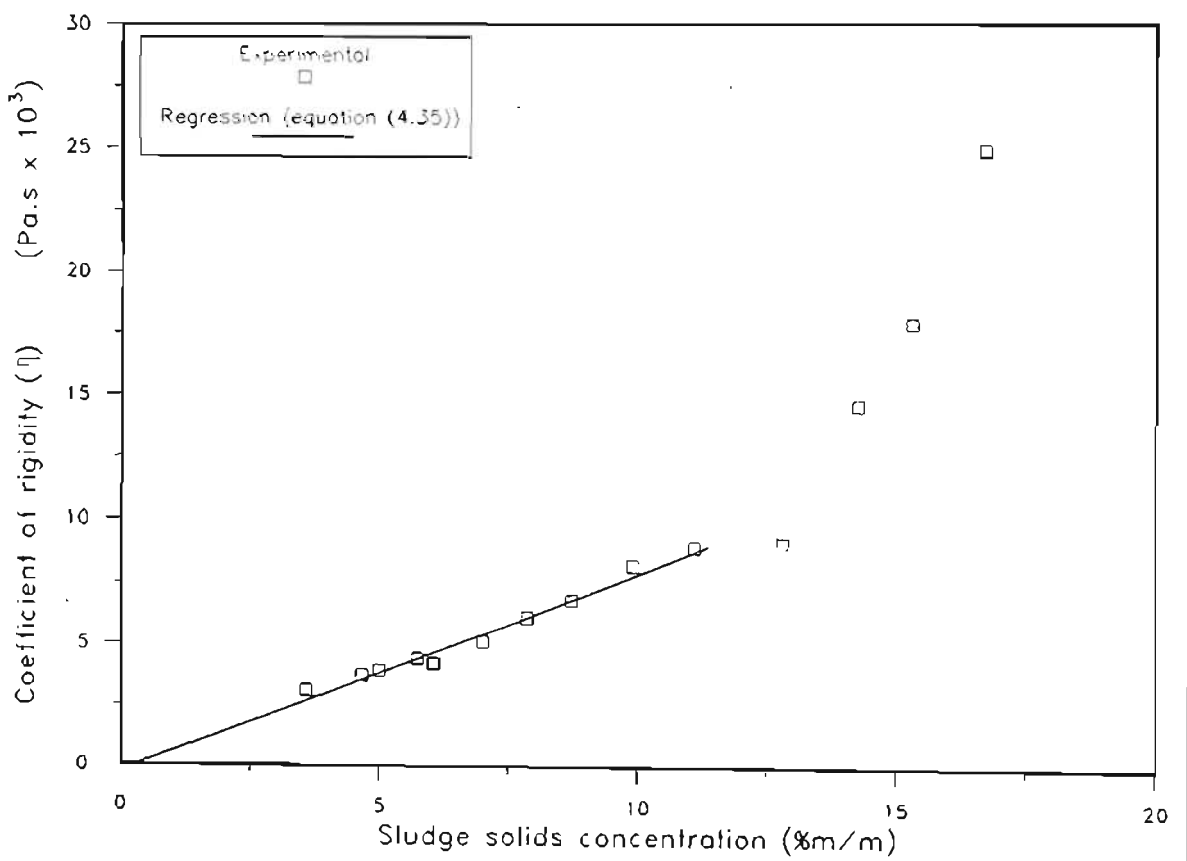

FIGURE 4.28(b) : Graph Showing the Variation of Coefficient of Rigidity with Sludge Solids Concentration (Experimental and Regression)

4.7 COMPARISON BETWEEN PROPOSED SHEAR MODEL AND EXPERIMENTAL RESULTS

4.7.1 Calculation of Radial Variation of τ_{oc} for Cake and τ_w for Cleaning Fluid

The computer program which was used in Chapter 3 for the modelling of internal cylindrical filtration was modified slightly to incorporate the shear model which was developed in section 4.3.

The modified computer program calculated the radial porosity (ϵ) profile from the solids compressive pressure (p_s) profile using set of equations (3.81), (3.82) or (3.83). The radial solids concentration profile through the cake was calculated from the radial porosity profile using equation (4.37) which was derived as follows.

From equation (3.53) :

$$\epsilon = \frac{\frac{z}{\rho_l}}{\frac{z}{\rho_l} + \frac{(1-z)}{\rho_s}} \qquad (3.53)$$

where z = mass fraction of moisture in cake, (-)
ϵ = local porosity of cake or sediment, (-)
ρ_l = liquid density, (kg/m^3)
ρ_s = solids density, (kg/m^3)

From the definition of c_s and z :

$$c_s = (1 - z) \times 100 \qquad (4.36)$$

Therefore, combining equations (3.53) and (4.36) :

$$c_s = \left[1 - \left(\frac{\frac{\epsilon}{\rho_s}}{\frac{\epsilon}{\rho_s} + \left(\frac{1-\epsilon}{\rho_l} \right)} \right) \right] \times 100 \qquad (4.37)$$

The radial yield stress (τ_{oc}) profile through the cake was calculated from the radial cake solids concentration profile using equation (4.34).

The radial variation of τ_w for a certain flow rate of the cleaning fluid was calculated from equations (4.5b), (4.6) and (4.7). The surface roughness in equation (4.6) was taken as the mass average particle size of the waterworks sludge; i.e. 5,90 μm. The mass average particle size for the sludge was determined from a particle size analysis as shown in Appendix F.

An example of the radial variation of τ_{oc} (for the cake) and τ_w (for the cleaning fluid) is shown in Figure 4.29. Set of equations (3.82) was used for the prediction of τ_{oc}. According to the hypothesis of the shear model, the theoretical internal cake radius (r_2) after the shearing of the deposited cake should occur where :

$$\tau_{oc} = \tau_{w} \qquad (4.38)$$

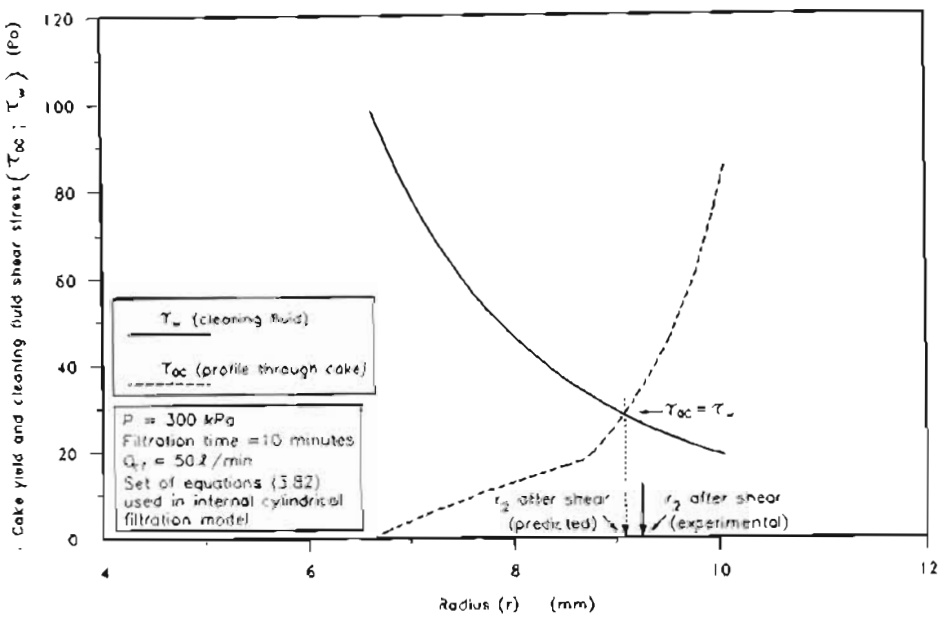

FIGURE 4.29 : Graph Showing the Radial Variation of Cake Yield Stress (τ_{oc}) and Cleaning Fluid Shear Stress (τ_w) as well as the Predicted and Experimental Internal Cake Radii After Shear of the Cleaning Fluid

The predicted and experimental internal cake radii are shown in Figure 4.29.

4.7.2 Comparison Between Predicted and Experimental Results

The predicted and experimental internal cake diameters (after shear) for various filtration times are shown in Figures 4.30(a) and 4.30(b) and Figures 4.31(a) and 4.31(b) for cleaning fluid (water) flow rates of approximately 25 ℓ/min and 50 ℓ/min and for filtration pressures of 100 kPa and 300 kPa, respectively.

As shown in Appendix H, the experimental internal cake diameters (after shear) were determined using two methods :

(i) indirectly by calculation from the mass of wet cake and the average cake dry solids concentration. The method was also used for the internal cylindrical filtration experiments in Chapter 3;

(ii) by direct measurement using a vernier calliper (where possible).

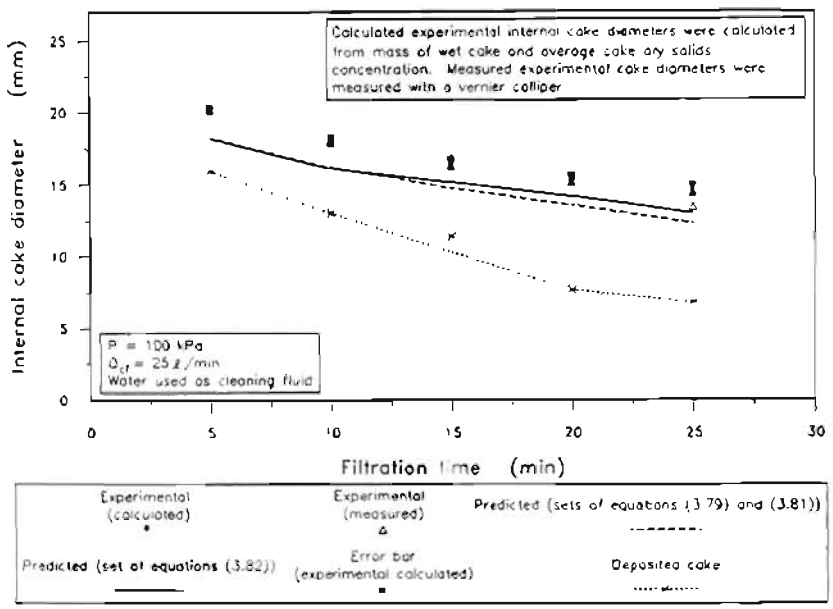

FIGURE 4.30(a) : Comparison Between Experimental and Predicted Internal Cake Diameters After Shear for P = 100 kPa and Q_{cf} = 25 ℓ/min (Water as Cleaning Fluid)

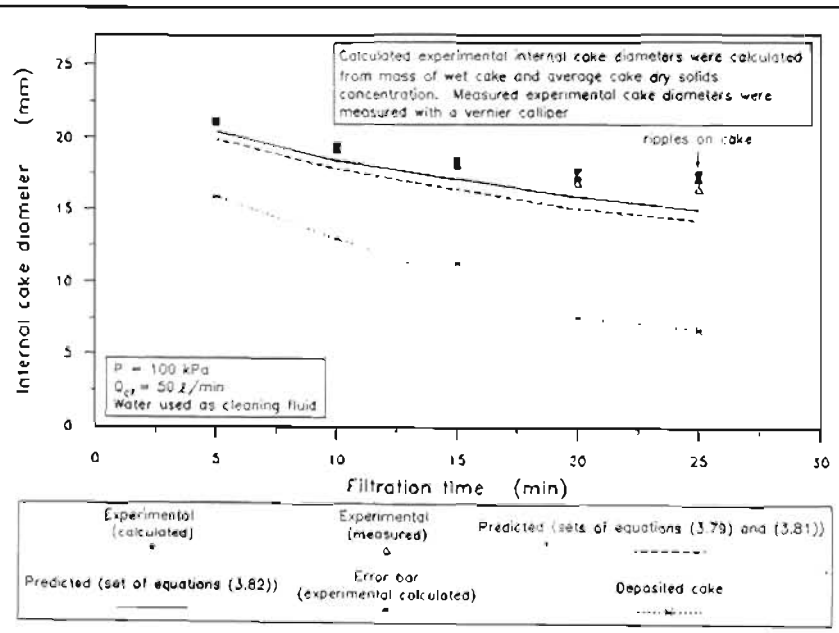

FIGURE 4.30(b) : Comparison Between Experimental and Predicted Internal Cake Diameters After Shear for P = 100 kPa and Q_{cf} = 50 ℓ/min (Water as Cleaning Fluid)

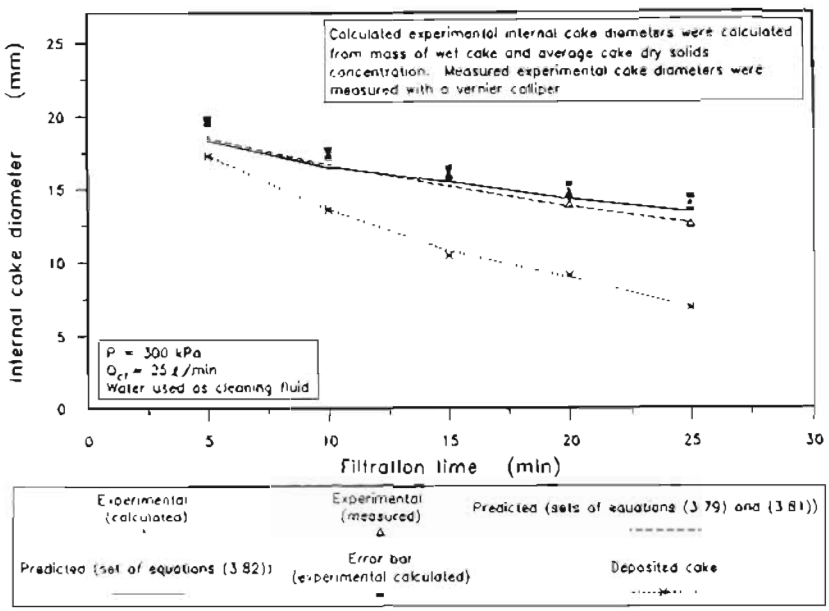

FIGURE 4.31(a) : Comparison Between Experimental and Predicted Internal Cake Diameters After Shear for P = 300 kPa and Q_{cf} = 25 ℓ/min (Water as Cleaning Fluid)

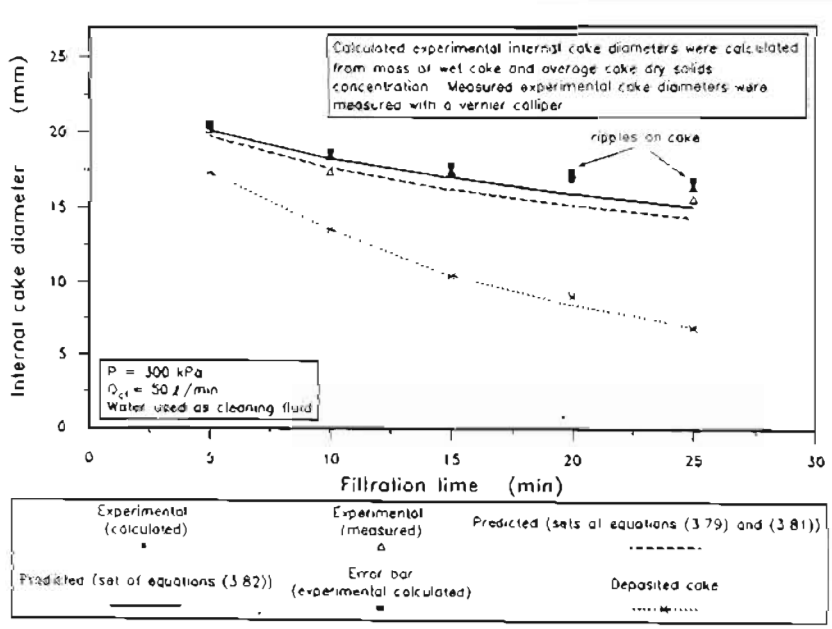

FIGURE 4.31(b) : Comparison Between Experimental and Predicted Internal Cake Diameters After Shear for P = 300 kPa and Q_{cf} = 50 ℓ/min (Water as Cleaning Fluid)

The calculated and measured (by vernier calliper) experimental internal cake diameters are shown in Figures 4.30(a) and (b) and 4.31(a) and (b). For most of the experimental points there was close agreement between the calculated and measured experimental internal cake diameters. For the cases where there was a discrepancy between the calculated and measured experimental internal cake diameters, the measured experimental internal cake diameters were closer to the *predicted* (from the model) internal cake diameters than the calculated experimental internal cake diameters.

The calculated experimental internal cake diameters for the *deposited* cakes (from the internal cylindrical filtration experiments in Chapter 3) are also shown in Figures 4.30(a) and (b) and 4.31(a) and (b). Predicted curves for sets of equations (3.79) and (3.81) and set of equations (3.82) in the internal cylindrical filtration model are shown in Figures 4.30(a) and (b) and 4.31(a) and (b). As shown, the predicted curves using set of equations (3.82) gave a slightly better fit than those using sets of equations (3.79) and (3.81). The error bars for the calculated experimental internal cake diameters (after shear) are based on the same error estimates that were used for the calculated experimental internal cake diameters for the internal cylindrical filtration experiments in Chapter 3. The agreement between experimental and predicted internal cake diameters was not as good for 100 kPa as for 300 kPa.

For both filtration pressures and cleaning fluid (water) flow rates the predicted internal cake diameters were lower than the experimental internal cake diameters (see section 4.9.2). For all experiments except for the three experiments marked in Figures 4.30(b) and 4.31(b) the internal cake surface after scouring had a smooth appearance. For these three experiments there were marked ripples on the internal cake surface after the applied fluid shear.

The comparison between predicted and experimental internal cake diameters for the experiments where *feed sludge* was used as the cleaning fluid, is shown in Figure 4.32. For the feed sludge experiments there was very close agreement between the experimental and predicted (using set of equations (3.82) in the internal cylindrical filtration model) internal cake diameters.

The wall shear stress, τ_w, for the feed sludge experiments was determined by assuming that the feed sludge was a *Newtonian* fluid. The solids concentration of the feed sludge was 53,32 g/ℓ or 5,17 % m/m. From Table 4.1 it is evident that the yield stress for this solids concentration was very low ($\approx$ 0,16 Pa). According to Wasp et al. (1979), various researchers have found that if the yield stress of a Bingham plastic fluid is low (< 24 Pa for thorium oxide suspensions), then the frictional pressure drop in the turbulent regime may be calculated by assuming that such a fluid is *Newtonian* with the coefficient of rigidity, η, equal to the viscosity, μ. The coefficient of rigidity of the feed sludge was estimated to be 4,03 x 10^{-3} Pa.s by interpolation between the coefficients of rigidity for sludge solids concentrations of 5,00 % m/m and 5,73 % m/m (see Table 4.1).

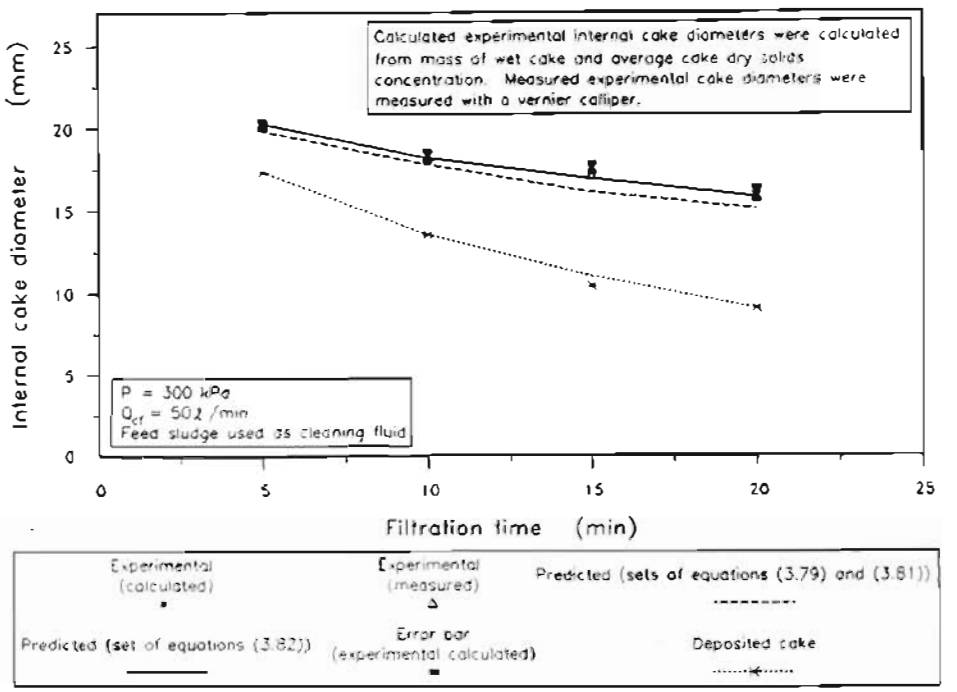

FIGURE 4.32 : Comparison Between Experimental and Predicted Internal Cake Diameters After Shear for P = 300 kPa and Q_{cf} = 50 ℓ/min (Feed Sludge as Cleaning Fluid)

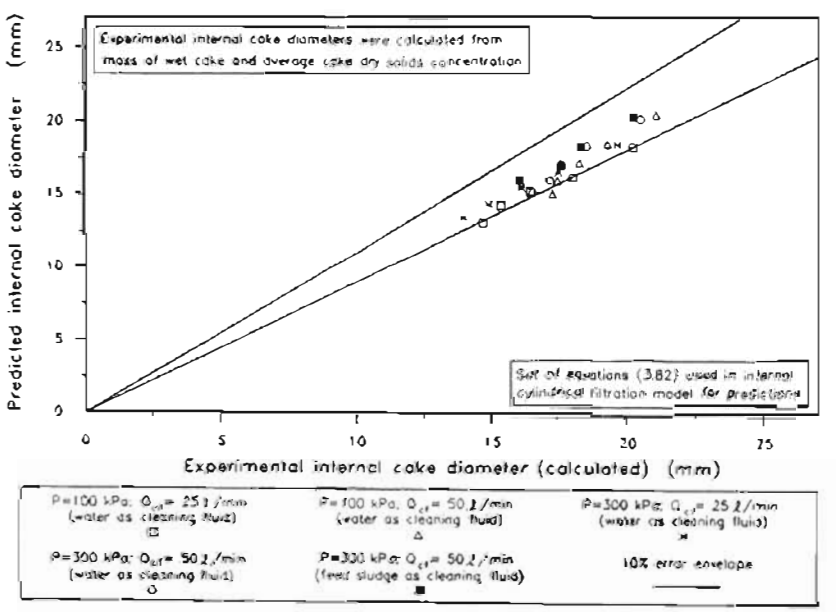

FIGURE 4.33 : Overall Comparison Between Experimental (Calculated) and Predicted Internal Cake Diameters

The overall comparison between experimental (calculated) and predicted internal cake diameters (using set of equations (3.82) in the internal cylindrical filtration model) is shown in Figure 4.33 for all experiments including those for which feed sludge was used as a cleaning fluid. With the exception of two data points, the bulk of the predictions lie within 10 % of the experimental observations.

The comparison between experimental and predicted average cake dry solids concentrations at various filtration times is shown in Figures 4.34(a) and (b) and Figures 4.35(a) and (b) for cleaning fluid (water) flow rates of approximately 25 ℓ/min and 50 ℓ/min and for filtration pressures of 100 kPa and 300 kPa, respectively. The comparison between experimental and predicted average cake dry solids concentrations for the experiments for which feed sludge was used as a cleaning fluid, is shown in Figure 4.36. The predicted average cake dry solids concentrations using sets of equations (3.79) and (3.81) and set of equations (3.82) in the internal cylindrical filtration model are shown in Figures 4.34(a) and (b), 4.35(a) and (b) and 4.36.

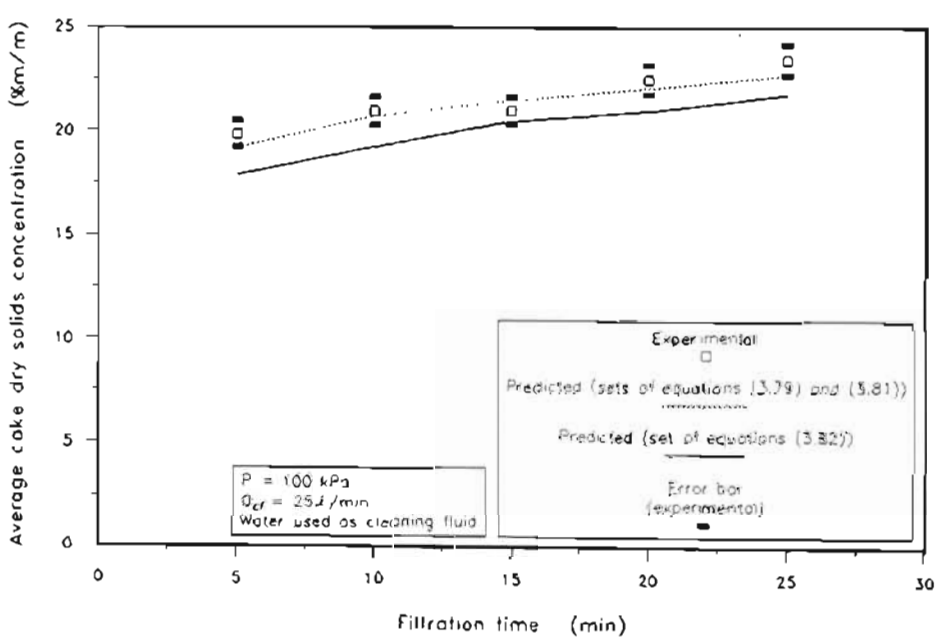

FIGURE 4.34(a) : Comparison Between Experimental and Predicted Average Cake Dry Solids Concentrations for P = 100 kPa and Q_{cf} = 25 ℓ/min (Water as Cleaning Fluid)

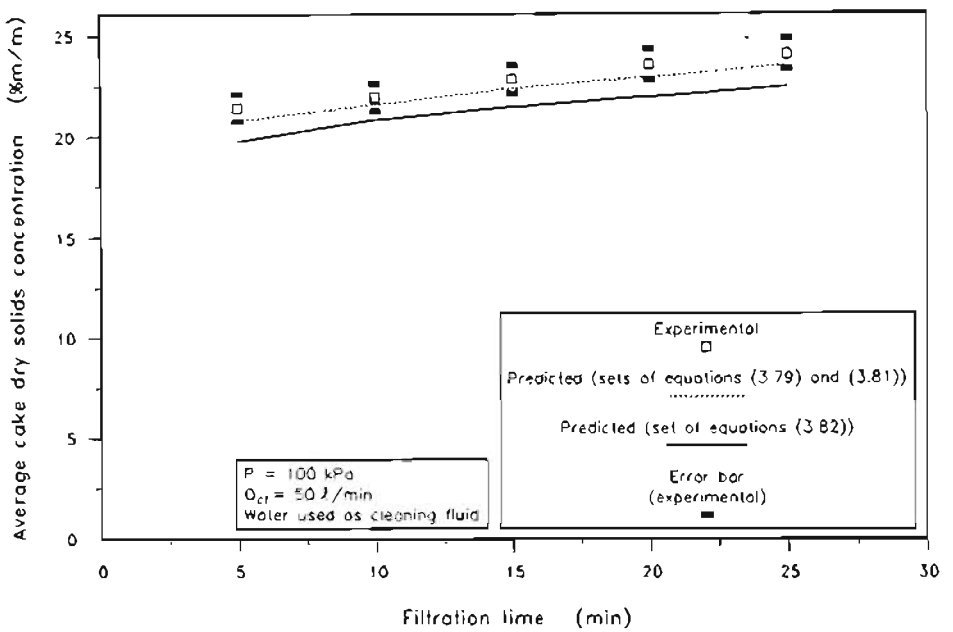

FIGURE 4.34(b) : Comparison Between Experimental and Predicted Average Cake Dry Solids Concentrations for P = 100 kPa and Q_{cf} = 50 ℓ/min (Water as Cleaning Fluid)

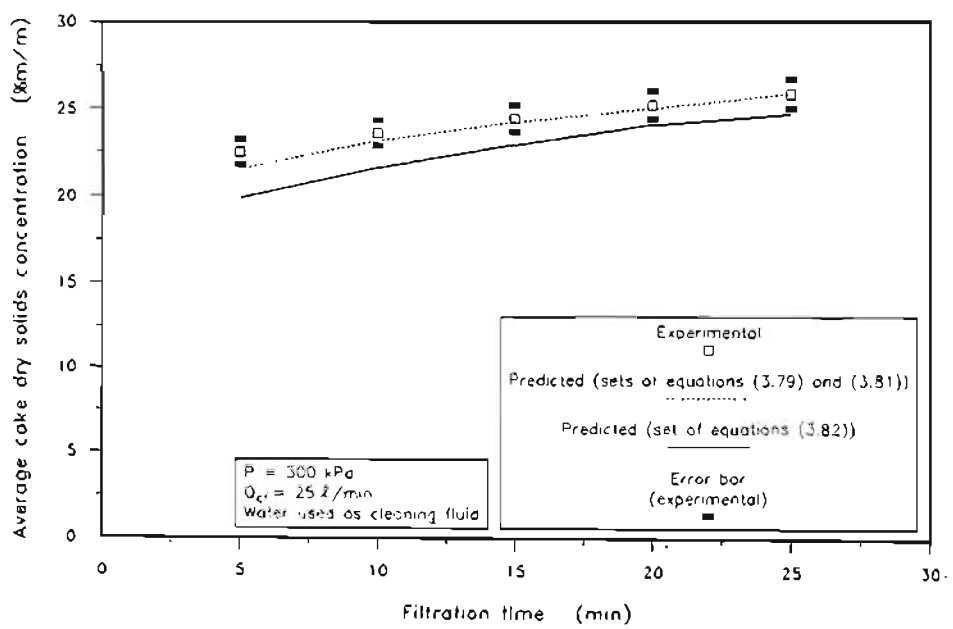

FIGURE 4.35(a) : Comparison Between Experimental and Predicted Average Cake Dry Solids Concentrations for P = 300 kPa and Q_{cf} = 25 ℓ/min (Water as Cleaning Fluid)

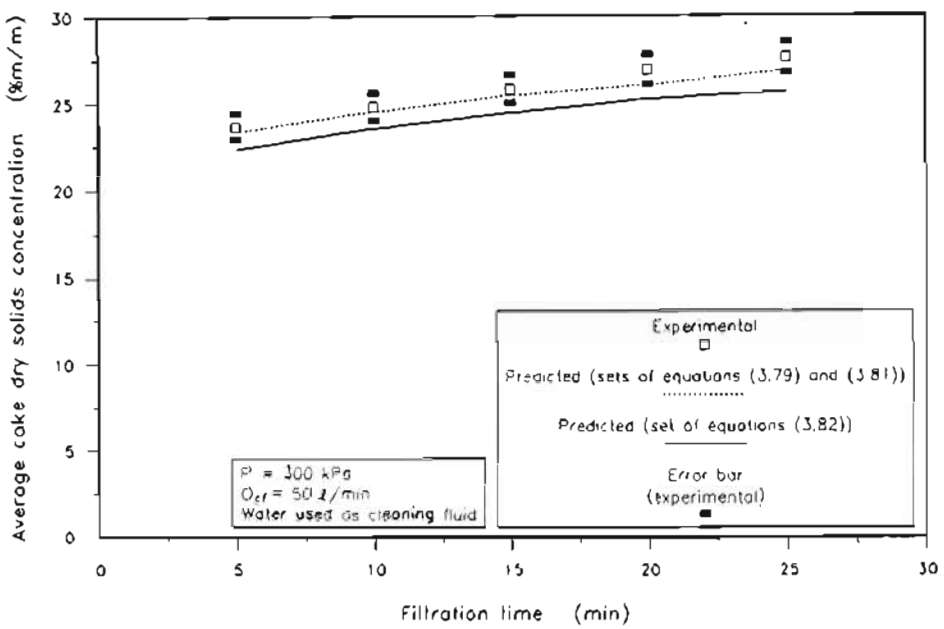

FIGURE 4.35(b) : Comparison Between Experimental and Predicted Average Cake Dry Solids Concentrations for P = 300 kPa and Q_{cf} = 50 ℓ/min (Water as Cleaning Fluid)

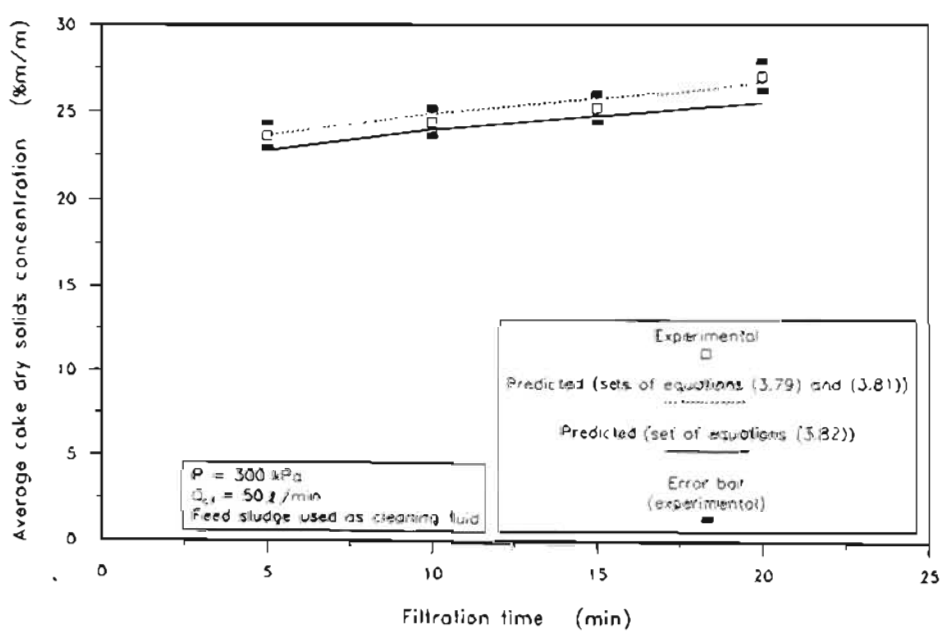

FIGURE 4.36 : Comparison Between Experimental and Predicted Average Cake Dry Solids Concentrations for P = 300 kPa and Q_{cf} = 50 ℓ/min (Feed Sludge as Cleaning Fluid)

The average porosity of the remaining cake after shear was calculated by modifying the computer program for internal cylindrical filtration as follows. For a certain filtration time the internal cake radius and the radial porosity profile of the deposited cake (without shear) were calculated as for the internal cylindrical filtration experiments in Chapter 3. The predicted internal cake radius after cleaning fluid shear was calculated as discussed before. The average porosity of the remaining cake after shear was calculated by substituting the predicted internal cake radius (r_2) (after shear) into equation (3.45) :

$$\epsilon_{av} = \frac{2\pi \int_{r_2}^{r_1} \epsilon r \, dr}{\pi (r_1^2 - r_2^2)} \qquad (3.45)$$

The average cake dry solids concentration of the remaining cake after shear was calculated from the average cake porosity by using equation (4.37).

As shown in Figures 4.34(a) and (b), 4.35(a) and (b) and 4.36, the agreement between the experimental and predicted average cake dry solids concentrations was better for sets of equations (3.79) and (3.81) than for set of equations (3.82). The error bars are based on the same errors that were used for the average cake dry solids concentrations for the internal cylindrical filtration experiments in Chapter 3.

The comparison between experimental and predicted cake losses due to shear (CL_s) (with water as cleaning fluid) is shown in Figures 4.37 and 4.38 for filtration pressures of 100 kPa and 300 kPa, respectively. The experimental and predicted cake losses due to shear for feed sludge as cleaning fluid are shown in Figure 4.39.

Set of equations (3.82) was used for the predicted cake losses due to shear since this set of equations gave the best overall fit in terms of internal cake diameters and average cake dry solids concentrations.

For water as cleaning fluid the agreement between experimental and predicted values at a filtration pressure of 100 kPa was not as good as the agreement for a filtration pressure of 300 kPa, as shown in Figures 4.37 and 4.38, respectively. This was mainly due to the fact that the agreement between experimental and predicted internal cake diameters was better for 300 kPa than it was for 100 kPa (see Figures 4.30(a) and (b) and 4.31(a) and (b)). The agreement between experimental and predicted cake losses for the experiments with feed sludge as cleaning fluid was good, as is shown in Figure 4.39.

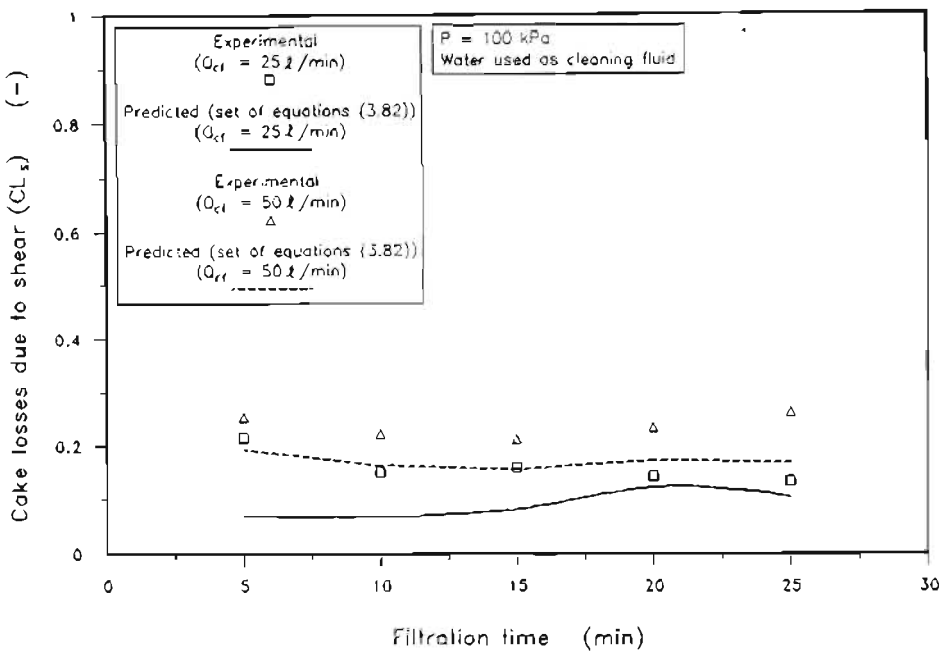

FIGURE 4.37 : Comparison Between Experimental and Predicted Cake Losses Due to Shear (CL_s) for P = 100 kPa (Water as Cleaning Fluid)

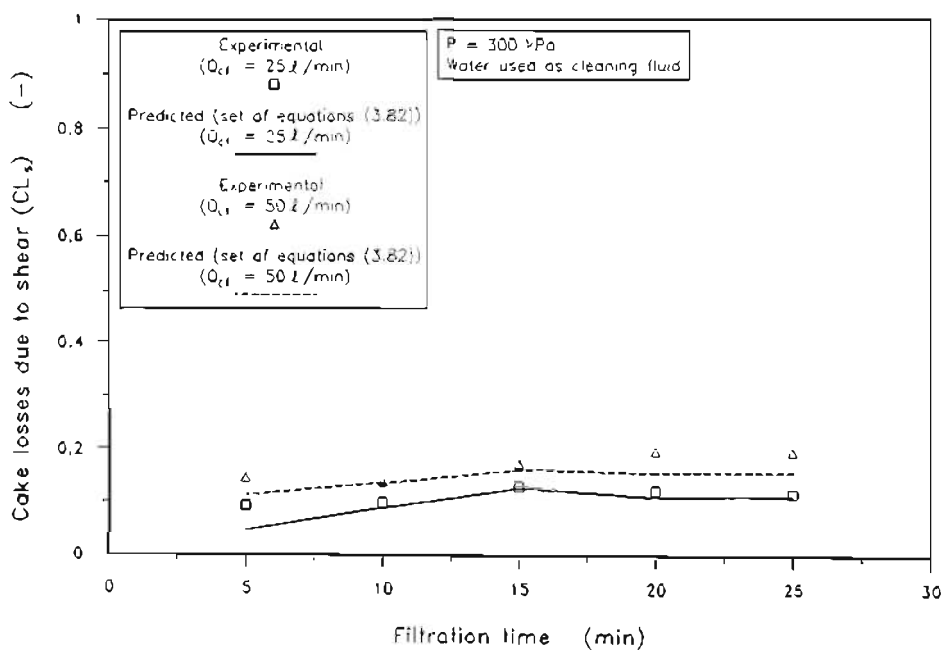

FIGURE 4.38 : Comparison Between Experimental and Predicted Cake Losses Due to Shear (CL_s) for P = 300 kPa (Water as Cleaning Fluid)

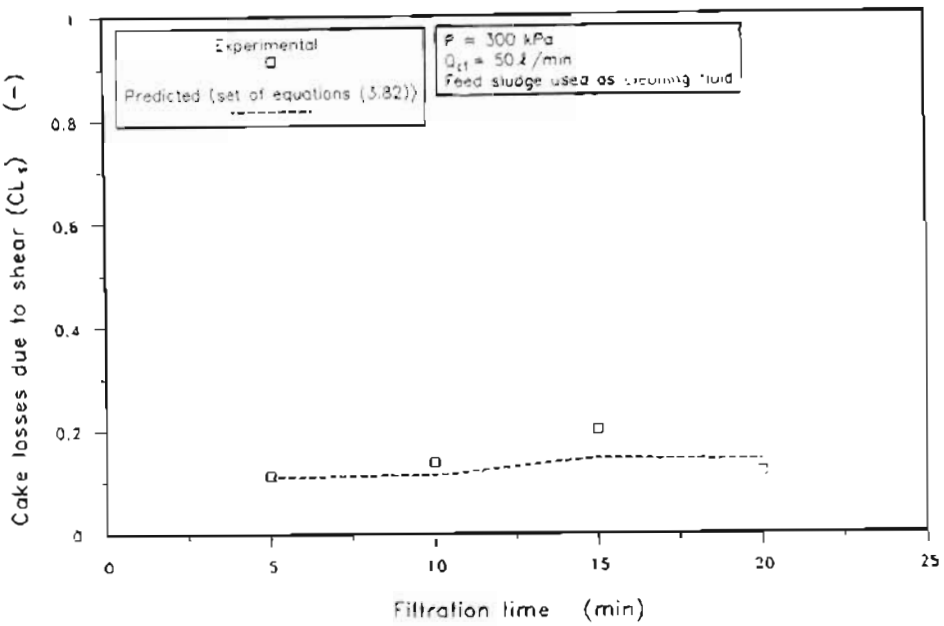

FIGURE 4.39 : Comparison Between Experimental and Predicted Cake Losses Due to Shear (CL_s) for P = 300 kPa (Feed Sludge as Cleaning Fluid)

4.8 PROCESS OPTIMIZATION

As discussed in Chapter 2 (section 2.2.3) process optimization for the tubular filter press process is more complex than for conventional planar filtration processes (see Figures 2.4 and 2.5), since optimization is very dependent on cake recovery during the cake removal cycle. Although process optimization is strictly speaking not part of the objectives of this study, it is included here for completeness, because of the dependence of process optimization on cake recovery.

During this study it was found that cake recovery during the cake removal cycle was a complex function of filtration pressure, filtration time (or mass of cake dry solids deposited per unit medium area), flow rate of cleaning fluid and path length for the hydraulic conveyance of cake flakes.

As discussed in section 4.6.1, it was found that in order to minimize cake losses the filtration pressure should be as *high* as possible, the flow rate of the cleaning fluid as *low* as possible and the path length for the hydraulic conveyance of cake flakes should be as *short* as possible.

Assuming that the process is constrained in terms of maximum filtration pressure, minimum flow rate of cleaning fluid and minimum path length for hydraulic conveyance of cake flakes, it is still necessary to determine the optimum filtration time.

The results of this study (see Figure 4.10) and those achieved on the prototype tubular filter press (see Figure 2.4) indicated that cake recovery is a strong function of filtration time. Cake recovery increased sharply with filtration time for relatively low filtration times until after a "threshold" filtration time the cake recovery seemed to level out and almost reach a "plateau". It therefore seems apparent that for a given set of operating parameters a tubular filter press should not be operated below a "threshold" filtration time, as this would lead to a disproportionately low cake recovery and resultant thickening of the feed sludge in the feed tank (see section 2.2.2.2).

For the waterworks clarifier sludge which was used during this study, excessive thickening of the feed sludge would result in an inordinate increase in yield stress and coefficient of rigidity (see Table 4.1). This can cause problems with the pumping of sludge (especially during the cake removal process) and poor sludge drainage and therefore flooding of the perforated conveyor belt during the cake removal cycle.

There is also an upper limit to filtration time above which there is a danger of either blocking the filter tubes or of the internal cake diameter after fluid shear being too small to allow the conveyance of dislodged flakes of cake.

Process optimization with respect to filtration time will be demonstrated in terms of the results achieved for the following set of experimental parameters :

(i) pressure = 300 kPa;
(ii) path length = 4 m;
(iii) Q_{cf} = 25 ℓ/min;
(iv) feed sludge solids concentration = 49 g/ℓ.

The variation of cake recovery and dry solids production rate (J_s) with filtration time is shown in Figure 4.40. The cleaning time (t_c) in Figure 4.40 is 150 s (2,5 minutes), which corresponds to the cleaning time used on the prototype tubular filter press. Dry solids production rate was calculated from equation (2.16) :

$$J_s = \frac{3\,600\, R\, w_c}{(t_d + t_c)} \qquad (2.16)$$

where J_s = mass of cake dry solids produced per unit medium area per hour, (kg/m².h)
t_c = time to remove cake during cake removal cycle, (s)
t_d = time to deposit cake, (s)

As shown in Figure 4.40 the dry solids production rate is not very sensitive to cake deposition time. A maximum occurs at a cake deposition time of 15 minutes which corresponds to a dry solids production rate of 2,48 kg/m².h and a cake recovery (R) of 0,54. The optimum mass of dry cake solids deposited per unit area (w_c) in a

cycle is 1,34 kg/m² (see Figure 4.42). A time of 15 minutes may be considered a "safe" time since the internal cake diameter of the deposited cake was measured to be 10,4 mm, while the internal cake diameter after shear was 16,1 mm.

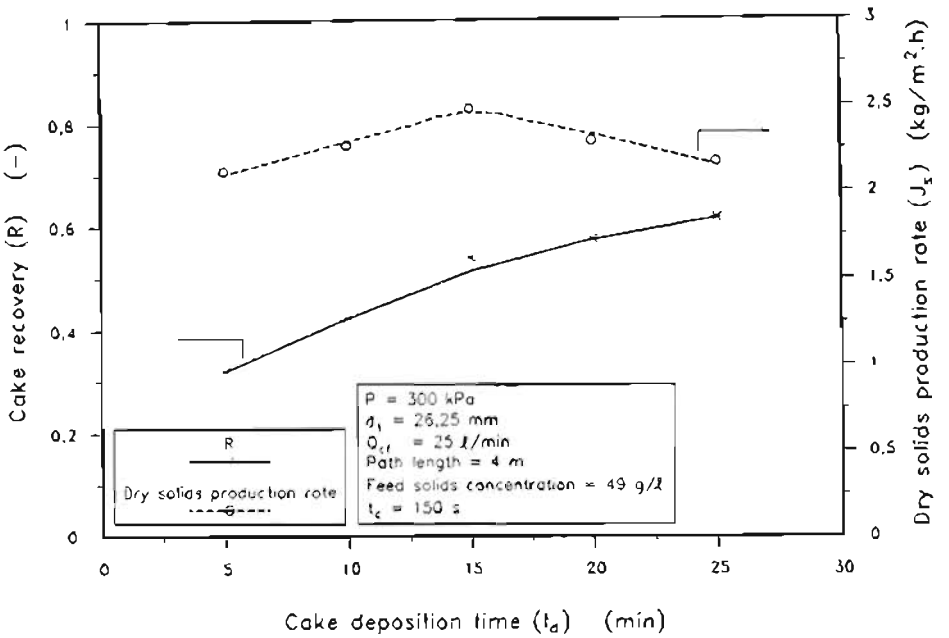

FIGURE 4.40 : Graph of Experimental Cake Recovery and Dry Solids Production Rate versus Cake Deposition Time

The effect of cleaning time (t_c) on dry solids production rate is shown in Figure 4.41. The dry solids production rates for cleaning times of 75 s, 150 s and 300 s are shown in Figure 4.41.

As shown in Figure 4.41 the dry solids production rate decreases as cleaning time is increased. However, the optimum cake deposition time remains at 15 minutes for all three cleaning times.

In Chapter 2 it was shown that if the cake recovery (R) is less than 1, then the solids concentration in the feed tank will increase so that the *average* solids concentration from equation (2.14) is :

$$x_s = \frac{x_f}{R} \qquad (2.14)$$

where x_f = mass of dry solids per unit volume of liquid in feed sludge which is pumped to the plant, (kg/m^3)

x_s = average steady-state mass of dry solids per unit volume of liquid in sludge which is filtered during pressing cycle, (kg/m^3)

Therefore for this example (for a cake deposition time of 15 minutes) if the feed sludge solids concentration is 49 g/ℓ, then the average steady-state solids concentration of the sludge in the feed tank (see Figure 1.1) would increase from 49 g/ℓ to approximately :

$$\frac{49}{0.54}\ g/l = 90.74\ g/l \qquad (R = 0.54)$$

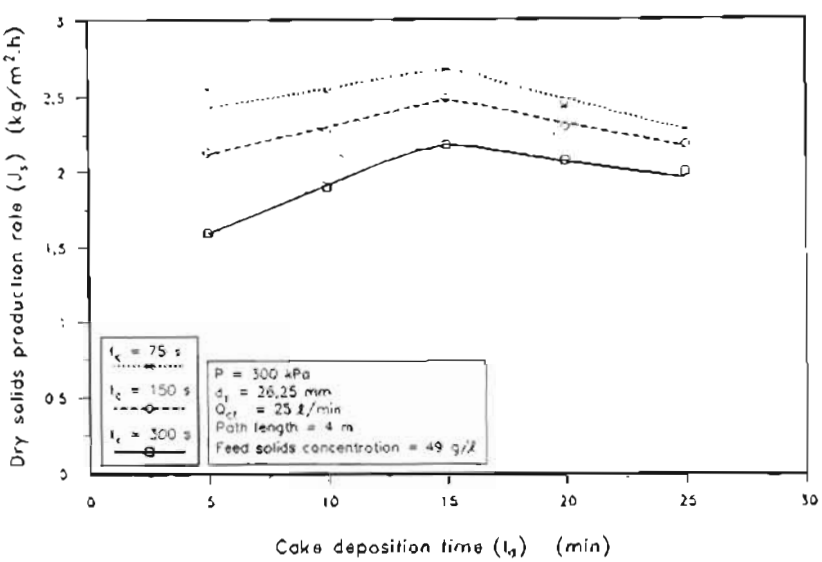

FIGURE 4.41 : Effect of Cleaning Time (t_c) on Dry Solids Production Rate (J_s)

The increased solids concentration in the feed tank results in a reduction in the time required to deposit a given mass of cake as shown in Figure 4.42. As shown in Figure 4.42, an approximate twofold increase in feed sludge solids concentration results in an approximate halving of the time required to deposit a given mass of cake. For a given cake deposition time the approximate twofold increase in solids concentration in the feed tank leads to a corresponding increase in dry solids production rate (compared to a feed sludge solids concentration of 49 g/ℓ) as shown in Figure 4.43. For Figure 4.43 the filtration performance for a feed sludge solids concentration of 90,74 g/ℓ was predicted by the internal cylindrical filtration model. It was also assumed that for a given value of w_c, cake recovery is independent of feed sludge solids concentration.

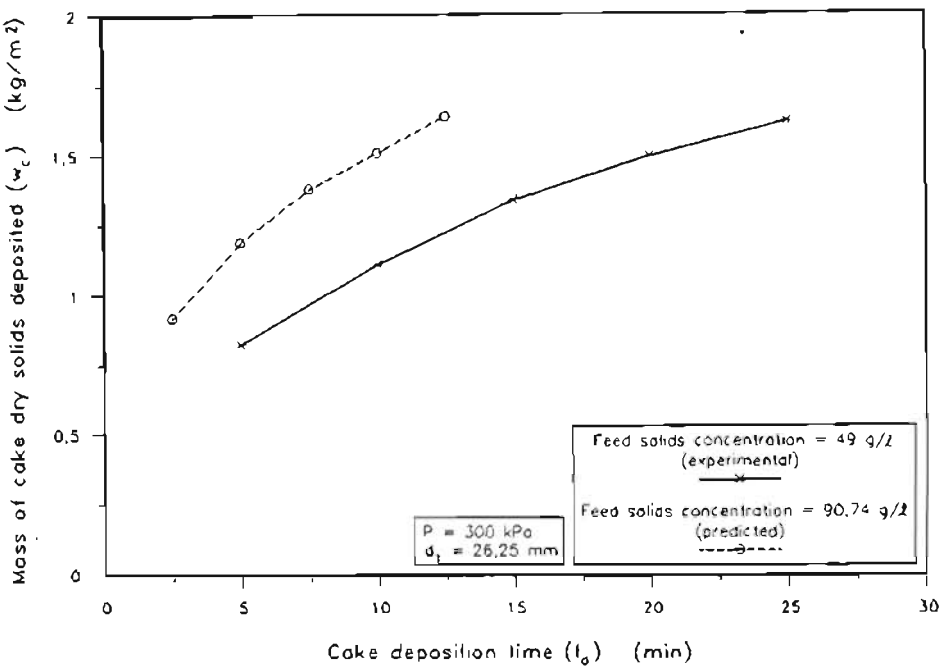

FIGURE 4.42 : Relationship Between Mass of Cake Dry Solids Deposited (w_c) and Cake Deposition Time for Two Feed Sludge Solids Concentrations

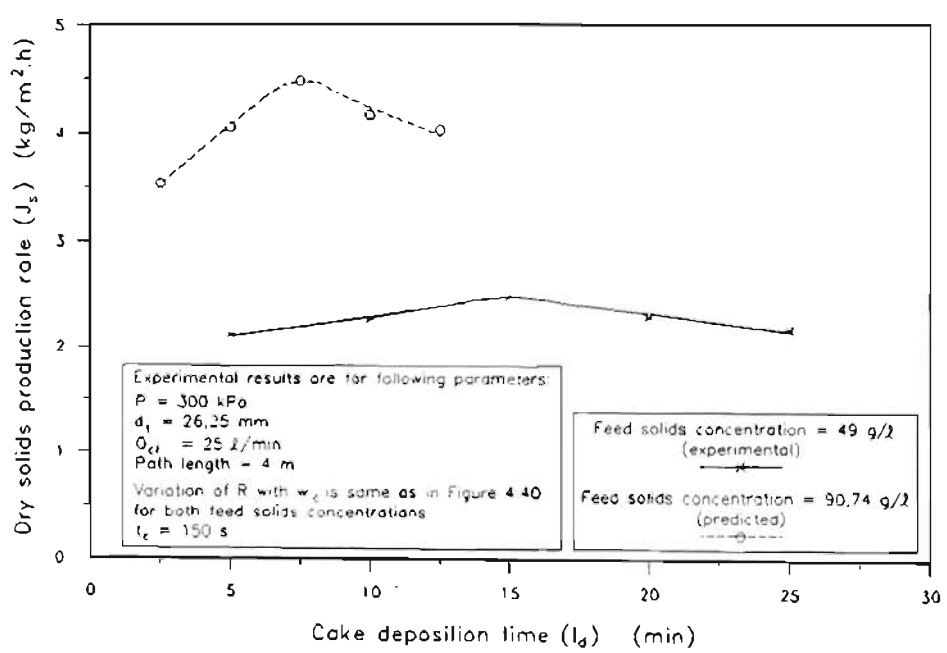

FIGURE 4.43 : Effect of Higher Average Steady-state Feed Sludge Solids Concentration on Dry Solids Production Rate

As shown in Figure 4.43, when the feed sludge solids concentration is approximately doubled the optimum dry solids production rate increases from 2,48 kg/m^2.h to 4,48 kg/m^2.h while the optimum cake deposition time is halved from 15 minutes to 7,5 minutes. At steady-state the optimum total cycle time (deposition and cleaning) for a feed sludge solids concentration of 90,74 g/ℓ is therefore 10 minutes.

Assuming that an increased solids concentration in the feed tank is acceptable, the increase in the feed sludge solids concentration to a certain extent compensates for the inefficiency in cake recovery. This is shown in Figure 4.44, where the dry solids production rate for the higher feed sludge solids concentration of 90,74 g/ℓ (R as in Figure 4.40) is compared with the dry solids production rate for the sludge if there were no inefficiency in cake recovery and all the cake were recovered during the cake removal cycle (i.e. R = 1 and feed sludge solids concentration = 49 g/ℓ). The curve for the latter case is based on the results of the internal cylindrical filtration experiments at P = 300 kPa and a feed sludge solids concentration of approximately 49 g/ℓ. As shown in Figure 4.44 the dry solids production rates are comparable at the optimum cake deposition time of 7,5 minutes for a feed sludge solids concentration of 90,74 g/ℓ.

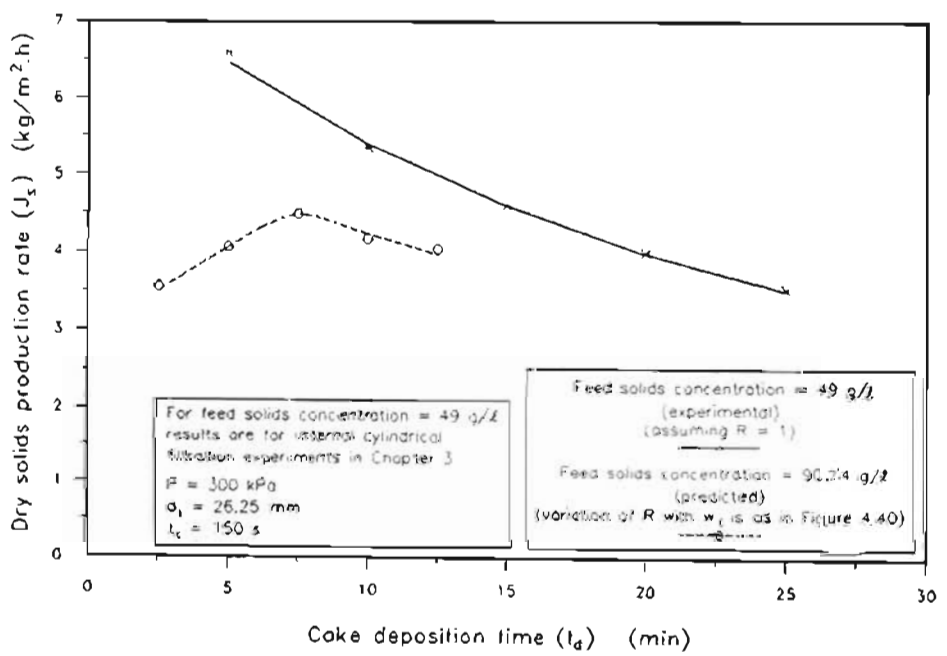

FIGURE 4.44 : Comparison Between Dry Solids Production Rate for Feed Solids Concentration of 49 g/ℓ (R = 1) (Experimental) and Feed Solids Concentration of 90,74 g/ℓ (R as in Figure 4.40) (Predicted)

Probably the major disadvantage of the inefficiency in cake recovery (apart from the potential problems mentioned before) is the fact that the energy required for cake removal per unit mass of dry cake solids *produced*, is *at least* inversely proportional to R, as shown by Rencken et al. (1990), i.e. :

$$\left\{\begin{array}{c}\textit{Energy required}\\ \textit{for cake removal}\\ \textit{for cake recovery, } R\\ \textit{(kWh/ton cake dry solids)}\end{array}\right\} = \left\{\begin{array}{c}\textit{Energy required for cake}\\ \textit{removal when } R = 1\\ \underline{\textit{(kWh/ton cake dry solids)}}\\ R\end{array}\right\} \quad (4.39)$$

Equation (4.39) does not incorporate any change in sludge rheology which may occur as a result of feed sludge thickening when $R < 1$.

4.8.1 Comparison Between Dry Solids Production Rate for Planar Filtration and the Tubular Filter Press

A comparison between the dry solids production rate for planar filtration and the tubular filter press is shown in Figure 4.45.

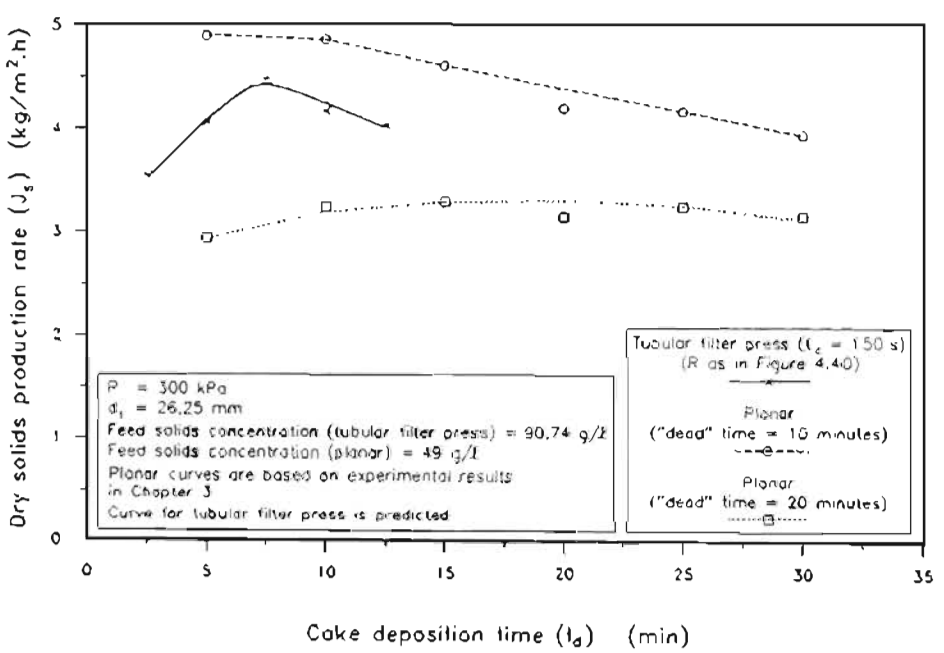

FIGURE 4.45 : Comparison Between Dry Solids Production Rate for Planar Filtration and the Tubular Filter Press Process

The parameters for the tubular filter press curve shown in Figure 4.45 are identical to those for the predicted curve in Figure 4.43 (feed solids concentration = 90,74 g/ℓ and R is as in Figure 4.40). The curves for planar filtration are based on the

experimental results for planar filtration shown in Chapter 3. Two "dead" times are shown for planar filtration, namely 600 s (10 minutes) and 1 200 s (20 minutes). These "dead" times are typical "dead" times (total time for filling of chambers and for removing cake) for modern plate and frame filter presses (Adam, 1991).

Despite an inherent lower dry solids production rate for internal cylindrical filtration than planar filtration (as shown in Figure 3.49), the dry solids production rate for the tubular filter press compares well with that for planar filtration for the example shown in Figure 4.45. This is because of the comparatively short cleaning time or "dead" time required for the tubular filter press.

4.9 DISCUSSION OF RESULTS

4.9.1 Results of Experiments to Determine Cake Losses Due to Shear of Cleaning Fluid

The main findings of the experiments to determine the cake losses due to cleaning fluid shear were as follows. It was found that the higher the flow rate of the cleaning fluid, the higher the cake losses due to shear. The shear of the cleaning fluid also caused a significant increase in internal cake diameter and average cake dry solids concentration when compared with the respective values for a deposited cake without fluid shear. It was found that the higher the flow rate of the cleaning fluid, the greater the internal cake diameter and the higher the average cake dry solids concentration after shear.

The shear experiments have shown that for the filtration (dewatering) of sludges which produce very compressible cakes, the tubular filter press process has a distinct advantage over conventional planar and external cylindrical filtration processes. Due to the shear of the cleaning fluid "undesirable sloppy" cake layers are scoured away during the cake removal cycle. This results in a cake with a significantly higher average cake dry solids concentration than the cake produced by conventional planar or external cylindrical filtration processes, if expression diaphragms are not installed.

4.9.2 Evaluation of Shear Model

Overall there was good agreement between the internal cake diameters and average cake dry solids concentrations after shear which were predicted by the shear model and those which were measured by experiment. For water as cleaning fluid the agreement between predicted and experimental results was better for a filtration pressure of 300 kPa than for 100 kPa. The agreement between predicted and experimental values for the limited experiments with sludge as cleaning fluid, was very good and better than for the experiments with water.

The agreement between predicted and experimental cake losses due to shear was not as good as the agreement between predicted and experimental internal cake diameters and average cake dry solids concentrations. The main reason for this was that the predicted cake losses were calculated from the *predicted* average cake dry solids

concentrations and internal cake diameters after shear. Therefore the errors between predicted and experimental internal cake diameters and average cake dry solids concentrations (after shear) were compounded in the calculation of the predicted cake losses due to shear.

Possible explanations for discrepancies between predicted and experimental results are given below.

For the shear experiments the cakes were sheared in the low solids compressive pressure region. In fact for all experiments the corresponding solids compressive pressures (in the deposited cakes) at which the cakes were sheared, were less than 9 kPa. An example of the predicted solids compressive pressures at which shear occurred, is shown in Figure 4.46 for various filtration times.

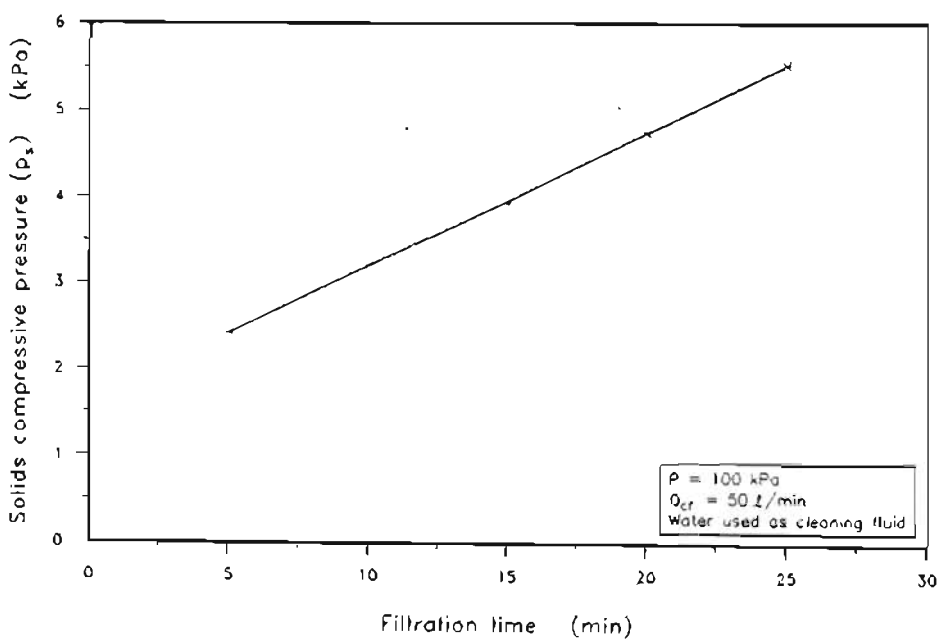

FIGURE 4.46 : Predicted Solids Compressive Pressures at which Cake was Sheared

It is well known that C-P cell experiments are not very accurate in the low solids compressive pressure region (Tiller and Leu, 1991). It is for this reason that settling experiments were done to obtain the variation of permeability and porosity in the low solids compressive pressure region, as discussed in Chapter 3. Although the combination of C-P cell and settling data gave good correlation between predicted and experimental values for the internal cylindrical filtration experiments (as shown in Chapter 3), Murase et al. (1989) expressed reservations about the accuracy of the settling tests. It is therefore feasible that the solids compressive pressure and therefore the cake solids concentration profiles as predicted by the incorporation of settling

and C-P cell data into the internal cylindrical filtration model were not very accurate in the low solids compressive pressure region. In fact various authors have expressed reservations about the accuracy of C-P cell tests to predict the liquid and solids compressive pressure profiles through certain cakes accurately (for example, Rushton and Arab, 1989). Unfortunately, because of the nature of internal cylindrical filtration, it was not practical to measure the liquid pressure profile through a cake directly using strain gauges as was done by Rushton and Arab (1989) for planar filtration, for example. The liquid and solids compressive pressure profiles therefore had to be obtained in an indirect manner by prediction. Recently developed non-intrusive measuring techniques such as synchrotron X-ray absorbance (Bierck et al., 1988) and possibly nuclear magnetic resonance (NMR) imaging techniques (Horsfield et al., 1989) seem to be ideally suited for the determination of the solids concentration profile through a compressible filter cake. Unfortunately the equipment for such techniques is very sophisticated and expensive and was not available for this study.

An indication of the sensitivity of the prediction of the internal cake diameter after shear to the solids compressive pressure profile, is shown in Figure 4.47 for a filtration pressure of 100 kPa.

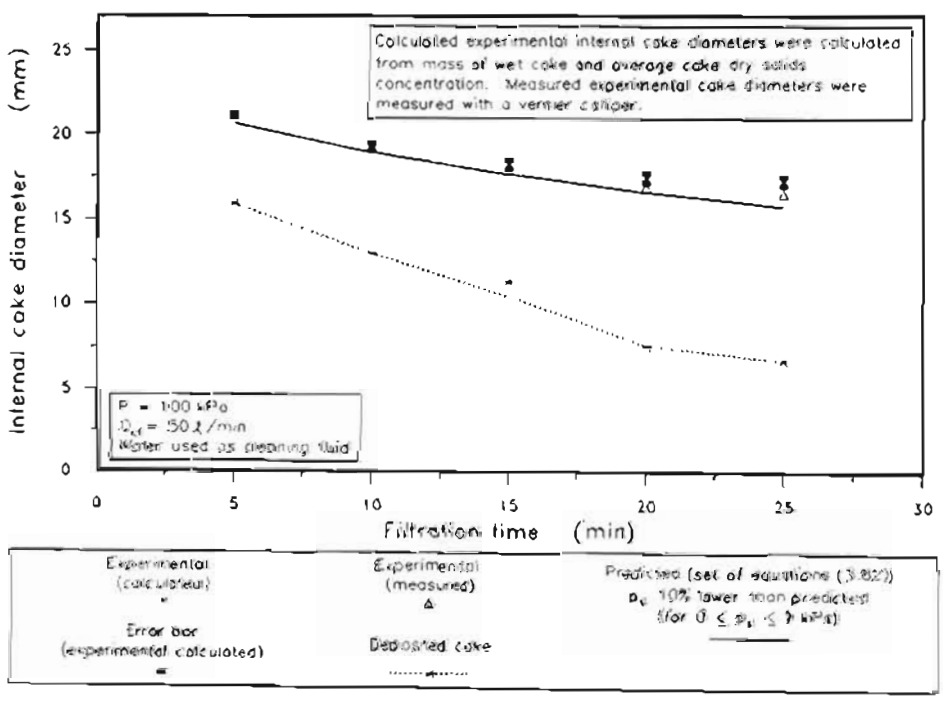

FIGURE 4.47 : Comparison Between Predicted and Experimental Internal Cake Diameters After Shear with the Solids Compressive Pressures 10 % Lower than those Predicted (In the Range $0 \leq p_s \geq 9$ kPa)

For the predicted curve in Figure 4.47 the solids compressive pressures in the range, $0 \leq p_s \geq 9$ kPa, were assumed to be 10 % lower than those predicted by incorporating set of equations (3.82) into the internal cylindrical filtration model. As shown in Figure 4.47 the fit is better than that shown in Figure 4.30(b). The reduction of 10 % in the solids compressive pressures in the range, $0 \leq p_s \geq 9$ kPa, hardly affected the average cake dry solids concentration of the deposited cake (before shear), as shown in Figure 4.48.

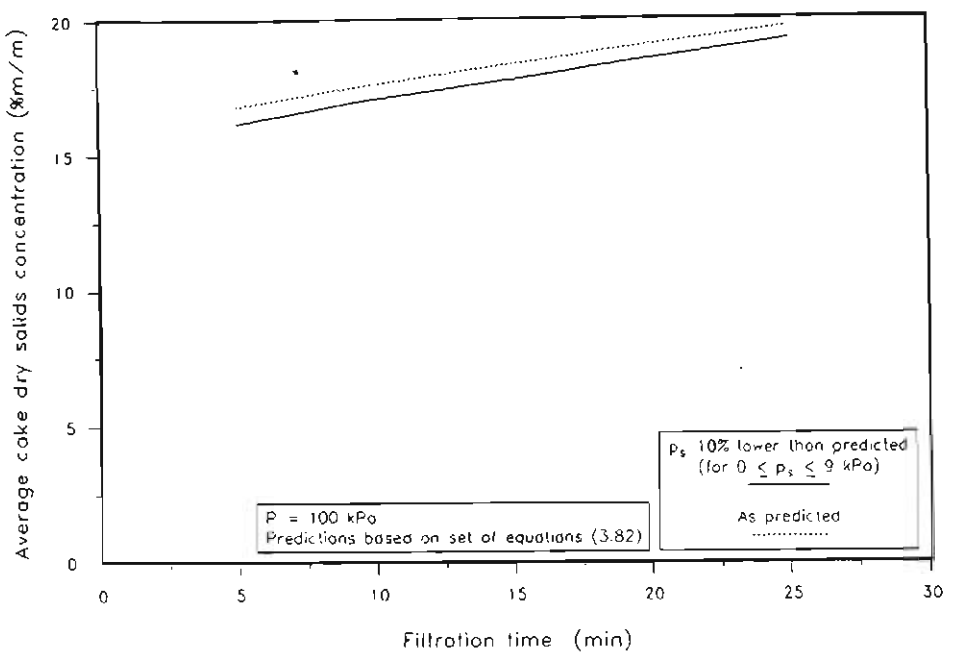

FIGURE 4.48 : Effect of 10 % Reduction in Solids Compressive Pressure (In the Range $0 \leq p_s \geq 9$ kPa) on Predicted Average Dry Solids Concentration of Deposited Cake (Before Shear)

Another factor which could have influenced the accuracy of the shear model is the estimate of the surface roughness of the filter cake. For the results predicted by the shear model it was assumed that the surface roughness of the filter cake was equal to the average particle size of the feed sludge i.e. 5,90 x 10^{-6} m. For all the experiments, except for the three experiments marked in Figures 4.30(b) and 4.31(b), the cake surface had a very smooth appearance after the shear of the cleaning fluid. The assumed surface roughness of 5,90 x 10^{-6} m compares well with the surface roughness values of *smooth* pipes given in the literature. Miller (1978) gives the surface roughness for smooth drawn brass and aluminium pipes as 2,5 x 10^{-6} m, while that for smooth steel pipes is given as 25 x 10^{-6} m.

Ideally, the surface roughness of the cake surface could have been determined by fluid pressure drop measurements across the upstream and downstream ends of the cake inside the porous tube. Such experiments were considered at one stage during the experimental study.

For the following reasons it was, however, decided not to continue with the pressure drop measurements :

(i) it was very difficult to install pressure sensors in the filter fabric and to seal the fabric against leaks;

(ii) as is mentioned below the filter tube was short (0,442 m) and there was a possibility that the flow profile of the cleaning fluid was not fully developed (inside the cake annulus), because of flow disturbances at the porous tube/cake interfaces at the upstream and the downstream ends of the cake.

Since the Reynolds numbers for the flowing cleaning fluid were less than 80 000 for all shear experiments, the predicted internal cake diameters were not that sensitive to the value of surface roughness. This is shown in Figure 4.49 for surface roughness values of 2,5 x 10^{-6} m; 5,90 x 10^{-6} m and 25 x 10^{-6} m.

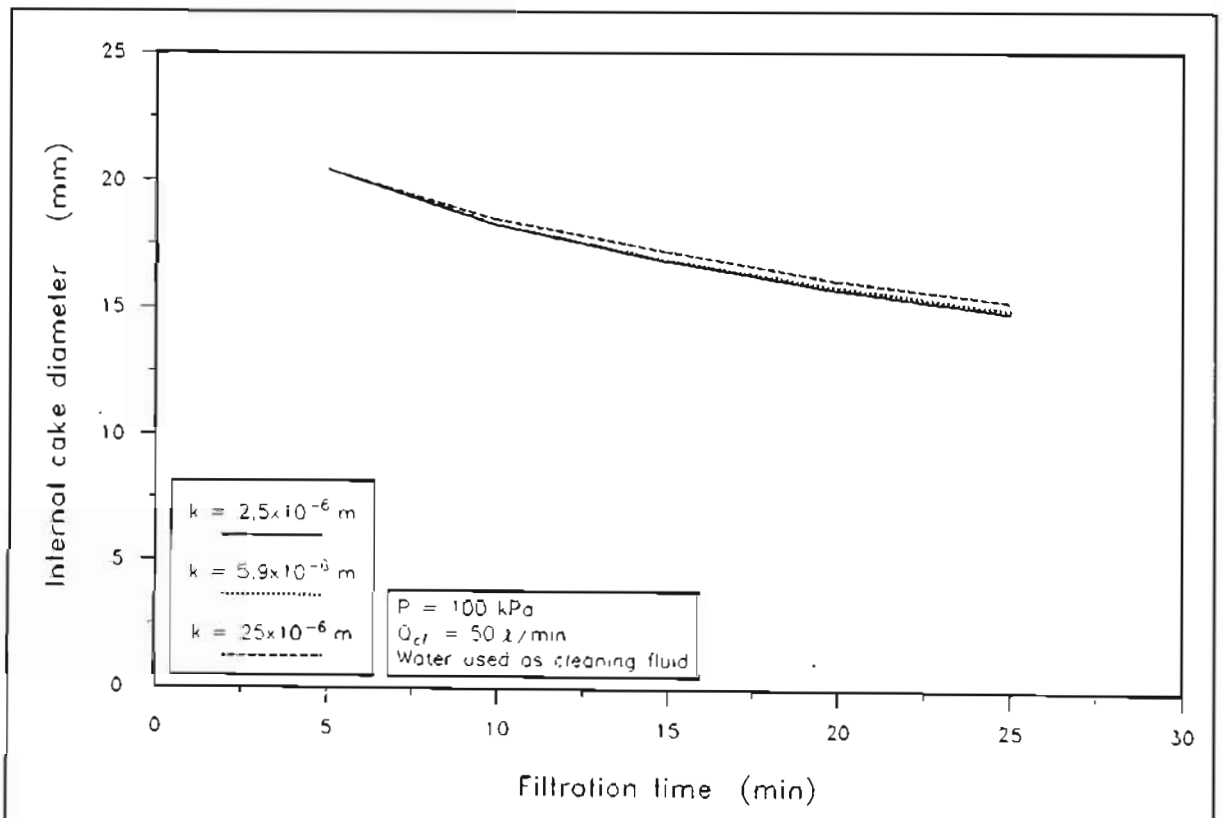

FIGURE 4.49 : Effect of Surface Roughness of Cake on Predicted Internal Cake Diameters After Shear

When assessing the accuracy of the shear model it also has to be borne in mind that for the shear experiments there was a sudden reduction in cross-sectional area at the beginning (upstream end) of the porous section and a sudden increase in cross-sectional area at the downstream end of the porous section, because of the deposited cake. These sudden changes in cross-sectional area must have caused flow disturbances in the flowing cleaning fluid at both ends of the porous section of the tube. Moreover, the porous section of the filter tube was relatively short (0,442 m). The flow disturbances in conjunction with the relatively short section of tube could have prevented the establishment of a well developed steady flow profile for the cleaning fluid flowing inside the cake. Since the shear model is based on the assumption of a well developed steady flow profile, these effects could have accounted for some of the discrepancy between experimental and predicted values.

Moreover, the flow disturbances due to the sudden changes in cross-sectional area would have been more pronounced, the longer the filtration time and the thicker the cake. This may offer an explanation for the appearance of ripples on the cake surface (after fluid shear) at longer filtration times as indicated in Figures 4.30(b) and 4.31(b).

Another explanation for the fact that the experimental internal cake diameters after fluid shear were larger than the predicted diameters for the experiments with water as cleaning fluid, is that the cake layers at the water/cake interface could have become progressively more diluted. Such dilution would have caused a decrease in the yield stress of these cake layers, with the result that they would have been scoured away, with a resultant increase in internal cake diameter.

A fact which militates against the above argument, however, is that for a few experiments the cleaning time was increased from 3 minutes to 10 minutes (see section 4.5.2.1). No significant difference between the cake losses obtained at a cleaning time of 3 minutes and those at 10 minutes was observed.

When considering all the above possible errors, then it is clear that the agreement which was achieved between predicted and experimental values can be considered to be good.

4.9.3 Significance of the Shear Model

The question may be asked as to the significance of the shear model, since it only predicts the cake losses due to the shear of the cleaning fluid and cannot be used to predict the *total* cake losses during the cake removal or cleaning process (including losses due to the action of the rollers and hydraulic conveyance of dislodged cake flakes).

The significance of the shear model for the tubular filter press process lies in the fact that it may be used to predict the following for *compressible* cake filtration :

(i) the average cake dry solids concentration of the final or product cake (after roller action and hydraulic conveyance);

(ii) internal cake diameter after cleaning fluid shear;

(iii) cake losses due to shear of the cleaning fluid.

4.9.3.1 Prediction of final average cake dry solids concentration (after roller action and hydraulic conveyance)

As shown in Figures 4.25 and 4.26 there was good agreement between the experimental final or product average cake dry solids concentration (after roller action and hydraulic conveyance) and the average cake solids concentration of the remaining cake after cleaning fluid shear, but before roller action. Since there was also good agreement between the predicted (from the shear model) and experimental average cake dry solids concentrations after shear, it may be concluded that for a compressible cake the shear model may be used to predict the average cake dry solids concentration of the final or product cake for the tubular filter press process.

4.9.3.2 Prediction of internal cake diameter after cleaning fluid shear

4.9.3.2.1 Prediction of maximum filtration time

By predicting the internal cake diameter after cleaning fluid shear, the shear model can assist in determining the maximum filtration time, so that during the cake removal cycle dislodged flakes of cake may be "safely" conveyed through the filter cake.

4.9.3.2.2 Design of manifold systems

The shear model predicts that the internal cake diameter after shear is dependent on the cleaning fluid flow rate. The higher the cleaning fluid flow rate, the larger the internal diameter and vice versa.

As discussed in Chapter 2, it is possible for maldistributions of flow to occur in manifold systems. For a tubular filter press, the filter tubes in a tube curtain are manifolded in parallel between an inlet and an outlet manifold. If such maldistributions of flow occur in a tube curtain (either during a "blow-down" during the pressing cycle (see section 2.2.1) or during the cleaning or cake removal cycle), then according to the shear model, for a compressible cake a corresponding variation in internal cake diameters (cake thicknesses) will result between the filter tubes in a curtain. A variation in internal cake diameters in a tube curtain can enhance the variation in flow rates (and therefore internal cake diameters) (see section 2.3.4) between filter tubes during successive "blow-downs" if the tubular filter press is operated with regular "blow-downs" during the pressing cycle. There were indications that this was occurring on the prototype tubular filter press (see Figure 2.19). Such variations in flow rates and internal cake diameters in a tube curtain could eventually result in some filter tubes becoming blocked.

If serious variations in flow rates and internal cake diameters occur in a tube curtain during the cake removal cycle, the flow rates (and internal cake diameters) in some tubes could be too low (small) to hydraulically convey the dislodged flakes of cake out of a tube curtain. This could also result in the blockage of such filter tubes.

From the predictions of the shear model and the above comments it is therefore essential to design the manifolds of a tubular filter press so that the variation in flow rates between filter tubes will be as low as possible.

4.9.3.2.3 Prediction of cake losses due to shear of cleaning fluid

Although the shear model cannot predict the total cake losses during the cake removal cycle, it can predict the cake losses, due to the shear of the cleaning fluid, for a compressible cake. A cake with excessive shear losses would not be suitable for the tubular filter press process.

4.9.4 Results of Experiments to Determine the Combined Cake Losses Due to the Action of the Rollers and Hydraulic Conveyance of Dislodged Flakes of Cake

The main findings of these experiments were that :

(i) filtration pressure had a significant effect on the combined cake losses due to the action of the rollers and hydraulic conveyance of dislodged flakes of cake. The higher the filtration pressure, the lower the cake losses. The reason for this is that at a higher filtration pressure the remaining cake after cleaning fluid shear is more consolidated than at a lower filtration pressure. This is shown by the higher average cake dry solids concentrations (after shear) at 300 kPa than at 100 kPa (see Figures 4.17 and 4.16, respectively);

(ii) cleaning fluid flow rate had no significant effect on these cake losses;

(iii) filtration time (or mass of cake deposited) had a significant effect on these cake losses. The longer the filtration time (higher mass of cake deposited) the lower the cake losses;

(iv) path length for hydraulic conveyance of dislodged flakes of cake had an effect on these cake losses although the effect was not as great as that of filtration pressure and filtration time. The longer the path length, the higher the cake losses.

The dimensions of the rollers used for this study were identical to those which were found to operate successfully on the prototype unit (as shown in Figure 4.8). The rollers were manually moved along the filter tube for these experiments and not mechanically at a controllable steady speed, as on the prototype unit. Future investigations should include the effect of such physical parameters as roller dimensions, gap size between rollers and speed of rollers on cake recovery.

As has been mentioned before, it seems almost impossible to develop a general model to predict the combined cake losses due to the action of the rollers and hydraulic conveyance of the dislodged flakes of cake. A pilot-scale test will always be necessary to *accurately* determine these cake losses. It should, however, be possible to develop a quick *screening* test (similar to that of Berger et al., 1990), in order to give a rough indication of whether the tubular filter press process is suitable for a certain sludge or not.

4.9.5 Experiments to Determine the Rheology of Sludge (Cake)

All solids concentrations of sludge (cake) which were investigated fitted the ideal Bingham plastic model well, as is shown by the regression coefficients in Table 4.1. The yield stress of the sludge increased sharply with sludge solids concentration for sludge solids concentrations greater than 10 % m/m.

The regression equation (4.34) to describe the variation of sludge (cake) yield stress with solids concentration fitted the experimental values well, as shown in Figure 4.28(a). The same applied to coefficients of rigidity. The regression equation (4.35) to describe the variation of sludge (cake) coefficient of rigidity with solids concentration also fitted the experimental data well (over the specified solids concentration range), as shown in Figure 4.28(b).

End effects were ignored in the calculation of shear stress at the wall (τ_w) and average shear rate for the pseudo-shear diagrams, since the $\frac{L_t}{D_t}$ ratios for all the tests were large ($250 < \frac{L_t}{D_t} < 2\,500$).

4.9.6 Type of Sludge

Although the sludge which was used for this investigation into cake recovery produced a cake for which the recovery was lower than the minimum recovery which is currently considered acceptable for the successful operation of a tubular filter press (minimum R = 0,7; Treffry-Goatley, 1991), this study nevertheless proved very valuable for quantifying the various cake losses during the cake removal cycle. The shear model which was developed is also significant for compressible cake filtration as explained in section 4.9.3. Moreover, process parameters for the optimization of cake recovery were identified.

A drawback of this investigation is that it concentrated on one type of sludge, which when filtered produced a *very* compressible cake. More work is required on other sludges to determine whether the findings of this study and the proposed shear model are applicable to other sludges which produce compressible cakes. Further investigations are also required to determine the cake losses for incompressible cakes.

4.10 CONCLUSIONS AND RECOMMENDATIONS

As discussed in Chapter 2, one of the objectives of this study was to investigate cake recovery (cake losses) during the cake removal cycle of the tubular filter press process. The motivation for this objective was that very low cake recoveries (high cake losses) were experienced, at various times, on the prototype tubular filter press. Low cake recoveries can result in reduced dry solids production rates and excessive thickening of the sludge in the feed tank (see Figure 1.1).

Since the tubular filter press is a novel process, the cake losses during the cake removal cycle have not been investigated before. For this reason an investigation was conducted into the cake losses which occur during the cake removal cycle of the tubular filter press process. The waterworks clarifier sludge which was used for the internal cylindrical filtration experiments (as discussed in Chapter 3) was also used for this study.

It was found that significant cake losses occurred :

(i) due to the shear of the cleaning fluid (prior to the action of the rollers);

(ii) due to the action of the rollers in dislodging the cake and the hydraulic conveyance of the dislodged flakes of cake from the filter tubes.

The experiments to quantify the cake losses due to cleaning fluid shear were conducted both with water and feed sludge as cleaning fluids. The experiments with water as cleaning fluid were done at two filtration pressures (100 kPa and 300 kPa) and two cleaning water flow rates (25 ℓ/min and 50 ℓ/min) and for various filtration times (in increments of 5 minutes up to 30 minutes), while those with feed sludge were conducted at one filtration pressure (300 kPa) and sludge flow rate (50 ℓ/min), and at filtration times in increments of 5 minutes up to 20 minutes. The objective of the experiments with sludge as cleaning fluid was to ascertain whether there was a difference between sludge and water as cleaning fluids, since current practice is to use feed sludge as cleaning fluid on all installed tubular filter presses. No significant difference was found between these two cleaning fluids.

It was found that the shear of the cleaning fluid resulted in a significant increase in internal cake diameter and average cake dry solids concentration compared with a deposited cake without shear. Cake losses, internal cake diameter and average cake dry solids concentration were all found to increase with cleaning fluid flow rate. There was no clear trend of these cake losses with filtration time or filtration pressure, however.

The shear experiments have shown that for the filtration (dewatering) of sludges which produce very compressible cakes, the tubular filter press process has a distinct advantage over conventional planar and external cylindrical filtration processes, if expression diaphragms are not installed. Due to the shear of the cleaning fluid, "undesirable sloppy" cake layers are scoured away during the cake removal cycle.

This results in a cake with a significantly higher average cake dry solids concentration than an equivalent cake produced by conventional planar or external cylindrical filtration processes.

A new shear model was developed to predict the cake losses due to cleaning fluid shear. For the shear model it was necessary to determine the sludge (cake) rheology. The sludge (cake) rheology was determined using a capillary-tube viscometer. It was found that the sludges (cakes) exhibited Bingham plastic behaviour (with a yield stress) over the solids concentration range : 3,58 % m/m $\leq c_s \geq$ 16,71 % m/m.

The essence of the new shear model is that when a cleaning fluid is allowed to flow inside the cake annulus of a compressible cake deposited inside a porous tube, those cake layers for which the yield stress is less than the shear stress exerted by the flowing cleaning fluid, are scoured away. Those cake layers for which the yield stress is greater than the shear stress exerted by the flowing cleaning fluid remain static. The internal cake diameter after shear coincides with the shear plane (in the cake) along which the yield stress of the cake is equal to the shear stress exerted by the flowing cleaning fluid.

For the cleaning fluid shear tests there was good agreement between most of the experimental results and the predictions by the proposed new shear model. Possible explanations for discrepancies have been discussed in detail in section 4.9.2.

The significance of the shear model for compressible cake filtration is that it can be used to predict :

(i) the average cake dry solids concentration of the cake produced by the tubular filter press process;

(ii) the cake losses due to shear of the cleaning fluid;

(iii) the internal cake diameter after shear of the cleaning fluid.

The prediction of the internal cake diameter after shear, can assist in determining the maximum filtration time, so that dislodged flakes of cake may be conveyed "safely" through the filter cake during the cake removal cycle.

From the results of the shear experiments and the predictions of the shear model it may be concluded that for compressible cake filtration it is very important that the filter tube manifold systems be designed so that maldistributions of flow are minimized, in order to prevent tube blockages in the tube curtains of a tubular filter press. The reasons for this have been discussed in detail in section 4.9.3.2.2.

Only one type of sludge was used for the shear experiments. More work is required to determine whether the findings of this study and the proposed shear model are applicable to other types of sludges which produce compressible cakes. Further investigations are also required to determine the shear losses for incompressible cakes.

Experiments were also conducted to determine the combined cake losses due to the action of the rollers and the hydraulic conveyance of the dislodged flakes of cake. Water was used as cleaning fluid for these experiments. The filtration pressures, filtration times and cleaning fluid flow rates were identical to those which were used for the experiments to determine the cake losses due to cleaning fluid shear. The main findings of these experiments were that the cake losses decreased markedly as filtration pressure and filtration time were increased. The decrease in cake losses as filtration pressure was increased was due to the greater consolidation of the cake at higher filtration pressures. Flow rate of the cleaning fluid did not have a marked effect on these cake losses, while an increase in path length for conveyance of dislodged flakes of cake resulted in a a mild increase in cake losses.

The experiments to quantify the combined cake losses due to the action of the rollers and the hydraulic conveyance of the dislodged flakes of cake were conducted with fixed roller dimensions. It is recommended that future investigations also consider the effect of roller dimensions on cake losses.

A pilot-scale test will always be necessary to *accurately* determine the cake losses due to roller action and hydraulic conveyance, since it seems almost impossible to develop a general model to predict these losses.

It is recommended, however, that a quick *screening* test be developed in order to give a rough indication of the cake losses due to roller action and hydraulic conveyance, which can be expected for a tubular filter press.

CHAPTER 5
INVESTIGATION OF THE CROSS-FLOW FILTRATION OF THE WATERWORKS CLARIFIER SLUDGE

5.1 INTRODUCTION

The objectives of this study were defined in Chapter 2. One of the objectives was to develop an unsteady-state internal cylindrical cross-flow microfiltration model for a sludge which has a non-Newtonian rheology and which when filtered produces a very compressible cake. The motivation for this objective was as follows.

The tubular filter press may be operated either in a cross-flow or in a dead-end filtration mode during the filtration cycle. The main advantage of cross-flow over dead-end filtration is that under ideal conditions if the flow rate in all filter tubes is the same, the internal cake diameters (in all tubes) will eventually reach an identical equilibrium or steady-state value. It is well known that this occurs in cross-flow microfiltration processes (see, for example, Pillay, 1991). Under these circumstances it would then be impossible for tube blockages (one of the main problems experienced on the prototype tubular filter press) to occur.

Since the objective of the tubular filter press is to *dewater* rather than to *thicken* sludges, the flow rate in the tubes for cross-flow filtration should not be too high, otherwise cake deposition would be hindered. This would lead to thickening of the feed sludge and to reduced efficiency of the cake formation process. Also, the higher the flow rate, the higher the energy consumption per unit mass of cake dry solids in the product cake.

It is therefore important to be able to predict a minimum flow rate which will give a "safe" equilibrium or steady-state internal cake diameter for the operation of a tubular filter press. For this purpose, a mathematical model which predicts the variation of internal cake diameter with filtration time for a given flow rate in a filter tube, is required. Such a mathematical model is also required for the prediction of the distribution of flow in the filter tube manifold system of a tubular filter press, as discussed in Chapter 2.

As discussed in Chapters 3 and 4, the cake which was produced from the filtration of the waterworks clarifier sludge was found to be very compressible, while the rheology of the sludge was found to be non-Newtonian (Bingham plastic). A literature review (see section 5.2) revealed that only one cross-flow microfiltration model (Pearson and Sherwood, 1988) has been developed for the unsteady-state cross-flow microfiltration of a non-Newtonian sludge, which when filtered produces a compressible cake. However the convection-diffusion model of Pearson and Sherwood (1988) had drawbacks which are discussed in section 5.2.6. For this reason

it was necessary to develop a predictive unsteady-state internal cylindrical cross-flow microfiltration model for a sludge which has a non-Newtonian (Bingham plastic) rheology and which when filtered produces a very compressible cake.

For the reasons mentioned above, only low flow rate cross-flow microfiltration is applicable to the tubular filter press. Consequently, a *laminar* cross-flow microfiltration model is developed in this chapter.

5.2 LITERATURE REVIEW OF MODELS FOR CROSS-FLOW MICROFILTRATION

In general if the particle size of the sludge to be filtered is greater than 0,1 μm and less than 10 μm, the filtration of such a sludge is termed *microfiltration*. Since the average particle size of the waterworks sludge used during this study was 5,90 μm, the filtration of this sludge could be classified as microfiltration.

A brief description of cross-flow microfiltration will be given. The technique of cross-flow microfiltration potentially permits the continuous filtration of particulate suspensions. The suspension is pumped into a porous tube (Figure 5.1).

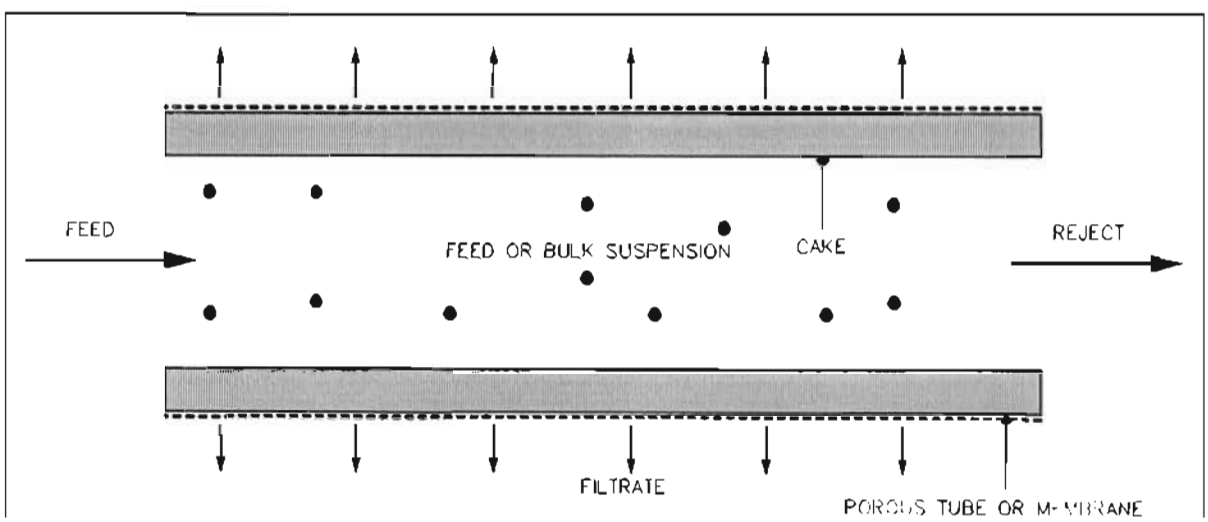

FIGURE 5.1 : The Principle of Cross-flow Microfiltration

Clear liquid permeates through the filter medium (or membrane) driven by the pressure difference across the filter medium (or membrane) and is recovered as filtrate. This flow of liquid normal to the medium convects particles to the wall where they accumulate to form a cake. As the cake thickness increases, the filtrate flux decreases. However, the flow of the feed or bulk suspension tangential to the cake tends to limit its growth, eventually resulting in a cake thickness and filtrate

flux, that is relatively constant with time - the *steady-state* condition. This can be contrasted to dead-end filtration, for which the cake thickness increases continuously with time, resulting in a filtrate flux that decreases continuously.

The cross-flow microfiltration of a sludge may therefore be divided into two phases or time periods :

(i) the unsteady-state or transient period during which initial cake growth occurs;

(ii) the steady-state period during which the cake thickness and filtrate flux are relatively constant with time. Various researchers (for example, Baker et al., 1985 and Pillay, 1991) have found that the flux slowly declines further during the so-called steady-state phase. For this reason the steady-state condition has been termed the *pseudo* steady-state phase.

There are numerous models for cross-flow microfiltration in the literature. Pillay (1991) provided a summary of the various cross-flow microfiltration models available in the literature. The majority of the models are only valid for laminar flow of the feed suspension and only focus on the steady-state condition. There are not many models available for the cake formation or build-up during the unsteady-state or transient time period.

The driving force for cake growth for cross-flow microfiltration inside a porous tube is the convection of solids towards the cake by the *radial* fluid (filtrate) flow. Even after the steady-state cake thickness has been attained, solids will still be convected towards the cake. Hence some mechanism must exist to prevent further cake growth. It is the identification of this mechanism that has posed the greatest challenge in the modelling of the steady-state in cross-flow microfiltration.

Initial models for cross-flow microfiltration were based upon the concentration polarization concept, which had been successfully applied to ultrafiltration of macromolecules (Blatt et al., 1970). In that approach, the steady-state is attained when the convection towards the medium is balanced by a Brownian or pseudo-Brownian back-diffusion away from the cake. However, when this theory is applied to the cross-flow microfiltration of particles, using the Stokes-Einstein Brownian diffusivity, predicted fluxes are orders of magnitude below those observed experimentally.

Subsequent modelling approaches have been aimed at suggesting alternative mechanisms for particle transport away from the cake surface or medium.

The models may be divided into four main categories :

(i) force balance models;

(ii) enhanced back-diffusion models;

(iii) axial convection models;

(iv) scour models.

5.2.1 Force Balance Models

For these models, the forces acting on individual particles are considered.

5.2.1.1 Inertial lift (lateral migration) models

Neutrally buoyant particles in a *laminar* flow field experience an inertial lift force which causes a migration away from the filter medium or membrane to some equilibrium position between the medium and centre line of the tube. Porter (1972) initially suggested that this "inward" migration towards the centre line of the tube could offset the convection of solids towards the medium. Green and Belfort (1980) proposed a lateral migration model which incorporates the build-up of an immobile cake at the wall. In this model it is proposed that particles are subject to two significant forces, namely, a fluid drag force directed towards the medium (due to the convection of solids towards the medium) and an inertial lift force directed away from the medium (see Figure 5.2). These correspond to a permeation velocity and to a lift velocity. When the permeation velocity exceeds the lift velocity, particles convect to the wall and cake growth occurs. Cake growth ceases when the lift velocity is equal to the permeation velocity.

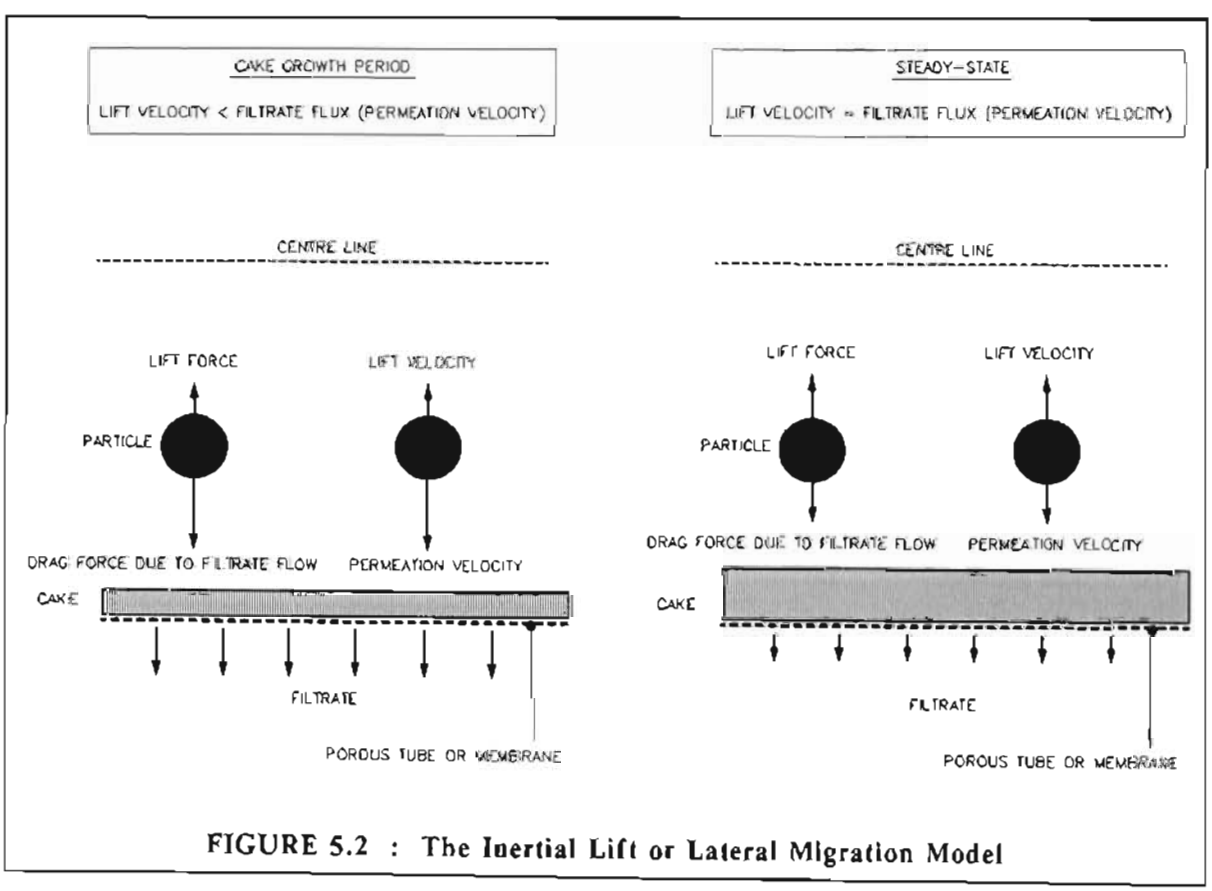

FIGURE 5.2 : The Inertial Lift or Lateral Migration Model

Green and Belfort (1980) found good agreement between their lateral migration model and the data obtained for the filtration of a dilute latex suspension. The model can also be used to model the initial unsteady-state cake growth phase.

Criticism which has been levelled against the model is that it is only applicable to dilute suspensions of non-interacting particles (Zydney and Colton, 1986).

5.2.1.2 Critical shear models

Fischer (1987), Rautenbach and Schock (1988) and Blake et al. (1990) have all proposed critical shear models. Conceptually all the proposed models are similar. However, unlike Fischer (1987) and Rautenbach and Schock (1988), Blake et al. (1990) also considered interparticle forces within the cake. Although the various models have all been developed for turbulent flow, the critical shear model could, in principle, relatively easily be extended to laminar flow.

For the critical shear models it is proposed that a critical force balance exists for particle stability on a membrane or cake surface. Below the critical condition particles which reach the cake surface will deposit stably. At or above this critical condition, particles which reach the surface will be destabilized and will not deposit (see Figure 5.3).

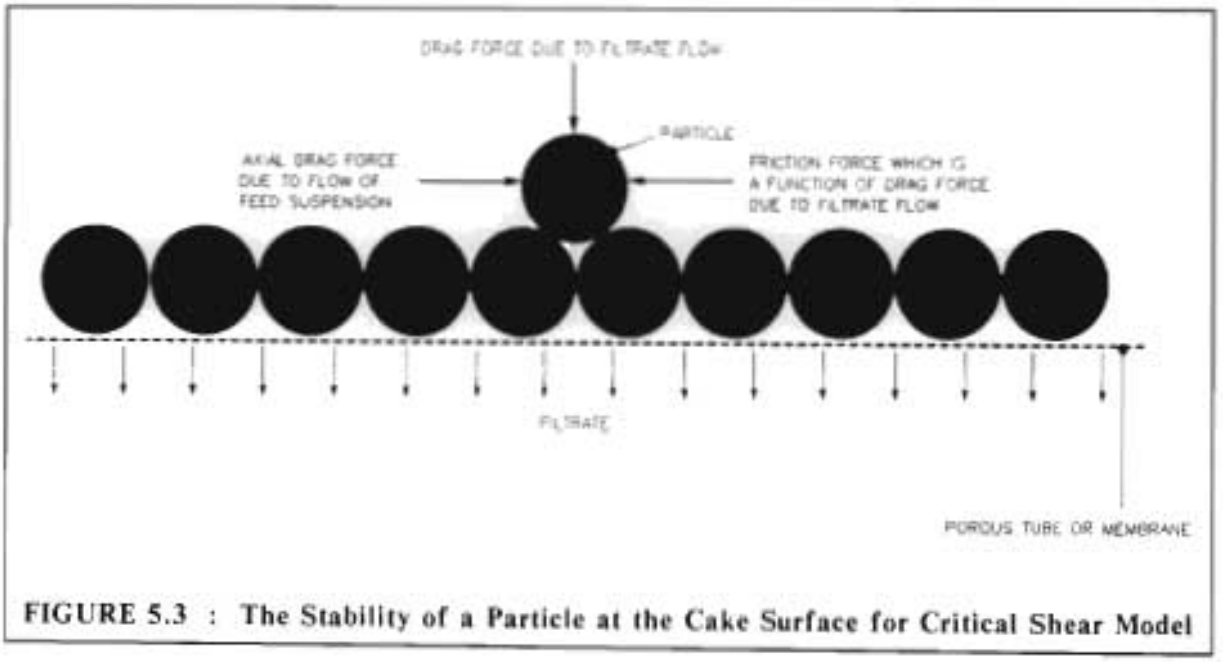

FIGURE 5.3 : The Stability of a Particle at the Cake Surface for Critical Shear Model

A consequence of the critical shear models is that (for a certain cross-flow velocity or flow rate), during the unsteady-state cake growth phase, the cake will grow in

an identical manner as for *dead-end* filtration. Once the critical condition is reached no further deposition will occur and the cake thickness will remain constant. This is shown in Figure 5.4.

5.2.2 Enhanced Back-diffusion Models

For this class of models it is proposed that the convection of solids towards the filter medium is offset by a simultaneous back-diffusion of particles from the cake to the bulk or feed suspension. The steady-state is attained when these rates are equal, and may be represented by the one-dimensional Fickian diffusion equation :

$$J\phi = D\frac{\partial \phi}{\partial y_m} \qquad (5.1)$$

where D = particle diffusion coefficient, (m^2/s)
J = filtrate flux, (m/s)
y_m = distance from membrane or filter medium, (m)
ϕ = volume fraction of particles, (-)

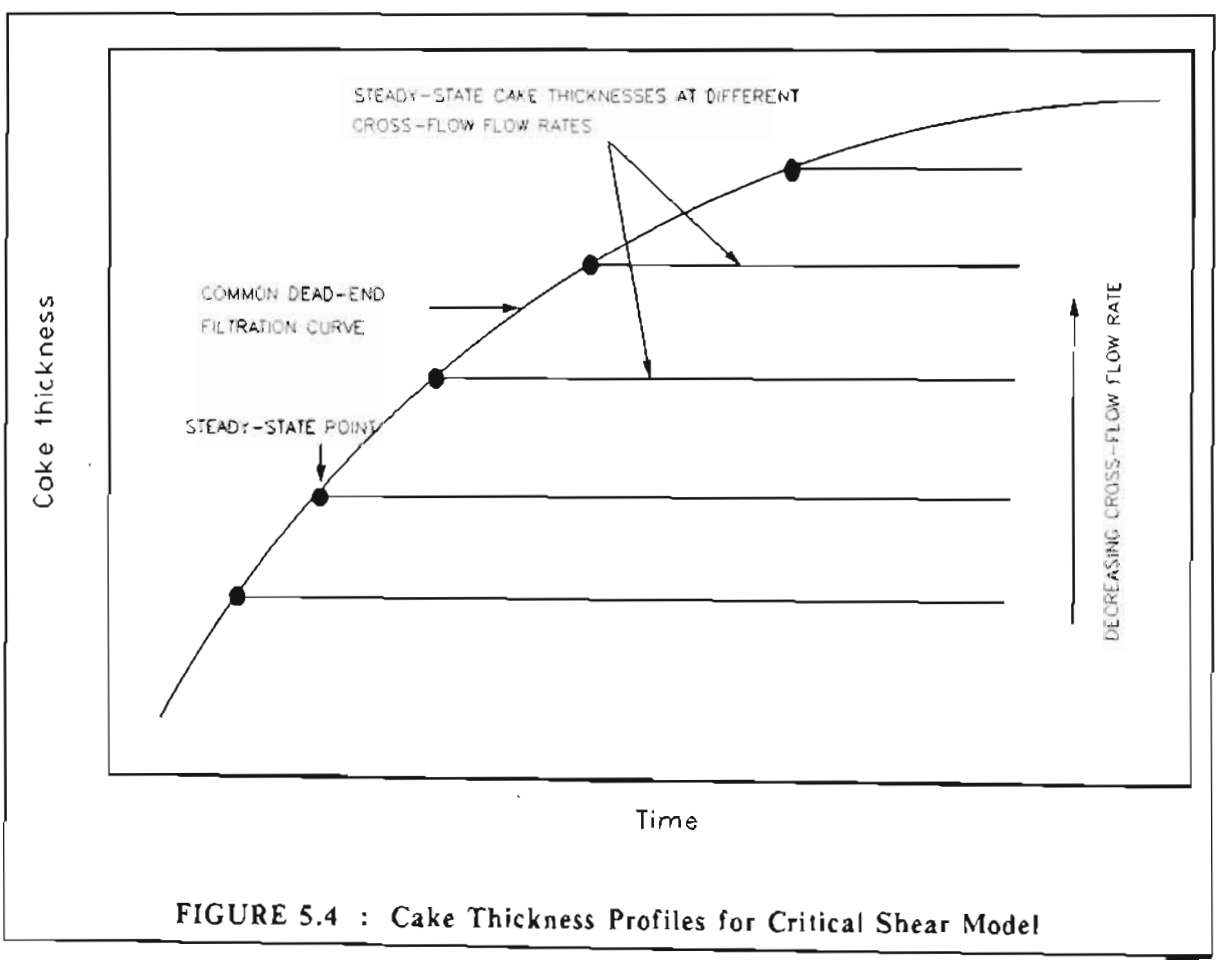

FIGURE 5.4 : Cake Thickness Profiles for Critical Shear Model

In contrast to the simple concentration polarization models, however, the diffusivity used in equation (5.1) is not the Stokes-Einstein diffusivity, but one which is augmented or enhanced by the shear of the flowing bulk suspension and resultant particle-particle interactions. The augmented diffusion has been termed shear induced hydrodynamic diffusion and shear enhanced diffusion.

Eckstein et al. (1977) and Leighton and Acrivos (1986) investigated the enhanced diffusivity for small rigid spheres.

Zydney and Colton (1986) substituted the correlation for the shear enhanced diffusion coefficient obtained by Eckstein et al. (1977) for the Stokes-Einstein diffusion coefficient in equation (5.1). On this basis they developed a laminar cross-flow microfiltration model which is identical to the earlier concentration polarization models for the ultrafiltration of macromolecules (for example, Blatt et al., 1970), except for the shear enhanced diffusion coefficient. The steady-state model of Zydney and Colton (1986) did not include the hydraulic resistance of the cake.

Hunt (1987) also incorporated a shear enhanced diffusion coefficient into his steady-state model for the cross-flow microfiltration of a limestone slurry. Although Hunt's (1987) model was developed for turbulent flow of the bulk suspension it can in principle be extended to laminar flow and is therefore mentioned here. On the basis of Hunt's (1987) steady-state model, Hunt et al. (1987) also developed an unsteady-state model for the turbulent cross-flow microfiltration of a limestone slurry. Hunt (1987) and Hunt et al. (1987) assumed that the cake is incompressible.

5.2.3 Axial Convection Models

The axial convection models propose that the convection of solids towards the filter medium is offset by a simultaneous *axial* convection of solids along the porous tube or inner cake wall and out of the filter tube (see Figure 5.5).

Leonard and Vassilieff (1984) proposed a simple axial convection or moving cake model for laminar flow of the feed suspension along a filter *channel* of square cross-section. They assumed that there was a sharp boundary between the feed suspension and the axially moving cake layer. The solids concentration within the moving filter cake was assumed to be uniform and the filtrate flux was assumed to be *invariant* in the axial direction (i.e. the resistance of the moving cake layer was assumed to be negligible compared with that of the filter medium or membrane). The moving cake and the bulk suspension were assumed to be Newtonian fluids and their viscosities were assumed to be equal. It is important to note that for this model the cake had no yield stress and the *whole* cake was assumed to flow. The compressibility of the cake was also not incorporated into the model.

The model by Leonard and Vassilieff (1984) incorporated both the unsteady-state time period (when a filter cake is established) and the steady-state during which no further growth in cake occurs. Solutions for the steady-state regime showed that the thickness of the moving cake increases as it flows along the filter channel.

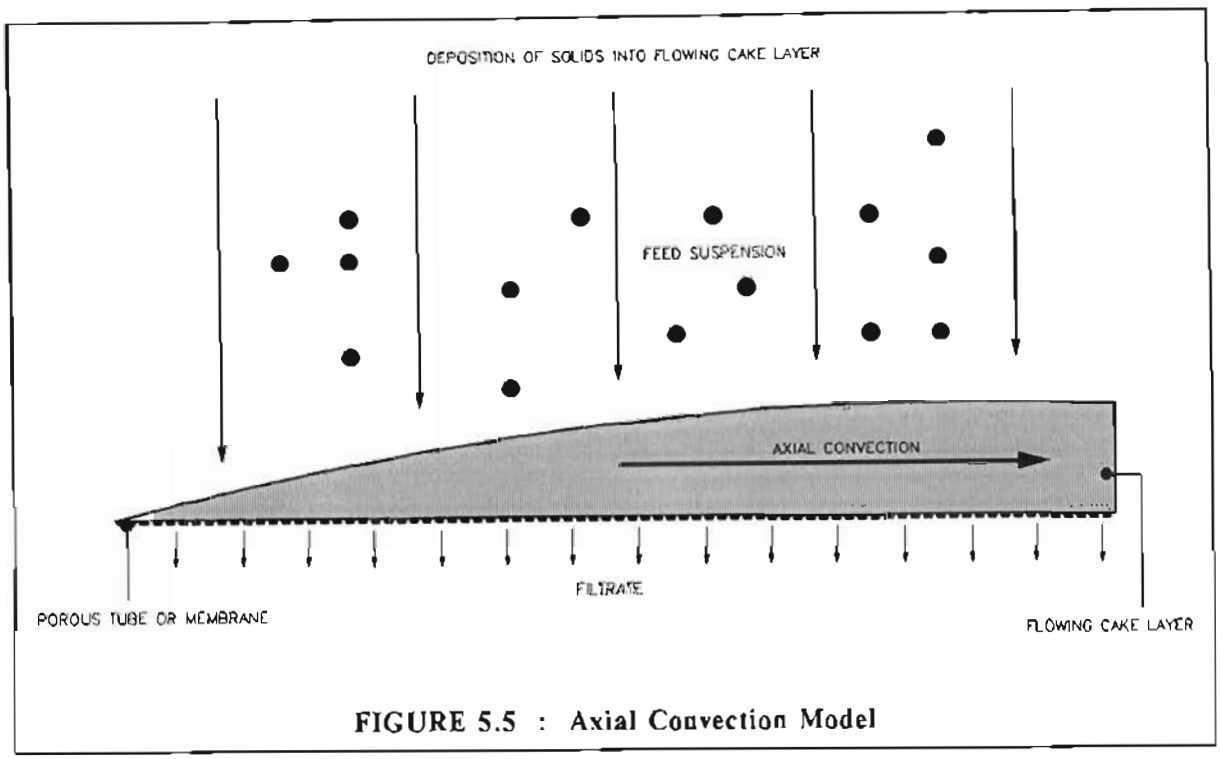

FIGURE 5.5 : Axial Convection Model

The model of Leonard and Vassilieff (1984) was subsequently extended by Davis and Birdsell (1987). Davis and Birdsell (1987) also assumed a constant particle concentration in the moving cake layer, but allowed for the cake viscosity to be greater than the viscosity of the bulk suspension. Both phases were treated as Newtonian fluids in parabolic laminar flow. Filtrate fluxes were allowed to vary axially. The model by Davis and Birdsell (1987) was developed for a filter channel of square cross-section and only the steady-state was considered.

The numerical solutions provided by Davis and Birdsell (1987) showed an axial increase in cake thickness similar to that given by the model of Leonard and Vassilieff (1984).

To test model predictions and to visually monitor the axial convection of cake layers, a channel with transparent side walls was constructed (Davis and Birdsell, 1987). Relatively large (150 to 212 μm) acrylic latex beads were suspended in a glycerol-water mixture. Experimental conditions were therefore remote from current industrial practice. At high fluxes Davis and Birdsell (1987) observed that thick stagnant cake layers were formed. At lower fluxes thin layers formed. It was observed that particles did indeed flow axially within the thin cake layers. Theoretical predictions for the thickness of these flowing layers were in order of magnitude agreement with observations, except for large thicknesses (Davis and Birdsell, 1987).

Hoogland et al. (1990) developed a *steady-state* axial convection model for the cross-flow filtration of silica particles. The model was developed for turbulent flow of the bulk suspension, but it could in principle be extended to laminar flow. The solids concentration within the moving cake was assumed to be uniform. The rheology of the cake was measured and found to be non-Newtonian. However, the cake exhibited no *yield stress*, and therefore the whole cake was assumed to flow. It was also assumed that the resistance of the membrane was small compared to that of the moving cake. The cake was assumed to be incompressible and the resistance of the cake was calculated using the Carman-Kozeny (Carman, 1938) equation.

Extensive experiments were conducted by Hoogland et al. (1990). The agreement between the results of experiments and predictions by the model was fair (Hoogland et al., 1990).

5.2.4 Convection-diffusion Models

Davis and Leighton (1987) combined the shear enhanced diffusion model with the simple axial convection model. The combined model is termed a convection-diffusion model. After the studies of Leighton and Acrivos (1986) on viscous resuspension of particles, Davis and Leighton (1987) proposed that the mechanism of shear enhanced diffusion results in fluidization and resuspension of cake layers, which consequently flow axially. The significant transport mechanisms in this model are depicted in Figure 5.6.

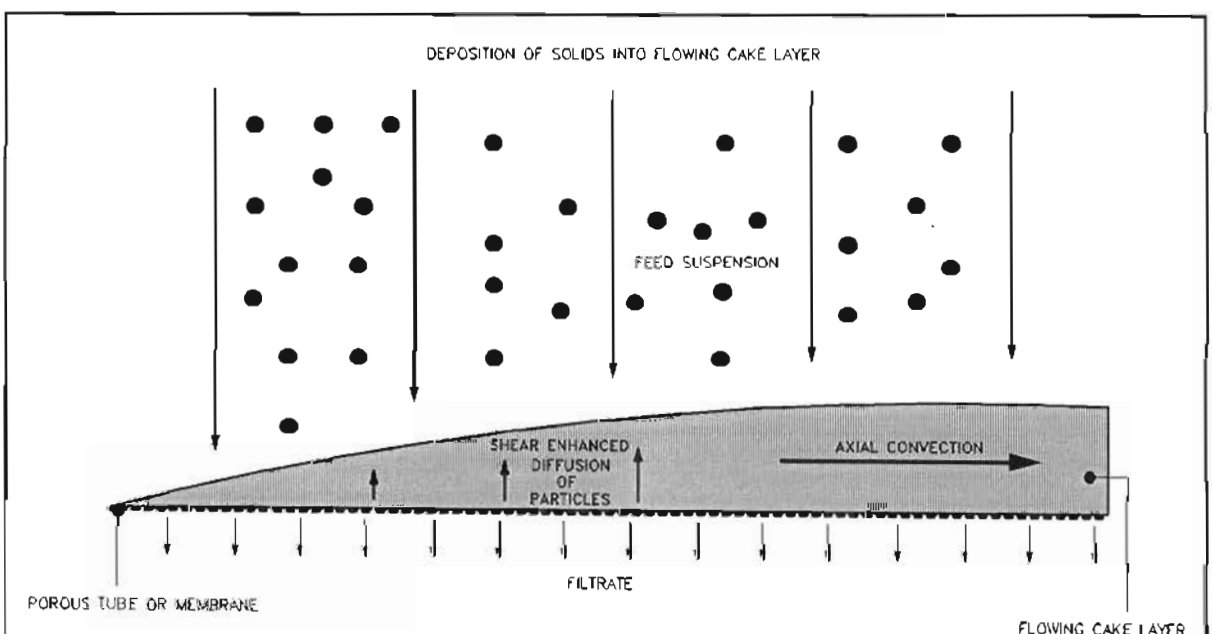

FIGURE 5.6 : Convection-diffusion Model

Davis and Leighton (1987) developed a "local" steady-state model for laminar flow conditions in a channel of square cross-section. This model does not make allowance for the resistance of the moving cake layer. The shear enhanced diffusion coefficients that were measured by Leighton and Acrivos (1986) for rigid spheres (size range 40 to 400 μm) were used in the model. Davis and Leighton (1987) also assumed that the rheology of the moving cake layers is *Newtonian*.

The model by Davis and Leighton (1987) allowed the prediction of the thickness of the moving layer, velocity and concentration profiles within the layer and the particle concentration at the filter medium at any point along the tube, for an assumed filtrate flux. The "local" model by Davis and Leighton (1987) also predicted the conditions at which a stagnant cake layer will form below the flowing layer.

The "local" model of Davis and Leighton (1987) was subsequently incorporated into a "global" steady-state laminar flow model by Romero and Davis (1988). The "global" model permits the prediction of the variations of the thickness of the moving layer, the thickness of the stagnant cake layer (if any) and the filtrate flux with *axial* distance along the filter medium. For the "global" model by Romero and Davis (1988) only the resistance of the stagnant layers was considered. The resistance of the moving layers was assumed to be negligible. No allowance was made for cake compressibility. Romero and Davis (1990) extended their "global" model (Romero and Davis, 1988) to an unsteady-state or so-called transient model. The unsteady-state model allows the prediction of the moving and stagnant cake layers with time and axial distance along a filter medium. No direct comparisons with experimental observations were made for either the aforementioned "local", "global" or unsteady-state models, although it was shown that the models are in qualitative agreement with experimental trends observed by other researchers.

Pearson and Sherwood (1988) developed a very complex unsteady-state convection-diffusion model for a sludge which, when filtered, produces a compressible cake. The model combined a convection-diffusion model for cross-flow filtration with a model for *dead-end* compressible cake filtration for a *planar* configuration. Allowance was made for non-Newtonian rheology of the feed suspension and the moving cake layers. It was assumed that there is a yield stress profile through a compressible cake. It was also assumed that under cross-flow conditions there is a shear plane within the compressible cake. Along the shear plane the shear stress exerted by the flowing bulk or feed sludge is equal to the yield stress of the cake layer at the shear plane. Those cake layers for which the yield stress is less than the shear stress (exerted by the flowing feed sludge) will flow, while those for which the yield stress is greater than the shear stress will form a static cake.

Pearson and Sherwood (1988) compared their convection-diffusion model with the results of Fordham and Ladva (1989) for the cross-flow filtration of bentonite suspensions. Unfortunately the model predictions were contradictory to the experimental results.

5.2.5 Scour Models

In this class of models, correlations and models developed for the fields of sedimentation and slurry transport in pipelines are adapted for cross-flow microfiltration. An example of a scour model is that by Fane (1984) which was based on the analogy between suspension flow across a filter cake (cross-flow filtration) and the motion of a sediment-laden stream over a layer of settled sediment. Such a model for a sediment-laden stream had earlier been proposed by Raudkivi (1967).

However, according to Pillay (1991), scour models are limited since they generally rely on empirical or semi-empirical correlations which have been developed for systems for which the hydrodynamic conditions are very different from those in cross-flow microfiltration. These models are therefore not considered further.

5.2.6 Conclusions of Literature Review

From the literature review, it is thus clear that numerous mathematical models have been developed for cross-flow microfiltration. The majority of the models consider only the case of *steady-state* laminar cross-flow microfiltration. For many models the resistance and nature of the cake have not been considered. In most instances where cake resistance has been considered, however, the cake has been assumed to be incompressible. Contradictions between theoretical predictions and experimental results, were found for one model which considered the cake to be *compressible* (Pearson and Sherwood, 1988). The majority of the axial convection and convection-diffusion models which have been developed recently, are based on slurries of rigid spheres. These artificial slurries are far removed from current industrial practice. There has also been limited experimental work done to compare theoretical predictions and experimental results.

For the majority of the models Newtonian rheology has been assumed for the feed suspension and moving cake layers (where applicable). Many of the models have also only been developed for flow in channels of square cross-section. It is plausible to expect similar differences between the performance of different filtration configurations in cross-flow mode, as were found in Chapter 3 for the dead-end filtration mode.

As has been mentioned, the waterworks clarifier sludge was used for the cross-flow experiments which are described in this chapter (see section 5.4). As was discussed in Chapter 3, this sludge produced a very compressible cake. Moreover, as was stated in Chapter 4, the rheology was found to be non-Newtonian.

The model of Pearson and Sherwood (1988) is the only cross-flow microfiltration model which has been developed for the unsteady-state cross-flow microfiltration of a non-Newtonian sludge, which when filtered produces a compressible cake. For

the following reasons the model of Pearson and Sherwood (1988) was found not to be suitable for the cross-flow filtration of the clarifier.sludge in a tubular filter press :

(i) the model by Pearson and Sherwood (1988) is a convection-diffusion model and incorporates shear enhanced diffusion coefficients which were measured by Leighton and Acrivos (1986) for relatively large rigid spheres (size range 40 to 400 μm) compared with the average particle size for the clarifier sludge of 5,90 μm (see Appendix F). (For the model which was developed during this study, shear enhanced back-diffusion of particles was assumed to be negligible);

(ii) the model (Pearson and Sherwood, 1988) is highly theoretical and difficult to apply practically. In fact Pearson and Sherwood (1988) did not give solutions to the full set of partial differential equations, but only similarity solutions;

(iii) the model (Pearson and Sherwood, 1988) was developed for a planar filtration configuration;

(iv) there were contradictions between model predictions and experimental results when the model of Pearson and Sherwood (1988) was compared with the experimental results of Fordham and Ladva (1989) for bentonite suspensions, which when filtered produced very compressible cakes. The model by Pearson and Sherwood (1988) predicted that the thickness of the filter cake grows in an axial direction along a filter, and that the filtrate flux therefore decreases in an axial direction along a filter. This was, however, not found to be consistent with the results of experiments by Fordham and Ladva (1989). Fordham and Ladva (1989) found that for their experiments with bentonite suspensions, the filter cakes were of uniform thickness in an axial direction along the filter and filtrate flux was independent of the axial length of a filter. As discussed in section 5.3.1, for the axial convection shear model, which was developed during this study, it was assumed that filtrate flux is invariant with axial distance along a filter tube. This model should therefore describe the results of Fordham and Ladva (1989) better than the model of Pearson and Sherwood (1988).

In the following section an *unsteady-state* mathematical model for the *laminar* cross-flow filtration of the waterworks clarifier sludge inside a porous tube is developed.

5.3 DEVELOPMENT OF A SHEAR MODEL FOR THE LAMINAR CROSS-FLOW MICROFILTRATION OF A SLUDGE WHICH WHEN FILTERED PRODUCES A VERY COMPRESSIBLE CAKE

As described in Chapter 4, for the very compressible cake produced by the filtration of the waterworks clarifier sludge, significant cake layers were sheared away when a shear stress was applied to a filter cake formed under static or dead-end conditions. A shear model was developed to predict cake losses due to shear.

The shear model which is developed in this section for cross-flow microfiltration inside a porous tube combines the internal cylindrical compressible cake filtration model (for static or dead-end filtration), which was developed in Chapter 3, with the shear model for cake losses, which was developed in Chapter 4. This approach is very similar to that adopted by Pearson and Sherwood (1988) for their convection-diffusion cross-flow microfiltration model for a compressible cake and a planar filtration configuration (see section 5.2.4). In a similar manner to Pearson and Sherwood (1988) (for a planar configuration), it is assumed that for a compressible cake deposited inside a porous tube there is a radial yield stress profile through the cake (see Chapter 4). Under cross-flow conditions a shear plane is established within the cake. At the shear plane the *shear stress* exerted by the flowing feed suspension is equal to the *yield stress* of the cake layer at the shear plane. Those cake layers for which the yield stress is less than the shear stress exerted by the flowing feed sludge, move along the shear plane, while those cake layers for which the yield stress is greater than the shear stress form a static cake. Deposited solids are transported away from the cake surface and out of the filter tube by the moving cake layer. This is shown in Figure 5.7 in section 5.3.2. The model developed here is, however, different from that proposed by Pearson and Sherwood (1988), the main difference being that unlike Pearson and Sherwood's (1988) model, back-diffusion of particles is assumed to be negligible. Also Pearson and Sherwood's (1988) model was developed for a planar configuration, while the model developed here is valid for an internal cylindrical configuration.

In order to "avoid" the complex partial differential equations to describe the unsteady-state behaviour in Pearson and Sherwood's (1988) model, the mathematical technique for the unsteady-state time period, for the model developed during this study (see section 5.3.3), is entirely different to that given by Pearson and Sherwood (1988).

Because of the aforementioned differences between Pearson and Sherwood's (1988) model and the axial convection shear model developed during this study, there is hardly any resemblance between Pearson and Sherwood's (1988) model and the axial convection shear model.

5.3.1 Assumptions for Model

The following assumptions are made for the proposed model :

(i) the sludge when filtered produces a very compressible cake;

(ii) the physical characteristics of the cake deposited under *cross-flow* conditions (i.e. porosity and permeability profiles) are not markedly different from those for a cake which is deposited in *dead-end* mode, so that for purposes of modelling, a "dead-end" cake may be assumed to be identical to a "cross-flow" cake. For the validity of this assumption see sections 5.5.4 and 5.6.10;

(iii) the axial convection of solids in the moving cake layer along the shear plane is the sole mechanism for removal of solids deposited at the cake surface. Diffusive and shear induced diffusive back-mixing are assumed to be negligible for the size range of particles studied. This is different from the model of Pearson and Sherwood (1988) (see section 5.2.6);

(iv) the bulk of the hydraulic cake resistance is in the well-compressed, highly resistant skin of cake adjacent to the filter medium. This is true for a very compressible cake as discussed in Chapter 3. The hydraulic resistance of the moving cake layer is considered to be negligible. As a result the filtrate flux is assumed to be *invariant* with axial distance along the filter tube. This is different from the model of Pearson and Sherwood (1988) (see section 5.2.6);

(v) the filtrate flux (flow rate) is small compared with the volumetric flow rate of the feed sludge so that the equations for fluid mechanics in *non-porous* tubes may be used to describe the flow of the feed sludge in a *porous* filter tube;

(vi) the flow of the feed suspension is *laminar*;

(vii) the thickness of the moving cake layer is thin compared with the internal diameter of the cake and the thickness of the cake;

(viii) since the moving layer is thin, a *uniform* shear stress exists within the moving cake layer;

(ix) the feed sludge and "mushy" cake layers near the cake/feed sludge interface are *Bingham* plastic fluids;

(x) a differential length of filter tube is considered i.e. axial variations in feed sludge concentration and flow rate are considered negligible;

(xi) as for all cross-flow filtration processes the cake deposition process may be divided into two periods :

  (i) unsteady-state or transient period during which the rate of solids deposition along the differential length of filter tube exceeds the rate of solids removal in the *moving cake layer* at the outlet of the filter tube;

(ii) steady-state period during which the rate of solids deposition along the differential length of filter tube is equal to the rate of solids removal in the *moving cake layer* at the outlet of the filter tube.

The theory for the steady-state period will be discussed first since the model for the unsteady-state period is based on assumptions derived from the theory for the steady-state period.

5.3.2 The Steady-state Filtration Period

As has been discussed in section 5.3.1 under assumption (ii), it is assumed that the porosity and solids compressive pressure profiles of the cake deposited under cross-flow conditions, are identical to those for a cake deposited under dead-end conditions. Due to the shear stress exerted by the flowing feed sludge at the inner cake surface, the dead-end cake is sheared along a shear plane. Those cake layers with a yield stress less than the shear stress exerted by the flowing feed sludge, flow along the shear plane in the cake (see Figure 5.7).

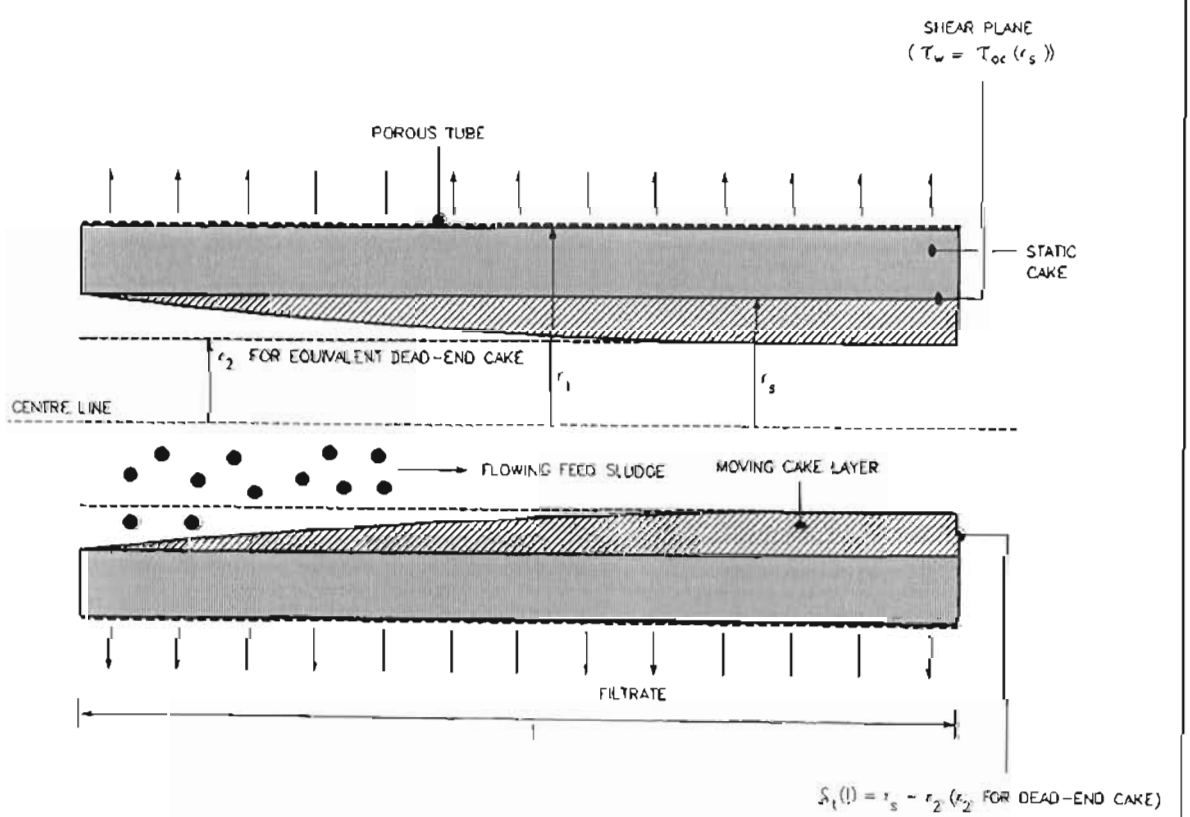

FIGURE 5.7 : Diagram to Explain Proposed Axial Convection Shear Model for Cross-flow Microfiltration Inside a Porous Tube

At steady-state, the rate of deposition of solids at the inner cake surface (over the whole length of the filter tube) is equal to the rate of removal of solids in the moving cake layer at the outlet of the filter tube. The thickness of the moving cake layer increases in an axial direction towards the outlet of the filter tube. The maximum thickness of the moving layer is at the outlet of the filter tube. It is assumed that the inner cake radius at the outlet of the filter tube corresponds to that of the corresponding dead-end cake from which the shear plane is determined. This is shown in Figure 5.7.

For the dead-end internal cylindrical filtration model developed in Chapter 3, it was assumed that the solids concentration of the feed sludge is sufficiently high so that sedimentation or settling occurs due to *consolidation* (see section 3.3.7.3). Under these conditions the settling rates of the solids in the feed sludge are very low and settling may be ignored. This also implies that for a cake deposited under static or dead-end conditions there will be no *discontinuity* in solids concentration at the cake/feed sludge interface, but rather a *continuous* progression from feed sludge to cake in the radial direction.

Under cross-flow conditions with an identical feed sludge it is highly probable that there will also be a *continuous* radial progression in solids concentration from feed sludge to moving cake layer through to static cake.

It is highly probable that there will be a complex *radial* and *axial* variation in solids concentration in the moving cake layer. However, since the moving cake layer is thin compared to the internal cake diameter and cake thickness (see assumption (vii) in section 5.3.1) it is assumed for the purposes of modelling that the solids concentration of the moving cake layer is *uniform*. This greatly simplifies the mathematical analysis which follows. The solids concentration of the moving layer is taken as the arithmetic mean of the solids concentration at the shear plane and that of the feed sludge, i.e. :

$$\phi_{sl} = \frac{\phi_{ss} + \phi_s}{2} \qquad (5.2)$$

where ϕ_s = volume fraction of solids in feed sludge, (-)

ϕ_{sl} = volume fraction of solids in moving cake layer, (-)

ϕ_{ss} = volume fraction of solids in cake at shear plane, (-)

The mathematical analysis for the laminar flow of a Bingham plastic fluid in a *non-porous* tube was given in section 4.4. These equations are rewritten for the laminar (see assumption (vi), section 5.3.1) flow of a Bingham plastic feed sludge (see assumption (ix), section 5.3.1) inside the annulus of a cake deposited inside a *porous* tube. From equation (4.22) the shear stress exerted at the inner cake wall or surface by the flowing feed sludge is :

$$\tau_w \cong \eta_{fs}\left(\frac{8\bar{u}_{fs}}{d_2}\right) + \frac{4}{3}\tau_{of} \qquad (5.3)$$

where d_2 = internal cake diameter, (m)

$\bar{u}_{fs}$ = average velocity of feed sludge, (m/s)

η_{fs} = coefficient of rigidity of feed sludge, (Pa.s)

τ_w = shear stress exerted by flowing fluid at internal wall of tube or cake, (Pa)

τ_{of} = yield stress of feed sludge, (Pa)

From equation (4.18) :

$$\bar{u}_{fs} = \frac{Q_{fs}}{\pi r_2^2} \qquad (5.4)$$

where Q_{fs} = volumetric flow rate of feed sludge, (m^3/s)

r_2 = internal radius of cake, (m)

Combining equations (5.3) and (5.4) :

$$\tau_w = \eta_{fs}\left(\frac{4Q_{fs}}{\pi r_2^3}\right) + \frac{4}{3}\tau_{of} \qquad (5.5)$$

At *steady-state* (since the liquid and solids are incompressible) the volumetric flow rate of solids into an element of the moving cake layer is equal to the volumetric flow rate of solids out of the element, as shown in Figure 5.8.

$$\therefore 2\pi\int_{r_s-\delta_t(x_t)}^{r_s} u_{mt}(r)\phi_{st}r\,dr + Q_{st}\phi_s\Delta x_t = 2\pi\int_{r_s-\delta_t(x_t+\Delta x_t)}^{r_s} u_{mt}(r)\phi_{st}r\,dr \qquad (5.6)$$

$$\left\{\begin{array}{c}\text{Volume of}\\ \text{solids into}\\ \text{differential}\\ \text{element due}\\ \text{to axial}\\ \text{convection}\end{array}\right\} + \left\{\begin{array}{c}\text{Volume of}\\ \text{solids into}\\ \text{differential}\\ \text{element due}\\ \text{to radial}\\ \text{convection}\end{array}\right\} = \left\{\begin{array}{c}\text{Volume of}\\ \text{solids out}\\ \text{of differential}\\ \text{element due}\\ \text{to axial}\\ \text{convection}\end{array}\right\}$$

where Q_{st} = volumetric flow rate of feed sludge to moving cake layer (due to radial convection) per unit length of tube, ($m^3/m.s$)

r = radius, (m)

r_s = radius of shear plane, (m)

u_{mt} = local axial velocity in moving cake layer, (m/s)

x_t = axial distance along filter tube, (m)

Δx_t = increment in axial distance along filter tube, (m)

δ_t = thickness of moving cake layer, (m)

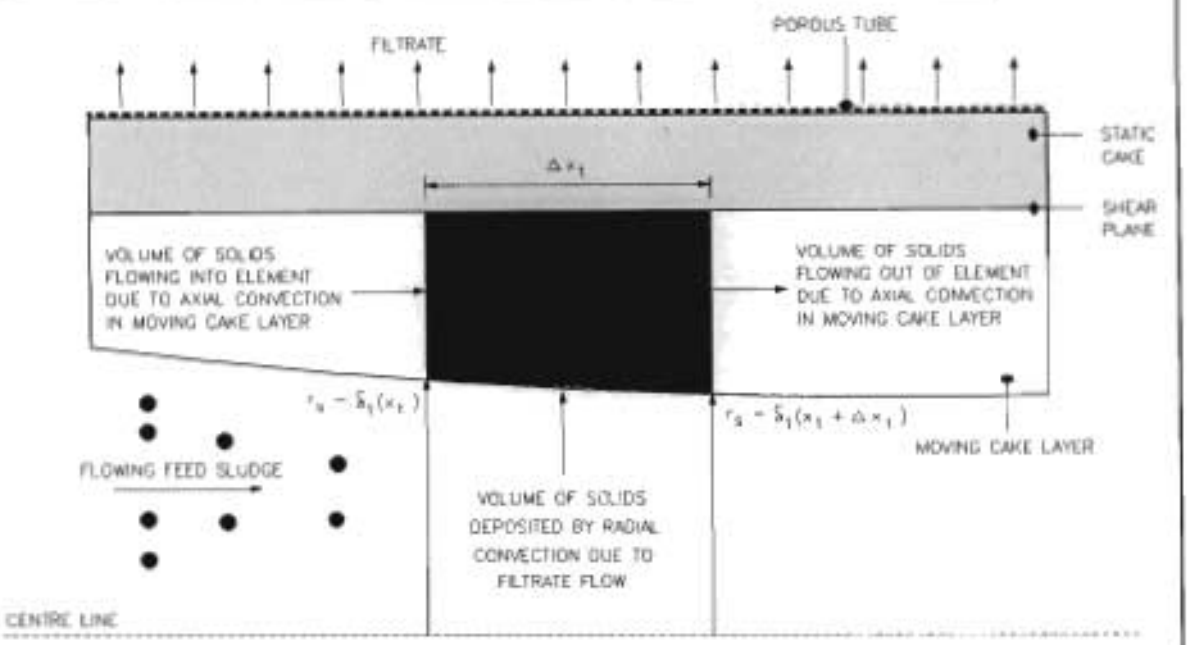

FIGURE 5.8 : Diagram to Show Solids Balance (at steady-state) Across a Differential Element of the Moving Cake Layer

The moving cake layer is a Bingham plastic fluid (see assumption (ix), section 5.3.1). Since the moving cake layer is thin compared to the internal cake diameter (see assumption (vii), section 5.3.1) and since the shear stress is uniform throughout the moving cake layer (see assumption (viii), section 5.3.1) (from equation (4.8)) :

$$\frac{du_{ml}}{dr} = -\left(\frac{\tau_w - \tau_{yl}}{\eta_l}\right) \tag{5.7}$$

where η_l = coefficient of rigidity of cake in moving layer, (Pa.s)

τ_{yl} = yield stress of cake in moving layer, (Pa)

Since $u_{ml} = 0$ at $r = r_s$, the integration of equation (5.7) gives :

$$\int_0^{u_{ml}} du_{ml} = -\int_{r_s}^{r} \frac{\tau_w - \tau_{yl}}{\eta_l} \tag{5.8}$$

$$\therefore\ u_{ml} = \left(\frac{\tau_w - \tau_{yl}}{\eta_l}\right)(r_s - r) \tag{5.9}$$

From equation (5.6) :

$$\frac{2\pi\int_{r_s-\delta_l(x_l-\Delta x_l)}^{r_s} u_{ml}(r)\phi_{sl}r\,dr \;-\; 2\pi\int_{r_s-\delta_l(x_l)}^{r_s} u_{ml}(r)\phi_{sl}r\,dr}{\Delta x_l} \;=\; Q_{sl}\phi_s \qquad (5.10)$$

By combining equations (5.9) and (5.10), as $\Delta x_l \rightarrow 0$:

$$Q_{sl}\phi_s \;=\; \frac{d}{dx_l}\left[\frac{2\pi(\tau_w-\tau_{ol})\phi_{sl}}{\eta_l}\int_{r_s-\delta_l(x_l)}^{r_s}(r_s-r)r\,dr\right] \qquad (5.11)$$

$$\therefore Q_{sl}\phi_s \;=\; 2\pi\left(\frac{\tau_w-\tau_{ol}}{\eta_l}\right)\phi_{sl}\frac{d}{dx_l}\left[\frac{r_s r^2}{2}-\frac{r^3}{3}\right]_{r_s-\delta_l(x_l)}^{r_s}$$

$$=\; 2\pi\left(\frac{\tau_w-\tau_{ol}}{\eta_l}\right)\phi_{sl}\frac{d}{dx_l}\left[\frac{r_s^3}{2}-\frac{r_s^3}{3}-\frac{r_s(r_s-\delta_l(x_l))^2}{2}+\frac{(r_s-\delta_l(x_l))^3}{3}\right] \qquad (5.12)$$

Since r_s does not vary along the length of the filter tube, equation (5.12) becomes :

$$Q_{sl}\phi_s \;=\; 2\pi\left(\frac{\tau_w-\tau_{ol}}{\eta_l}\right)\phi_{sl}\left[r_s(r_s-\delta_l(x_l))\left(\frac{d\delta_l(x_l)}{dx_l}\right)-(r_s-\delta_l(x_l))^2\left(\frac{d\delta_l(x_l)}{dx_l}\right)\right]$$

$$=\; 2\pi\left(\frac{\tau_w-\tau_{ol}}{\eta_l}\right)\phi_{sl}[r_s^2-r_s\delta_l(x_l)-r_s^2+2r_s\delta_l(x_l)-\delta_l^2(x_l)]\frac{d\delta_l(x_l)}{dx_l}$$

$$=\; 2\pi\left(\frac{\tau_w-\tau_{ol}}{\eta_l}\right)\phi_{sl}[r_s\delta_l(x_l)-\delta_l^2(x_l)]\frac{d\delta_l(x_l)}{dx_l} \qquad (5.13)$$

Since the filtrate flux is invariant with x_l (see assumption (iv), section 5.3.1), Q_{sl} is *constant* at steady-state and does not vary with x_l.

Therefore, the integration of equation (5.13) yields :

$$\int_o^{x_l} Q_{sl}\phi_s dx_l \;=\; 2\pi\left(\frac{\tau_w-\tau_{ol}}{\eta_l}\right)\phi_{sl}\int_o^{\delta_l(x_l)}(r_s\delta_l(x_l)-\delta_l^2(x_l))d\delta_l(x_l)$$

$$\therefore\; Q_{sl}\phi_s x_l \;=\; 2\pi\left(\frac{\tau_w-\tau_{ol}}{\eta_l}\right)\phi_{sl}\left(\frac{r_s\delta_l^2(x_l)}{2}-\frac{\delta_l^3(x_l)}{3}\right) \qquad (5.14)$$

Equation (5.14) describes the variation of the thickness of the moving cake layer with axial distance along the filter tube at *steady-state*.

At steady state, the rate of solids removal in the moving cake layer at the outlet of the filter tube is equal to the rate of solids deposition over the total length of the filter tube i.e. from equation (5.14) :

$$Q_{sl}\phi_s l \;=\; 2\pi\left(\frac{\tau_w-\tau_{ol}}{\eta_l}\right)\phi_{sl}\left(\frac{r_s\delta_l^2(l)}{2}-\frac{\delta_l^3(l)}{3}\right) \qquad (5.15)$$

where l = length of filter tube, (m)

The left hand side of equation (5.15) gives the rate of solids deposition along the total length of the filter tube, while the right hand side of equation (5.15) gives the rate of solids removal in the moving cake layer at the *outlet* of the filter tube.

However, the steady state values of Q_{st}, ϕ_{st} and r_s are not known a priori, so that equation (5.15) as it stands cannot be used to determine the steady-state values. In the following section a model is developed for the *unsteady-state* period. For the unsteady-state period *quasi steady-state* conditions are assumed to exist during short incremental time intervals. The right hand side of equation (5.15) is used to describe the rate of solids removal for the *quasi steady-state* conditions.

5.3.3 The Unsteady-state Filtration Period

As mentioned before, Pearson and Sherwood (1988) developed complex partial differential equations to describe the unsteady-state time period for their cross-flow microfiltration model. The mathematical technique for the unsteady-state time period for the axial convection shear model, has been simplified as discussed below.

At the beginning of the filtration cycle the internal cake diameter is large (cake thickness thin) and the filtrate flux is high. Under these conditions the shear stress exerted by the flowing feed sludge at the inner cake surface is small (from equation (5.3)) and the rate of deposition of solids exceeds the rate of removal of solids. As the inner cake diameter decreases, the shear stress exerted by the flowing feed sludge at the inner cake surface increases and the filtrate flux decreases. This means that the rate of removal of solids increases, while the rate of deposition of solids decreases. The cake thickness increases until at steady-state, the rate of deposition of solids is equal to the rate of removal of solids in the moving cake layer at the outlet of the filter tube, as was described in section 5.3.2.

During the unsteady-state filtration period the situation is very complex due to the fact that the rate of solids deposition exceeds the rate of solids removal and the cake thickness is continuously growing. This means that the shear plane is moving with time.

In order to simplify the situation for the purposes of modelling, the unsteady-state filtration period is divided into short incremental time intervals, Δt. It is assumed that during each time interval, Δt, a *quasi steady-state* exists. For the *quasi* steady-state it is assumed that the solids removal rate and axial thickness profile of the moving cake layer may be calculated from the right hand side of equation (5.15), which was developed for the steady-state. As for the steady-state, it is assumed that the thickness of the moving cake layer grows in an axial direction as it flows towards the outlet of the filter tube and the thickness of the moving cake layer is greatest at the outlet of the filter tube.

Under the previously mentioned assumption for the *quasi steady-state* case, the right hand side of equation (5.15) may be used to calculate the rate of solids removal during any time interval, Δt, during the unsteady-state filtration period :

$$R_{sr} = 2\pi\left(\frac{\tau_w - \tau_{ol}}{\eta_l}\right)\phi_{sl}\left(\frac{r_s\delta_l^2(l)}{2} - \frac{\delta_l^3(l)}{3}\right) \qquad (5.16)$$

where R_{sr} = volumetric rate of removal of solids in moving cake layer at outlet of filter tube during time interval, Δt, (m^3/s)

The thickness of the moving cake layer at the outlet of the filter tube, $\delta_l(l)$, is taken as the difference between the radius of the shear plane within an equivalent cake formed under *dead-end* conditions and the internal radius, r_2, of such a cake (see Figure 5.7). (It should be noted that for an equivalent cake formed under dead-end conditions the internal radius of the cake is uniform in the axial direction (see Figure 5.7) while under cross-flow conditions the thickness of the moving cake layer grows along the *shear plane* from zero thickness, at the inlet of the filter tube, to $\delta_l(l)$, at the outlet of the filter tube).

For the quasi-steady state the volume fraction of solids in the moving cake layer, ϕ_{sl}, is determined from equation (5.2).

During time interval, Δt, the rate of solids deposition along the whole filter tube is calculated using the left hand side of equation (5.15) :

$$R_{sd} = Q_{sl}\phi_s l \qquad (5.17)$$

where R_{sd} = volumetric rate of deposition of solids along whole filter tube in time interval, Δt, (m^3/s)

The calculation of solids deposition is described in greater detail in section 5.3.3.1.

The *net* rate of deposition of solids during time interval, Δt, is therefore :

$$N_{dep} = R_{sd} - R_{sr} \qquad (5.18)$$

where N_{dep} = *net* volumetric rate of deposition of solids during time interval, Δt, (m^3/s)

During the unsteady-state filtration period when the rate of solids deposition exceeds the rate of solids removal, the *net* rate of solids deposition, N_{dep}, is greater than zero. The *increase* in cake thickness (which is assumed to be uniform along the length of the filter tube, identical to dead-end filtration) during the time interval, Δt, may be calculated from the *net* rate of solids deposition. This is shown in Figure 5.9.

From equation (5.18) the steady-state is reached when $R_{sd} = R_{sr}$ and the *net* rate of deposition of solids is zero.

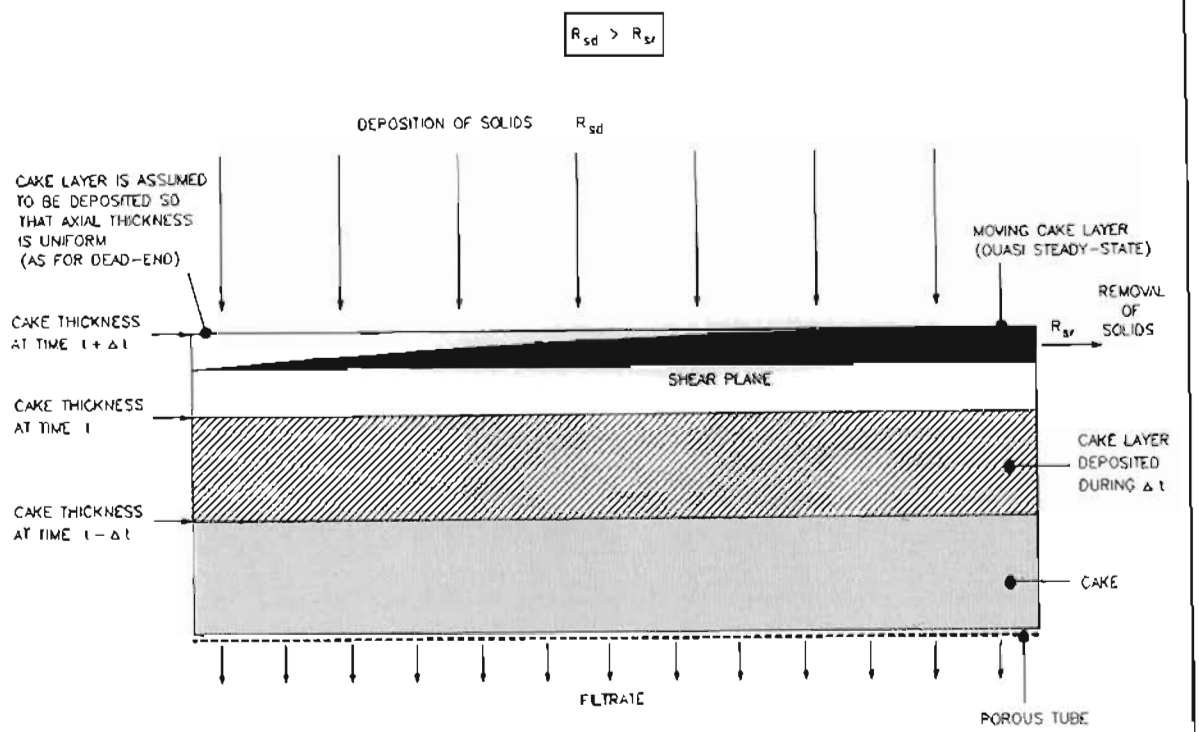

FIGURE 5.9 : Diagram to Explain Calculation of Cake Thickness During Unsteady-state Time Period

The calculation procedures for the unsteady-state model are discussed in greater detail in sections 5.3.3.1 and 5.3.3.2.

5.3.3.1 Method for calculation of rate of solids deposition

Before the unsteady-state cross-flow filtration model is developed further, the method for the calculation of the rate of solids deposition will first be described.

If the liquid in the cake is negligible compared with the volume of filtrate, then the rate of solids deposition may be calculated from the following equation :

$$Q_{sl}\phi_s = \frac{Q\phi_s}{1-\phi_s} \qquad (5.19)$$

where Q = overall volumetric flow rate of liquid (filtrate) per unit length of filter tube, ($m^3/m.s$)

However, if the liquid in the cake is not negligible compared with the volume of filtrate (as was true for this study), equation (5.19) cannot be used. The following iterative procedure may be employed to calculate Q_{sl}.

For a certain cake thickness or internal cake diameter, Q_{sl} will be the same for both dead-end and cross-flow filtration (see assumptions (ii) and (iv), section 5.3.1).

For a certain internal cake radius, r_2; and in time interval, Δt:

$$\left\{\begin{matrix}volume\ of\\ sludge\ filtered\end{matrix}\right\} = \left\{\begin{matrix}increment\ in\\ volume\ of\ filtrate\end{matrix}\right\} + \left\{\begin{matrix}increment\ in\\ volume\ of\ cake\end{matrix}\right\}$$

$$\Delta V_{sl} = \Delta V + \Delta V'_{cl} \qquad (5.20)$$

where Δt = time interval, (s)

ΔV = increment in volume of filtrate per unit length of tube in time interval, Δt, (m^3/m)

$\Delta V'_{cl}$ = increment in volume of cake per unit length of tube in time interval, Δt, (for dead-end filtration), (m^3/m)

ΔV_{sl} = volume of sludge filtered per unit length of tube in time interval, Δt, (m^3/m)

Also,

$$\Delta V'_{cl} = V'_{cl}|_{t+\Delta t} - V_{cl}|_t \qquad (5.21)$$

where V_{cl} = volume of cake per unit length of tube for cross-flow filtration, (m^3/m)

V'_{cl} = volume of cake per unit length of tube for dead-end filtration, (m^3/m)

The increment in volume of filtrate during time interval, Δt, may be calculated from the following equation :

$$\Delta V = Q(t)\Delta t \qquad (5.22)$$

$Q(t)$ may be calculated from the internal cylindrical filtration model for dead-end filtration (from assumption (ii), section 5.3.1).

The internal cake radius for dead-end filtration at time $t + \Delta t$ may be calculated from the following equation :

$$r_2|_{t+\Delta t} = \sqrt{r_1^2 - \frac{V'_{cl}|_{t+\Delta t}}{\pi}} \qquad (5.23)$$

From a solids balance :

$$\Delta V_{sl}\phi_s = V'_{cl}|_{t+\Delta t}(1-\epsilon_{av})|_{t+\Delta t} - V_{cl}|_t(1-\epsilon_{av})|_t \qquad (5.24)$$

$Q_{sl}(t)$ may be calculated from the following equation :

$$Q_{sl}(t) = \frac{\Delta V_{sl}}{\Delta t} \qquad (5.25)$$

ΔV_{sl} (and therefore $Q_{sl}(t)$) is calculated using an iterative procedure. An algorithm of this procedure is shown in Figure 5.10.

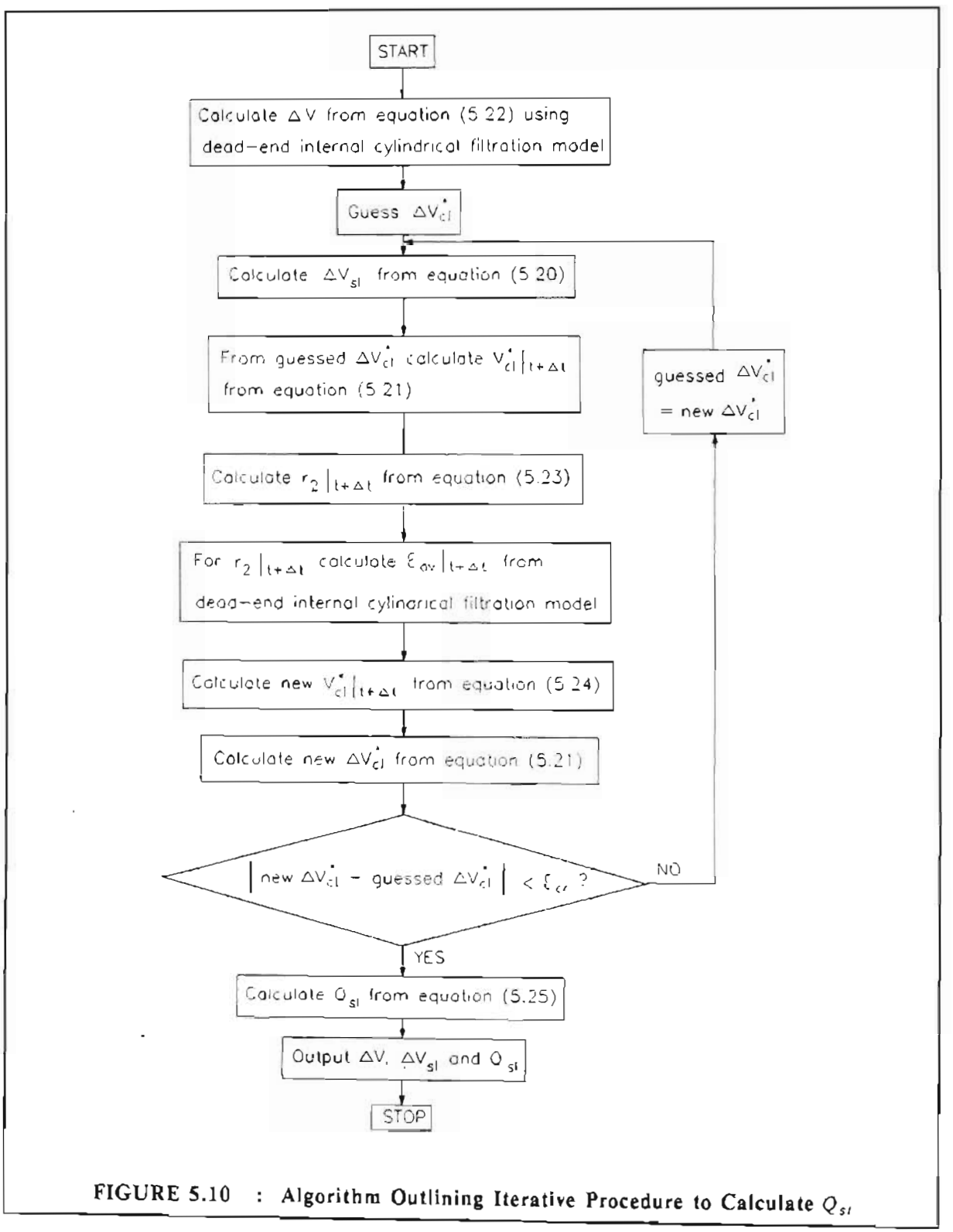

FIGURE 5.10 : Algorithm Outlining Iterative Procedure to Calculate Q_{sl}

For the calculation of Q and ϵ_{av} from the internal cylindrical filtration model for dead-end filtration, the procedure has to be slightly amended from that described in Chapter 3.

As discussed in section 3.5.7, the Euler technique was used to integrate ordinary differential equations (3.28) and (3.39) to obtain the p_s and p_L profiles through the cake for various internal cake diameters. For the Euler technique (see section 3.5.7), it was assumed that the cake is deposited in thin layers of *equal* thickness, Δr. This technique was used to allow for a decrease in solids compressive pressure in the cake layers in close proximity to the filter medium as the internal cake diameter decreases (see section 3.5.8).

As mentioned in section 3.6.3, the significance of the solids compressive pressure decreasing in the cake layers close to the filter medium (as internal cake diameter decreases), was found to be negligible.

For the calculation of Q and ϵ_{av} (as shown in Figure 5.10), the Runge-Kutta finite difference integration technique is used for the dead-end internal cylindrical filtration model. The major advantage of this technique is that the ordinary differential equations (3.28) and (3.39) can be solved for any arbitrary value of r_2 (which is required for the iterative technique shown in Figure 5.10), since the method is not limited to fixed increments in r_2 (as in the Euler technique).

5.3.3.2 Method of calculation for the unsteady-state filtration period

The modelling principles for the unsteady-state filtration period have been outlined earlier. An iterative calculation procedure for the unsteady-state is outlined in this section.

The volume of solids removed in time interval, Δt, due to the shear of the flowing feed sludge is :

$$\Delta V_{sh} = R_{sr}\Delta t \tag{5.26}$$

where ΔV_{sh} = volume of solids removed in moving cake layer at outlet of filter tube in time interval, Δt, (m^3)

When the solids removal due to shear is incorporated into a solids balance :

$$lV_{cl}|_{t+\Delta t}(1-\epsilon_{av})|_{t+\Delta t} - lV_{cl}|_t(1-\epsilon_{av})|_t = l\Delta V_{sl}\phi_s - \Delta V_{sh} \tag{5.27}$$

$$\therefore\ V_{cl}|_{t+\Delta t} = \frac{l\Delta V_{sl}\phi_s - \Delta V_{sh} + lV_{cl}|_t(1-\epsilon_{av})|_t}{l(1-\epsilon_{av})|_{t+\Delta t}} \tag{5.28}$$

The volume of cake per unit length of tube at time, $t+\Delta t$, may also be calculated using an iterative procedure which is shown in Figure 5.11.

The algorithm for the unsteady-state cross-flow microfiltration model is shown in Figure 5.11. A FORTRAN computer program was written for this algorithm.

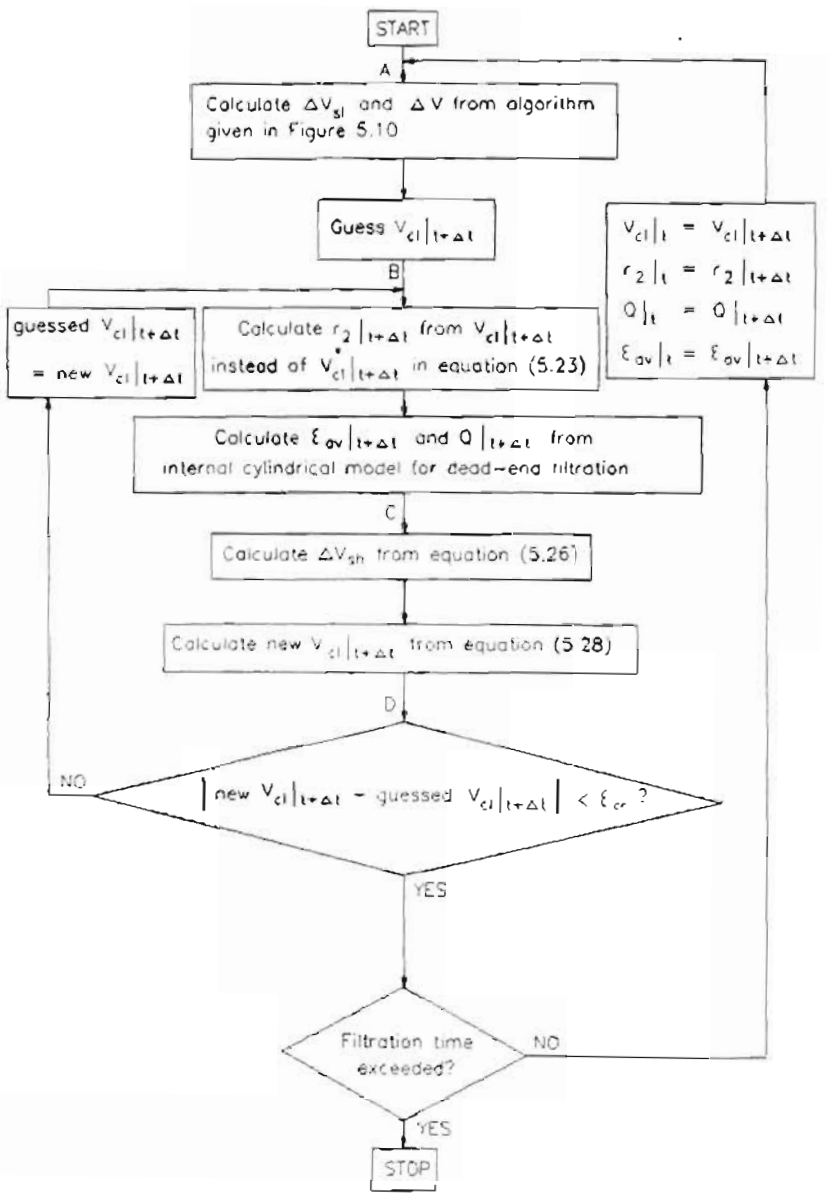

FIGURE 5.11 : Algorithm Outlining Iterative Procedure for Unsteady-state Cross-flow Microfiltration Model

One of the advantages of the axial convection shear model developed above, is that it does not require arbitrary fitting or regression parameters as is the case for many cross-flow microfiltration models. For Pearson and Sherwood's (1988) model, for example, the value of the shear enhanced diffusion coefficient has to be fitted to or regressed from experimental data, if the model is to be used for predictive purposes. The same applies to the models of Hunt (1987) and Pillay (1991).

For the axial convection shear model developed above, only the sludge and cake rheology and the variation of permeability and porosity with solids compressive pressure, have to be determined experimentally for a specific sludge, if the model is to be used for predictive purposes.

5.4 EXPERIMENTAL STUDY OF LAMINAR CROSS-FLOW FILTRATION OF THE WATERWORKS CLARIFIER SLUDGE INSIDE A POROUS TUBE

5.4.1 Introduction

The objectives of the experimental study were :

(i) to investigate the laminar cross-flow filtration of the waterworks clarifier sludge;

(ii) to compare the experimental results with those predicted by the unsteady-state (transient) laminar shear model which was developed in section 5.3.

5.4.2 Experimental Apparatus

The experimental apparatus was the same as that which was used for the dead-end internal cylindrical filtration experiments which were discussed in Chapter 3. The apparatus was amended slightly as shown in Figure 5.12. The cross-flow flow rate through the porous filter tube was controlled by means of "linear orifices". These were various lengths of nylon tubes (the same type as was used for the capillary-tube viscometer experiments discussed in Chapter 4). As the tube length was increased, the flow rate decreased and vice versa. "Linear orifices" were used for flow control instead of valves, because during earlier experiments it was found that the solids in the clarifier sludge would sometimes accumulate in the small throats of the valves, which were required for the low flow rates used during this study. This caused erratic flow rates and disturbances of flow. The pressure in the porous tube during an experiment was controlled by a programmable pressure controller which controlled the pressure within the porous tube by controlling the speed of the MONO pump.

5.4.3 Experimental Procedure

A batch of waterworks clarifier sludge was prepared in an identical manner as for the dead-end internal cylindrical filtration experiments (see section 3.4.3.2). A "linear orifice" (nylon tube) was installed to give the required cross-flow flow rate at the filtration pressure selected for an experiment (see Figure 5.12). Valve V10 was closed. The required pressure for an experiment was entered into the programmable pressure controller. Before an experiment the feed sludge was homogenized by switching on the stirrer in the feed tank (see Figure 5.12). Thereafter sludge was circulated by the MONO pump from the feed tank through the system

and back to the feed tank by opening valve V3 and keeping valves V4 and V5 closed. This was done to fill all pipes with sludge and to expel any air bubbles from the system.

After five minutes of pumping, valves V4, V5 and V10 were opened and by-pass valve V3 was closed to allow circulation of sludge through the porous tube for a short time period of 30 seconds. This allowed filling of the porous tube and the expelling of any air bubbles from the tube.

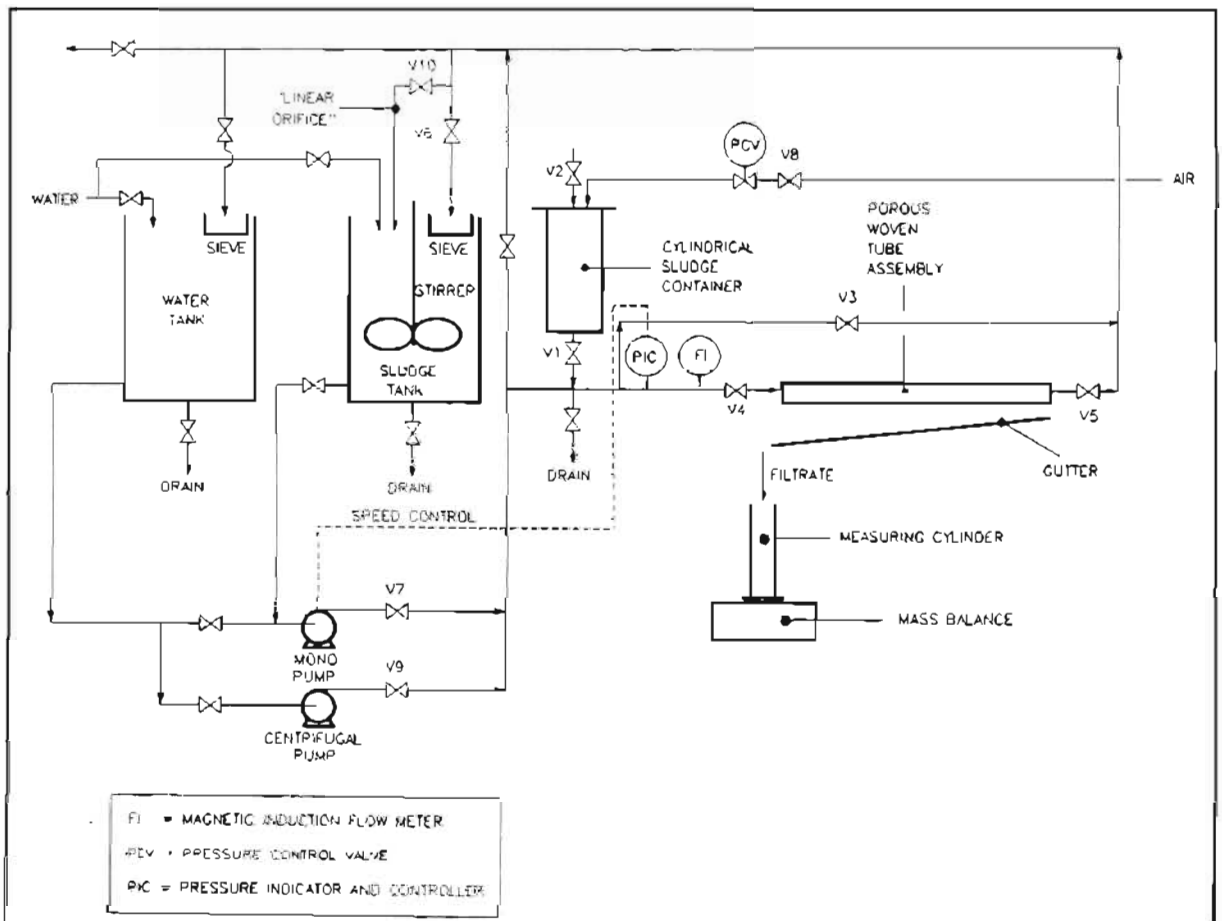

FIGURE 5.12 : Experimental Apparatus which was used for the Cross-flow Microfiltration Experiments

Valve V6 was closed and flow was directed through the "linear orifice". The pressure in the porous tube increased very rapidly until it reached the pre-selected filtration pressure. Thereafter the pressure was controlled by the pressure controller while the flow rate was controlled by the "linear orifice".

The filtrate was collected in the same manner as for the dead-end internal cylindrical filtration experiments (see section 3.4.3.2).

The sludge in the feed tank was intermittently homogenized during the course of an experiment.

At the end of the experiment the MONO pump was switched off and the pressure was released through the "linear orifice".

The porous tube assembly was dismantled and the cake was collected in the same manner as for the dead-end internal cylindrical filtration experiments (see section 3.4.3.2).

The experimental procedure was repeated for subsequent filtration experiments.

At the end of a day the pipes in the system were purged of sludge by pumping water from the water tank through the system by means of the centrifugal pump.

5.5 RESULTS

The results of the experimental study are tabulated in Appendix J. The experiments were all done at a single filtration pressure of 300 kPa. The following cross-flow flow rates for the feed sludge were considered : 0,84 ℓ/min; 1,58 ℓ/min; 2,43 ℓ/min and 4,44 ℓ/min. The filtration times were in the range of 5 minutes to 90 minutes. The feed sludge solids concentration for all experiments was the same as that for the dead-end internal cylindrical filtration experiments (Chapter 3), namely, approximately 49 g/ℓ (ϕ_s = 0,0206).

5.5.1 The Variation of Internal Cake Diameter with Filtration Time and Cross-flow Flow Rate

The variation of internal cake diameter with both filtration time and cross-flow flow rate is shown in Figure 5.13. Except for a cross-flow rate of 1,58 ℓ/min, the internal cake diameters shown in Figure 5.13 are calculated experimental internal cake diameters, as shown in Appendix J. The internal cake diameters for a cross-flow flow rate of 1,58 ℓ/min were measured with a vernier calliper. The internal cake diameters were calculated (from mass of wet cake and average cake dry solids concentration) using the same method as for the dead-end internal cylindrical filtration experiments (see Appendix D). (This method was acceptable since it was found by vernier calliper measurements that there was no significant *axial* variation in internal cake diameter (along the length of the filter tube) for the cross-flow filtration experiments). The internal cake diameters, as measured with a vernier calliper, are also tabulated in Appendix J. There was close agreement between *measured* (using a vernier calliper) and *calculated* (from mass of wet cake and average cake dry solids concentration) experimental internal cake diameters (see also Figures 5.22 (a) to (d)).

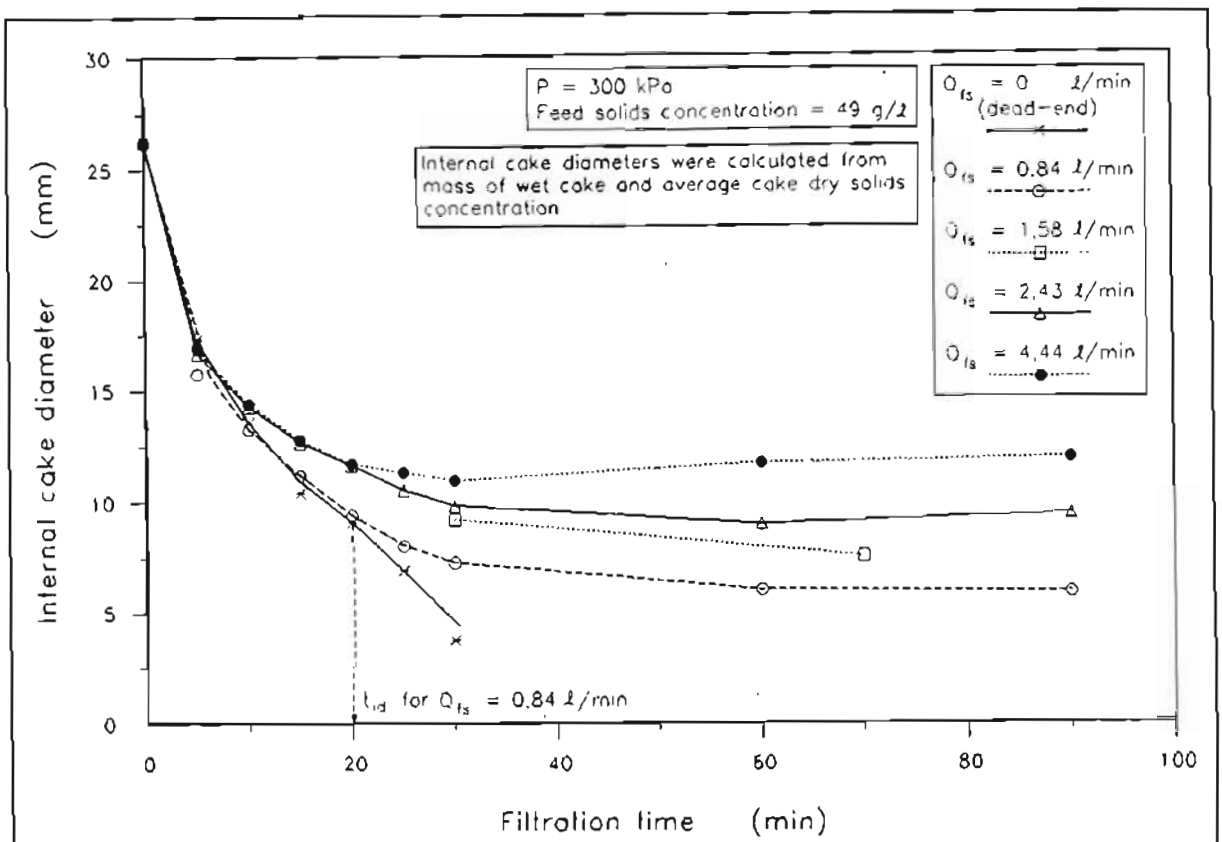

FIGURE 5.13 : The Variation of Calculated Experimental Internal Cake Diameter with Filtration Time and Cross-flow Flow Rate

As shown in Figure 5.13, for each cross-flow flow rate (the internal cake diameters for a flow rate of 1,58 ℓ/min were only measured at 30 and 70 minutes) it was found that below a threshold filtration time, t_{id} , the internal cake diameters were identical or very close to those for dead-end filtration. The threshold filtration times (t_{id}) for cross-flow rates of 0,84 ℓ/min; 2,43 ℓ/min and 4,44 ℓ/min were approximately 20 minutes, 10 minutes and 8 minutes, respectively. The threshold filtration time, t_{id} , was therefore dependent on the cross-flow flow rate. It was found that the lower the cross-flow flow rate, the higher the threshold filtration time, t_{id} . After the threshold filtration time, t_{id} ,the curve for each cross-flow flow rate *slowly deviated* from the curve for dead-end filtration, until an equilibrium internal cake diameter was reached. The equilibrium internal cake diameter remained essentially constant with filtration time. The equilibrium internal cake diameter was dependent on the cross-flow flow rate. It was found that the lower the cross-flow flow rate, the lower the equilibrium internal cake diameter.

The time required to reach an equilibrium internal cake diameter was also found to be dependent on cross-flow flow rate. For cross-flow flow rates of 0,84 ℓ/min; 2,43 ℓ/min and 4,44 ℓ/min the times were estimated to be 45 minutes, 30 minutes and 20 minutes, respectively. Therefore, the higher the cross-flow flow rate the shorter the time required to reach an equilibrium internal cake diameter.

5.5.2 The Variation of Filtrate Flux with Filtration Time and Cross-flow Flow Rate

The variation of filtrate flux with filtration time and cross-flow flow rate is shown in Figure 5.14. The shapes of the curves for filtrate flux are very similar to those for internal cake diameter, as shown previously in Figure 5.13. As shown in Figure 5.14, for cross-flow flow rates of 1,58 ℓ/min; 2,43 ℓ/min and 4,44 ℓ/min, it was found that below a threshold filtration time, t_{fi}, the filtrate fluxes were identical to those for dead-end filtration. (Fordham and Ladva (1989) achieved similar results for the cross-flow filtration of bentonite suspensions).

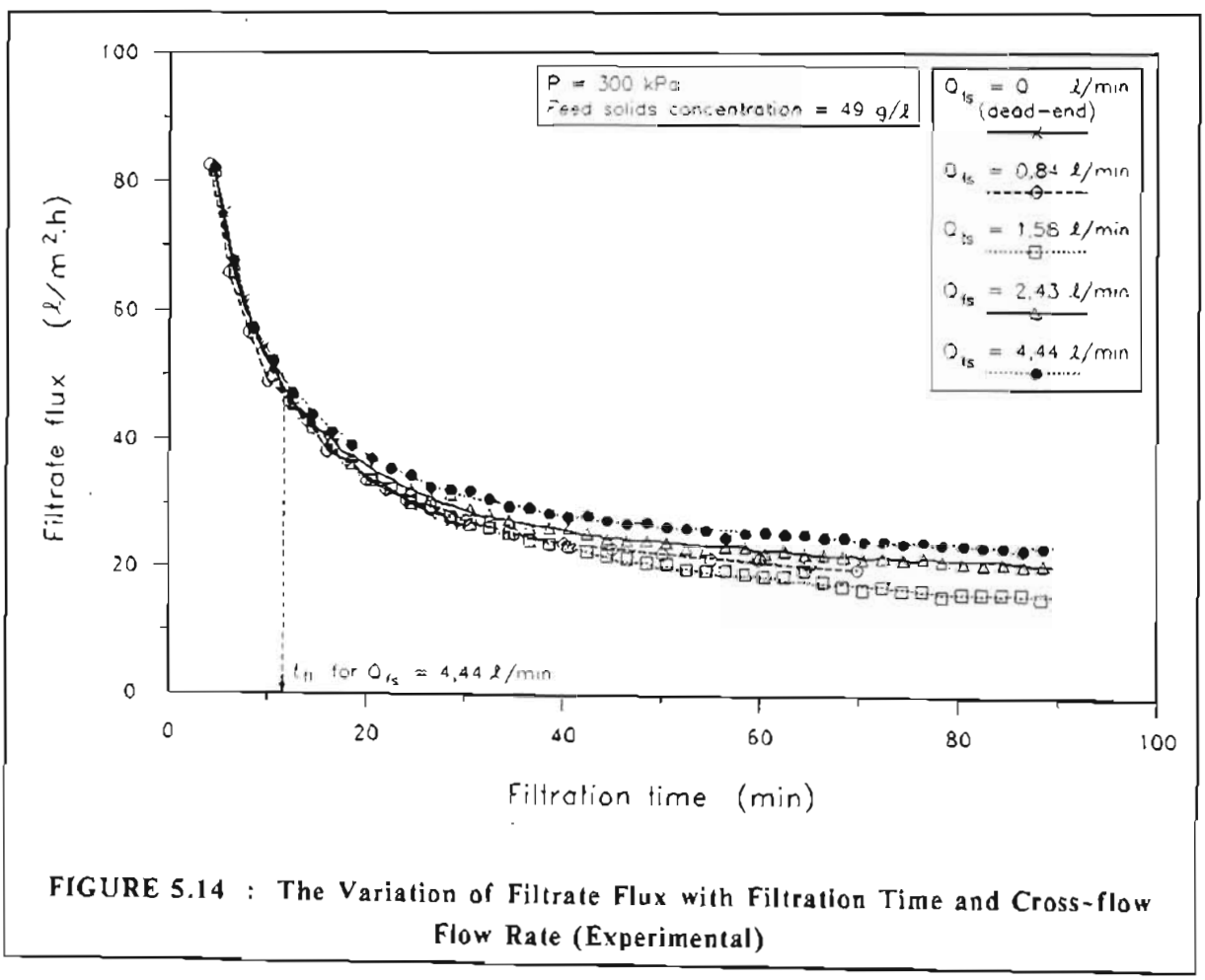

FIGURE 5.14 : The Variation of Filtrate Flux with Filtration Time and Cross-flow Flow Rate (Experimental)

The threshold filtration times, (t_{fl}) for cross-flow flow rates of 1,58 ℓ/min; 2,43 ℓ/min and 4,44 ℓ/min were estimated to be 27 minutes, 17 minutes and 12 minutes,respectively. Just as for the threshold filtration times, t_{id} , (see section 5.5.1), it was found that the lower the cross-flow flow rate, the higher t_{fl} . The threshold times, t_{fl} were slightly higher than the threshold times, t_{id} . The flux curve for a cross-flow flow rate of 0,84 ℓ/min was identical to that for dead-end filtration, so that no threshold filtration time could be determined.

After the threshold filtration time, t_{fl} , the flux curve for each cross-flow flow rate slowly deviated from the dead-end curve until a *pseudo* steady-state filtrate flux was reached. The *pseudo* steady-state filtrate flux was dependent on the cross-flow flow rate. It was found that the higher the cross-flow flow rate, the higher the pseudo steady-state flux.

As shown in Figure 5.15, the filtrate flux continued to decrease slowly even after the equilibrium internal cake diameter had been attained. Similar results were also reported by Baker et al. (1985) and Pillay (1991).

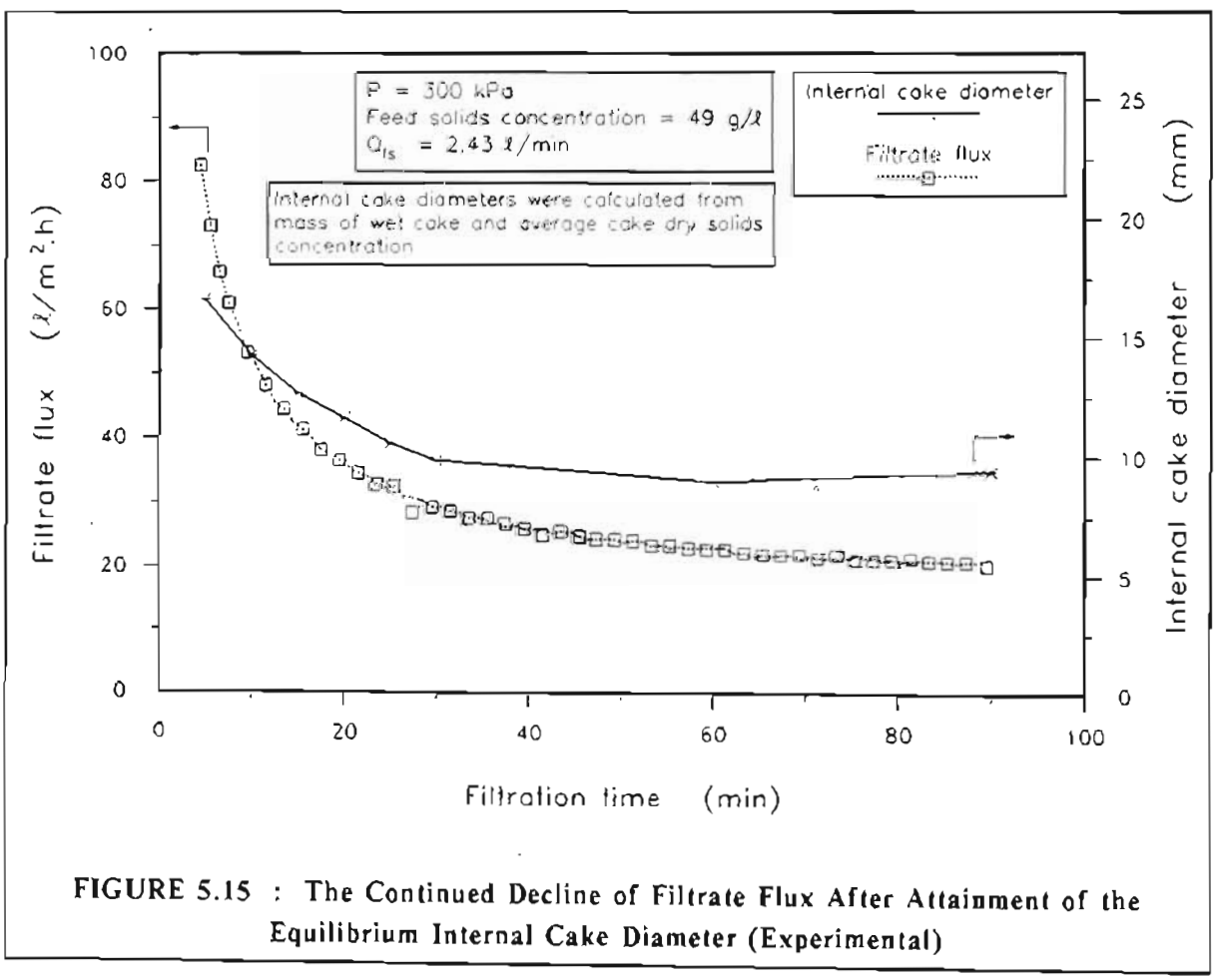

FIGURE 5.15 : The Continued Decline of Filtrate Flux After Attainment of the Equilibrium Internal Cake Diameter (Experimental)

5.5.3 The Variation of Average Cake Dry Solids Concentration with Filtration Time and Cross-flow Flow Rate

The variation of average cake dry solids concentration with filtration time and cross-flow flow rate is shown in Figure 5.16. When comparing Figures 5.13 and 5.16, it is evident that the average cake dry solids concentrations for dead-end filtration were not markedly different from those for cross-flow filtration in the time period prior to the attainment of an equilibrium internal cake diameter. This supports one of the assumptions for the theoretical model (assumption (ii), section 5.3.1), that the physical characteristics of a cake deposited under *dead-end* conditions are not markedly different from those of a cake deposited under *cross-flow* conditions. This is discussed further in section 5.7.3. However, after an equilibrium internal cake diameter was attained, the average cake dry solids concentration continued to increase further, as shown in Figure 5.17 for a cross-flow flow rate of 2,43 ℓ/min.

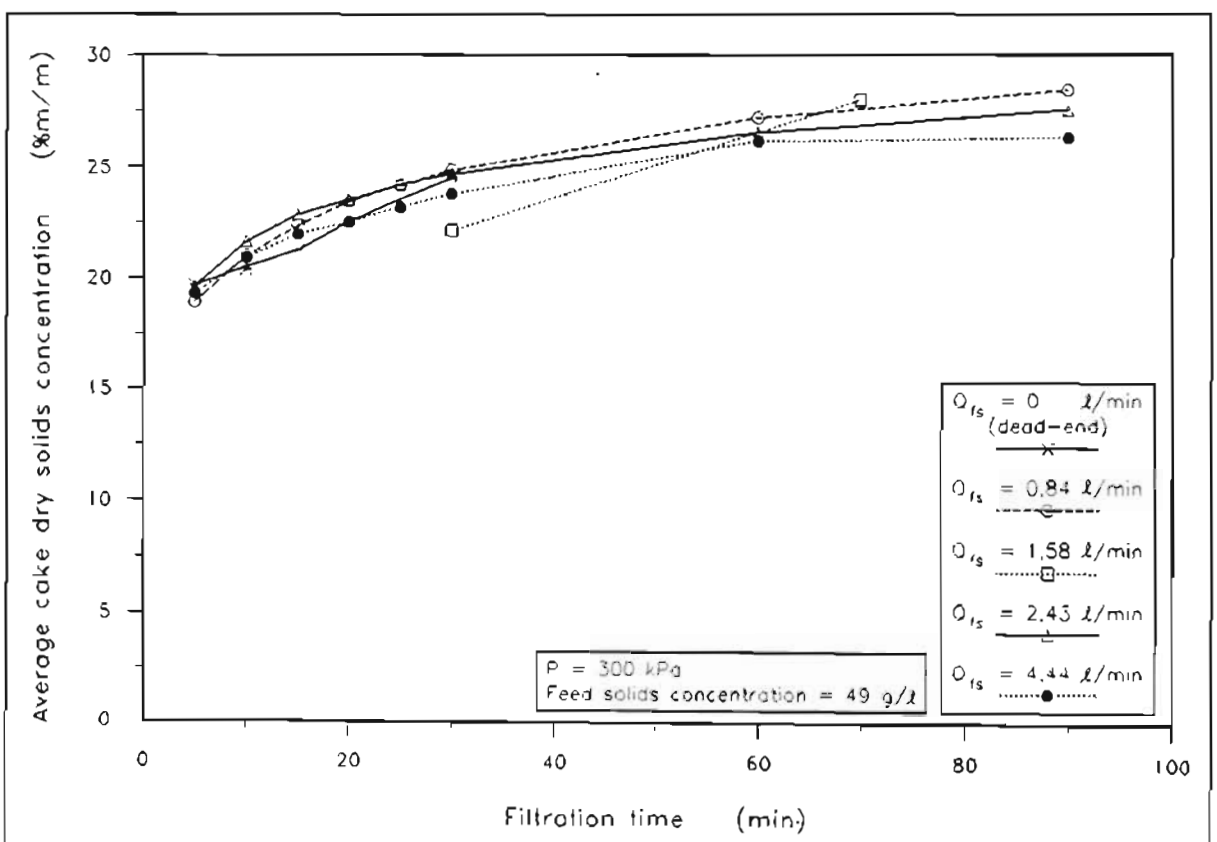

FIGURE 5.16 : The Variation of Average Cake Dry Solids Concentration with Filtration Time and Cross-flow Flow Rate (Experimental)

As shown in Figure 5.16, it was found that the *lower* the cross-flow flow rate, the *higher* the average cake dry solids concentration.

It was also found that the lower the cross-flow flow rate, the smaller the internal cake diameter (greater the cake thickness), as shown in Figure 5.13. The trend for average cake dry solids concentration shown in Figure 5.16 is the same as for *dead-end* internal cylindrical filtration. For dead-end internal cylindrical filtration it was found that the greater the cake thickness, the higher the average cake dry solids concentration (see Chapter 3).

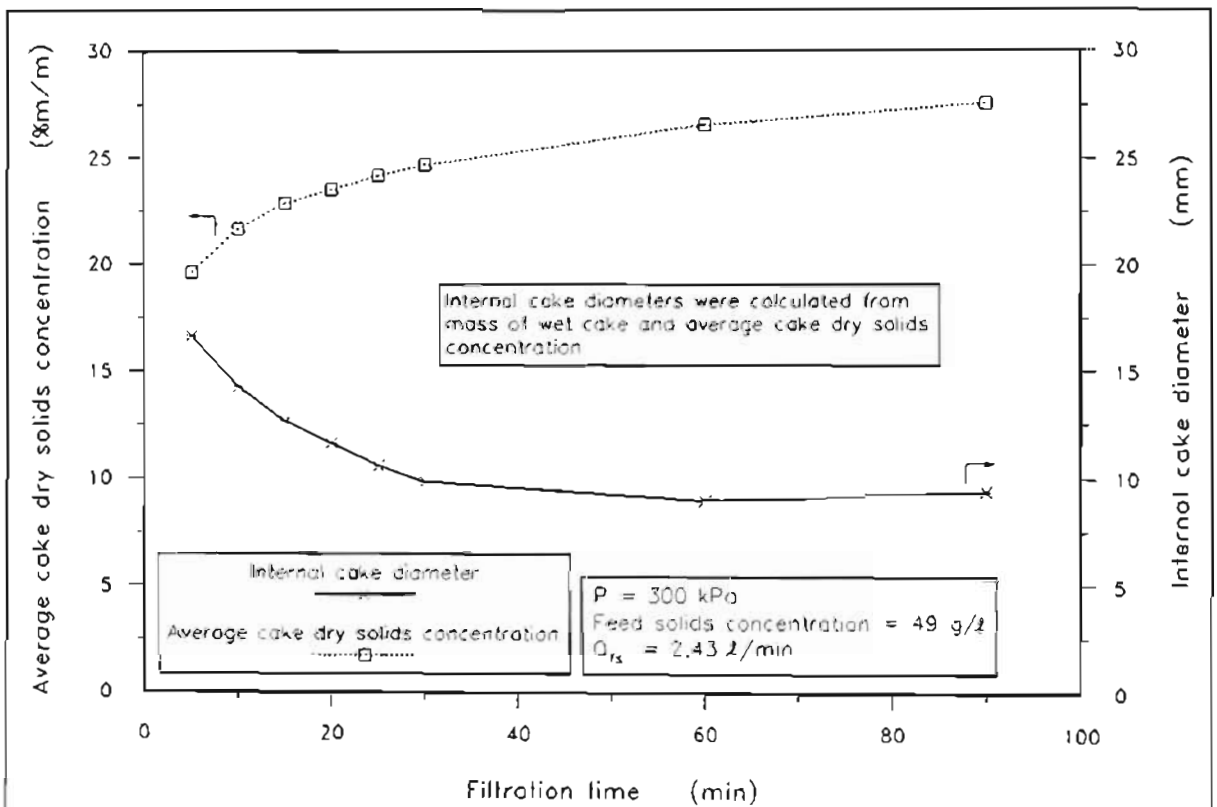

FIGURE 5.17 : The Continued Increase of Average Cake Dry Solids Concentration After Attainment of the Equilibrium Internal Cake Diameter (Experimental)

The fact that average cake dry solids concentration increased even after the attainment of an equilibrium internal cake diameter, means that solids deposition continued even after the attainment of an equilibrium internal cake diameter. The total mass of cake dry solids deposited per unit medium area (w_c) at various filtration times is shown in Figure 5.18, for a cross-flow flow rate of 2,43 ℓ/min. As shown in Figure 5.18, w_c increased even after the attainment of an equilibrium internal cake diameter.

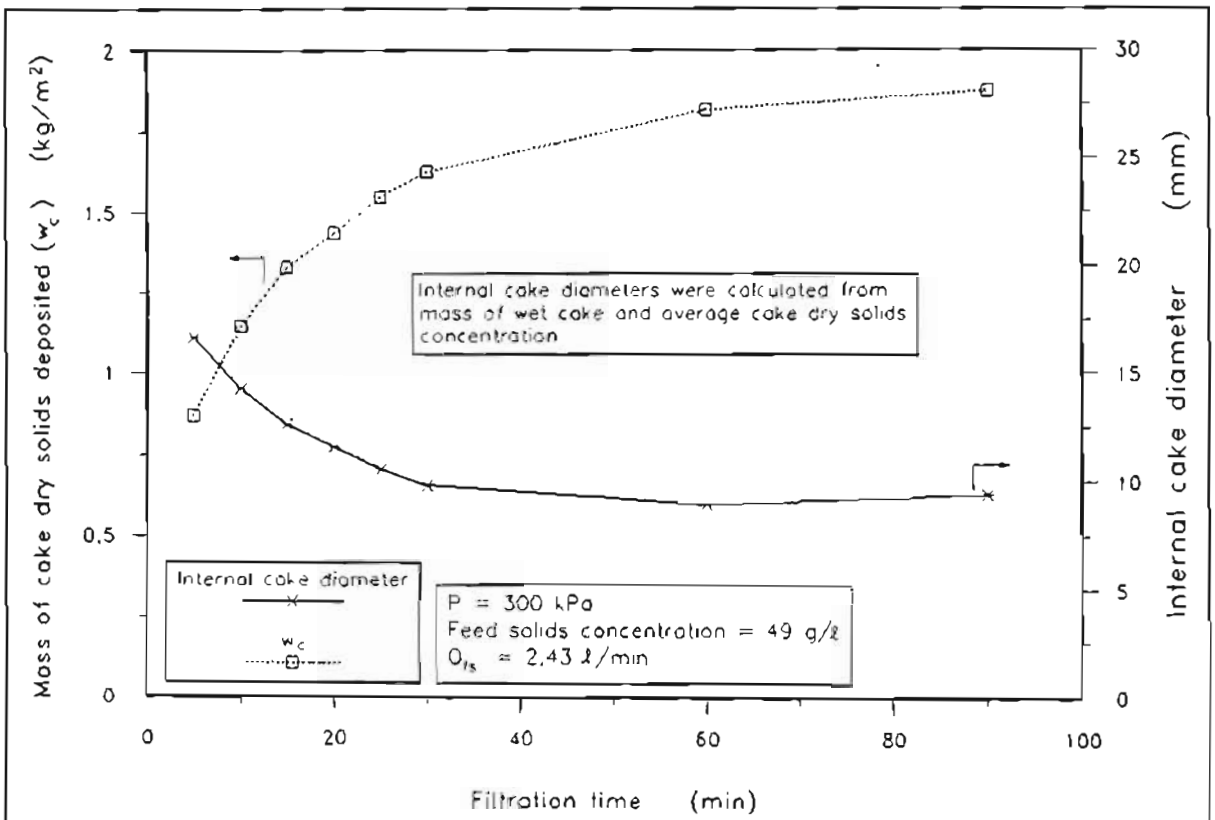

FIGURE 5.18 : Graph Showing Mass of Cake Dry Solids Deposited (w_c) versus Filtration Time for a Cross-flow Flow Rate of 2,43 ℓ/min (Experimental)

5.5.4 The Variation of Average Cake Permeability with Filtration Time and Cross-flow Flow Rate

The variation of average cake permeability (K_{av}) with filtration time and cross-flow flow rate is shown in Figure 5.19.

From equation (3.28) for dead-end internal cylindrical filtration the pressure drop through a layer of cake is :

$$\frac{dp_l}{dr} = -\frac{\mu_f Q}{2\pi r K} \qquad (3.28)$$

where K = local permeability of cake or sediment, (m^2)

p_l = liquid pressure, (kPa)

Q = overall volumetric flow rate of liquid (filtrate) per unit length of filter tube, ($m^3/m.s$)

r = radius, (m)

μ_f = viscosity of liquid (filtrate), (Pa.s)

If the resistance of the medium is ignored :

$$\int_0^P dp_t = -\frac{\mu_f Q}{2\pi}\int_{r_1}^{r_2}\frac{dr}{rK} \qquad (5.29)$$

where P = applied filtration pressure, (Pa)

r_1 = internal radius of filter medium, (m)

r_2 = internal radius of cake, (m)

$$\therefore\ P = \frac{\mu_f Q}{2\pi}\int_{r_2}^{r_1}\frac{dr}{rK} \qquad (5.30)$$

The average cake permeability for Figure 5.19 was defined as follows.

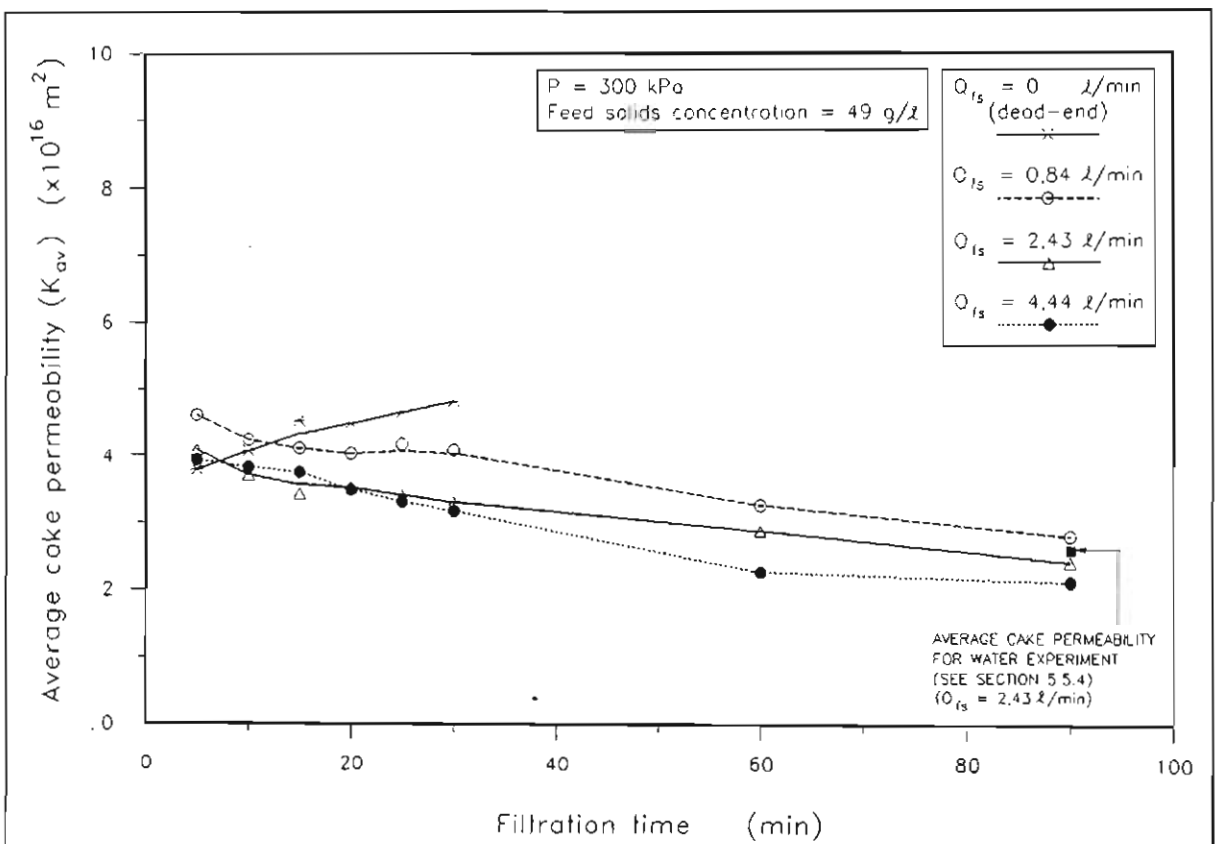

FIGURE 5.19 : The Variation of *Average* Cake Permeability with Filtration Time and Cross-flow Flow Rate (Experimental)

For a compressible cake, permeability, K, is a function of radius, r.

An *average* permeability, K_{av}, may be defined as follows (from equation (5.30)) :

$$P = \frac{\mu_f Q}{2\pi} \int_{r_2}^{r_1} \frac{dr}{rK}$$

$$= \frac{\mu_f Q}{2\pi K_{av}} \int_{r_2}^{r_1} \frac{dr}{r}$$

$$= \frac{\mu_f Q}{2\pi K_{av}} \ln\left(\frac{r_1}{r_2}\right) \qquad (5.31)$$

where K_{av} = average permeability of cake, (m^2)

From equation (5.31) :

$$K_{av} = \frac{\mu_f Q}{2\pi P} \ln\left(\frac{r_1}{r_2}\right) \qquad (5.32)$$

When comparing Figures 5.13 and 5.19, it is evident that for a certain cross-flow flow rate, for the time period up to the threshold time, t_{td} , the average permeability of the cake deposited under cross-flow conditions was not markedly different from that deposited under dead-end conditions. This was particularly evident for the cross-flow flow rate of 0,84 ℓ/min. After the threshold time the permeability of the cake declined slowly (unlike that for dead-end filtration) until the equilibrium internal cake diameter was attained. Thereafter the average cake permeability declined further although the internal cake diameter remained essentially constant. The average cake permeability was dependent on cross-flow flow rate. It was found that the higher the cross-flow flow rate, the lower the average cake permeability.

One of the assumptions for the proposed shear model for cross-flow microfiltration, was that the physical characteristics of the cake formed under *cross-flow* conditions are identical to a cake formed under dead-end conditions (see assumption (ii), section 5.3.1). When comparing Figures 5.13 and 5.19, it is evident that for cross-flow flow rates of 2,43 ℓ/min and 4,44 ℓ/min, the average cake permeability when the equilibrium internal cake diameter was attained, was approximately 20 % lower than the equivalent K_{av} for dead-end filtration. After 90 minutes, K_{av} for the cakes deposited under cross-flow conditions was approximately half of the K_{av} for the cakes deposited under dead-end conditions. The implications of this for the unsteady-state cross-flow microfiltration shear model are discussed further in section 5.7.3.

A point to consider is that for *optimized* sludge *dewatering* for the tubular filter press in cross-flow mode, the filtration times would not extend much beyond the time at which the equilibrium internal cake diameter is attained, otherwise the operation would become inefficient. The effect of a decrease in cake permeability would therefore be limited .

Other researchers (Baker et al., 1985 and Rushton and Aziz, 1983) have also found that cakes formed under cross-flow filtration conditions, from suspensions having a polydisperse size range, have different permeabilities to cakes formed under dead-end conditions. Baker et al. (1985) have shown that the permeability of a cake formed under cross-flow conditions can be a complex function of the cross-flow velocity, filtration pressure and time from start-up. They ascribed this to preferential deposition of smaller particles under cross-flow conditions. Other mechanisms which have been suggested are (Pillay, 1991) :

(i) the infiltration of smaller particles into the cake pores with time;

(ii) further compaction of the cake.

For this study an experiment was done where for a cross-flow flow rate of 2,43 ℓ/min, the feed suspension was switched from sludge to water after 20 minutes of filtration time. The experiment was terminated after 90 minutes total filtration time. The results of this experiment are tabulated in Appendix J. It was found that after 90 minutes the calculated internal cake diameter had increased from 11,63 mm at 20 minutes to 13,67 mm at 90 minutes, while the average cake dry solids concentration had increased from 23,51 % m/m to 24,89 % m/m. The average cake permeability (K_{av}) had decreased from 3,51 x 10^{-16} m^2 to 2,58 x 10^{-16} m^2, as shown in Figure 5.19. A mass balance revealed that no significant quantities of solids were purged away by the water.

The results of this one-off test would suggest that for the cake formed from the clarifier sludge, a major cause of the decline in cake permeability was cake compaction.

5.5.5 The Variation of Reynolds Number for the Flowing Feed Sludge with Filtration Time and Cross-flow Flow Rate

As mentioned previously this investigation of cross-flow filtration was restricted to the *laminar* flow of the feed sludge.

The variation of Reynolds number for the flowing feed sludge with filtration time and cross-flow flow rate is shown in Figure 5.20.

As was shown in Chapter 4 the waterworks clarifier sludges (cakes) were shown to be Bingham plastic fluids in the solids concentration range, 3,58 % m/m ≤ c_s ≤ 16,71 % m/m. The yield stress of the sludge was shown to be highly dependent on solids concentration. It was also shown in Chapter 4 that the yield stress may be calculated from equation (4.34) :

$$\tau_o = \frac{7.3268 \times 10^{-4} e^{0.1270 c_s}}{1.4292 c_s^{-3.5805}} \qquad (4.34)$$

where c_s = solids concentration of sludge (cake), (% m/m)

The coefficient of rigidity was also found to be dependent on solids concentration (see Figure 4.28(b)). A linear regression showed that the variation of coefficient of rigidity in the solids concentration range, 3,58 % m/m $\leq c_s \leq$ 11,1 % m/m, could be described by equation (4.35) :

$$\eta = 8.1422 \times 10^{-4} c_s - 2.1914 \times 10^{-4} \qquad (4.35)$$

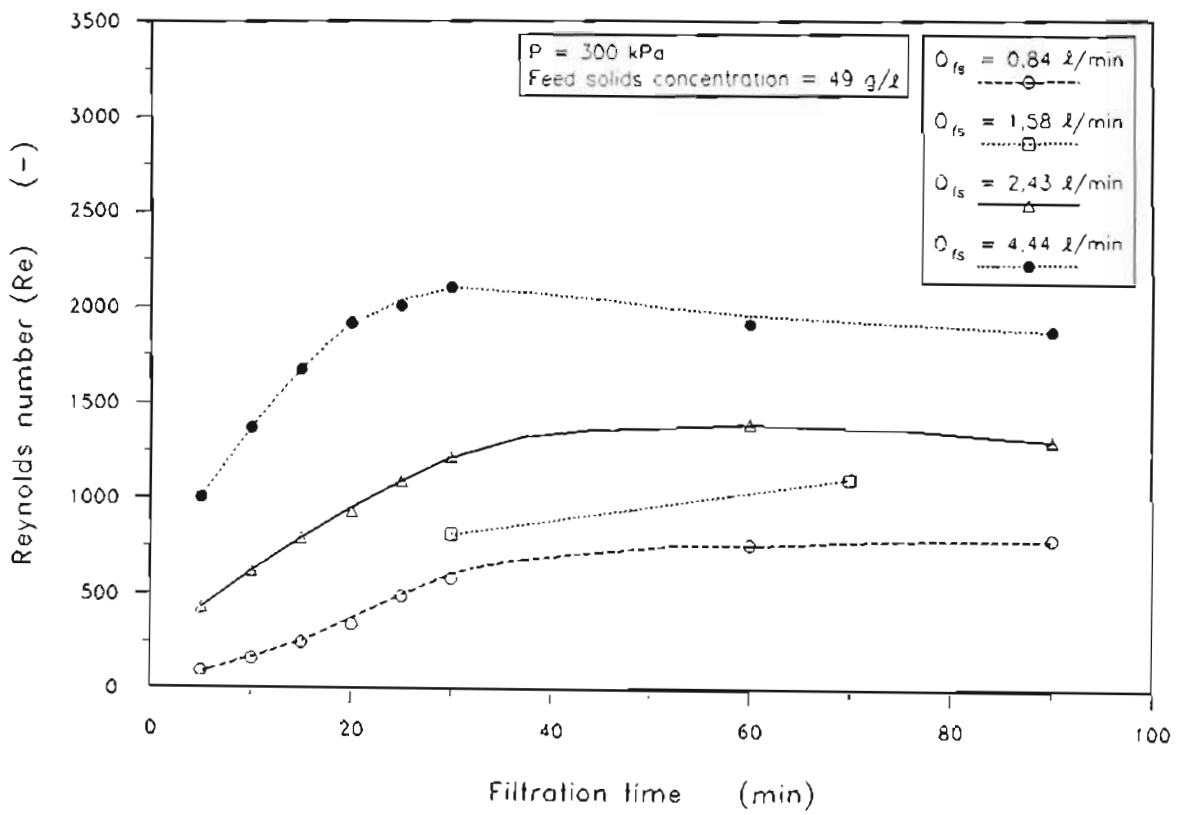

FIGURE 5.20 : The Variation of the Reynolds Number of the Flowing Feed Sludge with Filtration Time and Cross-flow Flow Rate (Experimental)

As was shown in Chapter 4, the Reynolds number for a Bingham plastic fluid flowing in a tube can be calculated from equation (4.29) :

$$Re = \frac{\rho_{fl} \bar{u}_{fl} D_t}{\eta\left(1 + \frac{\tau_o D_t}{6\eta \bar{u}_{fl}}\right)} \qquad (4.29)$$

where D_t = internal tube diameter, (m)

Re = Reynolds number, (-)

$\bar{u}_{fl}$ = average velocity of fluid, (m/s)

η = coefficient of rigidity, (Pa.s)
ρ_{fl} = density of fluid, (kg/m^3)
τ_o = yield stress, (Pa)

For a feed sludge flowing inside a cake annulus, equation (4.29) may be amended to :

$$Re = \frac{\rho_{fs}\bar{u}_{fs}d_2}{\eta_{fs}\left(1 + \frac{\tau_{of}d_2}{6\eta_{fs}\bar{u}_{fs}}\right)} \qquad (5.33)$$

where d_2 = internal cake diameter, (m)
$\bar{u}_{fs}$ = average velocity of feed sludge, (m/s)
η_{fs} = coefficient of rigidity of feed sludge, (Pa.s)
ρ_{fs} = density of feed sludge, (kg/m^3)
τ_{of} = yield stress of feed sludge, (Pa)

The solids concentration of the feed sludge was 4,76 % m/m. The yield stress (as calculated from equation (4.34)) was 0,25 Pa, while the coefficient of rigidity was 3,65 x 10^{-3} Pa.s (as calculated from equation (4.35)).

As shown in Figure 5.20, as the internal cake diameter decreased, the Reynolds number increased, until the equilibrium internal cake diameter was attained. Except for a cross-flow flow rate of 1,58 ℓ/min, the Reynolds numbers were based on *calculated* (from mass of wet cake and average cake dry solids concentration) experimental internal cake diameters. As shown in Figure 5.20, for a cross-flow flow rate of 4,44 ℓ/min the Reynolds numbers at the equilibrium internal cake diameter were very close to 2 100, the transition Reynolds number for a Newtonian fluid.

Wasp et al. (1979) have given a curve by Hanks and Pratt (1967) for estimating the transition Reynolds number (from laminar to turbulent flow) for a Bingham plastic fluid. This method is based on the Hedstrom number which (for the feed sludge) may be calculated from the following equation :

$$He = \frac{\tau_{of}\rho_{fs}d_2^2}{\eta_{fs}^2} \qquad (5.34)$$

where He = Hedstrom number as defined by equation (5.34), (-)

The variation of Hedstrom number with filtration time for a cross-flow flow rate of 4,44 ℓ/min is shown in Figure 5.21. The Hedstrom number at the equilibrium internal cake diameter was approximately 2 000. For a Hedstrom number of 2 000, the transition Reynolds number is approximately 2 500, according to the curve by

Hanks and Pratt (1967) given in Wasp et al. (1979). From this estimate of transition Reynolds number, the flow of the feed sludge for a cross-flow flow rate of 4,44 ℓ/min was well within the laminar regime.

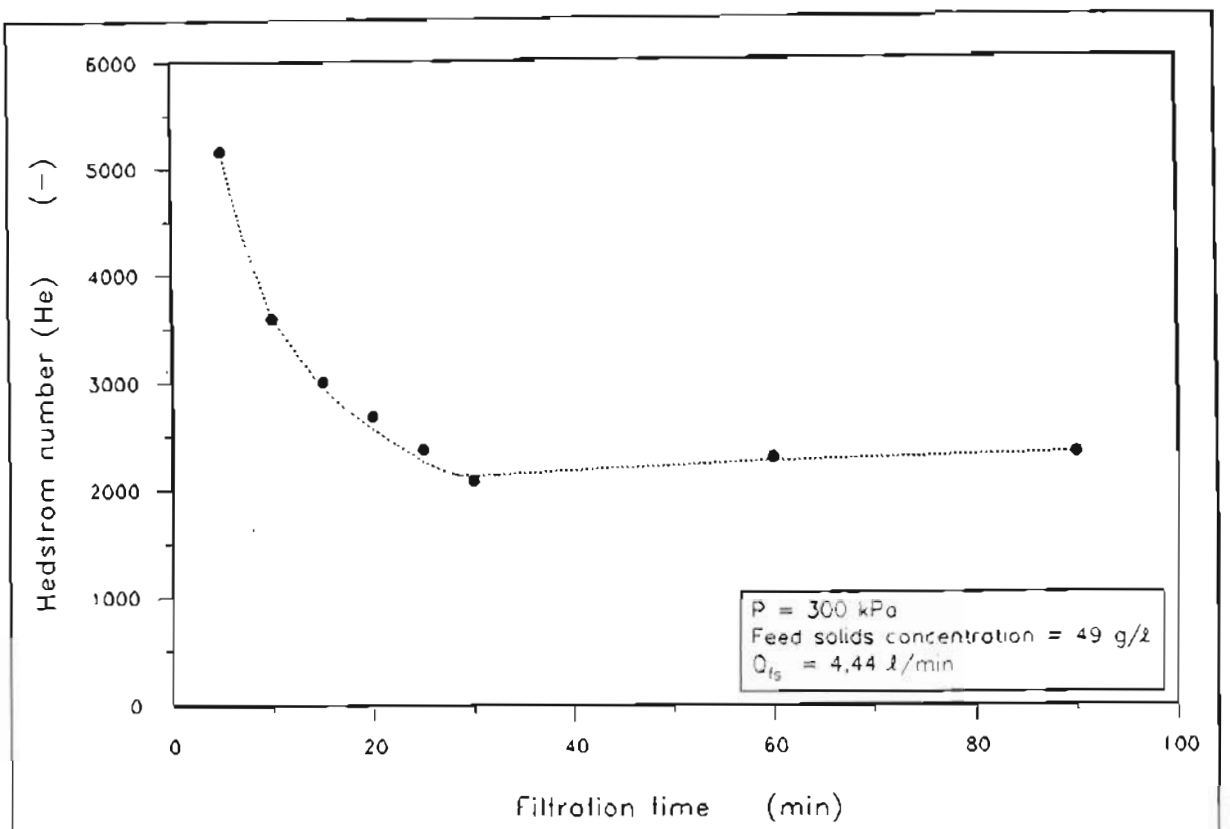

FIGURE 5.21 : The Variation of Hedstrom Number with Filtration Time for a Cross-flow Flow Rate of 4,44 ℓ/min (Experimental)

5.6 COMPARISON BETWEEN UNSTEADY-STATE AXIAL CONVECTION SHEAR MODEL FOR CROSS-FLOW MICROFILTRATION AND EXPERIMENTAL RESULTS

The proposed unsteady-state axial convection shear model for cross-flow microfiltration was compared to the experimental results in terms of internal cake diameters, filtrate fluxes and average cake dry solids concentrations.

5.6.1 Comparison Between Predicted and Experimental Internal Cake Diameters

The comparison between predicted and experimental internal cake diameters is shown in Figures 5.22(a), (b), (c) and (d) for cross-flow flow rates of 0,84 ℓ/min; 1,58 ℓ/min; 2,43 ℓ/min and 4,44 ℓ/min, respectively. Both *calculated* (from mass of wet cake

and average cake dry solids concentration) and *measured* (using a vernier calliper) experimental internal cake diameters are shown in Figure.5.22. The error bars for the calculated experimental internal cake diameters are based on the same errors as were used in Chapter 3 for the dead-end internal cylindrical filtration experiments. Sets of equations (3.79) and (3.81) were used in the model to describe the variation of permeability and porosity with solids compressive pressure, respectively.

As shown in Figure 5.22 there was close agreement between predicted and experimental internal cake diameters both during the unsteady-state and steady-state time periods. (The internal cake diameters for the unsteady-state time period were not measured for a cross-flow flow rate of 1,58 ℓ/min.)

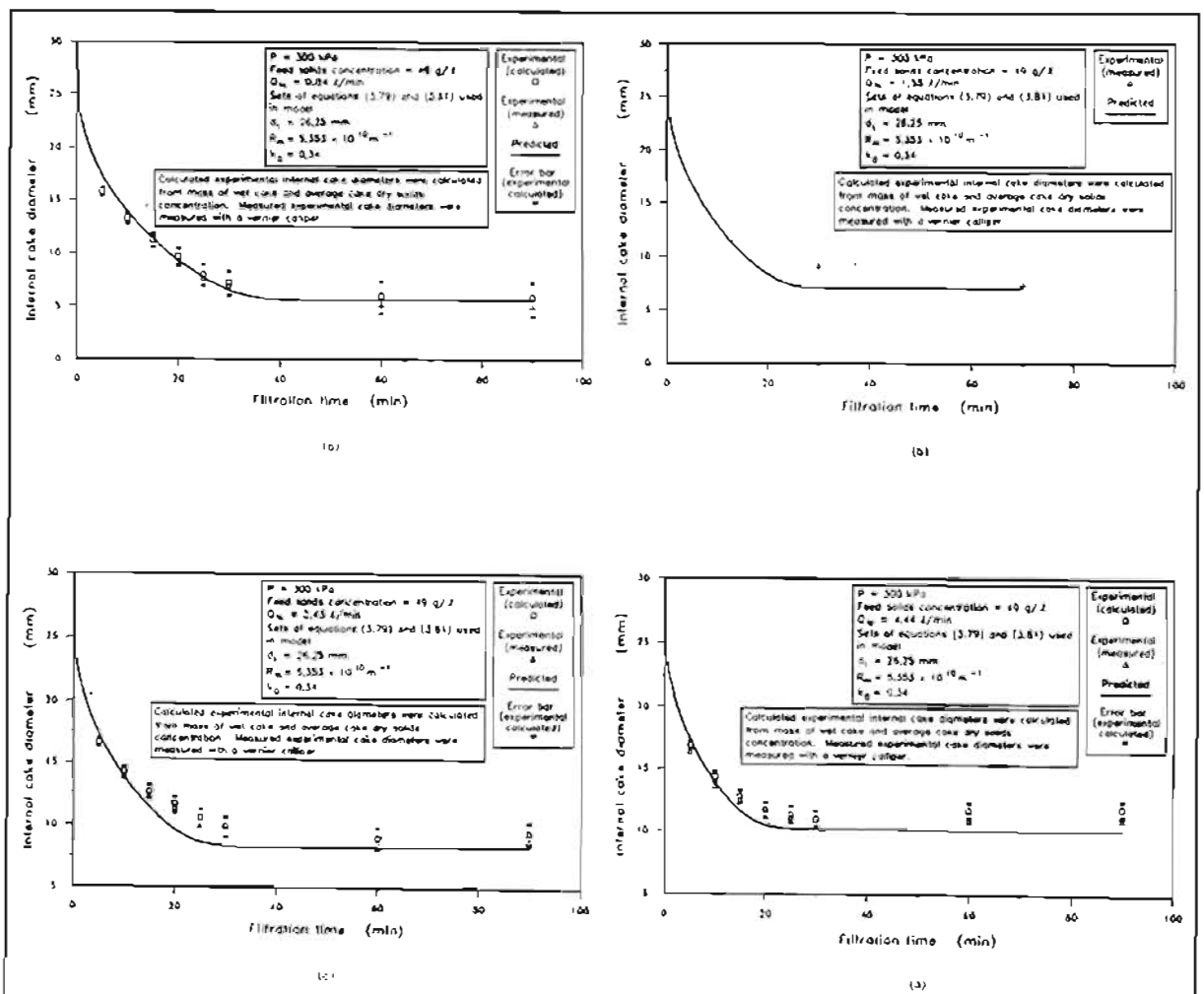

FIGURE 5.22 : Comparison Between Predicted and Experimental (Calculated and Measured) Internal Cake Diameters for Cross-flow Flow Rates of : (a) 0,84 ℓ/min; (b) 1,58 ℓ/min; (c) 2,43 ℓ/min and (d) 4,44 ℓ/min

For cross-flow flow rates of 2,43 ℓ/min and 4,44 ℓ/min the predicted internal cake diameters were slightly lower than the experimental values. This was mainly due to slight differences in average cake permeability (see Figure 5.19) between the cakes formed under *cross-flow* conditions and those formed under static conditions. It will be recalled that the model incorporates the average cake permeability of a cake deposited under dead-end conditions (see assumption (ii), section 5.3.1).

The model was subsequently amended or "extended" to incorporate the measured changes in cake permeability and porosity (see section 5.6.10). There was nevertheless good agreement between predicted and experimental equilibrium internal cake diameters even without making allowance for changes in average cake permeability under cross-flow conditions.

5.6.2 Comparison Between Predicted and Experimental Filtrate Fluxes

The comparison between predicted and experimental filtrate fluxes is shown in Figures 5.23(a), (b), (c) and (d) for cross-flow flow rates of 0,84 ℓ/min; 1,58 ℓ/min; 2,43 ℓ/min and 4,44 ℓ/min, respectively. Sets of equation (3.79) and (3.81) were used in the model to describe the variation of permeability and porosity with solids compressive pressure, respectively.

As shown in Figure 5.23, during the unsteady-state time period (between start-up and the attainment of an equilibrium internal cake diameter) there was close agreement between predicted and experimental filtrate fluxes. Once the steady-state (equilibrium internal cake diameter) was achieved the experimental filtrate fluxes continued to decline due to further decreases in average cake permeability (see Figure 5.19) while the predicted fluxes remained constant. This is because the model is based on the characteristics of a cake deposited under dead-end or static conditions (see assumption (ii), section 5.3.1). The model for a dead-end cake does not make allowance for cake compaction or consolidation and it is assumed that if the internal cake diameter remains constant the filtrate flux will also remain constant.

The discrepancy between experimental and predicted filtrate fluxes during the steady-state does not detract from the application or usefulness of the model for the tubular filter press. As mentioned in section 5.5.4, it has to be remembered that for *optimized* sludge *dewatering* for the tubular filter press in cross-flow mode, the filtration times would not extend much beyond the time at which the equilibrium internal cake diameter is attained, otherwise the operation would become inefficient. The filtration performance during the pseudo steady-state would therefore not be relevant for the tubular filter press.

As already mentioned the model was, however, "extended " further to include changes in permeability and porosity of the cake. The results for the "extended" model are shown in section 5.6.10.3.

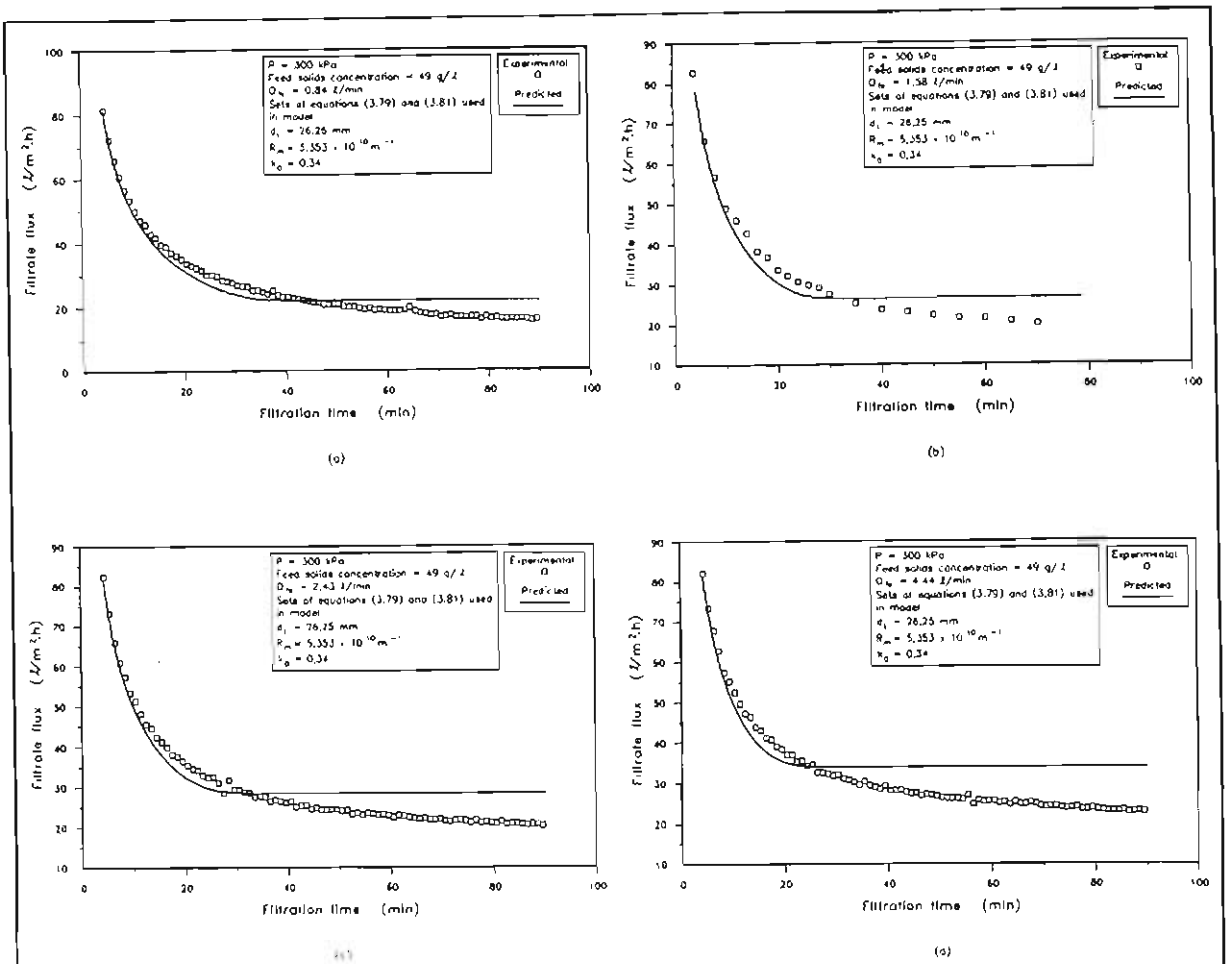

FIGURE 5.23 : Comparison Between Predicted and Experimental Filtrate Fluxes for Cross-flow Flow Rates of : (a) 0,84 ℓ/min; (b) 1,58 ℓ/min; (c) 2,43 ℓ/min and (d) 4,44 ℓ/min

5.6.3 Comparison Between Predicted and Experimental Average Cake Dry Solids Concentrations

The comparison between predicted and experimental average cake dry solids concentrations is shown in Figures 5.24(a), (b), (c) and (d) for cross-flow flow rates of 0,84 ℓ/min; 1,58 ℓ/min; 2,43 ℓ/min and 4,44 ℓ/min, respectively. The error bars for the average cake dry solids concentrations are based on the same errors as were used in Chapter 3 for the dead-end internal cylindrical filtration experiments. Sets of equations (3.79) and (3.81) were used in the model to describe the variation of permeability and porosity with solids compressive pressure, respectively.

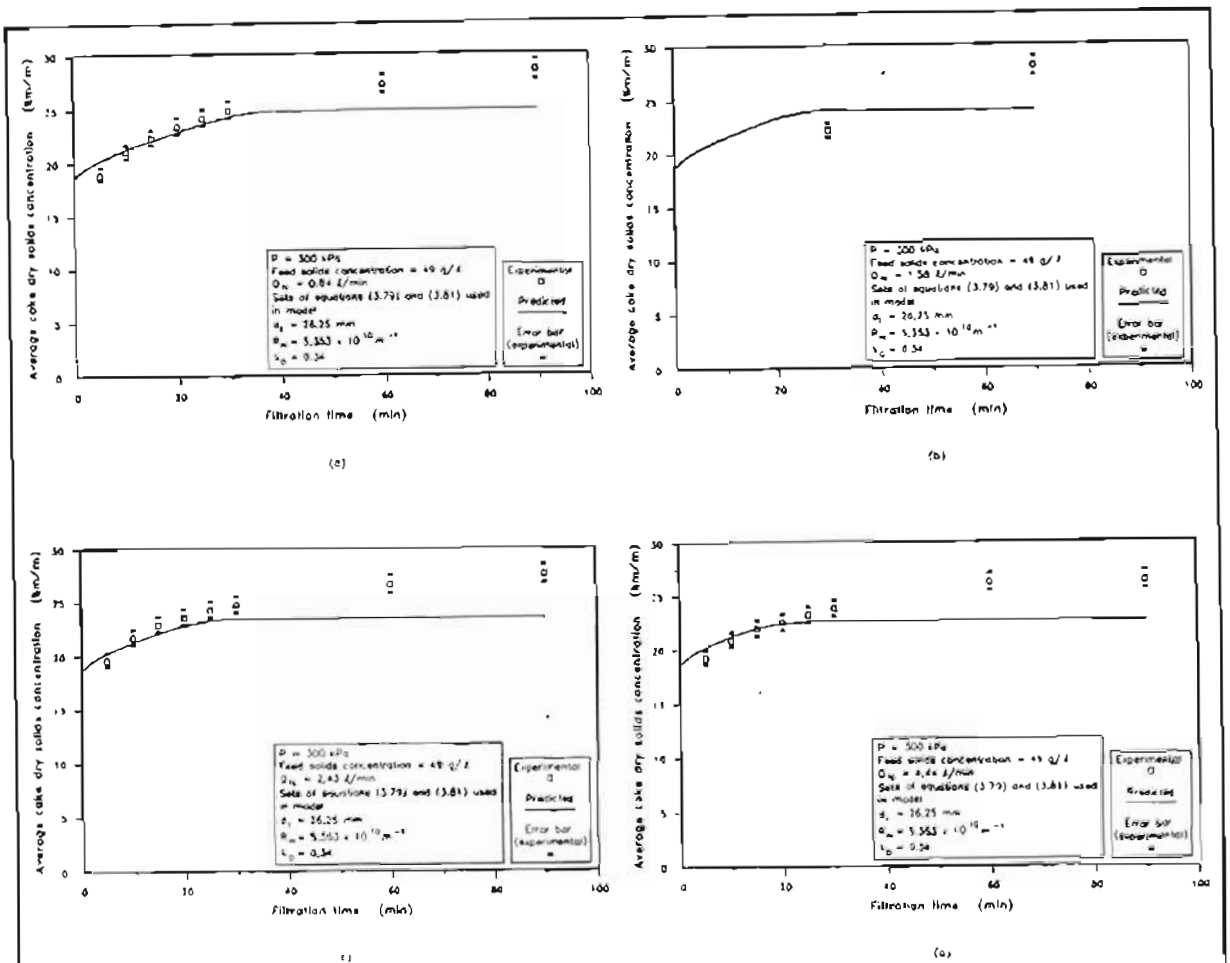

FIGURE 5.24 : Comparison Between Predicted and Experimental Average Cake Dry Solids Concentrations for Cross-flow Flow Rates of : (a) 0,84 ℓ/min; (b) 1,58 ℓ/min; (c) 2,43 ℓ/min and (d) 4,44 ℓ/min

As shown in Figure 5.24, the trends for the average cake dry solids concentrations were similar to those for the filtrate fluxes, in that during the unsteady-state time period there was close agreement between experimental and predicted values, while during the steady-state there was a further increase in average cake dry solids concentration.

However, for the reasons mentioned in section 5.6.2, although there were discrepancies between experimental and predicted average cake dry solids concentrations for the pseudo steady-state, the model is still useful for the operation of a tubular filter press in cross-flow mode.

As shown in section 5.6.10, the model was "extended" to include further increases in average cake dry solids concentrations during the pseudo steady-state time period.

5.6.4 Shear Stress at the Inner Cake Wall, τ_w

The predicted variation of the shear stress at the inner cake wall, τ_w, with filtration time is shown in Figure 5.25 for a cross-flow flow rate of 4,44 ℓ/min. The shear stress at the inner cake wall, τ_w, increases with filtration time, since the internal cake diameter decreases because of growth during the unsteady-state time period (see equation (5.3)). Once the equilibrium cake diameter is attained, τ_w remains essentially constant.

The predicted effect of cross-flow flow rate on τ_w at *steady-state*, is shown in Figure 5.26. As shown in Figure 5.26, τ_w at *steady-state* is essentially independent of cross-flow flow rate.

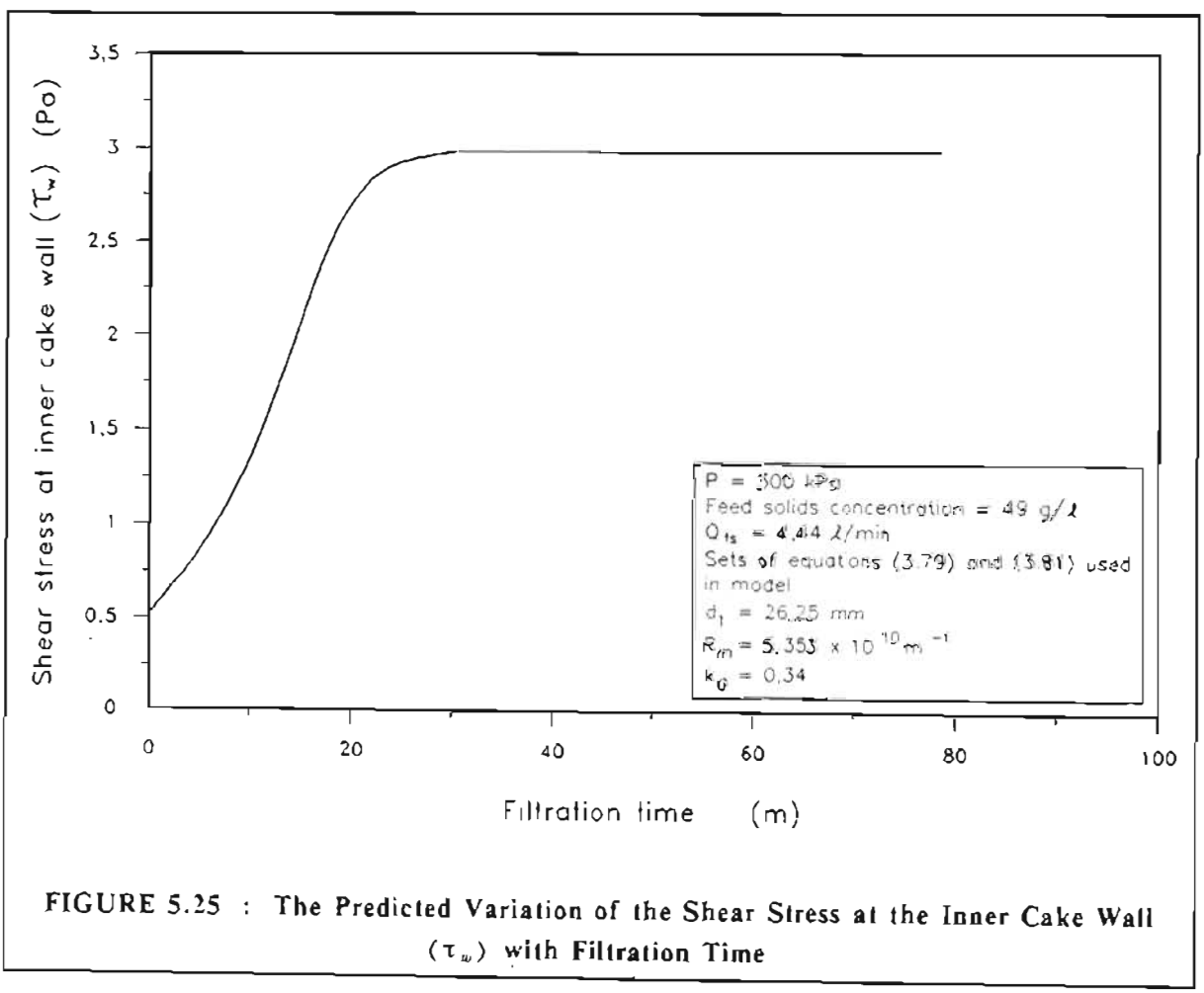

FIGURE 5.25 : The Predicted Variation of the Shear Stress at the Inner Cake Wall (τ_w) with Filtration Time

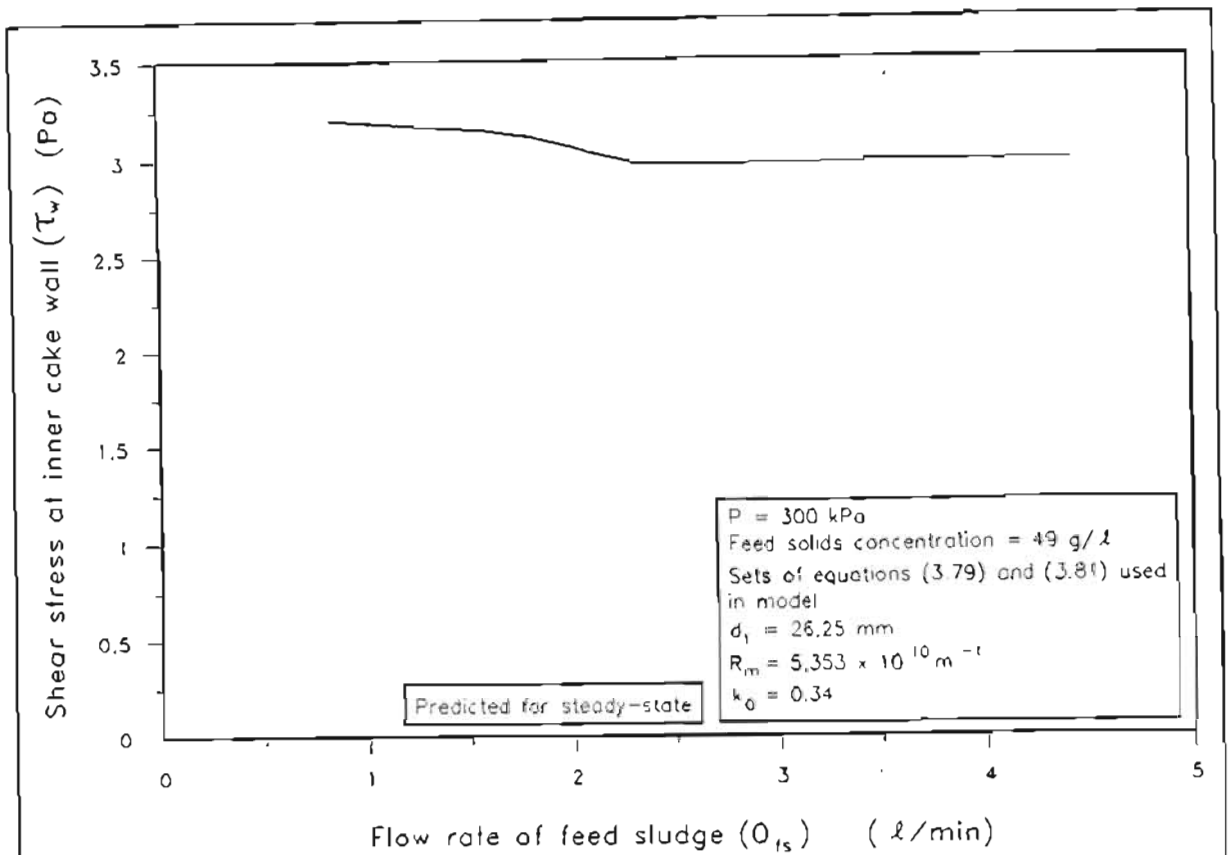

FIGURE 5.26 : The Predicted Effect of Cross-flow Flow Rate on the *Steady-state* Shear Stress at the Inner Cake Wall (τ_w)

5.6.5 Axial Thickness Profile of Moving Cake Layer

As shown in section 5.3.2, at *steady-state* the thickness of the moving cake layer grows in an axial direction. The steady-state axial thickness profile of the moving cake layer is described by equation (5.14). Equation (5.14) was numerically solved for δ_f by using Steffen's method (Burden et al., 1981).

The predicted effect of cross-flow flow rate on the steady-state axial thickness profile of the moving cake layer is shown in Figure 5.27. As shown in Figure 5.27, the axial thickness profile of the moving cake layer at steady-state is essentially independent of cross-flow flow rate.

As was discussed in section 5.3.3, for the axial convection shear model a quasi steady-state was assumed to exist during each time interval during the unsteady-state time period. As was shown in section 5.6.4, during the unsteady-state time period the shear stress at the wall, τ_w, increases as the internal cake diameter decreases because of cake growth (see equation (5.3)). As the shear stress at the inner cake wall, τ_w, increases, the yield stress (and therefore the solids concentration) of the

cake layers which may be moved, increases. This means that during the unsteady-state time period, the thickness of the moving cake layer increases with time. This is shown in Figure 5.28.

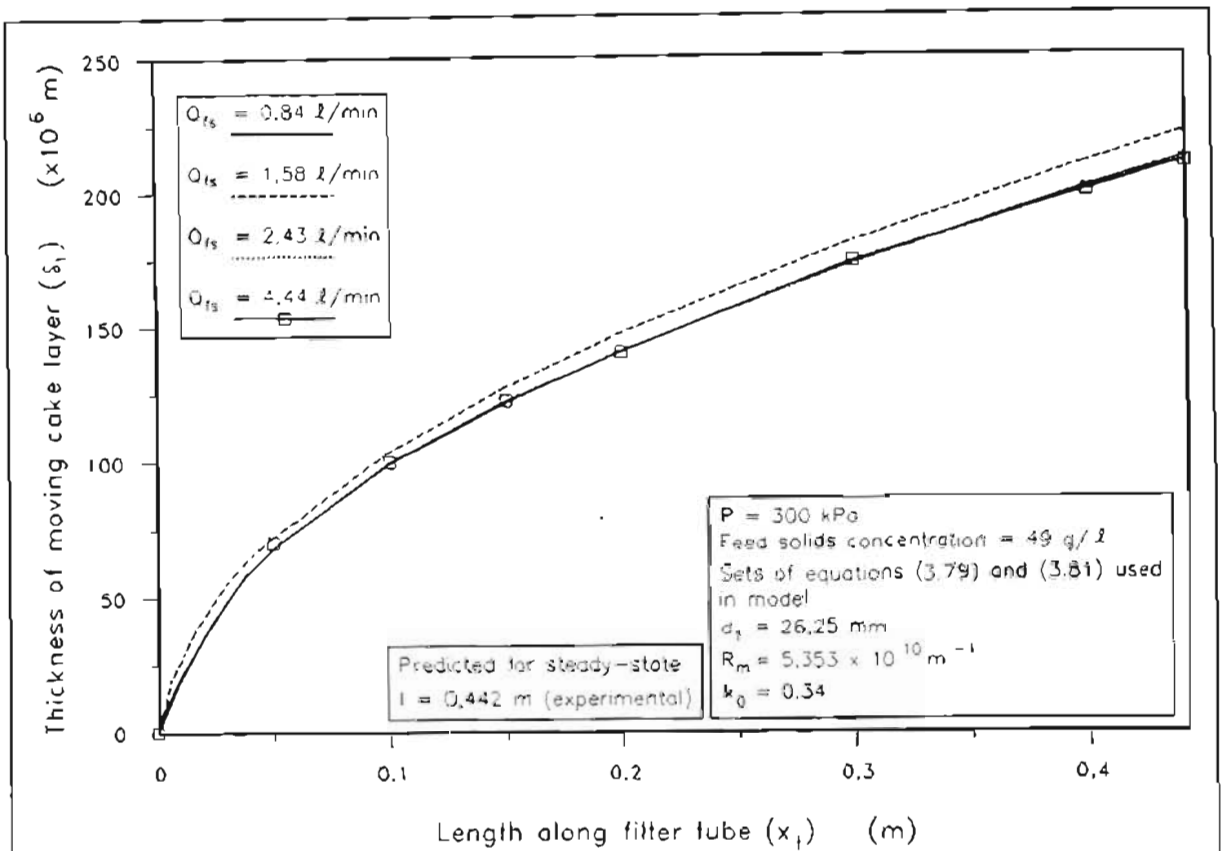

FIGURE 5.27 : The Predicted Effect of Cross-flow Flow Rate on the Axial Thickness Profile of the Moving Cake Layer at *Steady-state*

The moving cake layers which are shown in Figure 5.28 for filtration times of 10 minutes and 27 minutes (steady-state) are "realistic" in the sense that they are significantly greater than the mass average particle size for the clarifier sludge which was 5,90 μm (see Appendix F). At a short filtration time of 2 minutes the predicted thickness of the moving cake layer is approximately 15 μm at the outlet of the filter tube. This is only approximately 2 particle layers thick. This is obviously not very realistic. For further discussion see section 5.7.4.

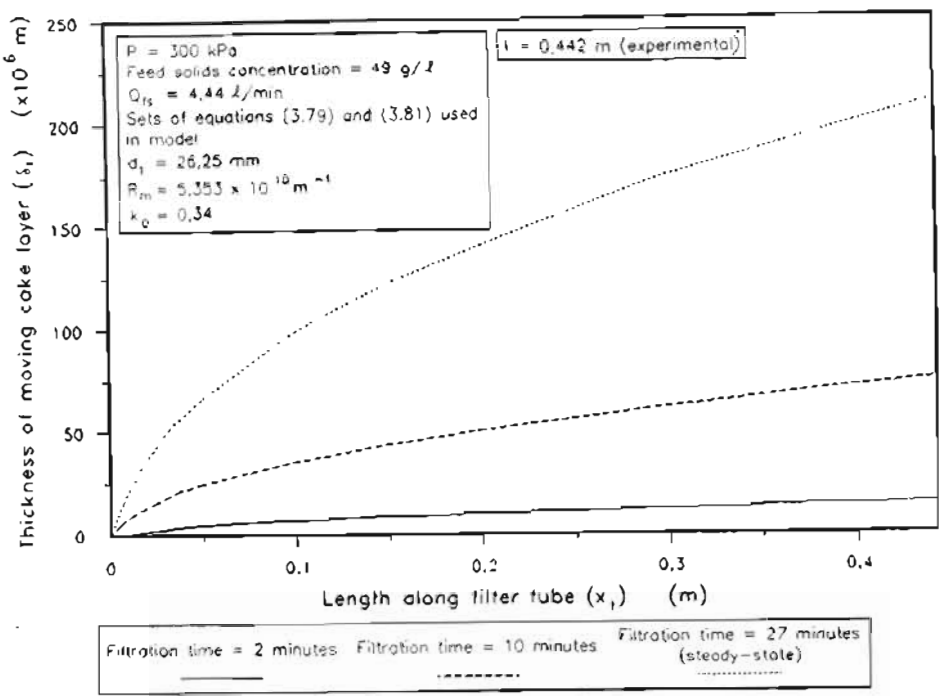

FIGURE 5.28 : The Predicted Variation of the Axial Thickness Profile of the Moving Cake Layer with Filtration Time for a Cross-flow Flow Rate of 4,44 ℓ/min

5.6.6 Solids Concentration of the Moving Cake Layer

As discussed in section 5.3.2, the solids concentration of the moving cake layer is assumed to be uniform and it is taken to be the arithmetic mean of the solids concentration of the feed sludge and the solids concentration of the cake at the shear plane, i.e.

$$\phi_{s1} = \frac{\phi_{ss} + \phi_s}{2} \qquad (5.2)$$

As the shear stress at the inner cake wall, τ_w, increases with time during the unsteady-state time period, the solids concentration at the *shear plane* will increase. From equation (5.2), this means that the solids concentration of the moving cake layer will increase with time during the unsteady-state time period. This is shown in Figure 5.29 for a cross-flow flow rate of 4,44 ℓ/min. Once an equilibrium internal cake diameter has been attained the solids concentration of the moving cake layer remains constant.

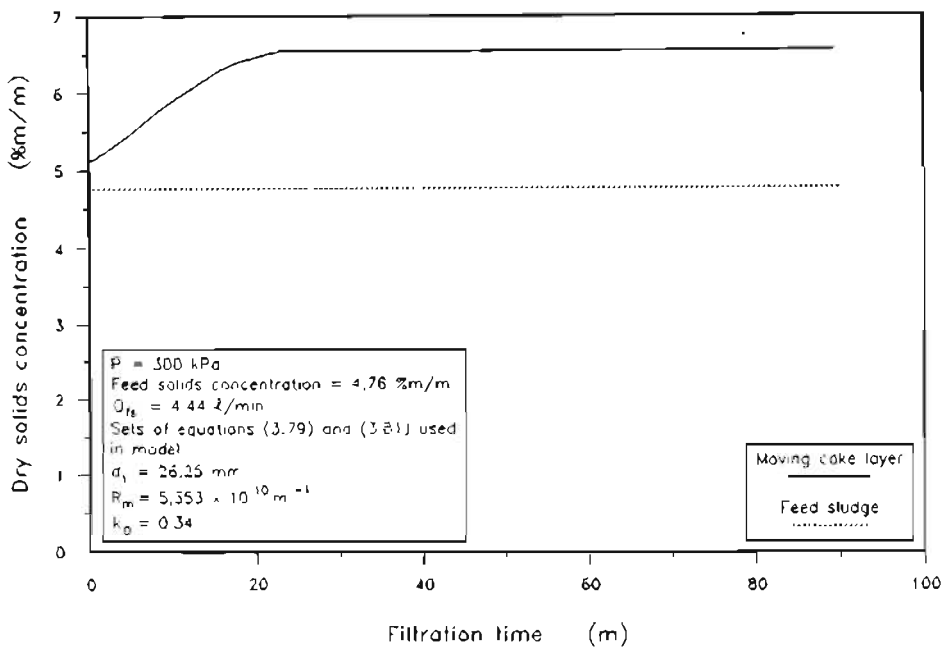

FIGURE 5.29 : The Predicted Variation of the Solids Concentration of the Moving Cake Layer with Filtration Time for a Cross-flow Rate of 4,44 ℓ/min

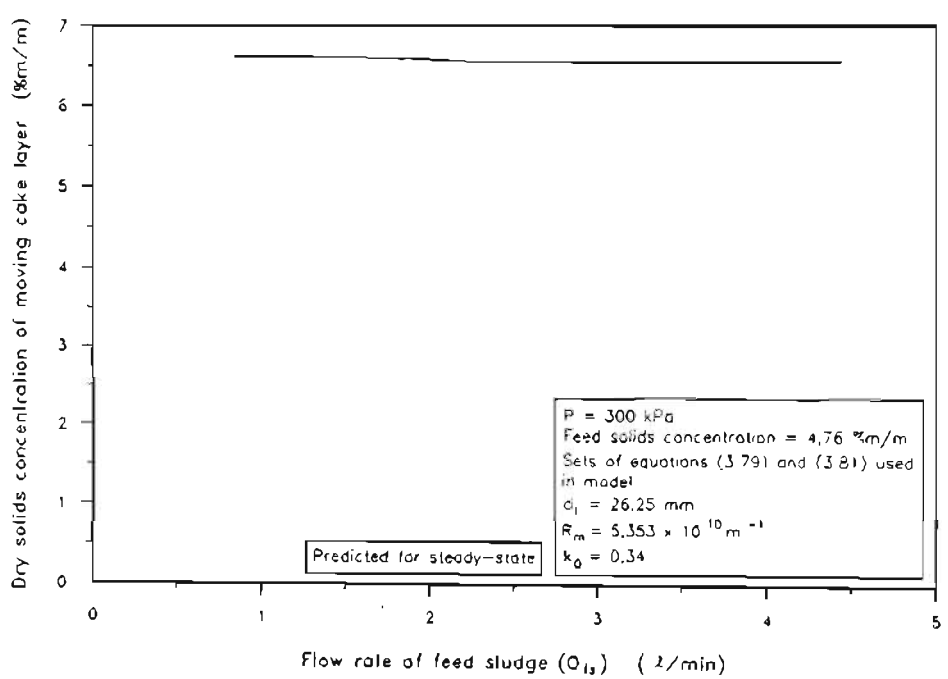

FIGURE 5.30 : The Predicted Effect of Cross-flow Flow Rate on the Solids Concentration of the Moving Cake Layer at *Steady-state*

The effect of cross-flow flow rate on the solids concentration of the moving cake layer at *steady-state* is shown in Figure 5.30. The solids concentration of the moving cake layer at steady-state is essentially independent of cross-flow flow rate.

5.6.7 Velocity Profile in Moving Cake Layer

As shown in section 5.3.2, the velocity profile in the moving cake layer is given by equation (5.9) :

$$u_{ml} = \left(\frac{\tau_w - \tau_{ol}}{\eta_l}\right)(r_s - r) \qquad (5.9)$$

The velocity profile in the moving cake layer at the outlet of the filter tube at *steady-state* is shown in Figure 5.31 for a cross-flow flow rate of 4,44 ℓ/min.

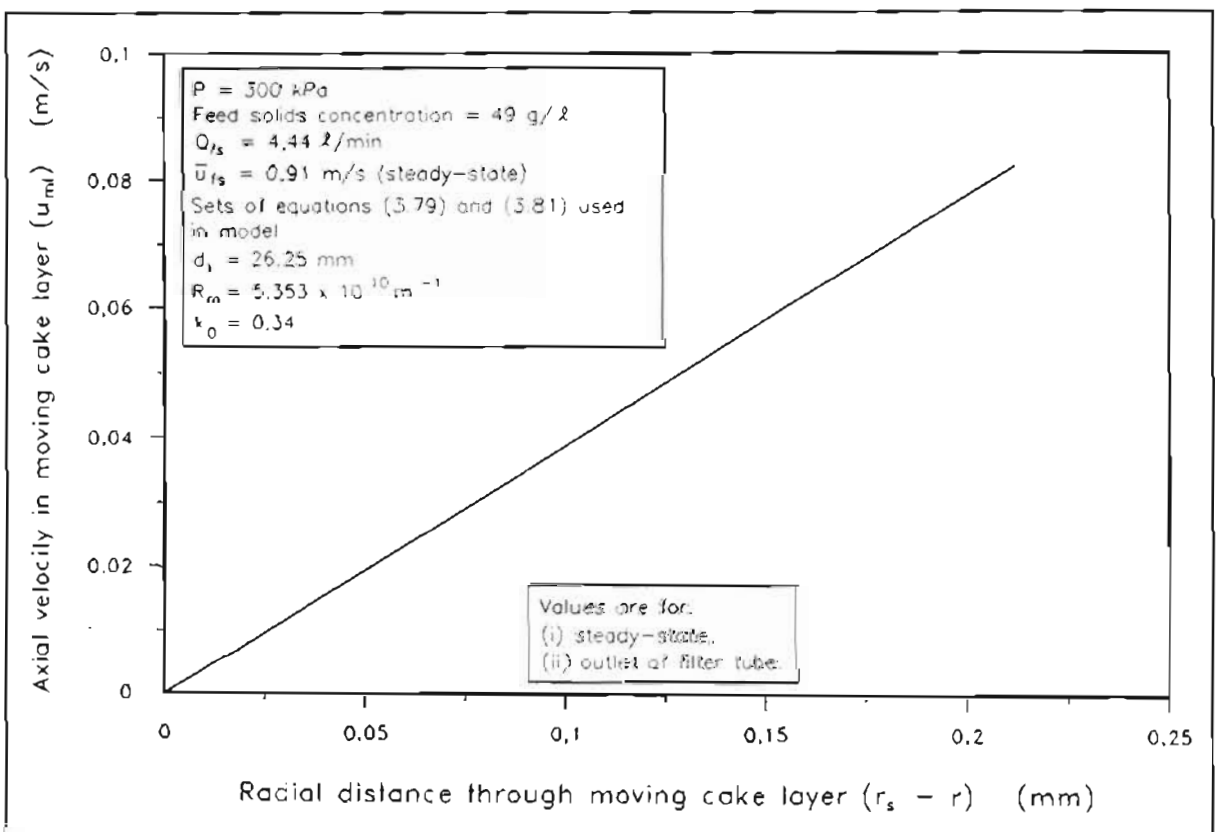

FIGURE 5.31 : The Predicted Radial Axial Velocity Profile in the Moving Cake Layer at the Outlet of the Filter Tube at *Steady-state* for a Cross-flow Flow Rate of 4,44 ℓ/min

5.6.8 Relationship Between Radial Volumetric Flow Rate of Feed Sludge to the Moving Cake Layer (Q_{sl}) and Volumetric Flow Rate of Filtrate (Q)

As discussed in section 5.3.3.1, for the very compressible cake used for this study, the liquid in the cake was not negligible compared with the volume of filtrate. This precluded the use of the relatively simple equation (5.19) for the calculation of Q_{sl} from the volume of filtrate :

$$Q_{sl}\phi_s = \frac{Q\phi_s}{(1-\phi_s)} \qquad (5.19)$$

Q_{sl} was determined using an iterative procedure which was described in section 5.3.3.1. The predicted variation of Q_{sl} and Q with filtration time is shown in Figure 5.32. The predicted values of Q_{sl} are approximately 15 to 20 % higher than those of Q for both the unsteady- and steady-state time periods. In comparison, from equation (5.19), Q_{sl} only exceeds Q by 2,1 % for a volumetric solids fraction in the feed sludge, ϕ_s, of 0.0206 (as was used for the experiments).

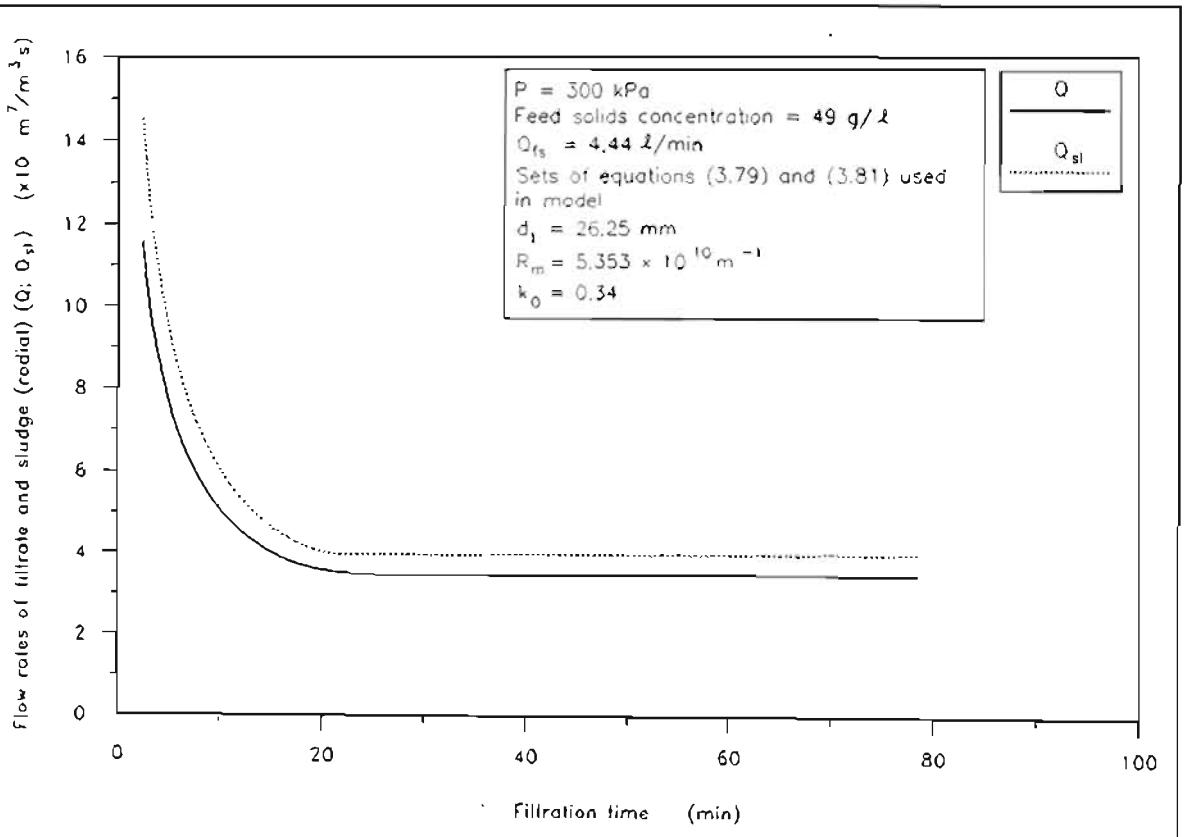

FIGURE 5.32 : The Predicted Variation of the Radial Volumetric Flow Rate of Feed Sludge to the Moving Cake Layer (Q_{sl}) and the Volumetric Flow Rate of Filtrate (Q) with Filtration Time

5.6.9 Use of Set of Equations (3.82) in Model

As was shown in Chapter 4, the use of set of equations (3.82) rather than sets of equations (3.79) and (3.81) (for permeability and porosity, respectively) in the "cleaning fluid" shear model gave a better agreement between predicted and experimental values.

As shown in Figure 5.33, there was hardly any difference between internal cake diameters predicted by incorporation of sets of equations (3.79) and (3.81) and set of equations (3.82) in the axial convection shear model for cross-flow microfiltration.

There was, however, a significant difference in average cake dry solids concentrations predicted by sets of equations (3.79) and (3.81) and set of equations (3.82), as shown in Figure 5.34. The use of sets of equations (3.79) and (3.81) in the model gave a better agreement between predicted and experimental average cake dry solids concentrations than the use of set of equations (3.82).

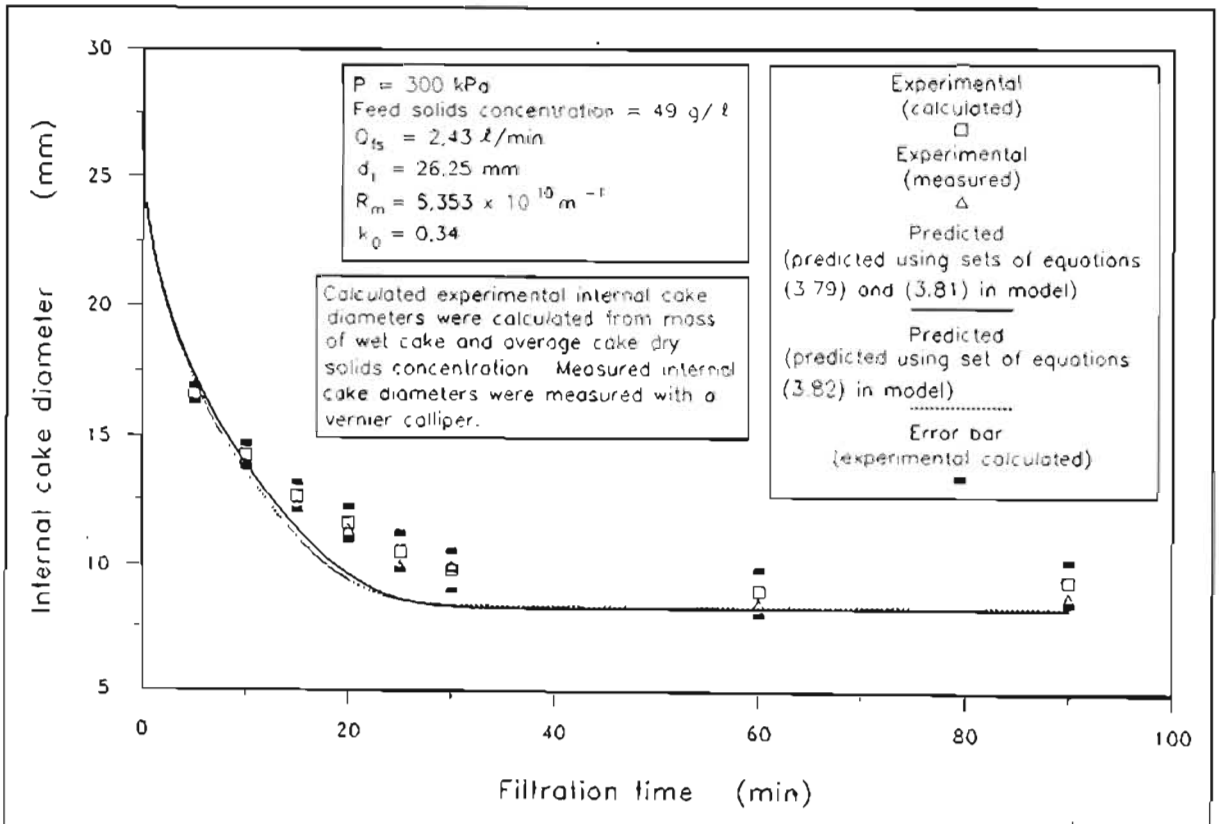

FIGURE 5.33 : Comparison Between Predicted and Experimental (Measured and Calculated) Internal Cake Diameters when using Sets of Equations (3.79) and (3.81) and Set of Equations (3.82) in the Axial Convection Shear Model for Cross-flow Microfiltration

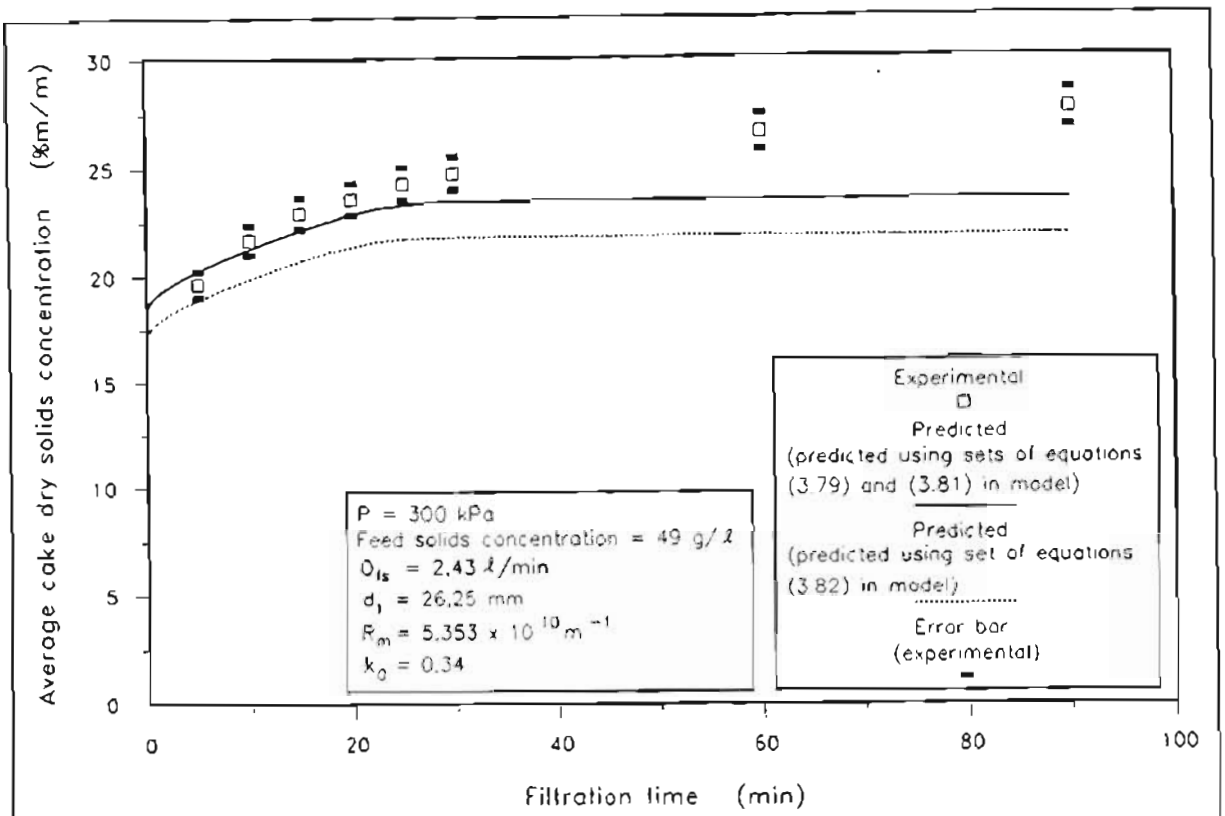

FIGURE 5.34 : Comparison Between Predicted and Experimental Average Cake Dry Solids Concentrations when using Sets of Equations (3.79) and (3.81) and Set of Equations (3.82) in the Axial Convection Shear Model for Cross-flow Microfiltration

5.6.10 "Extension" of Axial Convection Shear Model for Cross-flow Microfiltration to Incorporate Changes in Cake Permeability and Porosity

As discussed in section 5.5.4 and shown in Figure 5.19, in the time period between start-up and the threshold time, t_{ta}, the average permeability of a cake deposited under cross-flow conditions was similar to that of a dead-end cake. During the time period between the threshold time, t_{ta}, and the time required to attain an equilibrium internal cake diameter, the average permeability of the cross-flow cake decreased slightly when compared with that of the equivalent dead-end cake. The average cake permeability decreased further after the equilibrium internal cake diameter was attained. A similar trend was observed for average cake dry solids concentration. During the time period between start-up and the time required to attain an equilibrium internal cake diameter, the average cake dry solids concentration of the cross-flow cake was very similar to that of the equivalent dead-end cake. However, after the attainment of an equilibrium internal cake diameter, during the so-called steady-state, the average cake dry solids concentration continued to increase.

One of the assumptions for the axial convection shear model was that the physical characteristics of a cake deposited under cross-flow conditions are identical to an equivalent cake deposited under static conditions (see assumption (ii), section 5.3.1).

The agreement between the axial convection shear model and experimental results was close during the unsteady-state time period. However, after the attainment of an equilibrium internal cake diameter (during the pseudo steady-state) there were significant discrepancies between model predictions and experimental results. This was due to significant differences in average cake permeability and average cake dry solids concentrations between the cross-flow cakes and the equivalent dead-end cakes, during the pseudo steady-state. One of the major assumptions of the model was therefore invalid during the pseudo steady-state.

As has already been mentioned for the *efficient* operation of a tubular filter press in cross-flow mode, only the unsteady-state time period is of concern. In previous sections it has been shown that the model accurately predicted performance during the unsteady-state and is therefore adequate for the tubular filter press. In this section it is shown how the proposed model may be "extended" to a "proper" laminar cross-flow microfiltration model which predicts performance during both the unsteady- and pseudo steady-state time periods. This is achieved by incorporating empirical equations, to model the aforementioned changes in cake permeability and porosity, into the existing axial convection shear model.

The discussion has been kept brief, since in conformance with the title of this thesis the objective is to limit the investigation to matters directly related to the tubular filter press.

5.6.10.1 Modelling the dynamic changes in cake porosity and permeability under cross-flow conditions

In modelling dynamic changes in cake porosity and permeability, it was assumed that during the time interval from start-up to the threshold filtration time, t_{id} , the cake porosity and permeability for a cake deposited under cross-flow conditions are identical to those for an equivalent dead-end cake. The sets of equations which describe the variation of permeability and porosity with solids compressive pressure for the dead-end cake were developed in Chapter 3.

$$
\begin{aligned}
K &= 6.621 \times 10^{-13} p_{sl}^{-0.575} && 0 \leq p_s \leq p_{sl} \\
K &= 6.621 \times 10^{-13} p_s^{-0.575} && p_{sl} \leq p_s \leq 3781.7\ \text{Pa} \\
K &= 1.779 \times 10^{-10} p_s^{-1.254} && p_s \geq 3781.7\ \text{Pa}
\end{aligned}
\qquad (3.79)
$$

$$1-\epsilon = 0{,}0299\,p_{sf}^{0.0782} \qquad 0 \le p_s \le p_{sf}$$

$$1-\epsilon = 0{,}0299\,p_{s}^{0.0782} \qquad p_{sf} \le p_s \le 1285{,}1 \text{ Pa} \qquad (3.81)$$

$$1-\epsilon = 0{,}00785\,p_{s}^{0.265} \qquad p_s \ge 1285{,}1 \text{ Pa}$$

The following equations were proposed to describe the variation of average cake permeability and porosity with time after the threshold filtration time, t_{id} :

$$(K_{av}(t) - K_{av}^{\infty}) = (K_{av}^{ti} - K_{av}^{\infty})e^{\left[-A^c(t-t_{id})\right]} \qquad (5.35)$$

where A^c = constant in equation (5.35)

K_{av} = average permeability of cake, (m^2)

K_{av}^{ti} = average permeability of cake at threshold time, t_{id} , (m^2)

K_{av}^{∞} = average permeability of cake at infinity, (m^2)

t = time, (s)

t_{id} = threshold filtration time for internal cake diameter as defined in section 5.5.1, (s)

$$(\epsilon_{av}(t) - \epsilon_{av}^{\infty}) = -(\epsilon_{av}^{ti} - \epsilon_{av}^{\infty})e^{\left[-B^c(t-t_{id})\right]} \qquad (5.36)$$

where B^c = constant in equation (5.36)

ϵ_{av} = average porosity of cake, (-)

ϵ_{av}^{ti} = average porosity of cake at threshold time, t_{id} , (-)

ϵ_{av}^{∞} = average porosity of cake at infinity, (-)

As was shown in section 5.5.1, for a cross-flow flow rate of 4,44 ℓ/min, the threshold time, t_{id} , was 8 minutes. The average permeability of the dead-end cake at 8 minutes was estimated to be 3,93 x 10^{-16} m^2, while the average porosity was estimated to be 0,903. The values of A^c and K_{av}^{∞} in equation (5.35) were obtained by a SAS[1] non-linear regression package, using the experimental average cake permeabilities after the threshold time, t_{id} , for a cross-flow flow rate of 4,44 ℓ/min. The values for B^c and ϵ_{av}^{∞} in equation (5.36) were obtained in a similar manner. The following were the regressed values for a cross-flow flow rate of 4,44 ℓ/min :

A^c = 3,437 x 10^{-4}

K_{av}^{∞} = 1,640 x 10^{-16} m^2

B^c = 5,892 x 10^{-4}

ϵ_{av}^{∞} = 0,8664

The fit between predicted (using equations (5.35) and (5.36)) and experimental average cake permeabilities and porosities is shown in Figures 5.35 and 5.36, respectively.

1 SAS Institute Incorporated, Cary, North Carolina, USA.

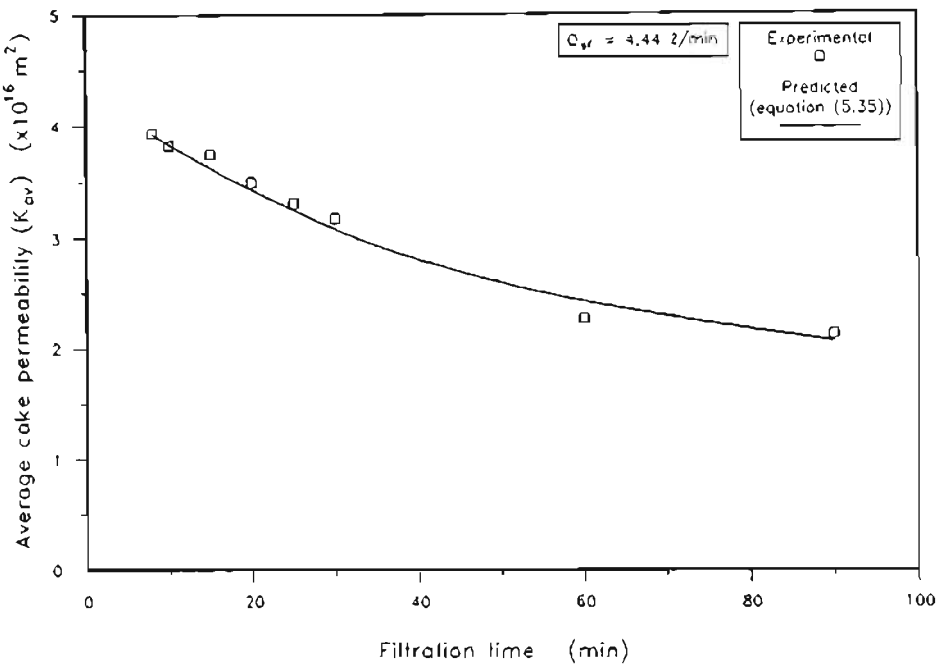

FIGURE 5.35 : Comparison Between Experimental and Predicted (from Equation (5.35)) Average Cake Permeabilities for a Cross-flow Flow Rate of 4,44 ℓ/min

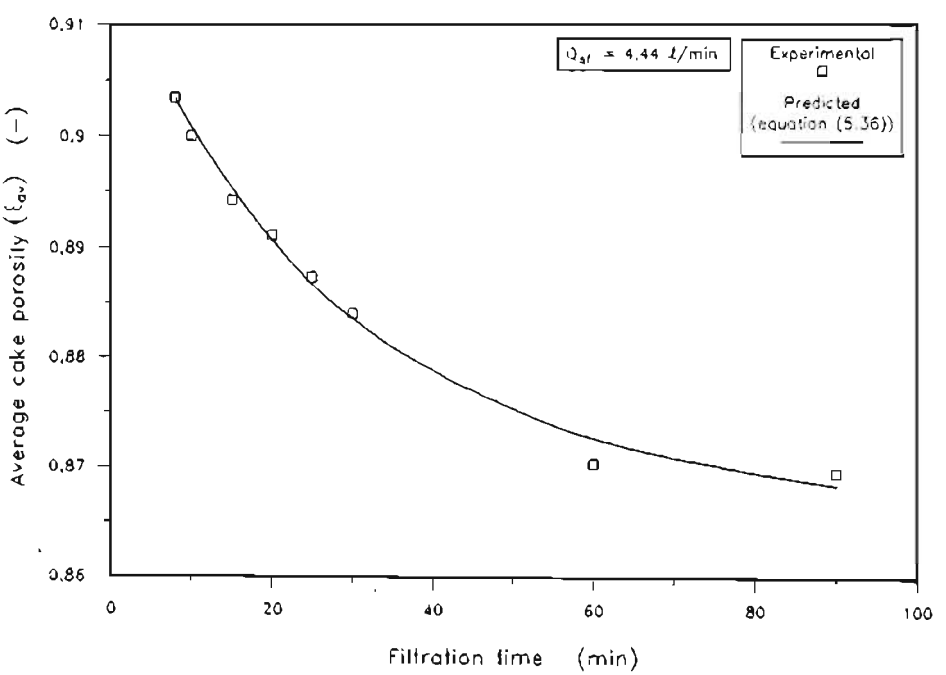

FIGURE 5.36 : Comparison Between Experimental and Predicted (from Equation (5.36)) Average Cake Porosities for a Cross-flow Flow Rate of 4,44 ℓ/min

5.6.10.2 Incorporation of equations (5.35) and (5.36) into the axial convection shear model for cross-flow microfiltration

A brief description will now be given of how the axial convection shear model was amended or "extended" to incorporate equations (5.35) and (5.36).

For the time period from start-up to the threshold filtration time, t_{id} , the procedure was identical to that for the model which was developed in section 5.3.

For the time period after the threshold filtration time, t_{id} , the average cake permeability and porosity were assumed to change in accordance with equations (5.35) and (5.36), respectively. The permeability and porosity of the cake after the threshold filtration time, t_{id} , was incorporated into the computer algorithm as follows :

$$PEF(t) = \frac{K_{av}(t)}{K_{av}^{d}} \qquad (5.37)$$

where K_{av}^{d} = average permeability of equivalent cake (with identical internal cake diameter) deposited under static or *dead-end* conditions, (m^2)

PEF = factor as defined by equation (5.37), (-)

$K_{av}(t)$ was calculated from equation (5.35).

In a similar manner for cake porosity :

$$POF(t) = \frac{\epsilon_{av}(t)}{\epsilon_{av}^{d}} \qquad (5.38)$$

where ϵ_{av}^{d} = average porosity of equivalent cake (with identical internal cake diameter) deposited under static or *dead-end* conditions, (-)

POF = factor as defined by equation (5.38), (-)

$\epsilon_{av}(t)$ was calculated from equation (5.36).

Sets of equations (3.79) and (3.81) were amended as follows in the computer algorithm shown in Figure 5.37.

$$\begin{aligned} K(t) &= 6.621 \times 10^{-13} p_{sf}^{-0.575} && 0 \le p_s \le p_{sf} \\ K(t) &= 6.621 \times 10^{-13} PEF(t)\, p_s^{-0.575} && p_{sf} \le p_s \le 3781.7\ \text{Pa} \\ K(t) &= 1.779 \times 10^{-10} PEF(t)\, p_s^{-1.254} && p_s \ge 3781.7\ \text{Pa} \end{aligned} \qquad (5.39)$$

$$\begin{aligned} \epsilon(t) &= 0.0299\, p_{sf}^{0.0782} && 0 \le p_s \le p_{sf} \\ \epsilon(t) &= 0.0299\, POF(t)\, p_s^{0.0782} && p_{sf} \le p_s \le 1285.1\ \text{Pa} \\ \epsilon(t) &= 0.00785\, POF(t)\, p_s^{0.265} && p_s \ge 1285.1\ \text{Pa} \end{aligned} \qquad (5.40)$$

It was however, assumed that the moving cake layer was *not subject to compaction* or dynamic changes in permeability and porosity as the bulk of the cake. The axial thickness profile and solids concentration of the *moving cake layer* were calculated from an *equivalent cake deposited under dead-end conditions* without compaction. A consequence of this assumption is that during the pseudo steady-state, it is possible for the model to predict that during some time intervals the rate of solids removal in the moving cake layer at the outlet of the filter tube is *greater* than the solids deposition along the filter tube. Since this is clearly not feasible, it was assumed for the purposes of the model that during such time intervals the rate of solids deposition was *equal* to the rate of solids removal.

A computer program was written to incorporate the abovementioned changes. A highly simplified algorithm is presented in Figure 5.37.

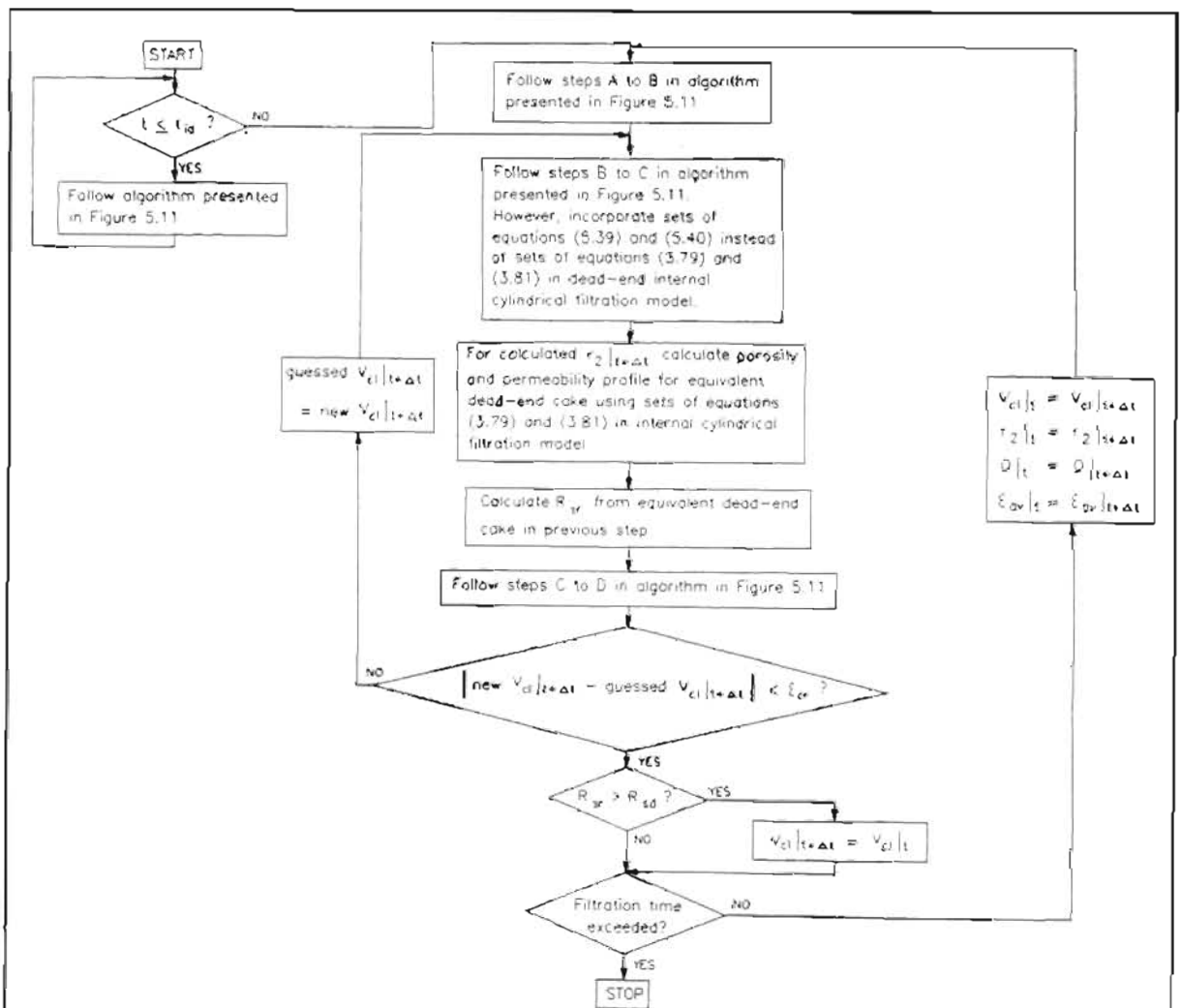

FIGURE 5.37 : Algorithm for "Extended" Axial Convection Shear Model for Cross-flow Microfiltration

5.6.10.3 Comparison between experimental results and "extended" axial convection shear model for cross-flow microfiltration

The comparison between experimental results and predictions by the "extended" axial convection shear model for cross-flow microfiltration is shown in Figures 5.38, 5.39 and 5.40 in terms of internal cake diameters, filtrate fluxes and average cake dry solids concentrations, respectively. The cross-flow flow rate for Figures 5.38, 5.39 and 5.40 is 4,44 ℓ/min.

When comparing Figures 5.22(d), 5.23(d) and 5.24(d) with Figures 5.38, 5.39 and 5.40, respectively, it is evident that the fit between experimental and predicted values was improved when the aforementioned dynamic changes in cake permeability and porosity were incorporated into the model. This was particularly true for the pseudo steady-state time period.

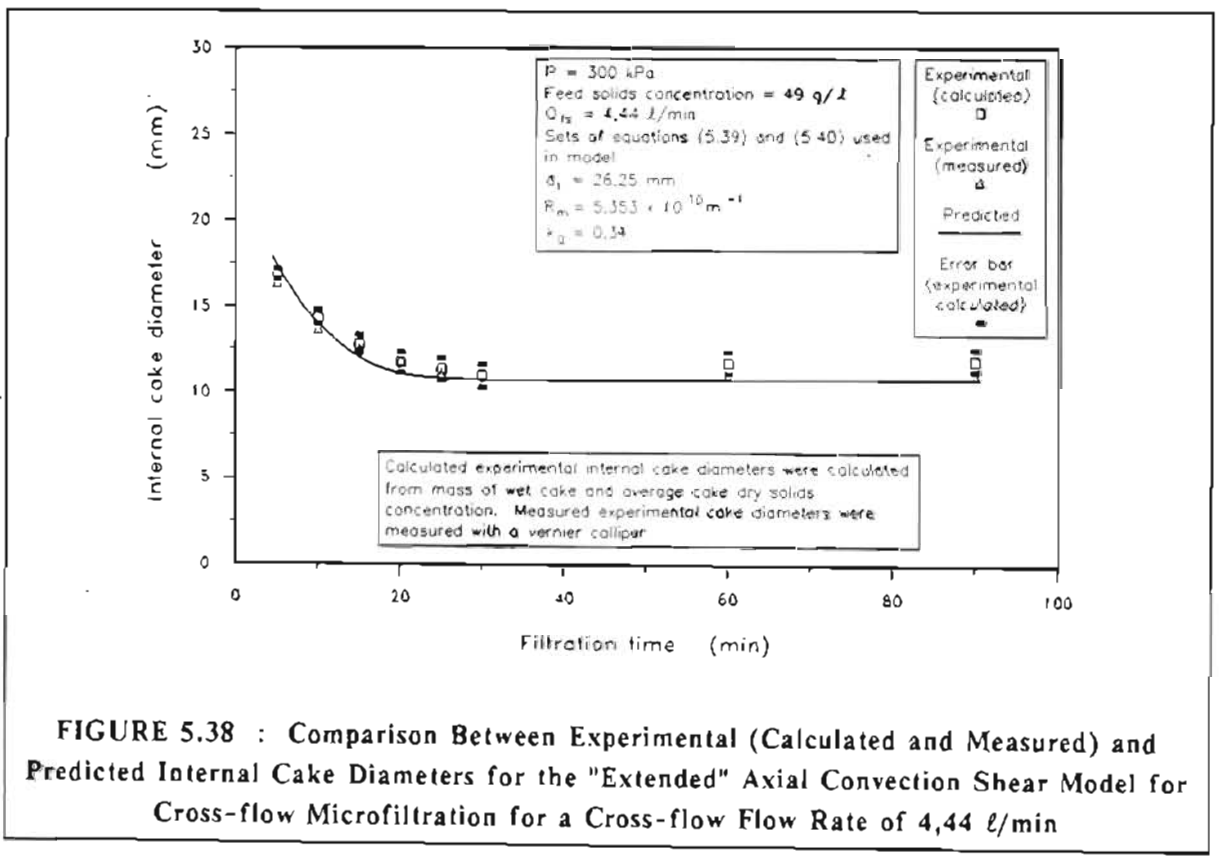

FIGURE 5.38 : Comparison Between Experimental (Calculated and Measured) and Predicted Internal Cake Diameters for the "Extended" Axial Convection Shear Model for Cross-flow Microfiltration for a Cross-flow Flow Rate of 4,44 ℓ/min

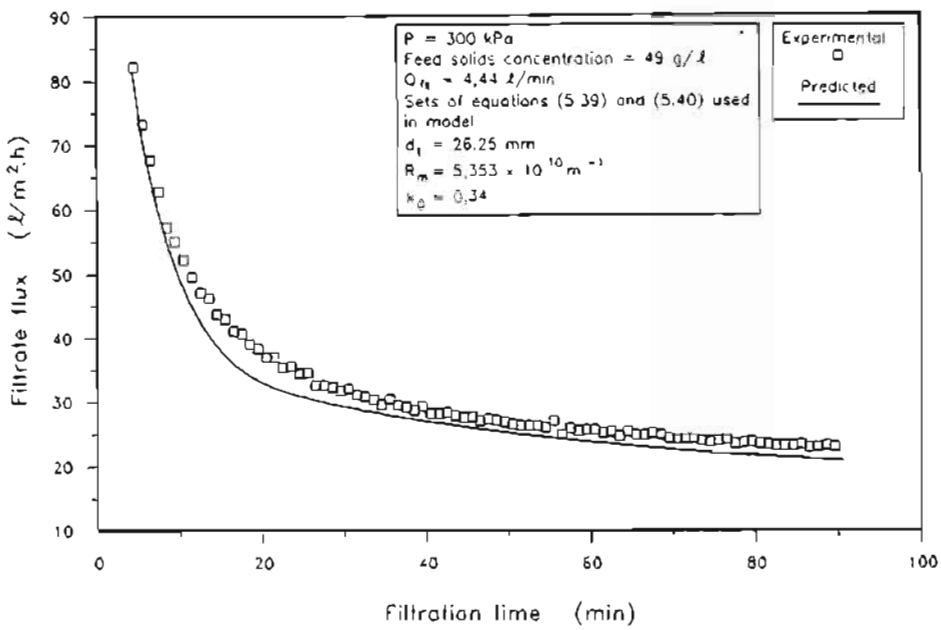

FIGURE 5.39 : Comparison Between Experimental and Predicted Filtrate Fluxes for the "Extended" Axial Convection Shear Model for Cross-flow Microfiltration for a Cross-flow Flow Rate of 4,44 ℓ/min

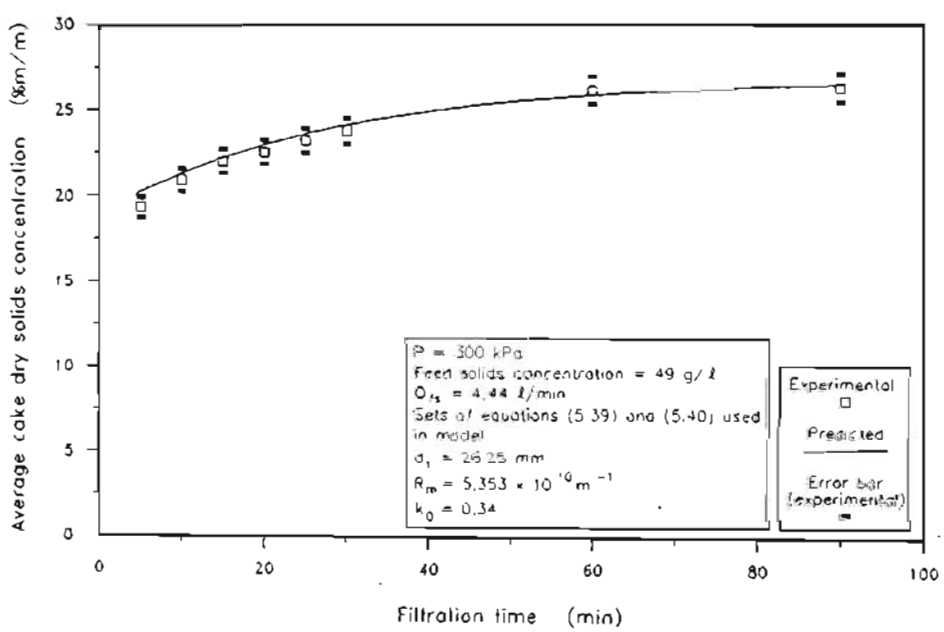

FIGURE 5.40 : Comparison Between Experimental and Predicted Average Cake Dry Solids Concentrations for the "Extended" Axial Convection Shear Model for Cross-flow Microfiltration for a Cross-flow Flow Rate of 4,44 ℓ/min

5.7 DISCUSSION OF RESULTS

5.7.1 Evaluation of Axial Convection Shear Model for Cross-flow Microfiltration

Overall there was good agreement between the axial convection shear model (based on equivalent static or dead-end cake characteristics) and experimental results for the *unsteady-state* time period. As was stated previously, it is primarily the unsteady-state phase which is applicable to the operation of a tubular filter press in cross-flow mode. For the so-called steady-state time period there were, however, significant discrepancies between experimental results and predictions by the axial convection shear model based on *dead-end cake characteristics*. These discrepancies were due to the fact that cake compaction caused a decrease in cake permeability and porosity (compared with those for an equivalent dead-end cake) after an equilibrium internal cake diameter was attained. The model was "extended" by incorporating changes in cake permeability and porosity into the model. For the "extended" model, good agreement between experimental and predicted values was achieved for both the unsteady-state and so-called steady-state time periods.

The experimental data for evaluation of the model was limited in that experiments were conducted at four cross-flow flow rates at a *single* filtration pressure and feed sludge solids concentration. It is recommended that more work be done to evaluate the model at other filtration pressures and feed sludge solids concentrations.

5.7.2 Validity of Model

5.7.2.1 Type of sludge

One of the advantages of the axial convection shear model (without "extension"), is that it does not require any arbitrary fitting or regression parameters for predictive purposes, as is the case for many cross-flow microfiltration models. For Pearson and Sherwood's (1988) model, for example, the value of the shear enhanced diffusion coefficient has to be fitted to or regressed from experimental data if the model is to be used for predictive purposes. The same applies to the models of Hunt (1987) and Pillay (1991).

For the proposed axial convection shear model (without "extension"), only the sludge and cake rheology and the variation of permeability and porosity with solids compressive pressure, have to be determined experimentally for a specific sludge if the model is to be used for predictive purposes.

For the "extended" axial convection shear model the cake permeability and porosity have to be fitted to or regressed from actual experimental data obtained from cross-flow microfiltration experiments (in accordance with equations (5.35) and (5.36)), if the model is to be used for predictive purposes.

The proposed axial convection shear model was evaluated using one type of sludge. It is important that tests be conducted on other types of sludges (which produce compressible cakes) to further evaluate the performance and predictive capability of the model.

However, in contrast to many research studies, the model was evaluated using a *real* sludge.

5.7.2.2 Flow regime

The model developed here is restricted to laminar flow conditions for the feed sludge. It could, however, in principle fairly easily be extended to turbulent flow. This needs to be further investigated.

5.7.3 Main Assumptions for Model

As has already been stated, the assumption that the cake characteristics under cross-flow conditions are identical to those for a cake deposited under static or dead-end conditions, gave a satisfactory fit between experimental and predicted values for the *unsteady-state* time period. However, for the so-called steady-state time period this assumption was no longer valid, since there were significant deviations from dead-end cake porosities and permeabilities due to further compaction of the cake. These findings are in agreement with those of other researchers (for example, Baker et al., 1985; Rushton and Aziz, 1983) who found that the nature of a cross-flow cake was different to that of an equivalent dead-end cake.

The assumption that the solids concentration of the moving cake layer is uniform and equal to the arithmetic mean of the solids concentration of the feed sludge and the solids concentration at the shear plane, may be an oversimplification, and a more complex relationship may be required for a more general model.

As mentioned in Chapter 4, recently developed non-intrusive measuring techniques such as synchrotron X-ray absorbance (Bierck et al., 1988) and NMR (nuclear magnetic resonance) imaging (Horsfield et al., 1989) could potentially be used to measure the solids concentration in and thickness of such a moving cake layer, if it exists.

According to assumption (x), section 5.3.1, a differential length of filter tube was considered for the model. This means that axial variations in flow rate and solids concentration of the feed sludge were considered to be negligible. This was true for the experiments, since even for the lowest cross-flow flow rate of 0,84 ℓ/min, the flow rate of the filtrate at the end of the unsteady-state time period was only approximately 2% of the cross-flow flow rate. Also, the length of the porous section of the filter tube was short (0,442 m).

Further work is required to extend or "integrate" the model for long filter tubes.

The assumption that the unsteady-state time period may be modelled by a series of *quasi* steady-state conditions may be an oversimplification and mechanistically incorrect. However, the model nevertheless gave a surprisingly good fit between predicted and experimental results during the unsteady-state time period.

5.7.4 Thickness of Moving Cake Layer

Except for the very early stages of filtration (see section 5.6.5 and Figure 5.28), the thickness of the moving cake layer was "realistic" in that it could "accommodate" several layers of the average particle size which for this sludge was determined as 5,90 μm (see Appendix F). During the early stages of filtration the internal cake diameters under cross-flow conditions were almost identical to those for static conditions (see Figure 5.13). The rate of solids removal during the early stages of filtration was therefore insignificant compared with the rate of solids deposition, so that the thickness of the moving cake layer during the early stages of filtration does not warrant further attention.

The thickness of the moving cake layer was also thin when compared with the internal cake diameter so that assumption (vii) (section 5.3.1) for the model was valid.

5.7.5 Accuracy of Solids Compressive Pressure Profiles in Low Solids Compressive Pressure Region

As shown in Chapter 3, the variation of porosity and permeability in the low solids compressive pressure region, was determined by means of settling tests. The accuracy of the settling tests has been questioned by Murase et al. (1989), as mentioned in section 3.6.4. Since yield stress was found to be an exponential power function of solids concentration (see equation (4.34)), the location of the shear plane (in the cake) and therefore the yield stress of the cake in the moving cake layer are very sensitive to the solids concentration and solids compressive pressure profiles in the low solids compressive pressure region. The location of the shear plane also determines the thickness, δ_t, of the moving cake layer. The thickness of the moving cake layer in turn has a significant impact on the calculation of the rate of solids removal (see equation (5.16)).

Inaccuracies in the low solids compressive pressure region could have been responsible for some of the discrepancies between experimental and predicted results.

5.7.6 Accuracy of Cake/Sludge Rheology

As described in Chapter 4, the rheology of the sludge (cake) was determined using a capillary-tube viscometer. The sludges (cakes) in the solids concentration range 3,58 % m/m to 16,71 % m/m were all found to be Bingham plastic fluids, as was assumed for the model. The rheology experiments have already been discussed in Chapter 4.

5.7.7 Implications of Model for Design of Manifold Systems for a Tubular Filter Press

The axial convection shear model predicts that the internal cake diameter for cross-flow filtration inside a porous tube is dependent on the cross-flow flow rate. The higher the cross-flow flow rate, the larger the internal cake diameter and vice versa.

As discussed in Chapter 2, it is possible for maldistributions of flow to occur in manifold systems. For a tubular filter press, the filter tubes are manifolded between an inlet and an outlet manifold. If maldistributions of flow occur in the filter tubes of a manifold system, then from the predictions of the axial convection shear model such maldistributions will result in variations in internal cake diameters in a filter tube curtain. As was discussed in Chapter 2, such variations in internal cake diameters may further enhance maldistributions of flow in a filter tube manifold system. Under such conditions it can be envisaged that tube blockages can occur.

From the results of this investigation it is therefore imperative that the manifolds for a tubular filter press be designed so that maldistributions of flow are minimized. This model when combined with a conventional manifold model, could assist in the design of such manifold systems.

5.8 CONCLUSIONS AND RECOMMENDATIONS

For the tubular filter press an alternative operating mode to dead-end filtration is that of low flow rate (unsteady-state) cross-flow filtration. The main advantage of cross-flow over dead-end filtration is that under ideal circumstances, if the flow rate in all filter tubes of a manifold system were the same during the pressing cycle, it would be impossible for tube blockages to occur.

The particle size of the sludge on the prototype tubular filter press was found to be such (average particle size : 5,90 μm (see Appendix F)) that the filtration of the sludge could be classified as microfiltration.

A literature review of mathematical models for cross-flow microfiltration revealed that although there are numerous mathematical models for cross-flow microfiltration, there is only one mathematical model (Pearson and Sherwood, 1988) currently available for the *unsteady-state* cross-flow microfiltration of a *non-Newtonian* sludge, which when filtered produces a *compressible* cake. However, for the reasons discussed in section 5.2.6, the model of Pearson and Sherwood (1988) was found not to be suitable for the filtration of the clarifier sludge inside a porous tube.

Consequently an investigation was conducted into the *laminar* cross-flow filtration of the same waterworks clarifier sludge which was used for the dead-end internal cylindrical filtration experiments (see Chapter 3) and the cake recovery experiments (see Chapter 4).

An unsteady-state or dynamic cross-flow (micro)filtration axial convection shear model was developed for *laminar* flow of the feed sludge.

The model combines the internal cylindrical compressible cake filtration model (for static or "dead-end" filtration) which was developed in Chapter 3 with the shear model for cake losses which was developed in Chapter 4. This approach is similar to that adopted by Pearson and Sherwood (1988) for their convection-diffusion model for cross-flow microfiltration.

Similarly to Pearson and Sherwood (1988), it was assumed that there is a shear plane in the cake under cross-flow conditions. The yield stress of the cake layer along the shear plane is equal to the shear stress exerted by the flowing feed sludge at the sludge/cake interface. It was assumed that those cake layers for which the yield stress is less than the shear stress exerted by the flowing feed sludge are convected along the shear plane to the outlet end of the filter tube. Those cake layers for which the yield stress is greater than the shear stress exerted by the flowing feed suspension form a static cake. However, unlike Pearson and Sherwood (1988), it was assumed that the axial convection of solids in the moving cake layer along the shear plane is the sole mechanism for removal of solids deposited at the cake surface. Diffusive and shear induced diffusive back-mixing (which were an integral part of the Pearson and Sherwood (1988) model) were assumed to be negligible for the size range of particles studied.

Further differences between the axial convection shear model developed during this study and Pearson and Sherwood's (1988) model, are as follows. Pearson and Sherwood's (1988) model was developed for a planar configuration, while the model developed during this study is valid for an internal cylindrical configuration. In order to "avoid" the complex partial differential equations to describe the unsteady-state behaviour in Pearson and Sherwood's (1988) model, the mathematical technique for the unsteady-state time period (as mentioned below) for the axial convection shear model is entirely different from that given by Pearson and Sherwood (1988). The main assumptions for the model are summarized below.

It was assumed that the solids concentration of the moving layer is uniform (i.e. there is no axial or radial solids concentration profile in the moving cake layer). A further assumption was that the feed sludge and moving cake layer are Bingham plastic fluids.

For the model it was assumed that the cake is very compressible and that the bulk of the cake resistance is concentrated in a well-compressed skin of cake adjacent to the filter medium. The resistance of the thin moving cake layer, which increases in thickness as it moves towards the outlet of the filter tube, was considered negligible, so that filtrate flux was assumed to be *invariant* with axial distance along the filter tube. A further assumption was that the physical characteristics of a cake deposited under cross-flow conditions are identical to those for a cake deposited under static or dead-end conditions.

As with all cross-flow microfiltration processes the filtration time was divided into an unsteady-state phase (during which the internal cake diameter decreases due to cake growth), and a so-called steady-state time period (during which the internal cake diameter remains constant).

Equations were developed for solids deposition and removal (in the cake layer) for the *steady-state* time period.

For the modelling of the unsteady-state, the time period was divided into successive short time intervals. For the purposes of modelling it was assumed that during each short time interval a *quasi* steady-state exists and that the equations for solids removal (in the moving cake layer), developed for the *steady-state* could be applied during each time interval during the *unsteady-state* phase.

One of the advantages of the axial convection shear model is that it does not require any arbitrary fitting or regression parameters for predictive purposes, as is the case for many cross-flow microfiltration models.

The model was compared with the results of cross-flow filtration experiments using the waterworks clarifier sludge. These experiments were conducted at a single filtration pressure and feed sludge concentration and four cross-flow flow rates in the laminar flow regime. The rheology of the waterworks sludge (which was measured for various solids concentrations as discussed in Chapter 4) was incorporated into the model. The same permeability and porosity equations as were used in Chapter 3 for the waterworks clarifier sludge were used for the cross-flow (micro)filtration axial convection shear model. The model accurately described the measured variation of average cake dry solids concentration, internal cake diameter and filtrate flux with time for the unsteady-state time period for all four cross-flow flow rates. The model also accurately predicted the equilibrium or steady-state internal cake diameter for all four cross-flow flow rates.

However, it was found that although the internal cake diameter remained essentially constant during the so-called (pseudo) steady-state time period and the model therefore predicted a constant flux, there was a further slow decline in filtrate flux and a slow increase in average cake dry solids concentration during this period. It was found that there were significant discrepancies between the measured average cake porosities and permeabilities for the steady-state period and those for an equivalent dead-end cake (based on the same internal cake diameter). These findings are in agreement with those of other researchers (for example, Baker et al., 1985; Rushton and Aziz, 1983) who found that the nature of a cake deposited under cross-flow conditions was different to one deposited under static conditions. It was also found that the average cake permeability and porosity was dependent on cross-flow flow rate. (In contrast there were contradictions when the model of Pearson and Sherwood (1988) was compared to the experimental results of Fordham and Ladva (1989) for bentonite suspensions).

Despite these discrepancies between the model and experimental results for the *steady-state* time period, the model is a useful predictive tool for cross-flow filtration for a tubular filter press, since for *optimized* sludge dewatering, filtration times will not extend much beyond the time required to reach an equilibrium or steady-state internal cake diameter. As mentioned there was close agreement between the model and experimental results for the *unsteady-state* time period.

It was also shown how the model may be "extended" by incorporating empirical equations to describe changes in cake porosity and permeability during the steady-state period. The "extended" model accurately described the experimental results both during the unsteady- and pseudo steady-state time periods. The "extended" model is a contribution to what is a complex problem, namely, the modelling of the unsteady-state cross-flow microfiltration of a non-Newtonian sludge which, when filtered, produces a very compressible cake.

The experiments were limited in that they were done at a single filtration pressure and feed sludge solids concentration. It is recommended that more work be done to evaluate the model at other filtration pressures and feed sludge solids concentrations.

Since this model was developed for a differential length of filter tube, future work should extend or "integrate" the model for long filter tubes. It is also recommended that more work be done on other types of sludges to further evaluate the performance and predictive capability of the model.

There is also a possibility that recently developed non-intrusive measuring techniques such as X-ray synchrotron absorbance (Bierck et al., 1988) and nuclear magnetic resonance imaging (Horsfield et al., 1989) may be employed to measure the solids concentration profile of the cake more accurately, especially in the vicinity of the moving cake layer (if such a layer exists). Such techniques could potentially also be employed to gather more data on the behaviour of the moving cake layer such as axial thickness profiles of and velocity profiles within the cake layer.

CHAPTER 6
CONCLUSIONS AND RECOMMENDATIONS

As discussed in Chapter 2, the objectives of this study were defined on the basis of the results achieved and the two main problems encountered on the prototype tubular filter press. The two main problems experienced on the prototype tubular filter press were :

(i) tube blockages during the filtration cycle;

(ii) low cake recoveries (high cake losses) during the cake removal cycle.

The objectives of this study were classified into three categories :

(i) to develop a predictive model for static or dead-end compressible cake filtration inside a porous tube. Such a model is fundamental to any solution of the tube blockage problems experienced during the dead-end filtration mode of the tubular filter press;

(ii) to investigate cake recovery (cake losses) during the cake removal cycle of the tubular filter press.

(iii) an alternative to dead-end filtration during the filtration cycle is to operate the tubular filter press in low axial velocity cross-flow mode during the filtration cycle. Under ideal circumstances this procedure should prevent tube blockages. The third objective of the study was therefore to develop a predictive unsteady-state internal cylindrical cross-flow microfiltration model for a sludge which has a non-Newtonian rheology and which, when filtered, produces a very compressible cake.

This study was divided into three investigations. Each of the three objectives involved a separate "self contained" investigation.

Although conclusions and recommendations have been given for each investigation, it is the purpose of this chapter to consolidate these into global conclusions and recommendations for the study as a whole.

6.1 INVESTIGATION OF STATIC OR DEAD-END COMPRESSIBLE CAKE FILTRATION INSIDE A POROUS TUBE

A literature review revealed that to date no one has developed a model which incorporates the cylindrical configuration of the filter medium, for dead-end internal cylindrical compressible cake filtration.

The most comprehensive model to date for dead-end *external* cylindrical compressible cake filtration is that of Tiller and Yeh (1985).

For this study, the model by Tiller and Yeh (1985) for external cylindrical compressible cake filtration was adapted for compressible cake filtration *inside* a cylindrical or tubular filter medium.

In essence the model by Tiller and Yeh (1985) for external cylindrical compressible cake filtration requires the solution of a system of two ordinary differential equations in order to obtain the radial liquid and solids compressive pressure profiles within the cake. The first differential equation relates the liquid (filtrate) flow rate to the radial liquid (filtrate) pressure drop :

$$\frac{dp_L}{dr} = \frac{\mu_f Q}{2\pi r K} \qquad (3.27)$$

The second equation gives a relationship between solids compressive pressure and liquid pressure :

$$\frac{dp_s}{dr} = \frac{\mu_f Q}{2\pi r K} - (1 - k_0)\frac{p_s}{r} \qquad (3.39)$$

The relevant equations for internal cylindrical compressible cake filtration were derived, and it was found that for internal cylindrical filtration, equation (3.27) changes to :

$$\frac{dp_L}{dr} = -\frac{\mu_f Q}{2\pi r K} \qquad (3.28)$$

Equation (3.39) remains unaltered for internal cylindrical compressible cake filtration.

A waterworks clarifier sludge was used for experiments to evaluate the performance of the internal cylindrical compressible cake filtration model. For the model, it was necessary to characterize the cake, which was produced by the filtration of this sludge. Since the cake was found to be very compressible, it was decided to obtain porosity and permeability data over a wide range of solids compressive pressures. A Compression-Permeability (C-P) cell was used to obtain permeability and porosity data in the *high* solids compressive pressure range, while a settling technique was used to determine permeability and porosity data in the *low* solids compressive pressure range. A recently developed centrifuge technique was used to obtain porosity data in the *intermediate* solids compressive pressure range.

The empirical equations which were derived from the C-P cell, settling and centrifuge tests, to relate permeability and porosity to solids compressive pressure, were slightly different from those proposed by Tiller and Cooper (1962). The main difference was that Tiller and Cooper (1962) assumed that for a compressible cake, permeability and porosity are constant below a certain value of solids compressive pressure, whereas the equations for this study propose that for a compressible cake, permeability and porosity *decrease continuously* (or steadily) as solids compressive pressure is increased from that corresponding to the feed sludge.

In order to evaluate the permeability and porosity data, the data were incorporated into a conventional *planar* filtration model. It was found that when the centrifuge data were ignored, there was close agreement between the planar filtration model and the results of constant pressure planar filtration experiments.

Incorporation of the centrifuge data into the internal cylindrical filtration model also resulted in significant discrepancies between predictions by the model and experimental results. The centrifuge data were therefore ignored.

The predictions by the *internal* cylindrical filtration model were compared to the results of constant pressure filtration experiments inside a porous tube, which could be dismantled. As already mentioned, a waterworks clarifier sludge, which when filtered produced a very compressible cake with a high resistance, was used for the experiments. Overall there was good agreement between the predictions by the model and experimental results at filtration pressures of 100 kPa, 200 kPa and 300 kPa.

The main findings of the investigation were as follows.

For internal cylindrical compressible cake filtration, the solids compressive and liquid pressures are not unique functions of the fractional distance through the cake, as is the case for planar filtration with negligible filter medium resistance.

As for external cylindrical filtration, it was found that for internal cylindrical filtration the effect of the value of the coefficient of earth pressure at rest, k_o, is negligible, except for long filtration times (small internal cake diameters).

Significant differences between planar, external cylindrical and internal cylindrical compressible cake filtration were highlighted. For planar filtration the average cake dry solids concentration remains essentially *constant* as the cake thickness increases. For external cylindrical filtration the average cake dry solids concentration *decreases*, while for internal cylindrical filtration the average cake dry solids concentration *increases* with cake thickness.

However, the dry solids production rate (ignoring time required for cake removal and other "dead" time) is lower for internal cylindrical filtration than for planar filtration or external cylindrical filtration. This is due to the decrease in available filtration area as the internal cake diameter decreases.

The model predicted that internal filter tube diameter has a significant effect on average cake dry solids concentration for internal cylindrical filtration. The average cake dry solids concentration *decreases* as the internal tube diameter *increases*.

The only experimental inputs required for the model are the variations of permeability and porosity with solids compressive pressure. It is recommended that the performance and predictive capability of the model be evaluated for other types of sludges. Further work is required to determine the effect of feed solids concentration (if any) on filtration performance. The relatively new centrifuge method for the measurement of porosity and permeability in the *intermediate* solids compressive pressure range also requires further evaluation. Experiments also need to be done with various internal filter tube diameters to substantiate the predictions of the model.

Finally, since the model which was developed, accurately predicted the variation of internal cake diameter with filtration time, it should be of great assistance in preventing or minimizing tube blockages in a tubular filter press.

6.2 INVESTIGATION INTO CAKE RECOVERY DURING THE CAKE REMOVAL CYCLE

At various times low cake recoveries (during the cake removal cycle) were experienced on the prototype tubular filter press. Low cake recoveries are undesirable since they result in a reduced dry solids production rate and can cause an excessive increase in feed solids concentration in the feed tank.

Since the tubular filter press is a novel process, the cake losses during the cake removal cycle have not been investigated before. For this reason an investigation was conducted into the cake losses which occur during the cake removal cycle of the tubular filter press process. The waterworks clarifier sludge which was used for the internal cylindrical filtration experiments (as discussed in section 6.1) was also used for this study.

It was found that significant cake losses occurred :

(i) due to the shear of the cleaning fluid (prior to the action of the rollers), and;

(ii) due to the action of the rollers in dislodging the cake, and the hydraulic conveyance of the dislodged flakes of cake from the filter tubes.

The experiments to quantify the cake losses due to cleaning fluid shear were conducted with both water and feed sludge as cleaning fluids. The effect of the following variables on shear losses was investigated :

(i) filtration pressure (100 kPa and 300 kPa);

(ii) cleaning fluid flow rate (25 ℓ/min and 50 ℓ/min);

(iii) filtration time (in increments of 5 minutes up to 30 minutes).

It was found that for the very compressible cake, the shear exerted by the flowing cleaning fluid resulted in the scouring away of "mushy" or "sloppy" layers of cake. This resulted in significant increases in internal cake diameters and average cake dry solids concentrations when compared with the deposited cakes (without shear). The cake losses, internal cake diameters and average cake dry solids concentrations all increased with cleaning fluid flow rate. There was no clear trend of shear losses with filtration time or pressure, however.

A new shear model was developed to predict cake losses (due to cleaning fluid shear) and average cake dry solids concentration and internal cake diameter (after shear), for compressible cake filtration. For the shear model it was assumed that when a cleaning fluid flows inside the annulus of a cake, which was deposited inside a porous tube, a shear plane exists within the cake. The yield stress of the cake layer along

the shear plane is equal to the shear stress exerted by the flowing cleaning fluid. Those cake layers for which the yield stress is less than the shear stress exerted by the flowing cleaning fluid are scoured away, while those for which the yield stress is greater than the shear stress exerted by the flowing cleaning fluid remain static.

The rheology for sludges (cakes) of various solids concentrations in the range, 3,58 % m/m $\leq c_s \geq$ 16,71 % m/m, was determined using a capillary-tube viscometer. The sludges were all found to exhibit yield stresses and their rheology resembled that of Bingham plastic fluids. The sludge rheology was combined with the internal cylindrical filtration model (see section 6.1) to obtain a *radial* yield stress profile for a deposited cake. This was incorporated into the shear model.

Overall there was good agreement between the predictions by the shear model and experimental results.

The results of the cleaning fluid shear experiments have shown that for the filtration (dewatering) of sludges which produce very compressible cakes, the tubular filter press process has a distinct advantage over conventional planar and external cylindrical filtration processes. Due to the scouring away of undesirable "sloppy" cake layers, the average dry solids concentration of the cake produced by a tubular filter press is significantly higher than that produced by conventional planar or external cylindrical filtration processes, if expression diaphragms are not installed.

From the results of the cleaning fluid shear experiments and the predictions of the shear model it may be concluded that for compressible cake filtration in a tubular filter press it is very important that the filter tube manifold systems be designed so that maldistributions of flow are minimized. The reasons for this were discussed in detail in section 4.9.3.2.2.

The only experimental inputs required for the shear model are the variations of permeability and porosity with solids compressive pressure and the variation of sludge (cake) rheology with sludge (cake) solids concentration.

Only one type of sludge was used for the cleaning fluid shear experiments. More work is required to determine whether the findings of this study and the proposed shear model are applicable to other types of sludges which produce compressible cakes, and to test the predictive capability of the model. Further investigations are also required to determine the shear losses for *incompressible* cakes.

As mentioned earlier, experiments were also conducted to determine the combined cake losses due to the action of the rollers and the hydraulic conveyance of the dislodged flakes of cake. The effect of the following variables was investigated :

(i) filtration pressure (100 kPa and 300 kPa);

(ii) cleaning fluid flow rate (25 ℓ/min and 50 ℓ/min);

(iii) filtration time (in increments of 5 minutes up to 30 minutes);

(iv) path length for conveyance of flakes of cake (1 m and 4 m).

These cake losses decreased markedly as filtration pressure and filtration time were increased, while a decrease in path length for hydraulic conveyance of cake flakes resulted in a mild decrease in these cake losses. The flow rate of the cleaning fluid did not have a marked effect on the combined cake losses due to the action of the rollers and the hydraulic conveyance of the dislodged flakes of cake.

The experiments to determine the combined cake losses due to roller action and hydraulic conveyance, were conducted with fixed roller dimensions. It is recommended that future investigations also consider the effect of roller dimensions on cake losses. It is further recommended that a quick screening test (similar to the one by Berger et al. (1990)) be developed, in order to give a rough indication of the cake losses due to roller action and hydraulic conveyance, which can be expected for a tubular filter press.

6.3 INVESTIGATION OF THE LAMINAR CROSS-FLOW FILTRATION OF THE WATERWORKS CLARIFIER SLUDGE INSIDE A POROUS TUBE

For the tubular filter press an alternative operating mode to dead-end filtration is that of low flow rate cross-flow filtration during the filtration cycle. The advantages of low flow cross-flow over dead-end filtration were discussed in section 5.1. An investigation was conducted into the *laminar* cross-flow filtration of the waterworks clarifier sludge, which was used for the dead-end internal cylindrical filtration experiments and the cake recovery experiments.

The average particle size of the sludge was found to be such that the filtration of the sludge could be categorized as microfiltration. As was mentioned in section 6.2, the rheology of the sludge was found to resemble that of a Bingham plastic fluid. A literature review revealed that although there are numerous mathematical models for cross-flow microfiltration, there is only one satisfactory model (Pearson and Sherwood, 1988) currently available for the unsteady-state cross-flow microfiltration of a non-Newtonian sludge, which when filtered produces a compressible cake. For various reasons (see section 5.2.6) the model of Pearson and Sherwood (1988) was found not to be suitable for the filtration of the clarifier sludge inside a porous tube.

An new unsteady-state or dynamic cross-flow microfiltration axial convection shear model was developed for a differential length of filter tube and *laminar* flow of the feed sludge.

The model is a combination of the internal cylindrical filtration model developed for dead-end or static filtration (see section 6.1) and the shear model for quantifying cake losses due to shear of the cleaning fluid during the cake removal cycle of a tubular filter press (see section 6.2).

As for the cleaning fluid shear model it was assumed that under cross-flow conditions there is a shear plane within the cake. The yield stress of the cake layer along the shear plane is equal to the shear stress exerted by the flowing feed sludge. It was assumed that those cake layers for which the yield stress is less than the shear stress exerted by the flowing feed sludge are convected along the shear plane to the outlet of the filter tube. Those cake layers for which the yield stress is greater than the shear stress form a static cake. This approach is very similar to that adopted by Pearson and Sherwood (1988) for their convection-diffusion cross-flow microfiltration model. However, unlike Pearson and Sherwood (1988) it was assumed that the axial convection of solids in the moving cake layer along the shear plane is the sole mechanism for removal of solids deposited at the cake surface. Diffusive and shear induced diffusive back-mixing, which were an integral part of the Pearson and Sherwood (1988) model, were assumed to be negligible for the size range of particles in the clarifier sludge.

Further differences between the axial convection shear model developed during this study and Pearson and Sherwood's (1988) model, are as follows :

(i) Pearson and Sherwood's (1988) model was developed for a planar configuration, while the axial convection shear model is valid for an internal cylindrical configuration;

(ii) in order to "avoid" the complex partial differential equations to describe the unsteady-state time period in Pearson and Sherwood's (1988) model, the mathematical technique for the unsteady-state time period in the axial convection shear model is entirely different to that given by Pearson and Sherwood (1988) (as mentioned below).

A major assumption for the model was that the physical characteristics of a cake deposited under *cross-flow* conditions are identical to those of an equivalent cake deposited under *dead-end* conditions.

This meant that the model for dead-end internal cylindrical compressible cake filtration (see section 6.1) could be combined with the sludge rheology (which was determined for the cake recovery experiments) (see section 6.2) to calculate radial permeability, porosity and yield stress profiles for a cake under cross-flow conditions.

The cross-flow filtration was divided into an unsteady-state time period during which the internal cake diameter decreases due to cake growth and a steady-state time period during which the internal cake diameter remains constant.

Equations were developed for solids deposition and removal for the steady-state time period. For the modelling of the unsteady-state, the time period was divided into successive short time intervals. For the purposes of modelling it was assumed that during each time interval during the *unsteady-state* time period a *quasi* steady-state exists, and that the equations for solids removal developed for the steady-state may be applied during each time interval during the unsteady-state time period.

One of the advantages of the axial convection shear model is that it does not require any arbitrary fitting or regression parameters for predictive purposes, as is the case for many cross-flow microfiltration models. The only experimental inputs required for the model are the variations of permeability and porosity with solids compressive pressure, and the variation of sludge rheology with sludge solids concentration.

Laminar cross-flow filtration experiments were conducted at a single filtration pressure (300 kPa) and feed sludge solids concentration (49 g/ℓ) and four cross-flow flow rates (0,84 ℓ/min; 1,58 ℓ/min; 2,43 ℓ/min and 4,44 ℓ/min). There was good agreement between the model and experimental results for the unsteady-state time period up to the attainment of an equilibrium internal cake diameter. It was found that the higher the cross-flow flow rate, the larger the equilibrium internal cake diameter. The model accurately predicted the equilibrium internal cake diameters for all four cross-flow flow rates. (In contrast there were contradictions between the model by Pearson and Sherwood (1988) and the experimental results of Fordham and Ladva (1989) for bentonite suspensions).

For optimized sludge dewatering using the tubular filter press, the unsteady-state time period up to the attainment of an equilibrium internal cake diameter is of prime concern. The model may therefore be used as a predictive tool for laminar cross-flow filtration for a tubular filter press.

However, it was found that although the measured internal cake diameter remained essentially constant during the steady-state time period and the model therefore predicted a constant filtrate flux (for the steady-state), there was a further slow decline in measured filtrate fluxes and a slow increase in measured average cake dry solids concentrations during this time period. Further investigations revealed that there were significant discrepancies between the measured cake permeabilities and porosities for the steady-state period and those for a dead-end cake (based on the same internal cake diameter), due to cake compaction. These findings are in agreement with those of other researchers (Baker et al., 1985; Rushton and Aziz, 1983), who found that the nature of a cake deposited under cross-flow conditions was different to one deposited under static conditions.

It was shown how the axial convection shear model may be "extended" by incorporating empirical equations to describe changes in cake porosity and permeability during the so-called steady-state period. The "extended" model accurately described the experimental results both during the unsteady- *and* steady-state time periods.

Since the experiments were done at a single filtration pressure and feed sludge solids concentration, it is recommended that the model be evaluated at other filtration pressures and feed sludge solids concentrations.

It is also recommended that more work be done on other types of sludges to further evaluate the performance and predictive capability of the model. The model should be "integrated" for long filter tubes.

Recently developed non-intrusive measuring techniques such as X-ray synchrotron absorbance (Bierck et al., 1988) and nuclear magnetic resonance imaging (Horsfield et al., 1989) could potentially be employed to test the validity of the model, by accurately measuring the radial solids concentration profiles in the vicinity of the cake/feed sludge interface.

Since the new axial convection shear model accurately predicted the variation of internal cake diameter with filtration time, it should be of great assistance in preventing or minimizing tube blockages in a tubular filter press which is operated in cross-flow filtration mode during the filtration cycle.

Finally, the results of all three investigations of this study (see sections 6.1, 6.2 and 6.3) provide a greater understanding of the cake deposition process (during both dead-end and cross-flow filtration modes) and the cake removal process for the tubular filter press. This should assist in finding solutions to the two main problems which were experienced on the prototype tubular filter press.

NOMENCLATURE

A	=	area of filter medium, (m^2)
A_c	=	area of cake in C-P cell, (m^2)
A_e	=	effective filtration area, (m^2)
A^c	=	constant in equation (5.35)
a	=	empirical constant in equation (3.57)
a_h	=	cross-sectional area of manifold header, (m)
B	=	empirical constant in set of equations (3.33)
B^c	=	constant in equation (5.36)
b	=	empirical constant in equation (3.57)
C	=	empirical constant in set of equations (3.34)
CL_r	=	fraction of cake dry solids which is lost due to the action of the rollers and hydraulic conveyance of flakes of cake, (-)
CL_s	=	fraction of cake dry solids which is lost due to the shear of the cleaning fluid, (-)
C_t	=	turning loss coefficient, (-)
c	=	mass of cake dry solids per unit volume of filtrate, (kg/m^3)
c_s	=	solids concentration of sludge (cake), (% m/m)
D	=	particle diffusion coefficient, (m^2/s)
D_h	=	internal diameter of manifold header, (m)
D_t	=	internal tube diameter, (m)
d_f	=	mean diameter of particle aggregates, (m)
d_{la}	=	internal diameter of lateral, (m)
d_1	=	internal diameter of filter medium, (m)
d_2	=	internal cake diameter, (m)
F	=	empirical constant in set of equations (3.32)
F_c	=	solids compressive force, (N)
F_s	=	accumulated frictional drag on particles, (N)

f = friction factor, (-)

f_c = correction factor for velocity, (-)

f_s = mass fraction of solids in cake, (-)

f_u = function of, (-)

g = constant of gravitational acceleration, (m/s^2)

H = height of interface between supernatant liquid and sediment, (m)

He = Hedstrom number as defined by equation (5.34), (-)

H_i = initial height of uniform suspension in cylinder, (m)

H_∞ = final equilibrium height of sediment, (m)

h = radial distance between mesh points in Euler numerical integration, (m)

h_B = height of reference point B in diagram I.1, (m)

h_1 = initial height difference between level of sludge in cylindrical sludge container and outlet of tube, (m)

h_2 = final height difference between level of sludge in cylindrical sludge container and outlet of tube, (m)

IJ = parameter in computer flowsheet in Appendix E, (-)

i = mesh point in Euler numerical integration, (-)

J = filtrate flux, (m/s)

J_s = mass of cake dry solids produced per unit medium area per hour, ($kg/m^2.h$)

j = effective filtration area factor defined by equation (3.4), (-)

K = local permeability of cake or sediment, (m^2)

KL = parameter in computer flowsheet in Appendix E, (-)

K_{av} = average permeability of cake, (m^2)

K_t = permeability of cake when $p_s \leq p_{st}$, (m^2)

K_o = permeability of cake when $p_s = 0$, (m^2)

K_{av}^{d} = average permeability of equivalent cake (with identical internal cake diameter) deposited under static or *dead-end* conditions, (m^2)

$K_{av}^{t_i}$ = average permeability of cake at threshold time, t_{id}, (m^2)

K_{av}^{∞} = average permeability of cake at infinity, (m^2)

k = surface roughness, (m)

k_o = coefficient of earth pressure at rest, (-)

L = thickness of filter cake (planar filtration), (m)

LJ = parameter in computer flowsheet in Appendix E, (-)

L_h = length of manifold header, (m)

L_{la} = length of lateral, (m)

L_t = length of tube, (m)

l = length of filter tube, (m)

m = parameter in computer flowsheet in Appendix E, (-)

ma = number of mesh points in thin element of cake with thickness, Δr, in computer flowsheet in Appendix E, (-)

N = number of tubes or laterals, (-)

NR = number of internal cake radii in computer flowsheet in Appendix E, (-)

N_{dep} = *net* volumetric rate of deposition of solids during time interval, Δt, (m^3/s)

n = empirical constant in set of equations (3.34) (compressibility coefficient)

n_1 = empirical constant in equation (3.37)

P = applied filtration pressure, (Pa)

PATMO = value for $(P - \Delta p_c - \Delta p_m)$ for Q(0) in computer flowsheet in Appendix E, (Pa)

PATM1 = value for $(P - \Delta p_c - \Delta p_m)$ for Q(1) in computer flowsheet in Appendix E, (Pa)

PATM2 = value for $(P - \Delta p_c - \Delta p_m)$ for Q(2) in computer flowsheet in Appendix E, (Pa)

PEF = factor as defined by equation (5.37), (-)

POF = factor as defined by equation (5.38), (-)

P_B = static pressure at point B in diagram I.1, (Pa)

P_C = air pressure applied to cylinder, (Pa)

P_h = pressure of fluid along header, (Pa)

P_{in} = inlet pressure for manifold system, (Pa)

P_o = empirical constant, (Pa)

P_L = liquid pressure, (Pa)

p_s = solids compressive pressure, (Pa)

p_{sf} = solids compressive pressure corresponding to porosity of feed sludge, (Pa)

p_{si} = solids compressive pressure below which permeability, porosity and specific filtration resistance of cake are assumed constant, (Pa)

p_{sm} = solids compressive pressure at filter medium, (Pa)

p_l = liquid pressure at medium, (Pa)

Δp_c = pressure drop across the cake, (Pa)

Δp_f = fractional liquid pressure drop across the cake as defined by equation (3.87), (-)

Δp_m = pressure drop across the medium, (Pa)

Δp_t = pressure difference between ends of tube, (Pa)

Q = overall volumetric flow rate of liquid (filtrate) per unit length of filter tube, ($m^3/m.s$)

Q_{cf} = flow rate of cleaning fluid, (m^3/s)

Q_f = overall volumetric flow rate of liquid (filtrate), (m^3/s)

Q_{fl} = flow rate of fluid, (m^3/s)

Q_{fs} = volumetric flow rate of feed sludge, (m^3/s)

Q_{in} = inlet flow rate for manifold system, (m^3/s)

Q_{sl} = volumetric flow rate of feed sludge to moving cake layer (due to radial convection) per unit length of tube, ($m^3/m.s$)

Q_1 = overall volumetric flow rate of liquid (filtrate) per unit length of filter tube at r_1, ($m^3/m.s$)

Q(0) = initial guess for Q for a particular cake thickness in interval halving technique in computer flowsheet in Appendix E, ($m^3/m.s$)

Q(1) = value of Q for PATM1 in interval halving technique in computer flowsheet in Appendix E, ($m^3/m.s$)

Q(2) = "mid-point" between Q(0) and Q(1) in interval halving technique in computer flowsheet in Appendix E, ($m^3/m.s$)

R = fraction of deposited cake dry solids recovered from the filter tubes, (-)

Re = Reynolds number as defined by equations (4.7), (4.23) and (5.33), (-)

R_c = distance between centre of centrifuge and bottom of centrifuge tube, (m)

R_m = resistance of medium, (m^{-1})

R_{sd} = volumetric rate of deposition of solids along whole filter tube in time interval, Δt, (m^3/s)

R_{sr} = volumetric rate of removal of solids in moving cake layer at outlet of filter tube during time interval, Δt, (m^3/s)

R_t = internal radius of tube, (m)

r = radius, (m)

r_c = distance from centre of centrifuge, (m)

r_i = distance from centre of centrifuge to surface of sediment, (m)

r_r = square root of the correlation coefficient, (-)

r_s = radius of shear plane, (m)

r_t = radius of centrifuge tube, (m)

r_1 = internal radius of filter medium, (m)

r_2 = internal radius of cake, (m)

r_3 = external radius of filter medium, (m)

r_4 = external radius of the cake for external cylindrical filtration, (m)

Δr = thickness of thin cake layer for Euler numerical integration, (m)

Δr_c = thickness of differential element of sediment, (m)

S = perimeter of header, (m)

t = time, (s)

t_c = time to remove cake during cake removal cycle, (s)

t_d = time to deposit cake, (s)

t_{fl} = threshold filtration time for filtrate flux as defined in section 5.5.2, (s)

t_{id} = threshold filtration time for internal cake diameter as defined in section 5.5.1, (s)

Δt = time interval, (s)

Δt_c = thickness of cake in C-P cell, (m)

u = superficial velocity of liquid (filtrate), (m/s)

u_{fl} = axial velocity of fluid at radius r, (m)

$\bar{u}_{fl}$ = average velocity of fluid, (m/s)

$\bar{u}_{fs}$ = average velocity of feed sludge, (m/s)

u_l = average pore or true velocity of liquid, (m/s)

u_l = apparent liquid velocity relative to solids, (m/s)

u_{ml} = local axial velocity in moving cake layer, (m/s)

u_s = average solids velocity, (m/s)

V = volume of filtrate per unit length of tube, (m^3/m)

V_c = volume of liquid in cake which is not recovered per cycle, (m^3)

V_{cl} = volume of cake per unit length of tube for cross-flow filtration, (m^3/m)

V_f = volume of liquid in feed sludge which is pumped to the plant per cycle, (m^3)

V_s = volume of liquid in sludge which is filtered during pressing cycle, (m^3)

V_{sl} = volume of sludge collected, (m^3)

V'_{cl} = volume of cake per unit length of tube for dead-end filtration, (m^3/m)

v = volume of filtrate per unit medium area, (m^3/m^2)

v_c = volume of cake per unit medium area, (m^3/m^2)

v_h = average axial velocity in header, (m/s)

v_o = initial settling velocity of surface of sediment, (m/s)

ΔV = increment in volume of filtrate per unit length of tube in time interval, Δt, (m^3/m)

ΔV_{sh} = volume of solids removed in moving cake layer at outlet of filter tube in time interval, Δt, (m^3)

ΔV_{sl} = volume of sludge filtered per unit length of tube in time interval, Δt, (m^3/m)

$\Delta V'_{cl}$ = increment in volume of cake per unit length of tube in time interval, Δt, (for dead-end filtration), (m^3/m)

W = total mass of dry solids in cake, (kg)

W_c = mass of cake dry solids deposited per cycle, (kg)

w = mass of cake dry solids per unit medium area deposited in thickness x from medium (planar filtration), (kg/m^2)

w_c = total mass of cake dry solids deposited per unit medium area, (kg/m^2)

w_r = mass of cake dry solids recovered per unit medium area, (kg/m^2)

w_s = mass of cake dry solids per unit medium area remaining after shear of cleaning fluid, (kg/m^2)

x = distance from medium for planar filtration, (m)

x_c = mass of dry solids per unit volume of liquid in cake which is not recovered, (kg/m^3)

x_f = mass of dry solids per unit volume of liquid in feed sludge which is pumped to the plant, (kg/m^3)

x_h = distance along header, (m)

x_s = average steady-state mass of dry solids per unit volume of liquid in sludge which is filtered during pressing cycle, (kg/m^3)

x_t = axial distance along filter tube, (m)

Δx_h = increment in distance along header, (m)

Δx_t = increment in axial distance along filter tube, (m)

y = distance measured from bottom of cylinder, (m)

y_m = distance from membrane or filter medium, (m)

z = mass fraction of moisture in cake, (-)

GREEK SYMBOLS

α = local specific filtration resistance of cake or sediment, (m/kg)

α_{av} = average specific filtration resistance of cake, (m/kg)

α_t = specific filtration resistance of cake when $p_s \leq p_{st}$, (m/kg)

α_o = specific filtration resistance of cake when $p_s = 0$, (m/kg)

β = empirical constant in set of equations (3.33)

β_1 = empirical constant in equation (3.36)

δ = empirical constant in set of equations (3.32)

δ_t = thickness of moving cake layer, (m)

δ_1 = empirical constant in equation (3.35)

ϵ = local porosity of cake or sediment, (-)

ϵ_{av} = average porosity of cake, (-)

ϵ_{cr} = convergence criterion, (-)

ϵ_f = porosity of feed sludge, (-)

ϵ_i = porosity of cake when $p_s \leq p_{si}$, (-)

ϵ_{if} = internal porosity of particle aggregates, (-)

ϵ_{in} = initial porosity of suspension, (-)

ϵ_L = lower limit of porosity for dilute region where free or hindered settling of particle aggregates occurs, (-)

ϵ_o = porosity of cake when $p_s = 0$, (-)

ϵ_{av}^{d} = average porosity of equivalent cake (with identical internal cake diameter) deposited under static or *dead-end* conditions, (-)

ϵ_{av}^{ti} = average porosity of cake at threshold time, t_{ti}, (-)

ϵ_{av}^{∞} = average porosity of cake at infinity, (-)

η = coefficient of rigidity, (Pa.s)

η_{fs} = coefficient of rigidity of feed sludge, (Pa.s)

η_l = coefficient of rigidity of cake in moving layer, (Pa.s)

θ = cylindrical co-ordinate in cylindrical filtration, (radians)

μ = viscosity, (Pa.s)

μ_e = effective viscosity, (Pa.s)

μ_f = viscosity of liquid (filtrate), (Pa.s)

μ_{fl} = viscosity of fluid, (Pa.s)

ρ_{fl} = density of fluid, (kg/m^3)

ρ_{fs} = density of feed sludge, (kg/m^3)

ρ_l = liquid density, (kg/m^3)

ρ_s = solids density, (kg/m^3)

ρ_w = average bulk density of wet cake, (kg/m^3)

τ = shear stress, (Pa)

τ_w = shear stress exerted by flowing fluid at internal wall of tube or cake, (Pa)

τ_o = yield stress, (Pa)

τ_{oc} = yield stress of cake, (Pa)

τ_{of} = yield stress of feed sludge, (Pa)

τ_{ol} = yield stress of cake in moving layer, (Pa)

ϕ = volume fraction of particles, (-)

ϕ_s = volume fraction of solids in feed sludge, (-)

ϕ_{sl} = volume fraction of solids in moving cake layer, (-)

ϕ_{ss} = volume fraction of solids in cake at shear plane, (-)

Ω = angular velocity, (rad/s)

ω = volume of dry solids per unit cross-sectional area of tube or cylinder measured from bottom of tube or cylinder, (m^3/m^2)

ω_c = volume of cake dry solids per unit medium area, (m^3/m^2)

ω_o = total volume of dry solids per unit cross-sectional area of tube or cylinder, (m^3/m^2)

ABBREVIATIONS

C-P = Compression-Permeability

FI = Magnetic Induction Flow Meter

NTU = Nephelometric Turbidity Units

PCV = Pressure Control Valve

PI = Pressure Indicator

PIC = Pressure Indicator and Controller

V = Valve

(% m/m) = dry solids concentration of sludge or cake expressed in mass %.

REFERENCES

ADAM, H. (1991). **Private Communication**, Delkor Technik (Pty) Ltd., Johannesburg, Republic of South Africa, August.

ARAGAKI, T., HIROAKA, S., YAMADA, I., MURASE, T., IRITANI, E. and SHIRATO, M. (1989). **Generalized Relation Between Liquid Pressure and Solid Compressive Pressure in Non-unidimensional Filter Cakes**, *Journal of Chemical Engineering of Japan*, **22**(4), pp. 358-363.

BAJURA, R.A. and JONES, E.H. (1976). **Flow Distribution Manifolds**, *Journal of Fluids Engineering. Transactions of the American Society of Mechanical Engineers*, **98**, pp. 654-660.

BAKER, R.J., FANE, A.G., FELL, C.J.D. and YOO, B.H. (1985). **Factors Affecting Flux in Crossflow Filtration**, *Desalination*, **53**, pp. 81-93.

BERGER, W., ERNST, H. and QUANG KHAI, V. (1990). **Abtragung von Filterkuchen durch strömende Flüssigkeit**, *Chemische Technik*, **42**(3), pp. 123-125.

BIERCK, B.R., WELLS, S.A. and DICK, R.I. (1988). **Compressible Cake Filtration : Monitoring Cake Formation and Shrinkage Using Synchrotron X-rays**, *Journal Water Pollution Control Federation*, 60(5), pp. 645-650.

BIRD, R.B., STEWART, W.E. and LIGHTFOOT, E.N. (1960). *Transport Phenomena*, John Wiley and Sons Incorporated, New York.

BLAKE, N.J., CUMMING, I.W. and STREAT, M. (1990). **Prediction of Steady State Crossflow Filtration Using a Force Balance Model**, Proceedings Vth World Filtration Congress, Volume 1, pp. 579-585, Nice, 5-8 June.

BLATT, W.F., DAVID, A., MICHAELS, A.S. and NELSON, L. (1970). **Solute Polarization and Cake Formation in Membrane Ultrafiltration : Causes, Consequences and Control Techniques**, in *Membrane Science and Technology*, edited by J.E. Flim, Plenum Press, New York.

BÖMKES, F.J. and WAGENER, W. (1990). **Investigations on Pressing of Filter Cakes Subjected to High Pressure of One and Two Dimensions**, Proceedings Vth World Filtration Congress, Nice, Volume 2, pp. 191-196, Nice, 5-8 June.

BOWEN, R.L. (1961). **Scale-up for Non-Newtonian Fluid Flow, Part 6 : Best Methods for Obtaining Flow Data**, *Chemical Engineering*, pp. 119-122, 21 August.

BRODKEY, R.S. (1967). *The Phenomena of Fluid Motions*, Addison-Wesley Publishing Company, Reading, Massachusetts.

BROWN, A. (1979). **The Tube Press**, *Filtration and Separation*, pp. 468-474, September/October.

BURDEN, R.L., FAIRES, J.D. and REYNOLDS, A.C. (1981). *Numerical Analysis*, 2nd Edition, Prindle, Weber and Schmidt, Boston, Massachusetts.

CARMAN, P.C. (1938). **Fundamental Principles of Industrial Filtration**, *Transactions. Institution of Chemical Engineers*, **16**, pp. 168-188.

COULSON, J.M. and RICHARDSON, J.F. (1977). *Chemical Engineering*, Volume **1**, 3rd Edition, Pergamon Press, Oxford.

D'ARCY, H.P.G. (1856). *Les Fointaines publiques de la Ville de Dijon*, Dalmont, Paris.

DATTA, A.B. and MAJUMDAR, A.K. (1980). **Flow Distribution in Parallel and Reverse Flow Manifolds**, *International Journal of Heat and Fluid Flow*, **2**(4), pp. 253-262.

DAVIS, R.H. and BIRDSELL, S.A. (1987). **Hydrodynamic Model and Experiments for Cross-flow Microfiltration**, *Chemical Engineering Communications*, **49**, pp. 217-234.

DAVIS, R.H. and LEIGHTON, D.T. (1987). **Shear-Induced Transport of a Particle Layer Along a Porous Wall**, *Chemical Engineering Science*, **42**(2), pp. 275-281.

DOWNING, A.L. and SQUIRES, R.C. (1986). **Cross-flow Filtration**, British Patent, WO 86/05413.

ECKSTEIN, E.C., BAILEY, D.G. and SHAPIRO, A.H. (1977). **Self-diffusion of Particles in Shear Flow of a Suspension**, *Journal of Fluid Mechanics*, **79**, pp. 191-208.

FANE, A.G. (1984). **Ultrafiltration of Suspensions**, *Journal of Membrane Science*, **20**, pp. 249-259.

FISCHER, E. (1987). **Untersuchungen zum Trennprozess bei der Querstromfiltration**, *Fortschritt-Berichte, VDI Reihe* **3**(139), VDI-Verlag, Düsseldorf.

FORDHAM, E.J. and LADVA, H.K.J. (1989). **Cross-flow Filtration of Bentonite Suspensions**, Schlumberger Cambridge Research Institute, Copy of paper which was submitted to *Physicochemical Hydrodynamics*.

GREEN, G. and BELFORT, G. (1980). **Fouling of Ultrafiltration Membranes : Lateral Migration and the Particle Trajectory Model**, *Desalination*, **35**, pp. 129-147.

HANKS, R.W. and PRATT, D.R. (1967). **On the Flow of Bingham Plastic Slurries in Pipes and Between Parallel Plates**, *Society of Petroleum Engineers. American Institute of Mining, Metallurgical, and Petroleum Engineers Journal*, pp. 341-346, December.

HENRY, J.D., LUI, A.P. and KUO, C.H. (1976). **A Dual Functional Solid Liquid Separation Process Based on Filtration and Settling**, *Journal of the American Institution of Chemical Engineers*, **22**(3), pp. 433-441.

HOOGLAND, M.R., FELL, C.J.D., FANE, A.G. and JONES, D.A.R. (1990). **The Optimum Design of Crossflow Filtration Elements for Mineral Slurry Processing**, Proceedings Vth World Filtration Congress, Volume **1**, pp. 604-610, Nice, 5-8 June.

HORSFIELD, M.A., FORDHAM, E.J., HALL, C. and HALL, L.D. (1989). **^{1}H NMR Imaging Studies of Filtration in Colloidal Suspensions**, *Journal of Magnetic Resonance*, **81**, pp. 593-596.

HUNT, J.W. (1987). **Mathematical Modelling of Cross-flow Microfiltration**, MScEng Thesis, Department of Chemical Engineering, University of Natal, Republic of South Africa.

HUNT, J.W., BROUCKAERT, C.J., RAAL, J.D., TREFFRY-GOATLEY, K. and BUCKLEY, C.A. (1987). **The Unsteady-state Modelling of Cross-flow Microfiltration**, *Desalination*, **64**, pp. 431-442.

LEIGHTON, D. and ACRIVOS, A. (1986). **Viscous Resuspension**, *Chemical Engineering Science*, **41**(6), pp. 1377-1384.

LEONARD, E.F. and VASSILIEFF, C.S. (1984). **The Deposition of Rejected Matter in Membrane Separation Processes**, *Chemical Engineering Communications*, **30**, pp. 209-217.

LEU, W.F. (1981). **Cake Filtration**, Ph.D. Thesis, Department of Chemical Engineering, University of Houston.

MASSEY, B.S. (1979). *Mechanics of Fluids*, 4th Edition, van Nostrand Reinhold Company, New York.

MICHAELS, A.S. and BOLGER, J.C. (1962). **Settling Rates and Sediment Volumes of Flocculated Kaolin Suspensions**, *Industrial and Engineering Chemistry. Fundamentals*, 1(1), pp. 24-33.

MILLER, D.S. (1978). **Internal Flow Systems**, *BHRA Fluid Engineering, Series 5*, British Hydromechanics Research Association (BHRA).

MURASE, T., HAYASHI, N., SUZUKI, H. and SHIRATO, M. (1985). **Two-dimensional Expression on a Cylindrical Filter Element**, *International Chemical Engineering*, **25**(1), pp. 130-137.

MURASE, T., IWATA, M., ADACHI, T., GMACHOWSKI, L. and SHIRATO, M. (1989). **An Evaluation of Compression-Permeability Characteristics in the Intermediate Concentration Range by Use of Centrifugal and Constant-rate Compression Techniques**, *Journal of Chemical Engineering of Japan*, **22**(4), pp. 378-384.

NUIJENS, P.G.J.M. (1983). **A Discrete Model for the Flow Distribution in Manifolds**, Report CENG-467, Council for Scientific and Industrial Research (CSIR), Pretoria, Republic of South Africa.

PEARSON, J.R.A. and SHERWOOD, J.D. (1988). **Continuum Modelling of Cross-flow Filtration**, *Physicochemical Hydrodynamics*, **10**(5/6), pp. 647-661.

PERRY, R.H. and CHILTON, C.H. (1973). *Chemical Engineers' Handbook*, 5th Edition, McGraw Hill Kogakusha Ltd., Tokyo.

PILLAY, V.L. (1991). **Modelling of Turbulent Cross-flow Microfiltration of Particulate Suspensions**, Ph.D. thesis to be submitted, Department of Chemical Engineering, University of Natal, Republic of South Africa.

PILLAY, V.L., BROUCKAERT, C.J., BUCKLEY, C.A. and RAAL, J.D. (1989). **Predicted Performance Profiles Along a Long-tube Cross-flow Microfiltration System**, *Desalination*, **71**(3), pp. 247-264.

PORTER, M.C. (1972). **Concentration Polarization with Membrane Ultrafiltration**, *Industrial and Engineering Chemistry. Process Design and Development*, **11**(3), pp. 234-248.

RAUDKIVI, A.J. (1967). *Loose Boundary Hydraulics*, Pergamon Press, New York.

RAUTENBACH, R. and SCHOCK, G. (1988). **Ultrafiltration of Macromolecular Solutions and Cross-flow Microfiltration of Colloidal Suspensions. A Contribution to Permeate Flux Calculations**, *Journal of Membrane Science*, **36**, pp. 231-242.

RENCKEN, G.E. (1989). **Flow Distribution in Parallel and Reverse Cross-flow Microfiltration Manifold Systems**, Report to the Steering Committee for Water Research Commission Project No. 238, Design Criteria for Cross-flow Microfiltration.

RENCKEN, G.E. (1990). **Report on Measured Flow Distributions in a Tubular Filter Press Manifold System and the Flux Profile Down a Single Filter Tube**, Report to the Steering Committee for Water Research Commission Project No. 238, Design Criteria for Cross-flow Microfiltration.

RENCKEN, G.E., TREFFRY-GOATLEY, K. and BUCKLEY, C.A. (1990). **Operation and Theory of the Tubular Filter Press**, Proceedings Vth World Filtration Congress, Volume 2, pp. 197-204, Nice, 5-8 June.

RICHARDSON, J.F. and ZAKI, W.N. (1954). **Sedimentation and Fluidisation : Part I**, *Transactions. Institution of Chemical Engineers*, **32**(1), pp. 35-53.

ROMERO, C.A. and DAVIS, R.H. (1988). **Global Model of Crossflow Microfiltration Based on Hydrodynamic Particle Diffusion**, *Journal of Membrane Science*, **39**(2), pp. 157-185.

ROMERO, C.A. and DAVIS, R.H. (1990). **Transient Model of Crossflow Microfiltration**, *Chemical Engineering Science*, **45**(1), pp. 13-25.

ROWE, P.W. and BORDEN, L. (1966). **A New Consolidation Cell**, *Geotechnique*, **16**(2), pp. 162-170.

RUSHTON, A. and ARAB, M.A.A. (1989). **Internal Pressure Variations During the Filtration and Dewatering of Thick Cakes**, *Filtration and Separation*, pp. 181-186, May/June.

RUSHTON, A. and AZIZ, R. (1983). **Cross-flow Microfiltration of Slurries**, Extended Abstracts of International Membrane Technology Conference, p. 172, Sydney, Australia, November.

RUSHTON, A., HOSSEINI, M. and RUSHTON, Alan. (1979). **Shear Effects in Cake Formation Mechanisms,** *Filtration and Separation*, pp. 456-459, September/October.

RUTH, B.F. (1935). **Studies in Filtration III - Derivation of General Filtration Equations,** *Industrial and Engineering Chemistry*, **27**(6), pp. 708-723.

SHERMAN, J. (1949). Internal Report, Research and Development Centre, The Babcock and Wilcox Company.

SHIRATO, M. and ARAGAKI, T. (1969). **The Relations Between Hydraulic and Compressive Pressures in Non-unidimensional Filter Cakes,** *Kagaku Kogaku*, **33**(2), pp. 205-207.

SHIRATO, M. and KOBAYASHI, K. (1967). **Studies in Non-unidimensional Filtration ; Filtration on Cylindrical, Spherical and Square Surfaces,** Memoirs of the Faculty of Engineering, Nagoya University, **19**(2), pp. 280-292, November.

SHIRATO, M., KOBAYASHI, K. and TANIMURA, M. (1973). **Analysis of Constant Pressure Filtration of Compressible Cakes on Cylindrical Surface,** *Kagaku Kogaku*, **37**(1), pp. 76-82.

SHIRATO, M., MURASE, T., HIRATE, H. and MUIRA, M. (1966). **Studies in Non-unidimensional Filtration, Definition of Effective Filtration Area Factor,** Kagaku Kogaku, **4**(1), pp. 194-198.

SHIRATO, M., MURASE, T., IRITANI, E. and HAYASHI, N. (1983). **Cake Filtration - A Technique for Evaluating Compression-Permeability Data at Low Compressive Pressure,** *Filtration and Separation*, pp. 404-406, September/October.

SHIRATO, M., MURASE, T. and KOBAYASHI, K. (1968). **The Method of Calculation for Non-unidimensional Filtration,** *Filtration and Separation*, pp. 219-224, May/June.

SHIRATO, M., SAMBUICHI, M., KATO, H. and ARAGAKI, T. (1969). **Internal Flow Mechanism in Filter Cakes,** *Journal of the American Institution of Chemical Engineers*, **15**(3), pp. 405-409.

THOMAS, D.G. (1960). **Heat and Momentum Transport Characteristics of Non-Newtonian Aqueous Thorium Oxide Suspensions,** *Journal of the American Institution of Chemical Engineers*, 6(4), pp. 631-639.

TILLER, F.M. and COOPER, H. (1962). **The Role of Porosity in Filtration Part V : Porosity Variation in Filter Cakes,** *Journal of the American Institution of Chemical Engineers*, **8**(4), pp. 445-449.

TILLER, F.M. and GREEN, T.C. (1973). **Role of Porosity in Filtration IX : Skin Effect with Highly Compressible Materials,** *Journal of the American Institution of Chemical Engineers*, **19**(6), pp. 1266-1269.

TILLER, F.M. and LEU, W.F. (1980). **Basic Data Fitting in Filtration,** *Journal of the Chinese Institute of Chemical Engineers*, **11**, pp. 61-70.

TILLER, F.M. and LU, W.M. (1972). **The Role of Porosity in Filtration VIII : Cake Nonuniformity in Compression-Permeability Cells,** *Journal of the American Institution of Chemical Engineers*, **18**(3), pp. 569-572.

TILLER, F.M. and YEH, C.S. (1985). **The Role of Porosity in Filtration Part X : Deposition of Compressible Cakes on External Radial Surfaces,** *Journal of the American Institution of Chemical Engineers*, **31**(8), pp. 1241-1248.

TILLER, F.M., YEH, C.S., CHEN, W. and TSAI, C.D. (1986). **Generalized Approach to Mathematical Solution of Solid-Liquid Separation Problems,** Proceedings World Congress III of Chemical Engineering, Volume 3, pp. 126-129, Tokyo.

TREFFRY-GOATLEY, K. (1991). **Private Communication,** Explochem Water Treatment (Pty) Ltd., Durban, Republic of South Africa, July.

TREFFRY-GOATLEY, K. and BUCKLEY, C.A. (1987). **Dewatering Slurries,** South African Patent No. 87/0553, assigned to the Water Research Commission.

WASP, E.J., KENNY, J.P. and GANDHI, R.L. (1979). *Solid-liquid Flow Slurry Pipeline Transportation*, Gulf Publishing Company, Book Division, Houston.

WEAST, R.C. (1984). *Handbook of Chemistry and Physics*, 65th Edition, CRC Press Incorporated, Florida.

WHITLOW, R. (1983). *Basic Soil Mechanics*, Longman Incorporated, New York.

YEH, S.H. (1985). **Cake Deliquoring and Radial Filtration,** Ph.D. Thesis, Department of Chemical Engineering, University of Houston.

YELSHIN, A. and TILLER, F.M. (1989). **Optimising Candle Filters for Incompressible Cakes,** *Filtration and Separation*, pp. 436-437, November/December.

ZYDNEY, A.L. and COLTON, C.K. (1986). **A Concentration Polarization Model for the Filtrate Flux in Cross-flow Microfiltration of Particulate Suspensions,** *Chemical Engineering Communications*, **47**, pp. 1-21.

APPENDIX A
RESULTS OF COMPRESSION-PERMEABILITY CELL EXPERIMENTS

A.1 RESULTS OF C-P CELL TEST A.1

Date : 1/2/1990
Diameter of C-P cell : 105,5 mm
Area of C-P cell : 8,7417 x 10^{-3} m^2
Head of filtrate : 1,298 m
Temperature of filtrate : 27,0 °C
Mass of wet C-P cell cake : 33,53 g
Mass of dry C-P cell cake : 14,11 g
Average dry solids concentration of cake : 42,08 % m/m
Calculated final cake thickness : 2,908 mm

Pressure (kPa)	Time after pressure change (min)	Permeate volume (m^3 x 10^6)	Time (s)	Dial gauge reading (m x 10^3)	Cake Thickness (m x 10^3)	Permeability (m^2 x 10^{16})	Porosity (-)
10	60	0,5	13,46	8,929	7,330	20,897	0,908
20	40	0,5	37,28	7,542	5,943	6,117	0,886
30	40	0,5	61,57	6,939	5,340	3,328	0,873
40	40	0,5	80,00	6,699	5,100	2,446	0,867
50	40	0,5	98,04	6,282	4,683	1,833	0,856
100	180	0,5	178,04	5,340	3,741	0,806	0,819
150	60	0,5	222,62	5,182	3,583	0,618	0,811
200	185	0,5	355,26	4,789	3,190	0,345	0,788
250	110	0,5	474,86	4,650	3,051	0,247	0,779
300	60	0,5	503,43	4,507	2,908	0,222	0,768

CALCULATION OF FINAL CAKE THICKNESS

$$\text{Volume of solids in final cake} = \frac{33.53 \times 0.4208 \times 10^{-3}}{2380.1} \; m^3$$

$$= 5.928 \times 10^{-6} m^3$$

$$\text{Volume of liquid in final cake} = \frac{33.53 \times (1 - 0.4208) \times 10^{-3}}{996.54}$$

($\rho_l = 996.54\ kg/m^3$ at 27°C : Perry, 1973)

$$= 1.949 \times 10^{-5} \; m^3$$

$$\therefore \text{Total volume of final cake} = 2.542 \times 10^{-5} \; m^3$$

$$\text{Thickness of final cake} = \frac{2.542 \times 10^{-5}}{\frac{\pi}{4} \times (0.1055)^2}$$

$$= 2.908 \times 10^{-3} \; m$$

A.2 RESULTS OF C-P CELL TEST A.2

Date : 31/8/1990
Diameter of C-P cell : 105,5 mm
Area of C-P cell : 8,7417 x 10^{-3} m^2
Head of filtrate : 1,298 m
Temperature of filtrate : 18,5 °C
Mass of wet C-P cell cake : 41,2721 g
Mass of dry C-P cell cake : 17,3598 g
Average dry solids concentration of cake : 42,06 % m/m
Calculated final cake thickness : 3,574 mm

Pressure (kPa)	Time after pressure change (min)	Permeate volume (m^3 x 10^6)	Time (s)	Dial gauge reading (m x 10^3)	Cake Thickness (m x 10^3)	Permeability (m^2 x 10^{16})	Porosity (-)
20	150	0,3	25,22	12,415	8,289	9,226	0,899
40	75	0,3	56,38	10,825	6,699	3,335	0,876
60	75	0,3	84,70	10,110	5,984	1,983	0,861
80	90	0,3	109,52	9,765	5,639	1,445	0,852
100	90	0,1	45,80	9,398	5,272	1,077	0,842
150	90	0,1	68,72	8,762	4,636	0,631	0,820
200	90	0,1	87,77	8,425	4,299	0,458	0,806
250	90	0,1	108,90	8,135	4,009	0,344	0,792
300	90	0,1	123,92	7,945	3,819	0,288	0,782
400	90	0,1	197,00	7,700	3,574	0,170	0,767

APPENDIX B
RESULTS OF SETTLING EXPERIMENTS

B.1 RESULTS OF THE SETTLING TEST B.1 TO DETERMINE POROSITY AT LOW p_s

Date of start of test : 14/3/1990
Temperature of sludge : between 21,0 °C and 23,5 °C
Initial concentration of sludge : 59,3 g/ℓ

Initial height, H_i (m)	Height of supernatant liquid/sediment interface, H (m)
Date	Date
14/3/1990	31/3/1990
1,500	0,846
1,205	0,667
0,902	0,522
0,615	0,355
0,293	0,186
0,205	0,136
0,105	0,075
0,050	0,035

Solids compressive pressure, p_s, may be calculated from equation (3.56) :

$$p_s = (\rho_s - \rho_l) g \omega_o \qquad (3.56)$$

The values of ω_o and p_s, for the various initial sludge heights in the cylinders for test B.1, are given in Table B.1.

TABLE B.1
Values of ω_o and p_s for the Various Initial Sludge Heights in the Cylinders (Test B.1)

Initial sludge height in cylinder, H_i (m)	ω_o (m x 10^{-2})	p_s (Pa)
1,500	3,737	506,82
1,205	3,002	407,15
0,902	2,247	304,77
0,615	1,532	207,80
0,293	0,730	99,00
0,205	0,511	69,27
0,105	0,262	35,48
0,050	0,125	16,89

B.2 RESULTS OF THE SETTLING TEST B.2 TO DETERMINE POROSITY AT LOW p_s

Date of start of test : 17/4/1990
Temperature of sludge : between 21,5 °C and 23,5 °C
Initial concentration of sludge : 61,7 g/ℓ

Initial height, H_i (m)	Height of supernatant liquid/sediment interface, H (m)		
Date	Date	Date	Date
17/4/1990	20/4/1990	26/4/1990	7/5/1990
1,495	0,936	0,898	0,888
1,203	0,730	0,726	0,726
0,839	0,507	0,499	0,495
0,7	0,370	0,360	0,360
0,296	0,202	0,194	0,194
0,210	0,145	0,138	0,138
0,106	0,077	0,074	0,074
0,049	0,039	0,038	0,038

The values of ω_o and p_s, for the various initial sludge heights in the cylinders for test B.2, are given in Table B.2.

TABLE B.2
Values of ω_o and p_s for the Various Initial Sludge Heights in the Cylinders (Test B.2)

Initial sludge height in cylinder, H_i (m)	ω_o (m x 10^{-2})	p_s (Pa)
1,495	3,876	525,58
1,203	3,119	422,92
0,839	2,175	294,95
0,597	1,548	209,88
0,296	0,767	104,06
0,210	0,544	73,83
0,106	0,275	37,27
0,049	0,127	17,23

B.3 RESULTS OF SETTLING TESTS TO DETERMINE PERMEABILITY AND SPECIFIC FILTRATION RESISTANCE AT LOW p_s

Settling tests were done at initial heights of 0,159 m; 0,239 m; 0,318 m and 0,397 m for initial dry solids concentrations of 9,9 g/ℓ ; 21,3 g/ℓ ; 32,5 g/ℓ ; 33,2 g/ℓ ; 48,0 g/ℓ ; 59,5 g/ℓ ; 67,6 g/ℓ ; 76,0 g/ℓ and 90,8 g/ℓ. The cylinders used were 1 ℓ polypropylene measuring cylinders.

The temperature during the tests varied between 20,5 °C and 23,0 °C.

As an example, the results of the tests for an initial solids concentration of 76,0 g/ℓ are shown in Table B.3.

TABLE B.3
Results of Settling Test for an Initial Solids Concentration of 76,0 g/ℓ

Time (min)	Height of interface in cylinder 1, H (m x 10^3)	Height of interface in cylinder 2, H (m x 10^3)	Height of interface in cylinder 3, H (m x 10^3)	Height of interface in cylinder 4, H (m x 10^3)
0	159,0	239,0	318,0	397,0
60	157,0	237,0	316,0	397,0
120	155,0	236,0	314,0	397,0
180	155,0	235,0	314,0	397,0
240	155,0	235,0	313,0	395,0
327	154,0	233,0	312,0	393,0
392	153,0	232,0	310,5	392,0
452	152,0	231,0	309,5	391,0
512	150,5	230,5	309,0	389,5
572	150,0	230,0	307,5	389,0
632	150,0	229,0	307,0	388,5
692	149,5	227,5	306,0	387,0
812	147,0	227,0	305,5	385,0
882	147,0	226,5	303,0	385,0
1 232	143,0	221,0	298,0	381,0
1 352	142,5	219,0	297,5	378,0
1 442	141,0	218,0	296,0	376,5
1 547	141,0	217,0	296,0	375,0
1 622	139,5	216,0	294,0	374,5
1 682	139,5	216,0	294,0	374,0
1 802	138,5	214,5	292,0	372,5
1 922	137,5	213,0	290,5	370,5
2 042	136,5	212,0	290,0	369,0
2 162	136,5	211,0	288,0	368,5
2 262	135,0	211,0	286,0	366,0
2 359	134,5	209,0	286,0	365,0
2 437	134,0	208,5	285,0	363,5
2 612	134,0	207,0	282,0	361,0
2 792	134,0	206,5	281,5	360,5
2 922	133,0	204,0	278,0	357,5
3 092	132,0	203,0	277,5	356,5
3 212	131,5	201,0	277,0	355,5

TABLE B.3 (cont.)
Results of Settling Test for an Initial Solids Concentration of 76,0 g/ℓ

Time (min)	Height of interface in cylinder 1, H (m x 10^3)	Height of interface in cylinder 2, H (m x 10^3)	Height of interface in cylinder 3, H (m x 10^3)	Height of interface in cylinder 4, H (m x 10^3)
3 332	131,5	201,0	276,0	354,0
3 482	131,0	199,5	274,5	353,0
3 632	131,0	199,0	274,0	351,0
3 782	131,0	199,0	272,5	349,5
3 902	131,0	198,5	272,0	348,0
4 022	131,0	198,5	271,0	347,5
4 112	131,0	197,0	270,0	346,5
4 232	131,0	196,0	268,5	345,5
4 352	129,0	196,0	268,5	344,5
4 412	129,0	195,5	267,5	343,5
4 682	129,0	195,0	266,5	341,0
4 832	128,5	195,0	264,5	339,5
5 012	128,5	194,5	263,0	338,0
5 132	128,5	194,0	263,0	337,5
5 252	128,5	193,0	262,5	335,5
5 372	128,5	191,0	262,5	335,5
5 492	127,0	191,0	260,0	333,5
5 612	127,0	191,0	260,0	333,0
5 732	127,0	191,0	259,0	332,0
5 852	127,0	191,0	258,5	331,5
6 032	127,0	191,0	258,5	330,5
6 212	127,0	191,0	258,0	329,5
6 332	127,0	191,0	258,0	328,5
12 812	127,0	187,0	250,5	313,5

A plot of (H/H_i) versus (t/H_i) for the four cylinders and the results shown in Table B.3 is shown in Figure B.1. As discussed in section 3.3.7.3 and as found by Shirato et al. (1983) the curves for the various initial heights all converge to a single straight line as time $t \rightarrow 0$. The gradient of this line gives the initial settling velocity of the surface of the sediment, v_o. The initial settling velocity for a sludge of solids concentration of 76,0 g/ℓ was determined from the gradient of the line shown in Figure B.1 and found to be 2,214 x 10^{-7} m/s.

The initial settling velocities, v_o, for the initial solids concentrations which were investigated, are shown in Table B.4.

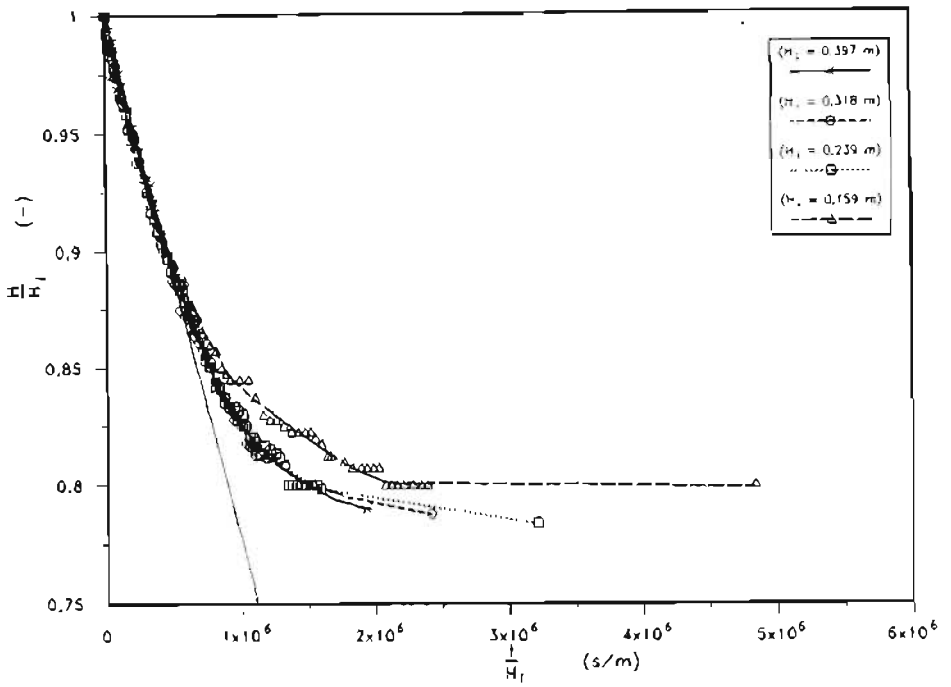

FIGURE B.1 : Graph of $\left(\frac{H}{H_i}\right)$ versus $\left(\frac{t}{H_i}\right)$ for Sludge with Initial Solids Concentration of 76 g/ℓ

TABLE B.4
The Variation of Initial Settling Velocity, v_o, with Initial Solids Concentration

Initial solids concentration (g/ℓ)	Initial porosity, ϵ_m (-)	v_o (m/s x 10^6)
9,9	0,9958	329,36
21,3	0,9911	48,56
32,5	0,9863	3,16
33,2	0,9861	3,53
48,0	0,9798	2,78
59,5	0,9750	0,869
67,6	0,9716	0,557
76,0	0,9681	0,221
90,8	0,9619	0,0436

A graph of $v_o^{(1/4.65)}$ versus ϵ_{in} is shown in Figure B.2. The porosity ranges for the three settling regimes described in section 3.3.7.3 are shown in the graph. The straight line represents equation (3.60) which is the modified Richardson and Zaki equation (Michaels and Bolger, 1962).

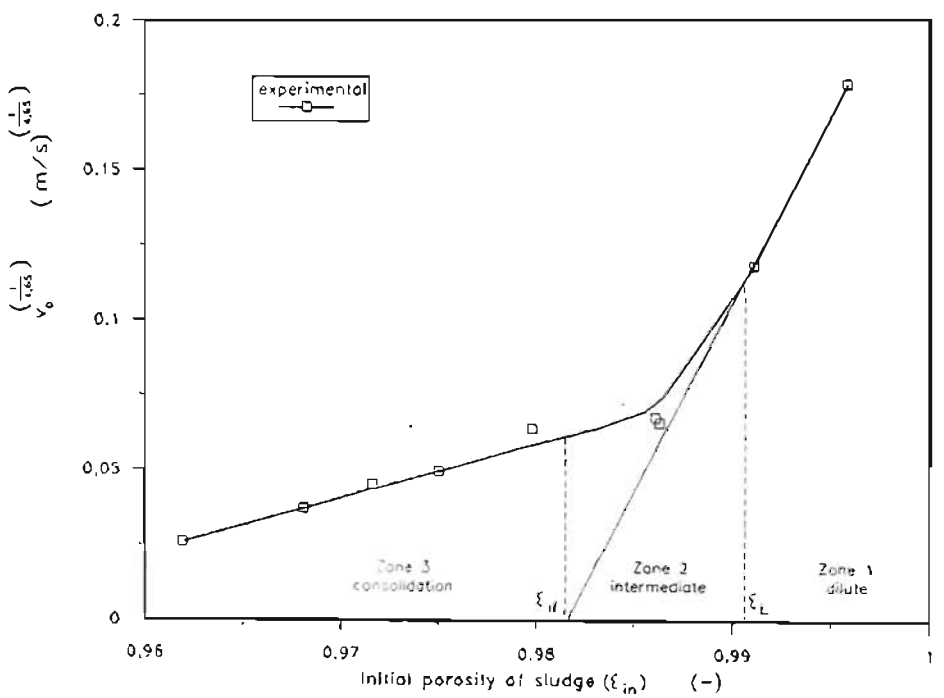

FIGURE B.2 : Graph of $v_o^{(\frac{1}{4.65})}$ versus Initial Porosity of Sludge (ϵ_{in}) for Settling Tests

The estimates for the porosity ranges of the three settling regimes from Figure B.2 are as follows :

Dilute region :

$$\epsilon_{in} > 0.991 \qquad \therefore \epsilon_L = 0.991$$

Intermediate region :

$$0.982 < \epsilon_{in} < 0.991 \qquad \therefore \epsilon_{if} = 0.982$$

Consolidation region :

$$\epsilon_{in} < 0.982$$

From equation (3.66)

$$K = \frac{v_o \mu_f}{(\rho_s - \rho_f)(1 - \epsilon_{in})g} \qquad (3.66)$$

ϵ_{in} for an initial solids concentration of 76,0 g/ℓ is 0,9681.

$$(\mu_l = 9.55 \times 10^{-4}\ Pa.s\ at\ 22°C;\ Weast, 1984)$$
$$(\rho_l = 997.8\ kg/m^3\ at\ 22°C;\ Perry, 1973)$$

$$\therefore\ K = \frac{(2.214 \times 10^{-7})(9.55 \times 10^{-4})}{(2380.1 - 997.8)(1 - 0.9681)9.81}$$

$$= 4.888 \times 10^{-13}\ m^2$$

In section 3.5.2.1, it was shown that the variation of porosity with p_s at low p_s for the sludge could be determined from the following equation :

$$(1 - \epsilon) = 0.0299\, p_s^{0.0782}$$

The solids compressive pressure corresponding to $\epsilon = 0.9681$ is therefore :

$$p_s = \left[\frac{(1 - 0.9681)}{0.0299}\right]^{\frac{1}{0.0782}}$$

$$= 2.316\ Pa$$

The variation of permeability with p_s in the higher concentration region, where settling occurs because of consolidation, is shown in Table B.5.

TABLE B.5
The Variation of Permeability with p_s

ϵ_{in} (-)	p_s (Pa)	K (m^2 x 10^{12})
0,9798	0,00650	9,708
0,9750	0,101	2,448
0,9716	0,518	1,382
0,9681	2,316	0,488
0,9619	22,554	0,0805

APPENDIX C
RESULTS OF CENTRIFUGE EXPERIMENTS

C.1 RESULTS OF THE CENTRIFUGE TEST C.1 TO DETERMINE POROSITY IN THE INTERMEDIATE SOLIDS COMPRESSIVE PRESSURE RANGE

Date : 17/8/1990
Temperature of sludge : 25,0 °C
Initial solids concentration of sludge : 4,49 % m/m
Inner diameter of jars : 40 mm
Height of jars : 93 mm
Distance from centre of arms to bottom of jars (R_c) : 158 mm
Average mass of sludge in jar : 115,24 g
Average ω_o : 1,730 x 10^{-3} m

Speed of centrifuge (r.p.m.)	Angular velocity, Ω (rad/s)	Height of interface in jar 1, $(R_c - r_i)$ (m x 10^3)	Height of interface in jar 2, $(R_c - r_i)$ (m x 10^3)	Height of interface in jar 3, $(R_c - r_i)$ (m x 10^3)	Height of interface in jar 4, $(R_c - r_i)$ (m x 10^3)	Average height of interfaces, $(R_c - r_i)$ (m x 10^3)
500	52,36	35,0	34,0	36,0	35,0	35,0
1 000	104,72	24,0	24,0	24,0	24,0	24,0
2 000	209,44	19,0	19,0	20,0	18,0	19,0
3 000	314,16	18,0	17,0	17,0	19,0	18,0
4 000	418,88	15,0	15,0	15,0	15,0	15,0

The average values of $(R_c - r_i)$ were used in the subsequent analysis.

The solids compressive pressure, p_s, may be calculated from equation (3.72) :

$$p_s(R_c) = (\rho_s - \rho_l)\,\Omega^2 \left(\frac{R_c + r_i}{2}\right)\omega_o \qquad (3.72)$$

The values of $\left(\frac{R_c + r_i}{2}\right)$ and p_s for test C.1 are shown in Table C.1.

TABLE C.1

Values of $\left(\frac{R_c - r_i}{2}\right)$ and p_s for the Various Angular Velocities, Ω

(Test C.1)

Ω (rad/s)	$\left(\frac{R_c - r_i}{2}\right)$ (m x 10^3)	p_s (Pa)
52,36	140,5	919,60
104,72	146,0	3 822,39
209,44	148,5	15 551,27
314,16	149,0	35 108,41
418,88	150,5	63 043,29

C.2 RESULTS OF THE CENTRIGUGE TEST C.2 TO DETERMINE POROSITY IN THE INTERMEDIATE SOLIDS COMPRESSIVE PRESSURE RANGE

Date : 1/11/1990
Temperature of sludge : 25,0 °C
Initial solids concentration of sludge : 7,13 % m/m
Inner diameter of jars : 50 mm
Height of jars : 100 mm
Distance from centre of arms to bottom of jars (R_c) : 174 mm
Average mass of sludge in jar : 178,48 g
Average ω_o : 2,723 x 10^{-3} m

Speed of centrifuge (r.p.m.)	Angular velocity, Ω (rad/s)	Height of interface in jar 1, $(R_c - r_1)$ (m x 10^3)	Height of interface in jar 2, $(R_c - r_1)$ (m x 10^3)	Average height of interfaces, $(R_c - r_1)$ (m x 10^3)
1 000	104,72	35,0	34,0	34,5
1 400	146,61	30,5	30,5	30,5
1 800	188,50	28,0	27,0	27,5
2 200	230,38	25,5	25,5	25,5
2 600	272,27	23,5	23,5	23,5

The values of $\left(\frac{R_c - r_1}{2}\right)$ and p_s for test C.2 are shown in Table C.2.

TABLE C.2

Values of $\left(\frac{R_c - r_1}{2}\right)$ and p_s for the Various Angular Velocities, Ω (Test C.2)

Ω (rad/s)	$\left(\frac{R_c - r_1}{2}\right)$ (m x 10^3)	p_s (Pa)
104,72	156,8	6 452,27
146,61	158,8	12 807,81
188,50	160,3	21 372,15
230,38	161,3	32 125,53
272,27	162,3	45 147,80

APPENDIX D
RESULTS OF CONSTANT PRESSURE FILTRATION EXPERIMENTS

D.1 RESULTS OF INTERNAL CYLINDRICAL FILTRATION EXPERIMENTS AT P = 100 kPa

Experiment D.1.1

Date : 5/10/1990
Temperature of filtrate : 20,0 °C
Feed solids concentration : 49,44 g/ℓ
Filtration time : 5 minutes

Pressure (kPa)	Time (min)	Mass of filtrate (g)
	0,0	0,0
101	0,5	118,4
101	1,0	164,8
100	1,5	198,7
101	2,0	227,9
101	2,5	254,8
101	3,0	277,7
101	3,5	298,1
101	4,0	318,3
102	4,5	336,8
102	5,0	354,7

Total mass of wet cake = 167,52 g.
Average dry solids concentration of cake = 16,64 % m/m.
Measured internal cake diameter = not measured, cake broken.
Calculated internal cake diameter = 15,89 mm.

SAMPLE CALCULATION FOR INTERNAL CAKE DIAMETER

Internal diameter of tube = 26,25 mm.

Mass of wet cake = 167,52 g.

Average cake dry solids concentration = 16,64 % m/m.

$$\textit{Volume of solids in cake} = \frac{167.52 \times 0.1664 \times 10^{-3}}{2380.1}$$

$$= 1.171 \times 10^{-5} \ m^3$$

$$\textit{Volume of liquid in cake} = \frac{167.52 \times (1 - 0.1664) \times 10^{-3}}{998.23}$$

$$= 1.399 \times 10^{-4} \ m^3$$

$$\textit{Volume of cake} = 1.171 \times 10^{-5} + 1.399 \times 10^{-4} \ m^3$$

$$= 1.516 \times 10^{-4} \ m^3$$

Length of tube = 0,442 m.

$$\textit{Volume of cake} = \pi (r_1^2 - r_2^2) \times 0.442 \ m^3$$

$$\therefore \quad \pi (r_1^2 - r_2^2) \times 0.442 = 1.516 \times 10^{-4}$$

$$\therefore \quad r_2 = \sqrt{r_1^2 - \frac{1.516 \times 10^{-4}}{0.442 \times \pi}}$$

$$= \sqrt{(13.125 \times 10^{-3})^2 - \frac{1.516 \times 10^{-4}}{0.442 \times \pi}}$$

$$= 7.943 \times 10^{-3} \ m$$

Internal cake diameter, d_i = 15,89 mm.

Experiment D.1.2

Date : 5/10/1990
Temperature of filtrate : 20,0 °C
Feed solids concentration : 49,44 g/ℓ
Filtration time : 10 minutes

Pressure (kPa)	Time (min)	Mass of filtrate (g)
	0,0	0,0
101	0,5	124,4
101	1,0	175,8
101	1,5	215,9
101	2,0	248,8
101	2,5	277,7
101	3,0	303,8
101	3,5	326,9
101	4,0	349,3
101	4,5	369,0
101	5,0	388,3
102	5,5	405,1
100	6,0	422,6
99	6,5	438,9
98	7,0	453,0
100	7,5	468,0
100	8,0	482,9
100	8,5	496,6
100	9,0	509,5
100	9,5	522,7
100	10,0	535,6

Total mass of wet cake = 201,49 g.
Average dry solids concentration of cake = 17,68 % m/m.
Measured internal cake diameter = not measured, cake broken.
Calculated internal cake diameter = 12,97 mm.

Experiment D.1.3

Date : 5/10/1990
Temperature of filtrate : 20,3 °C
Feed solids concentration : 49,44 g/ℓ
Filtration time : 15 minutes

Pressure (kPa)	Time (min)	Mass of filtrate (g)
	0,0	0,0
100	0,5	118,7
99	1,0	169,7
101	1,5	207,8
100	2,0	239,8
100	2,5	267,9
101	3,0	292,9
101	3,5	316,3
101	4,0	336,8
101	4,5	356,3
101	5,0	375,8
101	5,5	392,8
101	6,0	409,3
101	6,5	424,8
101	7,0	439,8
101	7,5	454,5
101	8,0	468,7
101	8,5	481,7
101	9,0	494,9
101	9,5	507,6
100	10,0	519,9
100	10,5	531,8
100	11,0	542,9
101	11,5	554,2
101	12,0	565,0
101	12,5	575,9
101	13,0	585,9
101	13,5	596,3
101	14,0	606,1
101	14,5	615,8
101	15,0	625,4

Total mass of wet cake = 218,63 g.
Average dry solids concentration of cake = 18,91 % m/m.
Measured internal cake diameter = not measured, cake broken.
Calculated internal cake diameter = 11,33 mm.

Experiment D.1.4

Date : 5/10/1990
Temperature of filtrate : 20,5 °C
Feed solids concentration : 49,44 g/ℓ
Filtrate time : 20 minutes

Pressure (kPa)	Time (min)	Mass of filtrate (g)
	0,0	0,0
101	0,5	121,8
101	1,0	174,5
101	1,5	215,8
101	2,0	247,8
100	2,5	276,4
100	3,0	301,8
100	3,5	325,3
100	4,0	347,3
100	4,5	367,4
100	5,0	385,9
100	5,5	403,6
100	6,0	420,6
101	6,5	436,9
100	7,0	452,5
100	7,5	467,3
100	8,0	481,7
100	8,5	495,4
100	9,0	508,5
100	9,5	521,7
99	10,0	533,9
98	10,5	546,4
100	11,0	558,0
100	11,5	569,3
101	12,0	580,7
101	12,5	591,8
101	13,0	602,4
100	13,5	613,1
100	14,0	623,3
100	14,5	633,5
100	15,0	643,0

Experiment D.1.4 (cont.)

Pressure (kPa)	Time (min)	Mass of filtrate (g)
100	15,5	652,8
100	16,0	662,2
101	16,5	671,5
100	17,0	680,4
100	17,5	689,4
100	18,0	697,8
100	18,5	706,9
100	19,0	715,1
100	19,5	723,6
100	20,0	731,9

Total mass of wet cake = 246,66 g.
Average dry solids concentration of cake = 19,28 % m/m.
Measured internal cake diameter = 7,4 mm.
Calculated internal cake diameter = 7,61 mm.

Experiment D.1.5

Date : 5/10/1990
Temperature of filtrate : 21,0 °C
Feed solids concentration : 49,44 g/ℓ
Filtration time : 25 minutes

Pressure (kPa)	Time (min)	Mass of filtrate (g)
	0,0	0,0
102	0,5	124,8
100	1,0	176,8
101	1,5	216,6
100	2,0	248,6
100	2,5	276,7
101	3,0	302,4
100	3,5	325,6
100	4,0	347,8
100	4,5	367,5
100	5,0	385,9
100	5,5	403,9
100	6,0	420,7
100	6,5	437,5
100	7,0	452,5
100	7,5	467,3
100	8,0	481,8
100	8,5	495,2
100	9,0	508,8
100	9,5	521,8
100	10,0	533,7
100	10,5	546,2
100	11,0	557,6
101	11,5	569,2
99	12,0	580,3
100	12,5	591,0
100	13,0	601,8
100	13,5	612,3
100	14,0	622,3
100	14,5	632,3
100	15,0	642,2

Experiment D.1.5 (cont.)

Pressure (kPa)	Time (min)	Mass of filtrate (g)
101	15,5	651,6
100	16,0	660,8
100	16,5	670,1
100	17,0	679,0
100	17,5	689,9
100	18,0	696,6
100	18,5	705,1
100	19,0	713,5
100	19,5	721,7
100	20,0	730,1
100	20,5	738,2
100	21,0	745,8
100	21,5	753,8
100	22,0	761,4
100	22,5	768,8
100	23,0	776,3
100	23,5	783,6
100	24,0	790,7
100	24,5	798,0
100	25,0	804,9

Total mass of wet cake = 253,26 g.
Average dry solids concentration of cake = 20,34 % m/m.
Measured internal cake diameter = 6,1 mm.
Calculated internal cake diameter = 6,76 mm.

D.2 RESULTS OF INTERNAL CYLINDRICAL FILTRATION EXPERIMENTS AT P = 200 kPa

Experiment D.2.1

Date : 10/12/1990
Temperature of filtrate : 23,0 °C
Feed solids concentration : 48,99 g/ℓ
Filtration time : 5 minutes

Pressure (kPa)	Time (min)	Mass of filtrate (g)
	0,0	0,0
200	0,5	145,1
200	1,0	210,8
200	1,5	259,7
200	2,0	299,5
202	2,5	334,3
200	3,0	365,5
200	3,5	393,9
200	4,0	419,6
200	4,5	444,2
200	5,0	467,4

Total mass of wet cake = 163,14 g.
Average dry solids concentration of cake = 18,14 % m/m.
Measured internal cake diameter = not measured, cake broken.
Calculated internal cake diameter = 16,39 mm.

Experiment D.2.2

Date : 10/12/1990
Temperature of filtrate : 23,0 °C
Feed solids concentration : 48,99 g/ℓ
Filtration time : 10 minutes

Pressure (kPa)	Time (min)	Mass of filtrate (g)
	0,0	0,0
201	0,5	151,7
203	1,0	217,9
203	1,5	267,8
201	2,0	304,5
200	2,5	343,8
200	3,0	374,8
200	3,5	403,6
199	4,0	429,7
199	4,5	454,0
199	5,0	477,3
199	5,5	498,8
199	6,0	519,4
200	6,5	538,9
200	7,0	557,6
200	7,5	575,8
200	8,0	593,1
200	8,5	609,8
200	9,0	626,1
200	9,5	641,6
200	10,0	656,9

Total mass of wet cake = 209,85 g.
Average dry solids concentration of cake = 19,18 % m/m.
Measured internal cake diameter = 12,7 mm.
Calculated internal cake diameter = 12,32 mm.

Experiment D.2.3

Date : 11/12/1990
Temperature of filtrate : 21,5 °C
Feed solids concentration : 48,99 g/ℓ
Filtration time : 15 minutes

Pressure (kPa)	Time (min)	Mass of filtrate (g)
	0,0	0,0
201	0,5	143,8
201	1,0	205,6
201	1,5	252,9
201	2,0	291,4
201	2,5	325,5
201	3,0	355,5
200	3,5	382,8
200	4,0	408,3
199	4,5	431,9
198	5,0	453,9
200	5,5	475,3
200	6,0	494,8
200	6,5	514,3
199	7,0	532,4
199	7,5	550,3
199	8,0	567,2
199	8,5	583,4
199	9,0	599,6
200	9,5	614,9
200	10,0	629,8
200	10,5	644,2
200	11,0	658,6
200	11,5	672,2
200	12,0	685,5
200	12,5	698,6
200	13,0	711,6
200	13,5	723,9
200	14,0	736,2
199	14,5	747,9
199	15,0	759,4

Total mass of wet cake = 230,95 g.
Average dry solids concentration of cake = 20,22 % m/m.
Measured internal cake diameter = 11,5 mm.
Calculated internal cake diameter = 10,09 mm.

Experiment D.2.4

Date : 11/12/1990
Temperature of filtrate : 22,0 °C
Feed solids concentration : 48,99 g/ℓ
Filtration time : 20 minutes

Pressure (kPa)	Time (min)	Mass of filtrate (g)
	0,0	0,0
201	0,5	148,8
201	1,0	214,8
201	1,5	263,8
201	2,0	304,3
201	2,5	338,9
201	3,0	369,8
201	3,5	397,8
201	4,0	423,9
201	4,5	448,4
201	5,0	470,9
202	5,5	492,8
202	6,0	513,4
201	6,5	532,4
201	7,0	550,8
200	7,5	568,9
200	8,0	585,9
200	8,5	602,4
200	9,0	618,3
200	9,5	633,8
200	10,0	648,7
200	10,5	663,2
200	11,0	677,3
200	11,5	691,3
200	12,0	704,7
200	12,5	717,9
200	13,0	730,8
200	13,5	743,6
200	14,0	755,8
199	14,5	767,7
199	15,0	779,7

Experiment D.2.4 (cont.)

Pressure (kPa)	Time (min)	Mass of filtrate (g)
199	15,5	791,3
199	16,0	802,6
199	16,5	813,4
199	17,0	824,6
199	17,5	834,9
199	18,0	845,4
199	18,5	855,7
199	19,0	856,9
199	19,5	876,0
199	20,0	885,6

Total mass of wet cake = 250,82 g.
Average dry solids concentration of cake = 21,07 % m/m.
Measured internal cake diameter = 6,7 mm.
Calculated internal cake diameter = 7,40 mm.

Experiment D.2.5

Date : 11/12/1990
Temperature of filtrate : 22,0 °C
Feed solids concentration : 48,99 g/ℓ
Filtration time : 25 minutes

Pressure (kPa)	Time (min)	Mass of filtrate (g)
	0,0	0,0
200	0,5	151,9
200	1,0	215,7
200	1,5	265,5
200	2,0	305,3
200	2,5	340,5
200	3,0	370,8
200	3,5	399,4
200	4,0	424,5
200	4,5	449,8
200	5,0	472,4
200	5,5	494,4
200	6,0	514,6
199	6,5	534,1
199	7,0	552,7
201	7,5	570,4
201	8,0	587,9
200	8,5	604,8
200	9,0	620,6
200	9,5	636,3
200	10,0	651,5
200	10,5	666,3
200	11,0	680,2
200	11,5	694,4
200	12,0	707,6
200	12,5	720,8
200	13,0	733,6
200	13,5	746,4
200	14,0	758,6
200	14,5	770,9
200	15,0	782,6

Experiment D.2.5 (cont.)

Pressure (kPa)	Time (min)	Mass of filtrate (g)
200	15,5	793,8
200	16,0	805,3
200	16,5	816,7
200	17,0	827,5
200	17,5	838,3
200	18,0	848,7
200	18,5	859,0
200	19,0	869,2
200	19,5	879,5
202	20,0	889,3
202	20,5	898,9
201	21,0	908,7
202	21,5	918,2
201	22,0	927,4
202	22,5	936,7
201	23,0	945,5
201	23,5	954,7
201	24,0	963,5
201	24,5	971,8
201	25,0	980,4

Total mass of wet cake = 262,2 g.
Average dry solids concentration of cake = 22,21 % m/m.
Measured internal cake diameter = 6,3 mm.
Calculated internal cake diameter = 5,57 mm.

Experiment D.2.6

Date : 11/12/1990
Temperature of filtrate : 22,0 °C
Feed solids concentration : 48,99 g/ℓ
Filtration time : 30 minutes

Pressure (kPa)	Time (min)	Mass of filtrate (g)
	0,0	0,0
202	0,5	150,9
200	1,0	215,9
200	1,5	264,4
200	2,0	304,8
200	2,5	339,9
200	3,0	371,4
200	3,5	399,5
200	4,0	425,8
200	4,5	450,3
200	5,0	472,8
200	5,5	494,5
200	6,0	515,0
200	6,5	534,7
200	7,0	553,4
200	7,5	571,3
200	8,0	588,8
200	8,5	605,6
200	9,0	621,9
199	9,5	637,0
199	10,0	651,9
200	10,5	666,4
200	11,0	680,8
200	11,5	694,6
200	12,0	707,8
200	12,5	721,4
200	13,0	734,0
199	13,5	746,8
199	14,0	759,0
199	14,5	771,1
199	15,0	782,6

Experiment D.2.6 (cont.)

Pressure (kPa)	Time (min)	Mass of filtrate (g)
200	15,5	794,4
200	16,0	805,6
200	16,5	816,8
200	17,0	827,9
200	17,5	838,4
199	18,0	848,9
199	18,5	859,5
199	19,0	869,7
199	19,5	879,7
199	20,0	889,5
199	20,5	899,3
200	21,0	908,8
200	21,5	918,3
200	22,0	927,7
200	22,5	936,9
200	23,0	945,9
200	23,5	954,8
200	24,0	963,5
200	24,5	972,2
200	25,0	980,8
200	25,5	989,0
200	26,0	997,6
200	26,5	1 005,7
200	27,0	1 013,7
200	27,5	1 021,8
200	28,0	1 029,7
200	28,5	1 037,6
200	29,0	1 045,2
200	29,5	1 052,8
199	30,0	1 060,3

Total mass of wet cake = 271,48 g.
Average dry solids concentration of cake = 22,82 % m/m.
Measured internal cake diameter = 4,6 mm.
Calculated internal cake diameter = 3,24 mm.

D.3 RESULTS OF INTERNAL CYLINDRICAL FILTRATION EXPERIMENTS AT P = 300 kPa

Experiment D.3.1

Date : 25/10/1990
Temperature of filtrate : 19,8 °C
Feed solids concentration : 49,13 g/ℓ
Filtration time : 5 minutes

Pressure (kPa)	Time (min)	Mass of filtrate (g)
	0,0	0,0
301	0,5	145,8
301	1,0	208,9
301	1,5	255,9
301	2,0	293,7
301	2,5	327,9
301	3,0	358,6
301	3,5	385,4
301	4,0	410,8
302	4,5	434,9
301	5,0	457,6

Total mass of wet cake = 152,55 g.
Average dry solids concentration of cake = 19,69 % m/m.
Measured internal cake diameter = not measured, cake broken.
Calculated internal cake diameter = 17,31 mm.

Experiment D.3.2

Date : 25/10/1990
Temperature of filtrate : 20,0 °C
Feed solids concentration : 49,13 g/ℓ
Filtration time : 10 minutes

Pressure (kPa)	Time (min)	Mass of filtrate (g)
	0,0	0,0
301	0,5	153,9
301	1,0	219,6
301	1,5	268,9
301	2,0	309,6
301	2,5	343,7
301	3,0	376,4
301	3,5	405,0
301	4,0	429,8
301	4,5	454,8
301	5,0	477,9
301	5,5	499,5
301	6,0	520,8
301	6,5	540,5
301	7,0	558,9
301	7,5	577,3
301	8,0	594,8
302	8,5	611,6
301	9,0	627,9
300	9,5	643,9
300	10,0	659,2

Total mass of wet cake = 199,15 g.
Average dry solids concentration of cake = 20,38 % m/m.
Measured internal cake diameter = 13,6 mm.
Calculated internal cake diameter = 13,53 mm.

Experiment D.3.3

Date : 25/10/1990
Temperature of filtrate : 20,0 °C
Feed solids concentration : 49,13 g/ℓ
Filtration time : 15 minutes

Pressure (kPa)	Time (min)	Mass of filtrate (g)
		Not monitored

Total mass of wet cake = 229,82 g.
Average dry solids concentration of cake = 21,25 % m/m.
Measured internal cake diameter = 12,1 mm.
Calculated internal cake diameter = 10,42 mm.

Experiment D.3.4

Date : 23/10/1990
Temperature of filtrate : 20,2 °C
Feed solids concentration : 49,808 g/ℓ
Filtration time : 20 minutes

Pressure (kPa)	Time (min)	Mass of filtrate (g)
	0,0	0,0
301	0,5	162,6
301	1,0	228,9
301	1,5	277,6
301	2,0	316,5
301	2,5	351,6
301	3,0	382,8
301	3,5	410,9
301	4,0	437,5
301	4,5	462,1
301	5,0	484,9
301	5,5	507,3
301	6,0	527,9
301	6,5	548,4
301	7,0	566,4
301	7,5	584,4
301	8,0	601,8
300	8,5	618,8
300	9,0	634,9
300	9,5	650,9
300	10,0	666,5
300	10,5	681,1
300	11,0	695,7
300	11,5	709,7
300	12,0	723,6
300	12,5	736,9
300	13,0	750,1
300	13,5	762,9
300	14,0	775,5
300	14,5	787,8
300	15,0	800,0

Experiment D.3.4 (cont.)

Pressure (kPa)	Time (min)	Mass of filtrate (g)
300	15,5	811,7
300	16,0	823,4
300	16,5	834,9
300	17,0	845,9
300	17,5	856,9
300	18,0	867,8
300	18,5	878,6
300	19,0	888,8
300	19,5	899,1
300	20,0	909,4

Total mass of wet cake = 238,95 g.
Average dry solids concentration of cake = 22,63 % m/m.
Measured internal cake diameter = 9,3 mm.
Calculated internal cake diameter = 9,54 mm.

Experiment D.3.5

Date : 23/10/1990
Temperature of filtrate : 20,3 °C
Feed solids concentration : 49,808 g/ℓ
Filtration time : 20 minutes

Pressure (kPa)	Time (min)	Mass of filtrate (g)
	0,0	0,0
302	0,5	155,0
300	1,0	219,0
300	1,5	267,8
300	2,0	307,6
300	2,5	342,7
300	3,0	373,6
300	3,5	401,8
300	4,0	428,5
300	4,5	452,9
300	5,0	476,6
300	5,5	497,8
300	6,0	518,7
300	6,5	538,4
300	7,0	557,6
300	7,5	575,9
300	8,0	593,3
300	8,5	610,2
300	9,0	626,4
300	9,5	641,8
300	10,0	657,4
300	10,5	672,5
300	11,0	686,9
300	11,5	701,1
300	12,0	714,9
300	12,5	728,3
300	13,0	741,3
300	13,5	754,5
301	14,0	767,3
301	14,5	779,4
301	15,0	791,3

Experiment D.3.5 (cont.)

Pressure (kPa)	Time (min)	Mass of filtrate (g)
301	15,5	803,1
301	16,0	814,6
300	16,5	825,9
300	17,0	837,1
300	17,5	848,4
300	18,0	859,1
300	18,5	869,9
300	19,0	880,3
300	19,5	890,5
300	20,0	900,8

Total mass of wet cake = 242,12 g.
Average dry solids concentration of cake = 22,55 % m/m.
Measured internal cake diameter = 10,1 mm.
Calculated internal cake diameter = 9,10 mm.

Experiment D.3.6

Date : 23/10/1990
Temperature of filtrate : 20,4 °C
Feed solids concentration : 49,808 g/ℓ
Filtration time : 20 minutes

Pressure (kPa)	Time (min)	Mass of filtrate (g)
	0,0	0,0
301	0,5	151,2
301	1,0	217,4
301	1,5	266,5
301	2,0	306,8
301	2,5	342,6
301	3,0	373,3
301	3,5	401,9
301	4,0	428,6
301	4,5	452,9
301	5,0	476,4
301	5,5	498,6
301	6,0	519,7
301	6,5	539,5
301	7,0	557,6
301	7,5	575,9
301	8,0	593,4
301	8,5	610,8
301	9,0	626,8
301	9,5	642,8
301	10,0	658,5
301	10,5	673,3
301	11,0	687,6
301	11,5	701,9
301	12,0	715,9
301	12,5	729,9
301	13,0	742,6
300	13,5	755,6
300	14,0	768,4
300	14,5	781,3
300	15,0	792,8

Experiment D.3.6 (cont.)

Pressure (kPa)	Time (min)	Mass of filtrate (g)
300	15,5	804,8
300	16,0	816,3
301	16,5	827,9
301	17,0	838,9
301	17,5	849,9
301	18,0	860,9
301	18,5	871,5
301	19,0	881,9
301	19,5	892,6
301	20,0	902,5

Total mass of wet cake = 243,93 g.
Average dry solids concentration of cake = 21,94% m/m.
Measured internal cake diameter = 9,6 mm.
Calculated internal cake diameter = 8,71 mm.

Experiment D.3.7

Date : 25/10/1990
Temperature of filtrate : 20,0 °C
Feed solids concentration : 49,13 g/ℓ
Filtration time : 25 minutes

Pressure (kPa)	Time (min)	Mass of filtrate (g)
	0,0	0,0
300	0,5	155,9
300	1,0	219,6
300	1,5	268,9
300	2,0	308,5
300	2,5	343,6
300	3,0	374,7
301	3,5	403,5
300	4,0	429,5
301	4,5	454,5
300	5,0	476,9
300	5,5	498,8
300	6,0	519,4
300	6,5	539,4
300	7,0	558,2
300	7,5	576,0
300	8,0	593,7
300	8,5	611,3
300	9,0	627,3
300	9,5	643,1
300	10,0	658,4
300	10,5	673,5
300	11,0	687,8
300	11,5	701,9
300	12,0	715,9
300	12,5	729,4
300	13,0	742,4
300	13,5	755,7
300	14,0	768,1
300	14,5	780,4
300	15,0	792,6
300	15,5	804,9

Experiment D.3.7 (cont.)

Pressure (kPa)	Time (min)	Mass of filtrate (g)
300	16,0	816,4
300	16,5	827,7
300	17,0	839,0
300	17,5	850,3
300	18,0	860,9
300	18,5	871,8
300	19,0	882,3
300	19,5	892,7
300	20,0	902,8
300	20,5	912,6
300	21,0	922,3
300	21,5	932,3
300	22,0	942,0
300	22,5	951,5
300	23,0	960,9
300	23,5	970,3
300	24,0	979,2
300	24,5	988,3
300	25,0	997,0

Total mass of wet cake = 256,83 g.
Average dry solids concentration of cake = 23,00 % m/m.
Measured internal cake diameter = 7,5 mm.
Calculated internal cake diameter = 6,92 mm.

Experiment D.3.8

Date : 11/12/1990
Temperature of filtrate : 22,5 °C
Feed solids concentration : 48,99 g/ℓ
Filtration time : 30 minutes

Pressure (kPa)	Time (min)	Mass of filtrate (g)
	0,0	0,0
300	0,5	170,7
300	1,0	241,5
300	1,5	292,6
300	2,0	334,8
300	2,5	372,4
300	3,0	405,7
300	3,5	436,1
300	4,0	464,2
301	4,5	489,9
301	5,0	513,8
301	5,5	537,7
301	6,0	559,3
301	6,5	580,9
301	7,0	599,9
301	7,5	618,6
301	8,0	637,3
301	8,5	655,2
301	9,0	671,9
301	9,5	688,8
301	10,0	704,8
301	10,5	720,7
301	11,0	735,8
299	11,5	750,6
299	12,0	764,9
299	12,5	778,6
300	13,0	792,6
300	13,5	806,2
300	14,0	819,2
300	14,5	832,2
300	15,0	844,7

Experiment D.3.8 (cont.)

Pressure (kPa)	Time (min)	Mass of filtrate (g)
300	15,5	857,2
300	16,0	869,7
300	16,5	881,4
300	17,0	892,7
300	17,5	903,8
300	18,0	915,2
300	18,5	926,2
300	19,0	937,3
300	19,5	947,9
300	20,0	958,4
300	20,5	968,7
300	21,0	978,8
300	21,5	989,2
300	22,0	999,0
300	22,5	1 008,8
300	23,0	1 018,4
300	23,5	1 027,8
300	24,0	1 037,4
300	24,5	046,7
300	25,0	1 055,7
300	25,5	1 064,7
300	26,0	1 073,7
300	26,5	1 082,5
300	27,0	1 091,0
300	27,5	1 099,6
300	28,0	1 108,3
300	28,5	1 116,5
300	29,0	1 124,8
300	29,5	1 133,0
300	30,0	1 141,0

Total mass of wet cake = 273,15 g.
Average dry solids concentration of cake = 24,51 % m/m.
Measured internal cake diameter = 4,7 mm.
Calculated internal cake diameter = 3,75 mm.

D.4 RESULTS OF PLANAR FILTRATION EXPERIMENTS AT P =100 kPa

Experiment D.4.1

Date : 8/3/1991
Temperature of filtrate : 25,0 °C
Feed solids concentration : 50,17 g/ℓ
Filtration time : 5 minutes

Pressure (kPa)	Time (min)	Mass of filtrate (g)
	0,0	0,0
100	0,5	47,9
100	1,0	77,7
100	1,5	99,4
100	2,0	118,3
100	2,5	135,5
100	3,0	150,6
100	3,5	163,8
100	4,0	176,6
100	4,5	189,8
100	5,0	201,3

Total mass of wet cake = 116,24 g.
Average dry solids concentration of cake = 14,78 % m/m.
Calculated cake thickness = 6,46 mm.

SAMPLE CALCULATION FOR CAKE THICKNESS

Mass of wet cake = 116,24 g.

Average cake dry solids concentration = 14,78 % m/m

$$Volume\ of\ solids\ in\ cake = \frac{116.24 \times 0.1478 \times 10^{-3}}{2380.1}$$

$$= 7.218 \times 10^{-6}\ m^3$$

$$Volume\ of\ liquid\ in\ cake = \frac{116.24 \times (1 - 0.1478) \times 10^{-3}}{997.07}$$

$$= 9.935 \times 10^{-5}\ m^3$$

$$Volume\ of\ cake = 7.218 \times 10^{-6} + 9.935 \times 10^{-5}\ m^3$$

$$= 1.066 \times 10^{-4}\ m^3$$

$$Area\ of\ filter\ medium = \frac{\pi}{4}(0.145)^2$$

$$= 0.0165\ m^2$$

$$Thickness\ of\ filter\ cake = \frac{1.066 \times 10^{-4}}{0.0165}\ m$$

$$= 6.46 \times 10^{-3}\ m$$

$$= 6.46\ mm$$

Experiment D.4.2

Date : 8/3/1991
Temperature of filtrate : 25,0 °C
Feed solids concentration : 51,41 g/ℓ
Filtration time : 10 minutes

Pressure (kPa)	Time (min)	Mass of filtrate (g)
	0,0	0,0
100	0,5	60,4
100	1,0	90,5
100	1,5	113,6
100	2,0	132,6
100	2,5	148,5
100	3,0	164,1
100	3,5	177,4
100	4,0	190,1
100	4,5	202,6
100	5,0	214,4
100	5,5	225,5
100	6,0	235,6
100	6,5	245,7
100	7,0	255,3
100	7,5	266,5
100	8,0	273,3
100	8,5	281,1
100	9,0	290,2
100	9,5	298,5
100	10,0	305,8

Total mass of wet cake = 146,11 g.
Average dry solids concentration of cake = 15,99 % m/m.
Calculated cake thickness = 8,03 mm.

Experiment D.4.3

Date : 8/3/1991
Temperature of filtrate : 25,1 °C
Feed solids concentration : 50,51 g/ℓ
Filtration time : 15 minutes

Pressure (kPa)	Time (min)	Mass of filtrate (g)
	0,0	0,0
100	0,5	61,4
100	1,0	90,3
100	1,5	111,9
100	2,0	131,2
100	2,5	149,3
100	3,0	163,4
100	3,5	176,9
100	4,0	189,9
100	4,5	202,8
100	5,0	214,8
100	5,5	225,5
100	6,0	236,1
100	6,5	246,2
100	7,0	255,9
100	7,5	265,3
100	8,0	274,0
100	8,5	282,4
100	9,0	290,6
100	9,5	298,8
100	10,0	305,9

Experiment D.4.3 (cont.)

Pressure (kPa)	Time (min)	Mass of filtrate (g)
100	10,5	313,6
100	11,0	321,0
100	11,5	328,4
100	12,0	335,7
100	12,5	342,6
100	13,0	349,3
100	13,5	356,2
100	14,0	362,7
100	15,5	369,2
100	15,0	375,6

Total mass of wet cake = 167,55 g.
Average dry solids concentration of cake = 16,71 % m/m.
Calculated cake thickness = 9,16 mm.

Experiment D.4.4

Date : 8/3/1991
Temperature of filtrate : 25,3 °C
Feed solids concentration : 51,29 g/ℓ
Filtration time : 20 minutes

Pressure (kPa)	Time (min)	Mass of filtrate (g)
	0,0	0,0
100	0,5	61,6
100	1,0	90,4
100	1,5	112,3
100	2,0	131,0
100	2,5	147,0
100	3,0	162,3
100	3,5	175,0
100	4,0	187,4
100	4,5	199,4
100	5,0	210,3
100	5,5	219,9
100	6,0	231,1
100	6,5	241,6
100	7,0	251,2
100	7,5	260,4
100	8,0	268,8
100	8,5	277,1
100	9,0	284,3
100	9,5	293,4
100	10,0	302,2
100	10,5	311,3
100	11,0	318,3
100	11,5	325,9
100	12,0	333,4
100	12,5	340,7
100	13,0	347,7
100	13,5	354,7
100	14,0	361,5
100	14,5	368,2
100	15,0	374,7

Experiment D.4.4 (cont.)

Pressure (kPa)	Time (min)	Mass of filtrate (g)
100	15,5	381,1
100	16,0	387,2
100	16,5	393,5
100	17,0	399,6
100	17,5	405,5
100	18,0	411,6
100	18,5	417,4
100	19,0	423,1
100	19,5	429,0
100	20,0	434,0

Total mass of wet cake = 191,83 g.
Average dry solids concentration of cake = 16,86 % m/m.
Calculated cake thickness = 10,48 mm.

Experiment D.4.5

Date : 8/3/1991
Temperature of filtrate : 25,5 °C
Feed solids concentration : 50,62 g/ℓ
Filtration time : 25 minutes

Pressure (kPa)	Time (min)	Mass of filtrate (g)
	0,0	0,0
100	0,5	59,4
100	1,0	88,8
100	1,5	111,1
100	2,0	129,6
100	2,5	145,9
100	3,0	161,5
100	3,5	174,5
100	4,0	186,8
100	4,5	198,5
100	5,0	209,3
100	5,5	219,4
100	6,0	228,6
100	6,5	237,7
100	7,0	248,4
100	7,5	257,8
100	8,0	268,0
100	8,5	276,1
100	9,0	284,5
100	9,5	292,3
100	10,0	300,5
100	10,5	307,3
100	11,0	315,9
100	11,5	323,5
100	12,0	330,7
100	12,5	337,8
100	13,0	344,8
100	13,5	351,6
100	14,0	358,4
100	14,5	364,8
100	15,0	371,3

Experiment D.4.5 (cont.)

Pressure (kPa)	Time (min)	Mass of filtrate (g)
100	15,5	377,9
100	16,0	384,6
100	16,5	390,6
100	17,0	396,3
100	17,5	401,8
100	18,0	407,6
100	18,5	413,1
100	19,0	418,3
100	19,5	423,2
100	20,0	428,5
100	20,5	433,4
100	21,0	438,2
100	21,5	443,0
100	22,0	447,0
100	22,5	452,0
100	23,0	457,4
100	23,5	462,8
100	24,0	467,9
100	24,5	473,3
100	25,0	478,5

Total mass of wet cake = 204,37 g.
Average dry solids concentration of cake = 17,05 % m/m.
Calculated cake thickness = 11,15 mm.

Experiment D.4.6

Date : 8/3/1991
Temperature of filtrate : 25,8 °C
Feed solids concentration : 49,08 g/ℓ
Filtration time : 30 minutes

Pressure (kPa)	Time (min)	Mass of filtrate (g)
	0,0	0,0
100	0,5	61,0
100	1,0	91,4
100	1,5	112,0
100	2,0	133,4
100	2,5	151,3
100	3,0	167,0
100	3,5	181,2
100	4,0	194,3
100	4,5	206,7
100	5,0	218,9
100	5,5	230,1
100	6,0	240,8
100	6,5	251,0
100	7,0	260,9
100	7,5	270,1
100	8,0	279,4
100	8,5	288,0
100	9,0	296,8
100	9,5	305,2
100	10,0	313,0
100	10,5	320,5
100	11,0	328,3
100	11,5	335,6
100	12,0	343,2
100	12,5	350,3
100	13,0	357,3
100	13,5	364,1
100	14,0	370,6
100	14,5	377,0
100	15,0	383,2
100	15,5	389,0

Experiment D.4.6 (cont.)

Pressure (kPa)	Time (min)	Mass of filtrate (g)
100	16,0	395,1
100	16,5	400,8
100	17,0	406,5
100	17,5	411,8
100	18,0	417,3
100	18,5	422,5
100	19,0	427,4
100	19,5	432,7
100	20,0	437,5
100	20,5	442,5
100	21,0	447,0
100	21,5	451,6
100	22,0	456,2
100	22,5	460,3
100	23,0	465,2
100	23,5	469,3
100	24,0	473,3
100	24,5	477,8
100	25,0	482,0
100	25,5	485,9
100	26,0	489,9
100	26,5	493,9
100	27,0	497,6
100	27,5	501,5
100	28,0	505,4
100	28,5	510,0
100	29,0	515,2
100	29,5	520,2
100	30,0	524,9

Total mass of wet cake = 228,07 g.
Average dry solids concentration of cake = 16,78 % m/m.
Calculated cake thickness = 12,47 mm.

D.5 RESULTS OF PLANAR FILTRATION EXPERIMENTS AT P = 200 kPa

Experiment D.5.1

Date : 27/3/1991
Temperature of filtrate : 24,9 °C
Feed solids concentration : 54,18 g/ℓ
Filtration time : 5 minutes

Pressure (kPa)	Time (min)	Mass of filtrate (g)
	0,0	0,0
200	0,5	51,7
200	1,0	88,6
200	1,5	111,5
200	2,0	132,1
200	2,5	149,5
200	3,0	167,6
200	3,5	182,1
200	4,0	195,5
200	4,5	210,0
200	5,0	222,9

Total mass of wet cake = 123,62 g.
Average dry solids concentration of cake = 15,70 % m/m.
Calculated cake thickness = 6,80 mm.

Experiment D.5.2

Date : 27/3/1991
Temperature of filtrate : 25,0 °C
Feed solids concentration : 53,18 g/ℓ
Filtration time : 10 minutes

Pressure (kPa)	Time (min)	Mass of filtrate (g)
	0,0	0,0
200	0,5	58,7
200	1,0	90,2
200	1,5	116,7
200	2,0	137,7
200	2,5	155,3
200	3,0	171,9
200	3,5	187,4
200	4,0	200,9
200	4,5	213,5
200	5,0	225,9
200	5,5	237,8
200	6,0	249,2
200	6,5	260,2
200	7,0	270,5
200	7,5	280,5
200	8,0	289,6
200	8,5	299,2
200	9,0	308,5
200	9,5	317,7
200	10,0	325,6

Total mass of wet cake = 162,91 g.
Average dry solids concentration of cake = 16,97 % m/m.
Calculated cake thickness = 8,89 mm.

Experiment D.5.3

Date : 27/3/1991
Temperature of filtrate : 25,0 °C
Feed solids concentration : 52,19 g/ℓ
Filtration time : 15 minutes

Pressure (kPa)	Time (min)	Mass of filtrate (g)
	0,0	0,0
200	0,5	57,8
200	1,0	90,8
200	1,5	114,5
200	2,0	135,8
200	2,5	154,2
200	3,0	170,8
200	3,5	185,1
200	4,0	200,3
200	4,5	213,1
200	5,0	225,6
200	5,5	237,5
200	6,0	248,8
200	6,5	259,4
200	7,0	269,9
200	7,5	279,9
200	8,0	289,6
200	8,5	298,6
200	9,0	307,8
200	9,5	316,6
200	10,0	325,2

Experiment D.5.3 (cont.)

Pressure (kPa)	Time (min)	Mass of filtrate (g)
200	10,5	333,3
200	11,0	341,5
200	11,5	349,1
200	12,0	356,6
200	12,5	364,1
200	13,0	371,4
200	13,5	378,7
200	14,0	386,7
200	14,5	392,1
200	15,0	400,0

Total mass of wet cake = 186,32 g.
Average dry solids concentration of cake = 17,34 % m/m.
Calculated cake thickness = 10,15 mm.

Experiment D.5.4

Date : 27/3/1991
Temperature of filtrate : 25,0 °C
Feed solids concentration : 51,35 g/ℓ
Filtration time : 20 minutes

Pressure (kPa)	Time (min)	Mass of filtrate (g)
	0,0	0,0
200	0,5	60,3
200	1,0	94,3
200	1,5	119,5
200	2,0	138,1
200	2,5	157,6
200	3,0	174,2
200	3,5	188,1
200	4,0	202,5
200	4,5	215,3
200	5,0	227,8
200	5,5	239,9
200	6,0	251,5
200	6,5	262,3
200	7,0	272,5
200	7,5	282,3
200	8,0	292,2
200	8,5	301,7
200	9,0	310,7
200	9,5	319,7
200	10,0	327,7
200	10,5	336,7
200	11,0	344,3
200	11,5	352,2
200	12,0	359,6
200	12,5	367,8
200	13,0	375,9
200	13,5	382,7
200	14,0	390,2
200	14,5	397,2
200	15,0	403,9

Experiment D.5.4 (cont.)

Pressure (kPa)	Time (min)	Mass of filtrate (g)
200	15,5	410,1
200	16,0	418,1
200	16,5	424,1
200	17,0	430,6
200	17,5	437,1
200	18,0	443,4
200	18,5	449,6
200	19,0	455,7
200	19,5	461,8
200	20,0	467,7

Total mass of wet cake = 215,30 g.
Average dry solids concentration of cake = 17,45 % m/m.
Calculated cake thickness = 11,72 mm.

Experiment D.5.5

Date : 27/3/1991
Temperature of filtrate : 24,0 °C
Feed solids concentration : 54,73 g/ℓ
Filtration time : 25 minutes

Pressure (kPa)	Time (min)	Mass of filtrate (g)
	0,0	0,0
200	0,5	56,5
200	1,0	83,6
200	1,5	110,6
200	2,0	130,3
200	2,5	147,8
200	3,0	164,3
200	3,5	179,6
200	4,0	193,7
200	4,5	203,7
200	5,0	217,4
200	5,5	230,7
200	6,0	243,9
200	6,5	263,6
200	7,0	274,3
200	7,5	284,6
200	8,0	294,5
200	8,5	303,9
200	9,0	312,2
200	9,5	321,8
200	10,0	330,5
200	10,5	339,0
200	11,0	343,5
200	11,5	354,9
200	12,0	362,4
200	12,5	370,0
200	13,0	377,7
200	13,5	384,9
200	14,0	392,8
200	14,5	399,3
200	15,0	406,4

Experiment D.5.5 (cont.)

Pressure (kPa)	Time (min)	Mass of filtrate (g)
200	15,5	413,2
200	16,0	419,9
200	16,5	426,5
200	17,0	433,0
200	17,5	439,6
200	18,0	445,7
200	18,5	452,0
200	19,0	458,2
200	19,5	464,3
200	20,0	470,3
200	20,5	476,2
200	21,0	481,9
200	21,5	487,7
200	22,0	493,5
200	22,5	499,0
200	23,0	504,7
200	23,5	510,2
200	24,0	515,5
200	24,5	520,9
200	25,0	526,2

Total mass of wet cake = 245,03 g.
Average dry solids concentration of cake = 17,84 % m/m.
Calculated cake thickness = 13,30 mm.

Experiment D.5.6

Date : 27/3/1991
Temperature of filtrate : 24,0 °C
Feed solids concentration : 54,06 g/ℓ
Filtration time : 30 minutes

Pressure (kPa)	Time (min)	Mass of filtrate (g)
	0,0	0,0
200	0,5	59,6
200	1,0	91,9
200	1,5	117,6
200	2,0	138,2
200	2,5	156,6
200	3,0	173,4
200	3,5	189,2
200	4,0	203,3
200	4,5	216,9
200	5,0	229,5
200	5,5	240,7
200	6,0	252,5
200	6,5	263,5
200	7,0	274,2
200	7,5	284,6
200	8,0	294,3
200	8,5	303,3
200	9,0	312,6
200	9,5	321,6
200	10,0	330,3
200	10,5	338,6
200	11,0	346,4
200	11,5	354,4
200	12,0	362,2
200	12,5	370,1
200	13,0	377,5
200	13,5	384,5
200	14,0	392,4
200	14,5	399,6
200	15,0	406,5

Experiment D.5.6 (cont.)

Pressure (kPa)	Time (min)	Mass of filtrate (g)
200	15,5	413,3
200	16,0	420,1
200	16,5	426,7
200	17,0	433,2
200	17,5	439,8
200	18,0	446,2
200	18,5	452,5
200	19,0	458,7
200	19,5	464,7
200	20,0	470,6
200	20,5	476,6
200	21,0	482,5
200	21,5	488,2
200	22,0	493,9
200	22,5	499,6
200	23,0	505,4
200	23,5	510,7
200	24,0	516,0
200	24,5	521,5
200	25,0	526,8
200	25,5	532,3
200	26,0	537,4
200	26,5	542,5
200	27,0	547,7
200	27,5	552,9
200	28,0	558,0
200	28,5	562,7
200	29,0	567,8
200	29,5	572,6
200	30,0	577,5

Total mass of wet cake = 261,91 g.
Average dry solids concentration of cake = 18,20 % m/m.
Calculated cake thickness = 14,19 mm.

D.6 RESULTS OF PLANAR FILTRATION EXPERIMENTS AT P = 300 kPa

Experiment D.6.1

Date : 28/2/1991
Temperature of filtrate : 24,5 °C
Feed solids concentration : 50,04 g/ℓ
Filtration time : 5 minutes

Pressure (kPa)	Time (min)	Mass of filtrate (g)
	0,0	0,0
300	0,5	68,3
300	1,0	101,6
300	1,5	128,2
300	2,0	150,8
300	2,5	170,6
300	3,0	188,5
300	3,5	204,5
300	4,0	219,1
300	4,5	234,4
300	5,0	248,0

Total mass of wet cake = 122,60 g.
Average dry solids concentration of cake = 15,74 % m/m.
Calculated cake thickness = 6,74 mm.

Experiment D.6.2

Date : 28/2/1991
Temperature of filtrate : 24,5 °C
Feed solids concentration : 51,01 g/ℓ
Filtration time : 10 minutes

Pressure (kPa)	Time (min)	Mass of filtrate (g)
	0,0	0,0
300	0,5	76,7
300	1,0	114,5
300	1,5	139,8
300	2,0	162,9
300	2,5	182,3
300	3,0	201,3
300	3,5	217,4
300	4,0	233,7
300	4,5	247,9
300	5,0	261,7
300	5,5	274,4
300	6,0	286,5
300	6,5	298,7
300	7,0	310,0
300	7,5	321,3
300	8,0	332,0
300	8,5	342,4
300	9,0	352,4
300	9,5	362,0
300	10,0	371,2

Total mass of wet cake = 168,16 g.
Average dry solids concentration of cake = 16,64 % m/m.
Calculated cake thickness = 9,23 mm.

Experiment D.6.3

Date : 28/2/1991
Temperature of filtrate : 24,6 °C
Feed solids concentration : 51,42 g/ℓ
Filtration time : 15 minutes

Pressure (kPa)	Time (min)	Mass of filtrate (g)
	0,0	0,0
300	0,5	77,9
300	1,0	112,4
300	1,5	140,3
300	2,0	161,9
300	2,5	182,4
300	3,0	200,7
300	3,5	216,6
300	4,0	232,6
300	4,5	247,3
300	5,0	260,4
300	5,5	273,5
300	6,0	286,1
300	6,5	297,6
300	7,0	309,5
300	7,5	320,5
300	8,0	330,5
300	8,5	341,0
300	9,0	351,1
300	9,5	360,8
300	10,0	370,2

Experiment D.6.3 (cont.)

Pressure (kPa)	Time (min)	Mass of filtrate (g)
300	10,5	379,0
300	11,0	388,4
300	11,5	397,0
300	12,0	405,6
300	12,5	413,6
300	13,0	422,2
300	13,5	429,5
300	14,0	437,9
300	14,5	445,0
300	15,0	452,2

Total mass of wet cake = 186,91 g.
Average dry solids concentration of cake = 17,79 % m/m.
Calculated cake thickness = 10,15 mm.

Experiment D.6.4

Date : 28/2/1991
Temperature of filtrate : 25,0 °C
Feed solids concentration : 51,32 g/ℓ
Filtration time : 20 minutes

Pressure (kPa)	Time (min)	Mass of filtrate (g)
	0,0	0,0
300	0,5	70,2
300	1,0	107,9
300	1,5	135,6
300	2,0	158,9
300	2,5	179,0
300	3,0	197,7
300	3,5	214,7
300	4,0	230,5
300	4,5	244,5
300	5,0	258,7
300	5,5	271,9
300	6,0	284,5
300	6,5	296,5
300	7,0	307,8
300	7,5	318,7
300	8,0	325,9
300	8,5	340,7
300	9,0	350,2
300	9,5	360,0
300	10,0	368,6
300	10,5	378,4
300	11,0	387,3
300	11,5	396,3
300	12,0	404,8
300	12,5	413,0
300	13,0	421,6
300	13,5	428,9
300	14,0	437,6
300	14,5	444,7
300	15,0	452,3

Experiment D.6.4 (cont.)

Pressure (kPa)	Time (min)	Mass of filtrate (g)
300	15,5	459,9
300	16,0	467,2
300	16,5	474,5
300	17,0	481,6
300	17,5	488,8
300	18,0	495,7
300	18,5	502,5
300	19,0	509,2
300	19,5	515,9
300	20,0	522,4

Total mass of wet cake = 199,44 g.
Average dry solids concentration of cake = 18,21 % m/m.
Calculated cake thickness = 10,80 mm.

Experiment D.6.5

Date : 28/2/1991
Temperature of filtrate : 25,0 °C
Feed solids concentration : 50,10 g/ℓ
Filtration time : 25 minutes

Pressure (kPa)	Time (min)	Mass of filtrate (g)
	0,0	0,0
300	0,5	79,8
300	1,0	114,3
300	1,5	140,8
300	2,0	164,5
300	2,5	184,9
300	3,0	204,6
300	3,5	219,4
300	4,0	235,6
300	4,5	249,6
300	5,0	263,8
300	5,5	276,6
300	6,0	289,0
300	6,5	301,3
300	7,0	312,8
300	7,5	323,9
300	8,0	334,7
300	8,5	344,8
300	9,0	354,8
300	9,5	364,7
300	10,0	374,3
300	10,5	383,3
300	11,0	392,5
300	11,5	401,4
300	12,0	409,9
300	12,5	417,8
300	13,0	426,5
300	13,5	434,7
300	14,0	442,9
300	14,5	449,8
300	15,0	457,7

Experiment D.6.5 (cont.)

Pressure (kPa)	Time (min)	Mass of filtrate (g)
300	15,5	465,0
300	16,0	472,3
300	16,5	479,7
300	17,0	486,8
300	17,5	493,7
300	18,0	500,8
300	18,5	507,7
300	19,0	514,4
300	19,5	521,0
300	20,0	527,5
300	20,5	534,0
300	21,0	540,2
300	21,5	546,7
300	22,0	553,0
300	22,5	559,1
300	23,0	565,2
300	23,5	571,2
300	24,0	577,2
300	24,5	583,1
300	25,0	588,8

Total mass of wet cake = 233,05 g.
Average dry solids concentration of cake = 18,04 % m/m.
Calculated cake thickness = 12,64 mm.

Experiment D.6.6

Date : 28/2/1991
Temperature of filtrate : 25,0 °C
Feed solids concentration : 50,68 g/ℓ
Filtration time : 30 minutes

Pressure (kPa)	Time (min)	Mass of filtrate (g)
	0,0	0,0
300	0,5	78,3
300	1,0	114,8
300	1,5	142,9
300	2,0	166,7
300	2,5	186,6
300	3,0	205,4
300	3,5	222,2
300	4,0	237,4
300	4,5	252,5
300	5,0	266,1
300	5,5	279,5
300	6,0	291,4
300	6,5	304,0
300	7,0	315,5
300	7,5	326,8
300	8,0	337,1
300	8,5	347,7
300	9,0	357,8
300	9,5	367,9
300	10,0	377,4
300	10,5	386,6
300	11,0	395,5
300	11,5	404,6
300	12,0	413,4
300	12,5	421,7
300	13,0	430,0
300	13,5	437,9
300	14,0	445,9
300	14,5	453,3
300	15,0	460,9

Experiment D.6.6 (cont.)

Pressure (kPa)	Time (min)	Mass of filtrate (g)
300	15,5	469,0
300	16,0	475,8
300	16,5	483,3
300	17,0	490,5
300	17,5	497,0
300	18,0	504,6
300	18,5	511,5
300	19,0	518,3
300	19,5	524,9
300	20,0	531,5
300	20,5	538,1
300	21,0	544,4
300	21,5	550,1
300	22,0	557,1
300	22,5	563,3
300	23,0	569,5
300	23,5	575,4
300	24,0	581,8
300	24,5	587,4
300	25,0	593,2
300	25,5	599,0
300	26,0	604,6
300	26,5	610,4
300	27,0	616,1
300	27,5	621,6
300	28,0	627,0
300	28,5	632,6
300	29,0	637,9
300	29,5	643,4
300	30,0	648,7

Total mass of wet cake = 243,38 g.
Average dry solids concentration of cake = 18,63 % m/m.
Calculated cake thickness = 13,15 mm.

APPENDIX E
FLOWSHEET FOR INTERNAL CYLINDRICAL FILTRATION FORTRAN COMPUTER PROGRAM

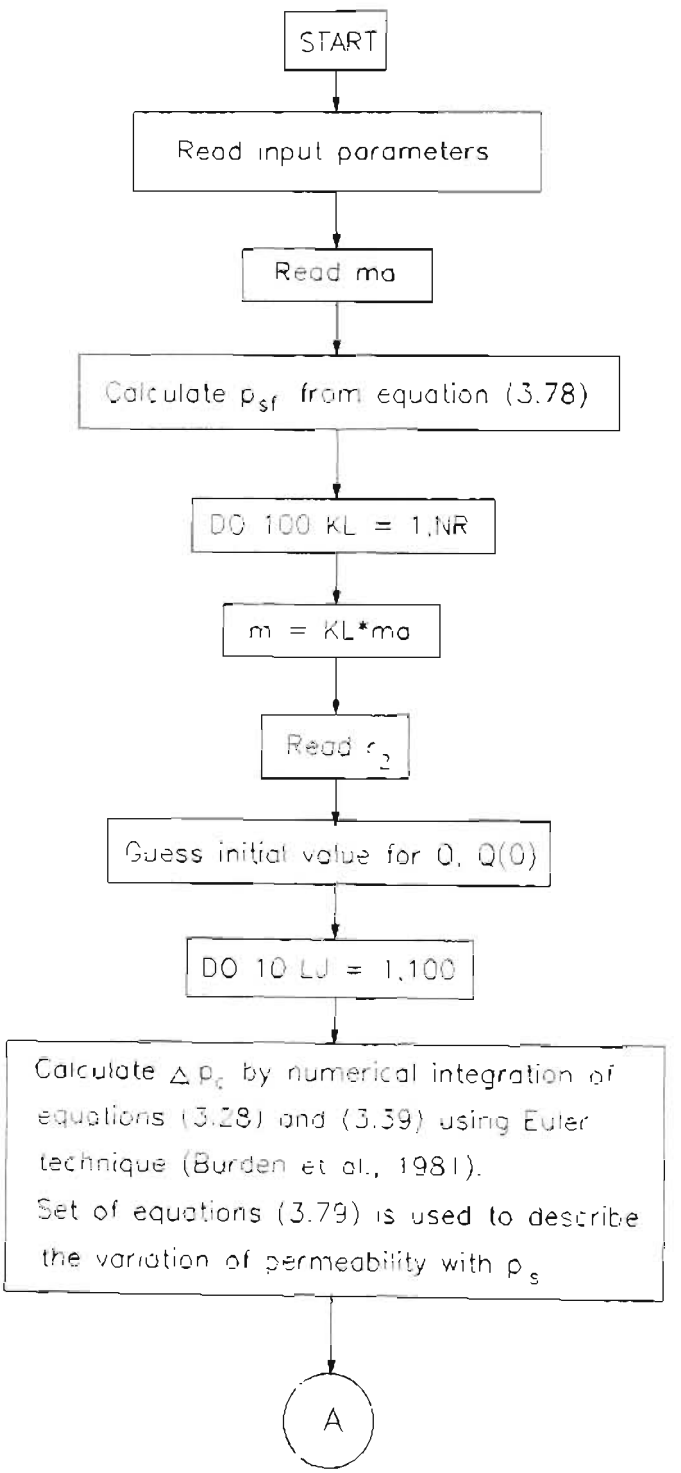

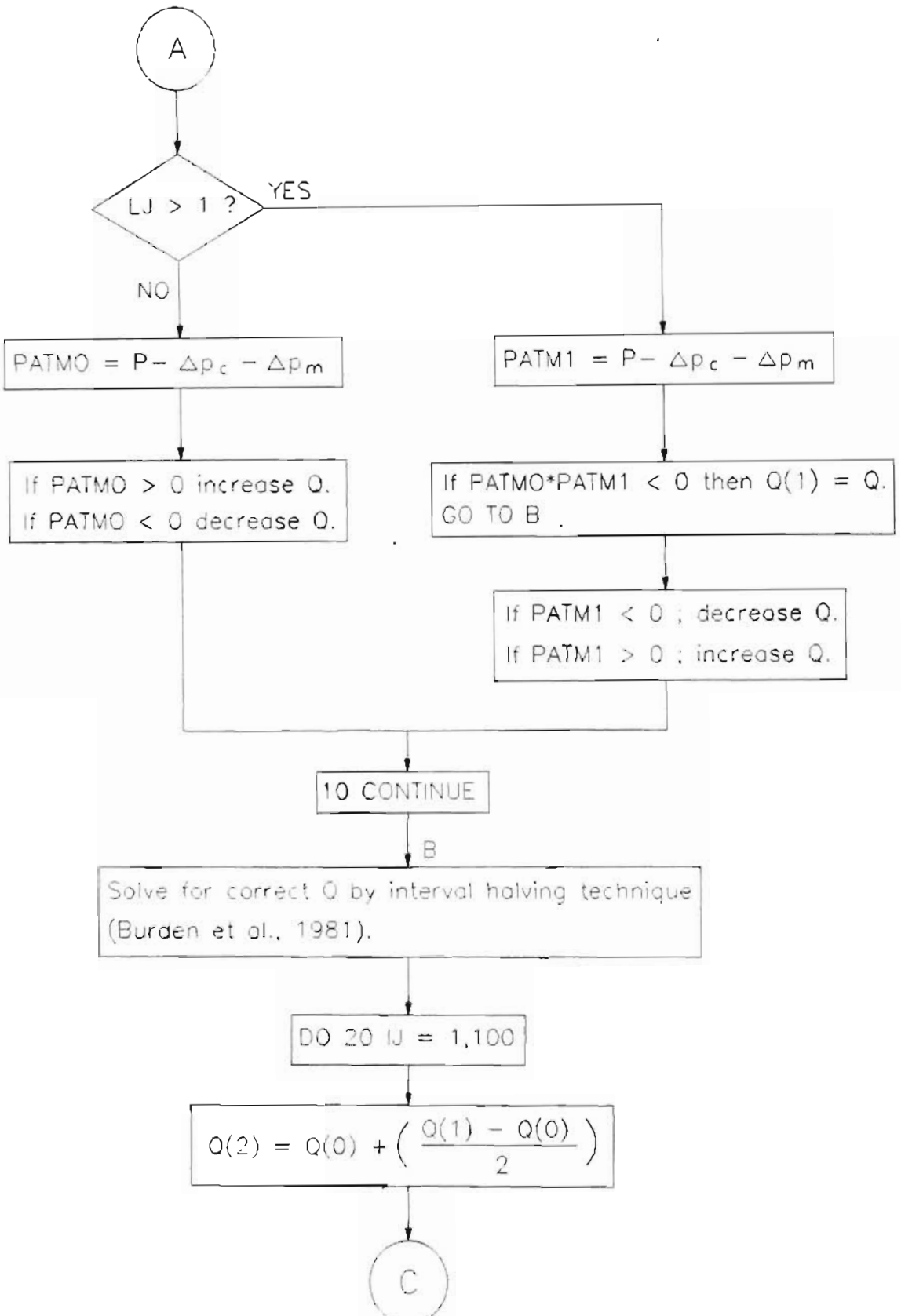
A
LJ > 1 ?
YES
NO
PATMO = P − Δp c − Δp m
PATM1 = P − Δp c − Δp m
If PATMO > 0 increase Q.
If PATMO < 0 decrease Q.
If PATMO*PATM1 < 0 then Q(1) = Q.
GO TO B .
If PATM1 < 0 ; decrease Q.
If PATM1 > 0 ; increase Q.
10 CONTINUE
B
Solve for correct Q by interval halving technique
(Burden et al., 1981).
DO 20 IJ = 1,100
Q(2) = Q(0) + (Q(1) − Q(0) / 2)
C

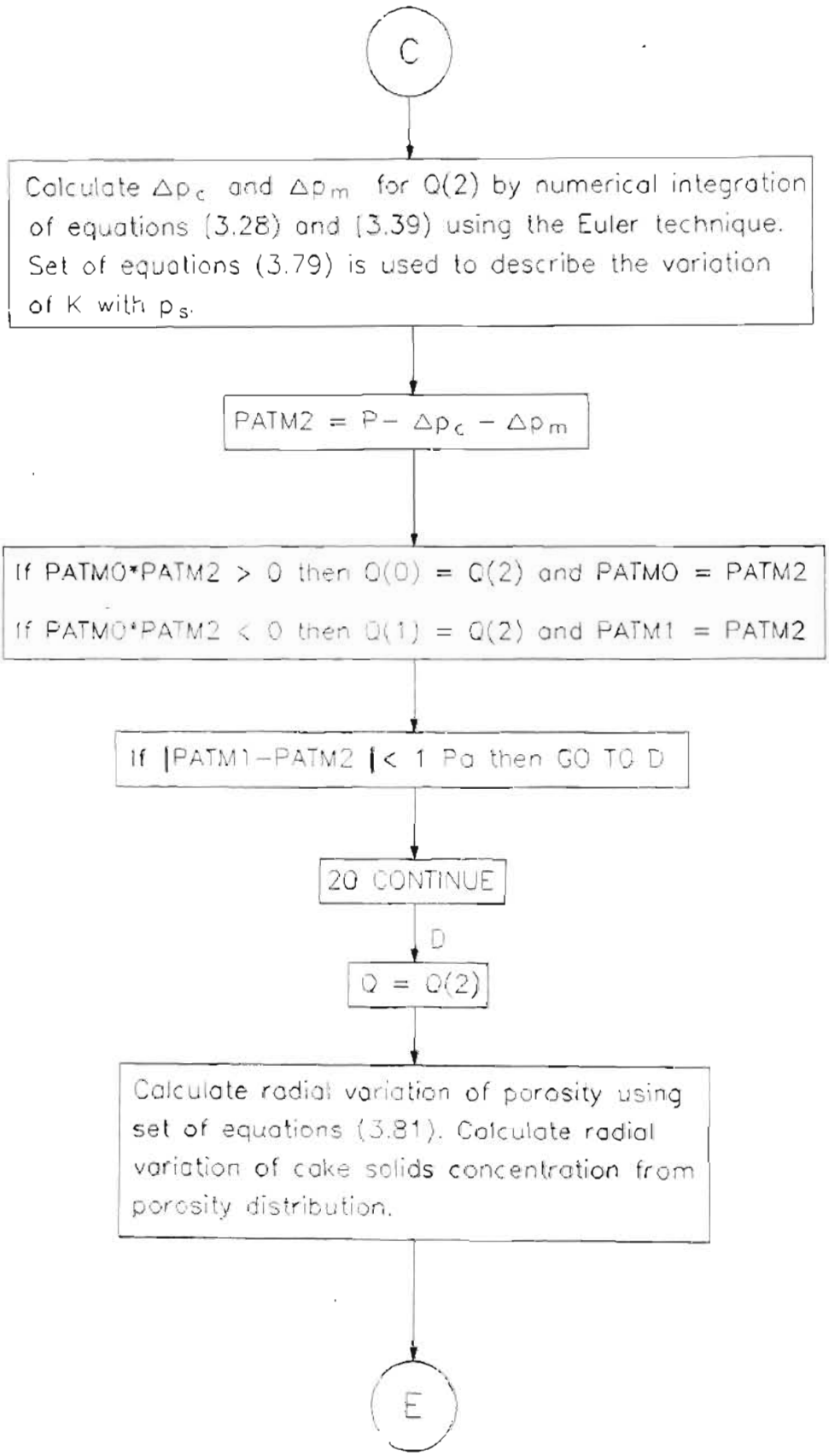
C
Calculate Δp_c and Δp_m for Q(2) by numerical integration of equations (3.28) and (3.39) using the Euler technique. Set of equations (3.79) is used to describe the variation of K with p_s.
PATM2 = P − Δp_c − Δp_m
If PATM0*PATM2 > 0 then Q(0) = Q(2) and PATM0 = PATM2
If PATM0*PATM2 < 0 then Q(1) = Q(2) and PATM1 = PATM2
If |PATM1−PATM2| < 1 Pa then GO TO D
20 CONTINUE
D
Q = Q(2)
Calculate radial variation of porosity using set of equations (3.81). Calculate radial variation of cake solids concentration from porosity distribution.
E

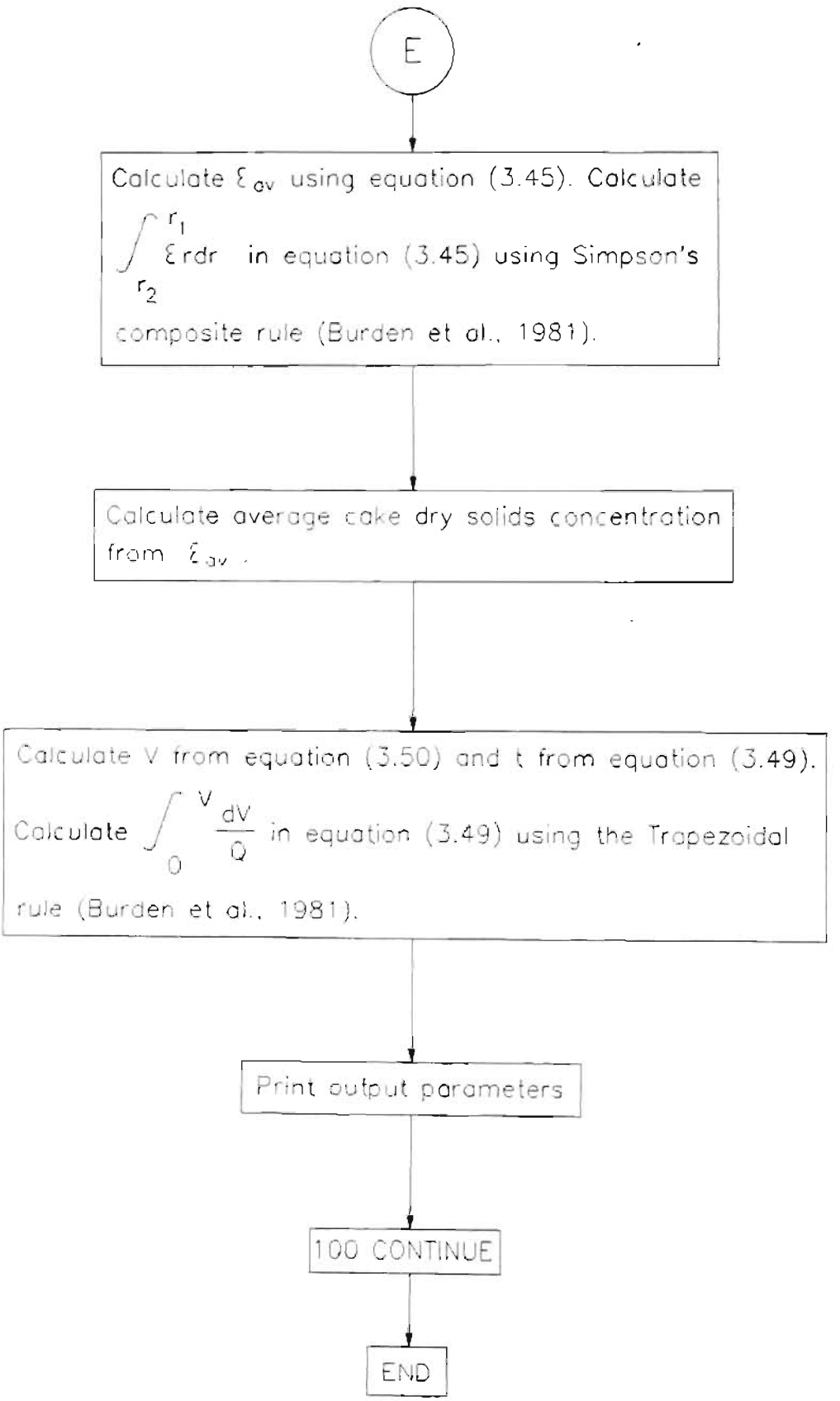
E
Calculate ξ_{av} using equation (3.45). Calculate $\int_{r_2}^{r_1} \xi r dr$ in equation (3.45) using Simpson's composite rule (Burden et al., 1981).
Calculate average cake dry solids concentration from ξ_{av}.
Calculate V from equation (3.50) and t from equation (3.49). Calculate $\int_0^V \frac{dV}{Q}$ in equation (3.49) using the Trapezoidal rule (Burden et al., 1981).
Print output parameters
100 CONTINUE
END

SYMBOLS FOR COMPUTER PROGRAM

IJ = parameter in computer flowsheet in Appendix E, (-)

KL = parameter in computer flowsheet in Appendix E, (-)

LJ = parameter in computer flowsheet in Appendix E, (-)

m = parameter in computer flowsheet in Appendix E, (-)

ma = number of mesh points in thin element of cake with thickness, Δr , in computer flowsheet in Appendix E, (-)

NR = number of internal cake radii in computer flowsheet in Appendix E, (-)

PATMO = value for $(P - \Delta p_c - \Delta p_m)$ for $Q(0)$ in computer flowsheet in Appendix E, (Pa)

PATM1 = value for $(P - \Delta p_c - \Delta p_m)$ for $Q(1)$ in computer flowsheet in Appendix E, (Pa)

PATM2 = value for $(P - \Delta p_c - \Delta p_m)$ for $Q(2)$ in computer flowsheet in Appendix E, (Pa)

$Q(0)$ = initial guess for Q for a particular cake thickness in interval halving technique in computer flowsheet in Appendix E, ($m^3/m.s$)

$Q(1)$ = value of Q for PATM1 in interval halving technique in computer flowsheet in Appendix E, ($m^3/m.s$)

$Q(2)$ = "mid-point" between $Q(0)$ and $Q(1)$ in interval halving technique in computer flowsheet in Appendix E, ($m^3/m.s$)

APPENDIX F
PARTICLE SIZE DISTRIBUTION FOR WATERWORKS CLARIFIER SLUDGE

The particle size distribution for the waterworks clarifier sludge was obtained using the Malvern particle size analyser type 3600E. The particle size distribution is shown in the following printout from the analyser.

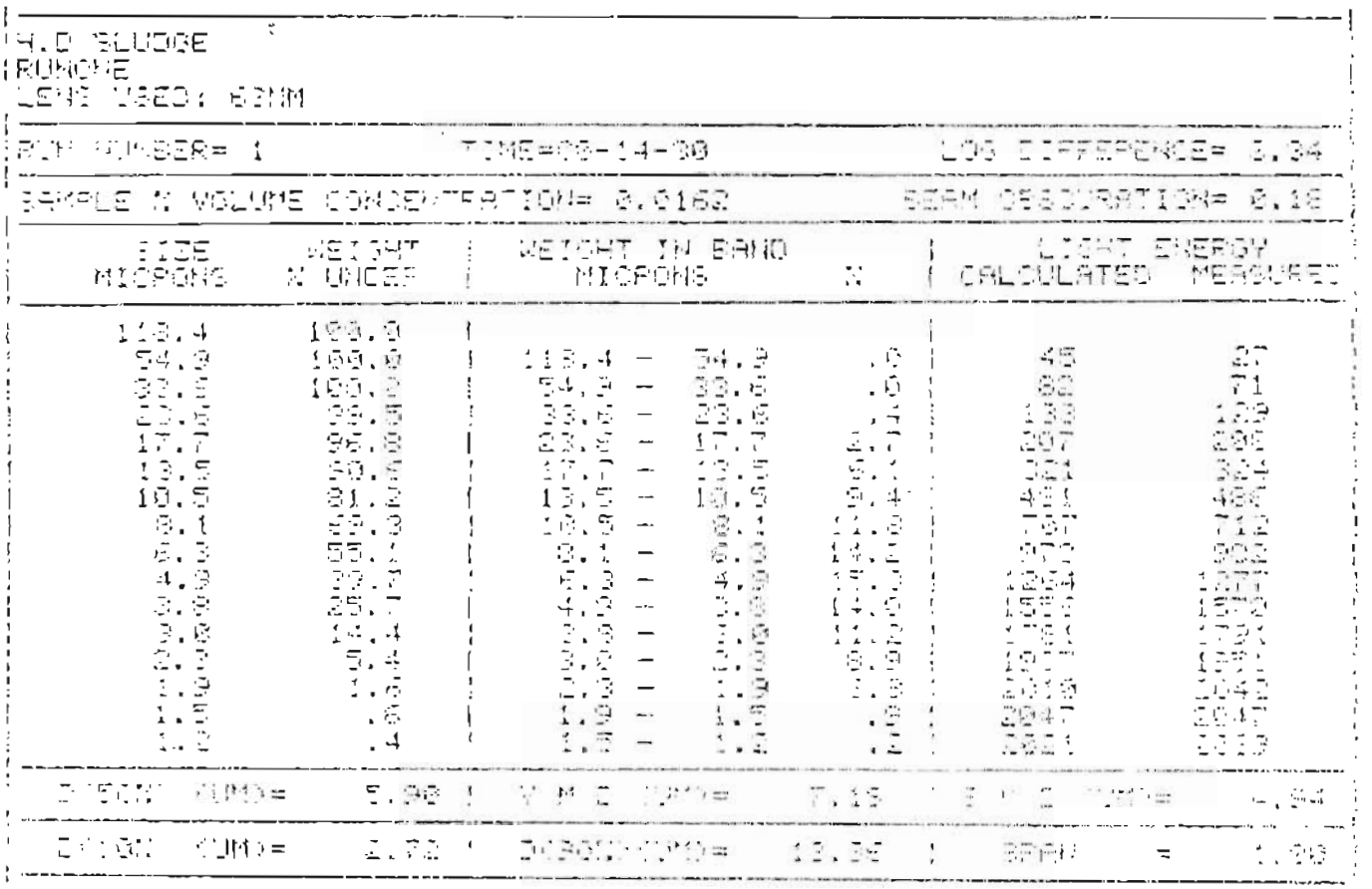

FIGURE F.1 : A Printout of the Particle Size Analysis for the Waterworks Clarifier Sludge Obtained from the Malvern Particle Size Analyser

The Malvern particle size analyser type 3600E operates on the principle of Fraunhofer diffraction of a laser beam by particles passing through the beam.

A process schematic of the Malvern particle size analyser is shown in Figure F.2.

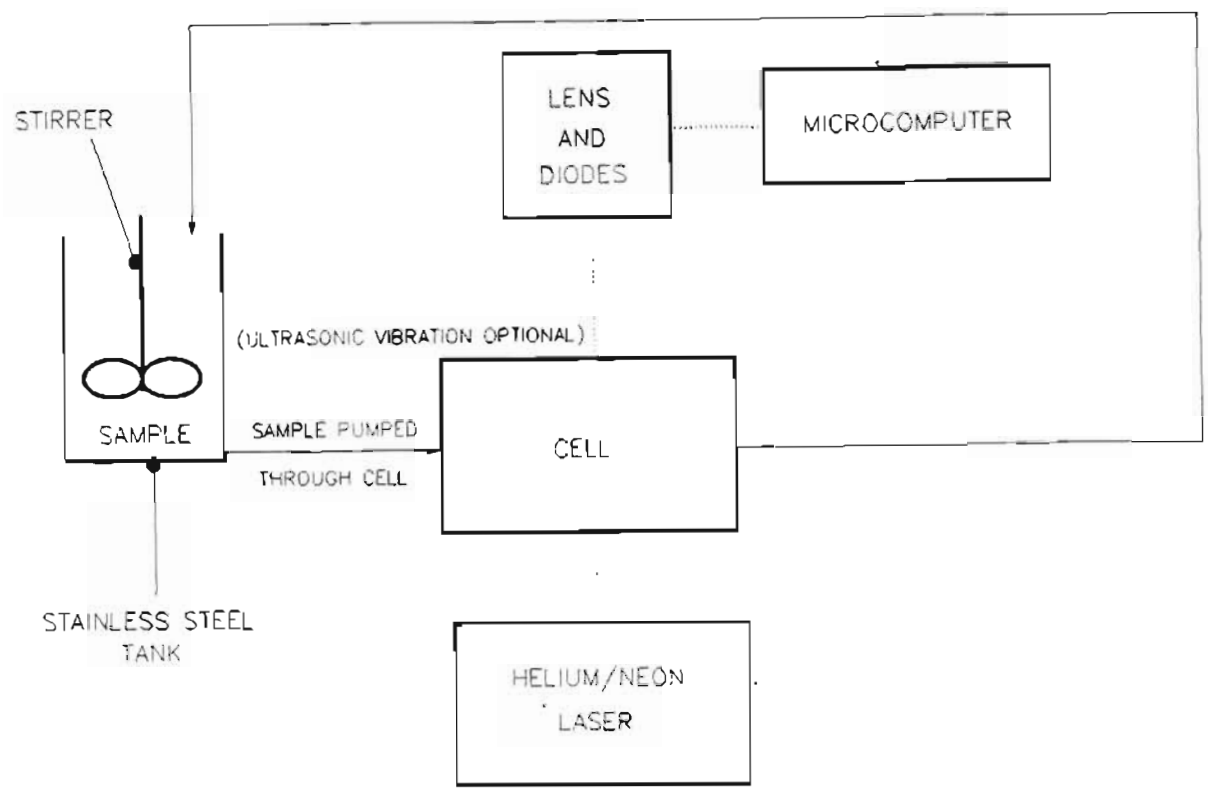

FIGURE F.2 : Process Schematic of the Malvern Particle Size Analyser Type 3600E

The sample to be sized is put into the stainless steel tank with water and pumped through a cell in the path of the helium/neon laser beam. If necessary, ultrasonic vibration can be applied to disperse the sample (as was done for the experiment shown above). A stirrer ensures that all the sample passes around the circuit. It is not the intention to give a detailed account of the theory involved. It is sufficient to say here that each sized particle diffracts the laser beam by a differing amount, and a transform lens focuses this pattern on a series of light sensitive diodes such that the motion of the particles has no effect on the pattern. The diffraction pattern is communicated to a microcomputer by the diodes. The necessary calculations are performed by the microcomputer. The particle size distribution of the sample is displayed in sixteen size bands.

For the calculations it is assumed that the particles are spherical. The average particle size for the waterworks clarifier sludge was taken as the mass average particle size of 5,90 μm. The mass average particle size means that for the sample half of the total mass of the particles had a particle size of less than or equal to 5,90 μm (assuming spherical particles).

The minimum measurable particle size is 0,5 μm and the lowest cut size reported is 1,2 μm.

APPENDIX G
MISCELLANEOUS CALCULATIONS FOR COMPRESSIBLE CAKE FILTRATION

G.1 DETERMINATION OF EMPIRICAL CONSTANTS C AND n FOR WATERWORKS CLARIFIER SLUDGE (see set of equations (3.34))

From equation (3.52)

$$\alpha = \frac{1}{\rho_s K (1-\epsilon)} \tag{3.52}$$

From set of equations (3.32) and (3.33) respectively :

$$K = F p_s^{-\delta} \tag{3.32}$$

$$(1-\epsilon) = B p_s^{\beta} \tag{3.33}$$

Substituting equations (3.32) and (3.33) into equation (3.52) gives :

$$\alpha = \frac{1}{\rho_s F p_s^{-\delta} B p_s^{\beta}}$$

$$= \left(\frac{1}{F B \rho_s}\right) p_s^{\delta-\beta} \tag{G.1}$$

However, from set of equations (3.34) :

$$\alpha = C p_s^{n} \tag{3.34}$$

From equations (G.1) and (3.34) :

$$C = \left(\frac{1}{F B \rho_s}\right) \tag{G.2}$$

$$n = \delta - \beta \tag{G.3}$$

For Combined C-P Cell Data (Tests A.1 and A.2)

$\delta = 1.254$

$F = 1.779 \times 10^{-10}$

$\beta = 0.265$

$B = 0.00785$

Therefore

$$C = \left(\frac{1}{1.779 \times 10^{-10} \times 0.00785 \times 2380.1}\right)$$

$$= 3.008 \times 10^{8}$$

$n = 1.254 - 0.265$

$= 0.989$

For Settling Data

$\delta = 0.575$

$F = 6.621 \times 10^{-13}$

$\beta = 0.0782$

$B = 0.0299$

Therefore

$$C = \left(\frac{1}{6.621 \times 10^{-13} \times 0.0299 \times 2380.1} \right)$$

$= 2.122 \times 10^{10}$

$n = 0.575 - 0.0782$

$= 0.497$

G.2 FILTRATION EQUATIONS FOR PLANAR COMPRESSIBLE CAKE FILTRATION

For planar filtration (from equation (3.10b)) :

$$\frac{dp_L}{dx} = -\frac{dp_s}{dx}$$

or in material co-ordinates :

$$\frac{dp_L}{dw} = -\frac{dp_s}{dw} \qquad (G.4)$$

For D'Arcy's law (D'Arcy, 1856) (assuming $u_s = 0$) from equations (3.16) and (G.4) :

$$\frac{dp_L}{dw} = -\frac{dp_s}{dw} = \mu_f \alpha u$$

where

$$u = \frac{Q_f}{A} \qquad (3.15)$$

from equation (3.15).

Therefore

$$-\frac{dp_s}{dw} = \mu_f \alpha \frac{Q_f}{A} \qquad (G.5)$$

or

$$-\frac{dp_s}{\alpha} = \mu_f \frac{Q_f}{A} dw \qquad (G.6)$$

Integrating equation (G.6) with the following boundary conditions :

x	o	L
w	o	w_c
p_s	$P - \Delta p_m = \Delta p_c$	o

$$\int_o^{\Delta p_c} \frac{dp_s}{\alpha} = \mu_f \frac{Q_f}{A} \int_o^{w_c} dw \qquad (G.7)$$

α_{av} is defined as follows :

$$\frac{1}{\alpha_{av}} = \frac{1}{\Delta p_c} \int_o^{\Delta p_c} \frac{dp_s}{\alpha} \qquad (G.8)$$

Therefore combining equations (G.7) and (G.8) :

$$\frac{Q_f}{A} = \frac{\Delta p_c}{\mu_f \alpha_{av} w_c} \qquad (G.9)$$

From equation (3.42), for planar filtration :

$$\Delta p_m = \mu_f \frac{Q_f}{A} R_m \qquad (3.42)$$

From equation (3.44)

$$P = \Delta p_c + \Delta p_m \qquad (3.44)$$

By combining equations (G.9), (3.42) and (3.44) :

$$\frac{Q_f}{A} = \frac{dv}{dt} = \frac{P}{\mu_f(\alpha_{av} w_c + R_m)} \qquad (G.10)$$

This is the conventional equation for planar compressible cake filtration.

If R_m is negligible compared to the resistance of the cake (as was true for the cake produced from the clarifier sludge) :

$$\frac{dv}{dt} = \frac{P}{\mu_f \alpha_{av} w_c} \qquad (3.1)$$

or

$$\frac{dt}{dv} = \frac{\mu_f \alpha_{av} w_c}{P} \qquad (2.1)$$

G.3 DETERMINATION OF α_{av} FOR CAKE DERIVED FROM PLANAR FILTRATION OF CLARIFIER SLUDGE

From equation (G.8) :

$$\frac{1}{\alpha_{av}} = \frac{1}{\Delta p_c}\int_o^{\Delta p_c}\frac{dp_s}{\alpha} \qquad (G.8)$$

The values of C and n for the C-P cell data and settling data are shown in section G.1.

By adapting set of equations (3.79) for specific filtration resistance, for the cake from the clarifier sludge :

$$\begin{aligned} \alpha &= 2,122\times10^{10}\,p_{sf}^{0,497} && 0 \le p_s \le p_{sf} \\ \alpha &= 2.122\times10^{10}\,p_s^{0,497} && p_{sf} \le p_s \le 3781,7\ \text{Pa} \\ \alpha &= 3,008\times10^{8}\,p_s^{0,989} && p_s \ge 3781,7\ \text{Pa} \end{aligned} \qquad (G.11)$$

From equation (G.8), if R_m is negligible compared to the cake resistance as was true for the cake from the clarifier sludge :

$$\frac{1}{\alpha_{av}} = \frac{1}{P}\int_o^{P}\frac{dp_s}{\alpha} \qquad (G.12)$$

The integral may be evaluated as follows (from equations (G.11) and (G.12)) :

$$\int_o^{P}\frac{dp_s}{\alpha} = \int_o^{p_{sf}}\frac{dp_s}{2,122\times10^{10}\,p_{sf}^{0,497}} + \int_{p_{sf}}^{3781,7}\frac{dp_s}{2.122\times10^{10}\,p_s^{0,497}} + \int_{3781,7}^{P}\frac{dp_s}{3,008\times10^{8}\,p_s^{0,989}} \qquad (G.13)$$

The first integral on the right hand side of equation (G.13) is negligible, since p_{sf} during this study was <1 Pa.

For a feed sludge with a solids concentration of 49 g/ℓ (p_{sf} = 0,0085 Pa) and P = 300 kPa, α_{av} was calculated (from equation (G.13)) to be 1,351 x 10^{13} (m/kg). The cake therefore had a very high resistance.

APPENDIX H
RESULTS OF CAKE RECOVERY EXPERIMENTS

H.1 EXPERIMENTS TO DETERMINE CAKE RECOVERY AFTER ROLLER ACTION AND HYDRAULIC CONVEYANCE OF DISLODGED CAKE FLAKES

H.1.1 Experiments at P = 100 kPa (flow rate of cleaning water = approximately 25 ℓ/min; path length = 1m)

Experiment H.1.1.1

Date	1/11/1990	
Filtration time	5	minutes
Feed solids concentration	49,71	g/ℓ
Temperature of filtrate	21,2	°C
Flow rate of cleaning water	25,8	ℓ/min
Temperature of cleaning water	22,0	°C
Path length	1	m
Mass of wet cake recovered	43,37	g
Average cake dry solids concentration	19,16	% m/m

Experiment H.1.1.2

Date	1/11/1990	
Filtration time	10	minutes
Feed solids concentration	49,71	g/ℓ
Temperature of filtrate	21,2	°C
Flow rate of cleaning water	25,3	ℓ/min
Temperature of cleaning water	22,0	°C
Path length	1	m
Mass of wet cake recovered	64,42	g
Average cake dry solids concentration	20,38	% m/m

Experiment H.1.1.3

Date	1/11/1990	
Filtration time	15	minutes
Feed solids concentration	49,71	g/ℓ
Temperature of filtrate	21,5	°C
Flow rate of cleaning water	24,6	ℓ/min
Temperature of cleaning water	22,0	°C
Path length	1	m
Mass of wet cake recovered	75,21	g
Average cake dry solids concentration	21,07	% m/m

Experiment H.1.1.4

Date	1/11/1990	
Filtration time	20	minutes
Feed solids concentration	49,71	g/ℓ
Temperature of filtrate	21,5	°C
Flow rate of cleaning water	25,7	ℓ/min
Temperature of cleaning water	22,0	°C
Path length	1	m
Mass of wet cake recovered	93,55	g
Average cake dry solids concentration	22,43	% m/m

Experiment H.1.1.5

Date	1/11/1990	
Filtration time	25	minutes
Feed solids concentration	49,71	g/ℓ
Temperature of filtrate	21,5	°C
Flow rate of cleaning water	25,8	ℓ/min
Temperature of cleaning water	22,0	°C
Path length	1	m
Mass of wet cake recovered	104,78	g
Average cake dry solids concentration	22,14	% m/m

H.1.2 Experiments at P = 100 kPa (flow rate of cleaning water = approximately 50 ℓ/min; path length = 1m)

Experiment H.1.2.1

Date	2/11/1990	
Filtration time	5	minutes
Feed solids concentration	47,17	g/ℓ
Temperature of filtrate	22,0	°C
Flow rate of cleaning water	51,7	ℓ/min
Temperature of cleaning water	22,0	°C
Path length	1	m
Mass of wet cake recovered	30,44	g
Average cake dry solids concentration	18,69	% m/m

Experiment H.1.2.2

Date	2/11/1990	
Filtration time	10	minutes
Feed solids concentration	47,17	g/ℓ
Temperature of filtrate	22,0	°C
Flow rate of cleaning water	51,7	ℓ/min
Temperature of cleaning water	22,0	°C
Path length	1	m
Mass of wet cake recovered	50,66	g
Average cake dry solids concentration	20,41	% m/m

Experiment H.1.2.3

Date	2/11/1990	
Filtration time	15	minutes
Feed solids concentration	47,17	g/ℓ
Temperature of filtrate	22,0	°C
Flow rate of cleaning water	51,6	ℓ/min
Temperature of cleaning water	22,0	°C
Path length	1	m
Mass of wet cake recovered	67,21	g
Average cake dry solids concentration	20,25	% m/m

Experiment H.1.2.4

Date	2/11/1990	
Filtration time	20	minutes
Feed solids concentration	47,17	g/ℓ
Temperature of filtrate	22,0	°C
Flow rate of cleaning water	50,8	ℓ/min
Temperature of cleaning water	22,0	°C
Path length	1	m
Mass of wet cake recovered	82,35	g
Average cake dry solids concentration	20,60	% m/m

H.1.3 Experiments at P = 300 kPa (flow rate of cleaning water = approximately 25 ℓ/min; path length = 1 m)

Experiment H.1.3.1

Date	31/10/1990	
Filtration time	5	minutes
Feed solids concentration	49,71	g/ℓ
Temperature of filtrate	21,5	°C
Flow rate of cleaning water	25,8	ℓ/min
Temperature of cleaning water	22,0	°C
Path length	1	m
Mass of wet cake recovered	62,77	g
Average cake dry solids concentration	23,72	% m/m

Experiment H.1.3.2

Date	31/10/1990	
Filtration time	10	minutes
Feed solids concentration	49,71	g/ℓ
Temperature of filtrate	21,5	°C
Flow rate of cleaning water	24,8	ℓ/min
Temperature of cleaning water	22,0	°C
Path length	1	m
Mass of wet cake recovered	88,33	g
Average cake dry solids concentration	24,59	% m/m

Experiment H.1.3.3

Date	31/10/1990	
Filtration time	15	minutes
Feed solids concentration	49,71	g/ℓ
Temperature of filtrate	21,5	°C
Flow rate of cleaning water	23,9	ℓ/min
Temperature of cleaning water	22,0	°C
Path length	1	m
Mass of wet cake recovered	104,96	g
Average cake dry solids concentration	25,14	% m/m

Experiment H.1.3.4

Date	31/10/1990	
Filtration time	20	minutes
Feed solids concentration	49,71	g/ℓ
Temperature of filtrate	21,5	°C
Flow rate of cleaning water	23,6	ℓ/min
Temperature of cleaning water	22,0	°C
Path length	1	m
Mass of wet cake recovered	133,65	g
Average cake dry solids concentration	25,46	% m/m

Experiment H.1.3.5

Date	31/10/1990	
Filtration time	25	minutes
Feed solids concentration	49,71	g/ℓ
Temperature of filtrate	21,0	°C
Flow rate of cleaning water	24,1	ℓ/min
Temperature of cleaning water	22,0	°C
Path length	1	m
Mass of wet cake recovered	145,13	g
Average cake dry solids concentration	26,82	% m/m

H.1.4 Experiments at P = 300 kPa (flow rate of cleaning water = approximately 50 ℓ/min; path length = 1 m)

Experiment H.1.4.1

Date	26/10/1990	
Filtration time	5	minutes
Feed solids concentration	49,13	g/ℓ
Temperature of filtrate	20,2	°C
Flow rate of cleaning water	52,6	ℓ/min
Temperature of cleaning water	21,0	°C
Path length	1	m
Mass of wet cake recovered	44,11	g
Average cake dry solids concentration	23,55	% m/m

Experiment H.1.4.2

Date	31/10/1990	
Filtration time	10	minutes
Feed solids concentration	49,71	g/ℓ
Temperature of filtrate	21,0	°C
Flow rate of cleaning water	51,5	ℓ/min
Temperature of cleaning water	22,0	°C
Path length	1	m
Mass of wet cake recovered	89,82	g
Average cake dry solids concentration	24,27	% m/m

Experiment H.1.4.3

Date	31/10/1990	
Filtration time	15	minutes
Feed solids concentration	49,71	g/ℓ
Temperature of filtrate	21,5	°C
Flow rate of cleaning water	51,9	ℓ/min
Temperature of cleaning water	22,0	°C
Path length	1	m
Mass of wet cake recovered	101,31	g
Average cake dry solids concentration	25,05	% m/m

Experiment H.1.4.4

Date	31/10/1990	
Filtration time	20	minutes
Feed solids concentration	49,71	g/ℓ
Temperature of filtrate	21,2	°C
Flow rate of cleaning water	51,6	ℓ/min
Temperature of cleaning water	22,0	°C
Path length	1	m
Mass of wet cake recovered	119,29	g
Average cake dry solids concentration	24,98	% m/m

Experiment H.1.4.5

Date	31/10/1990	
Filtration time	25	minutes
Feed solids concentration	49,71	g/ℓ
Temperature of filtrate	21,5	°C
Flow rate of cleaning water	51,1	ℓ/min
Temperature of cleaning water	22,0	°C
Path length	1	m
Mass of wet cake recovered	123,56	g
Average cake dry solids concentration	25,16	% m/m

H.1.5 Experiments at P = 300 kPa (flow rate of cleaning water = approximately 25 ℓ/min; path length = 4 m)

Experiment H.1.5.1

Date	18/10/1990	
Filtration time	5	minutes
Feed solids concentration	47,89	g/ℓ
Temperature of filtrate	19,0	°C
Flow rate of cleaning water	26,2	ℓ/min
Temperature of cleaning water	21,0	°C
Path length	4	m
Mass of wet cake recovered	44,11	g
Average cake dry solids concentration	21,95	% m/m

Experiment H.1.5.2

Date	18/10/1990	
Filtration time	10	minutes
Feed solids concentration	47,34	g/ℓ
Temperature of filtrate	19,0	°C
Flow rate of cleaning water	25,8	ℓ/min
Temperature of cleaning water	21,0	°C
Path length	4	m
Mass of wet cake recovered	73,49	g
Average cake dry solids concentration	23,51	% m/m

Experiment H.1.5.3

Date	19/10/1990	
Filtration time	20	minutes
Feed solids concentration	48,55	g/ℓ
Temperature of filtrate	18,0	°C
Flow rate of cleaning water	26,2	ℓ/min
Temperature of cleaning water	20,0	°C
Path length	4	m
Mass of wet cake recovered	121,64	g
Average cake dry solids concentration	25,78	% m/m

Experiment H.1.5.4

Date	19/10/1990	
Filtration time	25	minutes
Feed solids concentration	47,99	g/ℓ
Temperature of filtrate	19,0	°C
Flow rate of cleaning water	25,6	ℓ/min
Temperature of cleaning water	20,0	°C
Path length	4	m
Mass of wet cake recovered	141,95	g
Average cake dry solids concentration	25,56	% m/m

H.1.6 Experiments at P = 300 kPa (flow rate of cleaning water = approximately 50 ℓ/min; path length = 4 m)

Experiment H.1.6.1

Date	19/10/1990	
Filtration time	5	minutes
Feed solids concentration	47,44	g/ℓ
Temperature of filtrate	19,0	°C
Flow rate of cleaning water	48,5	ℓ/min
Temperature of cleaning water	20,0	°C
Path length	4	m
Mass of wet cake recovered	41,44	g
Average cake dry solids concentration	22,59	% m/m

Experiment H.1.6.2

Date	19/10/1990	
Filtration time	10	minutes
Feed solids concentration	46,89	g/ℓ
Temperature of filtrate	19,0	°C
Flow rate of cleaning water	49,6	ℓ/min
Temperature of cleaning water	20,0	°C
Path length	4	m
Mass of wet cake recovered	55,50	g
Average cake dry solids concentration	24,34	% m/m

Experiment H.1.6.3

Date	19/10/1990	
Filtration time	15	minutes
Feed solids concentration	46,79	g/ℓ
Temperature of filtrate	19,0	°C
Flow rate of cleaning water	50,4	ℓ/min
Temperature of cleaning water	20,0	°C
Path length	4	m
Mass of wet cake recovered	82,13	g
Average cake dry solids concentration	23,90	% m/m

Experiment H.1.6.4

Date	23/10/1990	
Filtration time	20	minutes
Feed solids concentration	49,81	g/ℓ
Temperature of filtrate	19,8	°C
Flow rate of cleaning water	50,3	ℓ/min
Temperature of cleaning water	21,0	°C
Path length	4	m
Mass of wet cake recovered	109,62	°C
Average cake dry solids concentration	25,36	% m/m

Experiment H.1.6.5

Date	23/10/1990	
Filtration time	25	minutes
Feed solids concentration	49,81	g/ℓ
Temperature of filtrate	20,0	°C
Flow rate of cleaning water	51,0	ℓ/min
Temperature of cleaning water	21,0	°C
Path length	4	m
Mass of wet cake recovered	129,56	g
Average cake dry solids concentration	25,84	% m/m

H.2 EXPERIMENTS TO DETERMINE CAKE LOSSES DUE TO THE SHEAR OF THE CLEANING FLUID (PRIOR TO ROLLER ACTION)

H.2.1 Experiments at P = 100 kPa (flow rate of cleaning water = approximately 25 ℓ/min)

Experiment H.2.1.1

Date	7/11/1990	
Filtration time	5	minutes
Feed solids concentration	48,56	g/ℓ
Temperature of filtrate	23,0	°C
Flow rate of cleaning water	26,9	ℓ/min
Temperature of cleaning water	21,0	°C
Mass of wet cake after shear	110,22	g
Average cake dry solids concentration	19,86	% m/m
Calculated internal cake diameter after shear	20,20	mm
Measured internal cake diameter after shear	cake broken (not measured)	
Duration of shear	3	minutes

Experiment H.2.1.2

Date	7/11/1990	
Filtration time	10	minutes
Feed solids concentration	48,56	g/ℓ
Temperature of filtrate	23,0	°C
Flow rate of cleaning water	26,7	ℓ/min
Temperature of cleaning water	21,0	°C
Mass of wet cake after shear	144,24	g
Average cake dry solids concentration	20,97	% m/m
Calculated internal cake diameter after shear	18,00	mm
Measured internal cake diameter after shear	18,1	mm
Duration of shear	3	minutes

Experiment H.2.1.3

Date	7/11/1990	
Filtration time	15	minutes
Feed solids concentration	48,56	g/ℓ
Temperature of filtrate	23,0	°C
Flow rate of cleaning water	26,8	ℓ/min
Temperature of cleaning water	21,0	°C
Mass of wet cake after shear	165,64	g
Average cake dry solids concentration	20,99	% m/m
Calculated internal cake diameter after shear	16,43	mm
Measured internal cake diameter after shear	16,9	mm
Duration of shear	3	minutes

Experiment H.2.1.4

Date	7/11/1990	
Filtration time	20	minutes
Feed solids concentration	47,50	g/ℓ
Temperature of filtrate	24,0	°C
Flow rate of cleaning water	26,6	ℓ/min
Temperature of cleaning water	22,0	°C
Mass of wet cake after shear	181,30	g
Average cake dry solids concentration	22,46	% m/m
Calculated internal cake diameter after shear	15,32	mm
Measured internal cake diameter after shear	15,6	mm
Duration of shear	3	minutes

Experiment H.2.1.5

Date	14/11/1990	
Filtration time	25	minutes
Feed solids concentration	48,93	g/ℓ
Temperature of filtrate	22,0	°C
Flow rate of cleaning water	26,5	ℓ/min
Temperature of cleaning water	23,0	°C
Mass of wet cake after shear	190,56	g
Average cake dry solids concentration	23,42	% m/m
Calculated internal cake diameter after shear	14,65	mm
Measured internal cake diameter after shear	13,4	mm
Duration of shear	3	minutes

H.2.2 Experiments at P = 100 kPa (flow rate of cleaning water = approximately 50 ℓ/min)

Experiment H.2.2.1

Date	6/11/1990	
Filtration time	5	minutes
Feed solids concentration	48,00	g/ℓ
Temperature of filtrate	23,0	°C
Flow rate of cleaning water	51,1	ℓ/min
Temperature of cleaning water	21,0	°C
Mass of wet cake after shear	97,18	g
Average cake dry solids concentration	21,42	% m/m
Calculated internal cake diameter after shear	21,06	mm
Measured internal cake diameter after shear	cake broken (not measured)	
Duration of shear	3	minutes

Experiment H.2.2.2

Date	6/11/1990	
Filtration time	10	minutes
Feed solids concentration	48,00	g/ℓ
Temperature of filtrate	23,0	°C
Flow rate of cleaning water	50,9	ℓ/min
Temperature of cleaning water	21,0	°C
Mass of wet cake after shear	126,37	g
Average cake dry solids concentration	21,91	% m/m
Calculated internal cake diameter after shear	19,27	mm
Measured internal cake diameter after shear	19,2	mm
Duration of shear	3	minutes

Experiment H.2.2.3

Date	6/11/1990	
Filtration time	15	minutes
Feed solids concentration	48,00	g/ℓ
Temperature of filtrate	23,0	°C
Flow rate of cleaning water	51,2	ℓ/min
Temperature of cleaning water	21,0	°C
Mass of wet cake after shear	142,84	g
Average cake dry solids concentration	22,80	% m/m
Calculated internal cake diameter after shear	18,22	mm
Measured internal cake diameter after shear	18,1	mm
Duration of shear	3	minutes

Experiment H.2.2.4

Date	7/11/1990	
Filtration time	20	minutes
Feed solids concentration	48,56	g/ℓ
Temperature of filtrate	22,5	°C
Flow rate of cleaning water	50,9	ℓ/min
Temperature of cleaning water	21,0	°C
Mass of wet cake after shear	155,01	g
Average cake dry solids concentration	23,53	% m/m
Calculated internal cake diameter after shear	17,42	mm
Measured internal cake diameter after shear	16,9	mm
Duration of shear	3	minutes

Experiment H.2.2.5

Date	7/11/1990	
Filtration time	25	minutes
Feed solids concentration	48,56	g/ℓ
Temperature of filtrate	22,5	°C
Flow rate of cleaning water	50,5	ℓ/min
Temperature of cleaning water	21,0	°C
Mass of wet cake after shear	158,26	g
Average cake dry solids concentration	24,03	% m/m
Calculated internal cake diameter after shear	17,22	mm
Measured internal cake diameter after shear	16,5	mm
Duration of shear	3	minutes
(Comments : ripples on cake surface!)		

H.2.3 Experiments at P = 300 kPa (flow rate of cleaning water = approximately 25 ℓ/min)

Experiment H.2.3.1

Date	17/10/1990	
Filtration time	5	minutes
Feed solids concentration	47,32	g/ℓ
Temperature of filtrate	19,5	°C
Flow rate of cleaning water	25,9	ℓ/min
Temperature of cleaning water	20,5	°C
Mass of wet cake after shear	121,06	g
Average cake dry solids concentration	22,49	% m/m
Calculated internal cake diameter after shear	19,64	mm
Measured internal cake diameter after shear	cake broken (not measured)	
Duration of shear	3	minutes

Experiment H.2.3.2

Date	17/10/1990	
Filtration time	10	minutes
Feed solids concentration	46,94	g/ℓ
Temperature of filtrate	19,5	°C
Flow rate of cleaning water	27,0	ℓ/min
Temperature of cleaning water	20,5	°C
Mass of wet cake after shear	154,85	g
Average cake dry solids concentration	23,58	% m/m
Calculated internal cake diameter after shear	17,44	mm
Measured internal cake diameter after shear	cake broken (not measured)	
Duration of shear	3	minutes

Experiment H.2.3.3

Date	17/10/1990	
Filtration time	15	minutes
Feed solids concentration	46,57	g/ℓ
Temperature of filtrate	20,0	°C
Flow rate of cleaning water	26,8	ℓ/min
Temperature of cleaning water	20,5	°C
Mass of wet cake after shear	174,09	g
Average cake dry solids concentration	24,43	% m/m
Calculated internal cake diameter after shear	16,08	mm
Measured internal cake diameter after shear	16,0	mm
Duration of shear	3	minutes

Experiment H.2.3.4

Date	18/10/1990	
Filtration time	20	minutes
Feed solids concentration	49,00	g/ℓ
Temperature of filtrate	19,8	°C
Flow rate of cleaning water	26,8	ℓ/min
Temperature of cleaning water	21,0	°C
Mass of wet cake after shear	190,20	g
Average cake dry solids concentration	25,20	% m/m
Calculated internal cake diameter after shear	14,87	mm
Measured internal cake diameter after shear	13,9	mm
Duration of shear	3	minutes

Experiment H.2.3.5

Date	18/10/1990	
Filtration time	25	minutes
Feed solids concentration	48,45	g/ℓ
Temperature of filtrate	19,8	°C
Flow rate of cleaning water	26,5	ℓ/min
Temperature of cleaning water	21,0	°C
Mass of wet cake after shear	202,15	g
Average cake dry solids concentration	25,84	% m/m
Calculated internal cake diameter after shear	13,92	mm
Measured internal cake diameter after shear	12,6	mm
Duration of shear	3	minutes

H.2.4 Experiments at P = 300 kPa (flow rate of cleaning water = approximately 50 ℓ/min)

Experiment H.2.4.1

Date	9/10/1990	
Filtration time	5	minutes
Feed solids concentration	49,44	g/ℓ
Temperature of filtrate	20,5	°C
Flow rate of cleaning water	49,5	ℓ/min
Temperature of cleaning water	21,0	°C
Mass of wet cake after shear	108,20	g
Average cake dry solids concentration	23,68	% m/m
Calculated internal cake diameter after shear	20,50	mm
Measured internal cake diameter after shear	20,2	mm
Duration of shear	3	minutes

Experiment H.2.4.2

Date	9/10/1990	
Filtration time	10	minutes
Feed solids concentration	48,98	g/ℓ
Temperature of filtrate	21,0	°C
Flow rate of cleaning water	50,7	ℓ/min
Temperature of cleaning water	21,0	°C
Mass of wet cake after shear	140,73	g
Average cake dry solids concentration	24,80	% m/m
Calculated internal cake diameter after shear	18,49	mm
Measured internal cake diameter after shear	17,4	mm
Duration of shear	3	minutes

Experiment H.2.4.3

Date	9/10/1990	
Filtration time	15	minutes
Feed solids concentration	48,52	g/ℓ
Temperature of filtrate	21,5	°C
Flow rate of cleaning water	50,6	ℓ/min
Temperature of cleaning water	21,5	°C
Mass of wet cake after shear	156,21	g
Average cake dry solids concentration	25,81	% m/m
Calculated internal cake diameter after shear	17,50	mm
Measured internal cake diameter after shear	17,4	mm
Duration of shear	3	minutes

Experiment H.2.4.4

Date	12/10/1990	
Filtration time	20	minutes
Feed solids concentration	48,06	g/ℓ
Temperature of filtrate	22,0	°C
Flow rate of cleaning water	50,6	ℓ/min
Temperature of cleaning water	21,0	°C
Mass of wet cake after shear	162,74	g
Average cake dry solids concentration	26,92	% m/m
Calculated internal cake diameter after shear	17,13	mm
Measured internal cake diameter after shear	17,3	mm
Duration of shear	3	minutes
(Comments : ripples on cake surface!)		

Experiment H.2.4.5

Date	12/10/1990	
Filtration time	25	minutes
Feed solids concentration	47,69	g/ℓ
Temperature of filtrate	22,5	°C
Flow rate of cleaning water	50,1	ℓ/min
Temperature of cleaning water	21,0	°C
Mass of wet cake after shear	171,91	g
Average cake dry solids concentration	27,62	% m/m
Calculated internal cake diameter after shear	16,53	mm
Measured internal cake diameter after shear	15,6	mm
Duration of shear	3	minutes
(Comments : ripples on cake surface!)		

H.2.5 Experiments at P = 300 kPa using feed sludge as cleaning fluid (flow rate of cleaning fluid = approximately 50 ℓ/min)

Experiment H.2.5.1

Date	18/5/1990	
Filtration time	5	minutes
Feed solids concentration	53,32	g/ℓ
Temperature of filtrate	23,0	°C
Flow rate of cleaning fluid (sludge)	47,3	ℓ/min
Temperature of cleaning fluid (sludge)	23,0	°C
Mass of wet cake after shear	112,87	g
Average cake dry solids concentration	23,63	% m/m
Calculated internal cake diameter after shear	20,21	mm
Measured internal cake diameter after shear	20,1	mm
Duration of shear	3	minutes

Experiment H.2.5.2

Date	18/5/1990	
Filtration time	10	minutes
Feed solids concentration	53,32	g/ℓ
Temperature of filtrate	23,0	°C
Flow rate of cleaning fluid (sludge)	47,0	ℓ/min
Temperature of cleaning fluid (sludge)	23,0	°C
Mass of wet cake after shear	143,38	g
Average cake dry solids concentration	24,41	% m/m
Calculated internal cake diameter after shear	18,29	mm
Measured internal cake diameter after shear	18,2	mm
Duration of shear	3	minutes

Experiment H.2.5.3

Date	23/5/1990	
Filtration time	15	minutes
Feed solids concentration	53,32	g/ℓ
Temperature of filtrate	17,0	°C
Flow rate of cleaning fluid (sludge)	47,1	ℓ/min
Temperature of cleaning fluid (sludge)	17,0	°C
Mass of wet cake after shear	154,89	g
Average cake dry solids concentration	25,20	% m/m
Calculated internal cake diameter after shear	17,55	mm
Measured internal cake diameter after shear	17,1	mm
Duration of shear	3	minutes

Experiment H.2.5.4

Date	17/10/1990	
Filtration time	20	minutes
Feed solids concentration	53,32	g/ℓ
Temperature of filtrate	22,0	°C
Flow rate of cleaning fluid (sludge)	47,1	ℓ/min
Temperature of cleaning fluid (sludge)	22,0	°C
Mass of wet cake after shear	178,22	g
Average cake dry solids concentration	27,01	% m/m
Calculated internal cake diameter after shear	16,00	mm
Measured internal cake diameter after shear	16,3	mm
Duration of shear	3	minutes

APPENDIX I
CAPILLARY-TUBE VISCOMETER EXPERIMENTS

I.1 RESULTS OF CAPILLARY-TUBE VISCOMETER EXPERIMENTS

Experiment I.1

Sludge solids concentration	:	3,58	% m/m
Sludge density	:	1019,2	kg/m^3
Sludge temperature	:	20,5	°C
Tube length	:	9,90	m

Mass of sludge (g)	Volume of sludge ($m^3 \times 10^6$)	Initial height difference (h_1) (m)	Final height difference (h_2) (m)	Average height difference $\left(\frac{h_1+h_2}{2}\right)$ (m)	Time (s)	Average velocity in tube ($\bar{u}_{ff}$) (m/s)	Air pressure (Pa)	Hydrostatic pressure (Pa)	Pressure loss (kinetic energy) (Pa)	Pressure loss (friction) (Pa)	(τ_w) (Pa)	$\left(\frac{8\bar{u}_{ff}}{D_i}\right)$ (s^{-1})	Re (-)
95	93,21	0,760	0,755	0,757	116,30	0,06	0	7 572	4	7 568	0,76	129,49	60,50
107	104,99	0,755	0,749	0,752	28,40	0,30	10 000	7 516	90	17 426	1,75	597,26	358,63
143	140,31	0,749	0,741	0,745	19,10	0,59	30 000	7 446	355	37 091	3,73	1186,86	741,76
190	186,42	0,741	0,730	0,736	19,10	0,78	45 000	7 354	627	51 727	5,20	1576,95	995,74

Experiment I.2

Sludge solids concentration	:	4,66	% m/m
Sludge density	:	1025,8	kg/m^3
Sludge temperature	:	20,5	^oC
Tube length	:	9,90	m

Mass of sludge (g)	Volume of sludge ($m^3 \times 10^6$)	Initial height difference (h_1) (m)	Final height difference (h_2) (m)	Average height difference $\left(\frac{h_1+h_2}{2}\right)$ (m)	Time (s)	Average velocity in tube ($\bar{u}_{fl}$) (m/s)	Air pressure (Pa)	Hydrostatic pressure (Pa)	Pressure loss (kinetic energy) (Pa)	Pressure loss (friction) (Pa)	(τ_w) (Pa)	$\left(\frac{8\bar{u}_{fl}}{D_t}\right)$ (s^{-1})	Re (-)
142	138,43	0,740	0,732	0,736	58,60	0,19	10 000	7 407	37	17 370	1,75	381,68	182,28
143	139,41	0,732	0,724	0,728	27,10	0,41	25 000	7 327	175	32 152	3,23	831,14	426,44
201	195,95	0,724	0,713	0,719	25,20	0,63	40 000	7 232	400	46 832	4,71	1256,32	658,67
244	218,38	0,713	0,701	0,707	16,70	1,05	75 000	7 114	1 133	80 981	8,14	2112,70	1127,15

Experiment I.3

Sludge solids concentration : 5,00 % m/m
Sludge density : 1027,8 kg/m^3
Sludge temperature : 20,5 ^oC
Tube length : 9,90 m

Mass of sludge (g)	Volume of sludge ($m^3 \times 10^6$)	Initial height difference (h_1) (m)	Final height difference (h_2) (m)	Average height difference $\left(\frac{h_1+h_2}{2}\right)$ (m)	Time (s)	Average velocity in tube ($\bar{u}_{fl}$) (m/s)	Air pressure (Pa)	Hydrostatic pressure (Pa)	Pressure loss (kinetic energy) (Pa)	Pressure loss (friction) (Pa)	(τ_w) (Pa)	$\left(\frac{8\bar{u}_{fl}}{D_t}\right)$ (s^{-1})	Re (-)
107	104,10	0,700	0,694	0,697	63,00	0,13	6 000	7 028	18	13 010	1,31	266,97	115,05
120	116,75	0,694	0,688	0,691	34,30	0,27	15 000	6 965	76	21 889	2,20	549,93	259,79
140	136,21	0,688	0,680	0,684	26,80	0,41	29 000	6 893	171	35 722	3,59	821,14	399,90
153	148,86	0,680	0,671	0,676	22,40	0,53	37 000	6 812	293	43 519	4,37	1073,66	530,70
169	164,42	0,671	0,662	0,667	20,20	0,65	48 000	6 722	439	54 283	5,46	1315,10	655,90
169	164,42	0,662	0,653	0,657	17,30	0,76	55 000	6 628	599	61 029	6,13	1535,55	770,28
191	185,83	0,653	0,642	0,648	17,10	0,87	65 000	6 529	784	70 745	7,11	1755,74	884,56

Experiment I.4

Sludge solids concentration : 5,73 % m/m
Sludge density : 1032,4 kg/m^3
Sludge temperature : 20,5 ^oC
Tube length : 9,90 m

Mass of sludge (g)	Volume of sludge ($m^3 \times 10^6$)	Initial height difference (h_1) (m)	Final height difference (h_2) (m)	Average height difference $\left(\frac{h_1+h_2}{2}\right)$ (m)	Time (s)	Average velocity in tube ($\bar{u}_{fl}$) (m/s)	Air pressure (Pa)	Hydrostatic pressure (Pa)	Pressure loss (kinetic energy) (Pa)	Pressure loss (friction) (Pa)	(τ_w) (Pa)	$\left(\frac{8\bar{u}_{fl}}{D_t}\right)$ (s^{-1})	Re (-)
51	49,40	0,735	0,732	0,734	178,30	0,02	6 500	7 429	0	13 929	1,40	44,77	3,69
97	93,96	0,732	0,727	0,730	31,90	0,24	25 000	7 388	57	32 331	3,25	457,89	154,53
141	136,58	0,727	0,719	0,723	17,10	0,64	55 000	7 322	425	61 897	6,22	1290,47	518,85
212	205,36	0,719	0,708	0,713	18,00	0,92	80 000	7 224	868	86 356	8,68	1843,26	773,38
193	186,95	0,735	0,724	0,730	13,40	1,12	105 000	7 390	1 298	111 092	11,17	2254,12	963,62

Experiment I.5

Sludge solids concentration	:	6,04	% m/m
Sludge density	:	1034,3	kg/m^3
Sludge temperature	:	20,5	^oC
Tube length	:	9,90	m

Mass of sludge (g)	Volume of sludge (m^3 x 10^6)	Initial height difference (h_1) (m)	Final height difference (h_2) (m)	Average height difference $\left(\frac{h_1+h_2}{2}\right)$ (m)	Time (s)	Average velocity in tube ($\bar{u}_{ff}$) (m/s)	Air pressure (Pa)	Hydrostatic pressure (Pa)	Pressure loss (kinetic energy) (Pa)	Pressure loss (friction) (Pa)	(τ_w) (Pa)	$\left(\frac{8\bar{u}_{ff}}{D_i}\right)$ (s^{-1})	Re (-)
35	33,84	0,700	0,698	0,699	142,60	0,02	9 000	7 092	0	16 092	1,62	38,34	2,48
106	102,49	0,698	0,692	0,695	49,10	0,17	20 000	7 053	29	27 024	2,72	337,24	94,23
206	199,17	0,692	0,681	0,687	41,30	0,39	35 000	6 967	155	41 812	4,20	779,17	287,16
216	208,84	0,681	0,669	0,675	33,30	0,50	45 000	6 850	263	51 587	5,18	1013,27	395,68
207	200,14	0,669	0,658	0,664	26,30	0,61	55 000	7 732	387	61 345	6,17	1229,50	497,47
210	203,04	0,658	0,646	0,652	21,90	0,75	65 000	6 616	574	71 042	7,14	1497,92	625,04
218	210,78	0,646	0,634	0,640	20,40	0,83	75 000	6 497	713	80 784	8,12	1669,32	706,96
211	204,01	0,634	0,623	0,629	16,90	0,97	89 000	6 379	974	94 405	9,49	1950,34	841,81

Experiment I.6

Sludge solids concentration	:	7,01	% m/m
Sludge density	:	1040,4	kg/m^3
Sludge temperature	:	20,5	^oC
Tube length	:	9,90	m

Mass of sludge (g)	Volume of sludge (m^3 x 10^6)	Initial height difference (h_1) (m)	Final height difference (h_2) (m)	Average height difference $\left(\frac{h_1+h_2}{2}\right)$ (m)	Time (s)	Average velocity in tube ($\bar{u}_{fl}$) (m/s)	Air pressure (Pa)	Hydrostatic pressure (Pa)	Pressure loss (kinetic energy) (Pa)	Pressure loss (friction) (Pa)	(τ_w) (Pa)	$\left(\frac{8\bar{u}_{fl}}{D_t}\right)$ (s^{-1})	Re (-)
72	69,21	0,735	0,731	0,733	199,70	0,03	20 000	7 481	1	27 480	2,76	55,99	2,92
114	109,58	0,731	0,725	0,728	29,10	0,30	45 000	7 429	95	52 334	5,26	608,39	151,16
130	124,96	0,735	0,728	0,735	16,80	0,60	70 000	7 501	372	77 129	7,75	1201,73	367,83
189	181,67	0,735	0,725	0,735	17,10	0,85	100 000	7 501	758	106 743	10,73	1716,48	565,73
209	200,89	0,735	0,724	0,735	14,30	1,13	130 000	7 501	1 326	136 175	13,69	2269,77	782,27

Experiment I.7

Sludge solids concentration	:	7,85	% m/m
Sludge density	:	1045,7	kg/m^3
Sludge temperature	:	20,5	^oC
Tube length	:	9,90	m

Mass of sludge (g)	Volume of sludge ($m^3 \times 10^6$)	Initial height difference (h_1) (m)	Final height difference (h_2) (m)	Average height difference $\left(\frac{h_1+h_2}{2}\right)$ (m)	Time (s)	Average velocity in tube ($\bar{u}_{fl}$) (m/s)	Air pressure (Pa)	Hydrostatic pressure (Pa)	Pressure loss (kinetic energy) (Pa)	Pressure loss (friction) (Pa)	(τ_w) (Pa)	$\left(\frac{8\bar{u}_{fl}}{D_i}\right)$ (s^{-1})	Re (-)
27	25,82	0,735	0,734	0,734	436,50	0,00	29 000	7 532	0	36 532	3,67	9,56	0,05
138	131,97	0,734	0,726	0,730	57,60	0,18	55 000	7 486	35	62 451	6,28	370,18	49,35
153	146,32	0,726	0,718	0,722	29,80	0,39	75 000	7 406	163	82 243	8,27	793,29	156,36
177	169,27	0,718	0,708	0,713	20,30	0,67	105 000	7 314	470	111 844	11,24	1347,21	320,77
206	197,00	0,708	0,697	0,703	16,70	0,95	140 000	7 207	940	146 267	14,70	1905,94	497,22
266	254,38	0,697	0,683	0,690	16,80	1,22	175 000	7 077	1 549	180 528	18,14	2446,42	672,49
222	212,30	0,683	0,671	0,677	12,40	1,38	205 000	6 941	1 980	209 961	21,10	2766,24	777,43

Experiment I.8

Sludge solids concentration : 8,72 % m/m
Sludge density : 1051,2 kg/m^3
Sludge temperature : 20,5 ^oC
Tube length : 9,90 m

Mass of sludge (g)	Volume of sludge ($m^3 \times 10^6$)	Initial height difference (h_1) (m)	Final height difference (h_2) (m)	Average height difference $\left(\frac{h_1+h_2}{2}\right)$ (m)	Time (s)	Average velocity in tube ($\bar{u}_{fl}$) (m/s)	Air pressure (Pa)	Hydrostatic pressure (Pa)	Pressure loss (kinetic energy) (Pa)	Pressure loss (friction) (Pa)	(τ_w) (Pa)	$\left(\frac{8\bar{u}_{fl}}{D_t}\right)$ (s^{-1})	Re (-)
26	24,73	0,745	0,744	0,744	306,50	0.01	39 000	7 676	0	46 676	4,69	13,04	0,08
144	136,98	0,744	0,736	0,740	211,20	0,05	50 000	7 629	3	57 626	5,79	104,79	4,58
143	136,03	0,736	0,728	0,732	45,90	0,24	75 000	7 549	60	82 489	8,29	478,82	63,31
166	157,91	0,728	0,719	0,724	26,70	0,48	100 000	7 463	238	107 225	10,78	955,54	176,21
211	200,72	0,719	0,708	0,714	22,90	0,70	125 000	7 358	521	131 837	13,25	1416,12	299,82
216	205,47	0,708	0,696	0,702	16,70	0,99	165 000	7 240	1 028	171 212	17,21	1987,88	461,66
224	213,08	0,696	0,684	0,690	13,90	1,23	200 000	7 118	1 596	205 522	20,66	2476,77	603,81
223	212,13	0,684	0,672	0,678	12,40	1,38	230 000	6 994	1 988	235 006	23,62	2763,99	688,30
252	239,72	0,672	0,659	0,665	12,40	1,55	255 000	6 861	2 538	259 323	26,06	3123,43	794,74

Experiment I.9

Sludge solids concentration : 9,90 % m/m
Sludge density : 1058,9 kg/m^3
Sludge temperature : 20,5 °C
Tube length : 9,90 m

Mass of sludge (g)	Volume of sludge ($m^3 \times 10^6$)	Initial height difference (h_1) (m)	Final height difference (h_2) (m)	Average height difference $\left(\frac{h_1+h_2}{2}\right)$ (m)	Time (s)	Average velocity in tube ($\bar{u}_{fl}$) (m/s)	Air pressure (Pa)	Hydrostatic pressure (Pa)	Pressure loss (kinetic energy) (Pa)	Pressure loss (friction) (Pa)	(τ_w) (Pa)	$\left(\frac{8\bar{u}_{fl}}{D_t}\right)$ (s^{-1})	Re (-)
204	192,66	0,770	0,759	0,765	200,00	0,08	45 000	7 941	6	52 935	11,53*	155,64	5,10
214	202,10	0,759	0,748	0,753	26,80	0,61	84 000	7 826	389	91 437	19,91*	1218,39	166,95
220	207,77	0,748	0,736	0,742	18,40	0,91	100 000	7 705	872	106 833	23,26*	1824,37	295,75
210	198,32	0,736	0,725	0,730	76,30	0,21	128 000	7 586	46	135 540	13,62	419,95	30,51
215	203,05	0,725	0,713	0,719	35,50	0,46	158 000	7 468	224	165 244	16,61	924,10	110,26
228	215,32	0,713	0,701	0,707	24,20	0,72	198 000	7 345	542	204 803	20,58	1437,56	212,04
215	203,05	0,701	0,690	0,695	17,90	0,91	218 000	7 222	880	224 342	22,55	1832,70	297,61
221	208,71	0,690	0,678	0,684	15,50	1,08	253 000	7 101	1 240	258 861	26,02	2175,54	374,97
259	244,60	0,678	0,664	0,671	14,70	1,34	292 000	6 968	1 894	297 074	29,86	2688,37	494,31
257	242,71	0,664	0,650	0,657	12,50	1,56	335 000	6 824	2 579	339 245	34,10	3137,11	601,18
223	210,60	0,650	0,638	0,644	9,70	1,75	372 000	6 691	3 225	375 466	37,74	3507,84	690,70
225	212,49	0,638	0,626	0,632	8,50	2,01	420 000	6 567	4 275	422 292	42,44	4038,97	820,37

*Tube length = 4,57 m

Experiment I.10

Sludge solids concentration : 11,10 % m/m
Sludge density : 1066,8 kg/m^3
Sludge temperature : 20,5 °C
Tube length : 4,57 m

Mass of sludge (g)	Volume of sludge ($m^3 \times 10^6$)	Initial height difference (h_1) (m)	Final height difference (h_2) (m)	Average height difference $\left(\frac{h_1+h_2}{2}\right)$ (m)	Time (s)	Average velocity in tube ($\bar{u}_{ll}$) (m/s)	Air pressure (Pa)	Hydrostatic pressure (Pa)	Pressure loss (kinetic energy) (Pa)	Pressure loss (friction) (Pa)	(τ_w) (Pa)	$\left(\frac{8\bar{u}_{ll}}{D_t}\right)$ (s^{-1})	Re (-)
208	194,98	0,850	0,839	0,844	260,30	0,06	78 000	8 837	3	86 834	18,91	121,02	1,45
204	191,23	0,839	0,828	0,834	55,90	0,27	115 000	8 723	81	123 642	26,92	552,72	25,64
213	199,67	0,828	0,817	0,822	25,30	0,63	140 000	8 607	429	148 178	32,26	1275,10	108,59
218	204,36	0,817	0,805	0,811	16,60	0,99	170 000	8 488	1 045	177 443	38,63	1988,99	219,84
228	213,73	0,805	0,793	0,799	12,60	1,36	200 000	8 364	1 983	206 381	44,93	2740,62	354,66
263	246,54	0,793	0,779	0,786	12,00	1,65	225 000	8 227	2 909	230 318	50,15	3319,39	466,32
256	239,98	0,779	0,766	0,772	10,00	1,93	250 000	8 083	3 969	254 114	55,33	2877,25	578,41
207	194,05	0,766	0,755	0,760	37,00	0,42	270 000	7 955	190	277 765	27,92*	847,33	54,55
211	197,80	0,755	0,743	0,749	28,20	0,56	295 000	7 839	339	302 500	30,40*	1133,23	89,35
215	201,54	0,743	0,732	0,738	19,20	0,84	340 000	7 720	759	346 961	34,87*	1695,98	171,67
221	207,17	0,732	0,720	0,726	13,70	1,22	395 000	7 600	1 576	401 024	40,30*	2443,18	299,68

*Tube length = 9,90 m

Experiment I.11

Sludge solids concentration : 12,80 % m/m
Sludge density : 1078,1 kg/m^3
Sludge temperature : 20,0 ^oC
Tube length : 2,00 m

Mass of sludge (g)	Volume of sludge ($m^3 \times 10^6$)	Initial height difference (h_1) (m)	Final height difference (h_2) (m)	Average height difference $\left(\frac{h_1+h_2}{2}\right)$ (m)	Time (s)	Average velocity in tube ($\bar{u}_{ff}$) (m/s)	Air pressure (Pa)	Hydrostatic pressure (Pa)	Pressure loss (kinetic energy) (Pa)	Pressure loss (friction) (Pa)	(τ_w) (Pa)	$\left(\frac{8\bar{u}_{ff}}{D_t}\right)$ (s^{-1})	Re (-)
5,77	5,35	1,205	1,205	1,205	65,44	0,01	10 000	12 743	0	22 743	11,31	13,21	0,01
10,95	10,16	1,205	1,204	1,204	41,48	0,02	30 000	12 738	0	42 738	21,26	39,56	0,11
130,42	120,97	1,204	1,197	1,201	30,54	0,32	50 000	12 699	109	62 590	31,14	639,96	24,47
168,22	156,03	1,197	1,188	1,193	19,04	0,66	70 000	12 616	467	82 149	40,87	1324,00	89,22
207,44	192,41	1,188	1,178	1,183	13,56	1,14	90 000	12 512	1 402	101 110	50,30	2292,50	221,11
217,85	202,06	1,178	1,166	1,172	9,90	1,64	110 000	12 394	2 902	119 492	59,45	3297,61	387,72
254,48	236,04	1,166	1,153	1,159	9,50	2,00	130 000	12 263	4 300	137 963	68,64	4014,28	518,20
360,50	334,37	1,153	1,134	1,143	10,62	2,53	150 000	12 092	6 905	155 187	77,21	5086,96	725,62
245,68	227,87	1,134	1,121	1,127	6,02	3,04	170 000	11 924	9 981	171 943	85,54	6115,76	934,11
222,63	206,50	1,121	1,109	1,115	4,38	3,79	200 000	11 794	15 482	196 312	97,67	7617,05	1249,60

Experiment I.12

Sludge solids concentration	:	14,27	% m/m
Sludge density	:	1088,2	kg/m^3
Sludge temperature	:	20,0	^oC
Tube length	:	2,00	m

Mass of sludge (g)	Volume of sludge ($m^3 \times 10^6$)	Initial height difference (h_1) (m)	Final height difference (h_2) (m)	Average height difference $\left(\frac{h_1+h_2}{2}\right)$ (m)	Time (s)	Average velocity in tube ($\bar{u}_{fl}$) (m/s)	Air pressure (Pa)	Hydrostatic pressure (Pa)	Pressure loss (kinetic energy) (Pa)	Pressure loss (friction) (Pa)	(τ_w) (Pa)	$\left(\frac{8\bar{u}_{fl}}{D_t}\right)$ (s^{-1})	Re (-)
13,32	12,24	1,205	1,204	1,205	47,67	0,02	60 000	12 859	0	72 859	36,25	41,49	0,07
79,71	73,25	1,204	1,200	1,202	42,01	0,14	80 000	12 833	21	92 812	46,17	281,72	3,11
98,16	90,21	1,200	1,195	1,198	24,44	0,30	100 000	12 784	95	112 689	56,06	596,33	12,87
120,69	110,91	1,195	1,189	1,192	16,94	0,53	120 000	12 723	301	132 422	65,88	1057,82	36,38
151,47	139,20	1,189	1,181	1,185	13,79	0,81	140 000	12 648	716	151 932	75,59	1630,86	76,78
270,01	248,13	1,181	1,167	1,174	16,78	1,19	160 000	12 531	1 537	170 994	85,07	2389,14	143,52
262,69	241,01	1,167	1,153	1,160	11,98	1,62	190 000	12 383	2 845	199 538	99,27	3250,34	231,69
236,70	217,52	1,153	1,141	1,147	7,59	2,30	230 000	12 245	5 774	236 471	117,64	4630,31	390,27
312,55	287,23	1,141	1,125	1,133	7,80	2,96	270 000	12 092	9 533	272 559	135,60	5949,84	554,27
281,60	258,78	1,125	1,110	1,117	6,03	3,45	310 000	11 928	12 949	308 979	153,72	6933,77	681,74

Experiment I.13

Sludge solids concentration	:	15,31	% m/m
Sludge density	:	1095,4	kg/m^3
Sludge temperature	:	20,0	^oC
Tube length	:	1,00	m

Mass of sludge (g)	Volume of sludge ($m^3 \times 10^6$)	Initial height difference (h_1) (m)	Final height difference (h_2) (m)	Average height difference $\left(\frac{h_1+h_2}{2}\right)$ (m)	Time (s)	Average velocity in tube ($\bar{u}_{fl}$) (m/s)	Air pressure (Pa)	Hydrostatic pressure (Pa)	Pressure loss (kinetic energy) (Pa)	Pressure loss (friction) (Pa)	(τ_w) (Pa)	$\left(\frac{8\bar{u}_{fl}}{D_t}\right)$ (s^{-1})	Re (-)
12,08	11,03	1,205	1,204	1,205	54,66	0,02	50 000	12 945	0	62 945	62,63	32,60	0,03
208,96	190,76	1,204	1,194	1,199	62,20	0,25	70 000	12 884	67	82 817	82,40	495,52	5,65
138,48	126,42	1,194	1,186	1,190	18,59	0,55	90 000	12 787	327	102 460	101,95	1098,73	24,92
181,18	165,40	1,186	1,177	1,182	13,82	0,96	110 000	12 699	1 014	121 685	121,08	1933,69	67,58
210,68	192,33	1,177	1,166	1,172	10,84	1,43	130 000	12 590	2 228	140 362	139,66	2866,68	130,39
238,66	217,88	1,166	1,154	1,160	8,84	1,98	150 000	12 465	4 299	158 166	157,38	3982,10	219,54
236,13	215,57	1,154	1,142	1,148	6,88	2,52	170 000	12 334	6 948	175 386	174,51	5062,29	315,83
312,96	285,71	1,142	1,125	1,134	7,86	2,92	190 000	12 181	9 351	192 830	191,87	5872,88	392,70
332,28	303,35	1,125	1,108	1,117	7,07	3,45	210 000	12 002	13 028	208 974	207,93	6932,17	497,63

Experiment I.14

Sludge solids concentration : 16,71 % m/m
Sludge density : 1105,3 kg/m^3
Sludge temperature : 20,0 ^oC
Tube length : 1,00 m

Mass of sludge (g)	Volume of sludge ($m^3 \times 10^6$)	Initial height difference (h_1) (m)	Final height difference (h_2) (m)	Average height difference $\left(\frac{h_1+h_2}{2}\right)$ (m)	Time (s)	Average velocity in tube ($\bar{u}_{ft}$) (m/s)	Air pressure (Pa)	Hydrostatic pressure (Pa)	Pressure loss (kinetic energy) (Pa)	Pressure loss (friction) (Pa)	(τ_w) (Pa)	$\left(\frac{8\bar{u}_{ft}}{D_t}\right)$ (s^{-1})	Re (-)
16,52	14,95	1,205	1,204	1,205	47,89	0,03	80 000	13 061	1	93 060	92,59	50,43	0,04
66,53	60,19	1,204	1,201	1,202	24,88	0,19	110 000	13 038	42	122 996	122,38	390,89	2,38
184,88	167,28	1,201	1,191	1,196	22,74	0,59	140 000	12 967	386	152 581	151,82	1188,48	19,35
167,62	151,66	1,191	1,183	1,187	12,11	1,01	170 000	12 870	1 120	181 750	180,84	2023,36	49,84
169,03	152,93	1,183	1,174	1,178	8,23	1,49	200 000	12 776	2 465	210 311	209,26	3002,31	93,03
257,48	232,96	1,174	1,161	1,167	8,98	2,09	230 000	12 658	4 806	237 852	236,66	4191,40	165,80
226,65	205,07	1,161	1,149	1,155	6,16	2,68	260 000	12 524	7 914	264 610	263,29	5378,57	243,11
280,28	253,59	1,149	1,135	1,142	6,01	3,39	290 000	12 383	12 713	289 670	288,22	6817,26	344,79
335,79	303,81	1,135	1,118	1,126	6,25	3,91	320 000	12 212	16 873	315 339	313,76	7853,80	421,97

I.2 SAMPLE CALCULATIONS

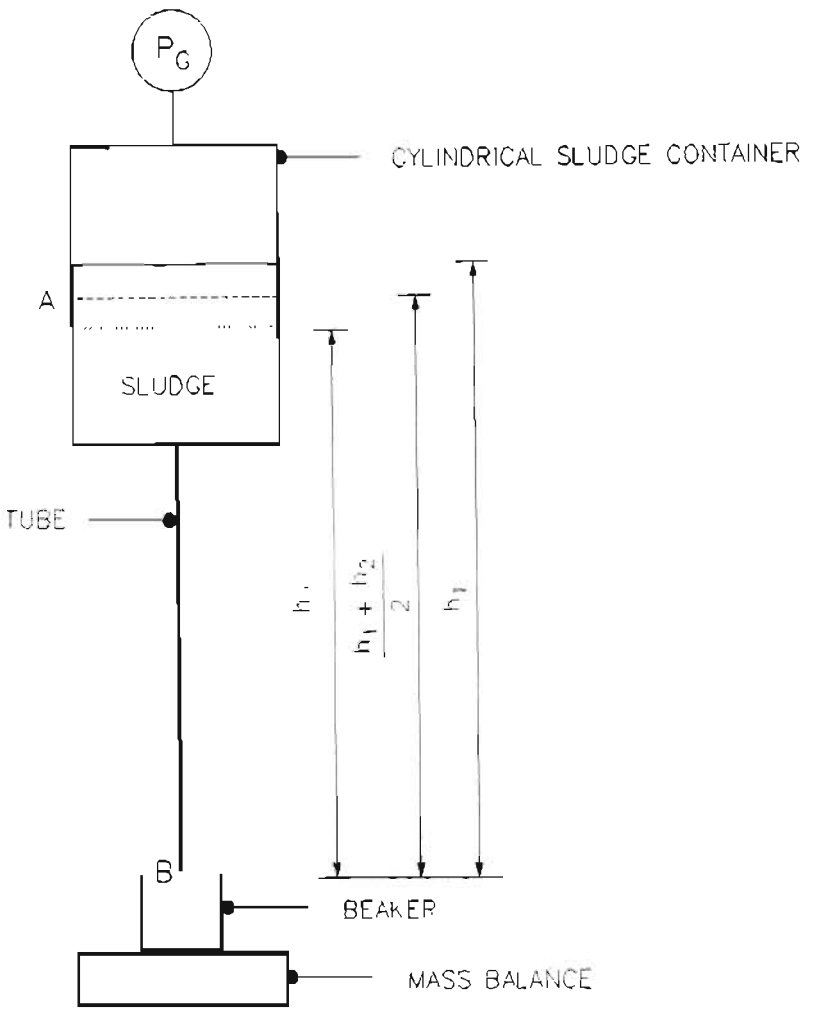

FIGURE I.1 : Diagram of Capillary-tube Viscometer to Explain Symbols for Sample Calculations

From Figure I.1 and Bernoulli's equation applied at points A and B with B as reference point (as shown in Figure I.1); and ignoring entrance and exit effects for the tube (Coulson and Richardson, 1977) :

$$\frac{P_c}{\rho_{ll} g} + \left(\frac{\bar{u}_{ll}^2}{2 f_c g}\right)_{at\,A} + \left(\frac{h_1 + h_2}{2}\right) - \frac{\Delta p_t}{\rho_{ll} g} = \frac{P_B}{\rho_{ll} g} + \left(\frac{\bar{u}_{ll}^2}{2 f_c g}\right)_{at\,B} + h_B \qquad (I.1)$$

where f_c = correction factor for velocity, (-)

g = constant of gravitational acceleration, (m/s^2)

h_1 = initial height difference between level of sludge in cylindrical sludge container and outlet of tube, (m)

h_2 = final height difference between level of sludge in cylindrical sludge container and outlet of tube, (m)

h_B = height of reference point B in diagram I.1, (m)

P_B = static pressure at point B in diagram I.1, (Pa)

P_C = air pressure applied to cylinder, (Pa)

Δp_t = pressure difference between ends of tube, (Pa)

$\bar{u}_{fl}$ = average velocity of fluid, (m/s)

ρ_{fl} = density of fluid, (kg/m^3)

But since $\bar{u}_{fl}$ at A is negligible compared to $\bar{u}_{fl}$ at B, $\bar{u}_{fl}$ at A can be ignored.

Also, $h_B = 0$ m since B is reference point and;

$P_B = 0$ Pa (gauge) since this pressure is atmospheric pressure.

According to Bowen (1961) some researchers have shown that for laminar flow of non-Newtonian fluids, $f_c = 0.5$.

Therefore, equation (I.1) becomes :

$$\Delta p_t = \rho_{fl} g \left(\frac{P_C}{\rho_{fl} g} + \left(\frac{h_1 + h_2}{2} \right) - \left(\frac{\bar{u}_{fl}^2}{g} \right)_{at\,B} \right)$$

$$= P_C + \rho_{fl} g \left(\frac{h_1 + h_2}{2} \right) - \rho_{fl} \left(\bar{u}_{fl}^2 \right)_{at\,B} \qquad (I.2)$$

(i) **Calculation of h_2** :

At the start of an experiment for a specific solids concentration, h_1 was measured. h_2 was calculated from the following equation :

$$h_2 = h_1 - \left(\frac{4 V_{sl}}{\pi (0.15)^2} \right) \qquad (I.3)$$

where V_{sl} = volume of sludge collected, (m^3)

The internal diameter of the cylindrical sludge container was 150 mm.

For subsequent experiments (at a fixed solids concentration), h_2 from the preceding experiment was taken as h_1 for the following experiment.

(ii) **Calculation of $\bar{u}_{fl}$ in tube** :

$\bar{u}_{fl}$ was calculated from the following equation :

$$\bar{u}_{fl} = \frac{4 V_{sl}}{\pi t D_t^2} \qquad (I.4)$$

where D_t = internal tube diameter, (m)

t = time, (s)

(iii) **Calculation of τ_w**:

τ_w was calculated from equation (4.11) :

$$\tau_w = \frac{\Delta p_t R_t}{2 L_t} = \frac{\Delta p_t D_t}{4 L_t} \qquad (I.5)$$

where L_t = length of tube, (m)

R_t = internal radius of tube, (m)

(iv) **Calculation of Re** :

The Reynolds number, Re, was calculated from equation (4.29) :

$$Re = \frac{\rho_{fl} \bar{u}_{fl} D_t}{\eta \left(1 + \frac{\tau_o D_t}{6 \eta \bar{u}_{fl}} \right)} \qquad (4.29)$$

where τ_o = yield stress, (Pa)

η = coefficient of rigidity, (Pa.s)

(v) **Density of sludge** :

The density of the sludge was calculated from the following equation :

$$\rho_{fl} = \frac{1}{\left(\frac{c_s}{100 \rho_s} \right) + \frac{\left(\frac{1 - c_s}{100} \right)}{\rho_l}} \qquad (I.6)$$

where c_s = solids concentration of sludge (cake), (% m/m)

ρ_l = liquid density, (kg/m^3)

ρ_s = solids density, (kg/m^3)

APPENDIX J
CROSS-FLOW FILTRATION EXPERIMENTS

J.1 EXPERIMENTS WITH FLOW RATE OF FEED SLUDGE = 0,84 ℓ/min AND P = 300 kPa

Note : For each feed sludge flow rate, the filtrate volumes at various filtration times are only given for the experiment with the longest total filtration time. The filtrate volumes for the experiments at shorter filtration times were very close to those for the experiment at the longest total filtration time.

Experiment J.1.1

Date	6/12/1990	
Filtration time	5	minutes
Temperature of filtrate	22,0	°C
Feed solids concentration	48,99	g/ℓ
Feed sludge flow rate	0,84	ℓ/min
Total mass of wet cake	171,91	g
Average cake dry solids concentration	18,91	% m/m
Measured internal cake diameter	cake broken	
Calculated internal cake diameter	15,75	mm

Experiment J.1.2

Date	6/12/1990	
Filtration time	10	minutes
Temperature of filtrate	22,0	°C
Feed solids concentration	48,99	g/ℓ
Feed sludge flow rate	0,84	ℓ/min
Total mass of wet cake	203,02	g
Average cake dry solids concentration	20,99	% m/m
Measured internal cake diameter	cake broken	
Calculated internal cake diameter	13, 24	mm

Experiment J.1.3

Date	6/12/1990	
Filtration time	15	minutes
Temperature of filtrate	22,0	°C
Feed solids concentration	48,99	g/ℓ
Feed sludge flow rate	0,84	ℓ/min
Total mass of wet cake	224,78	g
Average cake dry solids concentration	22,35	% m/m
Measured internal cake diameter	11,8	mm
Calculated internal cake diameter	11,20	mm

Experiment J.1.4

Date	6/12/1990	
Filtration time	20	minutes
Temperature of filtrate	22,0	°C
Feed solids concentration	48,99	g/ℓ
Feed sludge flow rate	0,84	ℓ/min
Total mass of wet cake	238,92	g
Average cake dry solids concentration	23,42	% m/m
Measured internal cake diameter	9,3	mm
Calculated internal cake diameter	9,71	mm

Experiment J.1.5

Date	6/12/1990	
Filtration time	25	minutes
Temperature of filtrate	22,0	°C
Feed solids concentration	48,99	g/ℓ
Feed sludge flow rate	0,84	ℓ/min
Total mass of wet cake	252,16	g
Average cake dry solids concentration	24,16	% m/m
Measured internal cake diameter	7,7	mm
Calculated internal cake diameter	8,03	mm

Experiment J.1.6

Date	6/12/1990	
Filtration time	30	minutes
Temperature of filtrate	22,0	°C
Feed solids concentration	48,99	g/ℓ
Feed sludge flow rate	0,84	ℓ/min
Total mass of wet cake	258,10	g
Average cake dry solids concentration	24,85	% m/m
Measured internal cake diameter	7,0	mm
Calculated internal cake diameter	7,26	mm

Experiment J.1.7

Date	6/12/1990	
Filtration time	60	minutes
Temperature of filtrate	22,0	°C
Feed solids concentration	48,99	g/ℓ
Feed sludge flow rate	0,84	ℓ/min
Total mass of wet cake	268,95	g
Average cake dry solids concentration	27,19	% m/m
Measured internal cake diameter	5,2	mm
Calculated internal cake diameter	6,04	mm

Experiment J.1.8

Date	7/12/1990	
Filtration time	90	minutes
Temperature of filtrate	20,5	°C
Feed solids concentration	48,99	g/ℓ
Feed sludge flow rate	0,84	ℓ/min
Total mass of wet cake	272,00	g
Average cake dry solids concentration	28,43	% m/m
Measured internal cake diameter	5,0	mm
Calculated internal cake diameter	5,89	mm

Experiment J.1.8 (cont. i)

Time (minutes)	Mass of filtrate (g)
0,0	0,0
1,5	262,8
2,0	304,8
2,5	341,1
3,0	374,0
3,5	403,7
4,0	430,5
4,5	456,0
5,0	480,0
5,5	502,7
6,0	523,9
6,5	544,6
7,0	563,8
7,5	582,8
8,0	600,7
8,5	618,4
9,0	635,0
9,5	651,8
10,0	667,5
10,5	682,8
11,0	697,8
11,5	712,2
12,0	726,4
12,5	740,4
13,0	754,2
13,5	767,6
14,0	780,3
14,5	793,1
15,0	805,7
15,5	818,0
16,0	829,7
16,5	841,7
17,0	853,4
17,5	864,9
18,0	875,9
18,5	887,0
19,0	897,9

Experiment J.1.8 (cont. ii)

Time (minutes)	Mass of filtrate (g)
19,5	908,6
20,0	919,3
20,5	929,7
21,0	939,8
21,5	949,9
22,0	960,0
22,5	969,9
23,0	979,7
23,5	989,3
24,0	998,9
24,5	1007,9
25,0	1017,2
25,5	1026,5
26,0	1035,5
26,5	1044,5
27,0	1053,5
27,5	1062,0
28,0	1070,7
28,5	1079,4
29,0	1087,7
29,5	1096,2
30,0	1104,5
31,0	1120,8
32,0	1136,9
33,0	1152,9
34,0	1168,2
35,0	1183,6
36,0	1198,7
37,0	1213,4
38,0	1228,7
39,0	1243,1
40,0	1257,1
41,0	1271,2
42,0	1285,0
43,0	1298,7
44,0	1312,1
45,0	1325,4

Experiment J.1.8 (cont. iii)

Time (minutes)	Mass of filtrate (g)
46,0	1338,5
47,0	1351,6
48,0	1364,3
49,0	1377,0
50,0	1389,6
51,0	1402,2
52,0	1414,4
53,0	1426,5
54,0	1438,6
55,0	1450,5
56,0	1462,2
57,0	1474,1
58,0	1485,6
59,0	1497,2
60,0	1508,7
61,0	1520,1
62,0	1531,5
63,0	1542,9
64,0	1554,3
65,0	1566,3
66,0	1577,6
67,0	1588,5
68,0	1599,3
69,0	1609,8
70,0	1620,5
71,0	1630,7
72,0	1641,0
73,0	1651,5
74,0	1661,6
75,0	1671,7
76,0	1681,7
77,0	1691,8
78,0	1702,0
79,0	1711,6
80,0	1721,7
81,0	1731,5
82,0	1741,4

Experiment J.1.8 - continued (iv)

Time (minutes)	Mass of filtrate (g)
83,0	1751,2
84,0	1760,8
85,0	1770,6
86,0	1780,2
87,0	1790,0
88,0	1799,6
89,0	1809,0
90,0	1818,8

J.2 EXPERIMENTS WITH FLOW RATE OF FEED SLUDGE = 1,58 ℓ/min AND P = 300 kPa

Experiment J.2.1

Date	5/4/1990	
Filtration time	30	minutes
Temperature of filtrate	24,0	°C
Feed solids concentration	53,32	g/ℓ
Feed sludge flow rate	1,58	ℓ/min
Average cake dry solids concentration	22,15	% m/m
Measured internal cake diameter	9,2	mm

Experiment J.2.2

Date	12/4/1990	
Filtration time	70	minutes
Temperature of filtrate	23,5	°C
Feed solids concentration	53,32	g/ℓ
Feed sludge flow rate	1,58	ℓ/min
Average cake dry solids concentration	28,00	% m/m
Measured internal cake diameter	7,5	mm

Experiment J.2.2 - continued (i)

(Filtrate volumes measured with measuring cylinder)

Time (minutes)	Volume of filtrate per minute (mℓ/min)
2	65,0
4	50,0
6	40,0
8	34,5
10	30,0
12	28,0
14	26,0
16	23,5
18	22,5
20	20,5
22	19,5
24	18,5
26	18,0
28	17,5
30	16,5
35	15,0
40	14,5
45	14,0
50	13,5
55	13,0
60	13,0
65	12,5
70	12,0

J.3 EXPERIMENTS WITH FLOW RATE OF FEED SLUDGE = 2,43 ℓ/min AND P = 300 kPa

Experiment J.3.1

Date	28/11/1990	
Filtration time	5	minutes
Temperature of filtrate	21,5	°C
Feed solids concentration	47,95	g/ℓ
Feed sludge flow rate	2,40	ℓ/min
Total mass of wet cake	161,26	g
Average cake dry solids concentration	19,62	% m/m
Measured internal cake diameter	cake broken	
Calculated internal cake diameter	16,63	mm

Experiment J.3.2

Date	28/11/1990	
Filtration time	10	minutes
Temperature of filtrate	22,0	°C
Feed solids concentration	47,95	g/ℓ
Feed sludge flow rate	2,43	ℓ/min
Total mass of wet cake	192,84	g
Average cake dry solids concentration	21,66	% m/m
Measured internal cake diameter	13,9	mm
Calculated internal cake diameter	14,26	mm

Experiment J.3.3

Date	28/11/1990	
Filtration time	15	minutes
Temperature of filtrate	22,5	°C
Feed solids concentration	47,95	g/ℓ
Feed sludge flow rate	2,37	ℓ/min
Total mass of wet cake	211,73	g
Average cake dry solids concentration	22,87	% m/m
Measured internal cake diameter	12,3	mm
Calculated internal cake diameter	12,65	mm

Experiment J.3.4

Date	28/11/1990	
Filtration time	20	minutes
Temperature of filtrate	22,5	°C
Feed solids concentration	47,95	g/ℓ
Feed sludge flow rate	2,43	ℓ/min
Total mass of wet cake	222,59	g
Average cake dry solids concentration	23,51	% m/m
Measured internal cake diameter	11,4	mm
Calculated internal cake diameter	11,63	mm

Experiment J.3.5

Date	29/11/1990	
Filtration time	25	minutes
Temperature of filtrate	22,0	°C
Feed solids concentration	48,99	g/ℓ
Feed sludge flow rate	2,43	ℓ/min
Total mass of wet cake	233,21	g
Average cake dry solids concentration	24,20	% m/m
Measured internal cake diameter	10,0	mm
Calculated internal cake diameter	10,56	mm

Experiment J.3.6

Date	29/11/1990	
Filtration time	30	minutes
Temperature of filtrate	22,5	°C
Feed solids concentration	48,99	g/ℓ
Feed sludge flow rate	2,46	ℓ/min
Total mass of wet cake	239,98	g
Average cake dry solids concentration	24,68	% m/m
Measured internal cake diameter	10,0	mm
Calculated internal cake diameter	9,83	mm

Experiment J.3.7

Date	29/11/1990	
Filtration time	60	minutes
Temperature of filtrate	23,0	°C
Feed solids concentration	48,99	g/ℓ
Feed sludge flow rate	2,43	ℓ/min
Total mass of wet cake	249,58	g
Average cake dry solids concentration	26,55	% m/m
Measured internal cake diameter	8,5	mm
Calculated internal cake diameter	8,99	mm

Experiment J.3.8

Date	29/11/1990	
Filtration time	90	minutes
Temperature of filtrate	23,0	°C
Feed solids concentration	48,99	g/ℓ
Feed sludge flow rate	2,43	ℓ/min
Total mass of wet cake	248,07	g
Average cake dry solids concentration	27,54	% m/m
Measured internal cake diameter	8,8	mm
Calculated internal cake diameter	9,41	mm

Time (minutes)	Mass of filtrate (g)
0,0	0,0
0,5	154,4
1,0	223,4
1,5	274,9
2,0	317,7
2,5	353,7
3,0	386,5
3,5	415,3
4,0	442,3
4,5	468,8
5,0	492,4
5,5	515,3
6,0	536,8
6,5	556,8

Experiment J.3.8 (cont. i)

Time (minutes)	Mass of filtrate (g)
7,0	576,8
7,5	595,8
8,0	611,7
8,5	631,2
9,0	648,6
9,5	664,8
10,0	680,9
10,5	696,8
11,0	712,0
11,5	726,6
12,0	741,2
12,5	755,4
13,0	768,8
13,5	782,4
14,0	795,8
14,5	808,4
15,0	821,5
15,5	834,3
16,0	846,5
16,5	858,8
17,0	870,7
17,5	882,4
18,0	893,8
18,5	905,4
19,0	916,6
19,5	927,8
20,0	938,8
20,5	949,6
21,0	960,2
21,5	970,7
22,0	981,2
22,5	991,5
23,0	1001,8
23,5	1012,8
24,0	1021,7
24,5	1031,7
25,0	1041,3

Experiment J.3.8 (cont. ii)

Time (minutes)	Mass of filtrate (g)
25,5	1050,8
26,0	1061,0
27,0	1079,8
27,5	1088,7
28,0	1097,1
28,5	1107,3
29,0	1116,3
29,5	1125,4
31,0	1151,9
33,0	1186,6
36,0	1236,8
37,0	1252,8
38,0	1269,0
39,0	1285,0
40,0	1300,8
41,0	1316,8
42,0	1332,0
43,0	1347,4
44,0	1362,9
45,0	1377,8
46,0	1392,9
50,0	1452,1
51,0	1466,7
52,0	1481,4
53,0	1495,5
54,0	1509,8
55,0	1523,8
56,0	1538,2
57,0	1552,3
58,0	1566,3
59,0	1580,4
60,0	1594,3
61,0	1607,9
62,0	1621,8
63,0	1635,6

Experiment J.3.8 (cont. iii)

Time (minutes)	Mass of filtrate (g)
65,0	1662,7
66,0	1676,1
67,0	1689,6
68,0	1702,9
69,0	1716,2
70,0	1729,6
71,0	1742,7
72,0	1755,7
73,0	1768,9
74,0	1782,2
75,0	1795,3
76,0	1808,1
77,0	1821,3
78,0	1834,1
79,0	1847,0
80,0	1859,8
81,0	1872,5
82,0	1885,5
83,0	1898,1
84,0	1910,8
85,0	1923,5
86,0	1936,1
87,0	1948,6
88,0	1961,2
89,0	1973,8
90,0	1986,1

Experiment J.3.9

(Filter for 20 minutes and then switch over to water instead of feed sludge)

Date	30/11/1990	
Filtration time	20 minutes with sludge and 70 minutes with water	
Temperature of filtrate	23,0	°C
Feed solids concentration	48,99	g/ℓ
Feed sludge (and water) flow rate	2,37	ℓ/min
Total mass of wet cake	203,68	g
Average cake dry solids concentration	24,89	% m/m
Measured internal cake diameter	13,2	mm
Calculated internal cake diameter	13,68	mm

Time (minutes)	Mass of filtrate (g)
0,0	0,0
0,5	151,8
1,0	215,8
2,0	304,8
2,5	339,9
3,0	371,5
3,5	399,7
4,0	426,7
4,5	450,9
5,0	474,4
5,5	496,4
6,0	517,3
7,0	556,8
7,5	575,7
8,0	593,3
8,5	610,5
9,0	627,5
9,5	643,7
10,0	659,5
11,0	689,8
11,5	704,2

Experiment J.3.9 (cont. i)

Time (minutes)	Mass of filtrate (g)
12,0	718,4
12,5	732,5
13,0	746,1
13,5	759,3
14,0	772,5
14,5	785,2
15,0	797,8
15,5	810,3
16,0	822,4
16,5	834,6
17,0	846,1
17,5	858,6
18,0	869,1
18,5	880,7
19,0	891,6
19,5	903,0
20,0	913,3
21,5	944,8
22,5	965,5
23,0	975,5
23,5	985,6
24,0	995,7
25,0	1015,4
25,5	1025,3
26,0	1035,2
26,5	1045,0
27,0	1054,7
27,5	1064,3
28,0	1073,9
28,5	1083,6
29,0	1093,4
29,5	1103,3
31,0	1133,6
32,0	1153,4

Experiment J.3.9 (cont. ii)

Time (minutes)	Mass of filtrate (g)
33,0	1173,0
34,0	1192,3
35,0	1212,7
36,0	1233,0
37,0	1253,2
38,0	1273,2
39,0	1292,8
40,0	1312,3
41,0	1333,1
42,0	1353,9
43,0	1374,4
44,0	1394,8
45,0	1415,3
46,0	1436,2
47,0	1457,0
48,0	1477,6
49,0	1498,1
51,0	1539,1
52,0	1559,1
53,0	1579,3
54,0	1599,5
55,0	1619,9
56,0	1640,5
57,0	1660,8
58,0	1681,3
60,0	1722,0
61,0	1742,4
62,0	1762,5
63,0	1782,9
64,0	1802,9
65,0	1822,9
67,0	1862,8
68,0	1882,9
70,0	1922,8
71,0	1942,8
73,0	1982,8

Experiment J.3.9 (cont. iii)

Time (minutes)	Mass of filtrate (g)
74,0	2002,8
75,0	2222,8
76,0	2242,9
77,0	2262,6
79,0	2303,1
80,0	2323,4
82,0	2364,3
83,0	2385,0
84,0	2405,6
85,0	2426,5
86,0	2447,5
87,0	2468,4
88,0	2489,4
89,0	2510,4
90,0	2531,6

J.4 EXPERIMENTS WITH FLOW RATE OF FEED SLUDGE = 4,44 ℓ/min AND P = 300 kPa

Experiment J.4.1

Date	10/12/1990	
Filtration time	5	minutes
Temperature of filtrate	21,5	°C
Feed solids concentration	48,99	g/ℓ
Feed sludge flow rate	4,44	ℓ/min
Total mass of wet cake	158,24	g
Average cake dry solids concentration	19,30	% m/m
Measured internal cake diameter	16,4	mm
Calculated internal cake diameter	16,86	mm

Experiment J.4.2

Date	10/12/1990	
Filtration time	10	minutes
Temperature of filtrate	22,0	°C
Feed solids concentration	48,99	g/ℓ
Feed sludge flow rate	4,44	ℓ/min
Total mass of wet cake	190,70	g
Average cake dry solids concentration	20,91	% m/m
Measured internal cake diameter	13,7	mm
Calculated internal cake diameter	14,36	mm

Experiment J.4.3

Date	10/12/1990	
Filtration time	15	minutes
Temperature of filtrate	22,0	°C
Feed solids concentration	48,99	g/ℓ
Feed sludge flow rate	4,44	ℓ/min
Total mass of wet cake	209,30	g
Average cake dry solids concentration	21,97	% m/m
Measured internal cake diameter	12,5	mm
Calculated internal cake diameter	12,77	mm

Experiment J.4.4

Date	10/12/1990	
Filtration time	20	minutes
Temperature of filtrate	22,0	°C
Feed solids concentration	48,99	g/ℓ
Feed sludge flow rate	4,44	ℓ/min
Total mass of wet cake	220,53	g
Average cake dry solids concentration	22,53	% m/m
Measured internal cake diameter	11,8	mm
Calculated internal cake diameter	11,70	mm

Experiment J.4.5

Date	10/12/1990	
Filtration time	25	minutes
Temperature of filtrate	22,0	°C
Feed solids concentration	48,99	g/ℓ
Feed sludge flow rate	4,44	ℓ/min
Total mass of wet cake	224,96	g
Average cake dry solids concentration	23,19	% m/m
Measured internal cake diameter	11,1	mm
Calculated internal cake diameter	11,32	mm

Experiment J.4.6

Date	7/12/1990	
Filtration time	30	minutes
Temperature of filtrate	22,5	°C
Feed solids concentration	48,99	g/ℓ
Feed sludge flow rate	4,44	ℓ/min
Total mass of wet cake	229,16	g
Average cake dry solids concentration	23,78	% m/m
Measured internal cake diameter	10,4	mm
Calculated internal cake diameter	10,95	mm

Experiment J.4.7

Date	7/12/1990	
Filtration time	60	minutes
Temperature of filtrate	21,5	°C
Feed solids concentration	48,99	g/ℓ
Feed sludge flow rate	4,44	ℓ/min
Total mass of wet cake	225,86	g
Average cake dry solids concentration	26,17	% m/m
Measured internal cake diameter	10,9	mm
Calculated internal cake diameter	11,71	mm

Experiment J.4.8

Date	4/12/1990	
Filtration time	90	minutes
Temperature of filtrate	22,0	°C
Feed solids concentration	48,99	g/ℓ
Feed sludge flow rate	4,47	ℓ/min
Total mass of wet cake	224,51	g
Average cake dry solids concentration	26,32	% m/m
Measured internal cake diameter	11,0	mm
Calculated internal cake diameter	11,88	mm

Time (minutes)	Mass of filtrate (g)
0,0	0,0
0,5	156,8
1,0	230,9
1,5	282,2
2,0	325,9
2,5	363,4
3,0	396,4
3,5	425,8
4,0	453,9
4,5	479,9
5,0	503,8
5,5	526,9
6,0	548,3
6,5	569,4
7,0	589,4
7,5	609,0
8,0	627,5
8,5	644,8
9,0	662,3
9,5	679,8
10,0	695,8
10,5	711,9
11,0	727,6
11,5	742,6
12,0	757,7
12,5	772,2
13,0	786,3

Experiment J.4.8 (cont. i)

Time (minutes)	Mass of filtrate (g)
13,5	800,3
14,0	814,4
14,5	827,7
15,0	841,0
15,5	854,3
16,0	867,1
16,5	879,7
17,0	892,1
17,5	904,5
18,0	916,8
18,5	928,7
19,0	940,5
19,5	952,2
20,0	963,8
20,5	974,8
21,0	986,3
21,5	997,6
22,0	1008,8
23,0	1030,3
23,5	1040,9
24,0	1051,9
24,5	1062,2
25,0	1072,8
25,5	1082,8
26,0	1093,2
26,5	1103,8
27,0	1113,6
27,5	1123,5
28,0	1133,4
28,5	1143,4
29,0	1153,0
29,5	1162,8
30,0	1172,3
31,0	1191,8
32,0	1210,7
33,0	1229,4
34,0	1247,8
35,0	1265,8

Experiment J.4.8 (cont. ii)

Time (minutes)	Mass of filtrate (g)
36,0	1284,3
37,0	1302,2
38,0	1319,9
39,0	1337,3
40,0	1355,1
41,0	1372,2
42,0	1389,3
43,0	1406,5
44,0	1423,4
45,0	1440,1
46,0	1456,9
47,0	1473,3
48,0	1489,9
49,0	1506,4
50,0	1522,7
51,0	1538,8
52,0	1554,8
53,0	1570,8
54,0	1586,8
55,0	1602,6
56,0	1619,0
57,0	1634,1
58,0	1649,8
59,0	1665,3
60,0	1680,9
61,0	1696,5
62,0	1711,8
63,0	1727,2
64,0	1742,2
65,0	1757,6
66,0	1772,7
67,0	1787,8
68,0	1803,1
69,0	1818,2
70,0	1833,0
71,0	1847,7
72,0	1862,5
73,0	1877,3

Experiment J.4.8 (cont. iii)

Time (minutes)	Mass of filtrate (g)
74,0	1891,9
75,0	1906,4
76,0	1921,0
77,0	1935,7
78,0	1950,0
79,0	1964,4
80,0	1978,9
81,0	1993,2
82,0	2007,4
83,0	2021,5
85,0	2049,8
86,0	2064,0
87,0	2077,9
88,0	2091,9
89,0	2106,0
90,0	2120,0